1949

THE PHYSICAL REVIEW

Second Series

ST 1, 1949

Published for the

AMERICAN PHYSICAL SOCIETY

by the

AMERICAN INSTITUTE OF PHYSICS

[illegible] New York 18, N. Y.

THE PHYSICAL REVIEW

A journal of experimental and theoretical physics established by E. L. Nichols in 1893

Published by the American Institute of Physics
for the
AMERICAN PHYSICAL SOCIETY

Officers

President

F. W. Loomis
University of Illinois
Urbana, Illinois

Vice-President

I. I. Rabi
Columbia University
New York, New York

Secretary

K. K. Darrow
Bell Telephone Laboratories
Office:
Columbia University
New York 27, New York

Treasurer

G. B. Pegram
Columbia University
New York 27, New York

Local Secretary
for the Pacific Coast

J. Kaplan
University of California at Los Angeles
Los Angeles, California

Managing Editor

John T. Tate
University of Minnesota
Minneapolis, Minnesota

BOARD OF EDITORS

Editor

John T. Tate

Associate Editor

J. W. Buchta

Associate Editors

R. A. Bethe	S. A. Goudsmit	W. E. Lamb, Jr.
L. A. Ellenbogen	E. M. Purcell	R. G. Herb
W. H. Zachariasen	V. F. Weisskopf	J. Halpern

Manuscripts for publication should be submitted to John T. Tate, University of Minnesota, Minneapolis, Minnesota. The authors' institutions are requested to pay a publication charge of $4 per page which, if honored, entitles them to 100 free reprints. Instructions will be sent with galley proofs.

Proof and all correspondence concerning papers in the process of publication should be addressed to the Publication Manager, American Institute of Physics, 57 East 55 Street, New York 22, New York.

Subscription Price

United States and Canada $20.00
Elsewhere $27.00

Back Numbers[1]

Twenty-four monthly issues when complete year is available:
Prior to 1949: $20.00
Thereafter: $27.00
Single copies: $2.00 each, prior to July, 1929;
$1.00 each, July, 1929–December, 1941;
$2.00 each, January, 1942–December, 1946;
$1.00 each, January, 1947–December, 1948.
Current issues: $1.25 each.
General index, 1893–1920: $4.00.

Subscriptions and orders for back numbers should be addressed to Prince and Lemon Streets, Lancaster, Pennsylvania, or to the American Institute of Physics, 57 East 55 Street, New York 22, New York.

Changes of address in the case of members of the American Physical Society should be addressed to the Treasurer; in the case of other subscribers to the Business Manager, American Institute of Physics.

[1] Mrs. Series 1 Issues of Physics Department, Cornell University, Ithaca, New York.

The Physical Review is published monthly by the American Institute of Physics, Prince and Lemon Streets, Lancaster, Pennsylvania.

Entered as second-class matter March 6, 1917, at the Post Office at Lancaster, Pennsylvania, under the Act of March 3, 1879.

Acceptance for mailing at special rate of postage provided for in paragraph 4, section 538, P. L. & R., authorized January 23, 1925.

THE
PHYSICAL REVIEW

A journal of experimental and theoretical physics established by E. L. Nichols in 1893

SECOND SERIES, VOL. 76, NO. 3 AUGUST 1, 1949

Neutron-Hydrogen Mass Difference from the $T^3(p, n)He^3$ Reaction Threshold*

R. F. TASCHEK, H. V. ARGO, A. HEMMENDINGER, AND G. A. JARVIS
Los Alamos Scientific Laboratory, Los Alamos, New Mexico

(Received April 21, 1949)

The threshold for the $T^3(p, n)He^3$ reaction has been carefully measured using protons from the Los Alamos electrostatic generator and a thick target of tritium absorbed in a zirconium disk. The neutrons were observed at 0°, and the proton energy was measured relative to the accurately measured $Al^{27}(p, \gamma)Si^{28}$ resonance at 993.3 kev. The threshold for neutrons is found to be at a proton energy of 1019±1 kev, giving for this reaction $Q=-764\pm1$ kev. Assuming the rest mass of the neutrino to be zero, and the maximum energy of the β-particle from the decay of tritium to be 18.5 kev, 782±2 kev is obtained for the neutron-hydrogen mass difference.

INTRODUCTION

CONSIDERABLE interest in the neutron-hydrogen mass difference has been aroused by the remeasurement of the deuteron binding energy by Bell and Elliott.[1] They obtained a binding energy of 2.237±0.005 Mev measured relative to the ThC″ 2.620-Mev gamma-ray as a standard. This is approximately 50 kev higher than the previously accepted[2] deuteron binding energy. From the $H^1H^1-D^2$ separation of 1.433±0.002 Mev[3] they calculate the $n-H^1$ mass difference to be 804±9 kev. Tollestrup[4] and his collaborators have measured the Q values of the two $D-D$ reactions obtaining

$$D^2+D^2=T^3+H^1+4.036\pm0.022 \text{ Mev}$$
$$=He^3+n^1+3.265\pm0.018 \text{ Mev}$$

from which they calculate $n-H^1=789\pm6$ kev; the differences of the Q's is measurable with greater precision than the absolute value of either. The best previous value[2,5] of the mass difference has been taken to be 754±5 kev.

In view of the marked discrepancy between the recent measurements and the earlier work, the present measurement is considered particularly informative. The threshold for the $T^3(p, n)He^3$ reaction gives immediately the Q of the reaction. With the additional information of the maximum energy carried away by the β-particles in the decay of tritium one can calculate the $n-H^1$ mass difference.

$$T^3+H^1=He^3+n+Q$$
$$T^3=He^3+E_\beta+\mu, \quad (1)$$

where T^3, H^1, and He^3 are atomic masses, and E_β is the maximum energy of the particle from the decay of tritium. Assuming the rest mass μ of the neutrino to be zero, one gets

$$n-H^1=(T^3-He^3)-Q$$
$$=E_\beta-Q. \quad (2)$$

E_β is known to within one kilovolt,[6] and $n-H^1$ will be known to within the sum of the errors of E_β and Q.

EXPERIMENTAL PROCEDURE

The Los Alamos electrostatic generator was used to produce a monoergic beam of protons. The energy of the generator is controlled by an electrostatic analyzer which utilizes the diatomic beam in a feedback control loop. The recently determined highly accurate nuclear energy scale of Herb, Snowdon, and Sala[7] establishes a

* This paper is based on work performed under Government Contract No. W-7405-eng-36 at the Los Alamos Scientific Laboratory of the University of California.

[1] R. E. Bell and L. G. Elliott, Phys. Rev. 74, 1552 (1948).

[2] W. E. Stephens, Rev. Mod. Phys. 19, 19 (1947). D. J. Hughes, Phys. Rev. 70, 219 (1946).

[3] R. Cohen and W. R. Hornyak, Phys. Rev. 72, 1127 (1947).

[4] Tollestrup, Jenkins, Fowler, and Lauritsen, private communications, to be published soon.

[5] K. T. Bainbridge, *Isotopic Weights of the Fundamental Isotopes* (National Research Council, June, 1948), p. 4.

[6] E. R. Graves and D. Meyer, private communication, to be submitted for publication in Phys. Rev. J. L. McKibben and A. Shurig, private communication. G. C. Hanna and B. Pontecorvo, Phys. Rev. 75, 983 (1949). Curran, Angus, and Cockroft, Phil. Mag. 40, 53 (1949).

[7] Herb, Snowdon, and Sala, Phys. Rev. 75, 246 (1949).

TABLE I. Threshold voltage for three separate runs.

Run	$Al^{27}(p, \gamma)Si^{28}$ potentiometer setting	$T^3(p, n)He^3$ potentiometer setting	$T^3(p, n)He^3$ threshold Mev
1	0.4806	0.4933	1.0197
2	0.4815	0.4942	1.0196
3	0.4815	0.4939	1.0189
			Av. = 1.019±0.001

suitable energy scale against which to calibrate the electrostatic analyzer. They have made the following three energy determinations: $Li^7(p, n)Be^7$ threshold at 1.8822±0.0002 Mev, the $Al^{27}(p, \gamma)Si^{28}$ resonance at 0.9933±0.0002 Mev, and the $F^{19}(p\alpha', \gamma)O^{16}$ resonance at 0.8735±0.0001 Mev. To make use of these three energy points, a paddle wheel type of target assembly holding four different target materials was constructed, as shown in Fig. 1. The wheel was within the vacuum system, and was rotated by a horseshoe magnet from outside, making possible a rapid switching from one target to another. For the calibration points, a freshly scraped aluminum plate about $\frac{1}{32}$ of an inch thick was placed on one of the target holders, and a crystal of LiF about one-mm thick on another. Both of these targets were "thick" for protons in the energy range to be covered.

A clean disk of zirconium was placed on the third paddle, and a "thick" target of tritium absorbed in a zirconium disk on the fourth. This type of tritium target has been developed in this laboratory by E. R. Graves, A. A. Rodriguez, M. Goldblatt, and D. Meyer.[8] Measurements on neutron yield from this target show that for protons in the neighborhood of 1.5 Mev the zirconium served to "dilute" the tritium to about one-fifteenth the concentration of an equivalent thick gaseous tritium target.

A large liquid nitrogen trap was placed near the target between the target and the oil diffusion pumps. The distance from the mouth of the pumps to the target was 3 meters. The trap was kept full of liquid nitrogen throughout the course of the experiment, and at the conclusion there was no visible darkening of the aluminum or zirconium targets, indicating that the trap was very effective in preventing oil vapor from reaching the target chamber.

The neutrons were detected at 0° with a flat energy response counter[9] placed 141 cm from the target. The gamma-rays were detected at 90° with two thin-wall G-M tubes crossed and in coincidence. A $\frac{1}{4}$-inch lead converter was used immediately in front of the first tube. The G-M tubes were placed in a lead pig having 2-in. thick walls, and the pig was hung as closely as possible to the target without being in physical contact.

Since the primary energy standard was the position of the $Al^{27}(p, \gamma)Si^{28}$ resonance at 993.3 kev, the experimental procedure was to swing the aluminum target into the path of the proton beam and run a thick target yield curve for the gamma-radiation as a function of proton energy, locating precisely the resonance on our electrostatic analyzer scale. The background was determined by running on the clean zirconium target and was found to be negligible. The LiF crystal was then swung into position in the beam and observations of the $F(p\alpha', \gamma)$ resonance and the $Li^7(p, n)Be^7$ threshold made. A calculation of the energies of these points using the calibration factor obtained by assuming the $Al(p, \gamma)$ resonance to be at 993.3 kev gave an indication of the linearity of our scale, and in addition the consistency of the three measurements precluded any gross mistakes in our observations. The Zr+T target was then swung into place and the threshold for the $T(p, n)$ reaction observed.

The proton beam was monitored with a current integrator[10] and was kept below 3 microamperes while running on the Zr+T target to prevent over-heating and driving off any of the tritium. The Al and LiF targets were run at a dull red heat with a beam of from 7 to 10 microamperes.

EXPERIMENTAL RESULTS

Figure 2 shows a set of curves obtained in a typical run. The energy scale is broken to permit sufficient expansion of the scale to show the precision of the measurements. All energy points are calibrated against the $Al(p, \gamma)$ resonance at 993.3 kev as a standard. The total widths of the $Al(p, \gamma)$ and the $F(p\alpha', \gamma)$ resonances were very close to 2 kev. Since these were thick targets, the energy at the midpoint of the rise was taken to be the resonance energy in each case. The energy ripple of the electrostatic generator has previously been estimated at one to two kev, which is closely checked by the above measured resonance widths. It will be seen from the curves that the measured energy of the $F(p\alpha', \gamma)$ resonance and the $Li(p, n)$ threshold relative to the $Al(p, \gamma)$ resonance fall within one kev of the values given by Herb, *et al.*[7] A run on a piece of metallic lithium gave an identical threshold to that found with the LiF and was done to make sure that crystal charging did not shift the energy by a few kilovolts.

The "foot" on the $T^3(p, n)He^3$ threshold curve is approximately 2-kev wide, which also is in agreement with the expected ripple of the electrostatic generator. The true threshold for the reaction is obtained by extrapolating the straight portion of the curve until it

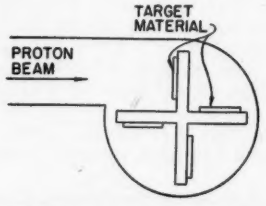

FIG. 1. Target assembly.

[8] E. R. Graves, A. A. Rodriguez, M. Goldblatt and D. Meyer, private communication, to be published in Rev. Sci. Inst.

[9] A. O. Hanson and J. L. McKibben, Phys. Rev. 72, 673 (1947).

[10] H. T. Gittings, LADC #520 (1948).

intersects the background. In this case the background is zero for all practical purposes.

The results of the three separate runs are shown in Table I. As the Al(p, γ) resonance was used as a primary calibration point for each run, the potentiometer setting corresponding to the electrostatic analyzer voltage for the resonance is listed for each run. The electrostatic analyzer controlled the energy of the incident proton beam. The potentiometer setting shifted slightly during the course of the measurements; the shift could be rather closely correlated to the time of day the measurement was being taken. Presumably this shift is a temperature effect in any or all of the energy controlling elements: the electrostatic analyzer, the resistor stack for the electrostatic analyzer and the standard cell in the potentiometer circuit. The same shift was observed in the $T^3(p, n)H^3$ threshold, but as the threshold was compared directly with the Al(p, γ) resonance measured at approximately the same time, we believe that any temperature effect has been eliminated from the final value. We wish to point out, however, that the maximum magnitude of this temperature shift was only of the order of 2 kev.

Run 3 was made after removing the zirconium +tritium disk from the target chamber and polishing it with number 600 carborundum. It was feared that an oxide coating might have built up on it prior to our use of it, but the shift in the threshold after the surface was polished was about -0.7 kev, and as this is within the voltage ripple of the machine we cannot attach much significance to it. There was essentially no neutron background below the two reaction thresholds.

The average value of the $T^3(p, n)He^3$ threshold is calculated to be 1019 ± 1 kev. Taking $(M_T/M_T+M_H)=0.7495$ as the mass factor for transforming from the laboratory system to the center of mass system, the Q value for this reaction is:

$$Q=-0.7495\times1019=-763.7\pm1 \text{ kev.}$$

Assuming the end point of the β-ray spectrum from the decay of tritium to be 18.5 kev[6] then from Eq. (2)

$$n-H^1=782\pm2 \text{ kev.}$$

This is 28 kev higher than the previously accepted[2, 5] value and approximately 20 kev lower than the recently determined values of Bell and Elliott.[1] The revised figures of Tollestrup, Jenkins, Fowler, and Lauritsen[4] are in agreement with these results. One calculates from this a neutron mass of 1.0089683 ± 0.0000049 A. M. U.

Bell and Elliott had to assume the value of the $H^1H^1-D^2$ mass spectrographic doublet in obtaining their value for the $n-H^1$ difference. K. T. Bainbridge[11] has suggested that the $n-H^1$ measurement reported in this paper, together with the deuteron binding energy measured by Bell and Elliott might be a good means of checking the $H^1H^1-D^2$ doublet separation.

We wish to express our appreciation for the help given in several phases of the experiment by H. T. Gittings and G. Everhart.

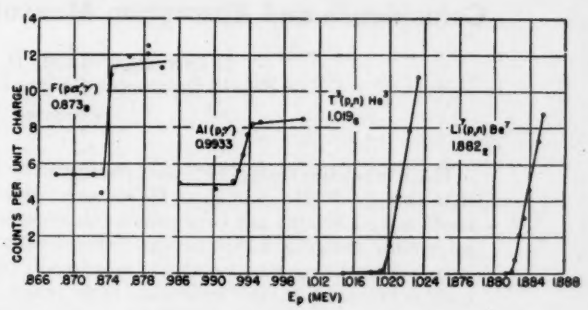

FIG. 2. Yield curves from a typical run.

[11] K. T. Bainbridge, private communication.

Coincidence and Absorption Measurements on Cs^{134}, I^{124}, Au^{199}, and Ca^{45}

J. LAWRENCE MEEM, JR. AND FRED MAIENSCHEIN
Physics Department, Indiana University, Bloomington, Indiana

(Received April 1, 1949)

The beta-ray spectrum of Cs^{134} was investigated by absorption and beta-gamma-coincidence measurements. Beta-rays of 0.60 Mev and about 90 kev were observed. In I^{124}, the maximum energy of the beta-rays was found to be 2.30 Mev and beta-gamma-coincidences showed the beta-spectrum to be simple. A maximum gamma-ray energy of 2.24 Mev was observed with several lower energy gamma-rays indicated. Gamma-gamma-coincidences were found, but coincidences between beta-particles and internal conversion electrons could not be detected. Au^{199} exhibited a beta-ray of 0.32 Mev, and the beta-gamma-coincidence rate per beta-ray was independent of absorber thickness. A maximum gamma-ray energy of about 0.21 Mev was found by coincidence absorption of photoelectrons and coincidences between beta-particles and internal conversion electrons. Gamma-gamma-coincidences were obtained. The 43-minute isomeric state of Hg sometimes attributed to Hg^{199} was not observed to grow from Au^{199}. Ca^{45} was found to have a single beta-ray of 0.22 Mev and no gamma-rays.

1. INTRODUCTION

COINCIDENCE and absorption measurements have been made on Cs^{134}, I^{124}, Au^{199}, and Ca^{45}. Cs^{134} has been investigated recently by Elliot and Bell[1] and Siegbahn and Deutsch.[2] Very little information has been available on I^{124}, but recent investigations on Au^{199} have been done by Peacock and Wilkinson[3] with a spectrometer, and by Mandeville, Scherb, and Keighton[4] using coincidence methods. Ca^{45} has been investigated by Solomon and Glendenin[5] and by Matthews and Pool.[6]

2. APPARATUS AND PROCEDURE

The coincidence apparatus used consisted of two Geiger-Müller tubes each connected to a pre-amplifier and then to one channel of a two-channel coincidence counting apparatus similar in principle to that of Jurney and Mitchell.[7] A resolving time of about 0.6 microsecond was used in all coincidence experiments described in this paper.

The arrangement of the counters with respect to the source was that generally used for coincidence and absorption measurements.[8] In general, cylindrical lead cathode counters were used for counting gamma-rays. However, for counting very low energy gamma-rays (of the order of 0.1 Mev), two silver cathode glass counters were used.

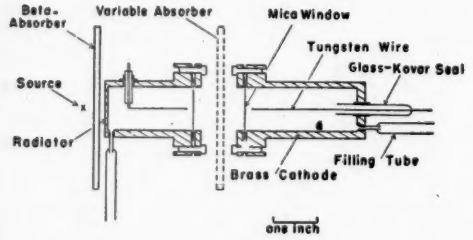

FIG. 1. Counter arrangement for coincidence absorption of Compton recoil electrons.

For counting beta-particles an end window counter with a mica window of 5.6 mg/cm² thickness was generally used. For counting very low energy particles (about 0.1 Mev) windows of condenser paper coated with Formvar were used. These windows had a thickness of 0.8 mg/cm² and the counters and source were placed in an airtight chamber which could be evacuated. Using this technique, beta-particles with ranges as low as 1 mg/cm² could be counted, corresponding to about 23-kev electron energy. All range energy relations for electrons were obtained from the curve of Glendenin.[9]

Coincidences between beta-particles and internal conversion electrons were measured using two end window counters in the evacuated chamber described above. The windows of the counters had a surface density of 0.8 mg/cm². In all cases the absorbers were placed before both counters.

The energy of the highest energy gamma-ray was determined by the coincidence absorption in aluminum of Compton recoil electrons. A special "Compton Counter" was devised for these experiments and is shown in Fig. 1. Using an end window counter with a 5.6-mg/cm² window, the center wire was introduced from the side rather than from the back of the counter. The tube for evacuating the counter was also inserted in the side. The back of the counter then served as a radiator for Compton electrons, when the source was placed behind it as shown. The Compton electrons which gave coincidences traveled through the window and into a second end window counter placed facing the first as shown. Absorbers were placed between the two counters. Knowing the thickness of the mica windows and the absorber thickness, the energy of the electrons[9] being counted could be determined closely. If W is the maxi-

[1] L. G. Elliot and R. E. Bell, Phys. Rev. **72**, 979 (1947).
[2] K. Siegbahn and M. Deutsch, Phys. Rev. **73**, 410 (1948).
[3] C. L. Peacock and R. G. Wilkinson, Phys. Rev. **75**, 329A (1949) and private communication.
[4] Mandeville, Scherb, and Keighton, Phys. Rev. **74**, 601 (1948).
[5] A. K. Solomon and L. E. Glendenin, Phys. Rev. **73**, 415 (1948).
[6] D. E. Matthews and M. L. Pool, Phys. Rev. **72**, 163 (1947).
[7] E. T. Jurney and A. C. G. Mitchell, Phys. Rev. **73**, 1153 (1948).
[8] A. C. G. Mitchell, Rev. Mod. Phys. **20**, 246 (1948).
[9] L. E. Glendenin, Nucleonics **2**, 12 (1948).

mum energy of the Compton recoil electrons, then $W=h\nu/(1+m_0c^2/2h\nu)$ and the energy of the gamma-ray, $h\nu$, may be calculated.

3. RESULTS

Cs^{134}

The disintegration scheme of Cs^{134} has been investigated by Elliot and Bell[1] and by Siegbahn and Deutsch[2] using spectrometer and coincidence techniques. From a Fermi plot of the beta-ray spectrum Elliot and Bell found two beta-ray groups with end-point energies of 0.658±0.030 Mev and about 0.090 Mev. They estimated that the low energy group represents about 28 percent of the total number of beta-rays. From absorption measurements using a windowless counter Siegbahn and Deutsch estimated the abundance of this group as 32±8 percent. Beta-gamma-coincidences have been measured by Wiedenbeck and Chu.[10] They obtained a constant ratio $N_{\beta\gamma}/N_\beta$, independent of beta-ray energy, but only one point was taken in the very low energy region.

The spectrum of Cs^{134} has been investigated by absorption and beta-gamma-coincidence methods. The source was obtained from Oak Ridge and was purified by an amberlite resin ion exchange column at this university. For absorption measurements an end window counter with a window thickness of 0.8 mg/cm² was used, the counter and source being placed in an evacuated chamber. For very low absorption thicknesses the absolute air pressure in the chamber was used as the absorbing medium, this pressure being varied from 1 cm to 76 cm of Hg. At 1 cm of Hg absolute pressure the air absorption plus the window thickness represented a window cut-off of about 23 kev. Figure 2 shows the beta-ray absorption curve obtained. By visual inspection of the end point, and using the curve of Glendenin[9] showing beta-ray energy *vs.* absorber thickness, a maximum beta-ray energy of 0.60±0.03 Mev was obtained. The insert in Fig. 2 shows an enlargement of the low energy end of the curve. In this region the high energy

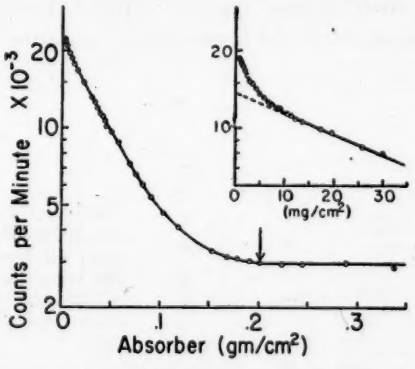

FIG. 2. Absorption of the beta-rays of Cs^{134}. The insert is an enlargement of the low energy region.

[10] M. L. Wiedenbeck and K. Y. Chu, Phys. Rev. **72**, 1164 (1947).

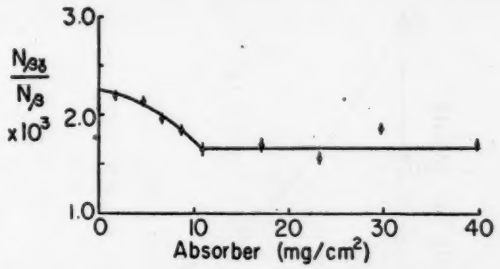

FIG. 3. Low energy beta-gamma-coincidences in Cs^{134}. The ratio $N_{\beta\gamma}/N_\beta$ remained constant for the higher absorber thicknesses not shown.

beta-ray curve is essentially a straight line and the low energy group may be clearly seen rising from it. An end point for the less energetic group may be readily determined and gives an energy of 96±8 kev. By extrapolating the curves back to zero absorber, the abundance of the low energy component was determined as 34±5 percent.

Using the same thin window beta-counter and a cylindrical lead counter to measure gamma-rays, a beta-gamma coincidence experiment was performed. The source and both counters were placed in the evacuated chamber for low energy determinations. The low energy end of the beta-gamma-coincidence curve is shown in Fig. 3. The curve extended on out to the right in the same straight line showing that except for very low energies the ratio $N_{\beta\gamma}/N_\beta$ was independent of beta-ray energy. However, again the presence of the very low energy beta-group may be clearly seen. The point of intersection of the sloping curve with the straight portion represents an energy of 85±10 kev. Gamma-gamma-coincidences were observed in Cs^{134} and the ratio $N_{\gamma\gamma}/N_\gamma$ had a value of $0.25\pm0.05\times10^{-3}$.

These results are in complete agreement with the disintegration scheme proposed by Elliot and Bell.

I^{124}

Nothing is to be found in the literature on the radiations from I^{124} other than that it is a positron emitter and has a half-life of 4 days.[11] I^{124} was made by bombarding antimony with 23-Mev alpha-particles in the Indiana University cyclotron. The irradiated material was dissolved in nitric acid and potassium iodide carrier added. The iodide was immediately oxidized to iodine and the mixture was boiled using a reflux condenser. The iodine sublimed and collected on the walls of the condenser in solid form. This was washed out with carbon tetrachloride, the iodine reduced to iodide ion, and then precipitated as silver iodide.

Since I^{126} (13.0 days) may also be produced by bombarding antimony with alpha-particles, the half-life was watched closely and when an appreciable amount of I^{126} began to appear, experiments on I^{124} were stopped. Figure 4 shows the half-life for one of the sources. All

[11] J. J. Livingood and G. T. Seaborg, Phys. Rev. **54**, 775 (1938).

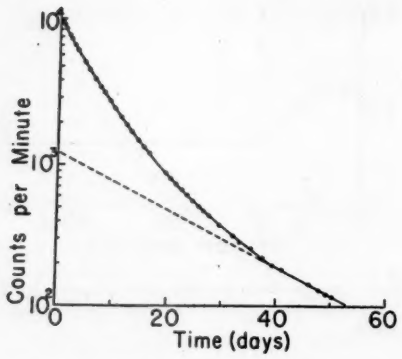

FIG. 4. Decay of I^{124}. Experiments were conducted for only the first four days.

measurements using this source were made during the first four days when the slope of the curve corresponded very closely to the reported half-life of I^{124}. The same procedure was followed with a second source. It was estimated that less than 15 percent of the total activity could be ascribed to I^{126} while measurements on I^{124} were being taken.

Figure 5 shows the results of absorbing the beta-rays in aluminum. The gamma-ray background was subtracted, and the resultant pure beta-ray curve analyzed by the method of Bleuler and Zunti.[12] The maximum energy of the beta-rays was found to be 2.30±0.15 Mev. The analysis gave no indication of the presence of a lower energy beta-ray group.

The maximum energy of the gamma-rays was measured by the coincidence absorption in aluminum of Compton recoil electrons using the counter arrangement shown in Fig. 1. The results are given in Fig. 6. The endpoint corresponds to an energy of 2.01 Mev for the electrons, or 2.24±0.15 Mev as the maximum gamma-ray energy. The curve shows several decided breaks at energies below the maximum indicating the presence of at least two lower energy gamma-rays.

Beta-gamma-coincidences are shown in Fig. 7. The ratio $N_{\beta\gamma}/N_{\beta}$ was found to be independent of beta-ray energy down to an energy of less than 0.1 Mev, again indicating the presence of only a single beta-ray group.

Gamma-gamma-coincidences were measured using two lead counters, first with the source located midway between the counters (the 180° position) and then with one counter at an angle of 90° with respect to its first location but at the same distance from the source. The source was contained in a copper tube so that all positrons would be stopped and the subsequent annihilation radiation emitted from the geometrical center of the arrangement. The value of $N_{\gamma\gamma}/N_{\gamma}\times 10^3$ in the 180° position was 0.975±0.027 and at 90° this ratio was 0.370±0.017, the two values being related to each other by a factor of 2.6. This is to be compared with results from Cu^{64} (a known positron emitter with no gamma-gamma-coincidences) which gave 2.83±0.14 in the 180° position and 0.25±0.05 in the 90° position, a factor of 11.3. Accordingly the observations on I^{124} showed that while annihilation radiation was present, it did not account for all of the coincidences. Gamma-gamma-coincidences were also present.

An attempt was made to measure coincidences between beta-particles and internal conversion electrons. No such coincidences were observed down to an energy of about 23 kev. It was concluded that if internal conversion electrons are present in I^{124} they do not arise from a gamma-ray which is in coincidence with the beta-ray, or that if the gamma-ray in coincidence with the beta-ray is internally converted, the conversion coefficient is quite small.

If a disintegration scheme is drawn for I^{124} and the 2.30-Mev positron is considered as in coincidence with the 2.24-Mev gamma-ray, the excited state of I^{124} would have to lie at least as high as 4.5 Mev plus $2m_0c^2$. It appears more logical to assume that the positron is in coincidence with a lower energy gamma-ray, and that the high energy gamma-ray results after K-capture. If K-capture were present, the characteristic x-rays of tellurium would be observed. By critical absorption in Ag, Cd, In, and Sn the characteristic x-rays of tellurium were found to be present. Since the number of internal-conversion beta-particle coincidences seems to be negligible, it would appear that the critical absorption experiments establish the presence of K-capture in I^{124}.

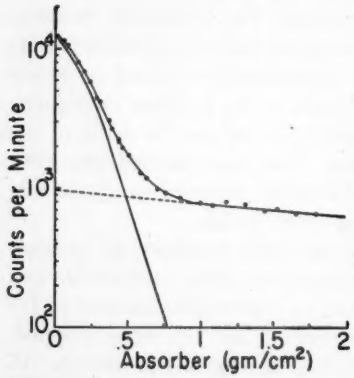

FIG. 5. Beta-ray absorption for I^{124}. The curve was analyzed by the method of Bleuler and Zunti.

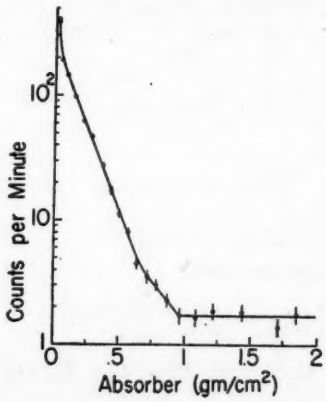

FIG. 6. Coincidence absorption of Compton recoil electrons in I^{124}. The breaks in the curve indicate the presence of lower energy gamma-rays.

[12] E. Bleuler and W. Zunti, Helv. Phys. Acta **XIX**, 375 (1946).

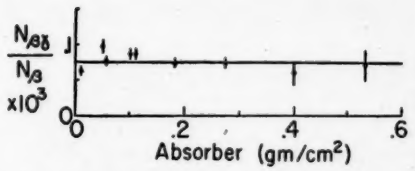

FIG. 7. Beta-gamma-coincidences in I^{124}.

Au^{199}

The radiations from Au^{199} have been studied recently by Peacock and Wilkinson[3] using a spectrometer and by Mandeville, Scherb, and Keighton[4] using coincidence and absorption methods. Peacock and Wilkinson observed several gamma-rays, one of approximately 0.22 Mev and others of lower energy, some of which were internally converted. In addition the beta-ray endpoint was 0.32 Mev. Mandeville, Scherb, and Keighton determined the beta-ray as 0.38 Mev but detected only one gamma-ray, by absorption in lead.

The source here investigated was obtained from Oak Ridge in the form of platinum which had been irradiated with neutrons. Au^{199} is formed from Pt^{199} which decays with a thirty minute half-life. The platinum was dissolved in aqua regia and gold carrier added. The gold was extracted from the platinum with ethyl acetate and the acetate solution washed with ammonium chloride solution to remove any mercury which might have been present. There is a 43-minute isomeric state of Hg which has been attributed[13] to either Hg^{199} or Hg^{201}. Since Au^{199} decays to Hg^{199}, one would expect to find this metastable state, if Hg^{199} is the correct assignment. The purified gold, which was dissolved in ethyl acetate, was allowed to stand for several hours to permit the supposed 43-min. Hg^{199} to form. The ethyl acetate solution was then washed with ammonium chloride to take out any mercury formed and the resultant mercury checked for activity. This procedure was repeated several times. No 43-minute activity was found.

The absorption of the beta-rays of Au^{199} in aluminum is shown in Fig. 8. An end point of 0.32 ± 0.01 Mev was obtained in agreement with Peacock and Wilkinson.

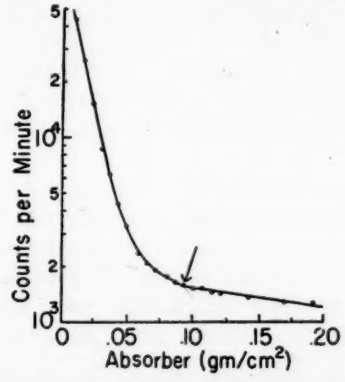

FIG. 8. Beta-ray absorption for Au^{199}.

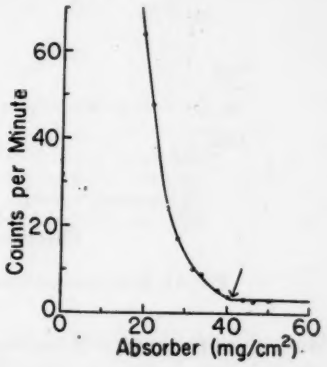

FIG. 9. Coincidence absorption of recoil electrons in Au^{199}.

The gamma-radiation was first investigated by absorption in lead. This indicated the presence of at least two gamma-ray energies of around 0.24 Mev and 0.14 Mev. A more exact determination of the maximum gamma-ray energy was obtained by measuring the coincidence absorption of recoil electrons in aluminum using the counter arrangement shown in Fig. 1. The results are given in Fig. 9, which shows the maximum energy of the recoil electrons to be 0.205 ± 0.015 Mev. If these recoils were Compton electrons, the gamma-ray energy would be 0.34 Mev, but if the recoils were photoelectrons ejected from the wall of the brass counter, 9 kev should be added giving 0.214 ± 0.015 Mev as the maximum gamma-ray energy. This value is approximately the same as that obtained by Peacock and Wilkinson. It may appear that the number of photoelectrons produced would be too small to give an absorption endpoint. However, for a 0.214-Mev gamma-ray the Compton recoil electrons would have a maximum energy of 0.095 Mev which energy would have been completely cut out by the thickness of the counter windows plus the air between the counters, a total of 14.2 mg/cm². With these Compton electrons cut out, the endpoint would have been that due to photoelectrons.

Absorption of the coincidences between beta-particles and internal conversion electrons, Fig. 10, gave an endpoint of 0.120 ± 0.015 Mev. Adding to this the binding energy of the K-electrons of mercury, 0.083

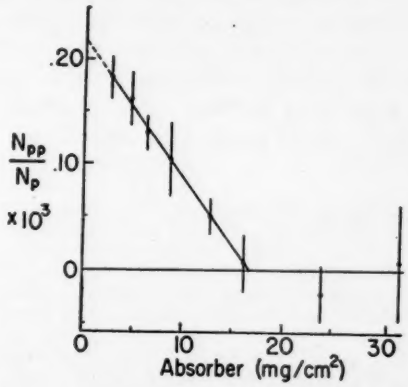

FIG. 10. Beta-beta-coincidences in Au^{199}. The absorber was either air or aluminum placed before both counters.

[13] M. Friedlander and C. Wu, Phys. Rev. **63**, 227 (1943). Sherr, Bainbridge, and Anderson, Phys. Rev. **60**, 473 (1941).

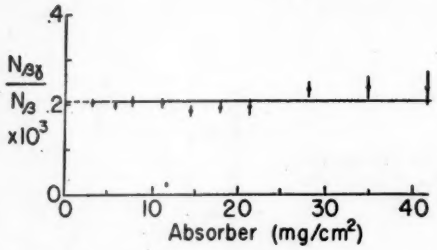

FIG. 11. Beta-gamma-coincidences in Au^{199}.

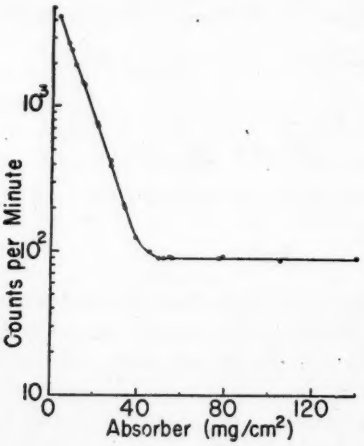

FIG. 12. Beta-ray absorption for Ca^{45}.

Mev, gives the energy of the most energetic gamma-ray, which is internally converted as 0.203±0.015 Mev, in agreement with the value obtained for the maximum gamma-ray energy from absorption of photoelectron coincidences.

A beta-gamma-coincidence rate per recorded beta-ray was obtained which was independent of beta-ray energy, as shown in Fig. 11. This indicated the presence of only a single beta-ray or that any lower energy beta-ray groups are of low abundance. Gamma-gamma coincidences were observed using two silver cathode glass counters and enough aluminum absorber to cut out all the beta-rays. The ratio $N_{\gamma\gamma}/N_\gamma$ was 0.19±0.01 $\times 10^{-3}$.

Ca^{45}

Measurements by Solomon and Glendenin[5] and by Matthews and Pool[6] have shown Ca^{45} to be a simple beta-ray emitter unaccompanied by gamma-rays. Solomon and Glendenin obtained a beta-ray endpoint of 0.26 Mev and Matthews and Pool obtained 0.21 Mev. In the present experiment, a source of Ca^{45} obtained from Oak Ridge, was chemically purified and an absorption curve taken. This absorption curve is shown in Fig. 12. The beta-ray endpoint is found to be 0.22±0.01 Mev, and in addition there were no gamma-rays present.

This work was assisted by the joint program of the ONR and the AEC. The authors wish to thank Professor A. C. G. Mitchell for his interest and advice in this work. They also express their appreciation to Mr. E. T. Jurney for many valuable suggestions.

Long-Lived Tellurium Isomers

R. D. HILL
Department of Physics, University of Illinois, Urbana, Illinois*
(Received April 25, 1949)

The internal conversion electron spectra of neutron-activated enriched tellurium isotopes have been studied. It has been shown that each odd mass-number isotope from 121 to 131 exists in a long-lived isomeric state. In all cases the initial isomeric transition is 2^4-pole magnetic, which appears to identify the long-lived isomeric states with a spin of 11/2. The spins of the ground states of Te^{127}, Te^{129}, Te^{131} would appear to be 3/2, and that of Te^{123} 1/2. Information about Te^{121} and Te^{125} ground states is incomplete.

INTRODUCTION

THE observation[1] that Sb when bombarded by energetic deuterons gave rise to a Te activity of about 140-day half-life and a profusion of internal conversion lines appeared to point to a particularly complicated Te^{121} isomeric decay. The assignment of the lines to Te^{121} had been made many times on the basis of the existence of 121 being the only gap which could be filled by a $d-2n$ reaction from Sb^{121} and Sb^{123}, as well as on the existence of only one period of decay of the activity. At the time of these experiments, however, it was felt that there was room for the existence of two isomers Te^{121} and Te^{123}, produced from Sb^{121} and Sb^{123}, which would have very similar lifetimes arising from the very similar 82 and 88.5-kev transitions. Separated Te isotopes were accordingly obtained from Oak Ridge and bombarded for a month in the pile there. This has led to a clarification of the Te^{121} radiations, the discovery of an isomer of Te^{123}, and a general survey of the Te isomers.

EXPERIMENTAL RESULTS

The internal conversion spectra of the activated Te isotopes were determined with a 180° focusing beta-ray spectrograph. The results are set down in Table I. The lifetime of Te^{123} has been inferred from the change in the intensities of the K-conversion lines of the 88.5 and 82-kev transitions over a period of 7 months. Immediately after separation of the Te fraction from the deuteron bombarded Sb, the intensity ratio of the (88.5-K) line to the (82-K) line was equal to 1.25. Approximately 7 months later, the ratio had diminished to 0.75. The half-life of Te^{123}, equal to 90 days, was calculated assuming a half-life for Te^{121} of 140 days. Both of these estimates are probably too low and the activities of the separate Te^{121} and Te^{123} isomers are now being followed.

The spectra from the activated Te isotopes are reproduced in Fig. 1. Certain lines are common to more than one spectrum. For example, the topmost spectrum is from deuteron bombarded Sb and is due to the mixed Te^{121}, Te^{123} isomers. The stable isotope Te^{120} was not obtainable in the enriched form. Analyses of the enriched isotopes which were bombarded are shown in Table II. The lines due to Te^{125} appear in Te^{123} and are due to 2.9 percent impurity of Te^{124}. The question might be raised as to whether the lines of the 88.5-kev transition in Te^{127} are not due to an impurity of Te^{122} in Te^{126}. This appears to be very unlikely since Te^{122} is present only to 0.1 percent in Te^{126} (95.4 percent), whereas the 88.5-kev lines are absent in the Te^{125} spectrum where Te^{122} is present to the extent of 1.5 percent in Te^{124} (84 percent). There is also no evidence for the 159-kev transition in the Te^{127} spectrum. A transition of 86 kev was observed by Helmholtz[4] present in the activity of Te^{127}.

For the 106-kev transition in Te^{129}, Helmholtz observed 102 kev. The value of 177 kev for the transition in Te^{131} is due to Helmholtz. This line was not observed in the present experiments although the irradiated Te^{130} was placed in the spectrograph within about 36 hours of removal from the pile. Activated Te^{130} gave, however, the 80 and 163.6-kev* transitions due to I^{131} (8 day) which grows from Te^{131}. The 80-kev transition provided a useful check on the energy calibration[5] of the spectrograph. A value of 80.4 kev was obtained from the K conversion line and 79.4 kev from the L-line, agreeing well with DuMond's value of 80.1 kev.

TABLE I. Half-lives and transitions of tellurium isomers.

Isomer	121	123	125	127	129	131
Half-life (day)	140[2]	90	58[3]	90[3]	32[3]	1.2[3]
Transitions (kev)	82	88.5	109.7	88.5	106	177[4]
	213	159	35.4			

Very rough activation isotopic cross sections can be obtained for the capture of slow neutrons and the production of Te^{123} and Te^{125} activities. The following values: $Te^{122}\sim 1$ barn, $Te^{124}\sim 5$ barn, were obtained from a comparison with Seren's[6] for Te^{130} (0.008), Te^{128} (0.015), Te^{126} (0.073).

* This work was assisted by the joint program of the ONR and the AEC.

[1] R. D. Hill and J. W. Mihelich, Phys. Rev. **74**, 1874 (1948).

* *Note added in proof:* It has since been recognized by Brosi, DeWitt, and Zeldes [Phys. Rev. **75**, 1615 (1949)] that this transition arises from a 12-day isomer of Xe^{131}.

[2] G. T. Seaborg and I. Perlman, Rev. Mod. Phys. **20**, 616 (1948).

[3] Friedlander, Goldhaber, and Scharff-Goldhaber, Phys. Rev. **74**, 981 (1948); Hill, Scharff-Goldhaber, and Friedlander, Phys. Rev. **75**, 324 (1949).

[4] A. C. Helmholtz, Phys. Rev. **60**, 415 (1941).

[5] Lind, Brown, Klein, Muller, and DuMond, Phys. Rev. **75**, 1633A (1949).

[6] Seren, Friedlander, and Turkel, Phys. Rev. **72**, 888 (1947).

DISCUSSION OF ISOMERISM

The similarity between the lifetimes and transition energies of the odd atomic mass isomers of Te is striking. (Only one odd isotope, Te^{125}, was bombarded with neutrons but no activity or transitions were detected, other than those due to the impurities of the already known odd isomers.)

In Table III are set down the relevant experimental and analytical data pertaining to the odd Te isomers. The angular momentum changes l of the long lived transitions were obtained from the relation

$$\tau_\gamma = [3(l!)^2/\rho^{2l}] \cdot (137/W)^{2l+1} \cdot (\hbar/mc^2),$$

where τ_γ is the experimental lifetime multiplied by (1+conversion coefficient in all shells). The estimated conversion coefficient in all shells was obtained using the experimental N_K/N_L ratio and the value of the K-conversion for a trial l value. In all the Te isomer cases, the angular momentum change of the transitions having the lowest N_K/N_L ratios is $l=4$ magnetic and/or $l=5$ electric. As shown by Drell,[7] the amount of magnetic multipole conversion is high, and in all cases amounts to approximately 95 percent.

Second transitions, following the long-lived transitions, occur in the three lowest mass number cases. The lifetime for the 213-kev transition was found[8] to be 5×10^{-8} sec.

From the N_K/N_L ratios, the angular momentum changes[9] of the 213 and 159 transitions are probably 3 electric and 1 magnetic, respectively. Assuming that the ratios of the intensities of the K-electrons of the 213 and 159 transitions to the total electron intensities[1] of the 82 and 88.5 kev transitions may yield the K-conversion coefficients of the former transitions, the values obtained are 0.13 and 0.17, respectively. Using the conversion tables of Rose,[10] then, one obtains for the 213-kev transition, $\alpha_K 2^2$-electric=0.10, $\alpha_K 2^3$-electric=0.39; $\beta_K 2^2$-magnetic=0.39; and for the 159-kev transition $\beta_K 2^1$-magnetic=0.17. The analysis for the 159 kev transition therefore seems to indicate $l=1$, magnetic, even parity change; but for the 213-kev transition the assignment of an angular momentum change is difficult to specify at present. The identity of the two weak electron lines[1] of 32.5 and 35 kev in the spectrum of Te^{121} also remains to be determined. In the case of Te^{125} only the L- and M-conversion lines have been observed, and values of the N_K/N_L or K-conversions are therefore not available.

According to Feenberg and Hammack,[11] on the basis of a one-particle nuclear shell structure theory, a region of isomerism should occur in the isotope table around Z or $N=63$ to 81 (approximately) where the $1h$, $2d$, $2p$ and $3s$ levels may cross.[12] The isotopes of Te^{121} to Te^{131} lie in this region with N equal to 69, 71$\cdots$79, and the

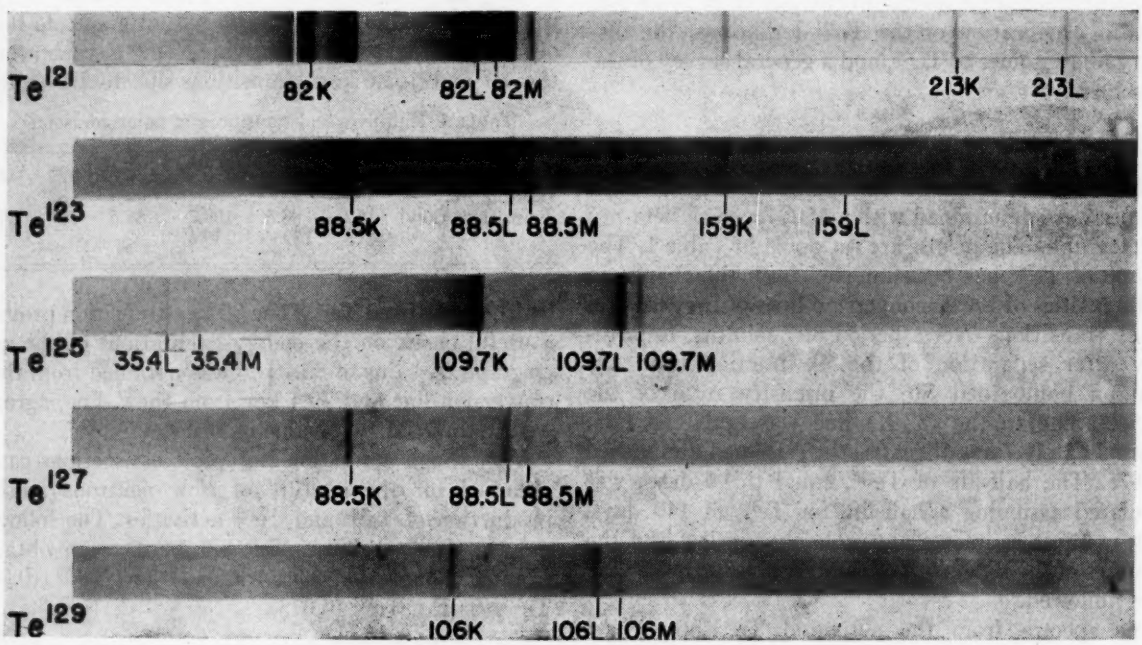

FIG. 1. Internal conversion spectra of Te isomers. The weak lines, caused by the following transitions, which are clearly visible on the original film, have been retouched for the purposes of reproduction: Te^{121} (213 kev), Te^{125} (35.4 kev), Te^{127} (88.5 kev), Te^{129} (106 kev).

[7] S. D. Drell, Phys. Rev. **75**, 132 (1949).
[8] P. T. Bittencourt and M. Goldhaber, Phys. Rev. **70**, 780 (1946).
[9] M. H. Hebb and E. Nelson, Phys. Rev. **58**, 486 (1940).
[10] M. E. Rose and others, "Tables of K-shell Internal Conversion Coefficients."
[11] E. Feenberg and K. C. Hammack, Phys. Rev. **75**, 1877 (1949). See also L. Nordheim, Phys. Rev **75**. 1894 (1949).
[12] The nomenclature is according to M. G. Mayer, Phys. Rev. **75**, 1969 (1949).

TABLE II. Isotopic abundances of enriched tellurium samples.

Stable isotope	Sample (1)	Sample (2)	Sample (3)	Sample (4)	Sample (5)	Sample (6)
122	79.4	1.5	0.1	0.1	<0.1	<0.1
123	1.4	0.7	0.3	0.0	<0.1	<0.1
124	2.9	83.9	1.4	0.6	<0.1	<0.1
125	2.6	4.7	87.9	0.7	0.2	<0.1
126	4.6	4.6	6.8	95.4	1.5	0.3
128	4.9	3.0	2.4	2.6	94.4	2.3
130	4.0	1.9	1.1	0.6	3.9	97.4

TABLE III. Angular momentum changes of telliurium isomer transitions.

Isomer	Te^{121}	Te^{123}	Te^{125}	Te^{127}	Te^{129}	Te^{131}
Half-life (days)	140	90	58	90	30	1.2
γ_1-transition (kev)	82	88.5	109.7	88.5	106	177
N_K/N_L	0.77	0.92	1.5	0.75	1	2
Ang. mom. change	4 mag.	4 mag.	4 mag.	4 mag.	4mag.	4 mag.
γ_2-transition (kev)	213	159	35.5			
N_K/N_L	4.2	7.7	?			
K-conv. coeff.	0.13	0.17	?			
Ang. mom. change	?	1 mag.				

required values of angular momentum changes for the isomeric transitions are also possible on the theory.

In order to obtain the large angular momentum changes associated with the long-lived isomeric states it is necessary to attribute the first transitions to ones to or from a $(1h)$ level. The possible transitions between the available levels are:

$$(1h_{11/2})\rightleftarrows(2d_{3/2});\quad (1h_{11/2})\rightleftarrows(2p_{3/2});$$
$$(1h_{9/2})\rightleftarrows(2p_{1/2});\quad (1h_{9/2})\rightleftarrows(3s_{1/2}).$$

Two of these transitions, those to the $2p$ level, can be ruled out since the selection rule for a 2^4-magnetic transition requires an odd parity change.

The second transitions must evidently be treated independently for each isotope. No second transitions have been observed at all for Te^{127}, Te^{129}, and Te^{131} but these cannot be ruled out entirely as the transitions might be low energy ones or might possibly be weakly converted. If we consider the best known case at present of Te^{123}, it appears that the second transition, between the available levels according to theory, may be one of the following:

$$(2d_{5/2})\rightleftarrows(2p_{3/2});\quad (2d_{3/2})\rightleftarrows(2p_{1/2});\quad (2d_{3/2})\rightleftarrows(3s_{1/2});$$
$$(2p_{3/2})\rightleftarrows(3s_{1/2});\quad (2p_{1/2})\rightleftarrows(3s_{1/2}).$$

All of the transitions to or from the $2p$ level are again ruled out on account of the selection rule for a 2^1-magnetic transition which requires an even parity change.

The transitions in Te^{123} thus indicate the existence of the $(1h_{11/2})$, $(2d_{3/2})$ and $(3s_{1/2})$ levels. These are just the levels which are being filled in the region of Te, $N=69-79$, according to Mayer's theory.[12]

ACKNOWLEDGMENTS

The tellurium isotopes used in this investigation were supplied by the Carbide and Carbon Chemicals Corporation, Oak Ridge, and obtained on allocation from the AEC.

Thanks are due M. Goldhaber for discussion of many points associated with the problem.

U-234 Specific Alpha-Activity*

A. S. GOLDIN, G. B. KNIGHT, P. A. MACKLIN**, AND R. L. MACKLIN
K-25 Research Laboratories, Carbide and Carbon Chemicals Corporation, Oak Ridge, Tennessee
(Received April 6, 1949)

The specific alpha-activity of U-234 has been determined using pure samples grown from UX. The half-life period was found to be 2.67 ± 0.04 (L. E.) $\times 10^5$ yr. The corresponding abundance in natural uranium is 0.0000580 ± 0.0000008 by weight in fair agreement with determinations by other methods.

INTRODUCTION

IN order to measure the specific alpha-activity of U-234 directly, two measurements are required. The first is the determination of the alpha-activity of a given sample. This is ordinarily done by pulse counting with an ionization chamber and linear amplifier using medium to high activity samples. If other alpha-active isotopes are present in the samples used, their effect must also be determined.

The second measurement required is a determination of the U-234 content of each sample. This has usually been obtained by measuring the relative ion currents produced by U-234, U-235 and U-238 in a mass spectrometer from samples of highly enriched uranium. Weighed samples then contain known fractions of U-234, U-235 and U-238. Highly enriched samples have been available in which the alpha-activity of the U-235 is less than five percent of the alpha-activity of the U-234. The activity of the U-238, of course, is completely negligible (less than 1/4000).

Determinations of this type have been reported from Los Alamos[1] together with indirect determinations based on the abundance of U-234 in natural uranium. An error of less than six percent is estimated by these authors for their average value of the specific alpha activity of U-234. Further measurements of the same type have been carried on at this laboratory[2] and at Y-12, a large enough series of results having been obtained to reduce the limit of error (95 percent probability) to two tenths percent, exclusive of possible bias.

The U-234 specific alpha-activity has now been determined without direct use of mass spectrometer measurements through a radioactive growth method similar to that of Gratias[3] and others. This work was undertaken to eliminate the effect of possible bias in the mass spectrometer measurements and the experimental difficulties in accurate high speed alpha-counting. A few micrograms of radioactively pure U-234 have been prepared and known fractions thereof have been alpha-counted at moderate counting rates (below 1500 counts per minute). This is very briefly the work to be described in more detail in the body of this report.

DETAILS OF METHOD

Starting Material

Quantities of a concentrate rich in UX_1 (Th-234) have been developed as a source of UX in cooperation with the Technical Division at X-10 where further purification has been carried out by ion exchange methods. As considerable quantities of crude UX became available, the preparation of small quantities (say, a few micrograms) of U-234 seemed possible. The UX_1 is formed by alpha-decay of U-238 and is then successively transformed by two beta-ray emissions to U-234.

The quantitative purification of such small quantities of U-234 for weighing by non-carrier methods was not deemed possible after extensive consultation with members of the Chemistry Division at X-10. It has been possible, however, to calculate the weight of U-234 from the weight of the parent U-238 and the several decay periods and constants involved. This required accurate knowledge of the specific alpha activity of U-238 and of the decay constant of UX_1.

Specific Activity of U-238

In special samples of nearly pure U-238 separated electromagnetically, by the use of fission counting with a moderated radium gamma-beryllium photo-neutron source, the U-235 content has been shown to be less than seven parts per million. Considering the method of preparation, the U-234 depletion factor compared with natural uranium is expected to be larger than that for U-235. Thus, less than one-thousandth as much U-234 was present in these samples as in natural uranium. Hence, the U-234 alpha-activity, which is nearly one-half of the total in natural uranium, has been reduced to less than one-tenth of one percent in these samples. The U-235 alpha-activity is about five-thousandths of one percent of the U-238 alpha-activity. Routine alpha-counting in this laboratory of such samples on nickel disks has led to a highly precise value for the specific activity of U-238, namely 742.7 disintegrations per minute per milligram.

Half-Life of UX_1

The decay of UX_1 (Th-234)[4] was followed by beta counting of several samples over periods ranging up to

* This document is based on work performed for the Atomic Energy Commission by Carbide and Carbon Chemicals Corporation, Oak Ridge, Tennessee.
** Present address: Columbia University, New York, N. Y.
[1] O. Chamberlain, D. Williams, and P. Yuster, Phys. Rev. **70**, 580 (1946).
[2] C. A. Kienberger, to be published.
[3] O. A. Gratias, Phil. Mag. **17**, 491 (1934).
[4] G. B. Knight, and R. L. Macklin, Phys. Rev. **74**, 540 (1948).

five half-lives. The samples were prepared from highly purified natural uranium by double precipitation with zirconium iodate carrier. The absence of longer lived contaminants was inferred from the linearity of the logarithms of the counting rates as a function of time. Statistical analysis of the data showed no significant curvature to this plot. The counters were frequently standardized with samples of natural U_3O_8 in equilibrium with UX_1, UX_2, UY, and UZ. As a result, the limit of error on the published half-life of UX_1 was reduced by an order of magnitude. The value found for the half-life was 24.101 ± 0.025 days.

UX_1 Standards

The UX_1 in equilibrium with 40 milligrams of natural uranium as black oxide was quantitatively removed, placed on a carefully standardized sample holder which provided for absorption of all UX_1 and UY beta-rays and beta-counted. Preliminary work on this separation using double precipitation with lanthanum fluoride as carrier was not found entirely reproducible. Natural thorium has proven a much more consistent carrier and the small blank correction required has not been serious. The use of oxalate as precipitant in place of fluoride (suggested by Mr. Whetzel of this laboratory) has decisively increased particle size and ease of handling. A series of eight UX standards (see Table I) prepared in this way gave a counting precision for the average of 0.41 percent limit of error (L. E.).

UX_1 Measurement

Accurately measured fractions of the main batch of UX_1 had then to be prepared and beta-counted for comparison. Some ten micrograms of UX had been treated at X-10 and about six micrograms recovered free of uranium. This material was diluted to one liter in a calibrated volumetric flask with four normal nitric acid. The fraction of the UX absorbed by the glass under these conditions ($4N-HNO_3$) had been shown in preliminary studies to be less than 0.1 percent although other conditions led to considerable absorption. Using specially calibrated one milliliter blow-out pipettes, three secondary liter dilutions were prepared. From these latter, five milliliter samples were withdrawn, mixed with 5 milligrams of natural thorium as carrier, and precipitated as oxalate. Another five milligrams of thorium were added after removal of the first precipitate, and a second precipitate formed. Repetition tests had shown that each precipitation removed from 97 to 99 percent of the UX_1 and natural thorium present.

Results from a series of such double precipitations are shown in Table II. No significant differences between the various pieces of volumetric equipment could be shown. The precision of the average was 0.68 percent L. E.

TABLE I. UX beta-counting rates from 40 mg samples of aged natural uranium as black oxide.

Observed rate (c/m)	Rate corrected for coincidence loss	Blank rate	Net UX rate	Net UX rate at equilibrium
5058.8	5139.4	61.9	5077.5	
5040.1	5120.1	61.9	5058.2	
5036.1	5116.2	61.9	5054.3	
5052.6	5133.0	61.9	5071.1	
5084.6	5166.0	61.9	5104.1	
5043.0	5123.1	61.9	5061.2	
5050.5	5130.8	113.6	5017.2	
5084.5	5165.9	113.6	5052.3	
			Av. 5062.0 $\pm$20.6 L. E.	5066.4 counts/minute

U-234 Preparation

The main batch of UX_1 was allowed to decay for several half-lives and the U-234 formed was then recovered. About thirty milligrams of U_3O_8 with low specific alpha-activity (about 320 counts per minute per milligram) were carefully weighed and added as carrier for the U-234. This was recovered by precipitation with ammonia gas and centrifugation. To reduce the high ionium (Th-230) alpha-activity to negligible proportions, several successive precipitations with lanthanum fluoride were carried out in a nitric acid solution of the ammonia precipitate. The decontamination factor was followed by beta-counting the UX_2 in transient equilibrium with successive precipitates. About 80 percent of the U-234 and carrier uranium was precipitated with hydrogen peroxide at a pH below 2 for purification and then ignited to constant weight. Thus a known fraction of the total U-234 was recovered in chemically pure form. This material was dissolved in nitric acid and twenty volumetrically measured fractions were quantitatively plated for alpha-counting. An equal weight of the uranium used as carrier was also prepared for alpha-counting to determine the blank correction. The average alpha-counting rates are included in Table III using the appropriate symbols from the section on calculations.

CALCULATIONS

Computation

The specific activity of U-234 in disintegrations per second per gram can be computed as

$$A=(N-B)/60f\times 1/M\times T/d\times 238.07/234.07 \times 2^{-k/d}\times C_1/C_2V\times \frac{1}{1-2^{\left(\frac{-L-K}{d}\right)}} \times W_1/W_2\times 1/S, \quad (1)$$

$$=2.119\times 10^8, \quad (2)$$

where N = average α-counts per minute of U-234 samples + carrier, B = average α-counts per minute of

TABLE II. UX aliquot beta-counting rates corrected to July 15, 1948 at 1:51 P.M.*

4320.4	4322.1
4445.3	4307.5
4363.3	4368.4
4409.6	4351.0
4293.3	4354.1
4285.5	4358.9

Av. 4348.3±29.6 counts per minute

* Also corrected for coincidence losses and blank sample counts.

carrier, f=efficiency of counter=0.5063[2], M=weight of U-238 used to prepare each UX standard, d=half-life of UX_1=24.101 days, T=half-life of U-238=4.49×10^9 years[2], k=length of time between purification and counting of main UX sample, C_2=average beta-counting rate of UX aliquots, V=volumetric dilution factor for UX aliquots, C_1=average counting rate of UX standards, L=length of time between counting of main UX sample and the purification of the U-234, W=weight of pure U_3O_8 carrier added, W_2=weight of pure U_3O_8 recovered, and S=volumetric fraction of U-234 and carrier used to prepare each sample for alpha-counting (routine quantitative plating procedure).

Equivalent values of the half-life, decay constant and equilibrium amount in natural uranium may be readily computed, giving

$$\text{Half-life of U-234}=2.67\times10^5 \text{ years}, \quad (3)$$

$$\text{Fraction decaying per second}=8.235\times10^{-14}, \quad (4)$$

$$\text{Weight fraction in natural uranium}=0.0000580. \quad (5)$$

Propagation of Errors

The error in the results arrived at in the work reported above has been calculated as follows. First, the error in each contributing observation has been evaluated. Where possible this has been done by statistical analysis of multiple determinations. In cases such as weighing and timing errors, conservative estimates have been used. These contributory errors are taken to represent in each case a sample at the 95 percent probability level drawn from a normal population of observations. The errors are then combined in accordance with the functional relationships outlined in formula (1) by the usual rules for propagation of error. In the case of several of the observations which contribute relatively negligible errors, combination functions have been used to reduce the complexity. For example, the symbol M represents a weight and tare of natural U_3O_8, the fraction of uranium in U_3O_8, the fraction of U-238 in the uranium, the volume of the pipette used to deliver standard samples and the reciprocal of the volume of the flask used for the stock solution. Likewise, the correction for decay of UX_1 in the half hour or so between isolation and sample counting has been included in the counting rates C_1 and C_2.

The propagation of error formula may be most readily presented with the aid of the function $\%^2$ defined as

$\%^2(X)=(100tS_x/X)^2$ where "t" is taken from the usual statistical table and S is the sample estimate of standard deviation.

$$\%^2A=(N^2\%^2N+B^2\%^2B/(N-B)^2)+\%^2f+\%^2M+\%^2T$$
$$+\frac{(k\ln2)^2 2^{2k/d}\%^2k+(L\ln2)^2 2^{-2L/d}\%^2L+d^2\%^2d\{2^{k/d}[(k\ln2/d)-1]+2^{-L/d}[1+(L\ln2/d)]\}^2}{d^2(2^{k/d}-2^{-L/d})^2}$$
$$+\%^2C_1+\%^2C_2+\%^2V+\%^2W_1+\%^2W_2+\%^2S \quad (6)$$

$$=1.776. \quad (7)$$

The values of the several variables, their "limits of error" and the contribution of each to $\%^2A$ are presented in Table III. It is realized that the formula used here is not rigorous. However, it is believed to give a more reliable estimate of total error than would be obtained by simple propagation of sample variance. The L. E. arrived at in this way is 1.3 percent.

COMPARISONS AND DISCUSSION

Perhaps the most convenient of the several values related to specific activity is the half-life. Recent values obtained for the U-234 half-life are listed in Table IV. The value of Gratias[3] was obtained by the radioactive growth method but based on alpha-activity determinations of low precision. The other values are based on mass spectrometer measurements. The values of Nier, Fox, and Rustad, and the lower value of Chamberlain, Williams, and Yuster were obtained from the U-234/U-238 ratio in natural uranium and the U-238 half-life. The higher value of Chamberlain, Williams, and Yuster was obtained by alpha-counting enriched samples of uranium (at high counting rates with questionable accuracy) and measuring their U-234 contents on a very high resolution mass spectrometer. The value reported by Kienberger was obtained by alpha-counting enriched samples of uranium after dilution or masking to reduce the counting rate by a known fraction as well as at high counting rates. The mass spectrometers used in connection with this latter work normally have sufficiently high resolution to make the so-called "toe correction"

TABLE III. Value of several variables, their limits of error and their contributions to $\%^2 A$.

Variable	Value	L. E.	Weight	Contribution to $\%^2 A$
N	1335 c/m	0.699%	1.62	0.791
B	306.8 c/m	1.173	0.075	0.103
f	0.5063	0.100	1	0.010
M	0.03370 g	0.223	1	0.050
d	24.101 day	0.104	9.80	0.106
T	1.640×10^{12} day	0.226	1	0.051
k	143.992 day	0.014	17.2	0.003
C_2	4348.3 c/m	0.681	1	0.463
V	2.0383×10^5	0.141	1	0.020
C_1	5066.4 c/m	0.407	1	0.166
L	6.0714 day	0.085	3×10^{-8}	0.000
W_1	30.393 mg	0.033	1	0.001
W_2	22.952 mg	0.043	1	0.002
S	0.04002	0.100	1	0.010
			Total	1.776
			Propagated % L. E. for $A=1.332$	

negligible. This correction attempts to account for the ions from U-235 appearing at the U-234 position and its omission probably introduces an error of less than 1½ percent. Differences between the ratio of peak heights and the ratio of peak areas might introduce a bias since the former was used in place of the latter. If such causes of bias can be ruled out, then we would have to conclude that a significant bias was inherent in the spectrometer method (i.e., mass discrimination) or a relatively large error had been made in the present work.

The procedures used in the present work are felt to be reliable in view of the following precautions. The sample preparation and handling were done by standard volumetric and gravimetric procedures, and, where possible were repeated several times. Beta-counting measurements involved only the activity ratios of samples prepared under identical conditions and having nearly equal activities. Alpha-counting measurements were made at rates below 1500 per minute and the equipment used was standardized using standard normal samples against the average of seven similar units used by Kienberger[2] in his redetermination of the half-life of U-238. Alpha- and beta-counts on each material used were repeated on from eight to twenty separate samples.

TABLE IV. Recent values of the half-life of U-234.

U-234 half-life	Source
1.7×10^5 yr.	Gratias[a]
2.7×10^5 yr. ±10%	Nier[b]
2.51×10^5 yr. ± 3%	Fox and Rustad[c]
2.29×10^5 yr. } ±6%	Chamberlain, Williams and Yuster[d]
2.35×10^5 yr. }	Chamberlain, Williams and Yuster[d]
2.52×10^5 yr.	Kienberger[e]
2.67×10^5 yr.	This paper

[a] See reference 3.
[b] A. O. C. Nier, Phys. Rev. **55**, 150 (1939).
[c] Fox and Rustad, Carbide and Carbon Chemicals Corporation, Report A-3828, January (1946).
[d] See reference 1.
[e] See reference 2.

It is felt that possible bias beyond 1⅓ percent could only be caused by outright mistakes in experimental manipulations.

SUMMARY

The half-life, specific activity, decay constant and fraction in natural uranium of U-234 have been redetermined by a radioactive growth method. A pure sample of U-234 was prepared by decay of isolated UX_1 and its alpha-activity measured and compared with the specific activity of pure U-238. The values obtained are estimated to be accurate to 1.3 percent but differ by more than this percentage from other values based on mass spectrometer data.

ACKNOWLEDGMENTS

The diversified character of the many components required to complete the work reported here has required the cooperation of many different groups and individuals. Members of the Chemistry and Production Divisions at Clinton National Laboratories have unstintingly given us the benefit of their chemical experience in addition to conducting the resin column purification of our UX concentrates. At the K-25 Laboratories, Mr. Kienberger and Mr. Flanders of the Counting Section, Mr. Greene of the Special Analysis Unit, Miss Pemberton and Mr. Simon of the Physics Research Department have been particularly generous with their help and advice.

Wave Amplification by Interaction with a Stream of Electrons

J. A. ROBERTS*
Department of Physics, University of Sydney, Sydney, Australia
(Received March 22, 1949)

A discussion is given of the propagation of plane electromagnetic waves in a uniform, ionized medium, in which the electrons possess a mean drift velocity. The treatment is based on the general theory developed by V. A. Bailey. It is shown that, for frequencies below a certain critical frequency (of the same order as the electron plasma frequency), one of the eight possible waves in general grows in amplitude as it progresses through the medium. The relation of this result to the theories of solar noise and of the traveling wave tube amplifier is discussed.

I. INTRODUCTION

RECENTLY Bailey [1] has published a general theory of the propagation of plane electromagnetic waves in an ionized gas, in which static electric and magnetic fields are present. It was shown that under certain conditions the coefficient of attenuation of a group of such waves becomes negative, and in more restricted circumstances the coefficient of damping may be negative.

For such growth to occur it is necessary that the electrons or positive ions have drift velocities and it has been found that static magnetic fields and random electron velocities are both favorable to the occurrence of the phenomenon. It will be shown here that waves with negative attenuation also exist when the static magnetic field is zero and the electron temperature negligible, provided only that the direction of propagation is oblique** to the drift velocity, and the frequency is below a certain critical frequency.

II. THE DISPERSION EQUATION

The theory investigates the propagation of uniform plane harmonic waves of small amplitude, of the form $\exp i(\omega t - lx)$, in a medium which is uniform in the static state, consisting of N_0 electrons and N_0 positive ions per cm^3, moving with drift velocities $\mathbf{U}_0$, $\mathbf{U}_{i0}$, respectively, together with neutral molecules. When the static magnetic field, random velocities and collisions are negligible*** and the motion of the positive ions is neglected, it was shown[2] that ω and l are related by the dispersion equation

$$R^2(Z+1)[(R^2-1)(Z+1)+U_T{}^2l^2]=0, \qquad (1)$$

where

$$R=\omega-U_1l, \quad Z=l^2-\omega^2,$$

and U_1, U_T are the components of $\mathbf{U}_0$, respectively, parallel and perpendicular to the direction of propagation. (U_1 and U_T are taken positive.)

In this equation, the unit of velocity is taken as c (the velocity of light in vacuum) and the unit of frequency as the electron density frequency p.**** As the theory is non-relativistic, values of $\mathbf{U}_0$ are restricted by the condition

$$|\mathbf{U}_0|^2\equiv U_1{}^2+U_T{}^2\ll 1.$$

According to Eq. (1), for any assigned value of ω there are eight values of l, namely,

$$l=U_1{}^{-1}\omega, \quad \text{(Two)}, \qquad (2)$$

$$l=\pm ia, \quad (a^2=1-\omega^2), \qquad (3)$$

and the four roots of the quartic

$$P(\omega,l)\equiv U_1{}^2l^4-2\omega U_1l^3+\{U_T{}^2-a^2(1-U_1{}^2)\}l^2 -2\omega a^2U_1l-a^4=0. \qquad (4)$$

All the corresponding waves are plane polarized,[3] the electric vector lying in the plane containing $\mathbf{U}_0$ and the direction of propagation. For the solutions (3) the field is entirely transverse to the direction of propagation. Each of these waves is associated with a finite Poynting vector.

If ω is real, the two solutions (2) correspond to unattenuated waves which have a phase velocity equal to U_1; the second pair (3) represent unattenuated waves when $\omega^2>1$, but for $\omega^2<1$ do not represent true waves.

III. GRAPHICAL SOLUTION OF THE QUARTIC

The quartic (4) is simpler when expressed in terms of ω and the phase velocity† $\sigma^{-1}=\omega/l$. Thus (4) becomes

$$\phi_4(\sigma)\omega^4+\phi_2(\sigma)\omega^2-1=0, \qquad (5)$$

where

$$\left.\begin{aligned}\phi_4(\sigma)&=(1-U_1\sigma)^2(\sigma^2-1),\\ \phi_2(\sigma)&=(1-U_1\sigma)^2+1-\sigma^2(1-U_T{}^2).\end{aligned}\right\} \qquad (6)$$

As Eq. (5) is a quadratic in ω^2, the (ω, l) curve may easily be plotted by solving (5) for ω, with selected values of σ. This curve is shown in Fig. 1 for the case

* Commonwealth Research Student.

[1] V. A. Bailey, Nature **161**, 599 (1948); J. Roy. Soc. NSW. **82**, 107 (1948); Austr. J. Sci. Research **1**, 351 (1948).

** Oblique is here taken to mean neither parallel nor perpendicular.

*** The phenomenon of growth is not due to collisions, but arises from the interaction of the wave with the electrons. Bailey has shown that the growth occurs with collisions present provided that the collision frequency is less than a certain value.

[2] V. A. Bailey, J. Roy. Soc. NSW. **82**, 112 (1948), Eq. (23.4) with W_1, W_T, ρ, and τ zero; Austr. J. Sci. Research **1**, 351 (1948), Eq. (21) with Ω_1, Ω_T, ν, and τ zero.

**** $p=(4\pi N_0e^2/m)^{\frac{1}{2}}=5.64\times10^4N_0{}^{\frac{1}{2}}$ rad./sec.

[3] V. A. Bailey, J. Roy. Soc. NSW. **82**, 110 (1948), Eq. (24.1).

† Following a method developed by Bailey, to be discussed in a joint paper on the graphical study of the dispersion of electromagneto-ionic waves.

$U_1=U_T=0.1$. Figure 2 shows the detail near $\omega=1$. In this region it is simpler to use the variables

$$x=1-\omega \quad \text{and} \quad y=l/x.$$

Equation (4) then becomes

$$\psi_2(y)x^2+2\psi_1(y)x+\psi_0(y)=0, \tag{7}$$

where

$$\left.\begin{aligned}\psi_2(y)&=(1+U_1y)^2(y^2-1),\\ \psi_1(y)&=-(1+U_1y)(y^2-U_1y-2),\\ \psi_0(y)&=U_T^2y^2-4U_1y-4.\end{aligned}\right\} \tag{8}$$

From these curves we see that for $|\omega|>\omega_c$, where $\omega_c\sim1$, there are four real values for l (four unattenuated waves), but for $|\omega|<\omega_c$ there are two real roots (l_1, l_2) and two complex roots (l_3, l_4). As the coefficients in (4) are real, l_3, l_4 must be complex conjugates

$$l_3,\ l_4=\alpha\pm i\beta.$$

Thus l_3, l_4 correspond to a pair of waves propagated in the same direction with the same phase velocity (ω/α), the attenuation being positive for one wave and negative for the other.††

The real roots of (4) may be read directly from the graph, and in the region $|\omega|<\omega_c$ the complex roots l_3, l_4 may be found from the two relations

$$l_1+l_2+l_3+l_4=-\text{coefficient of } l^3,$$

and

$$l_1l_2l_3l_4=\text{coefficient of } l^0.$$

Thus

$$\alpha=\omega U_1^{-1}-\tfrac{1}{2}(l_1+l_2), \tag{9a}$$

$$\beta=\left(-\frac{a^4U_1^{-2}}{l_1l_2}-\alpha^2\right)^{\frac{1}{2}}. \tag{9b}$$

It is convenient to replace (9a) by

$$\alpha=\tfrac{1}{2}(\Delta l_1+\Delta l_2), \tag{10}$$

where

$$\Delta l=l_a-l,$$

l_a being the value of l on the asymptotes

$$\omega=U_1l\pm(1-U_1^2-U_T^2)^{\frac{1}{2}}(1-U_1^2)^{-\frac{1}{2}}$$

corresponding to the given value of ω. In the neighborhood of ω_c, Δl_2 is negligible compared with Δl_1.

Values of α and β derived by the graphical method are shown in Fig. 3 for the values $U_1=U_T=0.01$.

In the two limiting cases $U_T=0$ and $U_1=0$ the real part of the complex roots vanishes, the solutions of the quartic then being, respectively,

$$U_T=0, \quad l=U_1^{-1}(\omega\pm1), \quad l=\pm ia; \tag{11}$$

and

$$U_1=0, \quad l=\pm ia^2(a^2-U_T^2)^{-\frac{1}{2}}, \quad l^2=\infty. \tag{12}$$

†† Bailey has shown that wave groups centered about the frequency ω also exhibit negative attenuation in the direction of the group velocity.

IV. A CUBIC APPROXIMATION

When x is very small (i.e., $\omega\sim1$) we may obtain good approximations to the complex roots (and the smaller of the two real roots) by neglecting the term in x^2 in Eq. (7). This then becomes

$$l^3-Al^2+Bl-C=0, \tag{13}$$

where

$$\begin{aligned}A&=U_1^{-1}\{\tfrac{1}{2}U_T^2-(1-U_1^2)x\},\\ B&=x(2-3x),\\ C&=-2U_1^{-1}x^2(1-x).\end{aligned}$$

This cubic may conveniently be solved by the use of tables.[4] Values for the complex roots ($\alpha\pm i\beta$) derived by this method are shown in Fig. 3. In this example the approximation is seen to be valid for α when $x<2\times10^{-4}$ and for β when $x<3\times10^{-3}$.

V. NEWTONIAN APPROXIMATION

Since $U_T^2\ll1$, we may take as first approximations the roots of (4) with $U_T=0$, namely (11), and obtain closer approximations by Newtonian iteration. The second approximations are therefore

$$l'=l-P(\partial P/\partial l)^{-1}, \tag{14}$$

where l on the right hand side is given the values (11).

For the complex roots we thus obtain

$$\left.\begin{aligned}\alpha&=\frac{\omega a^2U_1U_T^2}{\{U_T^2-a^2(1+U_1^2)\}^2+4U_1^2\omega^2a^2},\\ \beta&=a\left[1-\frac{U_T^2}{2}\frac{U_T^2-a^2(1+U_1^2)}{\{U_T^2-a^2(1+U_1^2)\}^2+4U_1^2\omega^2a^2}\right],\end{aligned}\right\} \tag{15}$$

or for small ω ($a^2\gg U_1^2$ and U_T^2)

$$\alpha\doteq\omega U_1U_T^2/a^2, \quad \beta\doteq a(1+U_T^2/2a^2). \tag{16}$$

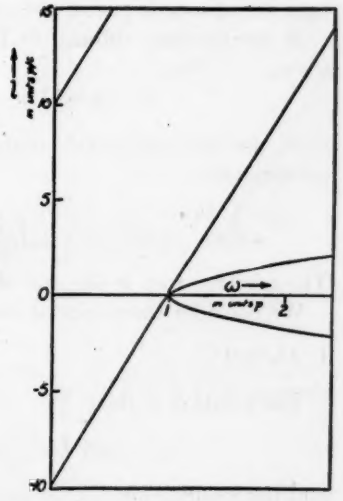

FIG. 1. l as a function of ω. $U_1=U_T=0.1$. (Solutions corresponding to Eq. (4).)

[4] For example, E. Jahnke and F. Emde, *Tables of Functions* (Dover Publications, New York, 1945), Addenda pp. 24–30.

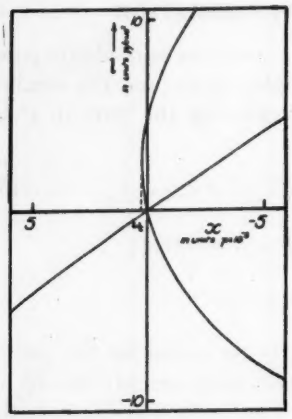

FIG. 2. Detail of the (ω, l) curve near $\omega=1$. $U_1=U_T=0.1$; $x=1-\omega$.

Points determined by (15) are included in Fig. 3. It is seen that a single iteration gives a good approximation at the lower frequencies. In the neighborhood of the critical frequency, the iterative process must be repeated to obtain sufficient accuracy.

VI. THE CRITICAL FREQUENCY AND THE MAXIMUM VALUE OF α

In the example of Fig. 3 the variation of α with the frequency is typical of the general behavior. The wave-length $2\pi/\alpha$ of the growing wave is infinite when the frequency $1-x$ is zero and decreases steadily as the frequency is increased. When $\omega=\omega_c$ the wave-length attains its minimum value $2\pi/\alpha_m$ where α_m is the maximum value of α in the amplifying range. The corresponding value of the phase velocity decreases steadily as the frequency increases ("normal" dispersion) and when $\omega=\omega_c$ has its minimum value which is approximately $2\pi/\alpha_m$. The dispersion of the medium is very large.

At the critical frequency (Fig. 2) there are two equal real roots, each equal to α_m. We may obtain an estimate of α_m, and of the critical frequency, from the condition that the discriminant of the cubic (13) should vanish.

If we assume, subject to confirmation, that when $\alpha=\alpha_m$

$$|x| \ll b \equiv \tfrac{1}{2}U_T^2/(1-U_1^2), \tag{17}$$

then the discriminantal condition reduces to the approximation

$$x=(1/54)\{-(8U_1^2+9U_T^2) \pm((8U_1^2+9U_T^2)^2+27U_T^4(1+U_1^{-2}U_T^2))^{\frac{1}{2}}\}. \tag{18}$$

The positive root is the one of interest here.

We consider three special cases:

I. $U_T^2 \ll U_1^2$.

The solution is then

$$x \doteqdot U_T^4/32U_1^2, \tag{19}$$

and the assumption (17) is justified. The corresponding value of α is

$$\alpha_m \doteqdot 0.25U_1^{-1}U_T^2. \tag{20}$$

II. $U_T=U_1$.

Then

$$x \doteqdot 0.028U_1^2. \tag{21}$$

Here $x \doteqdot 0.06b$, and the assumption (17) is not fully justified. Consequently the approximation may be somewhat rough. With this value for x, α assumes the value

$$\alpha_m \doteqdot 0.26U_1. \tag{22}$$

III. $U_T^2 \gg U_1^2$.

$$x \doteqdot 0.096U_1^{-1}U_T^3.$$

This solution violates the assumption (17) and is therefore inaccurate. This case may, of course, be treated graphically and leads to interesting results (see Fig. 4).

VII. EFFECT OF THE DIRECTION AND MAGNITUDE OF THE DRIFT VELOCITY

The effect of changing the angle ϕ between the drift velocity and the direction of propagation, while keeping the magnitude of the drift velocity constant, is illustrated by the example of Fig. 4. This shows α and β as functions of ϕ when $U_0=1.414\times10^{-2}$. Curves are drawn for four values of the frequency, namely $x=0.5$, 10^{-2}, 10^{-4}, and 10^{-5}, the last two values being those of the critical frequencies when $\phi=90°$ and 62°, respectively.

When the frequency is not in the immediate neighborhood of the critical frequency (e.g., when $x=0.5$ and 10^{-2}), as ϕ increases the wave-length $2\pi/\alpha$ at first decreases but reaches a minimum value when $\phi \doteqdot 55°$ (by Eqs. (15) and (16)). But when $x=10^{-5}$ the wave-length of the growing wave decreases steadily as ϕ increases up to 62°. At this point $\omega=\omega_c$ and amplification ceases. For values of ϕ greater than 62° l is always real. When $x=10^{-4}$ the behavior is similar, but when $\phi=90°$ the value of β is infinite, as is evident from Eq. (12).

The variation of the phase velocity parallels that of the wave-length. Near the critical frequency the velocity decreases with increasing ϕ until the critical frequency is reached, but at lower frequencies the phase velocity reaches a minimum value when $\phi \doteqdot 55°$.

The coefficient of attenuation β is approximately independent of ϕ except near the critical frequency.

With a fixed value of ϕ, for frequencies well away from the critical frequency, Eq. (16) shows that α is proportional to U_0^3, while β depends very little on U_0. On the other hand, it is evident from Eqs. (20) and (22) that near the critical frequency α is approximately proportional to U_0.

VIII. APPLICATIONS OF THE THEORY

This particular example of wave amplification is of importance primarily for its physical simplicity. Provided that the drift velocity is neither parallel nor perpendicular to the direction of propagation and that the frequency is less than the critical frequency ω_c,

groups of waves will increase in amplitude as they progress through the medium. As the associated Poynting vector is finite, the energy carried by the wave must also increase as the wave proceeds.

Bailey[1] has suggested that such growing waves may, in part, explain the electrical noise from discharge tubes, solar, cosmic and ionospheric noise, and terrestrial magnetic fluctuations. The use of such waves for the amplification of high frequency signals will also be considered.

We shall first apply our results for oblique propagation to the solar atmosphere. The drift velocities of electrons in the solar atmosphere not being accurately known, we may for purposes of illustration compute the wave magnitudes for the velocities 4.2×10^3 and 4.2×10^4 km/sec., and take ϕ as 45°. The values of electron density compiled by Smerd[5] have been used. Table I shows the critical frequency ω_c, wave-length and rate of growth of field strength, for various heights above the sun's surface.

It will be seen from this table that very large amplifications are possible in the sun's atmosphere, the lower regions of the chromosphere being most effective. The theory thus provides a very powerful mechanism for explaining the generation of abnormal noise at the frequencies which are observed. Thermal and other fluctuations at frequencies below the critical frequency will be greatly amplified, and if this radiation escapes from the sun,††† the equivalent blackbody temperature at radiofrequencies could be much greater than that observed at optical frequencies.

These waves are plane polarized and their associated Poynting vectors are finite. It is implicit in the general theory that in the presence of a static magnetic field the waves are in general elliptically polarized. The nonlinearity of the fundamental equations offers a means of limiting the amplitude ultimately attained, but this problem will not be discussed here.

We shall now consider the use of these growing waves in high frequency amplifiers. It is well known that the boundary conditions imposed on the field†††† by the surfaces of a conducting wave guide may be satisfied by a superposition of plane waves traveling in directions inclined to the axis of the guide. If electrons were projected longitudinally down the guide, the possible plane waves would include the growing waves discussed above and we would expect the corresponding modes to exhibit the negative attenuation characteristic of the component waves. If the guide were sufficiently long, the device would act as an amplifier, since the growing waves must ultimately predominate.

A rigorous discussion of the propagation of waves in a cylindrical guide containing electrons moving parallel to the axis has been given by Hahn,[6] in connection with the theory of the klystron. Hahn also considered the effect of an axial magnetic focusing field. Ramo[7] has discussed two specific cases of Hahn's theory namely the situation considered above in which there is no static magnetic field, and the corresponding case with an infinite axial magnetic field. In both cases separate E- and H-modes are possible, each mode of the charge free cylinder splitting into four sub-modes in the presence of the electrons. These correspond to the four values of l given by Eqs. (2) and (3) for the H-modes, and the four roots of Eq. (4) for the E-modes.‡

Although Hahn and Ramo derived the relevant equations they apparently did not discover the waves with negative attenuation. It may easily be verified that in certain frequency ranges Ramo's Eq. (37) for E-waves with zero static magnetic field, and his Eq. (15) for E-waves with an infinite axial magnetic field,

TABLE I. Characteristics of growing waves in the solar atmosphere, $\phi=45°$

Height above surface of sun (km)		10^3	10^4	10^5
Maximum frequency (ω_c) for amplification (Mc/sec.)		5600	176	6.8
Minimum wave-length (km)	$U_0=4.2\times10^3$ km/sec.	0.021	0.68	18
	$U_0=4.2\times10^4$ km/sec.	0.0021	0.068	1.8
Wave-length at half critical frequency (km)	$U_0=4.2\times10^3$ km/sec.	81	2.6×10^3	6.6×10^4
	$U_0=4.2\times10^4$ km/sec.	0.08	2.6	66
Rate of growth at half critical frequency (db/km)	$U_0=4.2\times10^3$ km/sec.	4.4×10^5	1.4×10^4	5.4×10^2
	$U_0=4.2\times10^4$ km/sec.	4.4×10^5	1.4×10^4	5.4×10^2

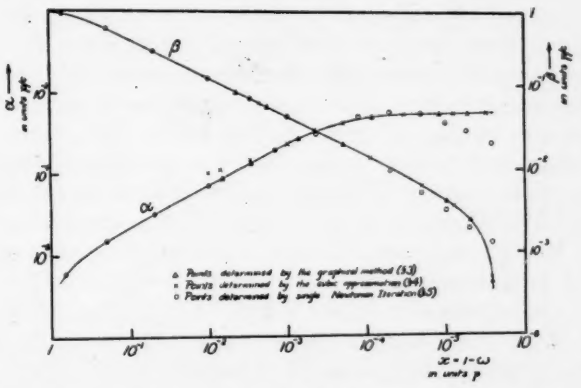
β
α
Points determined by the graphical method (3.3)
Points determined by the cubic approximation (34)
Points determined by single Newtonian Iteration (35)
x = 1 − ω
in units p

FIG. 3. Frequency dependence of the angular wave number α and the coefficient of negative attenuation β of the growing waves. $U_1=U_T=0.01$.

[5] S. F. Smerd, Australian Council for Scientific and Industrial Research R.P.L. 14 (1948).

††† It should be noted that if the electrons have a drift velocity, propagation, with amplification, is often possible in what is otherwise an over-dense medium.

†††† The boundary conditions imposed on the vibratory motions of the electrons also require consideration.

[6] W. C. Hahn, Gen. Elec. Rev. **42**, 258 (1939).

[7] S. Ramo, Phys. Rev. **56**, 276 (1939).

‡ E-modes have a longitudinal component of the electric but not the magnetic field; H-modes have a longitudinal component of the magnetic but not the electric field.

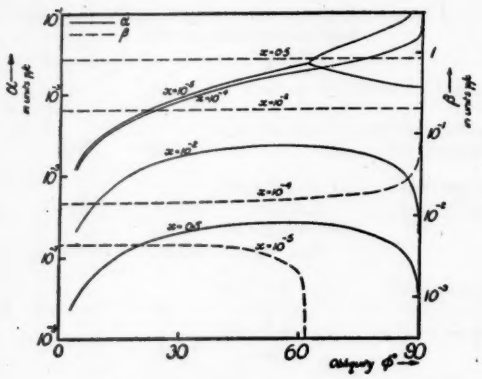

FIG. 4. α and β as functions of ϕ, the obliquity of propagation. $U_0=1.414\times10^{-2}$.

yield conjugate complex values for the axial wave number. The axial magnetic field has the effect of reducing the phase velocity in the guide and may in fact reverse the direction of phase propagation.

We now give an example of the solution of Ramo's Eq. (15). If a tube 0.3 cm in diameter is uniformly filled by a 100-ma beam of 30-volt electrons projected along the tube, and is pervaded by an infinite magnetic focusing field, then at a frequency of 3000 Mc/sec. the growing wave of the E_{01} mode has a wave-length of 4.14 cm in the guide and the field strength of the wave increases by 76 db/cm.

Amplifiers utilizing these growing waves have been constructed in a number of laboratories[8] and theories of their operation have been given by a number of authors.[9] In these "traveling wave tube" amplifiers, the cylindrical wave guide is replaced by a conducting helix, designed to reduce the longitudinal phase velocity in the charge free guide to approximately the same value as the electron drift velocity. Apparently these investigators believe that this is a necessary condition for amplification, but our analysis shows that amplification is possible in much less special circumstances. An amplifier of the same type, but operating on a somewhat different principle, has been discussed more recently by Haeff, Nergaard, Pierce and Hebenstreit,[10] and Hollenberg.[10]

A more complete study of propagation in cylindrical guides, based on Bailey's theory[1] in which the motion of the positive ions is also considered, will be given in another publication.

ACKNOWLEDGMENT

In conclusion I should like to thank Professor V. A. Bailey, who suggested this investigation, for much helpful advice and assistance. This work was carried out during the tenure of a Commonwealth Research Studentship.

---

[8] R. Kompfner, Proc. I.R.E. **35**, 124 (1947); J. R. Pierce and L. M. Field, Proc. I.R.E. **35**, 108 (1947); J. S. A. Tomner, Report No. 2 (1947). Research Laboratory of Electronics, Chalmers Institute of Technology, Sweden.

[9] J. R. Pierce, Proc. I.R.E. **35**, 111 (1947); L. J. Chu and D. Jackson, Proc. I.R.E. **36**, 853 (1948); O. E. H. Rydbeck, Report No. 1 (1947) Research Laboratory of Electronics, Chalmers Institute of Technology, Sweden; C. Shulman and M. S. Heagy, R.C.A. Rev. **8**, 585 (1947). A. Blanc-Lapierre et al., Ondé Élec. **27**, 194 (1947).

[10] A. V. Haeff, Phys. Rev. **74**, 1532 (1948); Proc. I.R.E. **37**, 4 (1949). L. S. Nergaard, R.C.A. Rev. **9**, 585 (1948). J. R. Pierce and W. B. Hebenstreit, Bell Syst. Tech. J. **28**, 33 (1949). A. V. Hollenberg, Bell. Syst. Tech. J. **28**, 52 (1949).

The Forbidden Transition of Yttrium[91] and Cesium[137] *,**

J. S. OSOBA
Department of Physics, Washington University, St. Louis, Missouri
(Received April 14, 1949)

Y^{91} decays by the emission of a single beta-particle with a maximum energy of 1.54 Mev, while Cs^{137} decays in two ways, (1) beta-decay (maximum energy=0.518 Mev) to Ba^{137*} followed by a gamma-transition to the ground state, and (2) beta-decay (maximum energy=1.2 Mev) directly to the ground state. Probably not more than 5 percent of the Cs^{137} nuclei decay directly to the ground state. Conventional (allowed transition) Kurie plots of Y^{91} and the low energy group of beta-particles of Cs^{137} display curvature which is concave toward the energy axis at high energies and concave upward at low energies. If it is assumed that Gamow-Teller selection rules govern the beta-process, the Fermi function $F(Z, W)$ for allowed spectra must be multiplied by a factor $G=(W^2-1)+(W_0-W)^2$ in a beta-transition for which there is a change of parity and for which the spin change is two units. If these conventional Kurie plots of Y^{91} and Cs^{137} are modified by the factor G, the resulting plots are approximately straight lines. This indicates that the beta-decay of Y^{91} and the low energy beta-decay of Cs^{137} involve a spin change of two units and a parity change. These results contribute evidence for the validity of the Fermi theory of beta-decay and the Gamow-Teller selection rules.

The K internal conversion coefficient for the 0.663-Mev gamma from the decay of Cs^{137} was found to be 0.081, while the ratio of the K conversion electrons to the L conversion electrons was 5.0. The gamma-radiation seems to be either magnetic 2^4-pole or electric 2^4-pole.

INTRODUCTION

In the beta-decay process the distributions of beta-particles as a function of energy are of two types, allowed and forbidden. Using the Kurie plot procedure to compare experimental results with the Fermi theory, allowed spectra should give straight line Kurie plots, while forbidden spectra are, in general, expected to yield Kurie plots which deviate from straightness. To date, experimental measurements of (presumably) allowed spectra have confirmed the theory fairly well, except perhaps in the very low energy region.[1] For many forbidden spectra, however, the type of deviation to be anticipated is not clearly understood because of a lack of uniqueness in the various possible formulations of the theory, and because the spins and parities of the initial and final nuclear states are frequently unknown. A third source of ambiguity is the possibility that more than one nuclear matrix element may appear in the distribution function, resulting in a spectrum which depends on the ratios and relative phases of the nuclear matrix elements.

Under certain circumstances, the shape of a forbidden spectrum can be predicted. If it is assumed that Gamow-Teller selection rules govern the beta-process, the distribution in a transition for which there is a change of parity and for which the spin change is two units will differ from that in an allowed transition by a simple function of the energy. Such a transition is classified as first-forbidden by the Gamow-Teller selection rules. In this case, the Fermi function $F(Z, W)$ for allowed spectra must be multiplied by a factor G, which, if $\alpha Z \ll 1$ and if the electron momentum is not too small, has the approximate form[2,3]

$$G=(W^2-1)+(W_0-W)^2.$$

Here W is the electron energy, and W_0 is the total energy available for the transition, both in units of mc^2. The omission of this correction tends to make the Kurie plot (computed as though the transition were allowed) concave toward the energy axis in the high energy region. If $W_0 \geqq 2$, the same omission also causes the Kurie plot to deviate upward at low energies.

In general, however, the link between theory and experiment is very weak for forbidden spectra. More often than not one or both spins of the parent and daughter nuclei in a beta-transition are not known. Initial and final parities of the nuclear states are even less well known. With so many unknown factors, theoretical predictions for the distribution of beta-particles in forbidden transitions, even on the assumption of a uniquely determined heavy-light particle interaction, is largely guesswork.

In some cases the shell model[4] of the nucleus may help to determine the spin and parity changes. For isotopes in certain regions of atomic number and atomic weight, this model predicts both the parities and the possible spin values for the nuclei involved. Ambiguities in the predictions of the shell model can be reduced by consideration of the energies and half-lives of beta- and gamma-transitions in a series of isobaric nuclei.

The isotope Y^{91}, which decays by β^--emission to Zr^{91} with a half-life of 57 days, is one for which both the spin and the parity change can be inferred from the shell model. For this transition, Feenberg and Hammack give a preferred spin change of 2 (from $\frac{1}{2}$ to 5/2) and a parity change from odd to even. Thus, if the shell model of the

* Part of a dissertation to be presented to the graduate school of Washington University in partial fulfillment of the requirements for the degree of Doctor of Philosophy.

** Assisted by the joint program of the ONR and AEC.

[1] C. S. Cook and L. M. Langer, Phys. Rev. 73, 601 (1948).

[2] Here α is the fine structure constant and Z is the charge on the nucleus.

[3] E. J. Konopinski and G. E. Uhlenbeck, Phys. Rev. 60, 308 (1941); E. J. Konopinski, Rev. Mod. Phys. 15, 226 (1943).

[4] E. Feenberg and K. C. Hammack (to be published in Phys. Rev.)

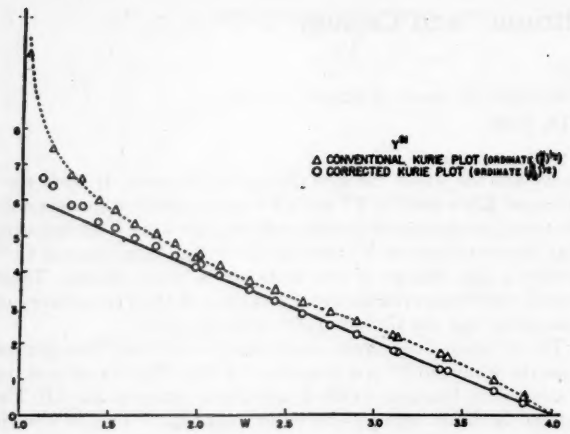

FIG. 1. Kurie plot of Y^{91} and a Kurie plot of the same element corrected by the factor $G=(W_0-W)^2+(W^2-1)$.

nucleus is at all reliable and if the Gamow-Teller selection rules apply, the decay of Y^{91} is an example of the particular kind of first-forbidden transition which was discussed above. Therefore, the distribution of the beta-particles as a function of energy should differ from the allowed distribution by the factor G. The recent work of Langer and Price[5] seems to confirm that this is the case. The Y^{91} spectrum thus provides a critical test of the Fermi theory for forbidden spectra and of the G-T selection rules. It also affords a minor test of the nuclear shell model. For these reasons it is felt that confirmation of the results published by Langer and Price is desirable.

The shell model again offers some help in understanding the decay of Cs^{137} since it predicts *even* parity for the ground states of both Cs^{137} and Ba^{137}. The transition is known to proceed by negatron emission to a mestastable state, Ba^{137*}, which then decays by gamma-emission (accompanied by internal conversion) to the ground state Ba^{137}. The known half-life of the metastable state requires an electric 2^5-pole transition with $\Delta I=5$ or a combination of electric 2^5-pole and magnetic 2^4-pole transitions with $\Delta I=4$. Either way the parity changes. A choice between these possibilities can be based on the internal conversion coefficients in the K and L shells. The spin of Ba^{137} is known to be $\frac{3}{2}$. Putting all this information together, one predicts $I=11/2$ or $13/2$ with odd parity for the metastable state Ba^{137*}. Mitchell and Peacock[6] have measured the K internal conversion coefficient (α_K) and the ratio N_K/N_L. Using the approximate theoretical equations of Dancoff and Morrison,[7] they conclude that $\Delta I=5$ and hence, $I=13/2$ in the isomeric state. The observations of Mitchell and Peacock[8] on the shape of the beta-spectrum lead them to conclude that the beta-transition $Cs^{137}\rightarrow Ba^{137*}$ is an example of the particular kind of first-forbidden transition discussed above with a distribution function modified by the presence of the factor G. Support for the latter conclusion may be derived from a comparison of ft values in the Y^{91} and Cs^{137} transitions. If f is derived from the theory of allowed transitions, the quantity W_0^2ft should be more nearly constant than ft in this particular type of decay. In fact, $W_0^2ft=9.7\times10^9(Cs^{137}\rightarrow Ba^{137*})$ and $W_0^2ft=8.6\times10^9(Y^{91}\rightarrow Zr^{91})$.

EXPERIMENTAL METHOD

The spectra of Cs^{137} and Y^{91} were studied in the double-focusing spectrometer described by Kurie, Osoba, and Slack.[9] The inherent resolution of this instrument is 0.29 percent as determined from a measurement of the thorium F-line, using a narrow source and a narrow counter window. For the present work, however, the high resolving power of the instrument was sacrificed to gain higher counting rates and to allow the use of thinner sources. With wide sources and a wide counter window, the resolving power was reduced to about one percent.

Radioactive sources were prepared by first defining the source area with insulin[10] on a thin Zapon film about 0.03 mg/cm^2 thick. The active material in solution was then applied to this area and fast-dried under an infrared lamp. The author feels it would be useless to give a figure for the source thickness since the active deposit seemed to be in small crystals. The source was prevented from charging[11] by painting two stripes of Aquadag on

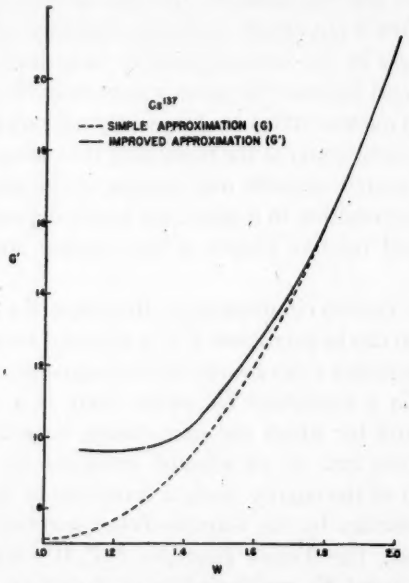

FIG. 2. A plot of $G=(W_0-W)^2+(W^2-1)$ and a plot of $G'=(W_0-W)^2+A(W^2-1)$ for Cs^{137}.

[5] L. M. Langer and H. C. Price, Phys. Rev. **75**, 1109 (1949).
[6] A. C. G. Mitchell and C. L. Peacock, Phys. Rev. **75**, 197 (1949).
[7] S. M. Dancoff and P. Morrison, Phys. Rev. **55**, 122 (1939).
[8] A. C. G. Mitchell and C. L. Peacock, Phys. Rev. **75**, 1272 (1949).
[9] Kurie, Osoba, and Slack, Rev. Sci. Inst. **19**, 771 (1948).
[10] It is found that when insulin is applied to an area and then allowed to dry, subsequent application of a solution will be limited to an area defined by the insulin.
[11] C. H. Braden, G. E. Owen, J. Townsend, C. S. Cook, and F. B. Shull, Phys. Rev. **74**, 1539 (1948).

the back side of the source support to hold the source at ground potential.

Detection of particles was accomplished by means of a Geiger-Müller counter with a Zapon film window which transmitted negatrons above 3.5 kev. The window was 0.25 inch wide and 0.625 inch high, with a 5-mil wire centered lengthwise across the window to help support the Zapon film. A window of this size made from thin Zapon film is difficult to make gas-tight. To keep the pressure in the counter unchanged, a constant pressure device similar to that developed by Ter-Pogossian, Robinson, and Townsend[12] was connected to the counter. The counter pressure changed less than 0.2 percent even though gas was always leaking out through the window.

RESULTS

Yttrium^{91}

The data obtained for Y^{91} is shown in Fig. 1, plotted as a conventional (allowed transition) Kurie plot, and displays curvature which is concave toward the energy axis at high energies and concave upward at low energies. For this plot, the value of $F(Z, W)$ was obtained from the curves found in the *Theoretical Nuclear Physics Course* lecture notes obtained from Oak Ridge. The chosen value of Z is 40, corresponding to the daughter nucleus Zr^{91}. Also shown in Fig. 1 is the Kurie plot which results when $F(Z, W)$ is multiplied by the correction factor G. The near-straightness of the corrected curve is in satisfactory agreement with the work of Langer and Price, although a slight upward deviation still remains at low energies. The deviation at low energy can probably be attributed to scattering due to the fact that the source was not sufficiently thin. The observed value of W_0 is 4.0 mc^2 or 1.54 Mev.

Cesium^{137}

Previous work done in this laboratory[13] indicated that Cs^{137} decays by simple beta-emission to a metastable state, Ba^{137*}, which then decays (half-life = 158 sec.) to the ground state of Ba^{137} by the emission of a 0.663-Mev gamma-ray. The present investigation confirms a result obtained by Mitchell and Peacock[8] that the decay of Cs^{137} occurs in two ways, (1) beta-decay ($W_0 = 0.518$ Mev) to Ba^{137*} followed by the gamma-transition to the ground state, and (2) beta-decay ($W_0 \sim 1.18$ Mev.) directly to the ground state. As will be shown, probably not more than 5 percent of the Cs^{137} nuclei decay directly to the ground state. This confirms the findings of Mitchell and Peacock.

A conventional Kurie plot of the more abundant negatron spectrum (Fig. 3, upper curve) reveals a curvature similar to that obtained for Y^{91}. When the function $F(Z, W)$ is multiplied by G, the re-computed

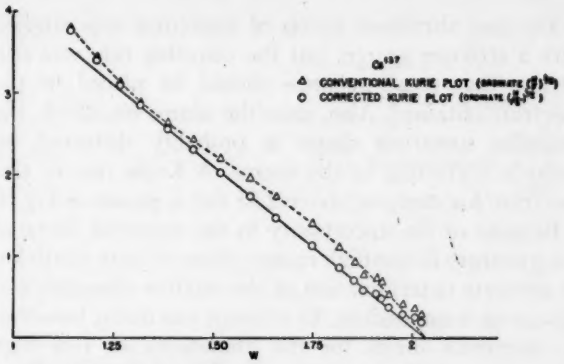

FIG. 3. Kurie plot of Cs^{137} and a Kurie plot of the same element corrected by the factor $G' = (W_0 - W)^2 + A(W^2 - 1)$.

Kurie plot yields a fairly good straight line (not shown in Fig. 3) at high energy. At low energy, however, the curve bends strongly upward. This latter behavior is caused in part by an imperfect approximation in evaluating the correction factor G. For $Z = 56$, the assumption that $\alpha Z \ll 1$ is not valid. Mr. J. Davidson of this laboratory has recomputed G, keeping terms in αZ and $(\alpha Z)^2$ which were previously neglected. His equation for the correction factor, now labeled G', and still subject to the assumption of reasonably large momentum, is

$$G' = (W_0 - W)^2 + A(W^2 - 1),$$

where

$$A = \left[\frac{2}{1+(1-\alpha^2Z^2)^{\frac{1}{2}}}\right]\left[\frac{2+(4-\alpha^2Z^2)^{\frac{1}{2}}}{4}\right] \times \left\{\frac{12\Gamma[1+2(1-\alpha^2Z^2)^{\frac{1}{2}}]}{\Gamma[1+2(4-\alpha^2Z^2)^{\frac{1}{2}}]}\right\}^2 (2P\rho)^{\alpha^2Z^2/2} \times \left|1-\frac{\alpha^2Z^2}{4}+\frac{i\alpha ZW}{P}\right|^2 \left|\left(1-\frac{\alpha^2Z^2}{4}C\right) + \frac{\alpha^2Z^2}{4}\cdot\frac{\alpha^2Z^2W^2}{P^2}\sum_{\nu=1}^{\infty}\frac{1}{\nu\left(\nu^2+\frac{\alpha^2Z^2W^2}{P^2}\right)} + i\left[\alpha^2Z^2\cdot\frac{\alpha ZW}{4P}\sum_{\nu=1}^{\infty}\frac{1}{\nu^2+\frac{\alpha^2Z^2W^2}{P^2}}\right]\right|^2,$$

where C = Gauss's number. Figure 2 compares G and G' for Cs^{137}. It should be noted that use of the simple form G would produce an upward deviation at low energies in the Kurie plot. Figure 3 shows how the Kurie plot for Cs^{137} is straightened out by the correction-factor G'. (It should be noted that G and G' would not differ appreciably from each other for Y^{91}, where $W_0 = 4.0$. This is because the term $(W_0 - W)^2$ is very large compared to $A(W^2 - 1)$ even at low W, where A is largest.)

[12] Ter-Pogossian, Robinson, and Townsend, Rev. Sci. Inst. **20**, 289 (1949).

[13] Townsend, Owen, Cleland, and Hughes, Phys. Rev. **74**, 99 (1948). Townsend, Cleland, and Hughes, Phys. Rev. **74**, 499 (1948).

The less abundant group of negatrons was studied with a stronger source, but the counting rate was still so low that small reliance should be placed in the spectrum obtained. Also, since the source was thick, the resulting spectrum shape is probably distorted by inelastic scattering in the source. A Kurie plot of this spectrum for energies above 2.35 mc^2 is shown in Fig. 4.

Because of the uncertainty in the expected shape of the spectrum of the high energy group of beta-particles, an accurate determination of the relative abundance of this group is impossible. An attempt was made, however, to determine limits for the abundance of this high energy group. In order to simplify the calculations, straight line Kurie plots were used though the spectrum, in all probability, does not have the Fermi allowed shape. In order to set a lower limit for the abundance of this group, the straight line (*A* in Fig. 4) passing from the expected end point (1.18 Mev$\approx$0.663+0.518) through the point at 2.35 mc^2 was assumed to represent the spectrum; the relative abundance of the high energy group was accordingly found to be 2 percent. The author feels that this procedure gives a value for the abundance which is almost certainly too low. In order to set an upper limit for the abundance of the high energy group, the straight line (*B* in Fig. 4) passing from the expected end point through the point indicated by a triangle was assumed to represent the spectrum. The point represented by the triangle was obtained using a thin source and was normalized to conform to the thick source counting rate. This point is located between the end point of the low energy beta-group (0.518 Mev) and the *K* conversion peak (0.625 Mev). Counts in this region are due to the high energy beta-group and possible scattering of some of the internal conversion electrons. The relative abundance of the high energy group corresponding to line *B* in Fig. 4 was found to be 5 percent. Even though the scattering was minimized by use of a thin source, the point represented by the triangle is probably too high and the value of 5 percent can be considered an upper limit for the relative abundance of the high energy group.

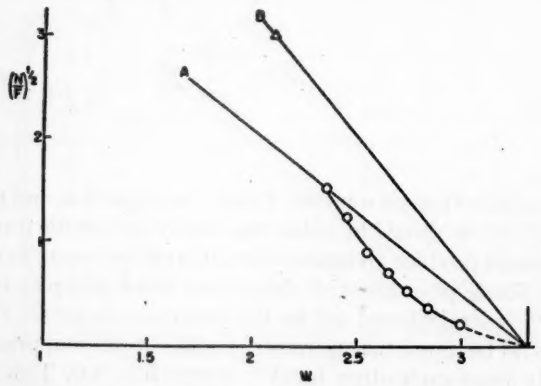

FIG. 4. Kurie plot of high energy group of beta-particles from Cs^{137} with two straight lines that were used to determine the abundance of this group.

The *K* internal conversion coefficient (α_K) for a transition is defined as the ratio of the number of *K* electrons ejected to the number of gammas which are emitted. This coefficient for the 0.663-Mev gamma was found to be $\alpha_K=0.081$, while the ratio N_K/N_L[14] was 5.0. The latter value agrees fairly well with the determination by Mitchell and Peacock who found $N_K/N_L=4.8$, but their value for α_K was 0.118. According to the Oak Ridge tables of internal conversion coefficients,[15] which are calculated from the relativistic formula, one finds that $\alpha_K=0.081$ for Ba^{137*} falls between the values for magnetic 2^4-pole ($\beta_K{}^4=0.094$) and electric 2^5-pole ($\alpha_K{}^5=0.053$) radiation, which in both cases requires a change of parity. (Since the tables of Rose *et al.*, were not specifically computed for $Z=56$ and energy 0.663 Mev, a careful graphical interpolation was carried out to obtain the values for $\beta_K{}^4$ and $\alpha_K{}^5$ which are quoted above.)

The value of 0.081 for the *K* internal conversion coefficient may be too high, because the window of the counter cuts out an undetermined part of the beta-spectrum. Even though the window of the counter has a cut-off of three kev, it probably attenuates the number of negatrons that reach the counter with energies below fifty kev. If there is inelastic scattering in the source, a portion of the beta-spectrum will be degraded to a region where there is attenuation in the counter window.

CONCLUSIONS

Yttrium[91]

The agreement observed by the present author and by Langer and Price between experimental results for Y^{91} and the theoretical predictions indicate that its decay involves a spin change of two units together with a change of parity. The results show the usefulness of the Feenberg-Hammack nuclear shell model in predicting spin and parity changes and also provide evidence for the validity of the Gamow-Teller selection rules and the Fermi theory for forbidden spectra.

Cesium[137]

The results for Cs^{137} are not so conclusive. Examination of the data leads to the following conclusions:

(1) There is branching in the decay of Cs^{137}, with the higher energy group accounting for between two and five percent of the total disintegrations. The end point of the low energy beta-group is 0.518 Mev, the energy of the gamma is 0.663 Mev, and the end point of the high energy betas is about 1.18-Mev.

(2) The shape of the low energy beta-spectrum indicates that this transition may involve a spin change of two together with a change of parity.

(3) A spin change of 4 or 5 and a change of parity appear to be most probable for the transition from metastable Ba^{137*} to the ground state.

[14] No use was made of this ratio because no theoretical curves which are calculated from the relativistic formula were available.

[15] Rose, Goertzel, Spinrad, Harr, Strong (prepublication copy).

Using the ground state of Ba^{137} ($I=\frac{3}{2}$, even) as a starting point, Fig. 5 shows two possible spin assignments which can be made for levels in the disintegration scheme of Cs^{137}.

In diagram *A*, Fig. 5, the spin change in the high energy transition is $\Delta I=2$ with no change in parity, placing it in the second-forbidden class, according to the G-T selection rules. The figure of 0.02 to 0.05 for the branching ratio is perhaps too small for this interpretation in view of the fact that the larger energy change partially compensates for the higher degree of forbiddenness. Unfortunately, there are no well established examples of similar transitions with which to make comparison.

If diagram *B*, Fig. 5, is accepted as correct, the high energy group will still be second forbidden according to the Gamow-Teller selection rules, but with $\Delta I=3$ and no change of parity. The probability for this transition is considerably smaller than for second-forbidden with $\Delta I=2$ (no), so that the number of beta-particles found in the high energy group may be now somewhat too high.

Even though the decay scheme for Cs^{137} is not definite, there is no pronounced disagreement with theoretical expectations. The shape of the low energy beta-spectrum seems to conform with the shell theory of the nucleus, the Gamow-Teller selection rules, and the Fermi theory for forbidden spectra.

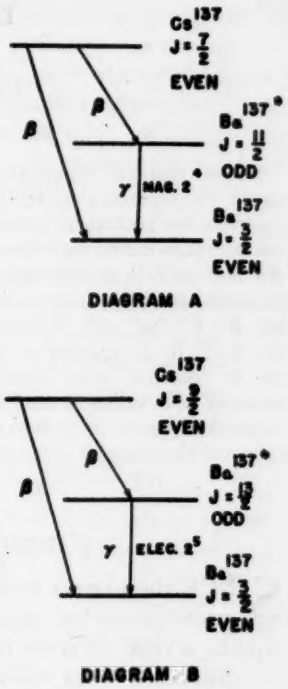

FIG. 5. Spin and parity assignments to the levels in the decay scheme of Cs^{137}.

ACKNOWLEDGMENTS

The author wishes to express his gratitude to Professor F. B. Shull, under whose direction this investigation was pursued, for his helpful advice and constant encouragement, and to Professor E. Feenberg for his many valuable suggestions. The author also wishes to express his gratitude to Mr. C. H. Braden and Mr. L. Slack for their assistance in the investigation.

Determination of Nuclear Gyromagnetic Ratios I

JOHN R. ZIMMERMAN* AND DUDLEY WILLIAMS
Mendenhall Laboratory of Physics, The Ohio State University, Columbus, Ohio
(Received February 11, 1949)

Nuclear magnetic resonance absorption peaks have been observed for seventeen nuclear species. The technique used in observing the resonances involves the use of super-regenerative oscillators and is different in many respects from the bridge method of Purcell and the nuclear induction method of Bloch. Resonance absorption has been observed for the following nuclei: H^1, H^2, Li^7, Be^9, B^{11}, F^{19}, Na^{23}, Al^{27}, P^{31}, Cu^{63}, Cu^{65}, Br^{79}, Br^{81}, Rb^{85}, Rb^{87}, I^{127}, and Cs^{133}. By comparison of various resonance peaks with the proton resonance peak observed simultaneously in the same magnetic field, values for nuclear gyromagnetic ratios and nuclear magnetic moments can be determined in terms of the gyromagnetic ratio and the magnetic moment of the proton. The following frequency ratios have been obtained:

Nucleus	Ratio of resonance frequency to proton frequency in same magnetic field
H^3	0.15355 ±0.03%
Li^7	0.38862 ±0.02
B^{11}	0.32076 ±0.03
F^{19}	0.94086 ±0.02
Na^{23}	0.26454 ±0.03
Al^{27}	0.26062 ±0.04
Cu^{63}	0.26515 ±0.02
Cu^{65}	0.28404 ±0.03
Br^{79}	0.25059 ±0.02
Br^{81}	0.27014 ±0.02
Rb^{87}	0.32718 ±0.05
I^{127}	0.20003 ±0.04

I. INTRODUCTION

SINCE the pioneer work of Purcell and his collaborators[1] on nuclear magnetic resonances in solids and liquids, several different methods have been developed for observing these resonances. Purcell employed a radiofrequency bridge, one arm of which included a coil containing a sample mounted in a strong magnetic field H, which could be modulated at a low audiofrequency. When the Larmor condition

$$h\nu = \mu H_R/I = gH_R \qquad (1)$$

was realized by variation of H, radiation of radiofrequency ν was absorbed by the sample and the bridge was unbalanced. By proper adjustment of the bridge, either absorption or dispersion effects could be observed.[2] In the contemporaneous work of Bloch and his colleagues[3–5] an entirely different approach to the problem was employed. Whereas in Purcell's method, it was necessary to work at extremely low radiofrequency power levels in order to avoid "saturation effects," which appear as a result of the de-population of the lower energy levels, Bloch's method involved the use of high radiofrequency power and involved adiabatic processes. In Bloch's experiment the sample was placed in a coil mounted with its axis perpendicular to a strong magnetic field; this coil formed a part of a radiofrequency oscillator. Resonances were observed by noting voltages induced at resonance in a second coil mounted with its axis perpendicular to the axis of the first coil and to the direction of the strong magnetic field; this is the so-called "nuclear induction" experiment. The ultimate sensitivities of the two methods are apparently the same.

Since the original work of Purcell[1] and Bloch,[3] other methods of detecting nuclear magnetic resonances have been developed by Roberts,[6] Pound,[7] and more recently by Torrey.[8]

In the work of Roberts, resonances were observed by noting the variation occurring in the output of a super-regenerative oscillator when condition (1) was realized; Roberts also reported experiments with an auto-dyne oscillator, which he found to be less sensitive than the super-regenerative oscillator. Pound has developed an ingenious method of detection which embodies principles similar to those involved in Roberts' work with the auto-dyne oscillator; Pound's system is arranged to permit an automatically controlled slow variation of frequency in a constant magnetic field and has been particularly effective in searching for magnetic resonances. An amplifier with an extremely narrow pass band can be used. Torrey has recently reported the development of a method using pulses of radiofrequency radiation; this method seems particularly well suited for studies of spin-lattice relaxation times.

Our own experiments[9–11] have been done with super-regenerative oscillator circuits operated under conditions apparently different from those used in Roberts' experiment. A super-regenerative oscillator consists of a vacuum-tube circuit which would execute normal oscillations at a radiofrequency were it not for an audiofrequency "quench voltage" which is applied to one of the tube elements in such a manner as to prevent the radiofrequency oscillations from attaining their normal amplitude; this type of oscillator can also be considered an amplitude-modulated radiofrequency oscillator with the amplitude-modulation occurring at the quench-

* Charles E. Coffin Fellow.
[1] E. M. Purcell, H. C. Torrey, and R. V. Pound, Phys. Rev. **69**, 37 (1946).
[2] Bloembergen, Purcell, and Pound, Phys. Rev. **73**, 679 (1948).
[3] Bloch, Hansen, and Packard, Phys. Rev. **69**, 127 (1946).
[4] F. Bloch, Phys. Rev. **70**, 460 (1946).
[5] Bloch, Hansen, and Packard, Phys. Rev. **70**, 474 (1946).
[6] A. Roberts, Rev. Sci. Inst. **18**, 845 (1947).
[7] R. V. Pound, Phys. Rev. **72**, 527 (1947).
[8] H. C. Torrey, Phys. Rev. **75**, 1326 (1949).
[9] J. R. Zimmerman and D. Williams, Phys. Rev. **73**, 94 (1948).
[10] J. R. Zimmerman and D. Williams, Phys. Rev. **74**, 1885 (1948).
[11] J. R. Zimmerman and D. Williams, Phys. Rev. **75**, 198 (1949).

voltage frequency. The spectrum of a super-regenerative oscillator consists of a central frequency ν_0 plus a large group of "side-bands" of frequency $\nu_0 \pm n\nu_q$, where n is an integer and ν_q is the quench frequency. In our work, ν_0 was of the order of 7 mc/sec. and the quench frequency was of the order of 10 kc/sec.; thus, the spectrum of our oscillator consisted of a central frequency of approximately 7 mc/sec. plus a large number of side-bands spaced at 10-kc/sec. intervals. The relative intensities of the various spectral components depend upon the conditions at which the oscillator is operated; for example, the relative intensities are functions of the bias voltages of the various electrodes in the tube, the quench voltage, the quench frequency, etc.

The central frequency may be easily identified by the method mentioned by Roberts;[6] small changes in quench frequency produce changes in side-band frequency but do not produce appreciable changes in the central frequency ν_0. In normal operation of our equipment, the central-frequency component was more intense than any of the side bands. Any of the frequencies

$$\nu = \nu_0 \pm n\nu_q \quad (n = 0, 1, 2, 3 \cdots) \tag{2}$$

is capable of producing a resonance absorption provided condition (1) is fulfilled. This fact can be used to advantage in *search* for resonances: for example, if the power level of the central frequency is so high as to produce saturation, one or more of the side-bands can be used for observing the absorption. Furthermore, as the search process involves changing the magnetic field H slowly while watching an oscilloscope display, it is usually easier to recognize a *series* of absorption peaks corresponding to the frequencies in (2) than to recognize a single peak which might be lost in the random noise signals.

Variations in the output of the super-regenerative oscillator when resonance occurs may be produced by absorption processes involved in transitions between energy levels or by the effects of nuclear-induction signals on the oscillator itself. Both effects are probably present; Roberts[6] reports that in his apparatus the latter effect was dominant. The relative magnitude of the circuit responses to the two effects depends upon conditions of operation. In our work, the radiofrequency power level was kept low, and the effects of resonance upon the circuit was analogous to the introduction of a resistive element in the tank circuit; the principal effect was a large variation of power level which could readily be observed by means of an a-m receiver. The chief effect observed was therefore more closely related to the Purcell experiment than to the Bloch experiment.

A small change in oscillation frequency could also be observed at resonance by means of an f-m receiver. The observed variation in frequency was small compared to the observed variation in amplitude. That the amplitude variation was dominant was further verified by comparison of the proton signal observed by means of an a-m receiver with the proton signal observed by means of an audio amplifier circuit which was insensitive to variations in radiofrequency. Although the a-m receiver proved more sensitive, the shapes of the proton signals obtained by the two methods showed marked similarity.

In initial search for nuclear magnetic resonances only one oscillator coil was placed in the strong magnetic field. In quantitative measurements two mutually perpendicular coils were mounted in the magnetic field; a proton sample was placed in one coil and a sample containing another nucleus was placed in the other coil. By simultaneous observation of resonances for the proton and for the other nucleus, the gyromagnetic ratio of the second nucleus could be determined in terms of the gyromagnetic ratio of the proton. Experimental details are given in the following section.

II. EXPERIMENTAL METHODS

The sample, S_x, to be investigated was placed within a small coil, L, in the homogeneous field of an electromagnet, M. This coil was the tank coil of a simple LC oscillator, the oscillations being interrupted by an external 10–15-kc quench voltage from an audio oscillator. When the condition of resonance, $h\nu = gH_R$, was realized by varying H, the energy absorbed from the tank circuit of the oscillator caused a marked change in the output of the oscillator. This change in output can be detected by several methods, two of which will be described briefly. A more detailed description of the apparatus will be given elsewhere in the near future.

(A) Direct Audio Detection

A block diagram of the experimental arrangement used in this method is shown in Fig. 1a. An audio bandpass amplifier, designed to suppress both 60-c and 10-kc frequencies, was used to detect any variation of the audio components in the plate current of the oscillator. By subjecting H_0 to a small 60-c modulation, amplitude variations occurring at resonance could be observed as amplitude signals on an oscilloscope as

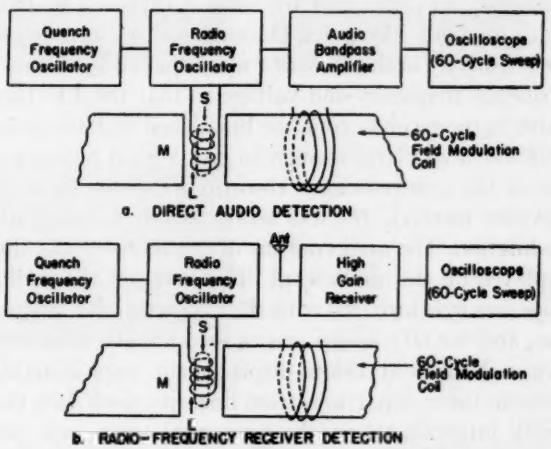

FIG. 1. Block diagram of apparatus used in search for nuclear magnetic resonances.

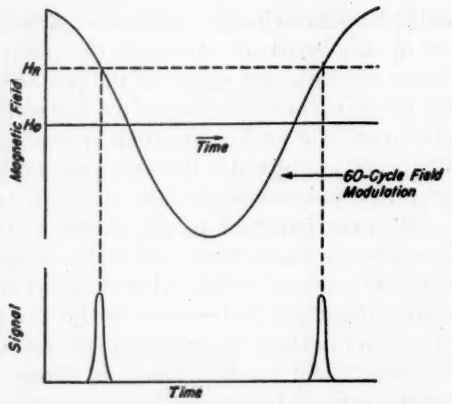

FIG. 2. Magnetic field applied to sample. H_0 is the large field (6000–7000 gauss) applied to sample. A small 60-cycle modulation (10–30 gauss) is superposed. Resonance absorption occurs at field H_R. On the oscilloscope employed trace length intervals $|\Delta l|$ are proportional to magnetic field variations $|\Delta H|$ when H_0 is adjusted so that $H_0=H_R$.

shown schematically in Fig. 2, where for a given frequency of the LC oscillator, H_R corresponds to the resonance condition $h\nu=gH_R$. These two oscilloscope "pips" coalesce into a single one if H_0 is increased to the value where H_R becomes tangent to the field modulation curve. Since no r-f tuning was required by this method, search for nuclear resonances could be carried out by varying the frequency of the r-f oscillator and holding H_0 constant.

(B) Radio Frequency Receiver Detection

A block diagram of the apparatus used in this method of detection is shown in Fig. 1b. When nuclear absorption occurs, there is a decrease in the radiated r-f power. This change in output of the oscillator was observed by means of a high gain receiver. The quench frequency modulation appearing in the output of the receiver was filtered out by the I.F. crystal band selector unit of the receiver. In searching for nuclear resonances, high sensitivity was obtained by using a crystal I.F. band width of about 300 cycles. Once resonances were found, the sensitivity of the oscillator was adjusted by variation of quench frequency and voltage so that the I.F. band width in the receiver could be broadened to 1000 cycles. This width was large enough to give a good representation of the true resonance absorption curves. As in the previous method, H_0 was subjected to a small 60-c modulation. The audio output of the receiver was then displayed on the oscilloscope. The sweep of the oscilloscope was synchronized with the magnetic field modulation, and the 60-c sweep was of such a wave form as to give a horizontal beam displacement approximately linear in time; departures from linearity were such that length intervals Δl on the horizontal trace were proportional to magnetic field variations ΔH in the immediate vicinity of the "pips" when $H_R=H_0$ in Fig. 2.

(C) Search Techniques

In initial search for nuclear resonances, the receiver detection method was employed because of its greater sensitivity as compared with that of the audio detection method. In Fig. 3 are shown typical absorption peaks observed with the "search" oscillator. A narrow crystal I.F. band width of 300 cycles/sec was used to increase the sensitivity of the apparatus. No attempt was made to obtain a true representation of the actual shape of the resonance curves for these pictures. In making frequency measurements, to be explained later, a broad I.F. band width was necessary to give an accurate reproduction of the absorption peaks. Some of the curves in Fig. 3 have two peaks and others appear to have only one. This can be explained by the fact that, for the narrow crystal I.F. setting, the amplitude of one peak can be enhanced and the other one suppressed by slightly detuning the receiver. The transient effect known as the "wiggles" can also be seen in several of the photographs in Fig. 3. These "wiggles" always occur *after* the magnetic field has passed through resonance; comprehensive discussions of this phenomenon have been given elsewhere.[2,12]

(D) Frequency Measurements

Making use of both the audio and receiver detection methods as shown in Fig. 4, one can measure the gyromagnetic ratio of an unknown nucleus in terms of the proton gyromagnetic ratio. Suppose that a sample, S_x, of an unknown nucleus is placed in the coil of oscillator B and a sample, S_p, of the proton is placed in the coil of oscillator A. With oscillator B remaining at a fixed frequency, the magnetic field, H_0, is then varied until a nuclear resonance indication appears on the oscilloscope trace. Then the frequency of oscillator A is varied until the proton resonance occurs at the same magnetic field H_R. These two resonances are observed simultaneously on an oscilloscope by use of an electronic switch. A typical double trace of F^{19} and H^1 is shown in Fig. 5. The resonance "pips" of the lower trace (H^1) are brought into coincidence with those of the upper trace by varying the frequency of oscillator A, the coil of which contains the proton sample.

It can be seen from Fig. 5 that two smaller proton resonances occur in addition to the two main resonances. These are merely side-band absorptions characteristic of super-regenerative oscillators described earlier in this paper. The side-bands serve several useful purposes. If the magnetic field H_0 is varied over a small range, the distance between one of the main resonances and its accompanying sideband will remain constant provided a portion of the oscilloscope sweep is linear with respect to magnetic field variations. Provided a portion of the sweep is found to be linear in gauss, the total sweep in gauss can be estimated, since the sweep is also linear in

[12] B. A. Jacobsohn and R. K. Wangsness, Phys. Rev. **73**, 940 (1948).

frequency and the distance between the main resonance and its sideband is merely the frequency of the audio quench voltage.

In Fig. 5a, the total sweep, i.e., twice the amplitude of the 60-c modulation, is 25 gauss; the distance between the main proton resonance "pips" and the corresponding sidebands is about 4 gauss or 15 kc.; the half-power widths of the F^{19} and H^1 resonances are approximately 1 gauss and 0.5 gauss, respectively. Figure 5b shows an expanded trace of the coincident F^{19} and H^1 amplitude "pips." This expansion gives an indication of what might be termed the resolving power of the instrument. As indicated in the discussion of frequency measurements and field inhomogeneities given below, the half-power resonance widths of the unknown samples apparently are not at present the limiting factors in the accuracy of the experiment. The proton resonance half-width is less than that of any of the nuclei to be measured.

Using the comparison method, one can write $h\nu = gH$ and $h\nu^1 = g^1H$ where ν is the frequency of oscillator B, and ν^1 is the frequency of oscillator A, g is the gyromagnetic ratio of nuclei in S_x, and g^1 is the gyromagnetic ratio of the proton. If the field H_0 is homogeneous throughout the region of S_p and S_x, then $g = (\nu/\nu^1)g^1$. When an oscilloscope double trace as in Fig. 5 is obtained, frequency measurements of oscillator A and oscillator B are obtained by tuning the frequencies of these oscillators, ν^1 and ν, in on the frequency calibration receiver of Fig. 4, and then zero beating these frequencies with a calibrated GR 805C signal generator. The coincident matching shown in Fig. 5 is displayed while frequency measurements are being made and serves to monitor the oscillator frequencies. Any drift in frequency of either oscillator A or B would be easily observed if such drift were to occur. This method of comparison, of course, is independent of magnetic field

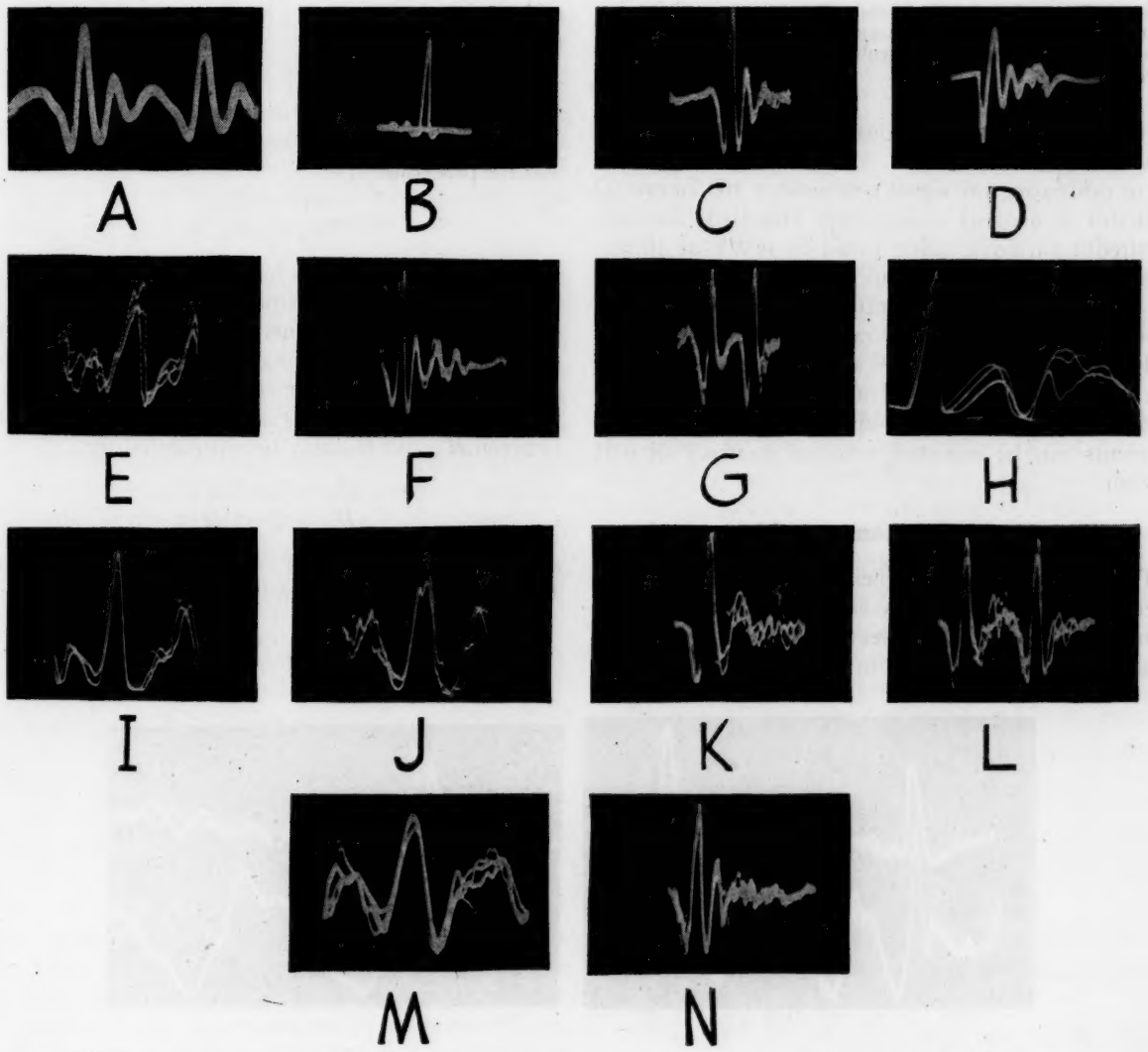

FIG. 3. Oscilloscope displays observed in search for resonances: (A) proton, (B) proton (audio detection), (C) deuteron, (D) lithium, (E) boron,[11] (F) fluorine,[19] (G) sodium,[23] (H) aluminum,[27] (I) copper,[63] (J) copper,[65] (K) bromine,[79] (L) bromine,[81] (M) rubidium,[87] and (N) iodine.[127] (Note: the oscilloscope sweep in (B) is different from that described.)

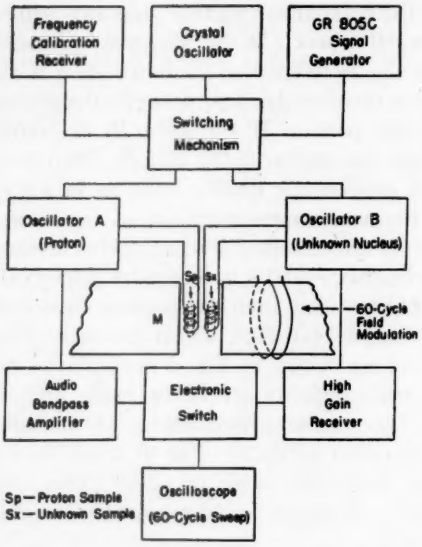

FIG. 4. Block diagram of apparatus used in determining frequency ratios. The coils containing samples S_p and S_x are actually placed with their axes perpendicular to each other and to the applied field.

fluctuations once the resonance "pips" have been matched.

For calibrating the signal generator, a 100-kc crystal oscillator is used as a secondary standard, the one-hundredth harmonic being tuned to WWV at 10 mc. Then, in terms of the harmonics of the crystal oscillator, the signal generator is calibrated at intervals of 0.1 mc over the expected frequency ranges of the oscillators A and B. By means of a vernier attachment, dial readings can be made to 0.001 percent of the operating frequency. Allowing a three-hour warm-up period, frequency measurements can be repeated with an accuracy of 0.01 percent.

(E) Field Inhomogeneities

The maximum inhomogeneity of the magnetic field over the region occupied by *one* of the samples can be estimated by observing directly the half-power resonance width of the protons in the given sample. Since even for the relatively large samples used, half-widths of proton signals are less than 0.5 gauss in a magnetic field of 6500 gauss for both S_p and S_x in Fig. 4, uncertainties due to this effect are small in comparison with other effects which limit the accuracy of the experiment.

The mean value of the magnetic field in the region occupied by S_p as compared with that in the region occupied by S_x is, however, of considerable significance in evaluating the gyromagnetic ratios. Suppose that S_p and S_x are both aqueous solutions of some compound containing unknown nuclei X. Then, first by comparing the H^1 resonance in oscillator A with the X resonance in B, and second by reversing this comparison procedure, the "inhomogeneity" between the two regions can be readily determined.

Let the superscript r denote the first comparison procedure, the superscript s denote the second comparison procedure, g^1 be the gyromagnetic ratio of H^1, g be the gyromagnetic ratio of X, H_A be the magnetic field in the region of S_p in Fig. 4, H_B be the magnetic field in the region of S_x in Fig. 4.

Then, for procedure r,

$$\begin{aligned} h\nu_B{}^r &= gH_B{}^r, \\ h\nu_A{}^r &= g^1H_A{}^r, \end{aligned} \tag{3}$$

and for procedure s,

$$\begin{aligned} h\nu_B{}^s &= g^1H_B{}^s, \\ h\nu_A{}^s &= gH_A{}^s. \end{aligned} \tag{4}$$

The magnetic field was in the range 6000–7000 gauss for all resonance measurements of unknown nuclei reported here, and the magnetization curve of the magnet material over this field range is essentially linear. To a good approximation over this range of magnetic field values, the ratio H_A/H_B is constant and the relationship between H_A and H_B may be represented by

$$\begin{aligned} H_A{}^r &= (k+1)H_B{}^r, \\ H_A{}^s &= (k+1)H_B{}^s, \end{aligned} \tag{5}$$

where k is the constant of inhomogeneity. A solution of Eqs. (3)–(5) yields two useful expressions,

$$\begin{aligned} k+1 &= (\nu_A{}^r\nu_A{}^s/\nu_B{}^r\nu_B{}^s), \\ g &= (\nu_B{}^r/\nu_A{}^r)(k+1)g^1. \end{aligned} \tag{6}$$

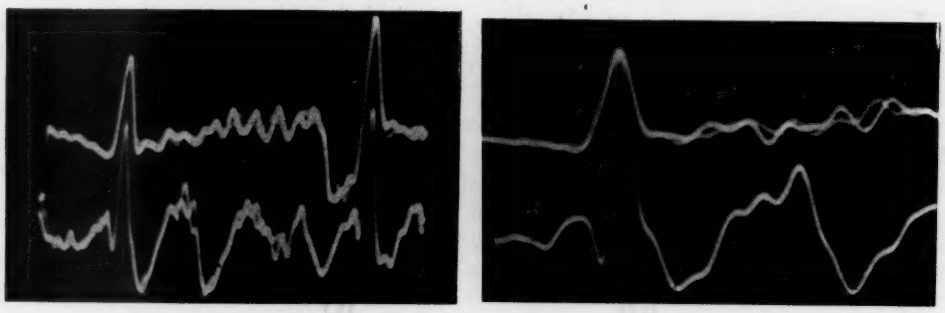

A B

FIG. 5. Oscilloscope displays used comparing resonance frequencies of fluorine[19] and the proton. In each photograph the upper trace shows the resonance for fluorine and the lower shows the proton resonance. The half-width of the proton peak is approximately 0.5 gauss.

In the determination of $(k+1)$, ten resonance frequency measurements using procedure r and ten comparisons using procedure s were obtained, the frequencies used in s corresponding to those used in r. The average value of $(k+1)$ obtained was

$$(k+1)\ (\text{average}) = 1.0011 \pm 0.0001.$$

Since both S_x and S_p cover the same regions of the magnetic field for all measurements, this factor of inhomogeneity was assumed to be the same for all gyromagnetic ratio measurements.

III. EXPERIMENTAL RESULTS

(A) Accuracy of Frequency Measurements

The experimental results for H^2, Li^7, B^{11}, F^{19}, Na^{23}, Al^{27}, Cu^{63}, Cu^{65}, Br^{79}, Br^{81}, Rb^{87}, I^{127} are summarized in Table II. Magnetic resonances for the nuclei Be^9, P^{31}, Rb^{85}, and Cs^{133} have also been observed by the receiver detection method of Fig. 1b. The resonance frequencies of these latter nuclei are being measured and will be reported later.

Each value listed in Table II represents the average of ten careful frequency-ratio determinations. Each of these determinations was made at a different value of the magnetic field H_0. A sample set of data for F^{19} is shown in Table I. The average deviation of the frequency ratio with sign disregarded was 0.02 percent.

In general, the average deviations for the individual measurements of a given unknown nucleus are about 0.03 percent. Since the error in estimating the inhomogeneity of the magnetic field might be as much as 0.01 percent, and since the frequency calibration of the GR 805C signal generator is allowed a variation of 0.01 percent of the measured frequency, it is easily seen that for any accuracy beyond that of the present average deviation, further refinement in frequency measurements and in the measurement of field inhomogeneities must be made. These factors, frequency measurements and determinations of field inhomogeneity, are the limitations of the accuracy in the present experiments.

(B) Summary of Results Obtained on Various Samples

A discussion of the results obtained on various samples containing the nuclei under investigation is desirable, since the intensity of the resonance peaks is strongly dependent upon the material used as a sample.

The basic datum obtained for any given nucleus in the present experiment is the ratio of its resonance frequency to the resonance frequency of the proton in the same *applied* magnetic field. In comparing our results with those of others, we have chosen to reduce their published results to a similar frequency ratio. Some of the earlier results have been stated in terms of the proton magnetic moment as determined by Millman and Kusch,[13] and others have been stated in terms of this value after application of the Schwinger[14] correction. Some of the values given in published summaries[15,16] include a correction for diamagnetism of the electrons,[17] which should be applied in calculation of a nuclear magnetic moment in view of the fact that the magnetic field at the nucleus is slightly different from the applied field. In view of the recent determination of the absolute value of the proton moment,[18] it seems desirable at present to use the measured frequency ratio as a basis of comparison. Actual values of the nuclear moments can be obtained in terms of the new value for the proton by using measured values of the spin and applying a suitable diamagnetism correction.

TABLE I. Typical data obtained in resonance frequency measurements (Fluorine[19]).

Fluorine frequency ν^{19}	Proton frequency ν^{1}	Observed ratio ν^{19}/ν^{1}	Corrected ratio $(\nu^{19}/\nu^{1})(k+1)$
25.192	26.816	0.93944	0.94047
24.839	26.424	0.94002	0.94105
24.913	26.506	0.93990	0.94093
25.195	26.805	0.93994	0.94097
25.300	26.913	0.94007	0.94110
24.932	26.534	0.93962	0.94065
24.540	26.120	0.93951	0.94054
24.943	26.536	0.93997	0.94100
24.827	26.413	0.93995	0.94098
24.938	26.534	0.93985	0.94088
		Average	0.94086

Each unknown sample S_x had a volume of about 6 cc, corresponding to physical dimensions of 5 cm in length and of 1.25 cm in diameter. The proton sample, S_p, consisted of about 3 cc of water placed in a test tube 2.5 cm. in length and 1.25 cm in diameter. Both samples, S_x and S_p, always occupied the same regions of the magnetic field throughout the measurements of all nuclei reported here. A paramagnetic salt was sometimes used in S_x to reduce the relaxation time of the nuclei, thereby raising the upper limit of the power level of the oscillator beyond which saturation of the nuclear energy levels would occur. The frequency of oscillator B in Fig. 4 was set at values corresponding to resonance values of the magnetic field in the range 6000–7000 gauss.

Hydrogen[2]. The nuclear resonance of H^2 was observed in a 95 percent solution of deuterium oxide. Rabi's group[19,15] using the method of molecular beams was the first to measure accurately the gyromagnetic ratio of H^2. Their value for the frequency ratio is 0.1535 ± 0.001. Bloch[20] has recently announced a very precise measure-

[13] S. Millman and P. Kusch, Phys. Rev. **60**, 91 (1941).

[14] J. Schwinger, Phys. Rev. **73**, 416 (1948).

[15] J. B. M. Kellogg and S. Millman, Rev. Mod. Phys. **18**, 323 (1946).

[16] J. Mattauch, *Nuclear Physics Tables* (Interscience Publishers, Inc., New York, 1946).

[17] W. E. Lamb, Phys. Rev. **60**, 817 (1941).

[18] Thomas, Driscoll, and Hipple, Phys. Rev. **75**, 902 (1949).

[19] Kellogg, Rabi, Ramsey, and Zacharias, Phys. Rev. **56**, 728 (1939).

[20] Bloch, Levinthal, and Packard, Phys. Rev. **72**, 1125 (1947), $(\mu'/\mu^2 = 3.257195 \pm 0.00002)$.

TABLE II. Summary of results.

Nucleus	Frequency ratios corrected $(\nu/\nu')(k+1)$
H^1	0.15355±0.00005
Li^7	0.38862±0.00002
B^{11}	0.32076±0.00009
F^{19}	0.94086±0.00017
Na^{23}	0.26454±0.00007
Al^{27}	0.26062±0.00011
Cu^{63}	0.26515±0.00005
Cu^{65}	0.28404±0.00009
Br^{79}	0.25059±0.00005
Br^{81}	0.27014±0.00005
Rb^{87}	0.32718±0.00016
I^{127}	0.20003±0.00007

ment which gives 0.1535063±0.00001 for the frequency ratio. Bitter,[21] using a bridge absorption method, reports a value of 0.153510±0.000003. Our corresponding value is 0.15355±0.00005.

Lithium[7]. An aqueous solution of $Li(C_2H_3O_2)$ was used as the sample for observing nuclear resonance of Li^7. About 1 cc of the saturated solution of $CuCl_2$ was added to the lithium solution to act as a paramagnetic catalyst. With a radiofrequency level satisfactory for other materials, saturation of nuclear levels in the lithium sample occurred even in the presence of paramagnetic ions. However, this saturation does not occur for the side-band frequencies of the quenched r-f oscillator. Making use of the side-band characteristic of super-regenerative oscillators, one can vary the magnetic field H_0 to nuclear resonance corresponding to a side-band frequency instead of the center frequency of the r-f oscillator. The side-band frequency used in this case was 10.0 kc higher than the center frequency. A previous measurement[15] of the gyromagnetic ratio of Li^7 gives a value of 0.38873±0.00017 for the frequency ratio. The corresponding value found here is 0.38862±0.00002.

Boron[11]. Strong resonances of both Na^{23} and B^{11} were observed in an aqueous solution of $Na_2B_2O_4$. However, only the measurements of B^{11} were obtained with this compound. There was no noticeable saturation of the nuclear levels at resonance. From molecular beam measurements[15] a value of 0.3081±0.0009 for the frequency ratio is obtained. In a recent private communication, F. Bitter reports a value of 0.32085±0.00006. These values are to be compared with the value 0.32076 ±0.00009 obtained in the present work.

Fluorine[19]. Nuclear resonances were first observed in an organic liquid $CF_3-CCl=CCl-CF_3$. Much stronger resonances have since been observed in an aqueous solution of SbF_3. In the organic liquid saturation effects set in at a much lower power operating level of the r-f oscillator than does the aqueous solution of the antimony trifluoride. Previous measurements[15] gave a frequency ratio of 0.9410±0.0009 as compared with the value of 0.94086±0.00017 measured at this laboratory.

[21] Bitter, Alpert, Nable, and Poss, Phys. Rev. 72, 1271 (1947).

Sodium[23]. Na^{23} seems to give a strong resonance in most soluble sodium salts. Resonances were observed in aqueous solutions of NaI, NaBr, $NaAsO_2$, and $Na_2B_2O_4$. Although the concentration of Na^{23} nuclei in the $NaAsO_2$ solution was about the same as the concentration of Na^{23} nuclei in the other mentioned solutions, the nuclear resonance of Na^{23} in $NaAsO_2$ is much stronger than that which occurs in the others. Rabi[15] has reported a value corresponding to a frequency ratio of 0.26494 ±0.00028. In a private communication, F. Bitter reports a value of 0.26450±0.00003. Measurements made in the present study give the value 0.26454±0.00007.

Aluminum[27]. Nuclear magnetic resonance absorption has been observed in aqueous solutions of both $AlCl_3$ and $Al_2(SO_4)_3$. Gyromagnetic ratio measurements were made with the $AlCl_3$ solution. Rabi[15] and his co-workers have reported a value giving a frequency ratio of 0.2603±0.0007. The average value determined here, 0.26062±0.00011, compares favorably with the above result.

Copper[63] *and Copper*[65]. The sample used was a mixture of Cu_2Cl_2 and a solution of $CuCl_2$. A considerable gain in nuclear absorption intensities of both Cu^{63} and Cu^{65} isotopes is obtained by the addition of the cupric ions. This increased intensity is, as earlier pointed out by R. V. Pound,[22] due to the cupric ion which decreases the relaxation time. Pound[23] has published the following frequency ratios for the isotopes of copper: $\nu(Cu^{63})/\nu(Na^{23})=1.0022$ and $\nu^{65}/\nu^{63}=1.0711$. Corresponding ratios computed from Table II are $\nu/(Cu^{63})/\nu(Na^{23})=1.0023$ and $\nu^{63}/\nu^{65}=1.0713$.

Bromine[79] *and Bromine*[81]. Nuclear resonances of both bromine isotopes were observed in NaBr and KBr aqueous solutions. Measurements were made with the NaBr solution. The only values published on the bromine isotopes are those reported by Pound.[23] He obtained $\nu^{81}/\nu^{79}=1.0778$ and $\nu^{81}/\nu(Na^{23})=1.0209$. Our corresponding values obtained from Table II are 1.0780 and 1.0212, respectively.

Rubidium[87]. An aqueous solution of Rb_2CO_3 was employed for observing the nuclear resonance of Rb^{87}. It should be mentioned here that resonance absorption was also observed for Rb^{85} with the same sample; and, although Rb^{87} is only about one-third as abundant as Rb^{85}, the intensity of the Rb^{87} peak observed in the present experiment is considerably greater than that of Rb^{85}. Our value for the frequency ratio is 0.32718 ±0.00016 as compared with 0.3266±0.0010 by molecular beam methods.

Iodine[127]. The absorption line resulting from I^{127} was first found by using an aqueous solution of NaI as a sample. A much stronger resonance was obtained from an aqueous solution of KI. Gyromagnetic measurements were made using the KI solution. Pound,[24] using his

[22] R. V. Pound, Phys. Rev. 73, 523 (1948).
[23] R. V. Pound, Phys. Rev. 72, 1273 (1947).
[24] R. V. Pound, Phys. Rev. 73, 1112 (1948).

recording radiofrequency spectrometer, found the ratio of the frequency of the I^{127} line to that of Na^{23} in a sample of NaI to be 0.75664. We have determined the same frequency ratio to be 0.75615.

IV. DISCUSSION OF RESULTS

From the results obtained thus far we are led to conclude that the sensitivity of the super-regenerative oscillator method of observing nuclear magnetic resonances is comparable with the sensitivities of the bridge and nuclear induction methods. The ultimate limitations of sensitivity have not yet been determined; these are of course determined by the effective noise factor associated with the oscillator and receiver or amplifier. The noise power can be decreased by decreasing the pass band of the receiver or amplifier. With 60-c modulation, the band width must of necessity be large, approximately 1000 cycles for a fair presentation of resonance line shapes; by decreasing the modulation frequency, one can decrease the band width. In observing a weak signal due to resonance absorption, there is an optimum radiofrequency power level which is probably determined by the spin-lattice relaxation time of the material used as a sample. The optimum power level had to be determined experimentally in the present work and there is at present no satisfactory method by which it can be calculated; it can be raised by adding magnetic catalysts. Further experimental work must be done before accurate estimates of ultimate sensitivity can be made.

An interesting check of some of the work done in the present study was made possible by the recent report of Bitter,[25] which appeared after the completion of our experimental work. Using two radiofrequency bridges, Bitter determined the ratio of resonance frequencies of several nuclei to the resonance frequency of the proton in the same magnetic field. In Table III is given a comparison of our results with those given by Bitter. In making the comparison, we have taken the ratio of our values for various nuclei to the corresponding values given by Bitter. It will be noted that in every case the results obtained by the two methods are in agreement within the limits stated. Except for B^{11} and Rb^{87} the frequency ratios obtained in the present work were slightly higher than the ones reported by Bitter. The average percentage difference between the values obtained by the two methods is 0.015 percent, which is extraordinarily good agreement in view of the fact that the details of the two experiments were quite different.

TABLE III. Comparison of present results with Bitter's results.

Nucleus	Present study / Bitter's results	Uncertainty: Present study	Uncertainty: Bitter
Li^{7}	1.0000	±0.0001	±0.0001
B^{11}	0.9997	3	2
Na^{23}	1.0002	3	1
Al^{27}	1.0002	4	1
Cu^{63}	1.0003	2	2
Cu^{65}	1.0004	2	2
Br^{81}	1.0004	2	3
Rb^{87}	1.0000	4	2

There is considerable room for improvement in our present methods of frequency measurements. If practical improvement in frequency measurements can be made, a more accurate determination of inhomogeneity factor k can also be made. It may then be advantageous to use smaller test samples in the hope of further reducing the widths of the observed resonance peaks. However, the agreement between our present results and those of Bitter indicates that fairly reliable results can be obtained with the super-regenerative oscillator even in its present form.

The writers take pleasure in expressing their appreciation to Professors E. M. Purcell and Arthur Roberts for helpful discussions during the early stages of the work; to Professors George Shortley, Ely Bell, and Fred Dickey for many valuable suggestions; to Mr. William Chambers, Mr. P. L. Reed, and Major Anthony J. Mony for assistance in various parts of the experimental work; to Mr. Carl McWhirt and his assistants for their cooperation in construction of needed instruments; and to Professor Harald H. Nielsen and Dean Alpheus Smith for their constant interest and encouragement. Grateful acknowledgment is also made to the Graduate School and Ohio State University Development Fund for research grants needed for the work, and to the General Electric Company for a research fellowship awarded to one of us (J.R.Z.).

[25] F. Bitter, Phys. Rev. 75, 1326 (1949).

TABLE II. Summary of results.

Nucleus	Frequency ratios corrected $(\nu/\nu^1)(k+1)$
H^2	0.15355±0.00005
Li^7	0.38862±0.00002
B^{11}	0.32076±0.00009
F^{19}	0.94086±0.00017
Na^{23}	0.26454±0.00007
Al^{27}	0.26062±0.00011
Cu^{63}	0.26515±0.00005
Cu^{65}	0.28404±0.00009
Br^{79}	0.25059±0.00005
Br^{81}	0.27014±0.00005
Rb^{87}	0.32718±0.00016
I^{127}	0.20003±0.00007

ment which gives 0.1535063±0.00001 for the frequency ratio. Bitter,[21] using a bridge absorption method, reports a value of 0.153510±0.000003. Our corresponding value is 0.15355±0.00005.

Lithium[7]. An aqueous solution of $Li(C_2H_3O_2)$ was used as the sample for observing nuclear resonance of Li^7. About 1 cc of the saturated solution of $CuCl_2$ was added to the lithium solution to act as a paramagnetic catalyst. With a radiofrequency level satisfactory for other materials, saturation of nuclear levels in the lithium sample occurred even in the presence of paramagnetic ions. However, this saturation does not occur for the side-band frequencies of the quenched r-f oscillator. Making use of the side-band characteristic of super-regenerative oscillators, one can vary the magnetic field H_0 to nuclear resonance corresponding to a side-band frequency instead of the center frequency of the r-f oscillator. The side-band frequency used in this case was 10.0 kc higher than the center frequency. A previous measurement[15] of the gyromagnetic ratio of Li^7 gives a value of 0.38873±0.00017 for the frequency ratio. The corresponding value found here is 0.38862±0.00002.

Boron[11]. Strong resonances of both Na^{23} and B^{11} were observed in an aqueous solution of $Na_2B_2O_4$. However, only the measurements of B^{11} were obtained with this compound. There was no noticeable saturation of the nuclear levels at resonance. From molecular beam measurements[15] a value of 0.3081±0.0009 for the frequency ratio is obtained. In a recent private communication, F. Bitter reports a value of 0.32085±0.00006. These values are to be compared with the value 0.32076 ±0.00009 obtained in the present work.

Fluorine[19]. Nuclear resonances were first observed in an organic liquid $CF_3-CCl=CCl-CF_3$. Much stronger resonances have since been observed in an aqueous solution of SbF_3. In the organic liquid saturation effects set in at a much lower power operating level of the r-f oscillator than does the aqueous solution of the antimony trifluoride. Previous measurements[15] gave a frequency ratio of 0.9410±0.0009 as compared with the value of 0.94086±0.00017 measured at this laboratory.

Sodium[23]. Na^{23} seems to give a strong resonance in most soluble sodium salts. Resonances were observed in aqueous solutions of NaI, NaBr, $NaAsO_2$, and $Na_2B_2O_4$. Although the concentration of Na^{23} nuclei in the $NaAsO_2$ solution was about the same as the concentration of Na^{23} nuclei in the other mentioned solutions, the nuclear resonance of Na^{23} in $NaAsO_2$ is much stronger than that which occurs in the others. Rabi[15] has reported a value corresponding to a frequency ratio of 0.26494 ±0.00028. In a private communication, F. Bitter reports a value of 0.26450±0.00003. Measurements made in the present study give the value 0.26454±0.00007.

Aluminum[27]. Nuclear magnetic resonance absorption has been observed in aqueous solutions of both $AlCl_3$ and $Al_2(SO_4)_3$. Gyromagnetic ratio measurements were made with the $AlCl_3$ solution. Rabi[15] and his co-workers have reported a value giving a frequency ratio of 0.2603±0.0007. The average value determined here, 0.26062±0.00011, compares favorably with the above result.

Copper[63] *and Copper*[65]. The sample used was a mixture of Cu_2Cl_2 and a solution of $CuCl_2$. A considerable gain in nuclear absorption intensities of both Cu^{63} and Cu^{65} isotopes is obtained by the addition of the cupric ions. This increased intensity is, as earlier pointed out by R. V. Pound,[22] due to the cupric ion which decreases the relaxation time. Pound[23] has published the following frequency ratios for the isotopes of copper: $\nu(Cu^{63})/\nu(Na^{23})=1.0022$ and $\nu^{65}/\nu^{63}=1.0711$. Corresponding ratios computed from Table II are $\nu/(Cu^{63})/\nu(Na^{23})=1.0023$ and $\nu^{63}/\nu^{65}=1.0713$.

Bromine[79] *and Bromine*[81]. Nuclear resonances of both bromine isotopes were observed in NaBr and KBr aqueous solutions. Measurements were made with the NaBr solution. The only values published on the bromine isotopes are those reported by Pound.[23] He obtained $\nu^{81}/\nu^{79}=1.0778$ and $\nu^{81}/\nu(Na^{23})=1.0209$. Our corresponding values obtained from Table II are 1.0780 and 1.0212, respectively.

Rubidium[87]. An aqueous solution of Rb_2CO_3 was employed for observing the nuclear resonance of Rb^{87}. It should be mentioned here that resonance absorption was also observed for Rb^{85} with the same sample; and, although Rb^{87} is only about one-third as abundant as Rb^{85}, the intensity of the Rb^{87} peak observed in the present experiment is considerably greater than that of Rb^{85}. Our value for the frequency ratio is 0.32718 ±0.00016 as compared with 0.3266±0.0010 by molecular beam methods.

Iodine[127]. The absorption line resulting from I^{127} was first found by using an aqueous solution of NaI as a sample. A much stronger resonance was obtained from an aqueous solution of KI. Gyromagnetic measurements were made using the KI solution. Pound,[24] using his

[21] Bitter, Alpert, Nable, and Poss, Phys. Rev. 72, 1271 (1947).

[22] R. V. Pound, Phys. Rev. 73, 523 (1948).
[23] R. V. Pound, Phys. Rev. 72, 1273 (1947).
[24] R. V. Pound, Phys. Rev. 73, 1112 (1948).

recording radiofrequency spectrometer, found the ratio of the frequency of the I^{127} line to that of Na^{23} in a sample of NaI to be 0.75664. We have determined the same frequency ratio to be 0.75615.

IV. DISCUSSION OF RESULTS

From the results obtained thus far we are led to conclude that the sensitivity of the super-regenerative oscillator method of observing nuclear magnetic resonances is comparable with the sensitivities of the bridge and nuclear induction methods. The ultimate limitations of sensitivity have not yet been determined; these are of course determined by the effective noise factor associated with the oscillator and receiver or amplifier. The noise power can be decreased by decreasing the pass band of the receiver or amplifier. With 60-c modulation, the band width must of necessity be large, approximately 1000 cycles for a fair presentation of resonance line shapes; by decreasing the modulation frequency, one can decrease the band width. In observing a weak signal due to resonance absorption, there is an optimum radiofrequency power level which is probably determined by the spin-lattice relaxation time of the material used as a sample. The optimum power level had to be determined experimentally in the present work and there is at present no satisfactory method by which it can be calculated; it can be raised by adding magnetic catalysts. Further experimental work must be done before accurate estimates of ultimate sensitivity can be made.

An interesting check of some of the work done in the present study was made possible by the recent report of Bitter,[25] which appeared after the completion of our experimental work. Using two radiofrequency bridges, Bitter determined the ratio of resonance frequencies of several nuclei to the resonance frequency of the proton in the same magnetic field. In Table III is given a comparison of our results with those given by Bitter. In making the comparison, we have taken the ratio of our values for various nuclei to the corresponding values given by Bitter. It will be noted that in every case the results obtained by the two methods are in agreement within the limits stated. Except for B^{11} and Rb^{87} the frequency ratios obtained in the present work were slightly higher than the ones reported by Bitter. The average percentage difference between the values obtained by the two methods is 0.015 percent, which is extraordinarily good agreement in view of the fact that the details of the two experiments were quite different.

TABLE III. Comparison of present results with Bitter's results.

Nucleus	Present study / Bitter's results	Uncertainty: Present study	Uncertainty: Bitter
Li^{7}	1.0000	±0.0001	±0.0001
B^{11}	0.9997	3	2
Na^{23}	1.0002	3	1
Al^{27}	1.0002	4	1
Cu^{63}	1.0003	2	2
Cu^{65}	1.0004	2	2
Br^{81}	1.0004	2	3
Rb^{87}	1.0000	4	2

There is considerable room for improvement in our present methods of frequency measurements. If practical improvement in frequency measurements can be made, a more accurate determination of inhomogeneity factor k can also be made. It may then be advantageous to use smaller test samples in the hope of further reducing the widths of the observed resonance peaks. However, the agreement between our present results and those of Bitter indicates that fairly reliable results can be obtained with the super-regenerative oscillator even in its present form.

The writers take pleasure in expressing their appreciation to Professors E. M. Purcell and Arthur Roberts for helpful discussions during the early stages of the work; to Professors George Shortley, Ely Bell, and Fred Dickey for many valuable suggestions; to Mr. William Chambers, Mr. P. L. Reed, and Major Anthony J. Mony for assistance in various parts of the experimental work; to Mr. Carl McWhirt and his assistants for their cooperation in construction of needed instruments; and to Professor Harald H. Nielsen and Dean Alpheus Smith for their constant interest and encouragement. Grateful acknowledgment is also made to the Graduate School and Ohio State University Development Fund for research grants needed for the work, and to the General Electric Company for a research fellowship awarded to one of us (J.R.Z.).

[25] F. Bitter, Phys. Rev. **75**, 1326 (1949).

Radioactive Tin 111

R. A. HINSHAW* AND M. L. POOL
The Ohio State University, Columbus, Ohio
(Received April 13, 1949)

A radioactive isotope of a half-life of 35.0±0.5 minutes has been found in the tin fraction of cadmium bombarded with alpha-particles. Using electromagnetically enriched cadmium the assignment can be made to Sn 111. Positrons of 1.45 Mev and x-rays are observed.

A 20-MINUTE tin activity has been reported[1] resulting from indium bombarded with protons. Positron emission was observed and the assignment was made to Sn^{113}.

Alpha-particle bombardment of cadmium has yielded a 25-minute tin activity.[2] Negative particle emission was reported, however; and the assignment could possibly be made to Sn^{113} also. The 105-day tin activity[3] which decays by K-electron capture is known to be due to Sn^{113}.

In so far that a short lived activity is strongly indicated in the light mass numbered isotopes of tin, it was thought that a positive identification could be made with the aid of electromagnetically separated isotopes.

The chemical identification of the activity is readily established by obtaining the tin chemical fraction from cadmium metal bombarded with 20 Mev alpha-particle. Hilger Lab. No. 10,677 of 99.9999 percent purity was used. The tin fraction was placed in a magnetic field and a Geiger counter was so located as to intercept either positrons or electrons.[4] The positron decay curve is shown in Fig. 1. Upon subtraction of longer period positron activities a new 35.0±0.5 minute activity was found.

Similar bombardments were made with stable isotopes of electromagnetically separated cadmium 106, 108 and 110 enriched to 32.9, 24.8 and 70 percent respectively.** The samples were mounted in sets of two on opposite sides of a rotating internal probe and thus given very nearly identical alpha-particle bombardments. The results showed that the activity was clearly obtained from the Cd^{108} isotope but not from the Cd^{106} or Cd^{110} isotopes. The assignment of the 35-minute activity is thus made to Sn^{111}.

Figure 2 shows a curve of the aluminum absorption measurements of the total activity of the tin fraction.

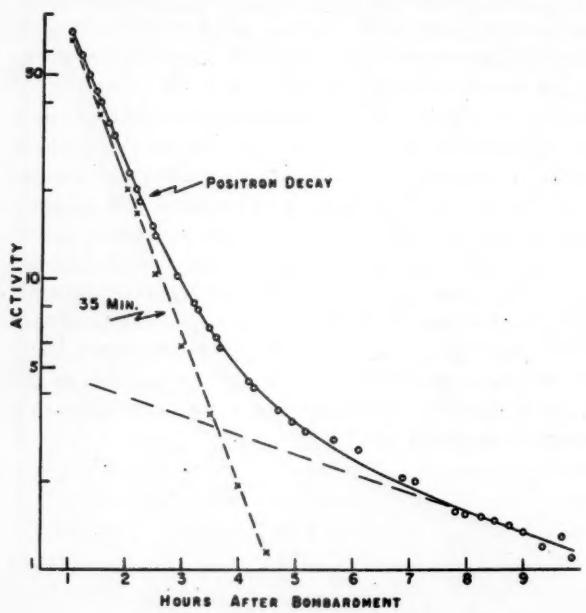

FIG. 1. Decay curve of the tin fraction of cadmium bombarded with 20 Mev alpha-particles.

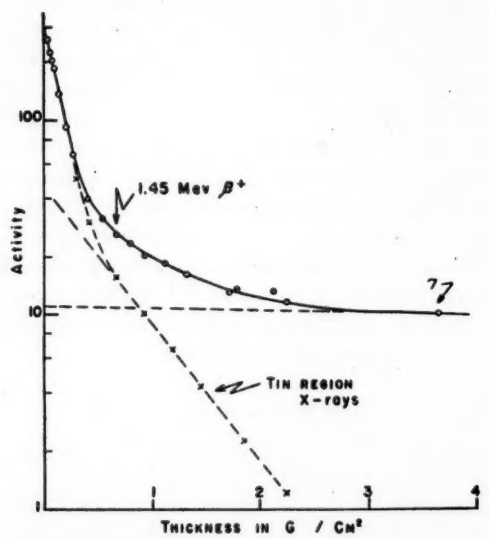

FIG. 2. Aluminum absorption curve taken in the 35.0-minute period of the tin fraction from an alpha-particle bombardment of cadmium. The positron end-point is 1.45 Mev. X-rays in the tin region are also indicated.

* Now at Muskingum College, New Concord, Ohio.
[1] S. W. Barnes, Phys. Rev. 55, 241 (1939).
[2] J. J. Livingood and G. T. Seaborg, Phys. Rev. 55, 667 (1939).
[3] S. W. Barnes, Phys. Rev. 56, 414 (1939); K. D. Coleman and M. L. Pool, Phys. Rev. 72, 1070 (1947).
[4] L. L. Woodward and D. A. McCown, Rev. Sci. Inst. 19, 823 (1948).
** Supplied by the Y-12 plant, Carbide and Carbon Chemicals Corporation through the Isotopes Division, U. S. Atomic Energy Commission, Oak Ridge, Tennessee.

During the time that the activity was in the 35-minute period the measurements were taken on a Wulf electrometer attached to an ionization chamber.

A beta-end point of 0.68 g/cm² was found corresponding to about 1.45 Mev. Evidence is also seen for the presence of x-rays of an absorption coefficient characteristic of the tin region. The ratio of K-electron process, as suggested by the x-rays, to the positron decay process is about 26.

Acknowledgment is gratefully made for support received from the Ohio State University Development Fund and the Graduate School. The chemical separations were performed by H. L. Finston and R. M. Dyer. E. C. Mallary kindly helped in taking some of the data.

PHYSICAL REVIEW VOLUME 76, NUMBER 3 AUGUST 1, 1949

A Note on Perturbation Theory as Applied to Collision Stimulated Processes

JAMES N. SNYDER* AND W. H. FURRY
Department of Physics, Harvard University, Cambridge, Massachusetts
(Received April 4, 1949)

If a particle which can decay spontaneously is subjected to collisions with other particles the transition probability may be changed. The calculation of such an effect by the usual time-dependent perturbation methods is complicated by the circumstance that energy can be conserved in some intermediate states, because of the possibility of elastic scattering. The perturbation calculation is here modified in such a way that the resulting expression for the whole transition probability does not contain any divergences or spurious effects. By suitable approximations the expression is separated into two parts, one of which gives the probability of elastic scattering followed by a spontaneous transition, and the other the true stimulated transition probability which causes a change in the lifetime.

I. INTRODUCTION

IF a particle which is subject to decay suffers a collision with another particle, it is conceivable that its lifetime will be altered. Such a process is exemplified by a meson interacting with a nucleon, for which the stimulated lifetime has been calculated.[1]

Such a stimulated decay is a three-step process, the collision accounting for two steps, and the decay, the third. If the collision be viewed as absorption and reemission, and standard time dependent perturbation theory[2] be applied, the result for the transition probability per unit time, $w_{f\leftarrow i}$ is

$$w_{f\leftarrow i}=2\pi/\hbar|H_{fi}|^2\rho_f, \tag{1}$$

where ρ_f is the density of final states, and

$$H_{fi}=\sum_{I\,II}\frac{H_{fII}H_{II\,I}H_{Ii}}{(E_i-E_{II})(E_i-E_I)}. \tag{2}$$

Here the H's are the matrix elements connecting the initial, first intermediate, second intermediate, and final states, and the E's are the energies of these states.

To calculate the stimulated decay of the incident particle it is necessary to integrate $w_{f\leftarrow i}$ over a set of variables describing the final state. Since momentum is conserved at every step of such a process, the energy of the second intermediate state, E_{II}, could be chosen as one of these variables. If this is done it is seen that the integrand (1) has a quadratic divergence at $E_{II}=E_i$. The origin of this difficulty is simply that energy *could* be conserved in the second intermediate state as well as in the final state. This corresponds to an elastic scattering of the particle followed by its spontaneous decay.

This divergence difficulty can be circumvented by re-examining the development of (1)–(2) and retaining those terms which are negligible in ordinary problems ($E_I, E_{II}\neq E_i$) but are important here. These are the boundary terms which arise at each step in the calculation of the probability amplitudes of the intermediate states, since all amplitudes except that of the initial state are required to vanish initially. If this is done the transition probability becomes

$$P_{f\leftarrow i}(t)=\sum\int\cdots\int dE_{II}dE_f\cdots\rho_f$$
$$\times\left|\frac{e^{i(E_f-E_i)t/\hbar}-1}{E_i-E_f}\sum_{I\,II}\frac{H_{f\,II}H_{II\,I}H_{I\,i}}{(E_i-E_{II})(E_i-E_I)}\right.$$
$$\left.-\sum_{I\,II}\frac{e^{i(E_f-E_{II})t/\hbar}-1}{(E_{II}-E_f)(E_i-E_{II})}\frac{H_{f\,II}H_{II\,I}H_{I\,i}}{(E_i-E_I)}\right|^2, \tag{3}$$

where the sum and integrals are to be performed over the variables of the final state; only the pertinent E_f and E_{II} integrals are shown. This integrand does not suffer from any singularity at $E_{II}=E_i$. But this line of attack is immediately precluded by the fact that (3)

* Now at Department of Physics, University of Illinois, Urbana, Illinois.

[1] W. H. Furry and J. N. Snyder, Phys. Rev. **75**, 1265 (1949).

[2] See W. Heitler, *The Quantum Theory of Radiation*, (Oxford University Press, London, 1944) Second Edition.

gives not only a contribution to the transition probability from $E_f=E_i\neq E_{II}$ but also from $E_{II}=E_f\neq E_i$, thus violating conservation of energy.

A more careful treatment of the problem is hence necessary.

II. SOLUTIONS OF THE PERTURBATION EQUATIONS

As notation, let

$$x=E_i-E_f \tag{4}$$

$$y=E_i-E_{II} \tag{5}$$

and let ξ represent generically the additional variables (angles, etc.) necessary to specify the second intermediate state, and η those to specify the final state: Hence:

$$\begin{aligned} &y,\ \xi \text{ specify an intermediate state,}\\ &x,\ \eta,\ y,\ \xi \text{ specify a final state.}\end{aligned} \tag{6}$$

In addition, for convenience, let the two matrix elements for the scattering process be replaced by a "second-order matrix element."

$$U=\sum_I \frac{H_{II\,I}H_{I\,i}}{E_i-E_I}, \tag{7}$$

and let the matrix element for the decay $H_{f\,II}$ be denoted by α. In general the variables ξ, η can be chosen, and indeed are most naturally chosen, so that both α and the density ρ_1 defined in Eq. (10) are independent of ξ; the quantity U, on the other hand, may depend strongly on ξ.

Then if $t/\hbar$ be for convenience replaced by t, the equations for the probability amplitudes of the second-intermediate and final states are:

$$i\dot{a}_{II}(y,\xi)=e^{-iyt}U(y,\xi)+\sum_f e^{-i(y-x)t}\alpha^*(x,\eta,y)a_f(x,\eta,y,\xi), \tag{8}$$

$$i\dot{a}_f(x,\eta,y,\xi)=e^{-i(x-y)t}\alpha(x,\eta,y)a_{II}(y,\xi), \tag{9}$$

where the transition probabilities have been assumed to be so small that the amplitude of the initial state a_i can be considered constant and equal to unity.

These equations differ from the conventional treatment by the retention of the second term in Eq. (8) which represents the effect of the excitation of a state on the probability amplitude of the preceding state. It is just the retention of this term that removes the divergence difficulty associated with the conventional treatment. The sum in (8) is to be carried over the restricted number of final states which can arise from a given intermediate state. No sum occurs in (9) since a given final state (x,η,y,ξ) can arise from only one intermediate state (y,ξ).

If the sum in (8) consisted only of one term (one-to-one correspondence of intermediate to final states), the equations could be integrated exactly, but this does not seem to correspond to any known physical problem.

If the sum in (8) were replaced by an integral and a_{II} eliminated by the use of (9), a second-order differentio-integral equation for a_f would be obtained. Such equations are met with in the theories of line breadth[3] and radiation damping,[4] where they are solved by assuming solutions of a convenient form. No such simple Ansatz suggests itself here.

Equations (8)–(9) are solved in an approximate manner by introducing a "density of final states," $\rho_1(x,\eta,y)$ with the significance

$$\begin{aligned}\rho_1(x,\eta,y)=&\text{Number of final states in the range } dxd\eta\\ &\text{about } x,\eta \text{ which arise from a given in-}\\ &\text{termediate state } y,\xi,\end{aligned} \tag{10}$$

and replacing the sum in (8) by an integral over the variables x',η' describing the final states. Equation (9) is then multiplied by $\rho_1(x,\eta,y)\alpha^*(x,\eta,y)$ and integrated over $d\eta$. With the notation[5]

$$\int d\eta'\rho_1(x,\eta',y)\alpha^*(x,\eta',y)a_f(x,\eta',y,\xi)=A_f(x,y,\xi), \tag{11}$$

$$\int d\eta'\rho_1(x,\eta',y)\,|\alpha(x,\eta',y)|^2=\beta(x,y). \tag{12}$$

Eqs. (8) and (9) become:

$$i\dot{a}_{II}(y,\xi)=e^{-iyt}U(y,\xi)+\int dx'e^{-i(y-x')t}A_f(x',y,\xi), \tag{13}$$

$$i\dot{A}_f(x,y,\xi)=e^{-i(x-y)t}\beta(x,y)a_{II}(y,\xi). \tag{14}$$

The substitution

$$b(y,\xi)=e^{iyt}a_{II}(y,\xi), \tag{15}$$

$$B(x,y,\xi)=e^{ixt}A_f(x,y,\xi) \tag{16}$$

reduces Eqs. (13) and (14) to

$$i\dot{b}(y,\xi)+yb(y,\xi)=U(y,\xi)+\int dx'B(x',y,\xi), \tag{17}$$

$$i\dot{B}(x,y,\xi)+xB(x,y,\xi)=\beta(x,y)b(y,\xi). \tag{18}$$

The initial conditions on a_{II} and a_f were:

$$a_{II}=a_f=0 \quad \text{at} \quad t=0, \tag{19}$$

so that

$$b=B=0 \quad \text{at} \quad t=0. \tag{20}$$

Equation (18) has the solution

$$B(x,y,\xi)=-ie^{ixt}\beta(x,y)\int_0^t e^{-ixt'}b(y,\xi;t')dt' \tag{21}$$

---

[3] V. F. Weisskopf and E. P. Wigner, Zeits. f. Physik. **63**, 54 (1930).

[4] W. Heitler, Proc. Camb. Phil. Soc. **37**, 291 (1941); W. Heitler and H. W. Peng, Proc. Camb. Phil. Soc. **38**, 296 (1942); A. H. Wilson, Proc. Camb. Phil. Soc. **37**, 301 (1941).

[5] Note that β is related to the spontaneous decay constant γ by $\gamma=(2\pi/\hbar)\beta(0,0)$.

which satisfies the initial condition. Then (17) becomes:

$$i\dot{b}(y,\xi;t)+yb(y,\xi;t)$$

$$=U(y,\xi)-i\int dx'e^{ix't}\beta(x',y)\int_0^t e^{-ix't'}b(y,\xi;t')dt'$$

$$=U(y,\xi)-i\int_0^t dt'b(y,\xi;t')\int dx'e^{ix'(t-t')}\beta(x',y). \quad (22)$$

In order to solve this equation simply, it is necessary to replace $\beta(x',y)$ by $\beta(0,y)$. This is the assumption that the density of final states ρ_1 and the matrix element α are not strongly varying functions of the final energy. Such an assumption is in accord with accepted quantum-mechanical practice and is equivalent to the assumption that most of the contribution to the integral in (22) comes from the region $x=0$ ($E_f=E_i$). Hence the hitherto unspecified range of the variable x' can be extended from $-\infty$ to ∞ and:

$$\int dx'e^{ix'(t-t')}\beta(x',y)\rightarrow 2\pi\beta(0,y)\delta(t-t'), \quad (23)$$

where δ is the Dirac δ-function. Hence the right-hand side of (22) becomes:

$$U(y,\xi)-2\pi i\beta(0,y)\int_0^t dt'b(y,\xi;t')\delta(t-t')$$

$$=U(y,\xi)-i\pi\beta(0,y)b(y,\xi;t). \quad (24)$$

This result, obtained by integrating up to the "middle" of a delta-function and getting half the usual result obtained by integrating across the delta-function, can be rigorously justified in this case by the application of the Fourier Integral Theorem.

The solution of (22) with its right-hand number replaced by (24) is

$$b(y,\xi)=\frac{U(y,\xi)}{y+i\pi\beta(0,y)}[1-\exp(iyt-\pi\beta(0,y)t)] \quad (25)$$

which satisfies the initial conditions (20). When Eqs. (25), (15), and (19) are used, the solution of Eq. (9) is found to be

$$a_f(x,\eta,y,\xi)=\frac{\alpha(x,\eta,y)U(y,\xi)}{y+i\pi\beta(0,y)}\left[\frac{e^{-ixt}-1}{x}\right.$$

$$\left.-\frac{\exp[-i(x-y)t-\pi\beta(0,y)t]-1}{x-y-i\pi\beta(0,y)}\right]. \quad (26)$$

The transition probability is given by

$$P(t)=\sum_{all\ f}|a_f|^2. \quad (27)$$

A density function $\rho(x,\eta,y,\xi)$ with the significance:

$\rho(x,\eta,y,\xi)$ = Number of final states in the range $dxd\eta dyd\xi$ about x,η,y,ξ (28)

is introduced so that the sum in (27) may be replaced by an integral, which yields with the use of (26):

$$P(t)=\int\int\int\int dxd\eta dyd\xi\rho(x,\eta,y,\xi)\frac{|\alpha(x,\eta,y)U(y,\xi)|^2}{y^2+\pi^2[\beta(0,y)]^2}$$

$$\times\left|\frac{e^{-ixt}-1}{x}-\frac{\exp[-i(x-y)t-\pi\beta(0,y)t]-1}{x-y-i\pi\beta(0,y)}\right|^2. \quad (29)$$

The limits on the integrals will be determined by the problem under consideration, and these integrals are also to be regarded as standing for any necessary spin sums.

III. DISCUSSION

The expression (29) does not suffer from any divergence difficulties, nor does it give any contribution to the transition probability except from the region around $x=0$ ($E_f=E_i$). In addition (29) provides the proper answer to the following classical analogy in which probabilities rather than probability amplitudes are treated by the standard methods of probability theory. (The word "classical" is here used in the sense that the quantum mechanically calculated transition probabilities, e.g., one for scattering and one for decay, both with energy conservation, are combined classically.)

Let transitions into the intermediate state "*II*" occur at the constant rate B, while transitions out of the state "*II*" into any one of final states "*f*" occur at a rate proportional to a coefficient A_f and the probability P_{II} of the state "*II*." Then with

$$P_{II}=P_f=0 \quad \text{at} \quad t=0, \quad (30)$$

we have

$$\dot{P}_{II}=B-\sum_f\dot{P}_f=B-\sum_f A_fP_{II}, \quad (31)$$

$$\dot{P}_f=A_fP_{II}. \quad (32)$$

Hence,

$$P_f=\frac{A_fB}{A}\left[t-\frac{e^{-At}-1}{A}\right], \quad (33)$$

where

$$A=\sum_f A_f. \quad (34)$$

This result is proportional to t^2 only initially, while if the "reaction" term describing the effect of the excitation of a state upon the probability of the preceding state were neglected in (31), the result would be proportional to t^2 for all t.

This "classical" process (i.e., particle is scattered elastically and then decays) is, of course, contained in and makes a large contribution to (29). The stimulated decay (i.e., scattering without conservation of energy, followed by decay) is also contained in (29) and is super-

imposed upon the "classical" answer. If in (29) the matrix elements and density of final states are assumed to be slowly varying functions of x and y so that they may be replaced by their values at $x=y=0$ ($E_i=E_{II}=E_f$), the result is

$$P_{\text{classical}}(t)=C\int_{-\infty}^{\infty}dx\int_{-\infty}^{\infty}\frac{dy}{y^2+\pi^2\beta^2}\left|\frac{e^{-ixt}-1}{x}-\frac{\exp[-i(x-y)t-\pi\beta t]-1}{x-y-i\pi\beta}\right|^2, \quad (35)$$

where the limits on the integrals have been extended from $-\infty$ to ∞ since the contributions to the integral all come from a narrow region of width β about $x=y=0$, and where

$$C=\int\int d\eta d\xi\rho(0,\eta,0,\xi)|\alpha(0,\eta,0)U(0,\xi)|^2.$$

The integral (35) can easily be evaluated by the method of residues, and yields the result:

$$P_{\text{classical}}(t)=C\{(2\pi t/\hbar\beta)+(e^{-2\pi\beta t/\hbar}-1)/\beta^2\}, \quad (36)$$

which is of the desired form (33). (The factor $\hbar$ in $t/\hbar$ has been restored.)

In order to obtain the complete transition probability, including both the "classical" part (36) and the part corresponding to stimulated transitions, it is necessary to take into account the energy dependence of the matrix elements and of the density of final states. Since there are no contributions except from very small values of x, it is permissible to set $x=0$ in the functions $\rho(x,\eta,y,\xi)$ and $\alpha(x,\eta,y)$ in the integrand of (29), but the dependence on y has to be retained. The exact calculation of the integral is in general not feasible, but simple approximations suffice to determine the parts which are of physical interest. These are the "classical" transition probability defined above and the "stimulated" transition probability; the latter comprises the remaining part of the result which is *proportional to the time*. In singling out these two contributions we are neglecting only small highly complicated contributions which decay exponentially in time.

The "classical" result of Eq. (36) was obtained from Eq. (29) by replacing the factor

$$\rho(x,\eta,y,\xi)|\alpha(x,\eta,y)U(y,\xi)|^2/\{y^2+(\pi\beta(0,y))^2\} \quad (37a)$$

by

$$\rho(0,\eta,0,\xi)|\alpha(0,\eta,0)U(0,\xi)|^2/\{y^2+(\pi\beta(0,0))^2\}, \quad (37b)$$

and $\beta(0,y)$ by $\beta(0,0)$. To get the "stimulated" transition probability we must correct for the replacement (37a)→(37b), but on the other hand, since we are now interested only in contributions linear in t, we can neglect the second term in the last factor in Eq. (29). Then since

$$\int dx|e^{-ixt/\hbar}-1|^2/x^2\to 2\pi t/\hbar, \quad (38)$$

with contribution only at $x=0$, we have as the formula for the stimulated transition probability:

$$P_{\text{stim.}}(t)=(2\pi t/\hbar)\int\int\int d\eta dy d\xi\times\left\{\rho(0,\eta,y,\xi)\frac{|\alpha(0,\eta,y)U(y,\xi)|^2}{y^2+(\pi\beta(0,y))^2}-\rho(0,\eta,0,\xi)\frac{|\alpha(0,\eta,0)U(0,\xi)|^2}{y^2+(\pi\beta(0,0))^2}\right\}. \quad (39)$$

In cases such as that of meson decay, in which β is very small and not very strongly dependent on y, the approximation of replacing $\beta(y,0)$ by $\beta(0,0)$ can be used to simplify the evaluation of this integral.

It may be pointed out that although the integrand in Eq. (39) is not everywhere positive, the result is certainly positive. This is true because the integrand of (29) is everywhere positive and the whole of the "classical" results (36) comes from a narrow region around $y=0$, whose contribution to the integral in Eq. (39) is negligible.

Note on the Resonance Scattering of High Energy γ-Rays by Nuclei of Carbon and Copper

E. R. GAERTTNER AND M. L. YEATER
Research Laboratory, General Electric Company, Schenectady, New York
(Received April 13, 1949)

A search has been made for the resonance scattering of high energy γ-rays in nuclei of carbon and copper using the 100-Mev betatron to provide the primary radiation. The scattering in carbon and copper is less than 1 percent and 3 percent, respectively, of the total cross section for resonance absorption.

EVIDENCE indicating that there is a resonance absorption of γ-rays at high energies has been obtained by several investigators[1,2] from a study of $\gamma-n$, reactions. Goldhaber and Teller[3] have suggested a nuclear model which may account for this absorption. According to Goldhaber and Teller there may also be a strong scattering of γ-rays at the resonance energy characteristic of each nucleus. The angular distribution of this scattered radiation, following the Goldhaber-Teller argument, is given by the classical Thomson formula

$$I(\theta) \propto (1+\cos^2\theta),$$

where θ is the angle between the primary beam and the scattered radiation. This is believed to hold for cases where the characteristic wave-length is greater than 2π times the nuclear radius.

We have investigated the scattering in copper and carbon, using the 100-Mev betatron for a source of γ-rays and a cloud chamber for a detector of the scattered radiation. Our data indicate the resonance scattering to be small in terms of the total nuclear absorption, and our result is an upper limit for this process.

A measurement of scattered radiation at a mean angle of $\theta=11°$ has afforded a means of making an absolute intensity calibration of the γ-ray beam. This is necessary for evaluating the cross section for resonance scattering. The Compton effect produces a relatively strong spectrum of scattered radiation at this angle. Since this spectrum is readily calculable, the intensity of the observed spectrum is a measure of the beam intensity. Figure 1 shows the pair spectrum obtained from the scattering of γ-rays in carbon, for a peak betatron energy, E_m, of 50 Mev. By pair spectrum is meant the number of pairs produced (in a lead foil 0.5 mm thick) in the chamber as a function of the pair energy. Taking account of the Klein-Nishina differential scattering cross section, the bremsstrahlung produced by secondary electrons in the carbon, the geometry, and the cloud-chamber efficiency, and assuming a primary quantum spectrum of the form $N(E)dE=K(dE/E)$,[4] we have calculated the theoretical pair spectrum in 5-Mev intervals down to 5 Mev. This is normalized to fit the experimental data and plotted in Fig. 1. The fit between the theoretical and experimental curves is satisfactory. The number of observed pairs is small above the "Compton cut-off" energy of 22 Mev, i.e., the maximum energy with which 50-Mev quanta can be scattered at our minimum angle of 9° by the Compton effect. Using the normalizing factor for this curve, we find the average number of quanta at a distance of 3 meters from the betatron target in a 1-Mev interval at 22 Mev (copper resonance energy) to be 1.9×10^3 per cm^2 per pulse for $E_m=50$ Mev.[5] (This is the greatest intensity, at this energy, which was available from the betatron during the period of the experiment.[6]) The corresponding constant for $E_m=100$ Mev follows from this, if one knows the relative γ-ray intensity for $E_m=50$ Mev and for 100 Mev. This ratio is obtained in a straightforward way by comparing the activation of copper samples placed directly in the beam. The quantum yield per pulse for $E_m=100$ Mev is found to be 6.0 times greater

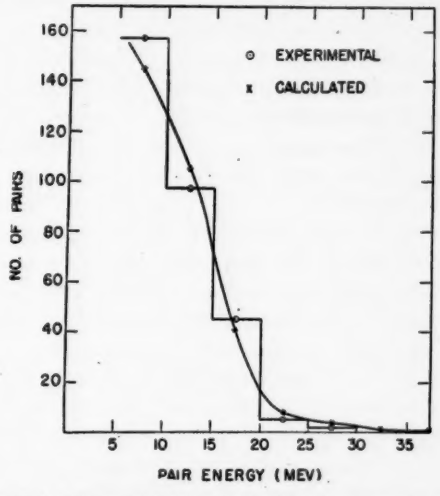

FIG. 1. Pairs observed in cloud chamber from quanta scattered in carbon at $\theta=11°$. The calculated values are for Compton scattering and bremsstrahlung from secondary electrons.

[1] G. C. Baldwin and G. S. Klaiber, Phys. Rev. **71**, 3 (1947); Phys. Rev. **73**, 1156 (1948).
[2] M. L. Perlman and G. Friedlander, Phys. Rev. **74**, 442 (1948).
[3] M. Goldhaber and E. Teller, Phys. Rev. **74**, 1046 (1948).
[4] Early measurements by J. L. Lawson, using the spectrum analyzer recently described, Phys. Rev. **75**, 436 (1949), indicate this spectrum to be approximately correct (private communication).
[5] These results can be shown to agree with those obtained by J. L. Lawson and M. L. Perlman, Phys. Rev. **74**, 1190 (1948), using a different method, when account is taken of the different experimental conditions.
[6] The relative betatron intensity is checked periodically by a Victoreen *R*-thimble placed directly in the beam, and is monitored continuously by an ionization chamber at one side of the beam.

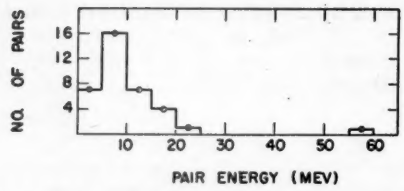

FIG. 2. Pairs observed in cloud chamber from quanta scattered in copper at $\theta=120°$.

than the number quoted above for $E_m=50$ Mev. These absolute intensities are estimated to be accurate within 40 percent.

The measurements at $\theta=11°$ do not constitute a sensitive test for the resonance scattering. The geometry is such that the calculated intensity of the scattered quanta is smaller than the expected bremsstrahlung in the carbon, assuming a scattering cross section equal to the total cross section of Goldhaber and Teller and a $(1+\cos^2\theta)$ distribution.

A value of θ near 90° is more favorable for the detection of resonance scattering because the distance from scatterer to detector is smaller and the contribution from Compton scattering and bremsstrahlung from secondary electrons is less. Scattering measurements in carbon and copper have been made with the following experimental conditions. The γ-rays from the betatron, operated at 100 Mev and maximum intensity, pass through a collimator which defines a beam 1 cm high and 3 cm wide at the scatterer. A magnetic field sweeps out electrons from the beam as it passes through the collimator. Carbon or copper of sufficient thickness to absorb 90 percent of the primary γ-rays is placed in the beam. The cloud chamber is placed at the side of the scatterer so that scattered quanta hitting the pair-forming lead foil in the chamber have a mean angle, with the forward direction of the beam, of 120°, and a spread in angle of 45°. Additional shielding of lead is placed between the betatron and the cloud chamber to absorb stray radiation from the betatron.

In the thick scatterers used, only a fraction of the primary quanta in the resonance energy interval are absorbed or scattered by the nucleus. This fraction is given by the ratio of the nuclear cross section to the sum of all absorption cross sections, including pair production and Compton scattering; these are averaged over the resonance interval. For assumed resonance widths between about 1 and 10 Mev the resonance cross section is expected to be smaller than the sum of the pair and Compton cross sections. For this range of widths, therefore, the number of nuclear resonance processes should be nearly independent of the width. If *all* of the resonance absorption resulted in *scattering* with a $(1+\cos^2\theta)$ distribution, we should expect to observe an average of 0.03 pairs of resonance energy per picture from the copper, and 0.01 resonance pairs per picture from the carbon. This expectation is based on the Goldhaber-Teller values of the total integrated cross section and on our measurement of the absolute beam intensity; it includes corrections for geometry, cloud-chamber detection efficiency, and absorption of the scattered quanta.

From 12,000 pictures taken with the carbon target and 5000 with the copper target, we have obtained no pairs which clearly result from nuclear scattering. From carbon we have observed one pair of energy 18 Mev and no others greater than 13 Mev; the few pairs observed can probably be accounted for as bremsstrahlung from secondary electrons in the carbon. The nuclear scattering in carbon of quanta of about 30 Mev, therefore, cannot amount to more than 1 percent of the total nuclear resonance absorption predicted by Goldhaber and Teller.[7] From copper we have observed the spectrum of pairs shown in Fig. 2. Since the multiple scattering of secondary electrons and the radiation probability are greater in copper than in carbon we should expect to observe a greater number of pairs from bremsstrahlung. It is probable that the observed pairs are of this origin. If one makes the assumption, however, that all five of the pairs lying between 15 and 30 Mev are due to nuclear resonance, this scattering is no greater than 3 percent of the nuclear resonance absorption.

It would be helpful to have a measurement of the total cross section and the total width of the absorption resonance. Early in our investigation we made a tentative measurement of the continuous spectrum of the γ-rays from the betatron transmitted through two feet of carbon, using the cloud chamber to measure the pair spectrum. Our data, although weak statistically so far, suggest a dip in the pair spectrum in the neighborhood of 30 Mev. Measurements of this type may provide information about the total resonance absorption.

We wish to thank Dr. E. E. Charlton and the betatron group for their generous cooperation. Dr. G. C. Baldwin kindly called our attention to this problem in advance of publication of the Goldhaber-Teller paper. We were fortunate in being able to discuss some of the theoretical aspects of the nuclear resonance effect with Professor H. A. Bethe and Dr. H. Hurwitz. Our program is supported by Contract N7 onr 332 with the ONR.

[7] In contrast to this result, the $\gamma-n$ absorption in carbon measured by J. L. Lawson and M. L. Perlman, Phys. Rev. 74, 1190 (1948), is about equal to the predicted total cross section.

PHYSICAL REVIEW VOLUME 76, NUMBER 3 AUGUST 1, 1949

On the Continuous Gamma-Radiation Accompanying the Beta-Decay of Nuclei*

C. S. WANG CHANG† AND D. L. FALKOFF‡
University of Michigan, Ann Arbor, Michigan
(Received April 22, 1949)

The quantum mechanical calculations of Knipp and Uhlenbeck, and F. Bloch of the continuous γ-spectrum associated with the sudden change of nuclear charge during β-decay have been extended to forbidden β-transitions and to the different types of β-interactions. It is shown that the γ-spectrum has practically the same shape, and the ratio of total γ-intensity to β-intensity is almost the same for forbidden transitions as for allowed transitions, irrespective of the β-interaction. This accounts for the good agreement of the theory for allowed transitions with the experiments of C. S. Wu on $_{15}P^{32}$, a "forbidden" β-emitter. A simple classical analogue is given to explain this uniformity and is shown to justify the interpretation that the probabilities for the β- and γ-emission processes may in a very good approximation be taken as independent.

I. INTRODUCTION

THE existence of a weak continuous γ-spectrum accompanying the β-decay of nuclei was first shown experimentally by Aston[1] in his measurements on RaE. Subsequently it has been observed in various β-radioactive elements by many investigators,[2] most recently by C. S. Wu[3] using $_{15}P^{32}$.

A satisfactory theory of this inhomogeneous low intensity radiation was given simultaneously by Knipp and Uhlenbeck,[4] and F. Bloch[5] who showed quantum mechanically that continuous radiation of the observed order of magnitude, e.g., roughly $\alpha=1/137$ quanta per β-particle could be attributed to the sudden change in nuclear charge when the particle is created and leaves the nucleus. This radiation has been called "internal" bremsstrahlung in contradistinction to the "external" bremsstrahlung which is the continuous electromagnetic radiation which is classically associated with the acceleration of a passing electron by the Coulomb field of the nucleus. The need to extend the calculations of Knipp, Uhlenbeck, and Bloch (henceforth denoted by KUB) becomes apparent when one seeks to compare theory and experiment. In the first place the theory was developed only for allowed β-transitions assuming the Fermi[6] polar vector interaction. On the other hand RaE and $_{15}P^{32}$ are generally classified[7] as first and second forbidden β-emitters, respectively. Hence any agreement between theory and experiment thus far might appear as fortuitous. Indeed, one knows that, for instance, the internal conversion of γ-radiation is quite different for the higher multipoles which correspond to the successive degrees of forbiddenness of the γ-transition. To check the theory, therefore, it is necessary to extend the calculations of KUB to forbidden β-transitions.

Since the Fermi polar vector interaction is but one of five linearly independent relativistically invariant interactions (see reference 7) which might be used in the β-decay theory, it is also of interest to see whether the calculated internal bremsstrahlung varies appreciably with the choice of interactions, in which case it could serve as a means of distinguishing between them. For this reason we have also extended the calculations of KUB to the different β-interactions for first and second degrees of forbiddenness.

The method of calculation is the same as in KUB. The joint probability per unit time $S(k)dk$ for emission of a quantum of energy k is obtained by a second order perturbation calculation, corresponding to the occurrence of the over-all process in two steps:

(1) The transition from initial to intermediate state consisting of the nuclear transformation accompanied by the creation and emission of a β-particle and a neutrino.

(2) The transition of the electron from its intermediate state to a final state by simultaneous emission of a light quantum of energy k.

The initial state, 0, of the unperturbed system is taken to be the state in which only the parent nucleus is present with an available energy W_0. The transition to the intermediate state, 1, is due to the electron neutrino interaction H_β. In this state of the system some neutron in the nucleus has been transformed into a proton, an electron has been created in a state s' of energy $W_{s'}$ and momentum $\mathbf{p}_{s'}$, and also an antineutrino in a state of energy W_σ and momentum $\mathbf{p}_\sigma$. The energy of the intermediate state is W_1. In the final state, f, the nucleus and neutrino remain unchanged, but in virtue of the interaction, H_γ, of the electron with the electromagnetic radiation field, a quantum of energy k and momentum $\mathbf{k}$ has been emitted leaving the electron with energy W_s and momentum $\mathbf{p}_s$.** The energy of the final state is $W_1=W_0=W_s+W_\sigma+k$. The total prob-

* A preliminary report was presented at the Chicago meeting of the American Physical Society, December 1947.

† Now at the Institute for Advanced Study, Princeton, New Jersey.

‡ Now at the University of Notre Dame, Notre Dame, Indiana.

[1] G. H. Aston, Proc. Camb. Phil. Soc. 23, 935 (1927).

[2] S. Bramson, J. de Phys. et Rad. 66, 721 (1930); E. Stahel and D. J. Commore, Physica 2, 707 (1935); G. J. Sizoo and D. J. Commore, Physica 3, 921 (1936); E. McMillan, Phys. Rev. 47, 801 (1935); G. V. Droste, Zeits. f. Physik 100, 529 (1936); Sizoo, Eickman, and Green, Physica 6, 1057 (1939); E. Stahel and J. Guillessen, J. de Phys. et Rad. 1, 12 (1940).

[3] C. S. Wu, Phys. Rev. 59, 481 (1941).

[4] J. K. Knipp and G. E. Uhlenbeck, Physica 3, 425 (1936).

[5] F. Bloch, Phys. Rev. 50, 272 (1936).

[6] E. Fermi, Zeits. f. Physik 88, 161 (1934).

[7] E. J. Konopinski, Rev. Mod. Phys. 15, 209 (1943); E. J. Konopinski and G. E. Uhlenbeck, Phys. Rev. 60, 308 (1941).

** The relativistic units will be used throughout, $\hbar=m=c=1$.

ability $S(k)dk$ for the emission of a γ-quantum with energy between k and $k+dk$ is

$$S(k)dk=\frac{1}{(2\pi)^8}dkk^2\int d\Omega_e\int d\Omega_\sigma\int d\Omega_k\int dW_e \times(W_0-W_e)^2(W_e-k)[(W_e-k)^2-1]^{\frac{1}{2}} \times\left|\sum_l\frac{(f|H_\gamma|l)(l|H_\beta|0)}{W_l-W_0}\right|^2, \quad (1)$$

where $W_e=W_0-W_\sigma$ is the energy with which the electron is "born," and where the integrations over Ω_e, Ω_σ and Ω_k are integrations over the directions of the momenta of the electron, anti-neutrino and the light quantum and summations over the polarizations of these particles respectively. The particular interaction H_β used by KUB was the "polar vector allowed." If one wanted only the probability per unit time for the non-radiative emission with energy between W and $W+dW$, this would be given by

$$P(W)dW=1/(2\pi)^5pW(W_0-W)^2|(0|H_\beta|l)|^2dW. \quad (2)$$

On comparing (1) and (2) there appears to be no good reason to suppose that the probability for the over-all process should be simply the product of the probability for each. Nevertheless, Knipp and Uhlenbeck[4] have given an alternative method for this calculation in which the two steps in the radiative β-decay are assumed to be independent. They first obtain the probability $P(W)dW$ for the emission of a β-particle with energy W using the conventional β-theory as indicated by Eq. (2), and then with a first order perturbation calculation they obtain the conditional probability per unit time $\Phi(W_e, k)$ that an electron coming from the nucleus with energy W_e will emit a quantum of energy k. (In this calculation the initial electron wave function is taken to be an outgoing wave solution of the Dirac equation divergent at the origin corresponding to a source of electrons at the nucleus. The final electron state is that for a free particle.) Then in virtue of the assumed independence of these two processes, they are able to write

$$S(k)=\int dW_eS(W_e, k)=\int dW_eP(W_e)\Phi(W_e, k). \quad (3)$$

This expression, if it were valid, has the advantage that for any given β-spectrum one can insert for $P(W)$ the experimentally observed energy distribution of the outgoing β-electrons thereby eliminating from the calculation of the radiative effects any lack of uniqueness inherent in the β-theory itself. For example, the question of which interaction to use is avoided, as is also any mention of the unobserved neutrino.

The sole justification of Knipp and Uhlenbeck for introducing this method of calculation is the *a posteriori* one that for allowed transitions it yields exactly the same result as the more rigorous second order perturbation method. But Morrison and Schiff[8] argue that it is only for allowed β-transitions that these two methods of calculation will agree, and that for forbidden β-transition in which the electron-neutrino coupling depends explicitly on the momenta of these particles these two methods should no longer agree.

Our calculations with the forbidden β-transition show that although the two different methods of evaluating the internal bremsstrahlung do not yield exactly the same results, they are nevertheless in good enough agreement to warrant the use of the simpler form (3) in practice for comparison with experiment. In addition, by way of making physically plausible the interpretation of the β-emission and radiation as independent processes, we show in Section III that the function $\Phi(W_e, k)$ may also be obtained classically.

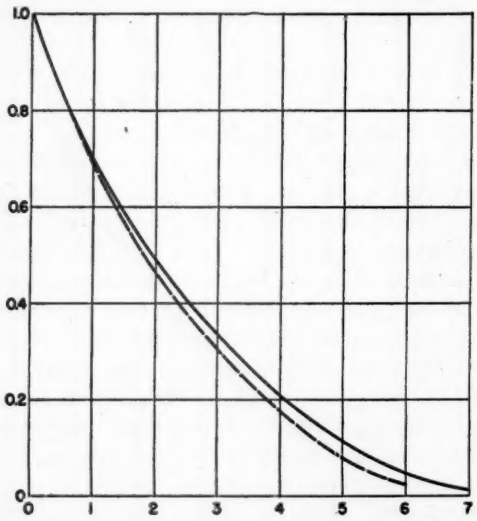

FIG. 1. Energy distribution of the γ-rays following allowed β-transitions, scalar and vector theory, for $W_0=10$ in relativistic units. Ordinate $kS(k)$ normalized to unity for $k=0$. Abscissa, k measured in relativistic units.

———— Exact, from Eq. (5).
– – – – – Approximate W_0 large, from Eq. (5a).

II. RESULTS

The electromagnetic interaction for emission of a γ-quantum of momentum $\mathbf{k}$ and polarization $\mathbf{e}_k$ is

$$H_\gamma=(2\pi\alpha/k)^{\frac{1}{2}}(\boldsymbol{\alpha}\cdot\mathbf{e}_k)e^{-i\mathbf{k}\cdot\mathbf{r}},$$

where α is the fine structure constant, $\boldsymbol{\alpha}$ the Dirac matrix operator. In the Born approximation one neglects the effect of the nuclear charge on the electron so that both the electron and anti-neutrino wave functions are the 4-component plane wave solutions of the Dirac equation

$$\psi_e=\frac{A_e}{(\Omega)^{\frac{1}{2}}}\exp(i\mathbf{p}_e\cdot\mathbf{r}), \text{ for the electron}$$

$$\varphi_\sigma=\frac{B_\sigma}{(\Omega)^{\frac{1}{2}}}\exp(-i\mathbf{p}_\sigma\cdot\mathbf{r}), \text{ for the anti-neutrino}$$

[8] P. Morrison and L. I. Schiff, Phys. Rev. **58**, 24 (1940)

normalized to unity in the volume Ω. For H_β we take the different interactions for the β-decay.

A. The Allowed Transitions. Scalar and Vector Interactions

For the polar vector interaction which KUB used, the matrix element of H_β is given by

$$(l|H_\beta|0)=G\int d\tau[(V^*QU)(\psi_e^*\varphi_\sigma)-(V^*\alpha QU)\cdot(\psi_e^*\alpha\varphi_\sigma)],$$

where G is the constant determining the strength of the coupling of the electron neutrino field to the nucleons, Q is an operator which transforms a neutron state into a proton state and U and V are the nuclear wave functions for the neutrons and protons respectively. For an allowed transition the second term is dropped. Writing M for the matrix element involving the unknown nuclear wave functions

$$M=\int d\tau V^*QU.$$

KUB obtained

$$S(k)=\frac{\alpha G^2|M|^2}{2\pi^4}\frac{1}{k}\int_{1+k}^{W_0}dW_e(W_0-W_e)^2 \times[(W_e^2+W_e^2)\ln(W_e+p_e)-2W_ep_e], \quad (4)$$

where $W_e=W_e-k$. After integration this becomes

$$S(k)=\frac{\alpha G^2|M|^2}{4\pi^4}\frac{1}{k}\left\{\left[W_0^2(\tfrac{2}{3}x^3+x)-W_0(x^4+x^2-\tfrac{1}{8})+\frac{7}{15}x^5-\frac{3}{8}x\right]\ln(x+(x^2-1)^{\frac{1}{2}})-\left[W_0^2\left(\frac{11}{9}x^2+\frac{4}{9}\right)-W_0\left(\frac{7}{4}x^3+\frac{1}{8}x\right)+\frac{689}{900}x^4-\frac{1021}{1800}x^2-\frac{8}{75}\right](x^2-1)^{\frac{1}{2}}\right\}, \quad (5)$$

with $x=W_0-k$. For W_0 large compared to unity one can simplify the above formula by keeping only the terms of the highest order in W_0 and x, and replacing $(x^2-1)^{\frac{1}{2}}$ by x, then one obtains

$$S(k)\cong\frac{\alpha G^2|M|^2}{4\pi^4}\frac{1}{k}\left\{\left[\frac{2}{3}W_0^2x^3-W_0x^4+\frac{7}{15}x^5\right]\ln 2x-\left(\frac{11}{9}W_0^2x^3-\frac{7}{4}W_0x^4+\frac{689}{900}x^5\right)\right\}. \quad (5a)$$

The comparison of this equation with the exact one (5) is given in Fig. 1.

The total intensity of the γ radiation is

$$I_\gamma=\int_0^{W_0-1}dkkS(k)$$

$$\cong\frac{\alpha G^2|M|^2}{4\pi^4}\left\{\left[\frac{2}{45}W_0^6+\frac{1}{6}W_0^4-\frac{1}{144}\right]\ln(W_0+(W_0^2-1)^{\frac{1}{2}})+W_0(W_0^2-1)^{\frac{1}{2}}\left[-\frac{22}{225}W_0^4-\frac{27}{200}W_0^2+\frac{103}{3600}\right]\right\}.$$

For large W_0, this simplifies to

$$I_\gamma\cong\frac{\alpha G^2|M|^2}{2\pi^4}\frac{1}{45}W_0^6(\ln 2W_0-2.22). \quad (6)$$

The β-energy distribution is given by

$$P(W_e)=(G^2|M|^2/2\pi^3)(W_0-W_e)^2W_ep_e, \quad (7)$$

whence in the approximation $W_0\gg1$, the total β-intensity becomes

$$I_\beta=\int_1^{W_0}dW_e(W_e-1)P(W_e)\cong\frac{G^2|M|^2}{2\pi^3}\frac{1}{60}W_0^6, \quad (8)$$

so that ratio of total γ-intensity to total β-intensity for this allowed transition becomes

$$I_\gamma/I_\beta=4\alpha/3\pi(\ln 2W_0-2.22). \quad (9)$$

Knipp and Uhlenbeck[4] rewrite $S(k)$ as given by (8) in the form

$$S(k)=\int_{1+k}^{W_0}dW_eP(W_e)\Phi(W_e,k) \quad (10)$$

where $P(W_e)$ is given by (11) and

$$\Phi(W_e,k)=\frac{\alpha p_e}{\pi p_ek}\left\{\frac{W_e^2+W_e^2}{W_ep_e}\ln(W_e+p_e)-2\right\}. \quad (11)$$

$\Phi(W_e,k)$ is interpreted as the conditional probability that a β-electron emitted with energy W_e will radiate a γ-quantum of energy k. In fact they show, further, that if one does not average over the direction of the quantum: $\int d\Omega_k$ in (5), then one may factor out a function depending on the angle θ between $\mathbf{k}$ and $\mathbf{p}_e$. This differential conditional probability is given by

$$d\Phi(W_e,k,\theta)=\frac{\alpha p_e}{p_ek}\left[\frac{W_e^2+W_e^2}{W_e(W_e-p_e\cos\theta)}-\frac{1}{(W_e-p_e\cos\theta)^2}-1\right]d\Omega_k \quad (12)$$

and integrates to (11).

Both the differential and integrated probabilities (11) and (12) are precisely the same as they obtained by the

alternative first order perturbation method mentioned in Section I.

By comparing the scalar β-interaction with the vector interaction one can easily convince oneself that one gets the same formulas (4)–(12) for an allowed scalar transition if one redefined M by

$$M=\int d\tau V^*\beta QU.$$

B. First Forbidden Transition; Scalar Interaction

For this case the matrix element depends explicitly on the electron and neutrino momenta

$$(l|H_\beta|0)=G/\Omega(A_{s'}{}^*\beta B_\sigma)[-i(\mathbf{p}_{s'}+\mathbf{p}_\sigma)\cdot\mathbf{M}]$$

with

$$\mathbf{M}=\int d\tau V^*\beta U\mathbf{r}.$$

Substituting this matrix element into (1) and performing the summation over the spins and the two directions of the polarization one finds

$$S(k)=\frac{2\alpha G^2}{(2\pi)^7}k\int dp_\sigma p_\sigma{}^2W_s p_s\int d\Omega_\sigma\int d\Omega_s\int d\Omega_k$$
$$\times\frac{1}{W_\sigma W_s(W_e{}^2-W_{s'}{}^2)^2}\times[(\mathbf{p}_{s'}+\mathbf{p}_\sigma)\cdot\mathbf{M}]^2$$
$$\times\left\{2W_eW_\sigma\left[W_sW_e-1-\frac{(\mathbf{k}\cdot\mathbf{p}_s)(\mathbf{k}\cdot\mathbf{p}_{s'})}{k^2}\right]\right.$$
$$-W_eW_s(W_e{}^2-W_{s'}{}^2)+\frac{(\mathbf{k}\cdot\mathbf{p}_e)(\mathbf{k}\cdot\mathbf{p}_s)}{k^2}(W_e{}^2-W_{s'}{}^2)$$
$$\left.+2(\mathbf{p}_\sigma\cdot\mathbf{p}_{s'})\left[1+\frac{(\mathbf{k}\cdot\mathbf{p}_s)(\mathbf{k}\cdot\mathbf{p}_{s'})}{k^2}-W_eW_s\right]\right\},\quad(13)$$

where $W_{s'}$ is related to k, p_s, W_e and θ by

$$W_e{}^2-W_{s'}{}^2=2k(W_s-p_s\cos\theta).$$

Remembering also the conservation of momentum: $\mathbf{p}_{s'}=\mathbf{p}_s+\mathbf{k}$, one sees that in the square bracket k enters either scalarly or through the scalar products with $\mathbf{p}_s$ and $\mathbf{p}_\sigma$. We can thus integrate first over-all directions of $\mathbf{k}$ keeping the angles $\hat{kp}_s$ and $\hat{kp}_\sigma$ fixed. After this integration and the integrations over all directions of $\mathbf{p}_s$ and $\mathbf{p}_\sigma$, and changing finally the last variable of integration from p_σ to W_e in order to compare the present result with the probability for the beta-decay, one finds

$$S(k)=\frac{\alpha G^2}{4\pi^3}\frac{|M|^2}{3}\frac{1}{k}\int_{1+k}^{W_0}dW_e p_\sigma$$
$$\times\{[2(p_\sigma{}^2+p_e{}^2)W_\sigma(W_e{}^2+W_s{}^2)$$
$$-(4/3)p_\sigma{}^2p_e{}^2(W_e+W_s)+4kW_eW_\sigma$$
$$-(4/3)kp_\sigma{}^2(2-W_\sigma W_s)]\ln(W_s+p_s)$$
$$+p_s[-4W_eW_\sigma(p_\sigma{}^2+p_e{}^2)+(8/3)p_\sigma{}^2p_e{}^2$$
$$-4kW_\sigma(W_e{}^2-W_eW_s+W_s{}^2)+(4/3)kW_ep_\sigma{}^2]\}.\quad(14)$$

The last integral is again elementary but the final expression is lengthy. For large W_0 one has the approximate expression,

$$S(k)=\frac{\alpha G^2|\mathbf{M}|^2}{9\pi^4}\frac{1}{k}\left\{\left[\frac{64}{105}x^7-\frac{31}{15}W_0x^6+\frac{11}{4}W_0{}^2x^5\right.\right.$$
$$\left.-\frac{7}{4}W_0{}^3x^4+\frac{1}{2}W_0{}^4x^3\right]\ln 2x$$
$$-\left[\frac{8081}{7350}x^7-\frac{281}{75}W_0x^6+\frac{1189}{240}W_0{}^2x^5\right.$$
$$\left.\left.-\frac{151}{48}W_0{}^3x^4+\frac{11}{12}W_0{}^4x^3\right]\right\}.\quad(15)$$

The total γ-energy emitted is to this approximation

$$I_\gamma=\frac{\alpha G^2|\mathbf{M}|^2}{2\pi^4}\frac{1}{315}W_0{}^8(\ln 2W_0-2.30).\quad(16)$$

The probability of β-emission for this case is

$$P_1(W_e)=\frac{G^2|\mathbf{M}|^2}{2\pi^3}\left[\frac{p_\sigma{}^2+p_e{}^2}{3}-\frac{2}{9}\frac{p_\sigma{}^2p_e{}^2}{W_eW_\sigma}\right]\quad(17)$$

from which it follows, to the same approximation as (16), the β-intensity:

$$I_\beta=(G^2|\mathbf{M}|^2/2\pi^3)(1/420)W_0{}^8.$$

The ratio of γ-intensity to β-intensity is

$$I_\gamma/I_\beta=4\alpha/3\pi(\ln 2W_0-2.30).\quad(18)$$

We see that for large W_0, this ratio is almost exactly the same as the ratio (9) calculated for the allowed β-transition.

The exact factorization of the integrand of (14) into a product of $P(W_e)$ and $\Phi(W_e, k)$ is not possible. But if we assume that k is small, so that $W_e\cong W_s$ and all the terms in the curly bracket involving k can be neglected, we can again write,

$$S(k)=\int_{1+k}^{W_0}dW_eP_1(W_e)\Phi(W_e, k),$$

where $\Phi(W_e, k)$ is precisely the same expression as (11), as obtained for the allowed β-transition. One can even show that for small k the factorization holds for the differential probability with the same $d\Phi$ as given by (12).

C. Second Forbidden, Scalar Theory

The matrix element for this case is

$$(l|H_\beta|0)=-(G/\Omega)A_{s'}{}^*\beta B_\sigma[\tfrac{1}{4}(p_{s'}+p_\sigma)_\alpha(p_{s'}+p_\sigma)_\beta M_{\alpha\beta}],$$

where now M is a symmetrical tensor of the second rank given by

$$M_{ij}=\int d\tau V^*\beta QU r_i r_j.$$

M_{ij} can be separated into two invariant parts,

$$M_{ij}=\tfrac{1}{3}M_{\alpha\alpha}\delta_{ij}+(M_{ij}-\tfrac{1}{3}M_{\alpha\alpha}\delta_{ij}).$$

The first term gives merely a small correction to the allowed transition. Only the second part gives a contribution to the second forbidden transition. We shall denote this spur zero tensor by R_{ij}. The calculation goes as before, and one obtains

$$\begin{aligned}S(k)=&\frac{\alpha G^2}{8\pi^4}\frac{2}{15}|R_{\alpha\beta}|^2\int dW_e p_\sigma\\
&\times\{[W_\sigma(W_e^2+W_s^2)(p_\sigma^2+p_e^2)^2\\
&+(4/3)W_\sigma p_\sigma^2 p_e^2(W_e^2+W_s^2)\\
&-(4/3)p_\sigma^2 p_e^2(p_\sigma^2+p_e^2)(W_e+W_s)\\
&+4kW_eW_\sigma((5/3)p_\sigma^2+p_e^2)\\
&+(4/3)kp_\sigma^2W_eW_s(p_\sigma^2+p_e^2)\\
&-(8/3)kp_\sigma^2(p_\sigma^2+2p_e^2)]\ln(W_s+p_s)\\
&+p_s[-2W_eW_\sigma(p_\sigma^2+p_e^2)^2-(8/3)W_eW_\sigma p_\sigma^2p_e^2\\
&+(8/3)p_\sigma^2p_e^2(p_\sigma^2+p_e^2)\\
&+(4/3)kp_\sigma^2(p_\sigma^2+3p_e^2)W_e\\
&-4kW_\sigma(W_e^2-W_eW_s+W_s^2)((5/3)p_\sigma^2+p_e^2)\\
&-(8/3)k^2W_eW_\sigma-(16/3)k^2p_\sigma^2W_eW_s\\
&+(40/9)k^2p_\sigma^2+4k^2W_\sigma W_s(W_e^2-W_eW_s+W_s^2)\\
&-(4k^2/3)W_eW_\sigma W_s^2+(8/9)k^2p_\sigma^2W_s^2]\}. \quad (19)\end{aligned}$$

Making the same approximation $W_0>1$, and integrating

$$\begin{aligned}S(k)=&\frac{\alpha G^2}{8\pi^4}\frac{2}{15}|R_{\alpha\beta}|^2\frac{1}{k}\left\{\left[\frac{58}{63}x^9-\frac{86}{21}W_0x^8+\frac{488}{63}W_0^2x^7\right.\right.\\
&-\frac{364}{45}W_0^3x^6+\frac{151}{30}W_0^4x^5-\frac{11}{6}W_0^5x^4\\
&\left.+\frac{1}{3}W_0^6x^3\right]\ln 2x-\left[\frac{151553}{79380}x^9-\frac{72661}{8820}W_0x^8\right.\\
&+\frac{33142}{2205}W_0^2x^7-\frac{1138}{75}W_0^3x^6+\frac{16577}{1800}W_0^4x^5\\
&\left.\left.-\frac{239}{72}W_0^5x^4+\frac{11}{18}W_0^6x^3\right]\right\}. \quad (20)\end{aligned}$$

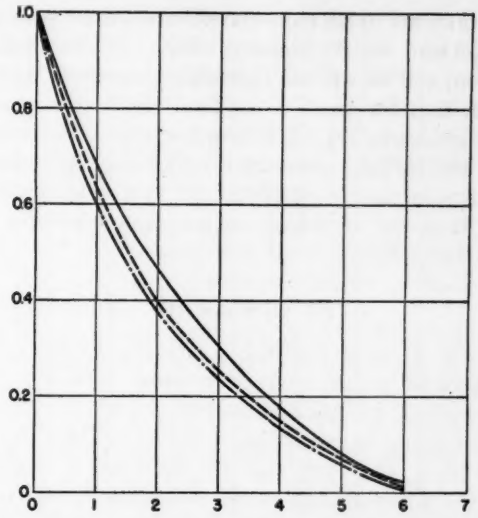

FIG. 2. Energy distribution of the γ-rays following β-transitions of different degree of forbiddenness, scalar theory. $W_0=10$. Ordinate $kS(k)$ normalized to unity for $k=0$, abscissa k measured in relativistic units.

——— Allowed.
– – – – First forbidden.
– – – – – Second forbidden.

The total gamma-intensity is to this approximation

$$I_\gamma=\frac{\alpha G^2|R_{\alpha\beta}|^2}{2\pi^4}\frac{1}{90\cdot 63}W_0{}^{10}(\ln 2W_0-2.35). \quad (21)$$

The corresponding β-emission probability and the total β-intensity are given respectively by

$$\begin{aligned}P_2(W_e)=&\frac{G^2|R_{\alpha\beta}|^2}{2\pi^3}p_eW_ep_\sigma^2\left[\frac{1}{30}(p_e^4+p_\sigma^4)+\frac{1}{9}p_e^2p_\sigma^2\right.\\
&\left.-\frac{2}{45}(p_e^2+p_\sigma^2)\frac{p_e^2p_\sigma^2}{W_eW_\sigma}\right] \quad (22)\end{aligned}$$

and

$$I_\beta=\frac{G^2}{2\pi^3}|R_{\alpha\beta}|^2\cdot\frac{1}{90\cdot 84}W_0{}^{10}. \quad (23)$$

The ratio

$$I_\gamma/I_\beta=4\alpha/3\pi(\ln 2W_0-2.35) \quad (24)$$

is again very nearly the same as (9) and (18).

As in the previous section the factorization of the integrand in Eq. (19) is not possible. By making the same assumption of k small, one gets exactly $P_s(W_e)\Phi(W_e,k)$ with the same function Φ as before.

D. Other Interactions

To investigate the effect of different interactions we have also made the calculations with the tensor interaction. For allowed transitions one gets exactly the same result as in A. The results for first forbidden

transitions are much more complicated, since more than one nuclear matrix element enters in the final expression, and we will not reproduce them here. We have shown, that for small k the final result can again be factorized as in Eq. (3) where the $P(W_e)$ is the complete first forbidden energy distribution containing *all* the nucleon matrix elements and Φ is again given by (11). It seems therefore certain that the same factorization will hold in all other cases.

III. DISCUSSION

In Fig. 1 are plotted the γ intensity $kS(k)$ *vs.* k for the allowed scalar interaction using both the exact expression (5) and the approximate one (5a) for $W_0=10$, corresponding to an upper limit of 5 Mev for the β-spectrum. It is seen that the difference is negligible over the whole energy range. Accordingly, we confine our discussion of the behavior of the γ- and β-intensities, I_γ and I_β, to this simplifying approximation.

To compare the shapes of the γ-intensity curves for the different degrees of forbiddenness we have plotted $kS(k)$ *vs.* k for the scalar interaction: allowed, first, and second forbidden in Fig. 2. The ordinates have been adjusted to coincide for $k=0$. It is clear that one could not hope to distinguish degrees of forbiddenness on account of the almost identical shapes of these curves.

The absolute γ-intensities do increase with successive degrees of forbiddenness. However, a striking feature of our results is that the ratio of total γ-intensity to total β-intensity is essentially independent of the degree of forbiddenness of the β-transition and is given by

$$I_\gamma/I_\beta=4\alpha/3\pi(\ln 2W_0-2.3). \tag{25}$$

This is in spite of the fact that the β-intensities $(W-1)P_L(W)$ vary strongly both in shape and magnitude for these same transitions. ($P_L(W)$ denotes the β-distribution for Lth forbidden transition.)

This behavior is not difficult to explain if one grants the factorization of $S(k)$ as given in Eq. (3) to be valid for forbidden as well as allowed β-transitions. For then the logarithmic energy dependence of $\Phi(W_e, k)$ will smooth out the variations in $P_L(W_e)$, and one can show easily that one will get for the ratio I_γ/I_β for large W_0 the value $(4\alpha/3\pi)\log(2W_0)$ for *all* values of L.

It is important to note that while the assumption of factorizability of $S(k)$ in the above form is sufficient to explain the uniformity of the ratio I_γ/I_β, this assumption has not been made in obtaining the formulae for I_γ/I_β. These were all obtained from the second order perturbation method (and evaluated for W_0 large). However, we have shown in Section II that the factorization is valid provided only that k is small compared to W_0 and W_e. But by inspection of the curves of Fig. 2, one sees that this restriction is *a posteriori* satisfied since most of the radiation intensity occurs at the low energy end of the spectrum and goes rapidly to zero as k approaches W_0. Hence the alternative method of Knipp and Uhlenbeck appears justified whatever the β-interaction, and it is clear why the experiments have been in such good agreement with the allowed theory of KUB.

The fact that the rather complicated calculations with different interactions all lead to the same result (25) suggests a simple underlying physical as well as formal reason. We now show that in the same approximation in which the method of Knipp and Uhlenbeck is valid, the function $\Phi(W_e k)$ may be obtained purely classically thus further corroborating their interpretation as to the independence of the β-decay and γ-emission processes.

We consider the following model for the γ-emission: An electron, having been created during the nuclear transformation, is ejected instantaneously with velocity v at time $t=0$, and since $Z=0$, moves with uniform velocity v ever after. Classically, of course, one cannot account for the creation of the electron or how it got its energy. However, once given this kinematical description of the electron's motion following the nuclear β-decay, one may ask: What is the spectral distribution of the energy radiated by the electron? This is a straightforward problem for classical electromagnetic theory, and we sketch its solution.

Starting with an arbitrary current distribution $\mathbf{J}(\mathbf{r}, t)$ having Fourier transform:

$$\mathbf{J}_\omega(\mathbf{r})=\frac{1}{2\pi}\int_{-\infty}^{\infty} dt\mathbf{J}(\mathbf{r}, t)e^{-i\omega t}$$

the transform of the vector potential in the radiation field will be given (in Gaussian units) by

$$\mathbf{A}_\omega(\mathbf{r})=\frac{e^{-(i\omega/c)r}}{cr}\int d\mathbf{r}'\mathbf{J}_\omega(\mathbf{r}')\exp[-(i\omega/c)\mathbf{n}\cdot\mathbf{r}'],$$

where the integral is taken over the coordinates $\mathbf{r}'$ of the current distribution and r is the distance from the source to the observation point in the wave zone; $\mathbf{n}$ is a unit vector in the direction $\mathbf{r}$.

For the total energy radiated in the angular frequency range $d\omega$ and in solid angle $d\Omega$ in the direction $\mathbf{n}$, one readily obtains

$$dW_\omega(\theta, \varphi)=\frac{\omega^2}{c^3}\left[\mathbf{n}\times\int \mathbf{J}_\omega(\mathbf{r}')\exp[(i\omega/c)\mathbf{n}\cdot\mathbf{r}']d\mathbf{r}'\right]^2 \tag{26}$$

For our case, the current is given by[9]

$$\begin{aligned}\mathbf{J}(\mathbf{r}, t)&=\mathbf{i}_z ev\delta(x)\delta(y)\delta(z-vt) && \text{for } t>0\\ &=0 && \text{for } t\leqslant 0,\end{aligned}$$

where $\mathbf{i}_z$ is a unit vector in the z-direction, taken as the direction of emission of the β-electron, and the δ's are

[9] I. Tamm, J. of Phys. (U.S.S.R.) **1**, 439 (1939).

Dirac δ-functions. Then

$$\mathbf{J}_\omega(\mathbf{r})=\mathbf{i}_z\frac{e}{2\pi}\delta(x)\delta(y)e^{-(i\omega z/v)},\quad z>0$$

Inserting this in the bracket of Eq. (26), one gets a factor $\sin\theta$ from $\mathbf{n}\times\mathbf{i}_z$, and the integral becomes

$$\int d\mathbf{r}'\mathbf{J}_\omega(\mathbf{r}')\exp[(i\omega/c)\mathbf{n}\cdot\mathbf{r}']$$

$$=\mathbf{i}_z\frac{e}{2\pi}\int_0^\infty dze^{-(i\omega/v)(1-\beta\cos\theta)z}$$

$$=\mathbf{i}_z\frac{e}{2\pi}\frac{v}{i\omega(1-\beta\cos\theta)}$$

so that the spectral distribution, differential in angle is

$$dW_\omega(\theta,\varphi)=\frac{e^2v^2}{4\pi^2c^3}\frac{\sin^2\theta}{(1-\beta\cos\theta)^2}d\Omega.$$

Dividing by $\hbar\omega$, we may interpret

$$d\Phi(v,\theta,\omega)\equiv dW_\omega(\theta,\phi)/\hbar\omega$$

as the probability for the electron with velocity v to emit a quantum of energy of frequency ω at an angle θ. Thus

$$d\Phi(v,\theta,\omega)=\frac{e^2v^2}{2\pi\hbar\omega c^3}\frac{\sin^2\theta}{(1-\beta\cos\theta)^2}\sin\theta d\theta$$

$$=\frac{\alpha}{2\pi\omega}\frac{\beta^2\sin^3\theta}{(1-\beta\cos\theta)^2}d\theta \tag{27}$$

where $\alpha=e^2/\hbar c$ and $\beta=v/c$. Integrating over θ, one gets

$$\Phi(v,\omega)=\frac{\alpha}{\pi\omega}\left[\frac{1}{\beta}\ln\frac{1+\beta}{1-\beta}-2\right]. \tag{28}$$

To see that the expressions (27) and (28) are the proper classical analogues of the quantum mechanically derived formulas (11) and (12), we need only remark that if one sets $W_e=W_e$, $P_e=P_e$ in (11) and (12), which is required by the assumption k small, and take into account the relations for a relativistic electron in relativistic units

$$P/W=\beta \quad\text{and}\quad W^2=1/(1-\beta^2)$$

then they become *exactly* the classical formulas (27) and (28) above.

The total energy radiated, gotten by integrating (28) over all frequencies will be infinite. But this is due to having assumed an instantaneous change in velocity from 0 to v. In reality, it will take a finite time τ for the acceleration of the electron to its final velocity v, and then the spectrum will go to zero for $\omega>2\pi/\tau$. This time must be of the order $\hbar/mc^2$ in order to correspond to the observed γ-spectrum and, of course, has nothing to do with the β-lifetime.

We remark finally on the angular distribution of the emitted γ-quanta. From (27) it is seen that for the fast electrons, $\beta\sim1$, almost all the radiation is in the forward direction in which the β-particle was emitted, while for small electron velocities, (27) reduces to a $\sin^2\theta$ distribution, as for a classical dipole. One can therefore expect an angular correlation between the β-rays and γ-quanta.

We should like to express our sincere appreciation to Professor G. E. Uhlenbeck for suggesting this problem and for many stimulating discussions and helpful suggestions concerning it. A major portion of this work was done while one of the authors (D.L.F.) was at the University of Michigan as a recipient of a National Research Council Pre-doctoral Fellowship. The preparation for publication was supported in part by the Joint Program of the ONR and AEC at the University of Notre Dame.

Single Production of Mesons by Gamma-Rays Near Threshold

LESLIE L. FOLDY
Case Institute of Technology, Cleveland, Ohio
(Received March 30, 1949)

The cross section for single charged meson production through absorption of a gamma-ray in a gamma-ray-nucleon collision has been calculated to order e^2g^2 in the charged scalar meson theory (scalar coupling) and charged pseudoscalar meson theory (pseudovector coupling). The nucleon was assumed to be infinitely heavy, thus restricting the validity of the results to gamma-ray energies less than a few times threshold. For a free nucleon the threshold for π-meson production is at 155 Mev in the rest system of the nucleon. Close to threshold, in the scalar theory the cross section varies as the three-halves power of the energy above threshold and the angular distribution is of the form $\sin^2\theta$, while in the pseudoscalar theory the cross section varies as the square root of the energy above threshold and the angular distribution of the mesons is approximately isotropic. At energies 50 percent above threshold, the total cross section is of order 10^{-28} cm^2 in the pseudoscalar theory and of order 10^{-29} cm^2 in the scalar theory.

THE recent completion of the 300-Mev synchrotron at the University of California has now made it possible to produce π-mesons by gamma-rays in the laboratory and thus measure the cross section for single π-meson production by a gamma-ray and the variation of the cross section with energy above threshold. It may therefore be of interest to report briefly on theoretical expectations for these quantities.[1]

The process of greatest interest here is that in which a gamma-ray of sufficient energy collides with a proton (neutron), the gamma-ray disappearing with the production of a single positive (negative) meson, the nucleon becoming a neutron (proton). For a free nucleon the threshold for this process in the system in which the nucleon is at rest is given by

$$E_\gamma=[1+(\mu/2M)]\mu c^2,$$

where μ is the mass of the meson and M is the mass of the nucleon. Using the Berkeley value[2] for the meson mass, $\mu=286m$ where m is the electron mass, the threshold is found to be 155 Mev so that energies nearly twice threshold are available with the 300-Mev synchrotron. We may note that the threshold for meson pair production in the Coulomb field of a free proton lies at 331 Mev, but in the Coulomb field of a heavy nucleus this threshold may be reduced to about 286 Mev. In the range of energies available at present, the production of meson pairs is negligible compared to the production of single mesons, except possibly in target materials of high atomic number.

In the following we calculate the cross section for single meson production by gamma-rays in the charged scalar meson theory (scalar coupling) and the charged pseudoscalar meson theory (pseudovector coupling). Quantum perturbation theory is employed retaining only terms of the lowest non-vanishing order (weak coupling approximation), and the nucleon is treated as infinitely heavy, thus restricting the validity of the results to gamma-ray energies below a few times the threshold energy. With the vector potential of the electromagnetic field and the meson potential expanded in plane waves in a volume V, the perturbation terms in the Hamiltonian are

$$H'=H_e+H_g+H_{eg}$$

with

$$H_e=e\left(\frac{4\pi}{V}\right)^{\frac{1}{2}}\sum_{\mathbf{k},\alpha}\sum_{\mathbf{K}}\sum_{\mathbf{K}'}\frac{[\boldsymbol{\lambda}_{\mathbf{k}}{}^{\alpha}\cdot(\mathbf{K}+\mathbf{K}')]}{(8k\omega_{\mathbf{K}}\omega_{\mathbf{K}'})^{\frac{1}{2}}}\times(A_{\mathbf{k}}{}^{\alpha}+A_{-\mathbf{k}}{}^{\alpha*})(a_{\mathbf{K}'}{}^{*}+b_{-\mathbf{K}'})\times(a_{\mathbf{K}}+b_{-\mathbf{K}}{}^{*})\delta(\mathbf{K}'-\mathbf{K}-\mathbf{k}).$$

In the scalar meson theory,

$$H_g=g\left(\frac{4\pi}{V}\right)^{\frac{1}{2}}\sum_{\mathbf{K}}\frac{1}{(2\omega_{\mathbf{K}})^{\frac{1}{2}}}\left[\left(\frac{\tau_x+i\tau_y}{2}\right)(a_{\mathbf{K}}+b_{-\mathbf{K}}{}^{*})e^{i\mathbf{K}\cdot\mathbf{r}}+\left(\frac{\tau_x-i\tau_y}{2}\right)(a_{\mathbf{K}}{}^{*}+b_{-\mathbf{K}})e^{-i\mathbf{K}\cdot\mathbf{r}}\right],$$

$$H_{eg}=0,$$

while in the pseudoscalar theory,

$$H_g=i\frac{g}{\mu}\left(\frac{4\pi}{V}\right)^{\frac{1}{2}}\sum_{\mathbf{K}}\frac{(\boldsymbol{\sigma}\cdot\mathbf{K})}{(2\omega_{\mathbf{K}})^{\frac{1}{2}}}\times\left[\left(\frac{\tau_x+i\tau_y}{2}\right)(a_{\mathbf{K}}+b_{-\mathbf{K}}{}^{*})e^{i\mathbf{K}\cdot\mathbf{r}}-\left(\frac{\tau_x-i\tau_y}{2}\right)(a_{\mathbf{K}}{}^{*}+b_{-\mathbf{K}})e^{-i\mathbf{K}\cdot\mathbf{r}}\right],$$

[1] Single meson production has been treated in the following papers: W. Heitler, Proc. Roy. Soc. **166**, 529 (1938); M. Kobayashi and T. Okayama, Proc. Phys. Math. Soc. Japan **21**, 1 (1939); H. S. W. Massey and H. C. Corben, Proc. Camb. Soc. **35**, 84 (1939) and **35**, 463 (1939); L. Nordheim and G. Nordheim, Phys. Rev. **54**, 254 (1938).

[2] A. S. Bishop, Phys. Rev. **75**, 1468 (1949).

$$H_{eg}=i\frac{eg}{\mu}\left(\frac{4\pi}{V}\right)\sum_{\mathbf{k},\alpha}\sum_{\mathbf{K}}\frac{(\boldsymbol{\sigma}\cdot\boldsymbol{\lambda}_{\mathbf{k}}{}^{\alpha})}{(4k\omega_{\mathbf{K}})^{\frac{1}{2}}}$$
$$\times\left[\left(\frac{\tau_x+i\tau_y}{2}\right)(A_{\mathbf{k}}{}^{\alpha}+A_{-\mathbf{k}}{}^{\alpha*})(a_{\mathbf{K}}+b_{-\mathbf{K}}{}^{*})e^{i(\mathbf{K}+\mathbf{k})\cdot\mathbf{r}}\right.$$
$$\left.-\left(\frac{\tau_x-i\tau_y}{2}\right)(A_{\mathbf{k}}{}^{\alpha*}+A_{-\mathbf{k}}{}^{\alpha})(a_{\mathbf{K}}{}^{*}+b_{-\mathbf{K}})e^{-i(\mathbf{K}+\mathbf{k})\cdot\mathbf{r}}\right].$$

In the above, g is the coupling constant of the meson field to the nucleon, $a_{\mathbf{K}}{}^{*}$, $a_{\mathbf{K}}$, $b_{\mathbf{K}}{}^{*}$, $b_{\mathbf{K}}$ are creation and destruction operators for positive and negative mesons of momentum $\mathbf{K}$, $A_{\mathbf{k}}{}^{\alpha*}$, $A_{\mathbf{k}}{}^{\alpha}$ are creation and destruction operators for photons of momentum $\mathbf{k}$, $\lambda_{\mathbf{k}}{}^{\alpha}$ ($\alpha=1, 2$) are unit polarization vectors of the photons, $\mathbf{r}$, $\boldsymbol{\sigma}$, $\boldsymbol{\tau}$ are the position, spin, and isotopic spin operators for the nucleon, and $\omega_{\mathbf{K}}=(\mu^2+K^2)^{\frac{1}{2}}$ with μ the mass of the meson. Units have been used in which $\hbar$ and c are unity.

The term H_{eg} in the pseudoscalar case is necessitated by considerations of gauge invariance and is present in any charged meson theory with gradient coupling. In spite of the fact that it leads to the dominant contribution to the cross section, it has been overlooked in some past calculations.

From the above expressions one may readily calculate the transition matrix element from a state in which there is a photon of momentum $\mathbf{k}$ and a nucleon in the spin state u_0 to a final state in which there is a meson of momentum $\mathbf{K}$ and the nucleon is in the spin state u. In the scalar theory the transition can only take place through an intermediate state, while in the pseudoscalar theory, because of the term H_{eg} in the perturbation, a direct transition is also possible. The results for the transition matrix element in the scalar and pseudoscalar theories, respectively, are

$$H_s{}'=-\frac{4\pi egV^{-1}}{(k\omega_{\mathbf{K}})^{\frac{1}{2}}\omega_{\mathbf{K}-\mathbf{k}}{}^{2}}(u^{*}|1|u_0),$$

$$H_{ps}{}'=-\frac{4\pi iegV^{-1}}{2\mu(k\omega_{\mathbf{K}})^{\frac{1}{2}}}\left[(u^{*}|\boldsymbol{\sigma}\cdot\boldsymbol{\lambda}_{\mathbf{k}}{}^{\alpha}|u_0)\right.$$
$$\left.-\frac{2(\boldsymbol{\lambda}_{\mathbf{k}}{}^{\alpha}\cdot\mathbf{K})(u^{*}|\boldsymbol{\sigma}\cdot(\mathbf{K}-\mathbf{k})|u_0)}{\omega_{\mathbf{K}-\mathbf{k}}{}^{2}}\right].$$

Squaring, summing over final spin states and averaging over initial spin states for the nucleon, and averaging over the direction of polarization of the gamma-ray, one obtains

$$\sum\langle|H_s{}'|^{2}\rangle_{Av}=\frac{8\pi^2e^2g^2V^{-2}K^2\sin^2\theta}{k\omega_{\mathbf{K}}\omega_{\mathbf{K}-\mathbf{k}}{}^{4}},$$

$$\sum\langle|H_{ps}{}'|^{2}\rangle_{Av}=\frac{4\pi^2e^2g^2V^{-2}}{\mu^2k\omega_{\mathbf{K}}}\left[1-\frac{2\mu^2K^2\sin^2\theta}{\omega_{\mathbf{K}-\mathbf{k}}{}^{4}}\right],$$

with θ the angle between the direction of emission of the meson and the direction of the incident gamma-ray.

From conservation of energy, one has $K=(k^2-\mu^2)^{\frac{1}{2}}$. The differential cross section for the process is then given by

$$d\sigma=2\pi\sum\langle|H'|^{2}\rangle_{Av}\frac{V^2K\omega_{\mathbf{K}}d\Omega_{\mathbf{K}}}{8\pi^3},$$

and substituting the above results, we obtain

$$d\sigma_s=\frac{2e^2g^2}{(\mu c^2)^2}\left(\frac{k^2-\mu^2}{\mu^2}\right)^{\frac{1}{2}}\left(\frac{\mu^5}{k\omega_{\mathbf{K}-\mathbf{k}}{}^{4}}\right)\sin^2\theta d\Omega_{\mathbf{K}},$$

$$d\sigma_{ps}=\frac{2e^2g^2}{(\mu c^2)^2}\left[\frac{1}{2}\left(\frac{k^2-\mu^2}{\mu^2}\right)^{\frac{1}{2}}\frac{\mu}{k}\right.$$
$$\left.-\left(\frac{k^2-\mu^2}{\mu^2}\right)^{\frac{1}{2}}\left(\frac{\mu^5}{k\omega_{\mathbf{K}-\mathbf{k}}{}^{4}}\right)\sin^2\theta\right]d\Omega_{\mathbf{K}}.$$

Integrating over all directions of emission for the meson we obtain, for the total cross sections,

$$\sigma_s=\frac{2\pi e^2g^2}{(\mu c^2)^2}\left(\frac{k^2-\mu^2}{\mu^2}\right)^{\frac{1}{2}}\frac{\mu}{k}$$
$$\times\left\{\frac{\mu^4}{k(k^2-\mu^2)^{\frac{1}{2}}}\ln\frac{k+(k^2-\mu^2)^{\frac{1}{2}}}{k-(k^2-\mu^2)^{\frac{1}{2}}}-\frac{2\mu^4}{k^2(k^2-\mu^2)}\right\},$$

$$\sigma_{ps}=\frac{4\pi e^2g^2}{(\mu c^2)^2}\left(\frac{k^2-\mu^2}{\mu^2}\right)^{\frac{1}{2}}\frac{\mu}{k}-\sigma_s.$$

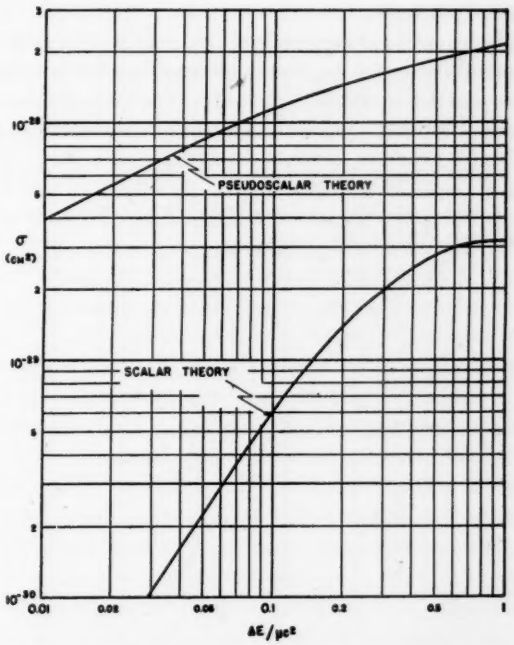

FIG. 1. Total cross section for single charged meson production by gamma-rays on nucleons as a function of the energy ΔE above threshold. Values assumed for the constants are: $g^2/\hbar c=\frac{1}{8}$, $\mu=286$ electron masses.

Here k now represents the energy of the gamma-ray divided by c^2.

We note that in the scalar theory the angular distribution of the mesons produced close to threshold has the form $\sin^2\theta$, and that the cross section increases as $(\Delta E)^{\frac{1}{2}}$ where $\Delta E=(k-\mu)c^2$ is the energy above threshold of the gamma-ray. In the pseudoscalar theory, on the other hand, the dominant term gives an isotropic angular distribution close to threshold and a cross section increasing as $(\Delta E)^{\frac{1}{2}}$. This latter behavior is a consequence of the term H_{eq} in the pseudoscalar Hamiltonian. It has been pointed out to the author[3] that if the anomalous magnetic moments of the proton and neutron are described by Pauli terms in the Hamiltonian, then this latter behavior will occur with any meson theory. In view of the great present difficulties of meson theory, we do not wish to imply much faith in the details of the present calculations beyond their usefulness for orientation purposes; however, if the anomalous moments of the neutron and proton are due to the interaction of these particles with the meson field, as is commonly assumed, then it is reasonable to expect that these two features of our result in the pseudoscalar theory, the isotropic angular distribution, and the $(\Delta E)^{\frac{1}{2}}$ variation of the cross section close to threshold, will be verified by experiment. In passing, we may also note the remarkable similarity between the results for the pseudoscalar theory and the results obtained for the cross section for photodisintegration of the deuteron.[4] In fact, our calculation may be considered as that of the photo-disintegration of the proton into a neutron and positive meson and of the neutron into proton and negative meson in a generalized sense.

The numerical magnitude of the cross sections may be in error both due to the inadequacies of the present theory and because of a lack of a reliable value for the meson coupling constant. The order of magnitude is probably reliable, however, and if we assume $g^2/\hbar c=\frac{1}{6}$, we obtain the values plotted in Fig. 1. Results for other meson theories may be expected to be comparable. It need hardly be pointed out that an accurate determination of the cross section at some known energy will yield a value for the coupling constant g which is likely to be more accurate than any estimated value from the meson theory of nuclear forces. In particular, the cross section of hydrogen would be of especial value.

From the above formulas one may readily calculate capture cross sections of nucleons for mesons with gamma-ray emission, but since this question is treated in detail in another paper[5] it will not be discussed here.

This work was supported in part by the Atomic Energy Commission.

Note added in proof: Since the submission of the present paper for publication, another paper[6] on this same subject has come to the author's attention. While it has not yet been possible for the author to see this paper, the results as quoted in another publication[7] appear to be in substantial agreement with the results published here.

Recently the production of π-mesons by 335 Mev gamma-rays has been announced by the group working with the synchrotron at Berkeley.[8] The target is essentially glass (nuclear plates) in one case and carbon in another and a cross section of approximately 3×10^{-30} cm^2 per nucleon was obtained though this result is admittedly very rough. Since only mesons with energies less than 20 Mev could be counted, the cross section may be considerably larger and the effect of binding of the nucleons into nuclei also makes any comparison with the cross section calculated in this paper unwarranted. It was also observed in this experiment that many more negative than positive mesons were produced (or at least detected in the emulsions). If this result is correct it would be extremely improbable that it could be reconciled with the theory we have presented which would predict at best only small differences in production probability between positive and negative mesons on the basis of the effect of the Coulomb field of the nucleons.

[3] Private communication from R. E. Marshak; see also reference 5.

[4] H. Bethe, *Elementary Nuclear Theory* (John Wiley & Sons, Inc., New York, 1947), p. 56.

[5] R. E. Marshak and A. S. Wightman, Phys. Rev. **76**, 114 (1949).

[6] J. Hamilton and H. W. Peng, Proc. Roy. Ir. Ac. **49A**, 197 (1944); see also C. Morette and H. W. Peng, Nature **160**, 59 (1947).

[7] W. Heitler, Rev. Mod. Phys. **21**, 113 (1949).

[8] E. M. McMillan and J. M. Peterson, Science **109**, 438 (1949).

The Fogging of Photographic Film by Radioactive Contaminants in Cardboard Packaging Materials

J. H. WEBB
Kodak Research Laboratories, Rochester, New York*
(Received April 18, 1949)

Following the detonation of the experimental atom bomb at Alamogordo, New Mexico, on July 16, 1945, a radioactive contaminant was encountered in strawboard material used by the Eastman Kodak Company for packaging photographic sensitive films. This paper board was manufactured in a mill situated at Vincennes, Indiana, on the Wabash River. A run of strawboard, produced on August 6, 1945, showed this new and unusual type of radioactive contaminant. X-ray film packed with this board showed fogged spots after about two weeks' exposure.

Measurements of the contaminated spots of strawboard showed no alpha-activity but fairly strong beta-activity. Absence of alpha-activity ruled out naturally radioactive materials. Measurements of the beta-activity showed a maximum energy of about 0.6 Mev. and a half-life of approximately 30 days. Radiochemical studies of the active ash from the strawboard indicated that the material was of the rare earth series. The energy value and half-life of the beta-radiation are compatible with the isotope, Ce 141.

All studies point to the conclusion that the radioactive contaminant was an artificially radioactive material which found its way into the mill through the river water. The most likely explanation seems to be that it was a wind-borne fission product derived from the atom-bomb detonation in New Mexico on July 16, 1945.

EXPERIMENTAL evidence is given in the present paper to show that radioactive fission products resulting from the detonation of the first atomic bomb in July, 1945, in the state of New Mexico, were detected by photographic means on paper stock derived from raw products and manufactured in a paper mill at a location approximately 1000 miles from the point of detonation. The experimental observations on this problem were carried out between September and December, 1945, and to the author's knowledge represent the only case of detection of fission products at a ground station so remote from the point of detonation. The magnitudes of the radioactive effects observed were exceedingly minute and were detected at all only because of unusual circumstances that resulted in very great sensitivity. In fact, the main reason for presenting the data at this time arises from the thought that the results obtained, and the experimental procedure used, might be of interest to other physicists who are concerned with detection of minute quantities of radioactive materials.

This work had its origin in a new and unusual type of radioactive contamination encountered in August, 1945, in cardboard material used by the Eastman Kodak Company for packaging sensitive photographic materials. Before discussing the principal subject of this paper, it will perhaps be of interest to present first certain background information on prior experience of the Eastman Kodak Company with radioactive contaminants, which will serve to introduce the main results to follow.

Preceding the time of appearance of the above-mentioned contaminants and during the war, a great deal of the cardboard in this country became contaminated with radioactive materials as a result of the paper salvage program. Paper and cardboard, salvaged from war plants where radium instrument dials were prepared, became mixed with general paper stocks and as a result, specks of radioactive material could be found sporadically distributed in almost any type of packaging paper. Although the amount of material of this sort was very small, nevertheless it was sufficient to cause fogged spots on film left in intimate contact with it for a period of several weeks. Radioactive contaminants of this type were discovered immediately upon their appearance and the source and nature of these contaminants recognized. Alpha-count measurements of radon emanation from such contaminants identified them with radium paint originating from the greatly expanded radium-dial production of the war period. As a result of this trouble with radium contaminants, it was essential in the photographic industry to obtain a new and uncontaminated source of material for packaging sensitive goods. The Eastman Kodak Company found it necessary to select a mill and to control carefully the raw materials when its orders were produced. One of the mills selected for this purpose was located at Vincennes, Indiana, which is situated in southern Indiana on the Wabash River. Strawboard from this mill was used by the Eastman Kodak Company as interleaving stiffener board between sheets of film. Strawboard procured in this way was completely satisfactory for a period extending over many months. However, a run of strawboard produced on August 6, 1945, showed a new type of radioactive contaminant not hitherto encountered.

Effects of this new type of radioactive contaminant were first observed on film which had been packed in contact with the stiffener strawboard. When a piece of double-coated x-ray film, which had been in contact with a piece of the strawboard for a period of three weeks, was developed, the film showed many small exposed areas. These exposed areas ranged in number from ten to several hundred on a piece of film 14 by 17 inches in size. The exposed areas were of the order of 1-millimeter diameter and were quite dark when developed. In many cases, the radiation had passed

* Communication No. 1253.

TABLE I.

Date	Counter	Description of sample	Beta-count	Time	Beta-count hour
		Vincennes strawboard (August 6 run)			
Oct. 11	(*A*)	200 Bad Spots	310	30 min.	620
		200 Bad Spots	233	30 min.	466
		Background	223	30 min.	446
Oct. 20	(*B*1)	350 Bad Spots	160	1 min.	9600
		Background	80	1 min.	4800
Oct. 24	(*A*)	300 Bad Spots	450	30 min.	900
		300 Good Spots	294	30 min.	588
		Background	238	30 min.	476
Oct. 29	(*A*)	600 Bad Spots	580	30 min.	1160
		600 Good Spots	280	30 min.	560
		Background	260	30 min.	520
Nov. 6	(*A*)	600 Bad Spots		1 hr.	1205
		600 Good Spots		1 hr.	760
		Background		1 hr.	700
		Tama strawboard (September run)			
Nov. 6	(*A*)	500 Bad Spots		1 hr.	1224
		600 Good Spots		1 hr.	760
		Background		1 hr.	604

TABLE II. Calibration of Bad-Spot Samples with Uranium Acetate Samples.

Date	Description of sample	Gross weight	Beta-activity (*A*)	Beta-activity (*B*1)
Oct. 30	400μ g U acetate+silica	0.274 g	1062/hr.	157/min.
	300 Bad Spots (Vincennes)	0.274 g	1014/hr.	154/min.
	Background		488/hr.	86/min.

through several layers of film and cardboard, indicating a penetrating radiation.

The usual type of tests that had been used previously to analyze radioactive contaminants showed conclusively that the new radioactive contaminant was not radium; it was therefore necessary to devise new methods of analysis for it. In order to obtain sufficient concentration of the radioactive contaminants for direct study by physical instruments, it was necessary to concentrate the active material from the strawboard. To accomplish this, a technique was adopted of punching out small circular areas of the strawboard which lay directly behind the exposed areas on the film. By cutting out hundreds of these spots from the strawboard, samples were obtained having a much higher concentration of the radioactive contaminants. These batches of strawboard spots were then ashed by heating in a porcelain crucible at a temperature of 900°C to reduce further the bulk of material to be dealt with. Using material prepared in this manner, measurements of beta-activity and alpha-activity were carried out. All samples of ashed strawboard corresponding to the exposed spots on the film showed a fairly strong beta-activity, easily measurable above the background, while samples of ashed strawboard not corresponding to spots on the film showed practically no beta-activity. Samples of ashed materials measured for alpha-activity gave no detectable effect above the background. These results strongly indicated that the new type of radioactive contaminant encountered was not one of the naturally radioactive elements—uranium, thorium, or actinium—since all of these elements emit alpha-rays in addition to the beta-rays. One other possible source of the radiation considered was potassium, which is a naturally radioactive element giving only beta-rays. However, potassium was ruled out on the basis that the large amounts of this material required to produce the observed beta-activity could be detected readily by chemical analysis. In order to rule out the possibility that alpha-radiation due to naturally radioactive elements was present but below the measurable limit, a synthetic sample of uranium acetate in inert powder was made up to match in total weight and beta-activity a sample of the contaminated ashed strawboard, and measured for alpha-activity. This synthetic sample gave easily measurable alpha-activity.

Measurements of the penetrating power of the beta-rays showed that about 0.2 g/cm^2 of aluminum was required to stop the highest energy beta-particles. The half-life period of decay of the contaminant was measured photographically between October and December, 1945, and was found to be of the order of 30 days though the decay curve was not truly exponential. Strawboard made in August, 1945, at Vincennes, Indiana, that had shown strong activity initially had dropped to a point of considerably less activity photographically by January, 1946. However, exposure of film to this strawboard for two months still gave strong effects at this time.

In September, 1945, production of similar strawboard was commenced at a mill in Tama, Iowa, located on the Iowa River. Strawboard made at this mill also was found to exhibit the same type of radioactive contaminant as that found in the strawboard manufactured at Vincennes, Indiana. This mill is situated several hundred miles away from the Indiana mill and derives its water from a different watershed.

EXPERIMENTAL RESULTS

Beta- and Alpha-Activity

The experimental results obtained during the study of this problem are presented in the Tables I to VI. The samples of strawboard spots used for the activity measurements are designated, respectively, as "bad spots" and "good spots." A bad spot consists of a $\frac{3}{16}$-inch diameter area punched out of the strawboard at a point directly behind a fogged spot on an adjacent piece of film. A good spot corresponds to a similar circular area punched out of the strawboard at a point *between* fogged spots on the film. In all cases, the spots of strawboard were ashed before measurements of activity were carried out.

The measurements of beta-activity were made with two different Geiger counter tubes. The first tube (*A*) was small in volume and had low sensitivity, as indicated by the low background count of about 8–10 counts per minute. This tube and its associated scale-of-2 circuit were far from elegant, but gave fairly consistent readings. The second tube (*B*) was a large volume tube, highly sensitive, and when unshielded gave a background count of about 80 counts per minute. When this tube was shielded with lead, its background count dropped to about 30 counts per minute. When unshielded, it is referred to as (*B*1), and when shielded, as (*B*2). The tube *B*, with its associated scaling circuit, was kindly placed at the writer's disposal by Dr. William Bale, of the University of Rochester Medical School, and measurements were made on these instruments with the co-operation of Dr. Bale, who was consulted frequently on this problem.

The alpha-counts on the samples were made on an air chamber alpha-counter which was also furnished by Dr. Bale. This alpha-counter was connected to a scaling circuit for recording counts, but the counts were also observed visually on the screen of a cathode-ray oscillograph in all cases to make sure there was one-to-one correspondence between alpha-counts and registered pulses.

Table I shows beta-counts made on a number of different samples of ashed spots selected from different samples of the contaminated strawboard. The first five samples were from strawboard manufactured at Vincennes, Indiana, and the sixth sample was from strawboard made at Tama, Iowa. It may be seen that measurements showed slightly higher than background activity for good spots, and an activity of about double background for the bad-spot samples. Also, it should be noted that the beta-activity of the Tama strawboard was about the same as that of the Vincennes strawboard.

Table II shows the results of calibration measurements of beta-activity of Vincennes strawboard spots against beta-activity of uranium acetate dispersed in silica powder. In order to determine the approximate amount of uranium acetate necessary to give the same beta-activity as a sample of 300 bad spots of strawboard, trial and error mixtures of uranium acetate with inert silica powder were made up and tested until a sample was obtained having the same gross weight and beta-activity as the sample of ashed spots. As may be seen, a mixture of silica powder and uranium acetate was obtained whose weight (0.274 gram) and beta-activity were closely the same as those of the comparison sample of ashed strawboard spots, this comparison sample of known radioactivity having about the same self-absorption characteristics as that of the ashed strawboard spots. This was necessary for alpha-particle measurements where it was feared that self-absorption might cut down the alpha-particle emission strongly.

TABLE III. Photographic alpha-count.

Date	Description of sample	Relative count	Relative no. of alpha-tracks
Oct. 29	0.2 g U acetate+silica	1	16.1
	0.2 g Bad-Spot Ash	1	2.3
	0.2 g Good-Spot Ash	—	1

TABLE IV.

		Alpha-Activity (Vincennes)		
Date	Description of sample	Gross weight	Beta-count *B*-1	Alpha-count
Oct. 30	400μ g U acetate+silica	0.274 g	157/min.	14.3/min.
	300 Bad Spots	0.274 g	154/min.	1.6
	Background	—	86/min.	2.3
		Alpha-Activity (Tama)		
Date	Description of sample	Gross weight	Beta-count *B*-2	Alpha-count
Nov. 26	400μ g U acetate+0.8 g Inert Strawboard Ash	~1 g	84.5/min.	4.6/min.
	500 Bad Spots	~1 g	87.1/min.	1.5
	Background	—	30.5	1.3

TABLE V. Activity of Vincennes and Tama strawboards.

Date	Description of sample	Gross weight	Beta-count (*B*-2)	Alpha-count
Nov. 7	400μ g U acetate+silica	0.274 g	385/5 min.	60/5 min.
	Tama Bad Spots	0.1747	237	3
	Vincennes Bad Spots	0.1747	183	6
	Background	—	128	4

With samples of the same weight and beta-activity, it was felt that alpha-measurements from the two samples would give strictly comparable values of emission of alpha-particles from the two types of materials.

Tables III, IV, and V give data on the measurements of alpha-activity from the ashed strawboard spots. Table III shows results obtained by a photographic method carried out by Dr. W. West of these Laboratories. Dr. West made up equal weight samples of uranium acetate and silica powder, bad-spot ash, and good-spot ash. Here again the sample of uranium and the sample of bad-spot ash were adjusted to equal beta-activity. For measurement of alpha-activity, these samples were placed in contact with one of the Eastman nuclear-track plates and left for a sufficient time to give a measurable number of alpha-tracks from the uranium sample. Tracks per unit area obtained from the three comparison samples were counted and the relative numbers are shown in Table III. It may be seen that the alpha-activity of the uranium sample (of equal beta-activity) was seven times as strong as that of the bad-spot sample. While the alpha-activity of the bad-spot sample is about twice that of the good-spot sample, the statistical error here was such that this value has only slight significance and the only conclusion to be drawn

TABLE VI. Beta-count of residue from gallon batches of Wabash River water.

Date	Description of sample	Time of count	Beta-count (A)
Nov. 2	(1) Residue	10 min.	12.1/min.
	Background	10 min.	11.4/min.
Nov. 2	(2) Residue	30 min.	12.1
	Background	30 min.	11.0
	(3) Ashed Residue	30 min.	11.6
	Background	30 min.	11.2

is that the two samples had approximately equal activity.

Table IV gives the beta- and alpha-counts made with electrical pulse counters on Vincennes and Tama bad spots *versus* the synthetic uranium acetate samples. In the first part of Table IV, the beta- and alpha-counts of a uranium-plus-silica sample are compared with the counts from the ash of 300 bad spots of Vincennes strawboard of the same weight. In the second part of Table IV, the beta- and alpha-counts of a uranium acetate plus inert strawboard ash are compared with the counts from the ash of 500 bad spots of Tama strawboard. In both cases, it is seen that, whereas the beta-activities of the synthetic and bad-spot samples are closely equal, the alpha-particle count for the synthetic samples of uranium acetate are much higher, being well above the limit of experimental error. In fact, the alpha-count from bad-spot ash was in no case found to be measurably above background. These results are considered to be strong evidence for the fact that the radioactive contaminant in the strawboard was not one of the naturally radioactive elements, such as Ra, Th, or Ac, all of which are alpha-emitters.

Table V shows beta- and alpha-counts made for different samples of Tama and Vincennes bad-spot ash compared with similar counts for the uranium acetate-plus-silica samples. While the gross weights of these samples are not equal, nevertheless, qualitatively it may be seen that the alpha-activity of the bad-spot ash is not significantly above the background, whereas the alpha-activity of the uranium sample of comparable beta-activity is well measurable above the background.

Table VI gives results of beta-activity on samples of residue from one-gallon batches of Wabash River water and it may be seen that the counts here are not significantly above the background, though in every case the residue count was slightly higher than background. It is felt that this method of testing the water was too insensitive for picking up the radioactive material. On the other hand, when the river water was filtered through the strawboard during manufacture, material particles to which the active material was adsorbed, were filtered out, thereby giving active specks in the strawboard which could and did exert a photographic effect on film held in contact with the speck for several weeks. This constituted a very sensitive method for detecting active specks of material. Photographic registration of the specks made it possible to punch out active spots of cardboard and thereby effect a further multifold concentration of the material for study by electrical means.

Energy of Beta-Radiation

Measurement of the penetrating power of the beta-radiation was carried out by the method of aluminum absorption and Geiger-counter registration. In Fig. 1 are shown measurements made on a sample of ash from 600 bad spots of the Vincennes strawboard. The activity of the contaminant had died down to some extent by the time these measurements were made, which accounts for the low readings. The values plotted in Fig. 1 are beta-counts per ten minutes above the cosmic-ray

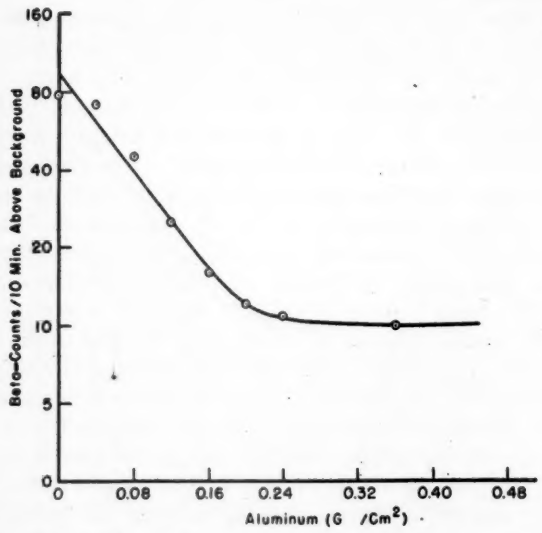

FIG. 1. Absorption measurements on beta-radiation by aluminum absorption and Geiger tube measurements for 600 bad spots of Vincennes strawboard.

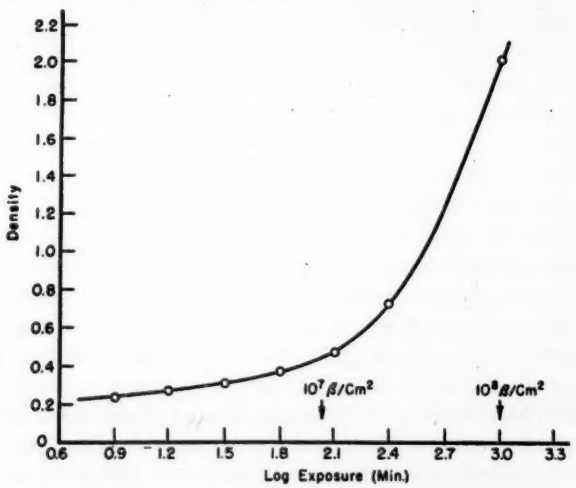

FIG. 2. Calibration characteristic curve for x-ray film exposed to beta-rays of uranium.

background. The abscissa values are given in terms of grams per square centimeter of aluminum. From these measurements it was apparent that there was a low gamma-ray background from the contaminant that was not stopped by a considerable thickness of aluminum. It may be seen that the toe of the curve, corresponding to the highest-energy beta-particles, falls at approximately 0.2 gram per square centimeter. This gives a maximum energy value of the beta-radiation of about 0.6 Mev.

Half-Life of Beta-Activity

The half-life of the beta-activity was measured by photographic methods. In brief, the method consisted in selecting a large piece of cardboard containing several strongly active specks of the contaminant, and exposing a piece of x-ray film to these specks for successive two-week periods over a total time of about two months. Photographic densities produced by these successive exposures showed a steady decline. By comparing the successive densities obtained in a characteristic exposure curve, such as that shown in Fig. 2, for beta-particle exposure, it was possible to read from the abscissa values the declining intensity values of the exposing radiations with time. These intensity values, plotted as a function of time, are shown by the experimental points in Fig. 3. A smooth curve drawn through these points shows an average half-life decay period of approximately thirty days.

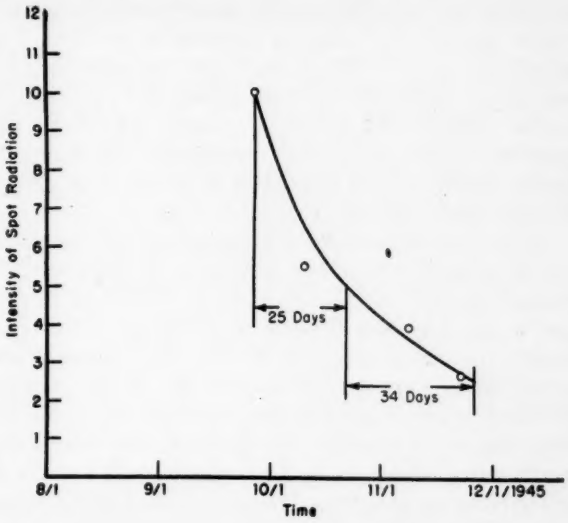

FIG. 3. Decay curve of beta-radiation from radioactive contaminant in strawboard (Vincennes, August 6, run).

DISCUSSION OF RESULTS

The experimental results obtained seem to show definitely that the radioactive contaminant encountered gives beta- and some gamma-radiation but no alpha-activity, indicating an artificially radioactive material. The large amount of material that must have been involved to show up over a period of several months in the water supply for the strawboard mill would seem to rule out the possibility that the material came from a moderate source of radioactive materials, such as a cyclotron. A check on possible sources of contamination of the river water from such nuclear laboratory by-products disclosed no such means of contamination. It was established that the contaminant was not carried by the straw going into the strawboard, since a run of strawboard made using straw that had not been in the field, but stored in warehouses for a considerable time prior to the trouble, showed the radioactive contaminant. Further evidence that the active material came from the river water was indicated by the fact that following each heavy precipitation in this locality, stronger activity occurred in the strawboard. This was attributed to the material being washed into the river water during heavy precipitation periods.

The most likely explanation of the source of this radioactive contaminant appears to be that it consisted of wind-borne radioactive fission products derived from the atom-bomb detonation in New Mexico on July 16, 1945. The evidence that the material was an artificially radioactive isotope, the occurrence of the same unusual type of contaminant in strawboard manufactured in two widely separated areas (Vincennes, Indiana, and Tama, Iowa) at the same time, and the timing of the appearance of this material immediately following the bomb detonation, are thought to lend strong support to the above tentative explanation. It is readily conceivable that radioactive atoms projected into the stratosphere, and carried by winds, could collect on dust particles and be brought down by precipitation and be washed into streams. It is well known that dust projected into the stratosphere from volcanic explosions has been scattered over wide areas in this way. The radioactive contaminants could have found their way into the products of the strawboard mills either by settling on the straw in the fields or through the river water used by the mills in the manufacture of the strawboard. Of these two possibilities, the latter seems to be much the more likely, since strawboard made from straw that was not in the field at the time of the explosion but stored indoors showed the contamination.

The measurements of the energy and half-life of the beta-particle radiation of the radioactive contaminant in the strawboard were found to be 0.6 Mev and thirty days, respectively. These values correspond closely to those for the radioactive isotope, Ce 141, which is one of the more prolific fission products of the atom bomb.

A simple calculation shows that if 50 grams of Ce 141 were formed in an atomic explosion, there would be approximately 2.2×10^{23} atoms. Since the area of the United States is about 7.5×10^{18} sq. mm, there would be about 0.3×10^{5} atoms for every square millimeter. Allowing for some local concentrations of these atoms such as that occurring under the circumstances sur-

rounding the manufacture of strawboard from river water, this number could be increased severalfold. The sensitivity of x-ray film is such that 10^5 beta-particles per square millimeter is just sufficient to produce a visible density. Therefore, it would appear readily possible from a theoretical standpoint for short-life fission products from the bomb to produce the photographic effects described above.

After carrying out the physical study just described of the radiations from the radioactive contaminants, a limited amount of radiochemical analysis was carried out to see if it were possible to follow by tracer techniques the chemical nature of the contaminant. These experiments were carried out by Mr. A. E. Ballard, of these laboratories. Enough work was done to show that the active material was probably one of the rare earth series. However, because of the small amount of material in the sample and because of the limited equipment available for such experiments at the time, a complete analytical determination of the radioactive isotope was not possible.

It is realized by the author that the measurements carried out in the study are not so complete nor so accurate as might be desired. However, the work was carried out hurriedly, and somewhat blindly at first, when it was important to get quick survey measurements. By the time sufficient knowledge was gained to make it possible to conduct the experiments more intelligently, the activity had died down to a considerable extent. In spite of this fact, however, it is thought that the results obtained are sufficiently good and of enough general interest to physicists to warrant their publication.

In conclusion, it is to be emphasized that the amounts of material considered throughout the discussion are exceedingly small and were observed only because of an accidental set of circumstances that proved particularly favorable for the detection of the contaminating substances. The river water carrying the substances was derived from a large area and specks of dust were filtered out of this water onto strawboard during passage of large quantities of water through the strawboard pulp. Photographic film placed in contact with this board for a period of weeks registered the radiation from the concentrated specks of the contaminant. The specific location of the radioactive specks through photographic registration made it possible to obtain large numbers of strawboard spots containing active specks and thereby to increase the concentration further. By ashing down these strawboard spots, the active material was concentrated sufficiently to make direct study possible.

ACKNOWLEDGMENT

The author desires to express his appreciation to Mr. A. E. Ballard, of these laboratories, who participated in some of the experimental work outlined and was frequently consulted on this problem throughout the course of the work. In particular, the analytical radiochemistry experiments were carried out by Mr. Ballard and the preparation of all ashed samples were made under his direction.

It is a pleasure to thank Dr. William Bale, of the University of Rochester, for the kind loan of beta- and alpha-counting equipment during this study and for his generous advice on different aspects of this work.

The photographic alpha-particle counts presented in Table II were carried out by Dr. West, of these Laboratories, and the author wishes to record his thanks to Dr. West for the use of these data.

Finally, the author would like to express appreciation to Mr. Harold Crouch and his co-workers, in the Department of Manufacturing Experiments, at Kodak Park, for the large amount of work contributed on this problem. All contaminated strawboard used in the experiments was selected on the basis of the photographic tests made by this group, who also supplied all of the punchings of the strawboard spots.

Diode Space Charge for Any Initial Velocity and Current

LEIGH PAGE AND NORMAN I. ADAMS, JR.
Sloane Physics Laboratory, Yale University, New Haven, Connecticut
(Received April 4, 1949)

The space charge equation is solved for any initial velocity which is the same for all electrons and for any realizable current, for (a) the plane diode, (b) the cylindrical diode. For the plane diode it is shown that all cases can be obtained from a single pair of master curves. For the cylindrical diode a series valid for large distances from the axis is obtained first, the form of which shows that the complete group of solutions form a bounded set. Next three solutions valid for small distances from the axis are obtained by means of which the first set of solutions can be extended. In addition to master curves representing these solutions, curves are plotted for special values of the initial velocity and current.

IN a recent paper[1] the authors presented a new solution of the space charge equation for the cylindrical diode which converges better the larger the ratio of the distance r from the axis of the diode to the radius a of the cathode. The solution was limited, however, to the case of saturation current and negligible initial velocity.

The present paper extends the solution to the case of any realizable current and any radial initial velocity u which is the same for all the ions (electrons). This initial velocity may be that of emission from a hot cathode, or the velocity with which the electrons pass through a screen or grid coaxial with the cathode after having been accelerated. The analysis is restricted to the case where all the ions at any one point are moving in the same direction.

Previous consideration has been given to this problem by several authors. Of these Crank, Hartree, Ingham, and Sloane[2] have presented the most extensive treatment. They employed mechanical integration by means of a differential analyzer and obtained portions of some of the complete set of curves for which analytical formulas are developed in the present paper.

Although the solution of the space charge equation for the plane diode, consisting of two parallel plane electrodes from one of which ions are emitted, has been given by others[3] for the case of arbitrary initial velocity and arbitrary current, we shall preface our discussion of the cylindrical diode, composed of coaxial cylindrical electrodes from the inner of which ions are emitted, by a brief treatment of the plane diode. This is undertaken for the purpose of making the theory of the cylindrical diode more easily comprehensible by putting the simpler solution for the plane diode in a form analogous to that found most convenient for the cylindrical diode, and also of pointing out the fact, apparently overlooked by previous writers, that all the curves showing the potential as a function of distance from the emitting electrode, are obtainable from a single pair of master curves.

[1] L. Page and N. I. Adams, Phys. Rev. **68**, 126 (1945).
[2] Crank, Hartree, Ingham, and Sloane, Proc. Phys. Soc. (London) **51**, 952 (1939).
[3] Plato, Kleen and Rothe, Zeits. f. Physik **101**, 509 (1936); W. Kleen and H. Rothe, Zeits. f. Physik **104**, 711 (1937); B. Salzberg and A. V. Haeff, RCA Rev. **II**, 336 (1937–8); Fry, Samuel and Shockley, Bell Sys. Tech. J. **17**, 49 (1938).

THE PLANE DIODE

Let x be the distance measured perpendicular to the parallel planes of the electrodes, u the initial velocity of the ions emerging normally from the electrode specified by the smaller value of x, V the excess of the potential at any point over that of the emitting electrode, ρ the charge density, j the current density and e/m the ratio of charge to mass of the ions. Then, in Heaviside-Lorentz units,

$$\dot{x}^2=-(2e/m)V+u^2, \tag{1}$$

$$d^2V/dx^2=-\rho, \tag{2}$$

$$j=\rho\dot{x}. \tag{3}$$

Eliminating ρ and $\dot{x}$, and putting

$$\chi\equiv(m/2ej)^{\frac{1}{3}}\{-(2e/m)V+u^2\}, \tag{4}$$

we find that χ satisfies the differential equation

$$d^2\chi/dx^2=\chi^{-\frac{1}{2}}, \tag{5}$$

of which the first integral is

$$d\chi/dx=2\{\chi^{\frac{1}{2}}+C\}^{\frac{1}{2}}. \tag{6}$$

Evidently $d\chi/dx$ is proportional to the accelerating field. Since $\chi^{\frac{1}{2}}$ is essentially positive, the electric field can become zero and change sign only when the constant C is zero or negative. The curve we obtain by making $C=0$ we shall call the *limiting curve*. It represents saturation current for the case of zero initial velocity.

Integrating a second time we have

$$\chi^{\frac{1}{2}}-3C\chi+4C^3=(9/4)x^2,$$

where we have made the second constant of integration zero by suitably choosing the position of the origin of x. Finally we solve this cubic in $\chi^{\frac{1}{2}}$, putting

$$\left.\begin{aligned} &k\equiv 8C^3/9x^2, \\ &\Psi\equiv\frac{\chi^{\frac{1}{2}}}{(3x/2)^{\frac{1}{2}}}=(2m/9ejx^2)^{\frac{1}{3}}\{-(2e/m)V+u^2\}^{\frac{1}{3}}. \end{aligned}\right\} \tag{7}$$

This gives

$$\left.\begin{aligned}\Psi&=\frac{1}{2^{\frac{1}{3}}}[k^{\frac{1}{3}}+\{1-k+(1-2k)^{\frac{1}{2}}\}^{\frac{1}{3}}\\&\qquad+\{1-k-(1-2k)^{\frac{1}{2}}\}^{\frac{1}{3}}],\quad k\leqslant\tfrac{1}{2};\\ \Psi&=(k/2)^{\frac{1}{3}}[1+2\cos(\theta/3)],\quad \tan\theta\equiv\frac{(2k-1)^{\frac{1}{2}}}{1-k},\\&\qquad k\geqslant\tfrac{1}{2}.\end{aligned}\right\}\tag{8}$$

When $k\to 0$, due either to $C\to 0$ or $x\to\infty$, $\Psi\to 1$. Thus, for the limiting curve, $\Psi=1$. Note that both k and Ψ are dimensionless ratios.

Actually we are not interested in Ψ but in the effective potential

$$W\equiv V+\left(-\frac{mu^2}{2e}\right)=\left(\frac{9ej}{2m}\right)^{\frac{1}{3}}\left(-\frac{m}{2e}\right)x^{4/3}\Psi^2.\tag{9}$$

If we put $\pm|k|^{\frac{1}{3}}=g/x$, where we choose the upper sign when k is positive and the lower when k is negative so that g has the same sign as C,

$$W=\left(\frac{9ej}{2m}\right)^{\frac{1}{3}}\left(-\frac{m}{2e}\right)g^{4/3}\left(\frac{\Psi}{k^{\frac{1}{3}}}\right)^2.\tag{10}$$

Consequently, if we plot $(\Psi/k^{\frac{1}{3}})^2$ against $1/|k|^{\frac{1}{3}}=x/|g|$, we have a pair of *master curves*, one for positive k and the other for negative k, from which all possible potential curves can be obtained by multiplying the ordinates by

$$(9ej/2m)^{\frac{1}{3}}(-m/2e)g^{4/3}$$

and the abscissas by $|g|$.

The curves on Fig. 1 are specified in terms of the values of the constant g, the one marked 0 being the limiting curve. The master curve for positive k is that for which $g=1$ and the master curve for negative k that for which $g=-1$.

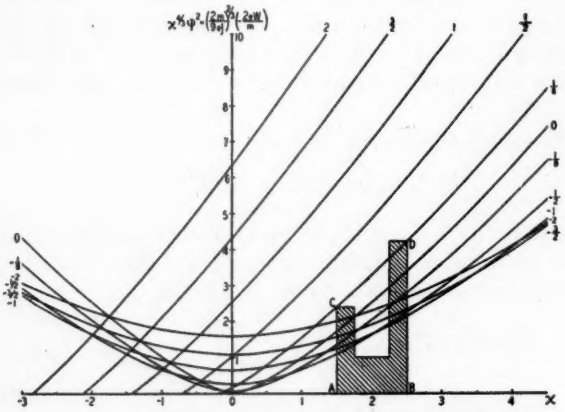

FIG. 1. Generalized potential curves for plane diodes.

Since

$$d/dx(x^{4/3}\Psi^2)=(2m/9ej)^{\frac{1}{3}}(-2e/m)dV/dx,\tag{11}$$

the electric field at any point is proportional to the slope of the curve.

Consider first the emission of ions with zero initial velocity. If ions are emitted in unlimited numbers, the potential as a function of x is given by the portion of the limiting curve 0 extending from the origin to the right. On the other hand, if saturation conditions do not exist, the potential is given by one of the curves with positive g, the distance from the emitting electrode being that from the intercept of the curve with the axis of abscissas. In the first case the field at the emitting electrode is zero, but in the latter case an accelerating field is present.

Next consider the general case in which the distance x_B-x_A between the emitting electrode A and the collecting electrode B and the effective potentials W_A and W_B at the two electrodes are given, as well as the current density j. From (9) we calculate the value of $x^{4/3}\Psi^2$ at each electrode and then cut a card (Fig. 1) so that the distance AB is equal to x_B-x_A and the ordinates AC and BD are equal to the values of $x^{4/3}\Psi^2$ at the electrodes A and B respectively. Sliding the card along the axis of abscissas, keeping AB on this axis, we find a curve (such as the curve $\frac{1}{8}$ in Fig. 1) which passes through the two points C and D. This curve specifies the distribution of potential between the two electrodes. If no curve passes through C and D, the current density j has been taken too large for realization. If C and D lie on the limiting curve 0 on opposite sides of the origin, a virtual cathode is present at the origin, whereas if they lie on a curve of negative k on opposite sides of the origin, a decelerating field exists in the neighborhood of the emitting electrode and the potential passes through a minimum in the region between the electrodes.

THE CYLINDRICAL DIODE

Here we have two coaxial cylindrical electrodes of radii a and b $(b>a)$, the inner of which emits ions (electrons) with the radial velocity u. The inner electrode may be a screen or grid through which electrons pass with velocity u, of course, instead of an actual electrode. Let r be the distance from the common axis of the electrodes and j_l the current per unit length. Then, if the remaining symbols have the same significance as in the previous case, we have, in Heaviside-Lorentz units,

$$\dot{r}^2=-(2e/m)V+u^2,\tag{12}$$

$$\frac{1}{r}\frac{d}{dr}\left(r\frac{dV}{dr}\right)=-\rho,\tag{13}$$

$$j_l=2\pi\rho r\dot{r}.\tag{14}$$

Eliminating ρ and $\dot{r}$, and putting[4]

$$\left.\begin{aligned} &\Psi^2\equiv(4\pi m/9ej_1r)^{\frac{1}{3}}\{-(2e/m)V+u^2\},\\ &z\equiv\tfrac{2}{3}\log(r/a),\\ &W\equiv V+\left(-\frac{mu^2}{2e}\right)=\left(\frac{9ej_1a}{4\pi m}\right)^{\frac{1}{3}}\left(-\frac{m}{2e}\right)\left(\frac{r}{a}\right)^{\frac{1}{3}}\Psi^2, \end{aligned}\right\} \quad (15)$$

we find that Ψ satisfies the non-linear differential equation

$$\Psi[d^2/dz^2(\Psi^2)+2d/dz(\Psi^2)+\Psi^2]=1. \quad (16)$$

Since z does not appear explicitly in this equation, Ψ must be a function of $z+\alpha$, where α is an arbitrary constant.

First we look for solutions of (16) which are valid for large z, then for solutions which are valid for small z. The first we shall refer to as "far" formulas, the second as "near" formulas.

FAR FORMULA

Clearly $\Psi=1$ is a solution of (16). Hence we suspect a solution of the form

$$\Psi=1+(\xi+\eta)+(a_{20}\xi^2+a_{11}\xi\eta+a_{02}\eta^2)+(a_{30}\xi^3+a_{21}\xi^2\eta+a_{12}\xi\eta^2+a_{03}\eta^3)+\cdots.$$

By substituting in (16) we find that a real solution of this form exists provided

$$\xi=\exp\{-[(z+\alpha')+i(2)^{-\frac{1}{2}}(z+\alpha'')]\}$$

and η is the complex conjugate of ξ.

The coefficients of the first six terms (in addition to the term unity) of this solution were calculated. The first five of these were obtained in fractional form and verified by substituting back in the differential equation. While the sixth term was calculated only in decimal form, it was checked by independent recalculation. The solution can best be expressed in terms of

$$\phi\equiv(2)^{-\frac{1}{2}}(z+\alpha''),\quad c\equiv\exp[-(z+\alpha')]. \quad (17)$$

Then

$$\begin{aligned}\Psi=1&+c[2.00000\cos\phi]+c^2[-1.09091\cos2\phi\\ &-0.51426\sin2\phi]\\ &+c^3[1.00000\cos3\phi+0.82496\sin3\phi\\ &+0.22727\cos\phi+0.93210\sin\phi]\\ &+c^4[-1.06618\cos4\phi-1.35505\sin4\phi\\ &-0.41786\cos2\phi-2.11568\sin2\phi-0.00957]\\ &+c^5[1.14794\cos5\phi+2.29087\sin5\phi\\ &+0.33420\cos3\phi+4.34538\sin3\phi\\ &-0.02034\cos\phi+1.94913\sin\phi]\\ &+c^6[-1.07982\cos6\phi-3.93115\sin6\phi\\ &+0.60929\cos4\phi-8.65663\sin4\phi\\ &+0.89535\cos2\phi-6.43121\sin2\phi\\ &-0.03878]\\ &+\cdots. \end{aligned} \quad (18)$$

[4] The function Ψ used here is the cube root of the function g used in reference 1.

TABLE I. Values of the coefficients a_1, a_2, etc.

ϕ	a_1	a_2	a_3	a_4	a_5	a_6
$0, \pi$	±2.00000	−1.09091	±1.22727	−1.49361	±1.46180	0.38605
$\pi/8, 9\pi/8$	±1.84776	−1.13503	±1.71152	−3.15611	±6.54679	−14.62605
$\pi/4, 5\pi/4$	±1.41421	−0.51426	±0.69603	−1.05907	±1.76859	−3.14813
$3\pi/8, 11\pi/8$	±0.76537	0.40775	∓0.29146	0.14494	±0.00518	−0.10611
$\pi/2, 3\pi/2$	0.00000	1.09091	±0.10714	−0.65789	∓0.10538	0.75498
$5\pi/8, 13\pi/8$	∓0.76537	1.13503	±1.38235	0.42687	∓1.48285	−2.76477
$3\pi/4, 7\pi/4$	∓1.41421	0.51426	±1.78883	3.17229	±3.89341	1.85198
$7\pi/8, 15\pi/8$	∓1.84776	−0.40775	±0.52620	2.54602	±7.20718	17.34181

This is a complete solution since it contains the two independent constants α' and α''. Since it is periodic in ϕ, we see that the solutions form a bounded set. We have computed the function Ψ for values of ϕ equal to the first sixteen positive integral multiples of $\pi/8$. If we designate the coefficient of c by a_1, that of c^2 by a_2, and so on, we obtain Table I, where, in each row, the upper sign goes with the first value of ϕ and the lower sign with the second.

Since the position of the origin of z is immaterial, we may, without any loss of generality, keep the constant α' in (17) fixed in plotting curves showing Ψ^2 as a function of z, increasing α'' by $(2)^{\frac{1}{2}}\pi/8=0.55536$ in passing from one curve to the next of higher ordinal number, so that when ϕ has increased by 2π we will have come back to the curve with which we started. In Fig. 2 we have made $\alpha'=1.11072$ and numbered the curves so that $\alpha''=N(2)^{\frac{1}{2}}\pi/8$, where N is the ordinal number of the curve. Under these circumstances, even though the series converge less rapidly the smaller z, the convergence is sufficiently good to give an accuracy of one percent for most of the curves at $z=0$. Hence, if we can obtain a near formula which converges satisfactorily for negative values of z, we can use it to extend into this region the curves given for positive values of z by the far formula. The near formula, must, of course, be a complete solution of (16), containing the two independent arbitrary constants necessary to enable us to fit both the function and its derivative. Actually, it has not been found possible to obtain a single near formula which converges sufficiently well to enable us to extend by means of it all of the sixteen curves obtained from the far formula. On the contrary, it has been found necessary to develop three different near formulas. Before discussing them, however, we shall give the formula for the limiting curve which represents the saturation current for zero initial velocity.

LIMITING CURVE

The limiting curve representing saturation current for zero initial velocity has been discussed in reference 1. In terms of our present more convenient notation, it is specified for small and moderate values of z by the near formula

$$\begin{aligned}\Psi=(1.5z)^{\frac{1}{3}}[1&-0.400{,}000z+0.097{,}500z^2\\ &-0.015{,}212z^3+0.001{,}799z^4-0.000{,}184z^5\\ &+0.000{,}014z^6+\cdots]. \end{aligned} \quad (19)$$

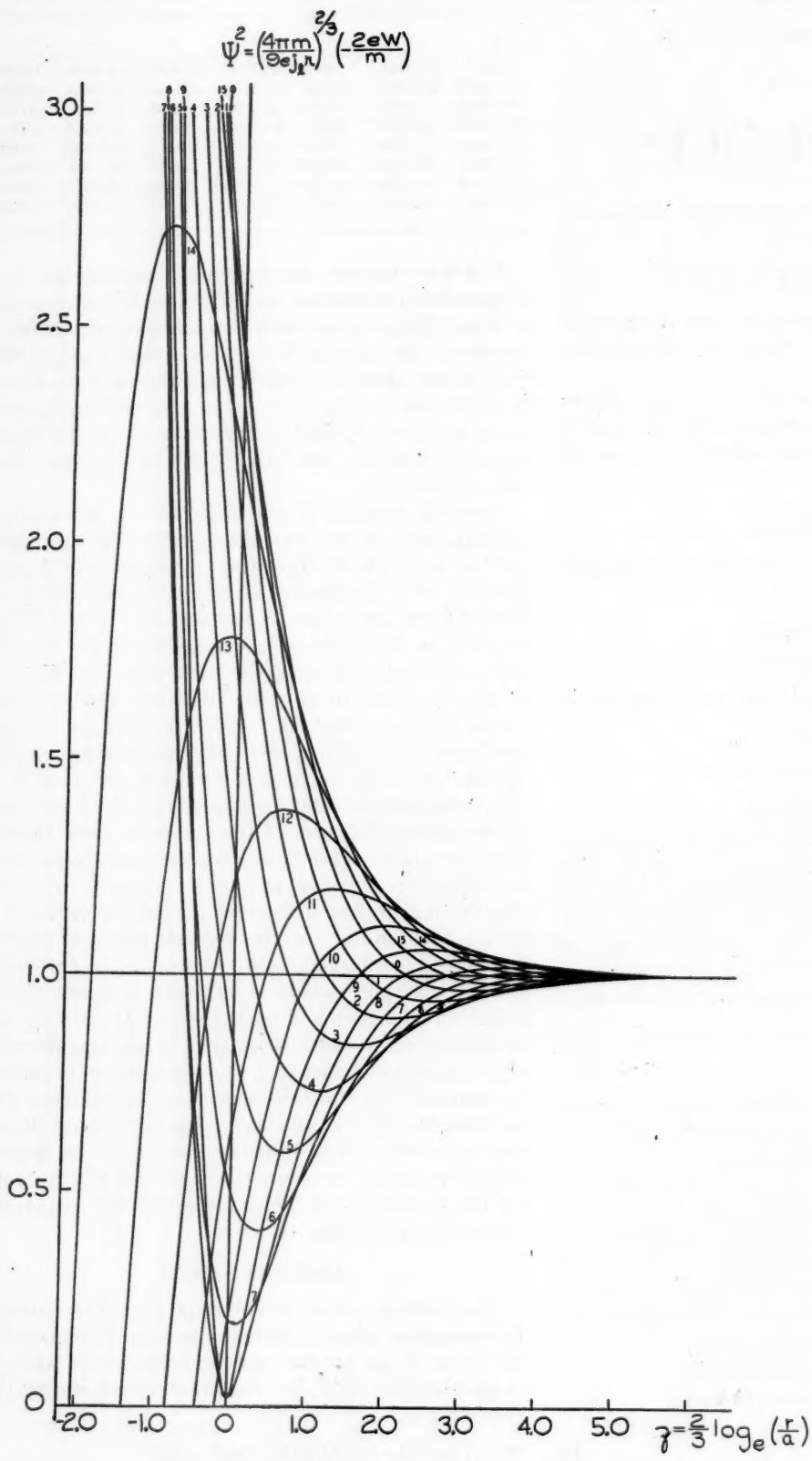

FIG. 2. Complete solution of space charge equation for cylindrical diode.

To fit this curve the constants in the far formula must be given the values

$$\phi=40°.5142z+202°.83, \quad \alpha'=1.12086, \tag{20}$$

so that

$$\begin{aligned}\Psi=1&+\epsilon^{-z}[0\cdot 65200\cos\phi]-\epsilon^{-2z}[0.11594\cos 2\phi\\ &+0.05465\sin 2\phi]\\ &+\epsilon^{-3z}[0.03465\cos 3\phi+0.02858\sin 3\phi\\ &+0.00787\cos\phi+0.03229\sin\phi]\\ &-\epsilon^{-4z}[0.01204\cos 4\phi+0.01530\sin 4\phi\\ &+0.00472\cos 2\phi+0.02390\sin 2\phi+0.00011]\\ &+\epsilon^{-5z}[0.00423\cos 5\phi+0.00844\sin 5\phi\\ &+0.00123\cos 3\phi+0.01600\sin 3\phi\\ &-0.00007\cos\phi+0.00718\sin\phi]\\ &-\epsilon^{-6z}[0.00130\cos 6\phi+0.00472\sin 6\phi\\ &-0.00073\cos 4\phi+0.01039\sin 4\phi\\ &-0.00107\cos 2\phi+0.00772\sin 2\phi+0.00005]\\ &+\cdots.\end{aligned} \tag{21}$$

The following values show how good the fit is and how well the series is converging:

z	From Near Formula (19) Ψ	From Near Formula (19) $d\Psi/dz$	From Far Formula (21) Ψ	From Far Formula (21) $d\Psi/dz$
0.55536	0.7131		0.7132	
1.11072	0.9242	0.2299	0.9242	0.2299
1.66608	1.0049		1.0048	

NEAR FORMULA I

The most obvious near formula for curves other than the limiting curve is a simple power series in z of the form

$$\Psi=A[1+a_1(z-\alpha)+a_2(z-\alpha)^2+a_3(z-\alpha)^3+\cdots], \tag{22}$$

where α is the value of z at which the curve described by this formula is to be fitted to the specified curve described by the far formula. Evidently A is the value of the function and Aa_1 the value of its derivative at $z=\alpha$.

As might be expected, a power series formula does not converge satisfactorily in regions where Ψ is small compared with unity, but is very satisfactory where Ψ is the order of magnitude of unity or greater. It was used to extend curves 15, 0, 1, 2, 3, 4, 5, 6. In some cases the fit was secured from the values of the function and its derivative at one point, in others from the values of the function at two nearby points, and in the case of curve 6 it was necessary to fit twice, using two different values of α. The coefficients for the curves specified above are given in Table II.

TABLE II. Values of the coefficients for the curves specified above.

Curve	α	A	a_1	a_2	a_3	a_4	a_5	a_6
15	0.5554	1.3458	−0.2492	0.0708	−0.0002	−0.0023		
0	0.5554	1.3171	−0.2854	0.1041	−0.0089	−0.0012		
1	0.5554	1.2525	−0.3083	0.1381	−0.0167	−0.0015		
2	0.5554	1.1574	−0.3139	0.1759	−0.0257	−0.0039		
3	0.0000	1.2875	−0.4651	0.2241	−0.0216	−0.0001		
4	0.0000	1.115	−0.5014	0.3016	−0.0207	−0.0078		
5	0.0000	0.916	−0.5240	0.4620	−0.0133	−0.0461	−0.0429	0.0041
6	0.0000	0.709	−0.5925	0.8684	0.0559	−0.2621	−0.2756	0.0912
6	−0.5554	1.119	−0.9160	0.4249	0.0334	0.0599		

The accuracy is least, of course, for curve 6. To give an indication of the goodness of the fit, and also of the convergence of the series used, we note the following values for curve 2:

z	Ψ from (22) Near Formula	Ψ from (18) Far Formula
0.0000	1.427	1.425
0.5554	1.1574	1.1574
1.1107	1.0130	1.0129
1.6661	0.9575	0.9571

NEAR FORMULA II

For curves near the limiting curve representing saturation for zero initial velocity, it should be possible to develop a solution in the form of a power series in a parameter γ, which reduces to (19) when γ becomes zero. After some labor the following near solution was found. Let

$$\beta\equiv-\frac{9}{4}\frac{(z-\alpha)^2}{\gamma^3}, \quad w\equiv(\beta-2)\{(\beta-2)^2-3\}. \tag{23}$$

Then

$$\begin{aligned}\Psi=\gamma[&\{w^{1/9}+1+w^{-1/9}-(1/9)w^{-17/9}\\ &+(1/9)w^{-19/9}+\cdots\}\\ &-1.5(z-\alpha)\{0.26667w^{1/9}+0.53333\\ &+0.80000w^{-1/9}-0.53333w^{-5/9}+0.53333w^{-7/9}\\ &-0.53333w^{-11/9}+0.53333w^{-13/9}+\cdots\}\\ &+2.25(z-\alpha)^2\{0.04333w^{1/9}+0.11651\\ &+0.22222w^{-1/9}+0.01873w^{-2/9}+0.17302w^{-4/9}\\ &-0.40029w^{-5/9}+\cdots\}\\ &-3.375(z-\alpha)^3\{0.00451w^{1/9}+0.01469\\ &+0.03371w^{-1/9}-0.00853w^{-2/9}\\ &+0.00748w^{-3/9}+\cdots\}\\ &+5.0625(z-\alpha)^4\{0.00036w^{1/9}+0.00139\\ &+0.00375w^{-1/9}+\cdots\}\\ &-7.5938(z-\alpha)^5\{0.000{,}024w^{1/9}\\ &+0.000{,}110+\cdots\}\\ &+11.391(z-\alpha)^6\{0.000{,}001w^{1/9}+\cdots\}\\ &+\cdots].\end{aligned} \tag{24}$$

This formula was used to extend curves 7, 8, 9. The fitting of the near formula to a specified curve described by the far formula was extremely laborious, since the only feasible method was to fit the one curve to the other at two points by trial and error. The following are the values found for the constants α and γ:

Curve	α	γ
7	0.018	−0.450
8	0.010	−0.250
9	0.000	−0.0085

TABLE III. Values of the coefficients in Eq. (30).

y	B	b_1	b_2	b_3	b_4	b_5	b_6	b_7	b_8
0.05	0.1357	0.6279	−0.3450	0.3095	−0.3316	0.3905	−0.4879		
0.10	0.2154	0.5926	−0.3062	0.2588	−0.2616	0.2903	−0.3417	0.4193	−0.5298
0.20	0.3420	0.5255	−0.2416	0.1814	−0.1626	0.1603	−0.1676	0.1827	−0.2050
0.30	0.4481	0.4674	−0.1911	0.1276	−0.1017	0.0891	−0.0829	0.0804	−0.0802
0.40	0.5429	0.4161	−0.1514	0.0900	−0.0639	0.0498	−0.0412	0.0356	−0.0317
0.50	0.6300	0.3707	−0.1201	0.0636	−0.0402	0.0279	−0.0206	0.0159	−0.0126
0.60	0.7113	0.3311	−0.0957	0.0453	−0.0255	0.0158	−0.0104	0.0073	−0.0051
0.70	0.7884	0.2959	−0.0764	0.0323	−0.0163	0.0090	−0.0053	0.0033	−0.0021
0.80	0.8618	0.2648	−0.0612	0.0231	−0.0104	0.0052	−0.0027	0.0015	−0.0009
0.90	0.9322	0.2373	−0.0491	0.0166	−0.0067	0.0029	−0.0014	0.0007	−0.0004
1.00	1.0000	0.2129	−0.0395	0.0120	−0.0043	0.0017	−0.0007	0.0003	−0.0002
1.10	1.0657	0.1914	−0.0318	0.0087	−0.0028	0.0010	−0.0004	0.0002	−0.0001
1.30	1.1912	0.1554	−0.0209	0.0046	−0.0012	0.0004	−0.0001		
1.40	1.2515	0.1406	−0.0171	0.0034	−0.0008	0.0002	−0.0001		
1.80	1.4797	0.0947	−0.0077	0.0010	−0.0002				
2.00	1.5874	0.0786	−0.0053	0.0006	−0.0001				

For curve 9, the nearest to the limiting curve, the fit is as follows:

z	Ψ from (24) Near Formula	Ψ from (18) Far Formula
0.5554	0.7078	0.7077
1.1107	0.921	0.922
1.6661	1.003	1.004

This is very satisfactory, but the fit is not as close for curves 7 and 8.

An unfortunate defect of the solution (24) is that the series does not converge for very small values of w.

Curve 9 lies so close to the limiting curve that it is impossible to distinguish the one from the other on the graph of Fig. 2 except in the immediate neighborhood of the origin, where the limiting curve has been indicated by a broken line. At the origin the limiting curve makes tangential contact with the axis of abscissas.

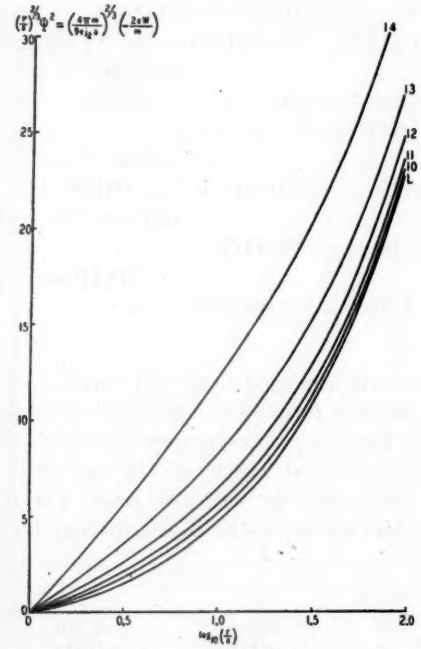

FIG. 3. Generalized potential curves for cylindrical diode with zero emission velocity.

NEAR FORMULA III

It follows from the definition (15) of Ψ that this quantity becomes infinite when there is no emission of ions. In such a case (16) reduces to

$$d^2/dz^2(\Psi^2)+2d/dz(\Psi^2)+\Psi^2=0, \tag{25}$$

of which the complete solution is

$$\Psi^2=(A_0+B_0z)e^{-z}=\{A_0+\tfrac{2}{3}B_0\log(r/a)\}(a/r)^{\frac{1}{3}}, \tag{26}$$

giving for the effective potential

$$W=A+B\log(r/a)$$

in agreement with the elementary expression for the potential between the plates of a cylindrical condenser.

It would be expected, therefore, that for small emission currents, a series solution should exist the first term of which is the equivalent of (26). If, for convenience in writing this solution, we put $y\equiv z-\alpha$, we find such a solution in the form

$$\begin{aligned}\Psi=&cy^{\frac{1}{2}}e^{-y/2}+\frac{1}{c^2}ye^{y}[0.66667p]\\&+\frac{1}{c^6}y^{\frac{1}{2}}e^{5y/2}[-0.38889p^2s_2]+\frac{1}{c^8}y^2e^{4y}[0.37037p^3s_3]\\&+\frac{1}{c^{11}}y^{5/2}e^{11y/2}[-0.42130p^4s_4]+\frac{1}{c^{14}}y^3e^{7y}[0.52675p^5s_5]\\&+\frac{1}{c^{17}}y^{7/2}e^{17y/2}[-0.69882p^6s_6]+\frac{1}{c^{20}}y^4e^{10y}[0.96571p^7s_7]\\&+\frac{1}{c^{23}}y^{9/2}e^{23y/2}[-1.37499p^8s_8]+\cdots\end{aligned} \tag{27}$$

where

$$\begin{aligned}p\equiv&1-\frac{2}{5}(3y)+\frac{3}{5\cdot7}(3y)^2-\frac{4}{5\cdot7\cdot9}(3y)^3+\cdots\\&+(-1)^n\frac{n+1}{5\cdot7\cdot9\cdots(2n+3)}(3y)^n+\cdots,\end{aligned} \tag{28}$$

$$\begin{aligned}s_2\equiv&1-0.003{,}675y^2-0.001{,}471y^3-0.000{,}226y^4\\&+0.000{,}027y^5+0.000{,}021y^6+\cdots,\\s_3\equiv&1-0.004{,}286y^2-0.001{,}590y^3\\&-0.000{,}182y^4+0.000{,}049y^5+\cdots,\\s_4\equiv&1-0.006{,}940y^2-0.002{,}421y^3\\&-0.000{,}206y^4+\cdots,\end{aligned}$$

$s_5 \equiv 1-0.010{,}205y^2-0.003{,}438y^3+\cdots,$

$s_6 \equiv 1-0.013{,}118y^2+\cdots,$

$s_7 \equiv 1+\cdots,$

$s_8 \equiv 1+\cdots.$

Putting

$$t \equiv (y^{\frac{1}{2}}e^{3y/2}/c^3) \tag{29}$$

we can write (27) in the form

$$\Psi = (B/t^{\frac{1}{3}})[1+b_1t+b_2t^2+b_3t^3+\cdots:] \tag{30}$$

where the coefficients of t are, of course, functions of y although not of c. In Table III we list the values of the coefficients for various values of y.

We have used (27) to extend the curves 10, 11, 12, 13, 14. Since the fitting of the function and its derivative had to be done by trial and error it was very laborious. It should be noted that, after a hump which becomes higher the greater the ordinal number of the curve, the curve drops abruptly to the axis of abscissas and ends there. While the accuracy of the fit is diminished as the ordinal number of the curve decreases, this lessened accuracy is compensated by the fact that the extended portion of the curve is shortened. The values of α and c found for these curves are as follows:

Curve	α	c
10	−0.14	1.031
11	−0.41	1.295
12	−0.81	1.568
13	−1.38	1.955
14	−2.06	2.584

DISCUSSION OF RESULTS

The solutions obtained are shown graphically by the curves in Fig. 2. Just as in the case of the plane diode, a sliding card (Fig. 1) can be used to pick out the potential curve for any assigned effective cathode potential W_a and anode potential W_b, any assigned anode to cathode ratio b/a, and any realizable current j_l per unit length. In this case, however, since the abscissa is $z=(\frac{2}{3})\log(r/a)$, the distance AB on the card must be made equal to

$$z_b-z_a=\tfrac{2}{3}\log(b/a) \tag{31}$$

and, since the ordinate is Ψ^2, the heights AC and BD must be made equal to the values of

$$(4\pi m/9ej_lr)^{\frac{1}{3}}\{-(2e/m)W\} \tag{32}$$

at each of the two electrodes, in accord with (15). It should be noted that the factor in the first parenthesis of (32) is of the dimensions of the reciprocal of the cube of a velocity and that in the second of the dimensions of the square of a velocity, so that the whole expression is a pure number.

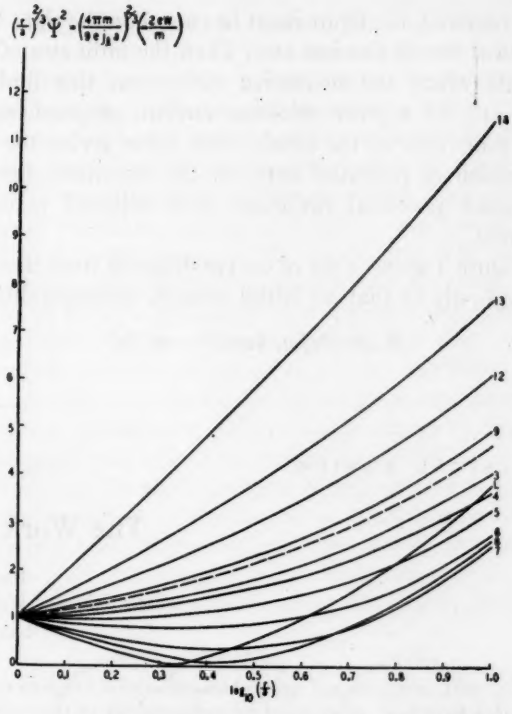

FIG. 4. Generalized potential curves for cylindrical diode with finite emission velocity.

If, when AB is slid along the axis of abscissas, the points C and D lie on the limiting curve on opposite sides of the origin, a virtual cathode is present. If no curve on which they both lie can be found, the value assumed for the current is too large.

Since

$$\frac{dV}{dr}=(2/3r)\left(\frac{9ej_lr}{4\pi m}\right)^{\frac{1}{3}}\left(-\frac{m}{2e}\right)\left[\frac{d}{dz}(\Psi^2)+\Psi^2\right], \tag{33}$$

the electric field is proportional to the slope of the curve only where $\Psi^2=0$. The limiting curve is the only one which meets the axis of abscissas with zero slope.

Any desired information regarding the cylindrical diode can be obtained from the master curves in Fig. 2. If, for instance, it is desired to study the characteristics of the cylindrical diode for the emission of ions with zero velocity but in varying numbers, we draw a new graph from the curves numbered 14 to 9 inclusive, taking as origin in each case the point where the curve intersects the axis of abscissas, and using $\log_{10}(r/a)$ rather than z as abscissa and $(r/a)^{\frac{1}{3}}\Psi^2$ rather than Ψ^2 as ordinate. The new ordinates, then, are directly proportional to the effective potential W, and the slope of the curve is proportional to the electric field at any point. Such curves have been drawn in Fig. 3, the numbering of the curves corresponding to that of the master curves of Fig. 2. The limiting curve is indicated by L. If, now, it is desired to apply the graph to the specific case of a tube in which the ratio b/a is, say,

one hundred, the figure must be cut off on the right by a vertical line of abscissa two. Then the ordinates of the points where the successive curves cut this limiting line are, for a given emission current, proportional to the potentials on the anode, each curve giving the distribution of potential between the electrodes for the assigned potential difference and assigned emission current.

Figure 4 shows a set of curves differing from those of Fig. 3 only in that an initial velocity corresponding to

$$W_a=(9ej_1a/4\pi m)^{\frac{1}{2}}(-m/2e)$$

is assumed. The broken curve representing $(r/a)^{\frac{1}{2}}$ has been included for the sake of comparison. Now we have cases in which the field near the cathode retards the ions, causing a dip in the potential curve, and leading, in the extreme case, to the formation of a virtual cathode. While each curve represents a possible potential distribution, the theory developed here does not, of course, specify the experimental conditions under which a specified curve may be realized or the sequence in which different curves are reached when one of the parameters, such as the potential on the anode, is altered.

PHYSICAL REVIEW VOLUME 76, NUMBER 3 AUGUST 1, 1949

The Work Function of Copper

PAUL A. ANDERSON
State College of Washington, Pullman, Washington*
(Received April 7, 1949)

The work functions and aging characteristics of fourteen copper surfaces have been determined by measurement of their contact differences of potential with respect to barium reference surfaces of known work function. Measurement was by the retarding potential method in tubes sealed from the pumps and gettered with vaporized barium. The copper surfaces were prepared by subjecting Hilger's "spectroscopic standard" copper to forty vacuum fusions followed by fractional distillation, redistillation of the fractions, and condensation of the vapor on glass. The barium films were prepared by a similar, standardized technique which yields surfaces reproducible and constant to 0.01 ev or better. The time interval between the deposition and initial measurement of the metal films was of the order of ten seconds, obtained conveniently with a tube in which the target is returned to the measuring position automatically after deposition of a metal film upon it.

The copper surfaces, formed from successive fractions of the distillate, showed marked variability of the initial work function and marked drift toward lower work function in films 1–4, progressive improvement in films 5–8 and, finally, good reproducibility and negligible drift in films 9–14 inclusive. The range of variation in films 1–8 coincides almost exactly with the range of divergent values reported in the literature. Copper evidently retains dissolved gases, in free or combined form, with extraordinary tenacity and these contaminants, evaporated with the copper and reabsorbed by the condensing film, appear to be responsible for the variations observed in films 1–8. The work function value given by films 9–14 is 4.46±0.03 ev, and this value is to be taken as representative of the present work.

THIS report describes further results in a series of studies of the external work functions of the pure metals. The more significant features of the experimental method, described in detail in previous reports,[1] may be summarized briefly as follows: (1) The surfaces to be measured are prepared by condensation of the metal vapor on glass after an exhaustive outgassing which includes repetitive vacuum fusion, fractional distillation, and, when necessary, redistillation of the selected fractions. (2) Each work function determination is based on the measurement of an extended series of different surfaces, a procedure which either establishes the reproducibility of the measurements or reveals inadequacies in the outgassing technique. (3) The first measurement on each surface is obtained immediately after its deposition and within a time interval which is short compared to the time required to form an equilibrium layer of contaminating gas on the surface. This procedure supplies a definite means for estimating the degree of contamination of the surface at the time of measurement.[2] (4) The work function of each surface is determined by measuring its difference of potential with respect to a barium reference surface prepared by a technique which has been found[1] to give surfaces consistently reproducible and constant to 0.01 ev or better.

A large number of unpublished measurements on copper, taken in this laboratory in 1939–41 with tubes of several different types, gave work function values which varied in random fashion over a range of about 0.5 ev without showing any trend toward better reproducibility. These results were obtained after outgassing treatments which were comparable in all respects to those which have given[1] excellent results on silver, zinc, magnesium, and lithium. In the present work, outgassing of the copper has been carried to an extreme and our earlier tube designs so modified as to simplify the manipulations required for obtaining short deposition-

* Assisted by the ONR under Contract M6-ori-167, Task I.
[1] P. A. Anderson, Phys. Rev. 59, 1034 (1941); 57, 122 (1940) and earlier reports cited therein.

[2] Reference 1, 1940 paper.

measurement intervals. These procedures have given work functions reproducible to a few centivolts in the initial readings and drifts with aging which are so slow that the initial readings can probably be taken as characteristic of clean copper.

TUBE DESIGN AND EXPERIMENTAL PROCEDURES

The experimental procedure, insofar as it involves modifications of our previous techniques,[1] may be described in connection with the design of the measuring tube, Fig. 1. The target on which the films of copper and barium are laid down is a glass drum pivoted on glass bearings and operated as a pendulum. The "measuring position" at which the freshly deposited metal film is centered over the electron gun is the equilibrium position to which the pendulum returns automatically whenever it is released. When a film of either metal is to be deposited, the drum is rotated to the appropriate position by traction of a small Alnico magnet on the glass-enclosed armature. Friction in the bearings damps the pendulum oscillations sufficiently to bring the target to rest a second or two after release; the deposition-measurement interval is thus reduced to the time required for bringing the galvanometer to the selected reference reading. The drum serves the important purpose, also, of isolating the vaporizing compartments from each other and from the electron gun, i.e., of preventing contamination of the copper charge or gun by the barium. The glass spindles of the drum were sealed on with the aid of a glassblowing lathe to insure constant target-gun geometry at all positions of the target.

The barium vaporizing assembly, which provides fractional distillation of the metal and redistillation of the fractions used for preparing the measured surfaces, was similar to that employed in previous investigations of this series. The first copper vaporizer was designed to handle a relatively large charge (order of 1.0–1.5 g) of the metal without excessively heavy current leads and with reasonably high efficiency in terms of the ratio of distillate intercepted by the second vaporizer to the total quantity of copper vaporized. The usual horizontal tungsten foil boat is not satisfactory for this purpose; the fused copper flows along the foil and shorts most of it out.

The outgassing schedule, involving prolonged baking of the tube at 450°C before introduction of the metal charges, another extended bake at 350°C after charging, and repetitive high frequency treatment of all metal parts, was similar to that used for silver.[3] The treatment of the barium followed the procedure described in our recent report on lithium.[4] The copper used in this work was Hilger's spectroscopic material, Lot No. 10300, which was supplied with an exceptionally complete analysis showing 0.004 percent oxygen and 0.0007 percent iron as the only impurities present in amounts exceeding 0.0001 percent. During the outgassing of the tube and before seal-off, the copper charge was melted down five times. After seal-off, alternate fusions and solidifications of the copper interspersed with similar treatments of the barium were continued until approximately half of the charges had been vaporized. Since copper vaporizes rather slowly at temperatures slightly above the melting point, thirty-five fusions were included in this stage of the outgassing. The second vaporizers were flashed to remove the discarded fractions of copper and barium before proceeding with the measurements. The current through the first copper vaporizer was then increased to a value which was high enough to give a suitable deposit on the second vaporizer in about ten minutes, that is enough copper to form an opaque film on the target when the redistillation was carried out. As each new film of copper was deposited on the target it was measured as quickly as possible, usually within ten seconds of its deposition, and then at intervals of one minute to establish the rate of drift of the work function with aging. This procedure was

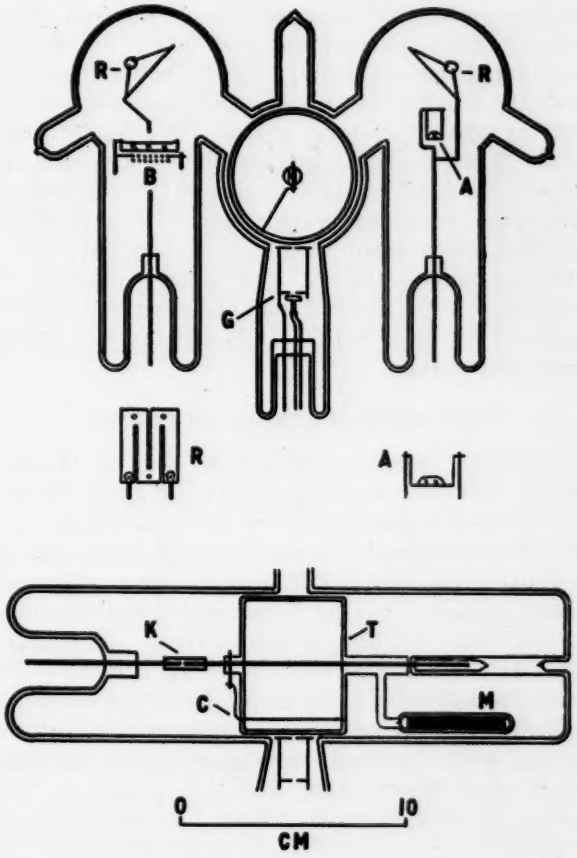

FIG. 1. Tube for measurement of contact difference of potential between vaporized films of Cu and Ba. Side view of complete tube above and of target section, rotated 90°, below. First Cu vaporizer *A* is 1-mil Ta foil 6-mm wide. Second vaporizers *R* of 1-mil Ta foil. Target *T* is Pyrex drum with 60-mil tungsten spindle rotating freely in nickel bearing *K*. Contact to metal film is by 20-mil Pt wire *C* embedded in face of drum. *M* is glass-enclosed soft iron armature. For detail of electron gun *G* and first Ba vaporizer *B*, see reference 1 of text. All leads 60-mil tungsten.

[3] Reference 1, 1941 paper.
[4] Paul A. Anderson, Phys. Rev. 75, 1205 (1949).

repeated until the copper charge on the first vaporizer was exhausted. A succession of barium films was then deposited on the copper and measured in like fashion. The electrical circuit used in these measurements has been described previously.[4]

THE CONTACT DIFFERENCE OF POTENTIAL BETWEEN COPPER AND BARIUM

The results to be described are based on measurements on fourteen copper surfaces and eight barium surfaces, prepared as described above. The retarding potential required to establish the reference electron current to the target in the measurement taken immediately after the deposition of a new film is referred to hereafter as the "initial reading." The barium films gave, as usual, initial readings which were consistently reproducible to 0.01 volt or better and constant to 0.01 volt for periods of hours or even days after deposition. The serial numbering of the copper surfaces, running from 1 through 14, conforms to the order in which these surfaces were prepared from successive fractions of the distillate. Copper films 1–4 inclusive gave initial readings which varied at random by amounts corresponding to an extreme variation of 0.24 ev in the work function, a reproducibility markedly better than that obtained in our earlier unpublished measurements but still far from satisfactory. In films 5–8 a regular trend in the initial readings, corresponding to a progressive increase in work function totaling 0.18 ev appeared. This trend then disappeared; films 9–14 gave initial readings which again varied at random but over a range of only ± 0.03 ev. The contact difference of potential Cu−Ba derived from the mean of the initial readings on films 9–14 is 1.94 ± 0.03 volts, copper negative to barium.

THE WORK FUNCTION OF COPPER

Neglecting deviations which arise from the Maxwell tails of the Fermi distributions and which are well within the limits of experimental error at room temperature, the difference between the work functions of two metals is equal to the contact difference of potential between them, multiplied by the elementary charge. Addition of our value for the contact difference of potential Cu−Ba to 2.52 ev, the work function of barium,[5] yields the value 4.46 ± 0.03 ev for the work function of copper. This value is to be taken as representative of the present work. Previously reported values[6] for the work function of copper range from 4.1 to 4.5 ev. The thermionic measurements of Goetz,[7] probably the most careful and thorough of the earlier investigations, gave 4.38 ev. It is interesting that this range of values, obtained in seven independent studies by a variety of methods and techniques, coincides almost exactly with the range of values obtained in our measurements on copper films 1–14, namely 4.04 to 4.49 ev. Our observations on the variation of the work function with the aging of freshly deposited copper films, described below, show in every case a trend toward lower work function and suggest that the work function of completely clean copper films deposited on glass at room temperature is probably close to 4.50 ev.

EFFECTS OF GASEOUS CONTAMINANTS ON THE WORK FUNCTION OF COPPER

We are concerned here not only with the initial readings on newly formed copper surfaces but with the behavior of these films on aging. The results of some two hundred measurements on the fourteen copper surfaces may be summarized as follows: (1) The first films to be deposited, characterized by poor reproducibility in the initial readings, showed a relatively rapid drift toward lower work function on aging. Film No. 1, the extreme example of drift, gave a work function of 4.32 ev ten seconds after its deposition, 4.27 at one minute, 4.23 at two minutes, 4.12 at eight minutes, and a slower drift thereafter. (2) Improvement in the reproducibility of the initial reading was accompanied by a striking decrease in both the rate and magnitude of the drift. Film No. 10, typical of the 9–14 group, gave an initial work function of 4.47 and successive readings of 4.47, 4.47, 4.47, 4.46, and 4.46 at one minute intervals without further drop within 12 minutes. (3) In no case was a drift toward higher work function observed. These observations seem to bear out the tentative conclusions reached in our earlier unpublished work, namely, that traces of gas retained by a copper charge through a series of fusions and solidifications are evaporated with the copper and are then reabsorbed by the condensed film. In the present measurements, the quantity of gas left in the copper charge on the first vaporizer appears to have been reduced to negligible proportions only after most of the copper had been evaporated. The fact that the residual gas, presumably oxygen, lowers the work function suggests further that solution in the condensed copper film rather than permanent adsorption on the surface is involved. It is well known that oxygen adsorbed on a clean tungsten surface raises the work function and a similar behavior would be expected of copper if the oxygen remained on the surface as an adsorbed film.

I am indebted to Mr. Frank Peters, departmental glassblower, for the skill and care which he has given to the construction of the tubes used in this work.

[5] N. C. Jamison and R. J. Cashman, Phys. Rev. **50**, 624 (1936).
[6] A. L. Hughes and L. A. DuBridge, *Photoelectric Phenomena* (McGraw-Hill Book Company, Inc., New York, 1932), p. 75.
[7] A. Goetz, Zeits. f. Physik **43**, 531 (1927).

PHYSICAL REVIEW VOLUME 76, NUMBER 3 AUGUST 1, 1949

On the Treatment of Quantum Electrodynamics without Eliminating the Longitudinal Field

NING HU*
Cornell University, Ithaca, New York
(Received April 7, 1949)

It is shown in the present paper that the supplementary condition in quantum electrodynamics can be satisfied identically without eliminating the longitudinal components of the electromagnetic field, provided certain rules on the summation over the polarizations of the photons are observed. The result is shown to be identical with that obtained by the usual method in which the longitudinal field is eliminated. This simplifies greatly the calculation since no separate treatment of longitudinal and transverse fields is needed.

RECENTLY Tomonaga,[1] Schwinger,[2] and others have succeeded in formulating quantum electrodynamics in a completely co-variant form. As in customary formulations, these authors showed that the longitudinal components of the electromagnetic field can be eliminated, and thus insured the identical satisfaction of the supplementary condition. As a consequence of this elimination, the application of the theory becomes very much involved, since one has to deal with the transverse field and the coulomb interaction separately for each virtual transition. On the other hand, it has been pointed out by Feynman[3] that one can treat the longitudinal and transverse fields on the same footing by dealing with four different polarizations of virtual photons and also obtain the correct results. The Coulomb interaction is thus replaced by virtual emission and re-absorption of longitudinal photons. This simplifies tremendously the calculations since no separate treatment of longitudinal and transverse field is needed. It is the aim of the present paper to derive this new method from the formalism of Tomonaga and Schwinger. Only the case of spin-$\frac{1}{2}$ particles interacting with the electromagnetic field is considered in the present paper.

It is perhaps of interest to mention here that as long as one is concerned only with the rigorous solution of the problem, the supplementary condition can be included in the initial condition[4] and will then be automatically preserved after the initial state of the system has been specified correctly. However, if the Schrödinger equation is solved by perturbation methods, a special treatment (such as the elimination of the longitudinal field) is needed to insure that the supplementary condition is satisfied by the approximate solution at all stages of approximation.

The first part of the present paper deals with the elimination of longitudinal field which is essentially not much different from that given by Koba, Tati, and Tomonaga.[1] The second part consists essentially of undoing the elimination, preserving, however, the identical satisfaction of the supplementary condition achieved in the first part. It seems that there should be a more direct way of obtaining the same results without following the round-about way of eliminating and then restoring the longitudinal field. The present derivation, however, shows the connection between Feynman's method and the conventional one in which the longtudinal field is eliminated.

In the following calculations the same notation as that of Schwinger's paper is used except that here in addition the unit $\hbar=c=1$ is in use. Therefore no detailed explanation of terms and concepts is given here that have been explained clearly in Tomonaga and Schwinger's papers. The state vector $\Psi[\sigma]$ of the system of electronic and electromagnetic fields satisfies the following generalized Schrödinger equation:

$$i\frac{\delta\Psi[\sigma]}{\delta\sigma(x)}=-j_\mu(x)A_\mu(x)\Psi[\sigma] \tag{1}$$

and the supplementary condition

$$\left[\frac{\partial A_\mu(x)}{\partial x_\mu}-\int_{\sigma(x)}D(x-x')j_\mu(x')d\sigma_\mu{}'\right]\Psi[\sigma]=0. \tag{2}$$

$A_\mu(x)$ can be expanded into the following Fourier integral

$$A_\mu(x)=\frac{1}{(2\pi)^{\frac{3}{2}}}\int[A_\mu(k)e^{i(kx)}+A_\mu{}^*(k)e^{-i(kx)}]\frac{d^3k}{k} \tag{3}$$

where $(kx)=k_0x_0-k_1x_1-k_2x_2-k_3x_3$, $x_\mu=(t,\mathbf{r})$ being the coordinates of any point in the space-time, and $A_\mu(x)=(\phi(t,\mathbf{r}),\mathbf{A}(t,\mathbf{r}))$ is the four-vector potential of the electromagnetic field. $\sigma(x)$ denotes an arbitrary space like surface passing through the point x_μ, and $\Psi[\sigma]$ is understood as a functional of σ. The meaning of other notations can easily be found in Schwinger's paper. $A_\mu(k)$ and $A_\mu{}^*(k)$ are q-numbers satisfying the following

* Now at University of Wisconsin.
[1] S. Tomonaga, Proc. Theor. Phys. **1**, 27 (1946); Koba, Tati, and Tomonaga, Proc. Theor. Phys. **2**, 101, 198 (1947).
[2] J. Schwinger, Phys. Rev. **73**, 416 (1948); **74**, 1439 (1948).
[3] R. P. Feynman, Phys. Rev. **74**, 939, 1430 (1948); and several papers still in the course of preparation.
[4] This follows from the fact that the supplementary condition and the Schrödinger equation are represented by operators commuting with each other. For earlier non-covariant derivation of the result see E. Fermi, Rev. Mod. Phys. **4**, 131 (1932); W. Heitler, *The Quantum Theory of Radiation* (Oxford University Press, London, 1944) §6.

commutation relations ($[A,B]=AB-BA$)

$$[A_0(k),A_0^*(k')]=-\tfrac{1}{2}k\delta(\mathbf{k}-\mathbf{k}')$$
$$[\mathbf{A}(k),\mathbf{A}^*(k')]=\tfrac{1}{2}k\delta(\mathbf{k}-\mathbf{k}'). \quad (4)$$

Introduce for each value of k_μ the following coordinate system: x_4 along any time-like direction, x_1 and x_2 perpendicular to each other and to both x_4 and k_μ and x_3 forms the fourth perpendicular direction which is parallel to $\mathbf{k}$, the space component of k_μ. Let $n_\mu^{(\alpha)}$ be unit vectors in the direction of $x_\alpha(\alpha=0,1,2,3)$ referred to any fixed coordinate system in the space-time. For different values of k_μ, the directions of $n_\mu^{(\alpha)}(k)$ are different. Introduce further the following two zero vectors:

$$n_\mu^{(\kappa)}(k)=1/\sqrt{2}[n_\mu^{(3)}(k)+n_\mu^{(0)}(k)],$$
$$n_\mu^{(l)}(k)=1/\sqrt{2}[-n_\mu^{(3)}(k)+n_\mu^{(0)}(k)]. \quad (5)$$

It can easily be verified that $(n^{(l)}n^{(l)})=(n^{(\kappa)}n^{(\kappa)})=0$ and $(n^{(\kappa)}n^{(l)})=-1$. $A_\mu(k)$ can then be written

$$A_\mu(k)=n_\mu^{(l)}A^{(l)}(k)+n_\mu^{(2)}A^{(2)}(k)+A_\mu'(k), \quad (6)$$

where

$$A_\mu'(k)=n_\mu^{(0)}A^{(0)}(k)+n_\mu^{(3)}A^{(3)}(k)$$
$$=n_\mu^{(\kappa)}A^{(\kappa)}(k)+n_\mu^{(l)}A^{(l)}(k), \quad (7)$$

and in coordinate space

$$A_\mu(x)=A_\mu^{(l)}(x)+A_\mu^{(2)}(x)+A_\mu'(x), \quad (6a)$$

and

$$A_\mu'(x)=A_\mu^{(3)}(x)+A_\mu^{(0)}(x)$$
$$=A_\mu^{(\kappa)}(x)+A_\mu^{(l)}(x), \quad (7a)$$

where

$$A_\mu^{(\alpha)}(x)=\int n_\mu^{(\alpha)}(k)[A^{(\alpha)}(k)e^{i(kx)}$$
$$+A^{*(\alpha)}(k)e^{-i(kx)}]\frac{d^3k}{k} \quad (\alpha=0,1,2,3,\kappa,l). \quad (8)$$

It can be shown from (4) that $A^{(\alpha)}(k)$ satisfy the following commutation relations

$$[A^{(\alpha)}(k),A^{*(\alpha)}(k')]=\tfrac{1}{2}g^{(\alpha)}k\delta(\mathbf{k}-\mathbf{k}') \quad (\alpha=0,1,2,3),$$
$$[A^{(l)}(k),A^{*(\kappa)}(k')]=-\tfrac{1}{2}k\delta(\mathbf{k}-\mathbf{k}'),$$
$$[A^{*(l)}(k),A^{(\kappa)}(k')]=-\tfrac{1}{2}k\delta(\mathbf{k}-\mathbf{k}'), \quad (8a)$$

(other commutators vanish) where $g^{(\alpha)}=-1$ when $\alpha=0$ and $g^{(\alpha)}=1$ when $\alpha=1,2,3$. This difference in sign of $g^{(0)}$ is important since it follows from (8a) that $A^{*(\alpha)}(k)$ should be considered as emission operator and $A^{(\alpha)}(k)$ as absorption operator when $\alpha\neq 0$, whereas $A^{(0)}(k)$ should be considered as emission operator and $A^{*(0)}(k)$ as absorption operator. This important fact should be borne in mind when applying Feynman's method.

The supplementary condition (2) will be satisfied if $\Psi[\sigma]$ is of the following form

$$\Psi[\sigma]=e^{i\chi[\sigma]}\Omega[\sigma], \quad (9)$$

where $\Omega[\sigma]$ is independent of $A^{(\kappa)}(k)$ and $A^{*(\kappa)}(k)$, i.e.,

$$A^{(l)}(k)\Omega[\sigma]=0, \quad A^{*(l)}(k)\Omega[\sigma]=0, \quad (9a)$$

and

$$\chi[\sigma]=\int_{-\infty}^{\sigma}j_\mu(x')A_\mu^{(\kappa)}(x')dx'. \quad (10)$$

It should be noted that χ contains operators at point x' which is on the past side of σ, whereas $\Omega[\sigma]$ on which χ is operated depends only on σ. One way of specifying the operation is to integrate χ with respect to x'. One finds readily

$$\chi=\int_\sigma j_\mu(x)B(x)d\sigma_\mu, \quad (11)$$

where

$$\frac{\partial}{\partial x_\mu}B(x)=A_\mu^{(\kappa)}(x), \quad (12)$$

or

$$B(x)=1/(2\pi)^{\frac{3}{2}}\int i[A^{(\kappa)}(k)e^{i(kx)}$$
$$-A^{*(\kappa)}(k)e^{-i(kx)}]d^3k/k^2. \quad (12a)$$

Then χ contains only operators referring to σ. An alternative way to specify the meaning of the operation is to follow the procedure of Dirac[5] who defines

$$j_\mu(x')A_\mu^{(\kappa)}(x')\Omega[\sigma]=j_\mu(x')A_\mu^{(\kappa)}(x')S[\sigma;\sigma']\Omega[\sigma'] \quad (13)$$

where σ' is a space like surface in the past side of σ and passing through the point x'. $S[\sigma;\sigma']$ is an unitary operator transforming a solution $\Omega[\sigma']$ of (1) at time σ' to the same solution $\Omega[\sigma]$ at time σ. $S[\sigma,\sigma']$ may contain other operators such as $j_\mu(x'')A_\mu^{(\alpha)}(x'')$, therefore care must be taken not to disturb the original order of different operators unless they commute. These two ways of specifying the meaning of operation are, of course, equivalent—at least in the following calculation only such properties of χ are used for which the equivalence of (10) with (11) is obvious.

Since from (6)–(8)

$$\partial A_\mu/\partial x_\mu=\partial A_\mu^{(l)}/\partial x_\mu=1/(2\pi)^{\frac{3}{2}}\int i[A^{(l)}(k)e^{i(kx)}$$
$$-A^{*(l)}(k)e^{-i(kx)}]d^3k/k,$$

and

$$\chi=\int_{-\infty}^{\sigma}j_\mu(x')dx'\int n_\mu^{(\kappa)}(k)[A^{(\kappa)}(k)e^{i(kx')}$$
$$+A^{*(\kappa)}(k)e^{-i(kx')}]d^3k/k.$$

It follows from Eq. (8)

$$\partial A_\mu/\partial x_\mu\chi=\int_{-\infty}^{\sigma}j_\mu(x')dx'\cdot\tfrac{1}{2}\int k_\mu[e^{i(k,x-x')}$$
$$+e^{-i(k,x-x')}]d^3k/k$$
$$=\int_{-\infty}^{\sigma}j_\mu(x')\frac{\partial}{\partial x_\mu}D(x-x')dx'$$
$$=\int_\sigma j_\mu(x')D(x-x')d\sigma_\mu', \quad (14)$$

[5] P. A. M. Dirac, Rev. Mod. Phys. **17**, 195 (1945).

where $(k,x-x')=k_0(x_0-x_0')-\mathbf{k}\cdot(\mathbf{x}-\mathbf{x}')$. If $\Omega[\sigma]$ is independent of $A^{(\kappa)}(k)$, and $A^{*(\kappa)}(k)$, or in other words, independent of $A^{(\kappa)}(x)$ then using (9a)

$$(\partial A_\mu/\partial x_\mu)e^{i\chi}\Omega[\sigma]=\int_\sigma j_\mu(x')D(x-x')d\sigma_\mu' e^{i\chi}\Omega[\sigma]. \quad (15)$$

This verifies that the supplementary condition is satisfied identically if (9a) is satisfied, i.e., if $\Omega[\sigma]$ is independent of $A^{(\kappa)}(x)$. It must now be shown that an $\Omega[\sigma]$ independent of $A^{(\kappa)}(x)$ is allowed by the Schrödinger Eq. (1).

It follows from (10)

$$e^{-i\chi}i(\delta/\delta\sigma)e^{i\chi}\Omega[\sigma]=i(\delta/\delta\sigma)\Omega[\sigma] -j_\mu(x)A_\mu^{(\kappa)}(x)\Omega[\sigma]. \quad (15a)$$

Since

$$\int_\sigma[j_\mu(x'),\ j_\alpha(x)]d\sigma_\mu'=0, \quad (15b)$$

$j_\mu(x')d\sigma_\mu'$ may be considered as commuting with $j_\alpha(x)$. Then with the help of the commutation relations (8a), it follows

$$e^{-i\chi}j_\mu A_\mu^{(\alpha)}e^{i\chi}=j_\mu A_\mu^{(\alpha)} \quad (\alpha=1,2,\kappa). \quad (16)$$

The following identity can easily be verified to be true

$$e^{-i\chi}j_\mu A_\mu^{(l)}e^{i\chi}=j_\mu A_\mu^{(l)}-[\chi,j_\mu A_\mu^{(l)}] +\frac{1}{2!}[\chi,[\chi,j_\mu A_\mu^{(l)}]] -\frac{1}{3!}[\chi,[\chi,[\chi,j_\mu A_\mu^{(l)}]]]+\cdots \quad (17)$$

From Eqs. (4), (12), and (15b), it follows, after some calculation,

$$[\chi,j_\mu A_\mu^{(l)}]=-\int j_\mu(x)j_\alpha(x')\mathfrak{L}_\mu(x-x')d\sigma_\alpha',$$

$$\mathfrak{L}_\mu(x-x')=\int n_\mu^{(l)}(k)[e^{i(k,x-x')}+e^{-i(k,x-x')}]\frac{d^3k}{k}. \quad (18)$$

It also follows from Eqs. (15b) and (18) that

$$[\chi,[\chi,j_\mu A_\mu^{(l)}]]=0.$$

Therefore, all the terms except the first two on the right-hand side of Eq. (17) vanish identically. Application of Eq. (17) on $\Omega[\sigma]$ gives further

$$e^{-i\chi}j_\mu A_\mu^{(l)}e^{i\chi}\Omega[\sigma]=-j_\mu A_\mu^{(l)}\chi\Omega[\sigma], \quad (19)$$

on account of the condition (9a). Finally the Schrödinger equation for $\Omega[\sigma]$ obtained by inserting (9) into (1) and using (15a), (16) and (19) is given by

$$i\frac{\delta\Omega[\sigma]}{\delta\sigma(x)}=-\sum_{r=1,2}j_\mu A_\mu^{(r)}\Omega[\sigma]+j_\mu A_\mu^{(l)}\chi[\sigma]\Omega[\sigma], \quad (20)$$

or, on inserting Eq. (18),

$$i\frac{\delta\Omega[\sigma]}{\delta\sigma(x)}=-\sum_{r=1,2}j_\mu A_\mu^{(r)}\Omega[\sigma] +\int_\sigma j_\mu(x)j_\alpha(x')\mathfrak{L}_\mu(x-x')d\sigma_\alpha'\Omega[\sigma]. \quad (21)$$

It is seen that the operators on the right hand side of (21) are independent of $A^{(\kappa)}(k)$ and $A^{*(\kappa)}(k)$. This furnishes the proof that (9a) is always satisfied if it is satisfied initially.

Equation (20) can be written in the following form

$$i\frac{\delta\Omega[\sigma]}{\delta\sigma(x)}=H(x)\Omega[\sigma], \quad (22)$$

where

$$H(x)=H_1(x)+H_2(x), \quad (23)$$

$$H_1(x)=-\sum_{r=1,2}j_\mu(x)A_\mu^{(r)}(x), \quad (24)$$

$$H_2(x)=-(-i)^2j_\mu(x)A_\mu^{(l)}(x)\int_\sigma j_\alpha(x')B(x')d\sigma_\alpha'. \quad (25)$$

Following Schwinger and Dyson,[6] the solution of (22) can be written down immediately:

$$\Omega[\sigma]=S[\sigma]\Omega_0, \quad (26)$$

$$S[\sigma]=1-i\int_{-\infty}^{\sigma}H_1(x_1)dx_1 +(-i)^2\int_{-\infty}^{\sigma}H(x_1)dx_1\int_{-\infty}^{\sigma_1}H(x_2)dx_2+\cdots. \quad (27)$$

The general term of Eq. (27) can be written:

$$(-i)^n\int^{\sigma}H(x_1)dx_1\int H(x_2)dx_2\cdots\int H(x_n)dx_n, \quad (28)$$

where the limits of the integrals have been omitted, it being understood that the integration of each factor $H(x)$ is from $-\infty$ to a space-like surface passing through the variable point x'' of the factor $H(x'')$ just in front of $H(x)$, with the order of the H's according to the order of time.

On inserting Eq. (23), the integrand of (28) can further be expanded into different combinations of products of factors H_1 and H_2. Consider first the terms of (28) which contain H_1 only and which contain no virtual emission and re-absorption of photons. (This does not exclude the processes in which a transverse virtual photon was emitted but has not been absorbed at time σ.) One of these terms can be written in the following form

$$I_n=(-i)^n\int^{\sigma}H_1(x_1)dx_1 \times\int H_1(x_2)dx_2\cdots\int H_1(x_n)dx_n. \quad (29)$$

[6] F. J. Dyson, Phys. Rev. **75**, 486 (1949).

Let $I_n(i)$ be another term of (27) constructed from (29) by adding a factor $\int H_2(x')dx'$ between $\int H_1(x_i)dx_i$ and $\int H_1(x_{i+1})dx_{i+1}$:

$$I_n(i)=(-i)^{n+2}\int^{\sigma} H_1(x_1)dx_1\int H_1(x_2)dx_2\cdots \times\int H_1(x_i)dx_i\int j_\mu(x')A_\mu^{(1)}(x')dx' \times\int_{\sigma(x')} j_\alpha(x'')B(x'')d\sigma_\alpha''\int H_1(x_{i+1})dx_{i+1}\cdots \times\int H_1(x_n)dx_n. \quad (30)$$

Now since $[A_\mu^{(1)}(x'),H_1(x)]=0$ and because of Eq. (15b), the added factor commutes with all the other factors of Eq. (30). By using the following identity

$$\int_{\sigma_i} j_\mu(x')B(x')d\sigma_{i\mu}'=\int_{\sigma_{i+1}}^{\sigma_i} j_\mu(x')A_\mu^{(s)}(x')dx' -\int_{\sigma_{i+1}} j_\mu(x')B(x')d\sigma'_{i+1,\mu}, \quad (31)$$

it can easily be seen that

$$\int_{\sigma(x')} j_\alpha(x')B(x')d\sigma'\int_{-\infty}^{\sigma(x')} H_1(x_{i+1})dx_{i+1} =\int_{-\infty}^{\sigma(x')} j_\alpha(x'')A_\alpha^{(s)}(x'')dx''\int_{-\infty}^{\sigma(x'')} H_1(x_{i+1})dx_{i+1} +\int_{-\infty}^{\sigma(x)} H_1(x_{i+1})dx_{i+1}\int_{\sigma_{i+1}} j_\alpha(x')B(x')d\sigma_\alpha'. \quad (32)$$

This relation can be used repeatedly to push the surface integral in Eq. (30) to the right side of the last factor $\int H_1(x_n)dx_n$ and then replace it by a volume integral Eq. (10) integrated from minus infinity to σ_n. The final expression of Eq. (30) will contain no surface integral and is given by

$$I_n(i)=\sum\int^{\sigma} H_1(x_1)dx_1\int H_1(x_2)dx_2\cdots \times\int H_1(x_i)dx_i\int j_\mu(x')A^{(1)}(x')dx' \times\int H_1(x_{i+1})dx_{i+1}\cdots\int j_\mu(x'')A^{(s)}(x'')dx''\cdots \times\int H_1(x_n)dx_n, \quad (33)$$

where $\sum$ means summation over all possible positions of $\int j_\mu(x'')A^{(s)}(x'')dx''$ between $\int H_1(x_i)dx_i$ and $\int H_1(x_n)dx_n$.

It will now be shown that the contribution due to the factors

$$\int j_\mu(x')A_\mu^{(1)}(x')dx', \quad \int j_\mu(x'')A_\mu^{(s)}(x'')dx'' \quad (34)$$

in Eq. (33) represent just the virtual exchange of longitudinal photons between σ' and σ''. Since from (7a)

$$A_\mu^{(1)}(x)+A_\mu^{(s)}(x)=A_\mu^{(0)}(x)+A_\mu^{(3)}(x),$$

it follows from the commutation relation that

$$A_\mu^{(1)}(x')A_\alpha^{(s)}(x'')+A_\mu^{(s)}(x')A_\alpha^{(1)}(x'') =A_\mu^{(0)}(x')A_\alpha^{(0)}(x'')+A_\mu^{(3)}(x')A_\alpha^{(3)}(x'') =\sum_{s=0,3}A_\mu^{(s)}(x')\cdot\sum_{t=0,3}A_\alpha^{(t)}(x'').$$

$A_\mu^{(s)}(x)A_\alpha^{(1)}(x'')$ vanishes identically because of the condition (9a). The above equation becomes

$$A_\mu^{(1)}(x')A_\alpha^{(s)}(x'')=\sum_{s=0,3}A_\mu^{(s)}(x')\cdot\sum_{t=0,3}A_\alpha^{(t)}(x''). \quad (35)$$

Therefore, the two factors (34) can be replaced by

$$\int j_\mu(x')]\textstyle\sum_s' A_\mu^{(s)}(x')dx', \qquad \int j_\mu(x'')\textstyle\sum_s' A_\mu^{(s)}(x'')dx'' \quad (36)$$

respectively, where the summation $\sum'$ is from 3 to 4. Now from (27), new groups of terms can be picked out which contain only H_1-factors and represent the same processes as (29), but in addition there is a virtual exchange of transverse protons between $\sigma(x')$ and $\sigma(x'')$. It is easily seen that the contribution of this new group of terms is just to replace $\sum'$ by another summation over all polarizations from 0 to 3.

So far only terms involving one pair of virtual emission and reabsorption have been considered. Let $I_n(i,j)$ be another term of (27) constructed from (29) by adding two H_2-factors in the following way:

$$I_n(i,j)=(-i)^{n+4}\int^{\sigma} H_1(x_1)dx_1\cdots\int H_1(x_j)dx_j \times\int j_\nu(x_b')A_\nu^{(1)}(x_b')dx_b'\int_{\sigma(x_b')} j_\beta(x_b'')B(x_b'')d\sigma_{b\beta}''\cdots \times\int H_1(x_i)dx_i\int j_\mu(x_a')A_\mu^{(1)}(x_a')dx_a' \times\int_{\sigma(x_a')} j_\alpha(x_a'')B(x_a'')d\sigma_{a\alpha}'\cdots\int H_1(x_n)dx_n. \quad (37)$$

It follows from Eq. (15b) that $j_\mu(x_a')dx_a'$ and $j_\nu(x_b')dx_b'$ commute with each other and also with all the other current vectors in Eq. (37). The operators $A_\mu^{(l)}(x_a')$, $B(x_a'')$, $A_\nu^{(l)}(x_b'')$ and $B(x_b'')$ commute with all the other operators in Eq. (37). It is seen from the foregoing result that the B's represent the emission operators of the longitudinal photon* and the $A_\mu^{(l)}$'s represent the corresponding absorption operator. The order of these operators in (37) shows that $A_\mu^{(l)}(x_a')$ absorbs only the photon emitted by $B(x_a'')$ and $A_\nu^{(l)}(x_b')$ absorbs only the photon emitted by $B(x_b'')$. If the order of $B(x_b'')$ and $A_\mu^{(l)}(x_a')$ is changed, new possibility arises that the photon emitted by $B(x_b'')$ may be absorbed by $A_\mu^{(l)}(x_a')$, which process is not included in (37). This situation is avoided if the photon emitted by $B(x_b'')$ is marked so that it cannot be absorbed by $A_\mu^{(l)}(x_a')$. This amounts formally to considering the pairs $A_\mu^{(l)}(x_a')$, $B(x_a'')$ and $A_\nu^{(l)}(x_b')$, $B(x_b'')$ as emission and absorption operators of two different kinds of particles a and b. This is the same as the rule introduced in Dyson's paper to group the operators into pairs with operators in different pairs commuting with each other. According to this rule the factor $N^{\frac{1}{2}}$ and $(N+1)^{\frac{1}{2}}$ of the matrix elements of the emission and absorption operators under customary convention should now be replaced by unity, where N is the number of photons in the same state. This reduction in the strength of the operators will be compensated exactly by the increase in the number of precesses due to different permutation of the order of the operators.

If the new rule is used, the argument that leads from (30) to (33) and (34) can be applied without any modification in the present case. Therefore Eq. (37) becomes

$$I_n(i,j)=(-i)^{n+4}\sum_p\int^\sigma H_1(x_1)dx_1\int H_1(x_2)dx_2\cdots$$
$$\times\int H'(x_a')dx_a'\cdots\int H'(x_a'')dx_a''\cdots$$
$$\times\int H'(x_b')dx_b'\cdots\int H'(x_b'')dx_b''\cdots\int H_1(x_n)dx_n,$$
$$H'(x)=\sum_{s=1}^{4}j_\mu(x)A_\mu^{(s)}(x), \quad (38)$$

where the summation $\sum_p$ is taken over all the positions of the four $H'(x)$ factors among all the other $H_1(x)$-factors. It should be understood that $H'(x_a')$ and $H'(x_a'')$ form a pair of virtual emission and absorption operators and $H'(x_b')$ and $H'(x_b'')$ form another pair whereas all the other H_1-factors contribute no virtual emission-reabsorption process.

The above result can easily be extended to the case when more than two pairs of virtual emission-absorption occur. It will not be difficult to see that terms constructed from Eq. (29) in this way will eventually include all the terms of Eq. (27). The general procedure of solving Eq. (22) can now be stated as follows:

First solve the following Schrödinger equation

$$\frac{\delta\Omega[\sigma]}{\delta\sigma(x)}=H(x)\Omega[\sigma], \quad H(x)=-\sum_s j_\mu A_\mu^{(s)}, \quad (39)$$

with the summation unspecified and obtain the following formal solution

$$\Omega[\sigma]=S[\sigma]\Omega_0$$
$$S[\sigma]=1-i\int_{-\infty}^{\sigma}H(x_1)dx_1+(-i)^2\int_{-\infty}^{\sigma}H(x_1)dx_1$$
$$\times\int_{-\infty}^{\sigma_1}H(x_2)dx_2+\cdots+(-i)^n\int_{-\infty}^{\sigma}H(x_1)dx_1$$
$$\times\int_{-\infty}^{\sigma_1}H(x_2)dx_2\cdots\int_{-\infty}^{\sigma_{n-1}}H(x_n)dx_n+\cdots. \quad (40)$$

Then the summation is specified as taken over all transverse and longitudinal polarizations for all the processes in which a photon has been emitted and then reabsorbed, and taken only over the transverse polarizations for all the other processes, namely, the processes in which either a real photon is emitted or absorbed or a virtual photon has been emitted but has not yet been absorbed. Equation (40) satisfies the supplementary condition identically even when a finite number of terms of $S[\sigma]$ are used as in the usual perturbation theory.

It should be noted that although emission and reabsorption of longitudinal photons can be considered as actually taken place in the *past*, the explicit expression of $S[\sigma]$ does not depend on the variables of the virtual longitudinal photons, as should be the case according to the condition (9a). In other words, no virtual longitudinal photon should be considered as existing at the *present*. On the other hand since the processes in which a transverse photon has been emitted but has not yet been absorbed are also included in Eq. (40), the expression of $S[\sigma]$ should therefore also depend on the variables of these virtual transverse photons. If however σ is put equal to infinity in Eq. (40), this remaining distinction between longitudinal and transverse virtual photons will disappear completely. $S[\infty]$ is just the representation used by Feynman.

It should further be pointed out that, strictly speaking, Ω_0 in (40) should satisfy the following condition as required by Eq. (9a):

$$A^{(l)}(k)\Omega_0=0, \quad A^{*(l)}(k)\Omega_0=0. \quad (41)$$

*The vacuum has been considered as free from longitudinal photons. Actually from (9a), vacuum should be considered as having an indefinite number of longitudinal photons. However this makes no difference on final results as far as virtual processes are concerned.

Now Ω_0 can be put into the following form

$$\Omega_0=\Omega_0'\Omega_0''$$

where Ω_0' depends only on the variables of the transverse photons and Ω_0'' depends only on those of the longitudinal photons belonging to the vacuum. Equation (41) becomes

$$A^{(l)}(k)\Omega_0''=0, \quad A^{*(l)}(k)\Omega_0''=0. \tag{42}$$

Since, as pointed out in the footnote before, the solution Eq. (40) does not depend on the exact form of Ω_0'', the factor Ω_0'' can simply be omitted from Eq. (40). This means that instead of choosing Ω_0 to satisfy Eq. (41), one can simply consider it as independent of the variables of the longitudinal photons. In other words, vacuum is considered as containing no longitudinal photons at all. This is just the convention adopted in the usual treatment in which the longitudinal field has been replaced by the Coulomb interaction.

In conclusion, the author wishes to express his thanks to Professor Bethe for helpful suggestions and discussions and also to Professor Feynman for detailed exposition of his theory before publication.

PHYSICAL REVIEW VOLUME 76, NUMBER 3 AUGUST 1, 1949

The Bose-Einstein Condensation for Thin Films

M. F. M. OSBORNE
Naval Research Laboratory, Washington, D. C.

(Received December 6, 1948)

The distinction is made between a condensation temperature in the thermodynamic sense, where the thermodynamic functions have a discontinuity, and an abrupt accumulation (in the statistical mechanical sense) of particles in the ground state of a system. The criterion for the latter is that an integral will not approximate one term of a sum. The problem of a thin film of gas is solved to illustrate this distinction. For films thicker than a critical thickness a condensation occurs at the same temperature as that for bulk material. The thinner films are effectively two dimensional and have an abrupt accumulation temperature lower than the bulk condensation temperature. Films of liquid helium are briefly considered.

INTRODUCTION

CONSIDERABLE interest has been provoked by London's proposal[1] that the λ-phenomenon of helium is a Bose-Einstein condensation, or accumulation of a finite fraction of all the particles in the ground state of a potential hole of macroscopic dimensions. Tisza[2] has extended this suggestion to discuss helium in terms of the hydrodynamics of a two-fluid system, and more recently Ogg[3] has proposed that phenomena which he has observed in metal-ammonia solutions and possibly also the phenomenon of superconductivity might be explained by the condensation of a gas of electron pairs formed from the free electrons of the material. It is the purpose of this paper to examine in some detail the conditions under which these condensations occur and to discuss some examples of physical interest. The particular examples we shall discuss are: (1) Three-dimensional gas of uncharged particles in a thin film, (2) Two-dimensional gas, and in a subsequent paper (3) Gas of charged particles in a magnetic field, neglecting electrostatic interactions.

Condensation and Accumulation Temperatures

In classical thermodynamics a condensation temperature implies a discontinuity in one of the thermodynamic functions which describe the system. Such discontinuities are also described by phase changes of first, second, third order, depending on whether the function or one of its higher derivatives becomes discontinuous.

From the standpoint of statistical mechanics we shall define an accumulation temperature T_0 as a temperature at which a finite fraction of all particles begin to accumulate in just one state or set of states with the same energy. By "finite" fraction we mean less than, but not a great deal less than unity, or very much greater than $1/N$, N being the total number of particles. We can speak of an "abrupt" accumulation if the fraction in a given state changes from "small" to "finite" in a small temperature range $\Delta T \ll T_0$. Such finite fractions can usually be expressed as $1-(T/T_0)^n$, $T<T_0$. We speak of a gradual accumulation if it occurs over a range $\Delta T \simeq T_0$. Only in the first case would it be appropriate to speak of a well-defined accumulation temperature, in the second case one might speak of an accumulation temperature band. Consider the expression for N, the total number of particles in a Bose-Einstein assembly.

$$N=\sum_{k,l,m} 1/(\exp(E(k,l,m)/kT+\alpha)-1)$$
$$=\sum_{k,l,m} f(E(k,l,m),\alpha,T), \tag{1}$$

where k, l, m are quantum numbers specifying the level of energy $E(k, l, m)$ and α is defined implicitly as a function of T by this relation.

[1] F. London, Phys. Rev. 54, 947 (1938).
[2] L. Tisza, Phys. Rev. 72, 838 (1947).
[3] R. A. Ogg, Preliminary Report to ONR, "Electronic Processes in Liquid Dielectric Media. The Constitution of Metal Ammonia Solutions." April 11, 1948, p. 20.

If the value of $\sum_{k,l,m} f(E(k,l,m),\alpha,T)$ can be replaced by $\int\int\int dkdldm f(E(k,l,m),\alpha,T)$ there is no accumulation of particles in any particular energy state. In general, on replacing a sum by an integral we have

$$\sum_{m=a}^{b} f(m)=\int_{a-\frac{1}{2}}^{b+\frac{1}{2}} f(m)dm-f'(m)/24\Big|_a^b, \qquad (2)$$

valid provided

$$f(n+\tfrac{1}{2})-f(n-\tfrac{1}{2})-f'(n)\ll f(n), \qquad (3)$$

where $a<n<b$, and n refers to any of the three indices k, l, m of summation.

The condition in Eq. (3) may fail in either of two ways: (a) If it fails for every value of n in the interval a, b, (as will be the case if in (1) kT is of the order of the spacing of the levels), then there is a gradual accumulation of the particles with diminishing temperature in the lowest energy state; (b) (3) may fail only for the lowest value of n in the interval a, b. If the value of the temperature at which this occurs is well defined, we have an abrupt accumulation of particles in the lowest state. If this accumulation temperature depends only on N/V as $N\to\infty$, i.e. is independent of the size of the system, we may expect discontinuities in the thermodynamic properties at this temperature. It is then a condensation temperature. This was first shown by Einstein,[4] and subsequently examined in detail by others.[5] Even when weak interactions between the particles are included the condensation occurs.[6]

THE IDEAL GAS IN A THIN FILM

In order to illustrate these points, let us consider the case of an ideal three-dimensional Bose-Einstein gas confined to a thin film. We shall show, using the above consideration, how thin the film must be for the well-known three-dimensional condensation to be prevented, and that for still thinner films (effectively two-dimensional gas[7]) an *abrupt accumulation* can still occur.

For the thin film, the expression for the total number of particles of mass M' in a box ($\psi=0$ on walls) of dimensions

$$L_x=L_y=L, \quad L_z=L/M, \quad M\gg 1$$

is

$$N=\sum_{k,l,m=1}^{\infty} 1/(\exp((k^2+l^2+m^2M^2)\epsilon/kT+\alpha)-1), \qquad (4)$$
$$\epsilon=h^2/8M'L^2.$$

Assuming for the moment that all these summations can be replaced by integrals (despite the large energy interval in m), we shall first examine the conditions under which the lower limits of integration on k, l, m can be replaced by 0, instead of $\frac{1}{2}$ as required by (2). This will give us an expression for N equivalent to that for a cubical box, plus correction terms which when large indicate that the film is too thin to be considered a three-dimensional system. The condition for largeness of the correction term will turn out to be the same as the condition forbidding replacement of a sum (over m) by an integral. From (4)

$$N=\int_{\frac{1}{2}}^{\infty}\int_{\frac{1}{2}}^{\infty}\int_{\frac{1}{2}}^{\infty} dkdldm \Big/ (\exp((k^2+l^2+m^2M^2)\epsilon/kT+\alpha)-1). \qquad (5)$$

Letting

$$k^2+l^2+M^2m^2=\rho^2, \quad \eta=(\tfrac{1}{2}+M^2/4)^{\frac{1}{2}}\simeq M/2$$

$$N=(1/M)\int_{\eta}^{\infty} (\pi/2)\rho^2 d\rho/(\exp(\rho^2\epsilon/kT+\alpha)-1), \qquad (6)$$

where the factor $\pi/2$ is a consequence of the fact we use box rather than periodic boundary conditions, and so integrate only over one octant in k, l, m space. Letting $\rho=\rho'+\eta$, and expanding that part of the exponential which is linear in ρ', and using the definition

$$U(p,\alpha)=(1/\Gamma(p+1))\int_0^{\infty} dz z^p/(\exp(z+\alpha)-1)$$
$$=\sum_{j=1}^{\infty}\exp(-\alpha j)/j^{p+1}, \qquad (7)$$

we find, after some manipulation

$$N=(\pi/2M)(kT/\epsilon)^{\frac{1}{2}}[\Gamma(3/2)U(\tfrac{1}{2},\eta^2\epsilon/kT+\alpha)/2 +\eta(\epsilon/kT)^{\frac{1}{2}}U(0,\eta^2\epsilon/kT+\alpha) +\eta^2\Gamma(1/2)(\epsilon/2kT)U(-\tfrac{1}{2},\eta^2\epsilon/kT+\alpha)] +\text{Order }(\eta(\epsilon/kT)^{\frac{1}{2}}). \qquad (8)$$

The four terms of (8) come in order from the three terms of $\rho^2=\rho'^2+2\eta\rho'+\eta^2$ in the numerator of (6) and the linear term in ρ' in the expansion of the denominator, the last being valid so long as $\eta\epsilon\rho'/kT$ is small in the region of the principal contribution to the integrand. This is so if $\eta\epsilon/kT$ is small. If one takes into account the following properties of the U functions,

$$U(\tfrac{1}{2},\alpha)\simeq U(\tfrac{1}{2},0),$$
$$U(0,\alpha)\simeq -\ln\alpha,$$
$$U(-\tfrac{1}{2},\alpha)\simeq\alpha^{-\frac{1}{2}},$$

for

$$0<\alpha\ll 1, \qquad (9)$$

and compares the above formulas with those of reference 1, one can easily verify the following statements. T_{01} is the condensation temperature for the three-dimensional case given in reference 1.

(1) For $\alpha>0$ and $\eta\epsilon/kT\ll 1$, $T>T_{01}$, the 2nd, 3rd,

[4] A. Einstein, Ber. Berl. Akad. (1924), 261; (1925), 3.
[5] R. H. Fowler and H. Jones, Camb. Phil. Soc. Proc. 34, 573 (1938).
[6] L. I. Shiff, Phys. Rev. 59, 758 (1941).
[7] Correspondence and conversation with F. London on this problem led to the distinction between "condensation" and "accumulation."

and 4th terms of Eq. (8) are negligible, and the first term gives just the conditions for determining α for the gas in a cubical box, given in reference 1.

(2) For $\alpha \leq 0$ and $\eta\epsilon/kT \ll 1$, the 2nd, 3rd and 4th terms of (8) are still negligible, and the first term determines the condensation temperature T_{01} as given in reference 1. Below this temperature, the condition (3) for integrating k, l or m fails for $k=l=m=1$. The first term of the summation must be separated from the integral, and α is determined by

$$\alpha+(2+M^2)\epsilon/kT=1/N(1-(T/T_{01})^{\frac{3}{2}}.$$

(3) For $\eta\epsilon/kT \simeq 1$, there is no condensation phenomenon. The 2nd, 3rd and 4th terms are not negligible, but (8) cannot be used to determine α, as $\eta\epsilon/kT \simeq 1$ is just the condition for a gradual accumulation in the lowest z direction level ($m=1$) and the failure of the integration condition (3) for all values of m.

(4) For $\eta\epsilon/kT \gg 1$ practically all of the particles are in the $m=1$ state, the gas can properly be considered as two dimensional, and must be reexamined for integrability on k and l.

Application to Liquid Helium

Before proceeding to a discussion of the two-dimensional case we can estimate for helium how thin a film has to be before condensation will be prevented. If $\eta\epsilon/kT \simeq 1$ we find for $T=T_{01}=3.4°$ (theoretical), $L_z \simeq 10^{-7}$ cm. This is small compared to the observed thickness of 5.10^{-6} cm for superfluid helium films.[8] Therefore, the observed thickness of superfluid helium films is not in contradiction with the idea that superfluidity is a consequence of a Bose-Einstein condensation. This calculation ignores the effect of the surface forces of the material on which the film lies in modifying the energy levels.

THE TWO DIMENSIONAL IDEAL GAS

Though primarily of academic interest, this problem has been the subject of some controversy, and is illuminating in showing the distinction between an abrupt accumulation and a condensation. It is also suggestive of the nature of the effects of geometry and impurities. The expression determining α for a square film is

$$N=\sum_{k,\,l=1}^{\infty} 1/(\exp((k^2+l^2)\epsilon/kT+\alpha)-1),$$
$$L_x=L_y=L, \quad \epsilon=h^2/8mL^2. \qquad (10)$$

If the conditions (3) for replacing the sums over k, l by integrals are met we have

$$N=\int_{\frac{1}{2}}^{\infty}\int_{\frac{1}{2}}^{\infty} dkdl \Big/ (\exp((k^2+l^2)\epsilon/kT+\alpha)-1) \qquad (11)$$

$$=-(\pi kT/4\epsilon)\ln(1-\exp(-\alpha')), \qquad (12)$$

where by definition

$$\alpha' \equiv \epsilon/kT+\alpha.$$

The expression (12), determining α, unlike its three dimensional analogue, does have a solution for α for all values of T. In fact for α small (low temperatures) we find

$$\alpha=\exp(-4\epsilon N/\pi kT)-\epsilon/kT, \qquad (13)$$

or in terms of α'

$$\alpha'=\exp(-T_{01}'/T), \qquad (14)$$

where by definition

$$T_{01}'=h^2N/2\pi mkS,$$
$$S=L_xL_y.$$

T_{01}' is very nearly the condensation temperature for a three-dimensional gas whose surface density is the same as that for the two dimensional case. But T_{01}' is not a condensation temperature in this problem.

However, it is not legitimate, in view of the integration criterion (3) to use the above expression (13) for $\alpha < \epsilon/kT$. When $\alpha < \epsilon/kT$, we must use

$$N=1/(\exp(2\epsilon/kT+\alpha)-1)$$
$$+\int_{3/2}^{\infty}\int_{3/2}^{\infty} dkdl \Big/ (\exp((k^2+l^2)\epsilon/kT+\alpha)-1), \qquad (15)$$

$$N=1/(\alpha'+3\epsilon/2kT)$$
$$-(\pi kT/4\epsilon)\ln(1-\exp(-5\epsilon/2kT-\alpha')). \qquad (16)$$

In Eq. (16) the first term represents the population of the ground state and the second term represents the population of all the higher states. We shall continue the discussion in terms of α' since it is the behavior of this quantity as a function of T, rather than α, which will simplify the argument. Let us ask at what temperature T_{02}', where we expect $T_{02}' \ll T_{01}'$, Eqs. (16) and (12) give different results for α', so that for $T < T_{02}'$ we must use the more exact expression Eq. (16).

T_{02}' is a temperature such that $\alpha'(T_{02}')=(5\epsilon/2)/kT_{02}'$. To see this we first observe that by (14) α' is a very violent function of the temperature for $T \ll T_{01}'$. Thus, since $T_{02}' \ll T_{01}'$, at temperatures slightly above T_{02}', α' dominates the logarithm in (16), and (16) and (12) are equivalent. However, at temperatures slightly less than T_{02}' in (16), the logarithm in Eq. (16) is practically independent of α'. Then (16) and (12) give different results for α', so one must use the more exact expression, Eq. (16), in which α' will primarily be determined by the first term.

Finally, we remark that the condition to determine T_{02}', $\alpha'(T_{02}')=5\epsilon/2kT_{02}'$ giving the temperature at which (16) and (12) begin to disagree, and the condition to use Eq. (16) given by $\alpha \simeq \epsilon/2kT_{02}'$ for the failure of the integration condition in Eq. (3), will in practice give almost exactly the same numerical value for T_{02}'. The reason for this is that α' is such a violent function of the

[8] J. G. Daunt and K. Mendelssohn, Proc. Roy. Soc. **170**, 423, 429 (1939).

temperature in the vicinity of T_{02}' that both of the equalities $\alpha'(T)=5\epsilon/2kT$ and $\alpha(T)=\epsilon/2kT$ are met in a very small temperature range.

Let us now determine what the relative populations of the ground, and all higher states are, above and below T_{02}'. Above T_{02}', since the right-hand side of Eq. (12) (the total population) and the second term of Eq. (16) agree, we see that the population of the ground state (1st term of Eq. (16)) is negligibly small. Below T_{02}' we have that the population of the higher states (2nd term of Eq. (16)), since $\alpha'\ll\epsilon/kT$, is $\simeq MT\ln MT$, where $M\sim k/\epsilon$ is *large*. Now $MT\ln MT$ varies approximately linearly in T, since its principal variation with T is in the factor of the logarithm. Moreover, it must provide, at the temperature T_{02}', practically all of the particles N, since above T_{02}' few of the particles are in the ground state. Therefore, we are compelled to conclude that, for $T<T_{02}'$ the population of the higher states must vary approximately like NT/T_{02}', and since the total number of particles must add up to N the ground state population varies like $N(1-T/T_{02}')$. In other words, since in Eq. (16), the second term is independent of α' (for $T<T_{02}'$, $\alpha'\ll 5\epsilon/2kT$) and is linear in T (like NT/T_{02}'), α' in the first term must vary in just such a way that the first term makes the total number of particles add up to N.

We, therefore, conclude that T_{02}' must be an accumulation temperature. We do not yet know how abrupt it is, and if it is also a condensation temperature.

To answer these questions we first determine T_{02}' by substituting $\alpha'=5\epsilon/2kT$, $T=T_{02}'$ in (16) and solving for T_{02}'. Doing this one finds

$$T_{02}'=T_{01}'(1+\delta)/\ln N, \tag{17}$$

where δ is small, of order $1/\ln N$. This shows that T_{02}' is not a condensation temperature since $T_{02}'\to 0$ as $N\to\infty$.

As an accumulation temperature T_{02}' is moderately "abrupt." To show this one calculates from Eq. (16) the relative population of ground and excited state *at* the temperature T_{02}', and also the maximum departure from linearity in T of the second term of (16), as α' varies in the range $\alpha'=5\epsilon/2kT$ to $\alpha'=-3\epsilon/2kT$ (the lowest allowed value according to first term of (16)).

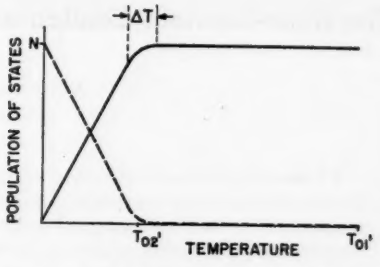

FIG. 1. Populations of the ground state (broken line) and all higher states (full line) of a two-dimensional B. E. gas. T_{01}' is the approximate condensation temperature of a three-dimensional B. E. gas of the same surface density.

Doing this one finds that the band of transition ΔT from condition "above" T_{02}' (negligible number of particles in ground state) to condition "below" T_{02}' (the ground state population $\simeq N(1-T/T_{02}')$) is given by

$$\Delta T\simeq T_{02}'/\ln N.$$

This means T_{02}' is a moderately abrupt accumulation temperature. Thus, if one had a "surface gram molecule" of material, $N=(N_{\text{Avogadro}})^{\frac{1}{2}}$ the accumulation at T_{02}' would occur at a temperature of 1/35 the corresponding three-dimensional condensation temperature, and in a temperature range about 3 percent of T_{02}' wide. All these conclusions are summarized in Fig. 1.

To interpret these results, one can say that in any physical situation where these calculations would be applicable, the results would be sensitive to any boundaries or impurities on the surface which would tend to modify the lowest energy state and break up the total number of particles N into subsystems. Effects of this type really represent the essence of surface and geometry effects in calculating from a statistical mechanical standpoint the properties of matter in the bulk. For example, one ordinarily considers the condensation temperature of water to be independent of the amount of material, but a moment's reflection shows that this is only approximately true. For small drops the condensation temperature (water-steam) is higher because of the increased pressure of surface tension. In this case, the condensation temperature also goes down (but not to zero) with an increased amount of material.

The Bose-Einstein Condensation for Charged Particles in a Magnetic Field

M. F. M. OSBORNE
Naval Research Laboratory, Washington, D. C.
(Received December 6, 1948)

The condensation and accumulation phenomena of charged Bose-Einstein particles in a magnetic field are examined, neglecting electrostatic interactions. For weak fields a single condensation occurs at the same temperature as that for uncharged particles; for strong fields there is a separate lower accumulation temperature, indicating the accumulation of particles in the lowest translational state. The total energy, free energy, and polarization are calculated, and applied to the properties of a gas of electron pairs, and a solution of deuterons in a metal, these being systems whose low temperature behavior might show a Bose-Einstein condensation. It is shown that the Bose-Einstein condensation of free electron pairs cannot provide a theory of superconductivity.

INTRODUCTION

IN the preceding paper[1] the distinction was made between a condensation in the thermodynamic sense, and an accumulation in the statistical mechanical sense. In this paper we use the conceptions and approximations there discussed to examine the properties of charged Bose-Einstein particles in a magnetic field, neglecting the effect of electrostatic interactions but including, where required, spin and intrinsic magnetic moment. We shall calculate the distribution of the population over the different classes of states, the total energy, the free energy, and the polarization.

We repeat here two expressions from *I* for convenience. To replace a sum by an integral we have

$$\sum_{m=a}^{b} f(m)=\int_{a-\frac{1}{2}}^{b+\frac{1}{2}} f(m)dm-f'(m)/24\Big|_{a}^{b}. \quad (1)$$

It is valid to use this approximation provided that for every point n within the interval, $a\leq n\leq b$

$$f(n+\tfrac{1}{2})-f(n-\tfrac{1}{2})-f'(n)\ll f(n). \quad (2)$$

For f of the form $1/(\exp(E(n)/kT+\alpha)-1)$, i.e. the B. E. integrand, it was found that if this criterion failed for one value of n in the interval (usually the lowest one) we could expect an abrupt accumulation of particles in the corresponding quantum state, and possibly a condensation. If it failed for every value we could expect a gradual accumulation in the lowest state.

THE GAS OF IONS IN A MAGNETIC FIELD, WITHOUT SPIN

Consider an assembly of N particles of mass m, charge e in a cylindrical container of volume V, radius R, height L with a magnetic field H along the axis. It is assumed that the energy levels which the particles occupy are given by the strength of the magnetic field and dimension L alone. Thus, we neglect electrostatic interactions, and ask: What is the behavior of this system as a function of the thermodynamic variables H and T? The energy levels are given by[2]

$$E(l, n_1, n_3)=\mu H(2(l+\tfrac{1}{2})+n_1+|n_1|)+\epsilon n_3^2$$
$$\epsilon=h^2/8mL^2, \quad \mu=eh/4\pi mc. \quad (3)$$

Let

$$g=\pi eHR^2/hc.$$

α is determined by

$$N=\sum_{n_1=-g}^{-1}\sum_{l=0}^{\infty}\sum_{n_3=1}^{\infty} 1/(\exp(E(l, n_1, n_3)/kT+\alpha)-1), \quad (4)$$

where the limits of summation on n_1, the azimuthal quantum number are determined by correspondence principle arguments.[2,3] l is the orbital quantum number and n_3 the translational quantum number for motion along the field.

Definitions and Approximations

In evaluating (4) we will utilize the following definitions (see Fig. 1):

(1) $U(p,\alpha)=(1/\Gamma(p+1))$

$$\times\int_0^{\infty} dzz^p/(\exp(z+\alpha)-1) \quad (5)$$

$$=\sum_{j=1}^{\infty}\exp(-\alpha j)/j^{p+1}. \quad (6)$$

(2) The temperature T_{01}, below which we must write separately the lowest term ($l=0$) in the integration over l (failure of Eq. (2))

$$T_{01}=(N/VU(\tfrac{1}{2}, 0))^{\frac{2}{3}}(h^2/2\pi mk). \quad (7)$$

T_{01} is also the condensation temperature in the absence of a field.[4]

(3) T_{02} is defined as the temperature below which, for $l=0$, we must write separately the lowest term ($n_3=1$) in the integration over n_3. It is defined so that

$$2gkT_{02}/3=N,$$

[1] M. F. M. Osborne, Phys. Rev. **76**, 396 (1949), hereafter referred to as *I*.

[2] J. H. Van Vleck, *The Theory of Electric and Magnetic Susceptibilities* (Clarendon Press, Oxford, 1932), pp. 354, 358.

[3] L. Landau, Zeits. f. Physik **64**, 262 (1930).

[4] F. London, Phys. Rev. **54**, 947 (1938).

or

$$T_{02}=3\epsilon Nhc/2\pi keHR^2 \tag{8}$$

$$=3h^3Nc/16LVmeHk. \tag{9}$$

Note that T_{02} depends on N/V, and also varies inversely as H and the dimensions of the system L in the direction of H. Roughly speaking T_{02} is the accumulation temperature of a one dimensional problem (see Fig. 1 of *I*), where the phenomenon is complicated by the presence of a magnetic field.

(4) T_H is defined as the temperature at which the spacing of the magnetic levels is of the order of magnitude of the thermal energy, $\mu H/kT_H=1$. When this is true it is certainly no longer valid to integrate over *any* of the magnetic levels. Note that this circumstance is not realized abruptly but gradually, so that T_H marks off an accumulation band rather than an accumulation temperature.

(5) For purposes of mathematical completeness rather than physical significance, we define a temperature T_t at which the average kinetic energy is equal to the average spacing of the translational levels ($\epsilon/kT_t=1$), and it is then no longer valid to integrate over any of the translational levels.

(6) H_c is defined as a critical field for which $T_{01}=T_{02}$

$$H_c=(N/V)^{\frac{1}{2}}(U(\tfrac{1}{2}, 0))^{\frac{1}{2}}3hc\pi/8Le. \tag{10}$$

For $H>H_c$ the accumulations at T_{01} and T_{02} occur separately. For $H<H_c$, the two accumulations occur at the same temperature T_{01} (case *C*). For $H<H_c$, $T_{02}>T_{01}$, and T_{02} is then simply a parameter by means of which the population of the lowest magnetic and higher translational states may simply be expressed as NT/T_{02}, an expression valid only for $T<T_{01}$.

Three other points should be noted in interpreting the formula which follows:

(1) The approximate behavior of the U functions for small parameter values, summarized in *I*, especially the fact that for

$$p=0, \quad \alpha\to 0, \quad U(p, \alpha)\to -\ln\alpha, \tag{11}$$

$$p<0, \quad \alpha\to 0, \quad U(p, \alpha)\to \alpha^p. \tag{12}$$

(2) The behavior of α in the neighborhood of the accumulation temperatures. Generally speaking, when a lowest energy term E_{low} has to be split off from an integration, in the separated term $\alpha\to -E_{\text{low}}/kT$ in just such a way that $(\alpha+E_{\text{low}}/kT)$ has the value to make the total population N. This is the explanation for the appearance of $\alpha+\mu H/kT$ and $\alpha+\mu H/kT+\epsilon/kT$ as effective normalization constants. A slightly different way of putting point (2) is as follows: if we have a series of complicated terms for N such as (14) or (17) which have a simple dependence on T, and only *one* of which is *sensitive* to α, then those terms effectively independent of α have the given dependence of population on T, and α is just such a complicated function of T to make the population of the term in which it does appear significantly vary as N minus the rest of the terms. Thus, if α only appears effectively in one term, we do not have to solve for α to get the relative populations of the different classes of states. This point will become apparent from the summary below, and be very useful in evaluating expressions for the total and free energy.

(3) In deriving the equations below, the lower limit of integration on n_3 must be chosen with care. In (13) for example, the lower limit zero for n_3 is a valid approximation, in some of the others, a half integral value as dictated by (1) must be used.

The Distribution of the Population

We can now write the expressions for α in the different regions of Fig. 1 as follows: N has been divided out so that the terms give the relative fractions of the populations in the different classes of states.

In region *A*

$$1=(T/T_{01})^{\frac{1}{2}}U(\tfrac{1}{2}, \alpha)/U(\tfrac{1}{2}, 0), \tag{13}$$

valid for

$$\alpha>\mu H/kT\ll 1, \quad T>T_{01}.$$

There is no accumulation in any particular class of states.

In region *B*

$$1=(2T_H/T_{01})(T/T_{01})^{\frac{1}{2}}U(-\tfrac{1}{2}, \alpha+\mu H/kT)/U(\tfrac{1}{2}, 0) + (T/T_{01})^{\frac{1}{2}}U(\tfrac{1}{2}, \alpha+2\mu H/kT)/U(\tfrac{1}{2}, 0), \tag{14}$$

valid for

$$\epsilon/kT<\alpha+\mu H/kT, \quad \alpha<\mu H/kT\ll 1, \quad T_{02}<T<T_{01}.$$

Since

$$U(\tfrac{1}{2}, \alpha+2\mu H/kT)\simeq U(\tfrac{1}{2}, 0), \tag{15}$$

the two terms of (14) vary like $1-(T/T_{01})^{\frac{1}{2}}$, $(T/T_{01})^{\frac{1}{2}}$,

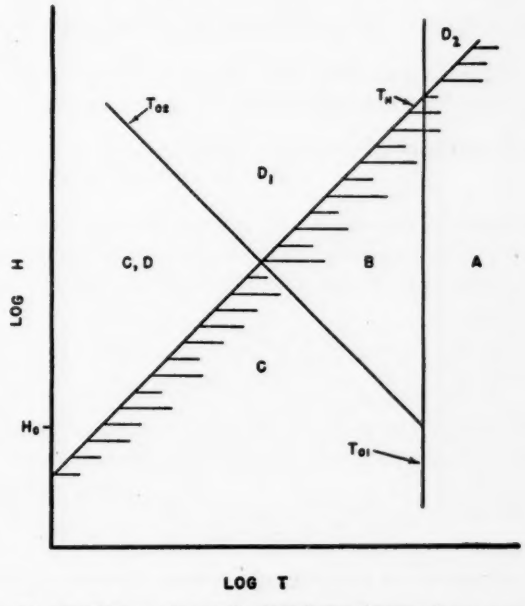

FIG. 1. (Schematic for Fig. 2.) Phase diagram for a gas of ions in a magnetic field.

these being the fractions of total population in ground magnetic and all higher magnetic states. From (14) we find

$$\alpha+\mu H/kT\simeq(\mu H/kT)^2(T/T_{01})^{\frac{3}{2}}\ll\mu H/kT. \quad (16)$$

In region C

$$1=(3T_t/2T_{02})/(\alpha+\mu H/kT+\epsilon/kT)+T/T_{02} +(T/T_{01})^{\frac{1}{2}}U(\tfrac{1}{2},\alpha+2\mu H/kT)/U(\tfrac{1}{2},0) \quad (17)$$

valid for

$$-\epsilon/kT<\alpha+\mu H/kT<\epsilon/kT,$$
$$T_H<T<(\text{the smaller of } T_{01},\ T_{02})$$

here also

$$U(\tfrac{1}{2},\alpha+2\mu H/kT)\simeq U(\tfrac{1}{2},0), \quad (18)$$

and the relative population of the states are

$$1-(T/T_{01})^{\frac{1}{2}}-T/T_{02},\quad T/T_{02},\quad (T/T_{01})^{\frac{1}{2}}, \quad (19)$$

in ground magnetic and ground translational, ground magnetic and higher translational, and higher magnetic and all translational states, respectively. Equation (19) is valid only if the first term is positive. Equation (17) is valid to the extent that $(2/3)\epsilon/kT$ represents the integral over n_3 for $l=0$ in (4), which is only approximately true (best when $|\alpha+\mu H/kT|\ll\epsilon/kT$). A detailed examination of this approximation will show that T/T_{02} in (19) indicates an abrupt accumulation in about the sense that T_{02}' in Fig. 1 of I represented an abrupt accumulation for the two-dimensional gas—perhaps not quite as abrupt. T_{02}, therefore, represents in Fig. 1 the center of a narrow accumulation band.

In region C, D

$$1=(3/2)(T_t/T_{02})/(\alpha+\mu H/kT+\epsilon/kT)+T/T_{02} +2(T_H/T_{01})(T/T_{01})^{\frac{1}{2}} \times U(-\tfrac{1}{2},\alpha+3\mu H/kT)/U(\tfrac{1}{2},0), \quad (20)$$

valid if

$$\mu H/kT\gg1,\quad -\epsilon/kT<\alpha+\mu H/kT<\epsilon/kT,\quad T<T_H.$$

This expression assumes that almost all the particles are in the first two magnetic states. This implies that

$$U(-\tfrac{1}{2},\alpha+3\mu H/kT)\simeq\exp(-2\mu H/kT) =\exp(-2T_H/T). \quad (21)$$

The relative population of ground translational and lowest magnetic, higher translational and ground magnetic, and next lowest magnetic and all translational states are

$$1-T/T_{02}-(2T_H/T_{02})(T/T_{01})^{\frac{1}{2}}\exp(-2T_H/T),$$
$$T/T_{02},\quad (2T_H/T_{02})(T/T_{01})^{\frac{1}{2}}\exp(-2T_H/T), \quad (22)$$

respectively. The first member of (22) must be positive.

In regions D_1 and D_2 we have α determined by

$$1=(2T_H/T_{01})(T/T_{01})^{\frac{1}{2}}[U(-\tfrac{1}{2},\alpha+\mu H/kT) +U(-\tfrac{1}{2},\alpha+3\mu H/kT)]/U(\tfrac{1}{2},0). \quad (23)$$

This assumes the population is almost entirely confined to the two lowest magnetic states, which these two terms represent. There is no accumulation in the lowest translational state as was the case in region CD. In region D_1 we may use the approximation

$$U(-\tfrac{1}{2},\alpha+\mu H/kT)\simeq(\pi/(\alpha+\mu H/kT))^{\frac{1}{2}},$$
$$U(-\tfrac{1}{2},\alpha+3\mu H/kT)\simeq\exp(-2\mu H/kT), \quad (24)$$

i.e.

$$(\alpha+\mu H/kT)\ll1,\quad \mu H/kT\gg1.$$

The relative populations are

$$1-(2T_H/T_{01})(T/T_{01})^{\frac{1}{2}}\exp(-2T_H/T), \quad (25)$$
$$(2T_H/T_{01})(T/T_{01})^{\frac{1}{2}}\exp(-2T_H/T).$$

In region D_2, the approximations (24) are not valid, and we must use exact expressions for the U functions.

In calculating Eqs. (13)–(25), the second term of (1) is neglected.

The Total Energy

We can also calculate expressions for the total energy

$$U=\sum_{l,\,n_1,\,n_3}E(l,n_1,n_3)n(l,n_1,n_3)$$

N_0 is Avogadro's number, R the gas constant.

In region A

$$U=(N/N_0)(3RT/2)(T/T_{01})^{\frac{1}{2}}U(\tfrac{3}{2},\alpha)/U(\tfrac{1}{2},0). \quad (26)$$

In region B

$$U=(N/N_0)[RT_H(1-(T/T_{01})^{\frac{1}{2}}) +(RTT_H/T_{02})(T/T_{01})^{\frac{1}{2}}U(\tfrac{1}{2},\alpha+\mu H/kT)/U(\tfrac{1}{2},0) +(3RT/2)(T/T_{01})^{\frac{1}{2}}U(\tfrac{3}{2},\alpha+2\mu H/kT)/U(\tfrac{1}{2},0) +2RT_H(T/T_{01})^{\frac{1}{2}}U(\tfrac{1}{2},\alpha+2\mu H/kT)/U(\tfrac{1}{2},0)]. \quad (27)$$

In region C

$$U=(N/N_0)[R(T_H+T_t)(1-(T/T_{01})^{\frac{1}{2}}-(T/T_{02})) +RTT_H/T_{02} +(3\pi^{\frac{1}{2}}RT/8)(T_t/T)^{\frac{1}{2}}(T/T_{02})U(\tfrac{1}{2},\alpha+\mu H/kT) +(3RT/2)(T/T_{01})^{\frac{1}{2}}U(\tfrac{3}{2},\alpha+2\mu H/kT)/U(\tfrac{1}{2},0) +2RT_H(T/T_{01})^{\frac{1}{2}}U(\tfrac{1}{2},\alpha+2\mu H/kT)/U(\tfrac{1}{2},0)]. \quad (28)$$

In region CD

$$U=(N/N_0)[R(T_H+T_t)(1-T/T_{02}-(2T_H/T_{01}) \times(T/T_{01})^{\frac{1}{2}}U(-\tfrac{1}{2},\alpha+3\mu H/kT)/U(\tfrac{1}{2},0)) +RTT_H/T_{02} +(3\pi^{\frac{1}{2}}/8)(RT^2/T_{02})(T_t/T)^{\frac{1}{2}}U(\tfrac{1}{2},\alpha+\mu H/kT) +(3RT_H^2/T_{01})(T/T_{01})^{\frac{1}{2}} \times U(-\tfrac{1}{2},\alpha+3\mu H/kT)/U(\tfrac{1}{2},0) +(3\pi^{\frac{1}{2}}/8)(RT^2/T_{02})(T_t/T)^{\frac{1}{2}} \times U(\tfrac{1}{2},\alpha+3\mu H/kT)]. \quad (29)$$

In regions D_1, D_2

$$U=(N/N_0)[RT_H(1-2(T_H/T_{01})(T/T_{01})^{\frac{1}{2}} \times U(-\tfrac{1}{2},\alpha+3\mu H/kT)/U(\tfrac{1}{2},0)) +RT(T_H/T_{01})(T/T_{01})^{\frac{1}{2}}U(\tfrac{1}{2},\alpha+\mu H/kT)/U(\tfrac{1}{2},0) +6RT_H(T/T_{01})^{\frac{1}{2}}U(-\tfrac{1}{2},\alpha+3\mu H/kT)/U(\tfrac{1}{2},0) +RT(T/T_{01})^{\frac{1}{2}}(T_H/T_{01}) \times U(\tfrac{1}{2},\alpha+3\mu H/kT)/U(\tfrac{1}{2},0)]. \quad (30)$$

The same approximations as in the corresponding equa-

tions for α also hold. The form of the above equations, when all the terms are written in the form const.$\times RT$ $\times$function of temperature ratios, is convenient when they are used with a diagram such as Fig. 1. Given an H, T point of interest, one can quickly estimate the values of different terms by reading the temperatures T_{01}, T_H, T_{02} at which a horizontal line through the H, T point of interest crosses the T_{01}, T_H or T_{02} line.

Equations (26)–(30) may be substantially simplified and condensed by using the valid approximations for each set, especially the facts that for all regions but B and D_2, $\alpha+\mu H/kT$ is very small and $U(p, \alpha)\simeq U(p, 0)$ for $\alpha\ll 1$ and $p>0$. However, they have been left in the form given so that the energy contribution of each type of level may be more explicitly identified, and the validity of the approximations more critically examined.

THE GAS OF IONS IN A MAGNETIC FIELD, WITH SPIN

The Relative Populations of the States

Let us reconsider the above problem when it is assumed that the particles have an intrinsic magnetic moment μ', and a spin I. In that case, we have to sum over $2I+1$ additional levels $\mu'H$ apart, in addition to the levels given in (3) above. The expression determining α becomes

$$N=\sum_{l=0}^{\infty}\sum_{n_3=1}^{\infty}\sum_{\sigma=-I}^{I} g/(\exp(E(\sigma, n_3, l)/kT+\alpha)-1) \quad (31)$$

with

$$E(\sigma, n_3, l)=\mu'H\sigma/I+\epsilon n_3^2+2(l+\tfrac{1}{2})\mu H,$$
$$\epsilon=h^2/8mL_z^2, \quad \mu=eh/4\pi mc.$$

Note that m refers to the (arbitrary) mass of the particle, so that in discussing particular particles such as deuterons μ'/μ is *not* the conventionally tabulated value for the intrinsic magnetic moment, but the mass number times it.

If all summations can be replaced by integrals, as will be the case so long as $\alpha>\mu H/kT$, (31) becomes

$$N=(2I+1)V(2\pi mkT)^{\frac{3}{2}}U(\tfrac{3}{2}, \alpha)/h^3. \quad (32)$$

When $\alpha<\mu H/kT$, it is no longer valid to replace the sum over the first terms of l by an integration. The behavior of α in this circumstance is a little subtle, but strict attention to the criterion (2) for integration, together with the expectation that α will approach close to the negative of the lowest energy state divided by kT, will show that when it no longer becomes valid to integrate over the first term of the l-summation, it will no longer be valid to integrate over the first term of the σ-summation either. Under these circumstances, splitting off the first term of the l- and σ-summation, (31) gives

$$1=(2\mu H/kT(2I+1))(T/T_{0\sigma})^{\frac{1}{2}}U(-\tfrac{1}{2}, \alpha_0)/U(\tfrac{1}{2}, 0)$$
$$+(\sum_{\sigma'=1}^{2I}(2\mu H/kT(2I+1))(T/T_{0\sigma})^{\frac{1}{2}}$$
$$\times U(-\tfrac{1}{2}, \alpha_0+\mu'H\sigma/I)/U(\tfrac{1}{2}, 0))+(T/T_{0\sigma})^{\frac{1}{2}}. \quad (33)$$

In (33) we have the following definition. $T_{0\sigma}$ is the condensation temperature in the absence of a field H. It is the solution of (32) for $\alpha=0$. $\alpha_0=\alpha+\mu H/kT$ $-\mu'H/kT$ is the effective normalization constant, and the first term of (33) is the only term sensitive to its value. It can be shown, as in the case of (16), that $\alpha_0\ll\mu H/kT$. This together with the fact that $U(-\frac{1}{2}, \alpha_0)$ $\simeq\alpha_0^{-\frac{1}{2}}$ will show that the terms of the summation in (33) are all small compared to the first term of (33).

The three terms of (33) represent the following classes of states:

(a) $l=0$, $\sigma=-I$, lowest magnetic and lowest spin, all translational.

(b) $l=0$, $\sigma=-I+1$ to $+I$, lowest magnetic and all higher spins, all translational.

(c) $l=1$ to ∞, $\sigma=-I$ to $+I$, excited magnetic, all spins, all translational.

The approximate relative orders of magnitude of the populations of these states are (a) $1-(T/T_{0\sigma})^{\frac{3}{2}}$, (b) Order $(\mu'H/kTI)^{\frac{1}{2}}$ (small), (c) $(T/T_{0\sigma})^{\frac{3}{2}}$.

The Free Energy and Polarization

We can now calculate the free energy $F=U-TS$ and magnetic polarization P. For $T>T_{0\sigma}$ and defining $\beta=\mu H/kT$, $\beta'=\mu'H/kTI$, $\gamma=\epsilon/kT$

$$F=-NkT\alpha+(gkT/4\beta)(\pi/\gamma)^{\frac{1}{2}}[-(2I+1)U(\tfrac{3}{2}, \alpha)$$
$$-\beta'^2(2I+1)^3U(-\tfrac{1}{2}, \alpha)/24$$
$$+\beta'^2U(-\tfrac{1}{2}, \alpha)/24$$
$$+\beta^2(2I+1)U(-\tfrac{1}{2}, \alpha)/6]. \quad (34)$$

In obtaining (34) we have expressed $\sum_{\sigma=-I}^{I} U(\frac{3}{2}, \alpha+\beta'\sigma)$ as an integral, using (1), including the correction term and also expanded this U function as a Taylor series about α.

For $T<T_{0\sigma}$

$$F=-NkT\alpha-gkT(\pi/\gamma)^{\frac{1}{2}}[\sum_{\sigma=-I}^{I} U(\tfrac{1}{2}, \alpha+\beta+\sigma\beta')$$
$$-\sum_{\sigma=-I}^{I} U(\tfrac{3}{2}, \alpha+2\beta+\sigma\beta')/4\beta$$
$$+\beta\sum_{\sigma=-I}^{I} U(-\tfrac{1}{2}, \alpha+2\beta+\sigma\beta')/24]. \quad (35)$$

The polarization, for $T>T_{0\sigma}$, is given by[5]

$$P=-(\partial F/\partial H)_\alpha/V,$$

$$P=(g(\pi/\gamma)^{\frac{1}{2}}\mu(2I+1)/V)$$
$$\times[(2I+1)^2(\mu'/\mu I)^2U(-\tfrac{1}{2}, \alpha)/48$$
$$-(\mu'/\mu I)^2U(-\tfrac{1}{2}, \alpha)/48-U(-\tfrac{1}{2}, \alpha)/12] \quad (36)$$

[5] See N. F. Mott and H. Jones, *Properties of Metals and Alloys* (Clarendon Press, Oxford, 1936), p. 204.

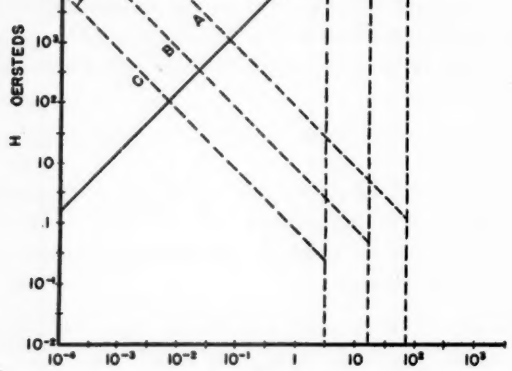

FIG. 2. Phase diagram for electron pairs. (A) 10^{19} pairs/cm^3, (B) 10^{18} pairs/cm^3, (C) 10^{17} pairs/cm^3. The Z dimension, along H, has been taken as 1 cm.

and for $T<T_{0\sigma}$

$$P=(g(\pi/\gamma)^{\frac{1}{2}}/V)\sum_{\sigma=-I}^{I}[\mu U(\tfrac{1}{2},\alpha+\beta+\sigma\beta')/2\beta - (\mu+\mu'\sigma/I)U(-\tfrac{1}{2},\alpha+\beta+\sigma\beta')/2 - (2\mu+\mu'\sigma/I)U(\tfrac{1}{2},\alpha+2\beta+\sigma\beta')/4\beta - \mu U(-\tfrac{1}{2},\alpha+2\beta+\sigma\beta')/12 + (2\mu+\mu'\sigma/I)\beta U(-\tfrac{3}{2},\alpha+2\beta+\sigma\beta')/24]. \quad (37)$$

Limiting Form for High Temperature

For high temperatures $\alpha\gg1$, $U(\frac{1}{2},\alpha)\simeq U(\frac{3}{2},\alpha)\simeq U(-\frac{1}{2},\alpha)\simeq\exp(-\alpha)$ and the polarization is, using (32) and (36)

$$P=\mu'^2HN(I+1)/3IkTV-N\mu^2H/3VkT. \quad (38)$$

For $I=\frac{1}{2}$

$$P=N\mu'^2H/kTV-N\mu^2H/3kTV \quad (39)$$

and these two terms can just be interpreted as the spin paramagnetism and the Langevin diamagnetism as given by Maxwell-Boltzmann statistics, which provides a convenient check on our work.

For $T<T_{0\sigma}$, the polarization is, using Eqs. (37) and (33) and neglecting quantities of order $(\mu H/kT)^{\frac{1}{2}}$

$$P=N(\mu'-\mu)(1-(T/T_{0\sigma})^{\frac{3}{2}})/V. \quad (40)$$

This expression has the quite plausible physical interpretation that there are $N(1-(T/T_{0\sigma})^{\frac{3}{2}})$ particles in the ground state of spin and circulation about the magnetic field, each of which contributes a positive magnetic moment μ' and a negative (diamagnetic) moment μ. In obtaining Eqs. (34)–(40) one has to include the correction term of Eq. (1) in replacing sums by integrals and also must utilize the approximate expressions for the U functions with small parameter.

Interpretation and Limitations of Formulas

It is appropriate to ask at this point if the temperature T_{01} (or $T_{0\sigma}$, for particles with spin) is a condensation temperature or merely an accumulation temperature, such as T_{02}. In the limiting case of no magnetic field we know that T_{01} is a condensation temperature. We also know that as the magnetic field increases and we go up along the T_{01} line (Fig. 1) eventually we reach the T_H band, in which we know there is a gradual accumulation in the ground magnetic state. Therefore, somewhere between 0 magnetic field and a magnetic field so strong that $kT_{01}\sim\mu H$, T_{01} ceases to be a condensation temperature and becomes an accumulation temperature. However, examination of the mathematics shows that it is fairly abrupt except in the immediate neighborhood of T_H. The exact problem of the field strength for which T_{01} ceases to be a condensation temperature has not been examined, though one might conjecture that it lies near H_c.

In the case of the accumulation temperature T_{02}, it should be observed that it is a function of N/V as $N\to\infty$ but it also depends on *how* $V\to\infty$ because of the factor L. If the thickness of the specimen $L\to\infty$, $T_{02}\to0$, otherwise it remains finite. This again is an example of how statistical mechanics shows the dependence of thermodynamic properties on geometry.

One can also point out here a limitation on the validity of the expressions derived above. It has been stated at the beginning that the magnetic field which determines the energy levels in which the particles move is H. Strictly speaking this is not true since the effective field acting on the particles is $H_{\text{eff.}}=H-\lambda P$ where λ is the depolarizing factor depending on the shape of the specimen, but in any event is not greater than 4π. However, it is valid to use H for $H_{\text{eff.}}$ if P is small compared to H. Now P, the polarization, was calculated to be $\sim(N\mu/V)(\mu H/kT)$ above the condensation temperature T_{01} and $\sim N\mu/V$ below it. If this latter expression is small compared to the applied H then the condition of applicability is met. As will be seen in the discussion of the numerical examples, this is the case for most problems of interest. $\mu\sim10^{-20}$ for electron pairs, and $\mu\sim10^{-23}$ for deuterons. For these examples the number of particles per unit volume has to be greater than 10^{20}, 10^{23}, respectively, for the theory to fail for fields less than one oersted.

Experimental Methods

We might now make a few remarks on the most suitable way in which these effects could be detected by measurement. Evidently, the orders of magnitude of the polarizations below and above the condensation tem-

measurement intervals. These procedures have given work functions reproducible to a few centivolts in the initial readings and drifts with aging which are so slow that the initial readings can probably be taken as characteristic of clean copper.

TUBE DESIGN AND EXPERIMENTAL PROCEDURES

The experimental procedure, insofar as it involves modifications of our previous techniques,[1] may be described in connection with the design of the measuring tube, Fig. 1. The target on which the films of copper and barium are laid down is a glass drum pivoted on glass bearings and operated as a pendulum. The "measuring position" at which the freshly deposited metal film is centered over the electron gun is the equilibrium position to which the pendulum returns automatically whenever it is released. When a film of either metal is to be deposited, the drum is rotated to the appropriate position by traction of a small Alnico magnet on the glass-enclosed armature. Friction in the bearings damps the pendulum oscillations sufficiently to bring the target to rest a second or two after release; the deposition-measurement interval is thus reduced to the time required for bringing the galvanometer to the selected reference reading. The drum serves the important purpose, also, of isolating the vaporizing compartments from each other and from the electron gun, i.e., of preventing contamination of the copper charge or gun by the barium. The glass spindles of the drum were sealed on with the aid of a glassblowing lathe to insure constant target-gun geometry at all positions of the target.

The barium vaporizing assembly, which provides fractional distillation of the metal and redistillation of the fractions used for preparing the measured surfaces, was similar to that employed in previous investigations of this series. The first copper vaporizer was designed to handle a relatively large charge (order of 1.0–1.5 g) of the metal without excessively heavy current leads and with reasonably high efficiency in terms of the ratio of distillate intercepted by the second vaporizer to the total quantity of copper vaporized. The usual horizontal tungsten foil boat is not satisfactory for this purpose; the fused copper flows along the foil and shorts most of it out.

The outgassing schedule, involving prolonged baking of the tube at 450°C before introduction of the metal charges, another extended bake at 350°C after charging, and repetitive high frequency treatment of all metal parts, was similar to that used for silver.[3] The treatment of the barium followed the procedure described in our recent report on lithium.[4] The copper used in this work was Hilger's spectroscopic material, Lot No. 10300, which was supplied with an exceptionally complete analysis showing 0.004 percent oxygen and 0.0007 percent iron as the only impurities present in amounts exceeding 0.0001 percent. During the outgassing of the tube and before seal-off, the copper charge was melted down five times. After seal-off, alternate fusions and solidifications of the copper interspersed with similar treatments of the barium were continued until approximately half of the charges had been vaporized. Since copper vaporizes rather slowly at temperatures slightly above the melting point, thirty-five fusions were included in this stage of the outgassing. The second vaporizers were flashed to remove the discarded fractions of copper and barium before proceeding with the measurements. The current through the first copper vaporizer was then increased to a value which was high enough to give a suitable deposit on the second vaporizer in about ten minutes, that is enough copper to form an opaque film on the target when the redistillation was carried out. As each new film of copper was deposited on the target it was measured as quickly as possible, usually within ten seconds of its deposition, and then at intervals of one minute to establish the rate of drift of the work function with aging. This procedure was

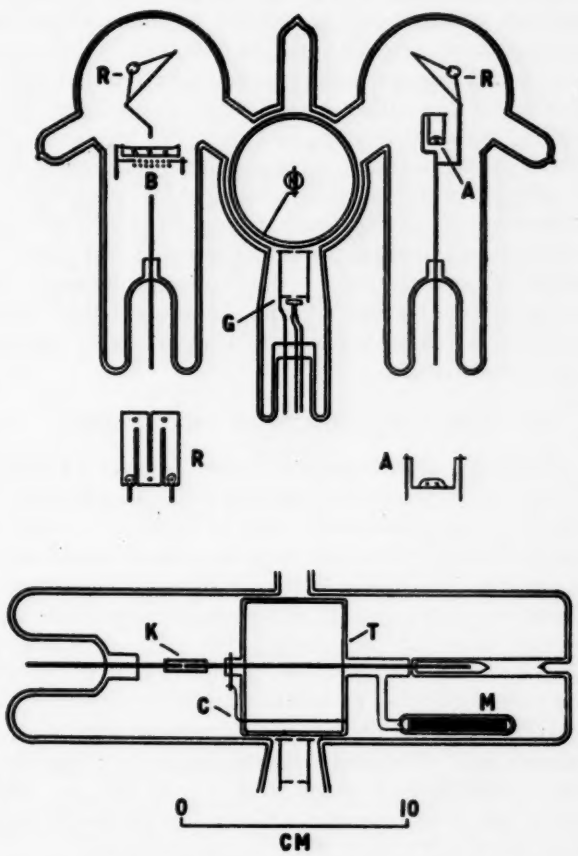

FIG. 1. Tube for measurement of contact difference of potential between vaporized films of Cu and Ba. Side view of complete tube above and of target section, rotated 90°, below. First Cu vaporizer *A* is 1-mil Ta foil 6-mm wide. Second vaporizers *R* of 1-mil Ta foil. Target *T* is Pyrex drum with 60-mil tungsten spindle rotating freely in nickel bearing *K*. Contact to metal film is by 20-mil Pt wire *C* embedded in face of drum. *M* is glass-enclosed soft iron armature. For detail of electron gun *G* and first Ba vaporizer *B*, see reference 1 of text. All leads 60-mil tungsten.

[3] Reference 1, 1941 paper.
[4] Paul A. Anderson, Phys. Rev. **75**, 1205 (1949).

repeated until the copper charge on the first vaporizer was exhausted. A succession of barium films was then deposited on the copper and measured in like fashion. The electrical circuit used in these measurements has been described previously.[4]

THE CONTACT DIFFERENCE OF POTENTIAL BETWEEN COPPER AND BARIUM

The results to be described are based on measurements on fourteen copper surfaces and eight barium surfaces, prepared as described above. The retarding potential required to establish the reference electron current to the target in the measurement taken immediately after the deposition of a new film is referred to hereafter as the "initial reading." The barium films gave, as usual, initial readings which were consistently reproducible to 0.01 volt or better and constant to 0.01 volt for periods of hours or even days after deposition. The serial numbering of the copper surfaces, running from 1 through 14, conforms to the order in which these surfaces were prepared from successive fractions of the distillate. Copper films 1–4 inclusive gave initial readings which varied at random by amounts corresponding to an extreme variation of 0.24 ev in the work function, a reproducibility markedly better than that obtained in our earlier unpublished measurements but still far from satisfactory. In films 5–8 a regular trend in the initial readings, corresponding to a progressive increase in work function totaling 0.18 ev appeared. This trend then disappeared; films 9–14 gave initial readings which again varied at random but over a range of only ± 0.03 ev. The contact difference of potential Cu−Ba derived from the mean of the initial readings on films 9–14 is 1.94 ± 0.03 volts, copper negative to barium.

THE WORK FUNCTION OF COPPER

Neglecting deviations which arise from the Maxwell tails of the Fermi distributions and which are well within the limits of experimental error at room temperature, the difference between the work functions of two metals is equal to the contact difference of potential between them, multiplied by the elementary charge. Addition of our value for the contact difference of potential Cu−Ba to 2.52 ev, the work function of barium,[5] yields the value 4.46 ± 0.03 ev for the work function of copper. This value is to be taken as representative of the present work. Previously reported values[6] for the work function of copper range from 4.1 to 4.5 ev. The thermionic measurements of Goetz,[7] probably the most careful and thorough of the earlier investigations, gave 4.38 ev. It is interesting that this range of values, obtained in seven independent studies by a variety of methods and techniques, coincides almost exactly with the range of values obtained in our measurements on copper films 1–14, namely 4.04 to 4.49 ev. Our observations on the variation of the work function with the aging of freshly deposited copper films, described below, show in every case a trend toward lower work function and suggest that the work function of completely clean copper films deposited on glass at room temperature is probably close to 4.50 ev.

EFFECTS OF GASEOUS CONTAMINANTS ON THE WORK FUNCTION OF COPPER

We are concerned here not only with the initial readings on newly formed copper surfaces but with the behavior of these films on aging. The results of some two hundred measurements on the fourteen copper surfaces may be summarized as follows: (1) The first films to be deposited, characterized by poor reproducibility in the initial readings, showed a relatively rapid drift toward lower work function on aging. Film No. 1, the extreme example of drift, gave a work function of 4.32 ev ten seconds after its deposition, 4.27 at one minute, 4.23 at two minutes, 4.12 at eight minutes, and a slower drift thereafter. (2) Improvement in the reproducibility of the initial reading was accompanied by a striking decrease in both the rate and magnitude of the drift. Film No. 10, typical of the 9–14 group, gave an initial work function of 4.47 and successive readings of 4.47, 4.47, 4.47, 4.46, and 4.46 at one minute intervals without further drop within 12 minutes. (3) In no case was a drift toward higher work function observed. These observations seem to bear out the tentative conclusions reached in our earlier unpublished work, namely, that traces of gas retained by a copper charge through a series of fusions and solidifications are evaporated with the copper and are then reabsorbed by the condensed film. In the present measurements, the quantity of gas left in the copper charge on the first vaporizer appears to have been reduced to negligible proportions only after most of the copper had been evaporated. The fact that the residual gas, presumably oxygen, lowers the work function suggests further that solution in the condensed copper film rather than permanent adsorption on the surface is involved. It is well known that oxygen adsorbed on a clean tungsten surface raises the work function and a similar behavior would be expected of copper if the oxygen remained on the surface as an adsorbed film.

I am indebted to Mr. Frank Peters, departmental glassblower, for the skill and care which he has given to the construction of the tubes used in this work.

[5] N. C. Jamison and R. J. Cashman, Phys. Rev. **50**, 624 (1936).
[6] A. L. Hughes and L. A. DuBridge, *Photoelectric Phenomena* (McGraw-Hill Book Company, Inc., New York, 1932), p. 75.
[7] A. Goetz, Zeits. f. Physik **43**, 531 (1927).

PHYSICAL REVIEW VOLUME 76, NUMBER 3 AUGUST 1, 1949

On the Treatment of Quantum Electrodynamics without Eliminating the Longitudinal Field

NING HU*
Cornell University, Ithaca, New York
(Received April 7, 1949)

It is shown in the present paper that the supplementary condition in quantum electrodynamics can be satisfied identically without eliminating the longitudinal components of the electromagnetic field, provided certain rules on the summation over the polarizations of the photons are observed. The result is shown to be identical with that obtained by the usual method in which the longitudinal field is eliminated. This simplifies greatly the calculation since no separate treatment of longitudinal and transverse fields is needed.

RECENTLY Tomonaga,[1] Schwinger,[2] and others have succeeded in formulating quantum electrodynamics in a completely co-variant form. As in customary formulations, these authors showed that the longitudinal components of the electromagnetic field can be eliminated, and thus insured the identical satisfaction of the supplementary condition. As a consequence of this elimination, the application of the theory becomes very much involved, since one has to deal with the transverse field and the coulomb interaction separately for each virtual transition. On the other hand, it has been pointed out by Feynman[3] that one can treat the longitudinal and transverse fields on the same footing by dealing with four different polarizations of virtual photons and also obtain the correct results. The Coulomb interaction is thus replaced by virtual emission and re-absorption of longitudinal photons. This simplifies tremendously the calculations since no separate treatment of longitudinal and transverse field is needed. It is the aim of the present paper to derive this new method from the formalism of Tomonaga and Schwinger. Only the case of spin-$\frac{1}{2}$ particles interacting with the electromagnetic field is considered in the present paper.

It is perhaps of interest to mention here that as long as one is concerned only with the rigorous solution of the problem, the supplementary condition can be included in the initial condition[4] and will then be automatically preserved after the initial state of the system has been specified correctly. However, if the Schrödinger equation is solved by perturbation methods, a special treatment (such as the elimination of the longitudinal field) is needed to insure that the supplementary condition is satisfied by the approximate solution at all stages of approximation.

The first part of the present paper deals with the elimination of longitudinal field which is essentially not much different from that given by Koba, Tati, and Tomonaga.[1] The second part consists essentially of undoing the elimination, preserving, however, the identical satisfaction of the supplementary condition achieved in the first part. It seems that there should be a more direct way of obtaining the same results without following the round-about way of eliminating and then restoring the longitudinal field. The present derivation, however, shows the connection between Feynman's method and the conventional one in which the longtudinal field is eliminated.

In the following calculations the same notation as that of Schwinger's paper is used except that here in addition the unit $\hbar=c=1$ is in use. Therefore no detailed explanation of terms and concepts is given here that have been explained clearly in Tomonaga and Schwinger's papers. The state vector $\Psi[\sigma]$ of the system of electronic and electromagnetic fields satisfies the following generalized Schrödinger equation:

$$i\frac{\delta\Psi[\sigma]}{\delta\sigma(x)}=-j_\mu(x)A_\mu(x)\Psi[\sigma] \tag{1}$$

and the supplementary condition

$$\left[\frac{\partial A_\mu(x)}{\partial x_\mu}-\int_{\sigma(x)}D(x-x')j_\mu(x')d\sigma_\mu'\right]\Psi[\sigma]=0. \tag{2}$$

$A_\mu(x)$ can be expanded into the following Fourier integral

$$A_\mu(x)=\frac{1}{(2\pi)^{\frac{3}{2}}}\int[A_\mu(k)e^{i(kx)}+A_\mu^*(k)e^{-i(kx)}]\frac{d^3k}{k} \tag{3}$$

where $(kx)=k_0x_0-k_1x_1-k_2x_2-k_3x_3$, $x_\mu=(t,\mathbf{r})$ being the coordinates of any point in the space-time, and $A_\mu(x)=(\phi(t,\mathbf{r}),\mathbf{A}(t,\mathbf{r}))$ is the four-vector potential of the electromagnetic field. $\sigma(x)$ denotes an arbitrary space like surface passing through the point x_μ, and $\Psi[\sigma]$ is understood as a functional of σ. The meaning of other notations can easily be found in Schwinger's paper. $A_\mu(k)$ and $A_\mu^*(k)$ are q-numbers satisfying the following

* Now at University of Wisconsin.
[1] S. Tomonaga, Proc. Theor. Phys. **1**, 27 (1946); Koba, Tati, and Tomonaga, Proc. Theor. Phys. **2**, 101, 198 (1947).
[2] J. Schwinger, Phys. Rev. **73**, 416 (1948); **74**, 1439 (1948).
[3] R. P. Feynman, Phys. Rev. **74**, 939, 1430 (1948); and several papers still in the course of preparation.
[4] This follows from the fact that the supplementary condition and the Schrödinger equation are represented by operators commuting with each other. For earlier non-covariant derivation of the result see E. Fermi, Rev. Mod. Phys. **4**, 131 (1932); W. Heitler, *The Quantum Theory of Radiation* (Oxford University Press, London, 1944) §6.

commutation relations ($[A,B]=AB-BA$)

$$[A_0(k),A_0^*(k')]=-\tfrac{1}{2}k\delta(\mathbf{k}-\mathbf{k}')$$
$$[\mathbf{A}(k),\mathbf{A}^*(k')]=\tfrac{1}{2}k\delta(\mathbf{k}-\mathbf{k}'). \quad (4)$$

Introduce for each value of k_μ the following coordinate system: x_4 along any time-like direction, x_1 and x_2 perpendicular to each other and to both x_4 and k_μ and x_3 forms the fourth perpendicular direction which is parallel to $\mathbf{k}$, the space component of k_μ. Let $n_\mu^{(\alpha)}$ be unit vectors in the direction of $x_\alpha(\alpha=0,1,2,3)$ referred to any fixed coordinate system in the space-time. For different values of k_μ, the directions of $n_\mu^{(\alpha)}(k)$ are different. Introduce further the following two zero vectors:

$$n_\mu^{(\kappa)}(k)=1/\sqrt{2}[n_\mu^{(3)}(k)+n_\mu^{(0)}(k)],$$
$$n_\mu^{(l)}(k)=1/\sqrt{2}[-n_\mu^{(3)}(k)+n_\mu^{(0)}(k)]. \quad (5)$$

It can easily be verified that $(n^{(l)}n^{(l)})=(n^{(\kappa)}n^{(\kappa)})=0$ and $(n^{(\kappa)}n^{(l)})=-1$. $A_\mu(k)$ can then be written

$$A_\mu(k)=n_\mu^{(1)}A^{(1)}(k)+n_\mu^{(2)}A^{(2)}(k)+A_\mu'(k), \quad (6)$$

where

$$A_\mu'(k)=n_\mu^{(0)}A^{(0)}(k)+n_\mu^{(3)}A^{(3)}(k)$$
$$=n_\mu^{(\kappa)}A^{(\kappa)}(k)+n_\mu^{(l)}A^{(l)}(k), \quad (7)$$

and in coordinate space

$$A_\mu(x)=A_\mu^{(1)}(x)+A_\mu^{(2)}(x)+A_\mu'(x), \quad (6a)$$

and

$$A_\mu'(x)=A_\mu^{(3)}(x)+A_\mu^{(0)}(x)$$
$$=A_\mu^{(\kappa)}(x)+A_\mu^{(l)}(x), \quad (7a)$$

where

$$A_\mu^{(\alpha)}(x)=\int n_\mu^{(\alpha)}(k)[A^{(\alpha)}(k)e^{i(kx)}$$
$$+A^{*(\alpha)}(k)e^{-i(kx)}]\frac{d^3k}{k} \quad (\alpha=0,1,2,3,\kappa,l). \quad (8)$$

It can be shown from (4) that $A^{(\alpha)}(k)$ satisfy the following commutation relations

$$[A^{(\alpha)}(k),A^{*(\alpha)}(k')]=\tfrac{1}{2}g^{(\alpha)}k\delta(\mathbf{k}-\mathbf{k}') \quad (\alpha=0,1,2,3),$$
$$[A^{(l)}(k),A^{*(\kappa)}(k')]=-\tfrac{1}{2}k\delta(\mathbf{k}-\mathbf{k}'),$$
$$[A^{*(l)}(k),A^{(\kappa)}(k')]=-\tfrac{1}{2}k\delta(\mathbf{k}-\mathbf{k}'), \quad (8a)$$

(other commutators vanish) where $g^{(\alpha)}=-1$ when $\alpha=0$ and $g^{(\alpha)}=1$ when $\alpha=1,2,3$. This difference in sign of $g^{(0)}$ is important since it follows from (8a) that $A^{*(\alpha)}(k)$ should be considered as emission operator and $A^{(\alpha)}(k)$ as absorption operator when $\alpha\neq0$, whereas $A^{(0)}(k)$ should be considered as emission operator and $A^{*(0)}(k)$ as absorption operator. This important fact should be borne in mind when applying Feynman's method.

The supplementary condition (2) will be satisfied if $\Psi[\sigma]$ is of the following form

$$\Psi[\sigma]=e^{i\chi[\sigma]}\Omega[\sigma], \quad (9)$$

where $\Omega[\sigma]$ is independent of $A^{(\kappa)}(k)$ and $A^{*(\kappa)}(k)$, i.e.,

$$A^{(l)}(k)\Omega[\sigma]=0, \quad A^{*(l)}(k)\Omega[\sigma]=0, \quad (9a)$$

and

$$\chi[\sigma]=\int_{-\infty}^{\sigma}j_\mu(x')A_\mu^{(\kappa)}(x')dx'. \quad (10)$$

It should be noted that χ contains operators at point x' which is on the past side of σ, whereas $\Omega[\sigma]$ on which χ is operated depends only on σ. One way of specifying the operation is to integrate χ with respect to x'. One finds readily

$$\chi=\int_\sigma j_\mu(x)B(x)d\sigma_\mu, \quad (11)$$

where

$$\frac{\partial}{\partial x_\mu}B(x)=A_\mu^{(\kappa)}(x), \quad (12)$$

or

$$B(x)=1/(2\pi)^{\frac{3}{2}}\int i[A^{(\kappa)}(k)e^{i(kx)}$$
$$-A^{*(\kappa)}(k)e^{-i(kx)}]d^3k/k^2. \quad (12a)$$

Then χ contains only operators referring to σ. An alternative way to specify the meaning of the operation is to follow the procedure of Dirac[5] who defines

$$j_\mu(x')A_\mu^{(\kappa)}(x')\Omega[\sigma]=j_\mu(x')A_\mu^{(\kappa)}(x')S[\sigma;\sigma']\Omega[\sigma'] \quad (13)$$

where σ' is a space like surface in the past side of σ and passing through the point x'. $S[\sigma;\sigma']$ is an unitary operator transforming a solution $\Omega[\sigma']$ of (1) at time σ' to the same solution $\Omega[\sigma]$ at time σ. $S[\sigma,\sigma']$ may contain other operators such as $j_\mu(x'')A_\mu^{(\alpha)}(x'')$, therefore care must be taken not to disturb the original order of different operators unless they commute. These two ways of specifying the meaning of operation are, of course, equivalent—at least in the following calculation only such properties of χ are used for which the equivalence of (10) with (11) is obvious.

Since from (6)–(8)

$$\partial A_\mu/\partial x_\mu=\partial A_\mu^{(l)}/\partial x_\mu=1/(2\pi)^{\frac{3}{2}}\int i[A^{(l)}(k)e^{i(kx)}$$
$$-A^{*(l)}(k)e^{-i(kx)}]d^3k/k,$$

and

$$\chi=\int_{-\infty}^{\sigma}j_\mu(x')dx'\int n_\mu^{(\kappa)}(k)[A^{(\kappa)}(k)e^{i(kx')}$$
$$+A^{*(\kappa)}(k)e^{-i(kx')}]d^3k/k.$$

It follows from Eq. (8)

$$\partial A_\mu/\partial x_\mu\chi=\int_{-\infty}^{\sigma}j_\mu(x')dx'\cdot\tfrac{1}{2}\int k_\mu[e^{i(k,x-x')}$$
$$+e^{-i(k,x-x')}]d^3k/k$$
$$=\int_{-\infty}^{\sigma}j_\mu(x')\frac{\partial}{\partial x_\mu}D(x-x')dx'$$
$$=\int_\sigma j_\mu(x')D(x-x')d\sigma_\mu', \quad (14)$$

[5] P. A. M. Dirac, Rev. Mod. Phys. **17**, 195 (1945).

where $(k,x-x')=k_0(x_0-x_0')-\mathbf{k}\cdot(\mathbf{x}-\mathbf{x}')$. If $\Omega[\sigma]$ is independent of $A^{(\kappa)}(k)$, and $A^{*(\kappa)}(k)$, or in other words, independent of $A^{(\kappa)}(x)$ then using (9a)

$$(\partial A_\mu/\partial x_\mu)e^{ix}\Omega[\sigma]=\int_\sigma j_\mu(x')D(x-x')d\sigma_\mu' e^{ix}\Omega[\sigma]. \quad (15)$$

This verifies that the supplementary condition is satisfied identically if (9a) is satisfied, i.e., if $\Omega[\sigma]$ is independent of $A^{(\kappa)}(x)$. It must now be shown that an $\Omega[\sigma]$ independent of $A^{(\kappa)}(x)$ is allowed by the Schrödinger Eq. (1).

It follows from (10)

$$e^{-ix}i(\delta/\delta\sigma)e^{ix}\Omega[\sigma]=i(\delta/\delta\sigma)\Omega[\sigma] - j_\mu(x)A_\mu^{(\kappa)}(x)\Omega[\sigma]. \quad (15a)$$

Since

$$\int_\sigma [j_\mu(x'),\ j_\alpha(x)]d\sigma_\mu'=0, \quad (15b)$$

$j_\mu(x')d\sigma_\mu'$ may be considered as commuting with $j_\alpha(x)$. Then with the help of the commutation relations (8a), it follows

$$e^{-ix}j_\mu A_\mu^{(\alpha)}e^{ix}=j_\mu A_\mu^{(\alpha)} \quad (\alpha=1,2,\kappa). \quad (16)$$

The following identity can easily be verified to be true

$$e^{-ix}j_\mu A_\mu^{(l)}e^{ix}=j_\mu A_\mu^{(l)}-[\chi,j_\mu A_\mu^{(l)}] +\frac{1}{2!}[\chi,[\chi,j_\mu A_\mu^{(l)}]] -\frac{1}{3!}[\chi,[\chi,[\chi,j_\mu A_\mu^{(l)}]]]+\cdots \quad (17)$$

From Eqs. (4), (12), and (15b), it follows, after some calculation,

$$[\chi,j_\mu A_\mu^{(l)}]=-\int j_\mu(x)j_\alpha(x')\mathfrak{L}_\mu(x-x')d\sigma_\alpha',$$

$$\mathfrak{L}_\mu(x-x')=\int n_\mu^{(l)}(k)[e^{i(k,x-x')}+e^{-i(k,x-x')}]\frac{d^3k}{k}. \quad (18)$$

It also follows from Eqs. (15b) and (18) that

$$[\chi,[\chi,j_\mu A_\mu^{(l)}]]=0.$$

Therefore, all the terms except the first two on the right-hand side of Eq. (17) vanish identically. Application of Eq. (17) on $\Omega[\sigma]$ gives further

$$e^{-ix}j_\mu A_\mu^{(l)}e^{ix}\Omega[\sigma]=-j_\mu A_\mu^{(l)}\chi\Omega[\sigma], \quad (19)$$

on account of the condition (9a). Finally the Schrödinger equation for $\Omega[\sigma]$ obtained by inserting (9) into (1) and using (15a), (16) and (19) is given by

$$i\frac{\delta\Omega[\sigma]}{\delta\sigma(x)}=-\sum_{r=1,2}j_\mu A_\mu^{(r)}\Omega[\sigma]+j_\mu A_\mu^{(l)}\chi[\sigma]\Omega[\sigma], \quad (20)$$

or, on inserting Eq. (18),

$$i\frac{\delta\Omega[\sigma]}{\delta\sigma(x)}=-\sum_{r=1,2}j_\mu A_\mu^{(r)}\Omega[\sigma] +\int_\sigma j_\mu(x)j_\alpha(x')\mathfrak{L}_\mu(x-x')d\sigma_\alpha'\Omega[\sigma]. \quad (21)$$

It is seen that the operators on the right hand side of (21) are independent of $A^{(\kappa)}(k)$ and $A^{*(\kappa)}(k)$. This furnishes the proof that (9a) is always satisfied if it is satisfied initially.

Equation (20) can be written in the following form

$$i\frac{\delta\Omega[\sigma]}{\delta\sigma(x)}=H(x)\Omega[\sigma], \quad (22)$$

where

$$H(x)=H_1(x)+H_2(x), \quad (23)$$

$$H_1(x)=-\sum_{r=1,2}j_\mu(x)A_\mu^{(r)}(x), \quad (24)$$

$$H_2(x)=-(-i)^2j_\mu(x)A_\mu^{(l)}(x)\int_\sigma j_\alpha(x')B(x')d\sigma_\alpha'. \quad (25)$$

Following Schwinger and Dyson,[6] the solution of (22) can be written down immediately:

$$\Omega[\sigma]=S[\sigma]\Omega_0, \quad (26)$$

$$S[\sigma]=1-i\int_{-\infty}^{\sigma}H_1(x_1)dx_1 +(-i)^2\int_{-\infty}^{\sigma}H(x_1)dx_1\int_{-\infty}^{\sigma_1}H(x_2)dx_2+\cdots. \quad (27)$$

The general term of Eq. (27) can be written:

$$(-i)^n\int^{\sigma}H(x_1)dx_1\int H(x_2)dx_2\cdots\int H(x_n)dx_n, \quad (28)$$

where the limits of the integrals have been omitted, it being understood that the integration of each factor $H(x)$ is from $-\infty$ to a space-like surface passing through the variable point x'' of the factor $H(x'')$ just in front of $H(x)$, with the order of the H's according to the order of time.

On inserting Eq. (23), the integrand of (28) can further be expanded into different combinations of products of factors H_1 and H_2. Consider first the terms of (28) which contain H_1 only and which contain no virtual emission and re-absorption of photons. (This does not exclude the processes in which a transverse virtual photon was emitted but has not been absorbed at time σ.) One of these terms can be written in the following form

$$I_n=(-i)^n\int^{\sigma}H_1(x_1)dx_1 \times\int H_1(x_2)dx_2\cdots\int H_1(x_n)dx_n. \quad (29)$$

[6] F. J. Dyson, Phys. Rev. **75**, 486 (1949).

Let $I_n(i)$ be another term of (27) constructed from (29) by adding a factor $\int H_2(x')dx'$ between $\int H_1(x_i)dx_i$ and $\int H_1(x_{i+1})dx_{i+1}$:

$$I_n(i)=(-i)^{n+2}\int^{\sigma} H_1(x_1)dx_1\int H_1(x_2)dx_2\cdots \times\int H_1(x_i)dx_i\int j_\mu(x')A_\mu^{(l)}(x')dx' \times\int_{\sigma(x')} j_\alpha(x'')B(x'')d\sigma_\alpha''\int H_1(x_{i+1})dx_{i+1}\cdots \times\int H_1(x_n)dx_n. \quad (30)$$

Now since $[A_\mu^{(l)}(x'),H_1(x)]=0$ and because of Eq. (15b), the added factor commutes with all the other factors of Eq. (30). By using the following identity

$$\int_{\sigma_i} j_\mu(x')B(x')d\sigma_{i\mu}'=\int_{\sigma_{i+1}}^{\sigma_i} j_\mu(x')A_\mu^{(s)}(x')dx' -\int_{\sigma_{i+1}} j_\mu(x')B(x')d\sigma'_{i+1,\mu}, \quad (31)$$

it can easily be seen that

$$\int_{\sigma(x')} j_\alpha(x')B(x')d\sigma'\int_{-\infty}^{\sigma(x')} H_1(x_{i+1})dx_{i+1} =\int_{-\infty}^{\sigma(x')} j_\alpha(x'')A_\alpha^{(s)}(x'')dx''\int_{-\infty}^{\sigma(x'')} H_1(x_{i+1})dx_{i+1} +\int_{-\infty}^{\sigma(x)} H_1(x_{i+1})dx_{i+1}\int_{\sigma_{i+1}} j_\alpha(x')B(x')d\sigma_\alpha'. \quad (32)$$

This relation can be used repeatedly to push the surface integral in Eq. (30) to the right side of the last factor $\int H_1(x_n)dx_n$ and then replace it by a volume integral Eq. (10) integrated from minus infinity to σ_n. The final expression of Eq. (30) will contain no surface integral and is given by

$$I_n(i)=\sum\int^{\sigma} H_1(x_1)dx_1\int H_1(x_2)dx_2\cdots \times\int H_1(x_i)dx_i\int j_\mu(x')A^{(l)}(x')dx' \times\int H_1(x_{i+1})dx_{i+1}\cdots\int j_\mu(x'')A^{(s)}(x'')dx''\cdots \times\int H_1(x_n)dx_n, \quad (33)$$

where $\sum$ means summation over all possible positions of $\int j_\mu(x'')A^{(s)}(x'')dx''$ between $\int H_1(x_i)dx_i$ and $\int H_1(x_n)dx_n$.

It will now be shown that the contribution due to the factors

$$\int j_\mu(x')A_\mu^{(l)}(x')dx', \quad \int j_\mu(x'')A_\mu^{(s)}(x'')dx'' \quad (34)$$

in Eq. (33) represent just the virtual exchange of longitudinal photons between σ' and σ''. Since from (7a)

$$A_\mu^{(l)}(x)+A_\mu^{(s)}(x)=A_\mu^{(0)}(x)+A_\mu^{(3)}(x),$$

it follows from the commutation relation that

$$A_\mu^{(l)}(x')A_\alpha^{(s)}(x'')+A_\mu^{(s)}(x')A_\alpha^{(l)}(x'') =A_\mu^{(0)}(x')A_\alpha^{(0)}(x'')+A_\mu^{(3)}(x')A_\alpha^{(3)}(x'') =\sum_{s=0,3}A_\mu^{(s)}(x')\cdot\sum_{t=0,3}A_\alpha^{(t)}(x'').$$

$A_\mu^{(s)}(x)A_\alpha^{(l)}(x'')$ vanishes identically because of the condition (9a). The above equation becomes

$$A_\mu^{(l)}(x')A_\alpha^{(s)}(x'')=\sum_{s=0,3}A_\mu^{(s)}(x')\cdot\sum_{t=0,3}A_\alpha^{(t)}(x''). \quad (35)$$

Therefore, the two factors (34) can be replaced by

$$\int j_\mu(x')[\textstyle\sum_s{}'A_\mu^{(s)}(x')dx', \quad \int j_\mu(x'')\sum_s{}'A_\mu^{(s)}(x'')dx'' \quad (36)$$

respectively, where the summation $\sum'$ is from 3 to 4. Now from (27), new groups of terms can be picked out which contain only H_1-factors and represent the same processes as (29), but in addition there is a virtual exchange of transverse protons between $\sigma(x')$ and $\sigma(x'')$. It is easily seen that the contribution of this new group of terms is just to replace $\sum'$ by another summation over all polarizations from 0 to 3.

So far only terms involving one pair of virtual emission and reabsorption have been considered. Let $I_n(i,j)$ be another term of (27) constructed from (29) by adding two H_2-factors in the following way:

$$I_n(i,j)=(-i)^{n+4}\int^{\sigma} H_1(x_1)dx_1\cdots\int H_1(x_j)dx_j \times\int j_\nu(x_b')A_\nu^{(l)}(x_b')dx_b'\int_{\sigma(x_b')} j_\beta(x_b'')B(x_b'')d\sigma_{b\beta}''\cdots \times\int H_1(x_i)dx_i\int j_\mu(x_a')A_\mu^{(l)}(x_a')dx_a' \times\int_{\sigma(x_a')} j_\alpha(x_a'')B(x_a'')d\sigma_{a\alpha}'\cdots\int H_1(x_n)dx_n. \quad (37)$$

It follows from Eq. (15b) that $j_\mu(x_a')dx_a'$ and $j_\nu(x_b')dx_b'$ commute with each other and also with all the other current vectors in Eq. (37). The operators $A_\mu^{(l)}(x_a')$, $B(x_a'')$, $A_\nu^{(l)}(x_b'')$ and $B(x_b'')$ commute with all the other operators in Eq. (37). It is seen from the foregoing result that the B's represent the emission operators of the longitudinal photon* and the $A_\mu^{(l)}$'s represent the corresponding absorption operator. The order of these operators in (37) shows that $A_\mu^{(l)}(x_a')$ absorbs only the photon emitted by $B(x_a'')$ and $A_\nu^{(l)}(x_b')$ absorbs only the photon emitted by $B(x_b'')$. If the order of $B(x_b'')$ and $A_\mu^{(l)}(x_a')$ is changed, new possibility arises that the photon emitted by $B(x_b'')$ may be absorbed by $A_\mu^{(l)}(x_a')$, which process is not included in (37). This situation is avoided if the photon emitted by $B(x_b'')$ is marked so that it cannot be absorbed by $A_\mu^{(l)}(x_a')$. This amounts formally to considering the pairs $A_\mu^{(l)}(x_a')$, $B(x_a'')$ and $A_\nu^{(l)}(x_b')$, $B(x_b'')$ as emission and absorption operators of two different kinds of particles a and b. This is the same as the rule introduced in Dyson's paper to group the operators into pairs with operators in different pairs commuting with each other. According to this rule the factor $N^{\frac{1}{2}}$ and $(N+1)^{\frac{1}{2}}$ of the matrix elements of the emission and absorption operators under customary convention should now be replaced by unity, where N is the number of photons in the same state. This reduction in the strength of the operators will be compensated exactly by the increase in the number of precesses due to different permutation of the order of the operators.

If the new rule is used, the argument that leads from (30) to (33) and (34) can be applied without any modification in the present case. Therefore Eq. (37) becomes

$$I_n(i,j)=(-i)^{n+4}\sum_p\int^\sigma H_1(x_1)dx_1\int H_1(x_2)dx_2\cdots$$
$$\times\int H'(x_a')dx_a'\cdots\int H'(x_a'')dx_a''\cdots$$
$$\times\int H'(x_b')dx_b'\cdots\int H'(x_b'')dx_b''\cdots\int H_1(x_n)dx_n,$$
$$H'(x)=\sum_{s=1}^{4}j_\mu(x)A_\mu^{(s)}(x), \quad (38)$$

where the summation $\sum_p$ is taken over all the positions of the four $H'(x)$ factors among all the other $H_1(x)$-factors. It should be understood that $H'(x_a')$ and $H'(x_a'')$ form a pair of virtual emission and absorption operators and $H'(x_b')$ and $H'(x_b'')$ form another pair whereas all the other H_1-factors contribute no virtual emission-reabsorption process.

* The vacuum has been considered as free from longitudinal photons. Actually from (9a), vacuum should be considered as having an indefinite number of longitudinal photons. However this makes no difference on final results as far as virtual processes are concerned.

The above result can easily be extended to the case when more than two pairs of virtual emission-absorption occur. It will not be difficult to see that terms constructed from Eq. (29) in this way will eventually include all the terms of Eq. (27). The general procedure of solving Eq. (22) can now be stated as follows:

First solve the following Schrödinger equation

$$\frac{\delta\Omega[\sigma]}{\delta\sigma(x)}=H(x)\Omega[\sigma], \quad H(x)=-\sum_s j_\mu A_\mu^{(s)}, \quad (39)$$

with the summation unspecified and obtain the following formal solution

$$\Omega[\sigma]=S[\sigma]\Omega_0$$
$$S[\sigma]=1-i\int_{-\infty}^{\sigma}H(x_1)dx_1+(-i)^2\int_{-\infty}^{\sigma}H(x_1)dx_1$$
$$\times\int_{-\infty}^{\sigma_1}H(x_2)dx_2+\cdots+(-i)^n\int_{-\infty}^{\sigma}H(x_1)dx_1$$
$$\times\int_{-\infty}^{\sigma_1}H(x_2)dx_2\cdots\int_{-\infty}^{\sigma_{n-1}}H(x_n)dx_n+\cdots. \quad (40)$$

Then the summation is specified as taken over all transverse and longitudinal polarizations for all the processes in which a photon has been emitted and then reabsorbed, and taken only over the transverse polarizations for all the other processes, namely, the processes in which either a real photon is emitted or absorbed or a virtual photon has been emitted but has not yet been absorbed. Equation (40) satisfies the supplementary condition identically even when a finite number of terms of $S[\sigma]$ are used as in the usual perturbation theory.

It should be noted that although emission and reabsorption of longitudinal photons can be considered as actually taken place in the *past*, the explicit expression of $S[\sigma]$ does not depend on the variables of the virtual longitudinal photons, as should be the case according to the condition (9a). In other words, no virtual longitudinal photon should be considered as existing at the *present*. On the other hand since the processes in which a transverse photon has been emitted but has not yet been absorbed are also included in Eq. (40), the expression of $S[\sigma]$ should therefore also depend on the variables of these virtual transverse photons. If however σ is put equal to infinity in Eq. (40), this remaining distinction between longitudinal and transverse virtual photons will disappear completely. $S[\infty]$ is just the representation used by Feynman.

It should further be pointed out that, strictly speaking, Ω_0 in (40) should satisfy the following condition as required by Eq. (9a):

$$A^{(l)}(k)\Omega_0=0, \quad A^{*(l)}(k)\Omega_0=0. \quad (41)$$

Now Ω_0 can be put into the following form

$$\Omega_0=\Omega_0'\Omega_0''$$

where Ω_0' depends only on the variables of the transverse photons and Ω_0'' depends only on those of the longitudinal photons belonging to the vacuum. Equation (41) becomes

$$A^{(l)}(k)\Omega_0''=0, \quad A^{*(l)}(k)\Omega_0''=0. \tag{42}$$

Since, as pointed out in the footnote before, the solution Eq. (40) does not depend on the exact form of Ω_0'', the factor Ω_0'' can simply be omitted from Eq. (40). This means that instead of choosing Ω_0 to satisfy Eq. (41), one can simply consider it as independent of the variables of the longitudinal photons. In other words, vacuum is considered as containing no longitudinal photons at all. This is just the convention adopted in the usual treatment in which the longitudinal field has been replaced by the Coulomb interaction.

In conclusion, the author wishes to express his thanks to Professor Bethe for helpful suggestions and discussions and also to Professor Feynman for detailed exposition of his theory before publication.

PHYSICAL REVIEW VOLUME 76, NUMBER 3 AUGUST 1, 1949

The Bose-Einstein Condensation for Thin Films

M. F. M. OSBORNE
Naval Research Laboratory, Washington, D. C.
(Received December 6, 1948)

The distinction is made between a condensation temperature in the thermodynamic sense, where the thermodynamic functions have a discontinuity, and an abrupt accumulation (in the statistical mechanical sense) of particles in the ground state of a system. The criterion for the latter is that an integral will not approximate one term of a sum. The problem of a thin film of gas is solved to illustrate this distinction. For films thicker than a critical thickness a condensation occurs at the same temperature as that for bulk material. The thinner films are effectively two dimensional and have an abrupt accumulation temperature lower than the bulk condensation temperature. Films of liquid helium are briefly considered.

INTRODUCTION

CONSIDERABLE interest has been provoked by London's proposal[1] that the λ-phenomenon of helium is a Bose-Einstein condensation, or accumulation of a finite fraction of all the particles in the ground state of a potential hole of macroscopic dimensions. Tisza[2] has extended this suggestion to discuss helium in terms of the hydrodynamics of a two-fluid system, and more recently Ogg[3] has proposed that phenomena which he has observed in metal-ammonia solutions and possibly also the phenomenon of superconductivity might be explained by the condensation of a gas of electron pairs formed from the free electrons of the material. It is the purpose of this paper to examine in some detail the conditions under which these condensations occur and to discuss some examples of physical interest. The particular examples we shall discuss are: (1) Three-dimensional gas of uncharged particles in a thin film, (2) Two-dimensional gas, and in a subsequent paper (3) Gas of charged particles in a magnetic field, neglecting electrostatic interactions.

Condensation and Accumulation Temperatures

In classical thermodynamics a condensation temperature implies a discontinuity in one of the thermodynamic functions which describe the system. Such discontinuities are also described by phase changes of first, second, third order, depending on whether the function or one of its higher derivatives becomes discontinuous.

From the standpoint of statistical mechanics we shall define an accumulation temperature T_0 as a temperature at which a finite fraction of all particles begin to accumulate in just one state or set of states with the same energy. By "finite" fraction we mean less than, but not a great deal less than unity, or very much greater than $1/N$, N being the total number of particles. We can speak of an "abrupt" accumulation if the fraction in a given state changes from "small" to "finite" in a small temperature range $\Delta T \ll T_0$. Such finite fractions can usually be expressed as $1-(T/T_0)^n$, $T<T_0$. We speak of a gradual accumulation if it occurs over a range $\Delta T \simeq T_0$. Only in the first case would it be appropriate to speak of a well-defined accumulation temperature, in the second case one might speak of an accumulation temperature band. Consider the expression for N, the total number of particles in a Bose-Einstein assembly.

$$N=\sum_{k,l,m} 1/(\exp(E(k,l,m)/kT+\alpha)-1)$$
$$=\sum_{k,l,m} f(E(k,l,m),\alpha,T), \tag{1}$$

where k, l, m are quantum numbers specifying the level of energy $E(k, l, m)$ and α is defined implicitly as a function of T by this relation.

[1] F. London, Phys. Rev. 54, 947 (1938).
[2] L. Tisza, Phys. Rev. 72, 838 (1947).
[3] R. A. Ogg, Preliminary Report to ONR, "Electronic Processes in Liquid Dielectric Media. The Constitution of Metal Ammonia Solutions." April 11, 1948, p. 20.

If the value of $\sum_{k,l,m} f(E(k,l,m),\alpha,T)$ can be replaced by $\int\int\int dkdldm f(E(k,l,m),\alpha,T)$ there is no accumulation of particles in any particular energy state. In general, on replacing a sum by an integral we have

$$\sum_{m=a}^{b} f(m)=\int_{a-\frac{1}{2}}^{b+\frac{1}{2}} f(m)dm-f'(m)/24\Big|_a^b, \qquad (2)$$

valid provided

$$f(n+\tfrac{1}{2})-f(n-\tfrac{1}{2})-f'(n)\ll f(n), \qquad (3)$$

where $a<n<b$, and n refers to any of the three indices k, l, m of summation.

The condition in Eq. (3) may fail in either of two ways: (a) If it fails for every value of n in the interval a, b, (as will be the case if in (1) kT is of the order of the spacing of the levels), then there is a gradual accumulation of the particles with diminishing temperature in the lowest energy state; (b) (3) may fail only for the lowest value of n in the interval a, b. If the value of the temperature at which this occurs is well defined, we have an abrupt accumulation of particles in the lowest state. If this accumulation temperature depends only on N/V as $N\to\infty$, i.e. is independent of the size of the system, we may expect discontinuities in the thermodynamic properties at this temperature. It is then a condensation temperature. This was first shown by Einstein,[4] and subsequently examined in detail by others.[5] Even when weak interactions between the particles are included the condensation occurs.[6]

THE IDEAL GAS IN A THIN FILM

In order to illustrate these points, let us consider the case of an ideal three-dimensional Bose-Einstein gas confined to a thin film. We shall show, using the above consideration, how thin the film must be for the well-known three-dimensional condensation to be prevented, and that for still thinner films (effectively two-dimensional gas[7]) an *abrupt accumulation* can still occur.

For the thin film, the expression for the total number of particles of mass M' in a box ($\psi=0$ on walls) of dimensions

$$L_x=L_y=L, \quad L_z=L/M, \quad M\gg 1$$

is

$$N=\sum_{k,l,m=1}^{\infty} 1/(\exp((k^2+l^2+m^2M^2)\epsilon/kT+\alpha)-1), \qquad (4)$$
$$\epsilon=h^2/8M'L^2.$$

Assuming for the moment that all these summations can be replaced by integrals (despite the large energy interval in m), we shall first examine the conditions under which the lower limits of integration on k, l, m can be replaced by 0, instead of $\frac{1}{2}$ as required by (2). This will give us an expression for N equivalent to that for a cubical box, plus correction terms which when large indicate that the film is too thin to be considered a three-dimensional system. The condition for largeness of the correction term will turn out to be the same as the condition forbidding replacement of a sum (over m) by an integral. From (4)

$$N=\int_{\frac{1}{2}}^{\infty}\int_{\frac{1}{2}}^{\infty}\int_{\frac{1}{2}}^{\infty} dkdldm \Big/ (\exp((k^2+l^2+m^2M^2)\epsilon/kT+\alpha)-1). \qquad (5)$$

Letting

$$k^2+l^2+M^2m^2=\rho^2, \quad \eta=(\tfrac{1}{2}+M^2/4)^{\frac{1}{2}}\simeq M/2$$

$$N=(1/M)\int_{\eta}^{\infty} (\pi/2)\rho^2 d\rho/(\exp(\rho^2\epsilon/kT+\alpha)-1), \qquad (6)$$

where the factor $\pi/2$ is a consequence of the fact we use box rather than periodic boundary conditions, and so integrate only over one octant in k, l, m space. Letting $\rho=\rho'+\eta$, and expanding that part of the exponential which is linear in ρ', and using the definition

$$U(p,\alpha)=(1/\Gamma(p+1))\int_0^{\infty} dz z^p/(\exp(z+\alpha)-1)$$
$$=\sum_{j=1}^{\infty}\exp(-\alpha j)/j^{p+1}, \qquad (7)$$

we find, after some manipulation

$$N=(\pi/2M)(kT/\epsilon)^{\frac{1}{2}}[\Gamma(3/2)U(\tfrac{1}{2},\eta^2\epsilon/kT+\alpha)/2 +\eta(\epsilon/kT)^{\frac{1}{2}}U(0,\eta^2\epsilon/kT+\alpha) +\eta^2\Gamma(1/2)(\epsilon/2kT)U(-\tfrac{1}{2},\eta^2\epsilon/kT+\alpha)] +\text{Order }(\eta(\epsilon/kT)^{\frac{1}{2}}). \qquad (8)$$

The four terms of (8) come in order from the three terms of $\rho^2=\rho'^2+2\eta\rho'+\eta^2$ in the numerator of (6) and the linear term in ρ' in the expansion of the denominator, the last being valid so long as $\eta\epsilon\rho'/kT$ is small in the region of the principal contribution to the integrand. This is so if $\eta\epsilon/kT$ is small. If one takes into account the following properties of the U functions,

$$U(\tfrac{1}{2},\alpha)\simeq U(\tfrac{1}{2},0),$$
$$U(0,\alpha)\simeq -\ln\alpha,$$
$$U(-\tfrac{1}{2},\alpha)\simeq\alpha^{-\frac{1}{2}},$$

for

$$0<\alpha\ll 1, \qquad (9)$$

and compares the above formulas with those of reference 1, one can easily verify the following statements. T_{01} is the condensation temperature for the three-dimensional case given in reference 1.

(1) For $\alpha>0$ and $\eta\epsilon/kT\ll 1$, $T>T_{01}$, the 2nd, 3rd,

[4] A. Einstein, Ber. Berl. Akad. (1924), 261; (1925), 3.
[5] R. H. Fowler and H. Jones, Camb. Phil. Soc. Proc. **34**, 573 (1938).
[6] L. I. Shiff, Phys. Rev. **59**, 758 (1941).
[7] Correspondence and conversation with F. London on this problem led to the distinction between "condensation" and "accumulation."

and 4th terms of Eq. (8) are negligible, and the first term gives just the conditions for determining α for the gas in a cubical box, given in reference 1.

(2) For $\alpha \leq 0$ and $\eta\epsilon/kT \ll 1$, the 2nd, 3rd and 4th terms of (8) are still negligible, and the first term determines the condensation temperature T_{01} as given in reference 1. Below this temperature, the condition (3) for integrating k, l or m fails for $k=l=m=1$. The first term of the summation must be separated from the integral, and α is determined by

$$\alpha+(2+M^2)\epsilon/kT=1/N(1-(T/T_{01})^{\frac{3}{2}}.$$

(3) For $\eta\epsilon/kT \simeq 1$, there is no condensation phenomenon. The 2nd, 3rd and 4th terms are not negligible, but (8) cannot be used to determine α, as $\eta\epsilon/kT \simeq 1$ is just the condition for a gradual accumulation in the lowest z direction level ($m=1$) and the failure of the integration condition (3) for all values of m.

(4) For $\eta\epsilon/kT \gg 1$ practically all of the particles are in the $m=1$ state, the gas can properly be considered as two dimensional, and must be reexamined for integrability on k and l.

Application to Liquid Helium

Before proceeding to a discussion of the two-dimensional case we can estimate for helium how thin a film has to be before condensation will be prevented. If $\eta\epsilon/kT \simeq 1$ we find for $T=T_{01}=3.4°$ (theoretical), $L_z \simeq 10^{-7}$ cm. This is small compared to the observed thickness of 5.10^{-6} cm for superfluid helium films.[8] Therefore, the observed thickness of superfluid helium films is not in contradiction with the idea that superfluidity is a consequence of a Bose-Einstein condensation. This calculation ignores the effect of the surface forces of the material on which the film lies in modifying the energy levels.

THE TWO DIMENSIONAL IDEAL GAS

Though primarily of academic interest, this problem has been the subject of some controversy, and is illuminating in showing the distinction between an abrupt accumulation and a condensation. It is also suggestive of the nature of the effects of geometry and impurities. The expression determining α for a square film is

$$N=\sum_{k,\,l=1}^{\infty} 1/(\exp((k^2+l^2)\epsilon/kT+\alpha)-1),$$
$$L_x=L_y=L, \quad \epsilon=h^2/8mL^2. \tag{10}$$

If the conditions (3) for replacing the sums over k, l by integrals are met we have

$$N=\int_{\frac{1}{2}}^{\infty}\int_{\frac{1}{2}}^{\infty} dkdl \Big/ (\exp((k^2+l^2)\epsilon/kT+\alpha)-1) \tag{11}$$
$$=-(\pi kT/4\epsilon)\ln(1-\exp(-\alpha')), \tag{12}$$

where by definition

$$\alpha' \equiv \epsilon/kT+\alpha.$$

The expression (12), determining α, unlike its three dimensional analogue, does have a solution for α for all values of T. In fact for α small (low temperatures) we find

$$\alpha=\exp(-4\epsilon N/\pi kT)-\epsilon/kT, \tag{13}$$

or in terms of α'

$$\alpha'=\exp(-T_{01}'/T), \tag{14}$$

where by definition

$$T_{01}'=h^2N/2\pi mkS,$$
$$S=L_xL_y.$$

T_{01}' is very nearly the condensation temperature for a three-dimensional gas whose surface density is the same as that for the two dimensional case. But T_{01}' is not a condensation temperature in this problem.

However, it is not legitimate, in view of the integration criterion (3) to use the above expression (13) for $\alpha < \epsilon/kT$. When $\alpha < \epsilon/kT$, we must use

$$N=1/(\exp(2\epsilon/kT+\alpha)-1)$$
$$+\int_{3/2}^{\infty}\int_{3/2}^{\infty} dkdl \Big/ (\exp((k^2+l^2)\epsilon/kT+\alpha)-1), \tag{15}$$

$$N=1/(\alpha'+3\epsilon/2kT)$$
$$-(\pi kT/4\epsilon)\ln(1-\exp(-5\epsilon/2kT-\alpha')). \tag{16}$$

In Eq. (16) the first term represents the population of the ground state and the second term represents the population of all the higher states. We shall continue the discussion in terms of α' since it is the behavior of this quantity as a function of T, rather than α, which will simplify the argument. Let us ask at what temperature T_{02}', where we expect $T_{02}' \ll T_{01}'$, Eqs. (16) and (12) give different results for α', so that for $T < T_{02}'$ we must use the more exact expression Eq. (16).

T_{02}' is a temperature such that $\alpha'(T_{02}')=(5\epsilon/2)/kT_{02}'$. To see this we first observe that by (14) α' is a very violent function of the temperature for $T \ll T_{01}'$. Thus, since $T_{02}' \ll T_{01}'$, at temperatures slightly above T_{02}', α' dominates the logarithm in (16), and (16) and (12) are equivalent. However, at temperatures slightly less than T_{02}' in (16), the logarithm in Eq. (16) is practically independent of α'. Then (16) and (12) give different results for α', so one must use the more exact expression, Eq. (16), in which α' will primarily be determined by the first term.

Finally, we remark that the condition to determine T_{02}', $\alpha'(T_{02}')=5\epsilon/2kT_{02}'$ giving the temperature at which (16) and (12) begin to disagree, and the condition to use Eq. (16) given by $\alpha \simeq \epsilon/2kT_{02}'$ for the failure of the integration condition in Eq. (3), will in practice give almost exactly the same numerical value for T_{02}'. The reason for this is that α' is such a violent function of the

[8] J. G. Daunt and K. Mendelssohn, Proc. Roy. Soc. **170**, 423, 429 (1939).

temperature in the vicinity of T_{02}' that both of the equalities $\alpha'(T)=5\epsilon/2kT$ and $\alpha(T)=\epsilon/2kT$ are met in a very small temperature range.

Let us now determine what the relative populations of the ground, and all higher states are, above and below T_{02}'. Above T_{02}', since the right-hand side of Eq. (12) (the total population) and the second term of Eq. (16) agree, we see that the population of the ground state (1st term of Eq. (16)) is negligibly small. Below T_{02}' we have that the population of the higher states (2nd term of Eq. (16)), since $\alpha'\ll\epsilon/kT$, is $\simeq MT\ln MT$, where $M\sim k/\epsilon$ is *large*. Now $MT\ln MT$ varies approximately linearly in T, since its principal variation with T is in the factor of the logarithm. Moreover, it must provide, at the temperature T_{02}', practically all of the particles N, since above T_{02}' few of the particles are in the ground state. Therefore, we are compelled to conclude that, for $T<T_{02}'$ the population of the higher states must vary approximately like NT/T_{02}', and since the total number of particles must add up to N the ground state population varies like $N(1-T/T_{02}')$. In other words, since in Eq. (16), the second term is independent of α' (for $T<T_{02}'$, $\alpha'\ll 5\epsilon/2kT$) and is linear in T (like NT/T_{02}'), α' in the first term must vary in just such a way that the first term makes the total number of particles add up to N.

We, therefore, conclude that T_{02}' must be an accumulation temperature. We do not yet know how abrupt it is, and if it is also a condensation temperature.

To answer these questions we first determine T_{02}' by substituting $\alpha'=5\epsilon/2kT$, $T=T_{02}'$ in (16) and solving for T_{02}'. Doing this one finds

$$T_{02}'=T_{01}'(1+\delta)/\ln N, \tag{17}$$

where δ is small, of order $1/\ln N$. This shows that T_{02}' is not a condensation temperature since $T_{02}'\to 0$ as $N\to\infty$.

As an accumulation temperature T_{02}' is moderately "abrupt." To show this one calculates from Eq. (16) the relative population of ground and excited state *at* the temperature T_{02}', and also the maximum departure from linearity in T of the second term of (16), as α' varies in the range $\alpha'=5\epsilon/2kT$ to $\alpha'=-3\epsilon/2kT$ (the lowest allowed value according to first term of (16)).

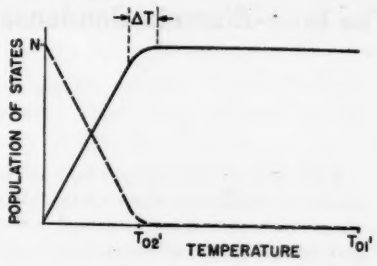

FIG. 1. Populations of the ground state (broken line) and all higher states (full line) of a two-dimensional B. E. gas. T_{01}' is the approximate condensation temperature of a three-dimensional B. E. gas of the same surface density.

Doing this one finds that the band of transition ΔT from condition "above" T_{02}' (negligible number of particles in ground state) to condition "below" T_{02}' (the ground state population $\simeq N(1-T/T_{02}')$) is given by

$$\Delta T\simeq T_{02}'/\ln N.$$

This means T_{02}' is a moderately abrupt accumulation temperature. Thus, if one had a "surface gram molecule" of material, $N=(N_{\text{Avogadro}})^{\frac{2}{3}}$ the accumulation at T_{02}' would occur at a temperature of 1/35 the corresponding three-dimensional condensation temperature, and in a temperature range about 3 percent of T_{02}' wide. All these conclusions are summarized in Fig. 1.

To interpret these results, one can say that in any physical situation where these calculations would be applicable, the results would be sensitive to any boundaries or impurities on the surface which would tend to modify the lowest energy state and break up the total number of particles N into subsystems. Effects of this type really represent the essence of surface and geometry effects in calculating from a statistical mechanical standpoint the properties of matter in the bulk. For example, one ordinarily considers the condensation temperature of water to be independent of the amount of material, but a moment's reflection shows that this is only approximately true. For small drops the condensation temperature (water-steam) is higher because of the increased pressure of surface tension. In this case, the condensation temperature also goes down (but not to zero) with an increased amount of material.

The Bose-Einstein Condensation for Charged Particles in a Magnetic Field

M. F. M. OSBORNE
Naval Research Laboratory, Washington, D. C.
(Received December 6, 1948)

The condensation and accumulation phenomena of charged Bose-Einstein particles in a magnetic field are examined, neglecting electrostatic interactions. For weak fields a single condensation occurs at the same temperature as that for uncharged particles; for strong fields there is a separate lower accumulation temperature, indicating the accumulation of particles in the lowest translational state. The total energy, free energy, and polarization are calculated, and applied to the properties of a gas of electron pairs, and a solution of deuterons in a metal, these being systems whose low temperature behavior might show a Bose-Einstein condensation. It is shown that the Bose-Einstein condensation of free electron pairs cannot provide a theory of superconductivity.

INTRODUCTION

IN the preceding paper[1] the distinction was made between a condensation in the thermodynamic sense, and an accumulation in the statistical mechanical sense. In this paper we use the conceptions and approximations there discussed to examine the properties of charged Bose-Einstein particles in a magnetic field, neglecting the effect of electrostatic interactions but including, where required, spin and intrinsic magnetic moment. We shall calculate the distribution of the population over the different classes of states, the total energy, the free energy, and the polarization.

We repeat here two expressions from I for convenience. To replace a sum by an integral we have

$$\sum_{m=a}^{b} f(m)=\int_{a-\frac{1}{2}}^{b+\frac{1}{2}} f(m)dm-f'(m)/24\Big|_{a}^{b}. \quad (1)$$

It is valid to use this approximation provided that for every point n within the interval, $a\leq n\leq b$

$$f(n+\tfrac{1}{2})-f(n-\tfrac{1}{2})-f'(n)\ll f(n). \quad (2)$$

For f of the form $1/(\exp(E(n)/kT+\alpha)-1)$, i.e. the B. E. integrand, it was found that if this criterion failed for one value of n in the interval (usually the lowest one) we could expect an abrupt accumulation of particles in the corresponding quantum state, and possibly a condensation. If it failed for every value we could expect a gradual accumulation in the lowest state.

THE GAS OF IONS IN A MAGNETIC FIELD, WITHOUT SPIN

Consider an assembly of N particles of mass m, charge e in a cylindrical container of volume V, radius R, height L with a magnetic field H along the axis. It is assumed that the energy levels which the particles occupy are given by the strength of the magnetic field and dimension L alone. Thus, we neglect electrostatic interactions, and ask: What is the behavior of this system as a function of the thermodynamic variables H and T? The energy levels are given by[2]

$$E(l, n_1, n_3)=\mu H(2(l+\tfrac{1}{2})+n_1+|n_1|)+\epsilon n_3^2$$
$$\epsilon=h^2/8mL^2, \quad \mu=eh/4\pi mc. \quad (3)$$

Let

$$g=\pi eHR^2/hc.$$

α is determined by

$$N=\sum_{n_1=-g}^{-1}\sum_{l=0}^{\infty}\sum_{n_3=1}^{\infty} 1/(\exp(E(l, n_1, n_3)/kT+\alpha)-1), \quad (4)$$

where the limits of summation on n_1, the azimuthal quantum number are determined by correspondence principle arguments.[2,3] l is the orbital quantum number and n_3 the translational quantum number for motion along the field.

Definitions and Approximations

In evaluating (4) we will utilize the following definitions (see Fig. 1):

(1) $U(p,\alpha)=(1/\Gamma(p+1))$

$$\times\int_0^{\infty} dzz^p/(\exp(z+\alpha)-1) \quad (5)$$

$$=\sum_{j=1}^{\infty}\exp(-\alpha j)/j^{p+1}. \quad (6)$$

(2) The temperature T_{01}, below which we must write separately the lowest term ($l=0$) in the integration over l (failure of Eq. (2))

$$T_{01}=(N/VU(\tfrac{1}{2}, 0))^{\frac{2}{3}}(h^2/2\pi mk). \quad (7)$$

T_{01} is also the condensation temperature in the absence of a field.[4]

(3) T_{02} is defined as the temperature below which, for $l=0$, we must write separately the lowest term ($n_3=1$) in the integration over n_3. It is defined so that

$$2gkT_{02}/3=N,$$

[1] M. F. M. Osborne, Phys. Rev. **76**, 396 (1949), hereafter referred to as I.

[2] J. H. Van Vleck, *The Theory of Electric and Magnetic Susceptibilities* (Clarendon Press, Oxford, 1932), pp. 354, 358.

[3] L. Landau, Zeits. f. Physik **64**, 262 (1930).

[4] F. London, Phys. Rev. **54**, 947 (1938).

or

$$T_{02}=3\epsilon Nhc/2\pi keHR^2 \tag{8}$$

$$=3h^3Nc/16LVmeHk. \tag{9}$$

Note that T_{02} depends on N/V, and also varies inversely as H and the dimensions of the system L in the direction of H. Roughly speaking T_{02} is the accumulation temperature of a one dimensional problem (see Fig. 1 of *I*), where the phenomenon is complicated by the presence of a magnetic field.

(4) T_H is defined as the temperature at which the spacing of the magnetic levels is of the order of magnitude of the thermal energy, $\mu H/kT_H=1$. When this is true it is certainly no longer valid to integrate over *any* of the magnetic levels. Note that this circumstance is not realized abruptly but gradually, so that T_H marks off an accumulation band rather than an accumulation temperature.

(5) For purposes of mathematical completeness rather than physical significance, we define a temperature T_t at which the average kinetic energy is equal to the average spacing of the translational levels ($\epsilon/kT_t=1$), and it is then no longer valid to integrate over any of the translational levels.

(6) H_c is defined as a critical field for which $T_{01}=T_{02}$

$$H_c=(N/V)^{\frac{1}{3}}(U(\tfrac{1}{2},0))^{\frac{2}{3}}3hc\pi/8Le. \tag{10}$$

For $H>H_c$ the accumulations at T_{01} and T_{02} occur separately. For $H<H_c$, the two accumulations occur at the same temperature T_{01} (case *C*). For $H<H_c$, $T_{02}>T_{01}$, and T_{02} is then simply a parameter by means of which the population of the lowest magnetic and higher translational states may simply be expressed as NT/T_{02}, an expression valid only for $T<T_{01}$.

Three other points should be noted in interpreting the formula which follows:

(1) The approximate behavior of the U functions for small parameter values, summarized in *I*, especially the fact that for

$$p=0,\quad \alpha\to 0,\quad U(p,\alpha)\to-\ln\alpha, \tag{11}$$

$$p<0,\quad \alpha\to 0,\quad U(p,\alpha)\to\alpha^p. \tag{12}$$

(2) The behavior of α in the neighborhood of the accumulation temperatures. Generally speaking, when a lowest energy term E_{low} has to be split off from an integration, in the separated term $\alpha\to-E_{\text{low}}/kT$ in just such a way that $(\alpha+E_{\text{low}}/kT)$ has the value to make the total population N. This is the explanation for the appearance of $\alpha+\mu H/kT$ and $\alpha+\mu H/kT+\epsilon/kT$ as effective normalization constants. A slightly different way of putting point (2) is as follows: if we have a series of complicated terms for N such as (14) or (17) which have a simple dependence on T, and only *one* of which is *sensitive* to α, then those terms effectively independent of α have the given dependence of population on T, and α is just such a complicated function of T to make the population of the term in which it does appear significantly vary as N minus the rest of the terms. Thus, if α only appears effectively in one term, we do not have to solve for α to get the relative populations of the different classes of states. This point will become apparent from the summary below, and be very useful in evaluating expressions for the total and free energy.

(3) In deriving the equations below, the lower limit of integration on n_3 must be chosen with care. In (13) for example, the lower limit zero for n_3 is a valid approximation, in some of the others, a half integral value as dictated by (1) must be used.

The Distribution of the Population

We can now write the expressions for α in the different regions of Fig. 1 as follows: N has been divided out so that the terms give the relative fractions of the populations in the different classes of states.

In region *A*

$$1=(T/T_{01})^{\frac{1}{2}}U(\tfrac{1}{2},\alpha)/U(\tfrac{1}{2},0), \tag{13}$$

valid for

$$\alpha>\mu H/kT\ll 1,\quad T>T_{01}.$$

There is no accumulation in any particular class of states.

In region *B*

$$1=(2T_H/T_{01})(T/T_{01})^{\frac{1}{2}}U(-\tfrac{1}{2},\alpha+\mu H/kT)/U(\tfrac{1}{2},0)$$
$$+(T/T_{01})^{\frac{1}{2}}U(\tfrac{1}{2},\alpha+2\mu H/kT)/U(\tfrac{1}{2},0), \tag{14}$$

valid for

$$\epsilon/kT<\alpha+\mu H/kT,\quad \alpha<\mu H/kT\ll 1,\quad T_{02}<T<T_{01}.$$

Since

$$U(\tfrac{1}{2},\alpha+2\mu H/kT)\simeq U(\tfrac{1}{2},0), \tag{15}$$

the two terms of (14) vary like $1-(T/T_{01})^{\frac{1}{2}}$, $(T/T_{01})^{\frac{1}{2}}$,

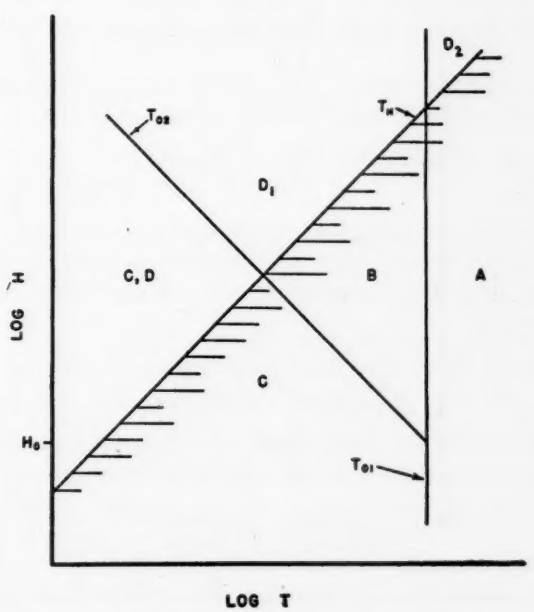

FIG. 1. (Schematic for Fig. 2.) Phase diagram for a gas of ions in a magnetic field.

these being the fractions of total population in ground magnetic and all higher magnetic states. From (14) we find

$$\alpha+\mu H/kT\simeq(\mu H/kT)^2(T/T_{01})^{\frac{3}{2}}\ll\mu H/kT. \quad (16)$$

In region C

$$1=(3T_t/2T_{02})/(\alpha+\mu H/kT+\epsilon/kT)+T/T_{02} +(T/T_{01})^{\frac{1}{2}}U(\tfrac{1}{2},\alpha+2\mu H/kT)/U(\tfrac{1}{2},0) \quad (17)$$

valid for

$$-\epsilon/kT<\alpha+\mu H/kT<\epsilon/kT,$$
$$T_H<T<(\text{the smaller of } T_{01},\ T_{02})$$

here also

$$U(\tfrac{1}{2},\alpha+2\mu H/kT)\simeq U(\tfrac{1}{2},0), \quad (18)$$

and the relative population of the states are

$$1-(T/T_{01})^{\frac{1}{2}}-T/T_{02},\quad T/T_{02},\quad (T/T_{01})^{\frac{1}{2}}, \quad (19)$$

in ground magnetic and ground translational, ground magnetic and higher translational, and higher magnetic and all translational states, respectively. Equation (19) is valid only if the first term is positive. Equation (17) is valid to the extent that $(2/3)\epsilon/kT$ represents the integral over n_3 for $l=0$ in (4), which is only approximately true (best when $|\alpha+\mu H/kT|\ll\epsilon/kT$). A detailed examination of this approximation will show that T/T_{02} in (19) indicates an abrupt accumulation in about the sense that T_{02}' in Fig. 1 of I represented an abrupt accumulation for the two-dimensional gas—perhaps not quite as abrupt. T_{02}, therefore, represents in Fig. 1 the center of a narrow accumulation band.

In region C, D

$$1=(3/2)(T_t/T_{02})/(\alpha+\mu H/kT+\epsilon/kT)+T/T_{02} +2(T_H/T_{01})(T/T_{01})^{\frac{1}{2}} \times U(-\tfrac{1}{2},\alpha+3\mu H/kT)/U(\tfrac{1}{2},0), \quad (20)$$

valid if

$$\mu H/kT\gg1,\quad -\epsilon/kT<\alpha+\mu H/kT<\epsilon/kT,\quad T<T_H.$$

This expression assumes that almost all the particles are in the first two magnetic states. This implies that

$$U(-\tfrac{1}{2},\alpha+3\mu H/kT)\simeq\exp(-2\mu H/kT) =\exp(-2T_H/T). \quad (21)$$

The relative population of ground translational and lowest magnetic, higher translational and ground magnetic, and next lowest magnetic and all translational states are

$$1-T/T_{02}-(2T_H/T_{02})(T/T_{01})^{\frac{1}{2}}\exp(-2T_H/T),$$
$$T/T_{02},\quad (2T_H/T_{02})(T/T_{01})^{\frac{1}{2}}\exp(-2T_H/T), \quad (22)$$

respectively. The first member of (22) must be positive.

In regions D_1 and D_2 we have α determined by

$$1=(2T_H/T_{01})(T/T_{01})^{\frac{1}{2}}[U(-\tfrac{1}{2},\alpha+\mu H/kT) +U(-\tfrac{1}{2},\alpha+3\mu H/kT)]/U(\tfrac{1}{2},0). \quad (23)$$

This assumes the population is almost entirely confined to the two lowest magnetic states, which these two terms represent. There is no accumulation in the lowest translational state as was the case in region CD. In region D_1 we may use the approximation

$$U(-\tfrac{1}{2},\alpha+\mu H/kT)\simeq(\pi/(\alpha+\mu H/kT))^{\frac{1}{2}},$$
$$U(-\tfrac{1}{2},\alpha+3\mu H/kT)\simeq\exp(-2\mu H/kT), \quad (24)$$

i.e.

$$(\alpha+\mu H/kT)\ll1,\quad \mu H/kT\gg1.$$

The relative populations are

$$1-(2T_H/T_{01})(T/T_{01})^{\frac{1}{2}}\exp(-2T_H/T), \quad (25)$$
$$(2T_H/T_{01})(T/T_{01})^{\frac{1}{2}}\exp(-2T_H/T).$$

In region D_2, the approximations (24) are not valid, and we must use exact expressions for the U functions.

In calculating Eqs. (13)–(25), the second term of (1) is neglected.

The Total Energy

We can also calculate expressions for the total energy

$$U=\sum_{l,\,n_1,\,n_3}E(l,n_1,n_3)n(l,n_1,n_3)$$

N_0 is Avogadro's number, R the gas constant.

In region A

$$U=(N/N_0)(3RT/2)(T/T_{01})^{\frac{1}{2}}U(\tfrac{3}{2},\alpha)/U(\tfrac{1}{2},0). \quad (26)$$

In region B

$$U=(N/N_0)[RT_H(1-(T/T_{01})^{\frac{1}{2}}) +(RTT_H/T_{02})(T/T_{01})^{\frac{1}{2}}U(\tfrac{1}{2},\alpha+\mu H/kT)/U(\tfrac{1}{2},0) +(3RT/2)(T/T_{01})^{\frac{1}{2}}U(\tfrac{3}{2},\alpha+2\mu H/kT)/U(\tfrac{1}{2},0) +2RT_H(T/T_{01})^{\frac{1}{2}}U(\tfrac{1}{2},\alpha+2\mu H/kT)/U(\tfrac{1}{2},0)]. \quad (27)$$

In region C

$$U=(N/N_0)[R(T_H+T_t)(1-(T/T_{01})^{\frac{1}{2}}-(T/T_{02})) +RTT_H/T_{02} +(3\pi^{\frac{1}{2}}RT/8)(T_t/T)^{\frac{1}{2}}(T/T_{02})U(\tfrac{1}{2},\alpha+\mu H/kT) +(3RT/2)(T/T_{01})^{\frac{1}{2}}U(\tfrac{3}{2},\alpha+2\mu H/kT)/U(\tfrac{1}{2},0) +2RT_H(T/T_{01})^{\frac{1}{2}}U(\tfrac{1}{2},\alpha+2\mu H/kT)/U(\tfrac{1}{2},0)]. \quad (28)$$

In region CD

$$U=(N/N_0)[R(T_H+T_t)(1-T/T_{02}-(2T_H/T_{01}) \times(T/T_{01})^{\frac{1}{2}}U(-\tfrac{1}{2},\alpha+3\mu H/kT)/U(\tfrac{1}{2},0)) +RTT_H/T_{02} +(3\pi^{\frac{1}{2}}/8)(RT^2/T_{02})(T_t/T)^{\frac{1}{2}}U(\tfrac{1}{2},\alpha+\mu H/kT) +(3RT_H^2/T_{01})(T/T_{01})^{\frac{1}{2}} \times U(-\tfrac{1}{2},\alpha+3\mu H/kT)/U(\tfrac{1}{2},0) +(3\pi^{\frac{1}{2}}/8)(RT^2/T_{02})(T_t/T)^{\frac{1}{2}} \times U(\tfrac{1}{2},\alpha+3\mu H/kT)]. \quad (29)$$

In regions D_1, D_2

$$U=(N/N_0)[RT_H(1-2(T_H/T_{01})(T/T_{01})^{\frac{1}{2}} \times U(-\tfrac{1}{2},\alpha+3\mu H/kT)/U(\tfrac{1}{2},0)) +RT(T_H/T_{01})(T/T_{01})^{\frac{1}{2}}U(\tfrac{1}{2},\alpha+\mu H/kT)/U(\tfrac{1}{2},0) +6RT_H(T/T_{01})^{\frac{1}{2}}U(-\tfrac{1}{2},\alpha+3\mu H/kT)/U(\tfrac{1}{2},0) +RT(T/T_{01})^{\frac{1}{2}}(T_H/T_{01}) \times U(\tfrac{1}{2},\alpha+3\mu H/kT)/U(\tfrac{1}{2},0)]. \quad (30)$$

The same approximations as in the corresponding equa-

tions for α also hold. The form of the above equations, when all the terms are written in the form const.$\times RT$ $\times$function of temperature ratios, is convenient when they are used with a diagram such as Fig. 1. Given an H, T point of interest, one can quickly estimate the values of different terms by reading the temperatures T_{01}, T_H, T_{02} at which a horizontal line through the H, T point of interest crosses the T_{01}, T_H or T_{02} line.

Equations (26)–(30) may be substantially simplified and condensed by using the valid approximations for each set, especially the facts that for all regions but B and D_2, $\alpha+\mu H/kT$ is very small and $U(p, \alpha)\simeq U(p, 0)$ for $\alpha\ll 1$ and $p>0$. However, they have been left in the form given so that the energy contribution of each type of level may be more explicitly identified, and the validity of the approximations more critically examined.

THE GAS OF IONS IN A MAGNETIC FIELD, WITH SPIN

The Relative Populations of the States

Let us reconsider the above problem when it is assumed that the particles have an intrinsic magnetic moment μ', and a spin I. In that case, we have to sum over $2I+1$ additional levels $\mu'H$ apart, in addition to the levels given in (3) above. The expression determining α becomes

$$N=\sum_{l=0}^{\infty}\sum_{n_3=1}^{\infty}\sum_{\sigma=-I}^{I} g/(\exp(E(\sigma, n_3, l)/kT+\alpha)-1) \quad (31)$$

with

$$E(\sigma, n_3, l)=\mu'H\sigma/I+\epsilon n_3^2+2(l+\tfrac{1}{2})\mu H,$$
$$\epsilon=h^2/8mL_z^2, \quad \mu=eh/4\pi mc.$$

Note that m refers to the (arbitrary) mass of the particle, so that in discussing particular particles such as deuterons μ'/μ is *not* the conventionally tabulated value for the intrinsic magnetic moment, but the mass number times it.

If all summations can be replaced by integrals, as will be the case so long as $\alpha>\mu H/kT$, (31) becomes

$$N=(2I+1)V(2\pi mkT)^{\frac{3}{2}}U(\tfrac{1}{2}, \alpha)/h^3. \quad (32)$$

When $\alpha<\mu H/kT$, it is no longer valid to replace the sum over the first terms of l by an integration. The behavior of α in this circumstance is a little subtle, but strict attention to the criterion (2) for integration, together with the expectation that α will approach close to the negative of the lowest energy state divided by kT, will show that when it no longer becomes valid to integrate over the first term of the l-summation, it will no longer be valid to integrate over the first term of the σ-summation either. Under these circumstances, splitting off the first term of the l- and σ-summation, (31) gives

$$1=(2\mu H/kT(2I+1))(T/T_{0\sigma})^{\frac{3}{2}}U(-\tfrac{1}{2}, \alpha_0)/U(\tfrac{1}{2}, 0)$$
$$+(\sum_{\sigma'=1}^{2I}(2\mu H/kT(2I+1))(T/T_{0\sigma})^{\frac{1}{2}}$$
$$\times U(-\tfrac{1}{2}, \alpha_0+\mu'H\sigma/I)/U(\tfrac{1}{2}, 0))+(T/T_{0\sigma})^{\frac{3}{2}}. \quad (33)$$

In (33) we have the following definition. $T_{0\sigma}$ is the condensation temperature in the absence of a field H. It is the solution of (32) for $\alpha=0$. $\alpha_0=\alpha+\mu H/kT$ $-\mu'H/kT$ is the effective normalization constant, and the first term of (33) is the only term sensitive to its value. It can be shown, as in the case of (16), that $\alpha_0\ll\mu H/kT$. This together with the fact that $U(-\frac{1}{2}, \alpha_0)$ $\simeq\alpha_0^{-\frac{1}{2}}$ will show that the terms of the summation in (33) are all small compared to the first term of (33).

The three terms of (33) represent the following classes of states:

(a) $l=0$, $\sigma=-I$, lowest magnetic and lowest spin, all translational.

(b) $l=0$, $\sigma=-I+1$ to $+I$, lowest magnetic and all higher spins, all translational.

(c) $l=1$ to ∞, $\sigma=-I$ to $+I$, excited magnetic, all spins, all translational.

The approximate relative orders of magnitude of the populations of these states are (a) $1-(T/T_{0\sigma})^{\frac{3}{2}}$, (b) Order $(\mu'H/kTI)^{\frac{1}{2}}$ (small), (c) $(T/T_{0\sigma})^{\frac{3}{2}}$.

The Free Energy and Polarization

We can now calculate the free energy $F=U-TS$ and magnetic polarization P. For $T>T_{0\sigma}$ and defining $\beta=\mu H/kT$, $\beta'=\mu'H/kTI$, $\gamma=\epsilon/kT$

$$F=-NkT\alpha+(gkT/4\beta)(\pi/\gamma)^{\frac{1}{2}}[-(2I+1)U(\tfrac{3}{2}, \alpha)$$
$$-\beta'^2(2I+1)^3U(-\tfrac{1}{2}, \alpha)/24$$
$$+\beta'^2U(-\tfrac{1}{2}, \alpha)/24$$
$$+\beta^2(2I+1)U(-\tfrac{1}{2}, \alpha)/6]. \quad (34)$$

In obtaining (34) we have expressed $\sum_{\sigma=-I}^{I} U(\frac{3}{2}, \alpha+\beta'\sigma)$ as an integral, using (1), including the correction term and also expanded this U function as a Taylor series about α.

For $T<T_{0\sigma}$

$$F=-NkT\alpha-gkT(\pi/\gamma)^{\frac{1}{2}}[\sum_{\sigma=-I}^{I} U(\tfrac{1}{2}, \alpha+\beta+\sigma\beta')$$
$$-\sum_{\sigma=-I}^{I} U(\tfrac{3}{2}, \alpha+2\beta+\sigma\beta')/4\beta$$
$$+\beta\sum_{\sigma=-I}^{I} U(-\tfrac{1}{2}, \alpha+2\beta+\sigma\beta')/24]. \quad (35)$$

The polarization, for $T>T_{0\sigma}$, is given by[5]

$$P=-(\partial F/\partial H)_\alpha/V,$$

$$P=(g(\pi/\gamma)^{\frac{1}{2}}\mu(2I+1)/V)$$
$$\times[(2I+1)^2(\mu'/\mu I)^2U(-\tfrac{1}{2}, \alpha)/48$$
$$-(\mu'/\mu I)^2U(-\tfrac{1}{2}, \alpha)/48-U(-\tfrac{1}{2}, \alpha)/12] \quad (36)$$

[5] See N. F. Mott and H. Jones, *Properties of Metals and Alloys* (Clarendon Press, Oxford, 1936), p. 204.

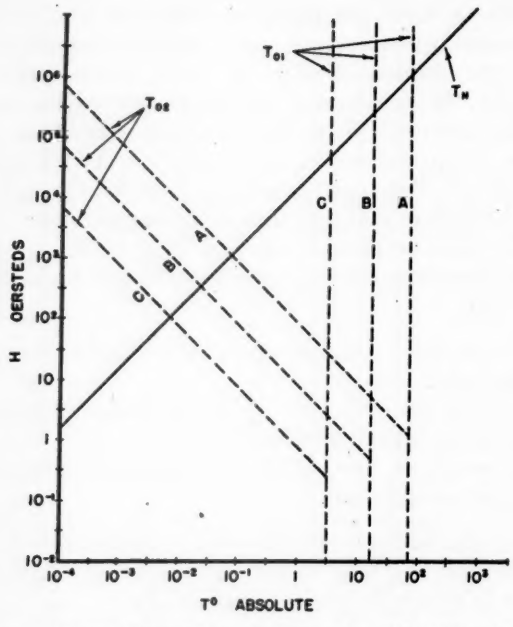

FIG. 2. Phase diagram for electron pairs. (A) 10^{19} pairs/cm^3, (B) 10^{18} pairs/cm^3, (C) 10^{17} pairs/cm^3. The Z dimension, along H, has been taken as 1 cm.

and for $T<T_{0\sigma}$

$$P=(g(\pi/\gamma)^{\frac{1}{2}}/V)\sum_{\sigma=-I}^{I}[\mu U(\tfrac{1}{2},\alpha+\beta+\sigma\beta')/2\beta - (\mu+\mu'\sigma/I)U(-\tfrac{1}{2},\alpha+\beta+\sigma\beta')/2 - (2\mu+\mu'\sigma/I)U(\tfrac{1}{2},\alpha+2\beta+\sigma\beta')/4\beta - \mu U(-\tfrac{1}{2},\alpha+2\beta+\sigma\beta')/12 + (2\mu+\mu'\sigma/I)\beta U(-\tfrac{3}{2},\alpha+2\beta+\sigma\beta')/24]. \quad (37)$$

Limiting Form for High Temperature

For high temperatures $\alpha\gg1$, $U(\frac{1}{2},\alpha)\simeq U(\frac{3}{2},\alpha)\simeq U(-\frac{1}{2},\alpha)\simeq\exp(-\alpha)$ and the polarization is, using (32) and (36)

$$P=\mu'^2HN(I+1)/3IkTV-N\mu^2H/3VkT. \quad (38)$$

For $I=\frac{1}{2}$

$$P=N\mu'^2H/kTV-N\mu^2H/3kTV \quad (39)$$

and these two terms can just be interpreted as the spin paramagnetism and the Langevin diamagnetism as given by Maxwell-Boltzmann statistics, which provides a convenient check on our work.

For $T<T_{0\sigma}$, the polarization is, using Eqs. (37) and (33) and neglecting quantities of order $(\mu H/kT)^{\frac{1}{2}}$

$$P=N(\mu'-\mu)(1-(T/T_{0\sigma})^{\frac{1}{2}})/V. \quad (40)$$

This expression has the quite plausible physical interpretation that there are $N(1-(T/T_{0\sigma})^{\frac{1}{2}})$ particles in the ground state of spin and circulation about the magnetic field, each of which contributes a positive magnetic moment μ' and a negative (diamagnetic) moment μ. In obtaining Eqs. (34)–(40) one has to include the correction term of Eq. (1) in replacing sums by integrals and also must utilize the approximate expressions for the U functions with small parameter.

Interpretation and Limitations of Formulas

It is appropriate to ask at this point if the temperature T_{01} (or $T_{0\sigma}$, for particles with spin) is a condensation temperature or merely an accumulation temperature, such as T_{02}. In the limiting case of no magnetic field we know that T_{01} is a condensation temperature. We also know that as the magnetic field increases and we go up along the T_{01} line (Fig. 1) eventually we reach the T_H band, in which we know there is a gradual accumulation in the ground magnetic state. Therefore, somewhere between 0 magnetic field and a magnetic field so strong that $kT_{01}\sim\mu H$, T_{01} ceases to be a condensation temperature and becomes an accumulation temperature. However, examination of the mathematics shows that it is fairly abrupt except in the immediate neighborhood of T_H. The exact problem of the field strength for which T_{01} ceases to be a condensation temperature has not been examined, though one might conjecture that it lies near H_c.

In the case of the accumulation temperature T_{02}, it should be observed that it is a function of N/V as $N\to\infty$ but it also depends on *how* $V\to\infty$ because of the factor L. If the thickness of the specimen $L\to\infty$, $T_{02}\to0$, otherwise it remains finite. This again is an example of how statistical mechanics shows the dependence of thermodynamic properties on geometry.

One can also point out here a limitation on the validity of the expressions derived above. It has been stated at the beginning that the magnetic field which determines the energy levels in which the particles move is H. Strictly speaking this is not true since the effective field acting on the particles is $H_{eff.}=H-\lambda P$ where λ is the depolarizing factor depending on the shape of the specimen, but in any event is not greater than 4π. However, it is valid to use H for $H_{eff.}$ if P is small compared to H. Now P, the polarization, was calculated to be $\sim(N\mu/V)(\mu H/kT)$ above the condensation temperature T_{01} and $\sim N\mu/V$ below it. If this latter expression is small compared to the applied H then the condition of applicability is met. As will be seen in the discussion of the numerical examples, this is the case for most problems of interest. $\mu\sim10^{-20}$ for electron pairs, and $\mu\sim10^{-23}$ for deuterons. For these examples the number of particles per unit volume has to be greater than 10^{20}, 10^{23}, respectively, for the theory to fail for fields less than one oersted.

Experimental Methods

We might now make a few remarks on the most suitable way in which these effects could be detected by measurement. Evidently, the orders of magnitude of the polarizations below and above the condensation tem-

perature are as $N\mu/V$ and as $(N\mu/V)\mu H/kT$, with $\mu H/kT \ll 1$. Now above the condensation temperature the phenomena are essentially the same as though determined by Maxwell-Boltzmann statistics, where Curie's law applies. Hence, for $T \gg T_{01}$, or $T \gg T_{0\sigma}$ as may be relevant, Bose-Einstein effects could not be distinguished from any others in which the susceptibility is independent of H and varies as $1/T$.

Experimentally, this means that the susceptibilities are of the order 10^{-6} and can best be detected by a weighing method in a strong inhomogeneous field. However, below the condensation temperature the polarization is essentially constant, or the susceptibility P/H varies as $1/H$. It is also larger by a quantity of order $kT/\mu H$ from what it is above. This means that it is not profitable in a weighing method to use a strong magnetic field since the force on the specimen would depend only on the gradient of the magnetic field and be independent of H. Also the fact that the polarization is so very much larger means that it would be simpler to detect it. Thus, a simple measurement of the self-induction of a coil around a specimen supposed to contain this peculiar gas would begin to change abruptly by a small amount as soon as the temperature T_{01} was reached. For the case of a needle-shaped specimen (depolarizing factor $\lambda=0$) filling a coil of inductance L_0, below the condensation temperature T_{01} the inductance would become $L=L_0(1+4\pi P/H)$ where H is the applied field, V the volume and P the total polarization as given by (40). This shows that the percentage change in the inductance would be larger the smaller H, with the restriction for applicability that $P/H \ll 1$.

Applications

Let us now consider some possible applications of these calculations. It was suggested by London,[4] among others, that superconductivity might be explained as a condensation phenomenon of Bose-Einstein particles and Ogg has added definiteness to this suggestion by supposing that these particles are electron pairs. Let us see whether or not this hypothesis is in accordance with the above calculations. Using twice the mass and charge of the electron, we see that for the condensation temperature to fall in the range of superconducting temperature, say less than 10° absolute, the concentration of particles must be $N/V < 10^{18}$. How large is the polarization under these conditions? It is of order $N\mu/V \simeq 10^{-2}$. However, it is one of the essential features of superconductivity that the material be perfectly diamagnetic, or that the $4\pi P$ be equal and opposite to the applied magnetic field H. This calculation shows that the polarization can never be larger than 10^{-2} oersteds, and since in practice superconductors are diamagnetic up to several hundred oersteds, we must reject this hypothesis, or modify in such a way that the accumulation takes place in states of much higher l than the lowest. This calculation does not exclude the possibility that there can be electron pairs either in a metal or in a metal-ammonia solution. If there are, and if they are mobile and can be treated as Bose-Einstein particles, then one can look for their condensation temperature in the manner described above, by a small fairly abrupt (like $1-(T/T_{01})^{\frac{1}{2}}$) change in the self-induction of a coil with diminishing temperature. It would be interesting to see if this effect can actually be observed, as it is intimately tied up with the vexatious question as to how far and in what particulars one can go in treating particles which are not free and do interact as though they were free and did not interact. This is done in the treatment of valence electrons inside a metal by Fermi-Dirac statistics. Figure 2 gives the phase diagram corresponding to Fig. 1, for particles of zero spin and twice the electronic mass and charge.

A second possibility for testing the above formulas is suggested by London's refinement of his theory of liquid helium. In order to fit the observations of the specific heat of He with a theoretical specific heat calculated by Bose-Einstein statistics, London[6] proposed that the helium atoms be divided into two classes. One of these was to be treated as a crystalline lattice obeying a Debye T^3 law, the other fraction was to be treated as a Bose-Einstein gas which occupied the allowed levels formed by this lattice. It was the condensation phenomenon of the second class of particles which accounted for the λ-phenomenon of liquid helium. Now the number of possible particles available to observation of condensation phenomenon are relatively limited, because the condensation temperature diminishes with increasing mass and for helium, already one of the lightest particles, it is ~3°K. One other possibility is deuterons, and fortunately, we have a mechanism whereby these might be treated as a gas just as the valence electrons of a metal are treated. It is known that certain metals[7,8] (Ce, Th, Zr, Ti, Ta, V, Pd, Cb, La) absorb large amounts of hydrogen and presumably also deuterium. These solutions cannot be strictly considered as chemical compounds, since the proportion increases with decreasing temperature. Therefore, it is suggested that for deuterium a fraction of the particles (as deuterons) may be treated as a Bose-Einstein gas in the sense that they can be imagined to be distributed throughout the metallic lattice rather than at fixed points, and for these we could seek a condensation temperature. If as many as 10^{+21} deuterons/cc could be considered free, the condensation temperature would be ~1°K.

A possible encouragement for this point of view can be taken for the case of hydrogen and palladium. Here it is known that the absorption of hydrogen by palladium

---

[6] F. London, J. Phys. Chem. **43**, 49 (1939).

[7] F. Ephraim, *Inorganic Chemistry*, 4th Rev. Ed. by P. C. L. Thorne and E. R. Roberts (Nordeman Publishing Company, New York, 1943), p. 875. There is a most striking correlation between the hydride forming and superconducting elements, the explanation of which is unknown.

[8] A. Sieverts, Zeits. f. angew Chem. **21**, 37 (1929).

decreases the susceptibility in a linear fashion to zero and that beyond that point the susceptibility remains zero.[9,10] This has been interpreted that the protons fill up the d levels (0.55 holes per atom). Presumably the excess ones wander about the lattice, and part of them could be treated as a gas of free particles in the desired way.[11] There is also evidence that hydrogen dissolved in the metal is dissolved as protons and if this were also true for deuterium the deuterons stripped of their external electrons could be considered as Bose-Einstein particles.

These considerations are at best speculative, and ignore completely interactions and the periodic nature of the potential in which the particles move. They do suggest that an experimental study of the relative low temperature behavior of solutions of hydrogen in a metal and of deuterium in a metal would be most illuminating in revealing the effect of the two different statistics on the behavior of the system, and in indicating the nature of possible modifications in the theoretical approach to such problems which might be made.

[9] See reference 5, p. 200.
[10] B. Svenson, Ann. d. Physik **18**, 294 (1933).
[11] It was pointed out to the author by S. Liebson that if one had a case where the "free proton theory of the hydrides" was approximately valid, one might expect that at very low temperatures there would be proton superconductivity, not to mention the formation of proton pairs!

PHYSICAL REVIEW VOLUME 76, NUMBER 3 AUGUST 1, 1949

On the Electromagnetic Surface Wave of Sommerfeld*

T. KAHAN AND G. ECKART
Office National d'Etudes et de Recherches Aeronautiques, Paris, France
(Received July 7, 1948)

It is proved that Sommerfeld's well-known electromagnetic surface wave does not exist in the radiation of a Hertzian dipole over a plane earth because it does not fulfill the so-called "radiation condition." The path of integration chosen by Sommerfeld is correct, but there is another saddle-point overlooked by this author which just annuls the surface wave due to the residue. These results are in agreement with Burrow's measurements.

IN a well-known paper published in 1909, Sommerfeld[1] treated the problem of the propagation of radio-waves along the surface of the (plane) earth. If we make the (ψ, ϕ) plane coincide with the plane of the earth surface (the z axis pointing upwards) and if we consider a vertically oscillating dipole in the air at the point $z=r=0$, the Hertzian vector Π describing the electromagnetic field may be expressed as follows:

$$\Pi=\frac{e^{ik_1R}}{R}=\int_0^\infty \frac{J_0(\lambda r)\lambda d\lambda \exp[-z(\lambda^2-k_1^2)^{\frac{1}{2}}]}{(\lambda^2-k_1^2)^{\frac{1}{2}}}; \quad z>0. \tag{1}$$

For $z<0$ we have a similar formula with k_2 replacing k_1. Here k_1 and k_2 denote the wave numbers of the upper and lower medium (air and earth). Taking into account the radiation reflected by the earth, we get in the upper medium (air), for the resulting Hertzian function

$$\Pi_1=\text{const.}\int_0^\infty \frac{J_0(\lambda r)\exp[-z(\lambda^2-k_1^2)^{\frac{1}{2}}]\lambda d\lambda}{k_1^2(\lambda^2-k_2^2)^{\frac{1}{2}}+k_2^2(\lambda^2-k_1^2)^{\frac{1}{2}}}. \tag{2}$$

Setting

$$J_0(\lambda r)=\tfrac{1}{2}[H_0^{(1)}(\lambda r)+H_0^{(2)}(\lambda r)], \tag{3}$$

where H and J are the usual cylindric functions. We can displace the path of integration of the integrand of (2) containing $H_0^{(1)}$ into the upper part of the complex plane λ, and the path of integration containing $H_0^{(2)}$ we can shift into the lower half-plane λ. The integrals effected along the circle of infinite diameter are zero, the two integrals conducted along the imaginary axis compensate each other. As the integrand of (2) has no singularities in the lower quadrant, we have left only the following integral in the upper half-plane λ:

$$\text{const.}\int \frac{H_0^{(1)}(\lambda r)\exp[-z(\lambda^2-k_1^2)^{\frac{1}{2}}]\lambda d\lambda}{k_1^2(\lambda^2-k_2^2)^{\frac{1}{2}}+k_2^2(\lambda^2-k_1^2)^{\frac{1}{2}}} \tag{4}$$

conducted along the following three paths (Fig. 1): (a) Along the loop 1 around the branch-cut going from the branch point k_1 of (4) to infinity in the upper half-plane; (b) along the loop 2 around the branch-cut going from the branch point k_2 of (4) to infinity; (c) and along the circle 3 around the pole P of (4). Path 1 provides the so-called space-wave; path 2 gives no appreciable contribution; path 3 gives rise to the famous surface wave expressed by:

$$w_0=\text{const.}e^{isr}\exp[-z(s^2-k_1^2)^{\frac{1}{2}}]/r^{\frac{1}{2}}, \tag{5}$$

s being the pole of the integrand of (4) defined by:

$$s=k_1\sin\phi_B; \quad \phi_B=\tan^{-1}(k_2/k_1), \tag{6}$$

ϕ_B being the Brewester angle.

In 1919 Weyl[2] tackled the same problem but with a different mathematical approach. His solution contains

* For a preliminary report see T. Kahan and G. Eckart, Comptes rendus **226**, 1513 (1948).
[1] A. Sommerfeld, Ann. d. Physik **28**, 665 (1909).
[2] H. Weyl, Ann. d. Physik **60**, 481 (1919).

only the part which in Sommerfeld's solution is given by loop 1, its solution did not therefore contain the surface wave (5). The discussion of this problem has been carried on for years by different authors. In 1937, Burrows[3] found in an experimental study, that the surface wave did not exist.[4]

In 1947, Epstein[4] went a step further in solving the problem without, however, reaching a complete solution. He points out that already in the primary radiation the path of integration may be taken, instead of along the real axis (path *I* in Fig. 2), along the path *II* which excludes the pole due to the presence of the second medium (earth). We have then only the integrals along the branch-cuts left. Epstein alleges now that the problem thus dealt with is not unique and states that Sommerfeld's proof of uniqueness loses its validity in the presence of sources, when there are singularities of sources such as the dipole. This remark about the singularity of sources such as the dipole is senseless, for Sommerfeld takes it into account expressly. The following demonstration proves it. Epstein declares himself satisfied in this non-uniqueness of the problem and points out eventually that the surface wave is not due to a dipole.

The scope of the following is to show how we can get rid of this indeterminateness in the solution, and how we can therefore solve the problem exactly.

Sommerfeld deals with this problem in a fundamental paper.[5] He points out that nature provides in fact a unique solution, and the problem is only to find the condition which determines the actual solution among the set of all possible solutions. This condition is the condition of outgoing waves or radiation condition ("Ausstrahlungsbedingung") established for the first time by Sommerfeld himself. This condition states that at a sufficient distance from the source, the field must have the character of outgoing waves; incoming waves would give rise to standing waves which have no reality whatever in our case, since we have no sources at infinity.

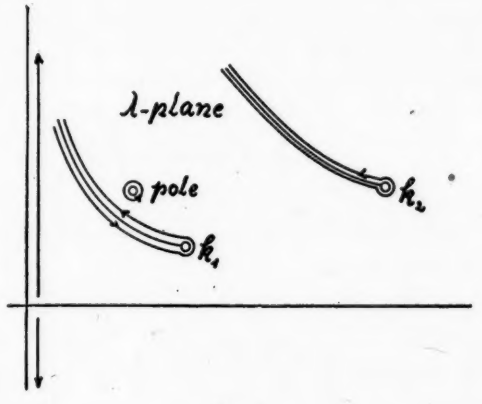

FIG. 1.

[3] C. W. Burrows, Proc. I.R E. **25**, 219 (1937).
[4] P. S. Epstein, Proc. Nat. Acad. Sci. **33**, 195 (1947).
[5] A. Sommerfeld, Jahresber. d. Deutsch. Math. Ver. **309** (1913).

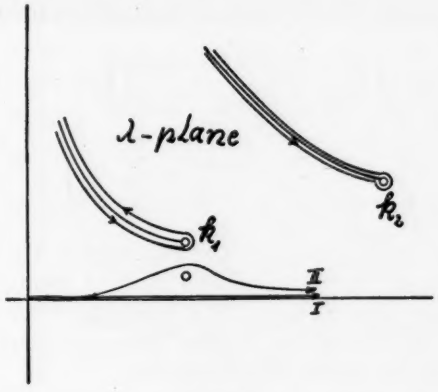

FIG. 2.

In order to avoid any experimental attenuation by absorption, let us suppose k_1 and k_2 to be real. If the time variation is supposed to be $e^{i\omega t}$, the condition of outgoing waves may be expressed as follows:

$$\lim_{R\to\infty} R(\partial\Pi_1/\partial n - ik\Pi_1)=0 \tag{7}$$

with

$$\lim_{R\to\infty} R\Pi_1 \neq \infty .$$

n is the normal to a surface at infinity. If we choose as such a large sphere around the source, n coincides with the direction of R (space vector). Now, as we shall see later on, the surface wave does not satisfy this condition.

We shall prove now that the condition of outgoing waves make our problem unique. We require two functions, Π_1 and Π_2, having the following characteristics:

I. We have

$$\Delta\Pi_1 + k_1^2\Pi_1 = 0, \quad z>0,$$
$$\Delta\Pi_2 + k_2^2\Pi_2 = 0, \quad z<0,$$

k_1 and k_2 both real, $\mu_1=\mu_2=\mu$.

II. At $z=0$,

$$\Pi_1=\Pi_2, \quad \partial\Pi_1/k_1^2\partial z = \partial\Pi_2/k_2^2\partial z.$$

III. $\Pi_1 - e^{ik_1R}/R$ for $z\geqq 0$ and $\Pi_2 - e^{ik_2R}/R$ for $z<0$ are finite and continuous with continuous derivatives, at $R=0$ included.

IV. $\lim_{R\to\infty} R[\partial\Pi_1/\partial n - ik_1\Pi_1]=0$,
$\lim_{R\to\infty} R\Pi_1 \neq \infty$, $z>0$,

$\lim_{R\to\infty} R[\partial\Pi_2/\partial n - ik_2\Pi]_2=0$,
$\lim_{R\to\infty} R\Pi_2 \neq \infty$, $z<0$.

We write condition IV in the form:

IVa. $\lim_{R\to m}[\partial\Pi_i/\partial n - ik_i\Pi_i]=\Pi_i^*$

with $\lim_{R\to\infty}\Pi_i^*\to 0$, $i=1, 2$.

Let us now suppose we have two different solutions; our purpose is to show that their difference is zero. Let Π_1, Π_2 be the first solution; Π_1', Π_2' the second one; $\overline{\Pi}_1$, $\overline{\Pi}_2$ the first conjugate solution; $\overline{\Pi}_1'$, $\overline{\Pi}_2'$ the second conjugate solution.

We introduce then the difference of our solutions:

$$\left.\begin{aligned} u_1&=\Pi_1-\Pi_1'; \quad \bar{u}_1=\overline{\Pi}_1-\overline{\Pi}_1' \\ u_2&=\Pi_2-\Pi_2'; \quad \bar{u}_2=\overline{\Pi}_2-\overline{\Pi}_2' \end{aligned}\right\} \tag{8}$$

Let us write the theorem of Green in the form:

$$\int u\Delta v dS+\int\left(\frac{\partial u}{\partial x}\frac{\partial v}{\partial x}+\frac{\partial u}{\partial y}\frac{\partial v}{\partial y}+\frac{\partial u}{\partial z}\frac{\partial v}{\partial z}\right)dS = \int u\frac{\partial v}{\partial n}d\sigma \quad (9)$$

where S represents the volume described in Fig. 3, and σ its surface. The latter consists of: (1) A hemisphere Σ of infinity large radius; (2) a hemisphere which surrounds the source D; (3) the horizontal plane $Z=0$ which lies between these hemispheres.

We shall also express the surface element of the large hemisphere as:

$$d\Sigma=r^2d\omega \quad (10)$$

where $\int d\omega=4\pi$ for the whole space.

We set in Green's theorem (9):

$$u=u_1, \quad v=\bar{u}_1. \quad (11)$$

We get then in view of I:

$$-k_1^2\int u_1\bar{u}_1dS+\int\left(\frac{\partial u_1}{\partial x}\frac{\partial \bar{u}_1}{\partial x}+\frac{\partial u_1}{\partial y}\frac{\partial \bar{u}_1}{\partial y}+\frac{\partial u_1}{\partial z}\frac{\partial \bar{u}_1}{\partial z}\right)dS=\int u_1\frac{\partial \bar{u}_1}{\partial n}d\sigma \quad (12)$$

where the surface integral is to be effected over the three mentioned surfaces.

1. The integral of the right-hand side extended over a small hemisphere tends to zero with ρ_2 if ρ is the radius of this sphere, for we chose according to III:

$$\Pi_1-e^{ik_1R}/R=w, \quad (13)$$

finite and continuous also at the origin.

$$\Pi_1'-e^{ik_1R}/R=w', \quad (14)$$

finite and continuous also at the origin. Therefore,

$$w-w'=\Pi_1-\Pi_1'=u_1 \quad (15)$$

also finite and continuous with their derivatives over the small sphere. Hence we have there

$$|u_1|<M, \quad |\partial\bar{u}_1/\partial u|<M, \quad (16)$$

if M means a fixed number which is sufficiently large. Therefore,

$$\left|\int u_1\frac{\partial\bar{u}_1}{\partial n}d\sigma\right|<M\rho^2 2\pi. \quad (17)$$

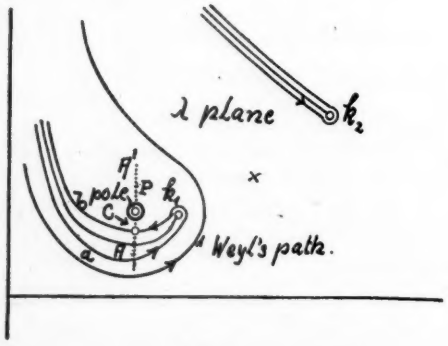

FIG. 3.

2. Consider now the integral of the right-hand side extended over the large hemisphere. The "Ausstrahlungsbedingung" demands for u_1:

$$\lim_{R\to\infty}R(\partial u_1/\partial n-ik_1u_1)=0$$

or

$$R\frac{\partial u_1}{\partial n}-ikRu_1=u' \text{ with } u'\to 0 \text{ for } R\to\infty.$$

We have therefore for the conjugate $\bar{u}_1$:

$$R\partial\bar{u}_1/\partial n+ik\bar{u}_1R=\bar{u}' \text{ with } \bar{u}'\to 0 \quad (18)$$

$$\partial\bar{u}_1/\partial n=ik\bar{u}_1+\bar{u}_1'/R \text{ with } u_1' \quad (19)$$

$$\Big\}R\to\infty.$$

Therefore:

$$\int u_1(-ik\bar{u}_1+\bar{u}_1')d\Sigma=\int(-iku_1\bar{u}_1+u_1\bar{u}_1'/R)d\Sigma, \quad (20)$$

with $d\Sigma=r^2d\omega$ the right-hand side becomes:

$$\int(-iku_1\bar{u}_1R^2+Ru_1\bar{u}_1')d\omega, \quad (21)$$

where Ru_1 is finite according to IV′ for $R\to\infty$, $\bar{u}_1'\to 0$ for $R\to\infty$, $d\omega$ is finite.

Therefore, the second term in the integral vanishes over the large hemisphere. $u_1\bar{u}_2$ is real and the integral which is finite because of IV′ is pure (negative) imaginary.

3. Consider now the integral extended over the plane. The formula of Green is reduced to:

$$-k_1^2\int u_1\bar{u}_1dS+\int\left(\frac{\partial u_1}{\partial x}\frac{\partial\bar{u}_1}{\partial x}+\frac{\partial u_1}{\partial y}\frac{\partial\bar{u}_1}{\partial y}+\frac{\partial u_1}{\partial z}\frac{\partial\bar{u}_1}{\partial z}\right)dS = -ik_1\int R^2u_1\bar{u}_1d\omega+\int u_1\frac{\partial\bar{u}_1}{\partial n}d\sigma. \quad (22)$$

The first member is real, the first term of the second member is imaginary.

In a similar way we get for the second medium:

$$-k_2^2\int u_2\bar{u}_2dS_2+\int\left(\frac{\partial u_2}{\partial x}\frac{\partial\bar{u}_2}{\partial x}+\cdots\right)dS_2 = -ik_2\int R^2u_2\bar{u}_2d\omega+\int u_2\frac{\partial u_2}{\partial n}d\sigma. \quad (23)$$

Multiply (22) by $1/k_1^2$, (23) by $1/k_2^2$ and add, we get:

$$\int u_1\bar{u}_1 dS_1+\int u_2\bar{u}_2 dS_2$$

$$-\frac{1}{k_1^2}\int\left(\frac{\partial u_1}{dx}\frac{\partial\bar{u}_1}{\partial x}+\cdots\right)dS_1$$

$$-\frac{1}{k_2^2}\int\left(\frac{\partial u_2}{\partial x}\cdot\frac{\partial\bar{u}_2}{\partial x}+\cdots\right)dS_2$$

$$=i\int_{\text{upper sphere}}\frac{R^2}{k_1}u_1\bar{u}_1 d\omega+i\int_{\text{lower sphere}}\frac{R^2}{k_2}u_2\bar{u}_2 d\omega$$

$$-\left\{\int_{\text{plane}}\frac{1}{k_1^2}u_1\frac{\partial\bar{u}_1}{\partial n}d\sigma+\int_{\text{plane}}\frac{1}{k_2^2}u_2\frac{\partial\bar{u}_2}{\partial n}d\sigma\right\}. \quad (24)$$

Since the direction of differentiation n means always the direction of the outside normal of the field considered, we have along the plane:

$$\partial/\partial n=-\partial/\partial z, \text{ in the upper space;}$$
$$\partial/\partial n=+\partial/\partial z, \text{ in the lower space.}$$

In view of the boundary condition *II*, the expression between brackets vanishes and an equation remains which is purely real on the left side and purely imaginary on the right side. Equation (24) is valid only if u_1 vanishes and similarly u_2. Hence the difference between our two admitted solutions II and II′ vanishes and the solution is unique. We admitted herein $k_{1,2}$ real, and the validity of the "Ausstrahlungsbedingung."

Our purpose is now to show that the surface wave does not meet the "Ausstrahlungsbedingung." This wave has the expression (if we confine ourselves to positive z and large r):

$$P=(\text{const.}/r^{\frac{1}{2}})\exp(-ik_1 z\cos\phi_B+ik_1 r\sin\phi_B)$$

with $\cos\phi_B>0$.

It is evident that this corresponds to a convergent wave, coming from infinity. We prove that also by substitution in formula IV′.

To do this, we fix the value of r; we have for $z\gg r$ $\partial/\partial n=\partial/\partial z=(\partial/\partial R)(\partial R/\partial z)$. We set therefore $z\approx R$, and we get then:

$$\lim_{z\to\infty}\left(\frac{\partial}{\partial z}-ik\right)u=\lim_{z\to\infty}\left(\frac{2\pi}{sr}\right)\exp(ik_1\sin\phi_B r)$$

$$\times(-ik_1\cos\phi_B-ik_1)\exp(-ik_1 z\cos\phi_B)$$

$$\to\infty \text{ for } z\to\infty$$

and does not vanish.

The wave equation is analytic in the constants k_2^2. If we possess the solution for k real, it may be analytically prolonged for k complex. We reach then solutions which do not contain the surface wave.

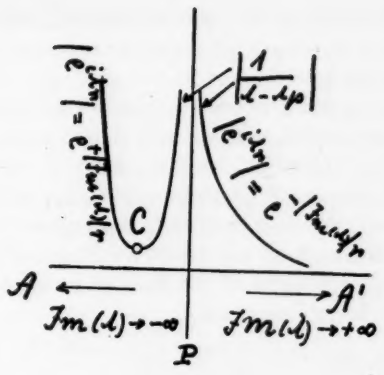

FIG. 4.

We have just shown that the radiation condition plays a decisive role in the present problem. The radiation from sources placed in a homogeneous medium over a conducting plane cannot contain any term corresponding to a surface wave, because such a wave would not fulfill this condition. The integration paths, therefore, must be chosen so as to fulfill this condition. We reach then the result shown in Fig. 3. By evaluating the integrals taken along path 1, which correspond to those of Weyl, no term belonging to the surface wave appears, as this author points out. That is why this path leads to the correct solution. By making the integration path pass through the pole placed at point P (Fig. 3), the integral of the problem breaks into two parts, namely, the residue of the pole which precisely gives rise to a surface wave, and the integral taken along the cut. According to Cauchy's theorem, the sum of these two parts must be equal to the integral extended over path 1. In other words, the integral taken along the cut must contain in itself a term corresponding to a surface way, but with the opposite sign so as to annul the term due to the pole. We are now going to show the existence of a saddle-point C in the neighborhood of pole P (Fig. 4). To this end, let us plot the modulus of the integrand (4) along the dotted line AA' of Fig. 3. When starting from the pole, the modulus decreases according to $\exp(i\lambda)/(\lambda-\lambda_p)$ as soon as we walk off in the positive direction along the axis AA' parallel to the positive imaginary axis. In the opposite (negative) direction, this modulus decreases at first, according to $1/(\lambda-\lambda_p)$, whereas $\exp(i\lambda)$ increases when $I_m(\lambda)$ decreases and becomes negative. The residue can be calculated, as we shall show, by the saddle-point method. Taking into account the directions of the two paths, a and b, (Fig. 3) we see that the two terms of opposite sign corresponding to the two surface waves compensate each other. The cut thus provides, in addition to the space wave, a term which annuls the residue, as Cauchy's theorem requires. Therefore, Epstein's remarks are not correct: It is the integration path 1 which alone is to be chosen. Sommerfeld seems to have overlooked the existence of this saddle-point. Though this author's integral taken along the cut con-

tains this saddle-point, the asymptotic development used by him does not contain it. That is the root of the present problem.

We wish to point out that most of the authors place the pole between k_1 and k_2, at a point (indicated by a cross on Fig. 3) where it does not exist.

Now we can easily find the saddle-point. We restrict ourselves to the case $z=0$ and develop the integral in the neighborhood of the pole. By making use of the asymptotic expression of the Hankel function, we may write, with a coefficient a:

$$\frac{H_0^{(1)}(\lambda r)}{k_1^2(\lambda^2-k_2^2)^{\frac{1}{2}}+k_2^2(\lambda^2-k_1^2)^{\frac{1}{2}}}\sim\frac{a}{(\lambda r)^{\frac{1}{2}}}\frac{e^{i\lambda r}}{\lambda-\lambda_P}$$

$$=\frac{a}{(\lambda r)^2}\exp[i\lambda r-\ln(\lambda-\lambda_P)].$$

By annulling the derivative of the exponent, we get

$$ir-(1/\lambda-\lambda_p)=0,\quad \lambda=\lambda_p-i/r.$$

SUMMARY

It results from the above considerations that:

1. The surface wave is not contained in the radiation of the dipole.
2. The problem is unique also for k_1 and k_2 real if we take into account the radiation condition.
3. The surface wave does not meet this condition.
4. The paths of integration of the primary radiation can be chosen so as to fulfill this condition.
5. Weyl fulfills this condition in his method.
6. Sommerfeld overlooked in his work the existence of a saddle-point.
7. The theory is in agreement with the measurements of Burrows.

PHYSICAL REVIEW VOLUME 76, NUMBER 3 AUGUST 1, 1949

Further Deductions from the ℵ-Theorem

HARVEY EINBINDER
Pupin Physics Laboratories, Columbia University, New York

(Received March 16, 1949)

For an ideal statistical gas, where $PV=sE$, all thermodynamic functions can be derived from $G(V, T)$, i.e., $A(V, T)$ is given by a suitable integration over $G(V, T)$. Since $G=N\mu$, the normalization constant, $\mu(V, T)$, of the distribution function is sufficient to provide a complete thermodynamic description of such a system. With the aid of the ℵ-theorem it is shown that there is a sharp physical distinction between the degenerate and non-degenerate Bose-Einstein gases; to any given density there corresponds a transition temperature between them. The method developed is applied to the general (relativistic and non-relativistic) non-degenerate quantum and degenerate Fermi-Dirac gases.

INTRODUCTION

EVERY gas composed of mechanically non-interacting particles in equilibrium in an n dimensional space[1] obeys the state equation[2]

$$PV=sE(V, T), \tag{1}$$

where $s=1/\sigma=2/n$, non-relativistic ($E\ll mc^2$), and $s=1/\sigma=1/n$, completely relativistic ($E\gg mc^2$). A number of important consequences follow from this equation.[3] It imposes a restriction on the possible functional forms which the thermodynamic functions may take. In particular,

$$E(V, T)=T\phi(z), \quad (2) \qquad G(V, T)=Tm(z), \quad (3)$$

where $z=TV^s$. If the individual particles obey quantum mechanics, then, from the ℵ(Aleph)-theorem, such an ideal statistical gas obeys the third law, and as $T\to 0$ has either a zero-point energy $E=BV^{-s}$, $(\partial E/\partial V)_T<0$, or condenses $P=BT^{\sigma+1}$, $(\partial E/\partial V)_T>0$. In the latter case, $G(V, T)\equiv 0$.

These results allow a notable simplification in the calculation of the thermodynamic functions for such systems in quantum statistics. The standard procedure[4] is to evaluate the normalization constant, $\mu(V, T)$, of the distribution function, $f(\epsilon, \mu/kT)$, by

$$N=\int_0^\infty C(\epsilon, z)f(\epsilon, \mu/kT)d\epsilon=N(z, \mu/kT), \tag{4}$$

where $C(\epsilon, z)$ is the number of energy states in a range $d\epsilon$. Since it can be shown that $\mu(V, T)$ is the chemical potential,[5] then

$$G=N\mu. \tag{5}$$

Solving Eq. (4) for μ is, therefore, equivalent to finding

[1] This is to allow for two-dimensional statistics. R. H. Fowler and E. A. Guggenheim, *Statistical Thermodynamics* (Cambridge University Press, London, 1939), p. 239; B. N. Singh, Ind. J. Phys. 15, 73 (1941).

[2] H. Einbinder, Phys. Rev. 74, 803 (1948).

[4] R. C. Tolman, *Principles of Statistical Mechanics* (Oxford University Press, London, 1938), p. 384. J. E. Mayer and M. G. Mayer, *Statistical Mechanics* (John Wiley & Sons, Inc., New York, 1940), pp. 378, 416.

[5] See reference 4, J. E. Mayer and M. G. Mayer, p. 121.

$G(V, T)$, Eq. (3). The energy is given by

$$E=\int_0^\infty \epsilon C(\epsilon, z) f(\epsilon, \mu/kT)d\epsilon = E(z, \mu/kT), \quad (6)$$

and eliminating μ between (6) and (4), $E(V, T)$, Eq. (2), is obtained. As $N(z, \mu/kT)$ and $E(z, \mu/kT)$ are infinite series in μ/kT, this elimination process becomes extremely laborious as the number of terms found increases.

It will be demonstrated that the use of Eq. (6) and the elimination of μ are wholly unnecessary; Eq. (4) is sufficient to provide a complete thermodynamic description of such a system.

$G(V, T)$ AS A COMPLETE FUNCTION

In general, $G(V, T)$ is not a complete (characteristic)[6] function, i.e., one from which all the others can be derived. However, because of Eq. (1), $G(V, T)$ is a complete function for an ideal statistical gas.

The Gibbs-Helmholtz equation can be written as

$$\left(\frac{\partial}{\partial T}\right)_V\left(\frac{A}{T}\right)=\left(\frac{\partial}{\partial T}\right)_V\left(\frac{G-sE}{T}\right)=-\frac{E}{T^2}. \quad (7)$$

Using Eqs. (2) and (3),

$$\phi'-\sigma\phi=\sigma m'(z), \quad (8)$$

where $\sigma=1/s$, $m(z)$ is a known function and the primes denote derivatives with respect to z. The solution of this differential equation for ϕ is

$$\phi=\sigma m(z)-\sigma z^\sigma\left[B-\sigma\int m(z)z^{-(\sigma+1)}dz\right]. \quad (9)$$

Multiplying through by T, and rearranging the resulting equation, then,

$$A(V, T)=Tz^\sigma\left[B-\sigma\int m(z)z^{-(\sigma+1)}dz\right]. \quad (10)$$

If it is more convenient to set $G=V^{-s}n(z)$ in Eq. (10), then T and $m(z)$ should be replaced by $V^{-s}z$ and $zn(z)$, respectively.

$A(V, T)$ is a complete function; differentiation yields all the other thermodynamic functions. However, here, where both $G=(1+s)E-TS$ and $A=E-TS$ are known functions, it is simpler to algebraically eliminate between them.

As ϕ is obtained by solving a first-order differential equation, the arbitrary constant B, which contributes a term $E/V=\sigma BT^{\sigma+1}$, must be evaluated. Now

$$N_j/C_j=[\exp(\epsilon_j-\mu/kT)+\beta]^{-1}. \quad (11)$$

For Fermi-Dirac statistics, where $\beta=1$, μ is a continuous function for all ϵ_j. When V/N and T are large, Eq. (11) reduces to Maxwell-Boltzmann statistics; in this limit $E=NkT$. Therefore, $B=0$ in Fermi-Dirac statistics. Here the distinction between the degenerate and non-degenerate gases is one of mathematical convenience only; it has no physical significance.

Such is not the case in Bose-Einstein statistics where $\beta=-1$. Since the distribution function must always be positive, μ cannot be positive. With decreasing V/N and T (degenerate gas), μ becomes virtually zero; an appreciable fraction of the particles are in the state of zero energy, $E/V=\sigma BT^{\sigma+1}$, $B\neq 0$. The existence of this zero-energy state as $T\to 0$ is also a direct consequence of the ℵ-theorem due to the statistical attraction of bosons $(\partial E/\partial V)_T>0$. For the non-degenerate limit, large V/N and T, where (11) reduces to Maxwell-Boltzmann statistics, $E=NkT$ and $B=0$. Thus, there is a sharp physical distinction between the degenerate and non-degenerate states where $B\neq 0$ and $B=0$, respectively, i.e., for a given V/N there is a characteristic transition temperature between them (3.14°K for a gas with molecular weight and density of liquid He).[7] Note that for black-body radiation the number of photons is not fixed, $\mu\equiv 0$, so $E/V=\sigma BT^3$ (Stefan-Boltzmann law) at all temperatures; it represents the degenerate case of relativistic Bose-Einstein statistics.[8]

The distinction between these two states for bosons is brought out more clearly by reconsidering the conditions used to prove the ℵ-theorem.[3] Since $E(V, T)$ is a continuous function, using Eq. (2) it can be represented by the series expansion

$$E(V, T)=T\sum_{j=0}^{\infty} a_j z^{b_j} \quad (b_j>-1). \quad (12)$$

As $T\to 0$, the lowest power of T will be the only important term; but the uncertainty principle requires that $V(P, T)>0$ when $0\leq P<\infty$ and $0\leq T<\infty$, whence, $b_j\geq\sigma$. Thus, in the low temperature (degenerate) region, $E(V, T)$ is given by an *ascending* series in z whose first and dominant term, a_0Tz^σ, corresponds to the condensing gas. Actual statistical calculation shows that there is only one non-zero coefficient, namely a_0.

As $T\to\infty$ (non-degenerate gas) the highest power in T dominates the expansion, but $b_j\leq\sigma$ to maintain dynamic stability, $(\partial P/\partial V)_T<0$. Therefore, in this case the expansion is a *descending* series in z whose dominant term, $a_0'Tz^\sigma$, is again the condensing gas. With this expansion, B can be eliminated from Eq. (10) for the Fermi-Dirac and non-degenerate Bose-Einstein gases without a resort to the energy of the Maxwell-Boltzmann gas. The only assumption required is that as $T\to\infty$, $P=P(V, T)$, i.e., the gas does not condense.

From the two separate series expansions for $E(V, T)$

[6] J. W. Gibbs, *Collected Works* (Longmans Green and Company, New York, 1928), Vol. 1, p. 86.

[7] See reference 4, J. E. Mayer and M. G. Mayer, p. 418.

[8] D. S. Kothari and B. N. Singh, Proc. Roy. Soc. **A178**, 135 (1941).

which have been derived, the sharp distinction between the degenerate and non-degenerate states is evident. Further, it is not surprising that at the transition (condensation) point between them there should be discontinuities in the thermodynamic derivatives,[9] e.g., dC_v/dT.

APPLICATIONS

Since $B=0$ for the general non-degenerate quantum and degenerate Fermi-Dirac gases, Eq. (10) may be used to calculate $A(V, T)$ from their respective $G(V, T)$, but cannot be used for the degenerate Bose-Einstein gas, where $G\equiv 0$, as B cannot be evaluated for this gas. However, here the calculation of $E(V, T)$ by standard methods, Eqs. (4) and (6), is quite simple.

For the general non-degenerate quantum gas[8, 9]

$$G=NkT\{\ln x+2a_1\beta x-(3/2)a_2(\beta x)^2+(4/3)a_3(\beta x)^3-\cdots\} \quad (13)$$

where

$$a_1=1/2^{(\sigma+1)},\quad a_2=2/3^{(\sigma+1)}-1/4^{\sigma},$$

$$a_3=3/4^{(\sigma+1)}+5/2^{3\sigma+1}-3/6^{\sigma},$$

$$x=(\Gamma(n/2)/\Gamma(\sigma))(h^2/\pi)^{n/2}(N/CgV(kT)^{\sigma}),$$

non-relativistic: $C=(2m)^{n/2}$, $\sigma=1/s=n/2$;
relativistic: $C=c^{-n}$, $\sigma=1/s=n$;

Fermi-Dirac: $\beta=1$; Bose-Einstein: $\beta=-1$.

[9] F. London, Phys. Rev. **54**, 947 (1938); B. N. Singh, Ind. J. Phys. **14**, 459 (1940).

Substituting (13) into Eq. (10),

$$A=-NkTz^{\sigma}\int\{-\sigma\ln\beta^{\sigma}az+2a_1(az)^{-\sigma}-(3/2)a_2(az)^{-2\sigma}+(4/3)a_3(az)^{-3\sigma}\}z^{-(\sigma+1)}dz, \quad (14)$$

where $\beta x=(az)^{-\sigma}$. So

$$A=-NkT\{1-\ln x-a_1\beta x+\tfrac{1}{2}a_2(\beta x)^2-(1/3)a_3(\beta x)^3-\cdots\}. \quad (15)$$

This also includes the Maxwell-Boltzmann gas as a special case, i.e., when all the a_j are zero.

For the general degenerate Fermi-Dirac gas,[10]

$$G=\{NkT/(s+1)y\}\{s+1+(s-1)c_1y^2-(s-\tfrac{1}{3})c_2y^4+\cdots\}, \quad (16)$$

where

$$c_1=(\sigma+1)\pi^2/6,\quad c_2=(\sigma+1)(\sigma-1)(9-2\sigma)\pi^4/120,$$

$$y=[\Gamma(\sigma+1)x]^{-s}.$$

So with $y=bz$ and $G=V^{-s}n(z)$, then

$$A=-\{\sigma NkTz^{\sigma+1}/(s+1)bz\}\int\{s+1+(s-1)c_1(bz)^2-(s+\tfrac{1}{3})c_2(bz)^4\}z^{-(\sigma+2)}dz \quad (17)$$

and

$$A=\{NkT/(s+1)y\}\{1-c_1y^2+(1/3)c_2y^4-\cdots\}. \quad (18)$$

[10] B. N. Singh, Ind. J. Phys. **15**, 73 (1941); D. S. Kothari and B. N. Singh, Proc. Roy. Soc. **A180**, 414 (1942).

Magnetic Susceptibility of Zinc at Liquid Hydrogen Temperatures*

JULES A. MARCUS**
*Sloane Physics Laboratory, Yale University,*** *New Haven, Connecticut*
(Received April 21, 1949)

The magnetic susceptibility of zinc has been investigated down to liquid hydrogen temperatures in fields ranging from 3 to 10.5 kilogauss. Measurements were made on single and polycrystalline specimens by the Faraday method. At 20°K, the susceptibility parallel to the hexagonal axis shows a marked field dependence similar to that found by de Haas and van Alphen for the susceptibility of bismuth perpendicular to the trigonal axis. Maxima were observed at 4.1, 5.6, and 9.8 kilogauss; minima at 4.8 and 7.1 kilogauss. The amplitude of the oscillations decreases with temperature increase but some field dependence persists to 64°K. The susceptibility in a plane perpendicular to the hexagonal axis remains isotropic down to the lowest temperature investigated (14°K) and is independent of the field. Oscillations in susceptibility characteristic of the de Haas-van Alphen effect were not observed in measurements on a polycrystal.

The results are compared with those for bismuth, and it is noted that the observation of the de Haas-van Alphen effect in zinc supports the view that this effect is closely related to the anomalous field dependence of resistance which has been previously observed for both metals at low temperatures.

INTRODUCTION

IN 1930, de Haas and van Alphen[1] observed that at liquid hydrogen temperatures, the diamagnetic susceptibility of bismuth single crystals becomes a complicated periodic function of the magnetic field. This has come to be known as the de Haas-van Alphen effect. The effect is confined to a plane perpendicular to the trigonal axis and is such that the susceptibility which is isotropic at high temperatures, becomes anisotropic at temperatures for which the field dependence occurs. Subsequently de Haas and van Alphen[2] investigated several additional metals and found no field dependence of susceptibility. Since the latter measurements were made on polycrystalline specimens, the results cannot be regarded as conclusive.

Shoenberg and Uddin[3,4] studied the effect in greater detail for pure bismuth and bismuth alloys. In every case, the result of alloying was to reduce the magnitude of the field dependence. They concluded that such dependence must be limited to an extremely narrow range of bismuth-like electronic structures and was therefore unlikely to occur in other pure metals. In this connection, they[5] also investigated antimony at 4°K and found the susceptibility to be independent of the field.

In the first attempt to formulate a theory of the de Haas-van Alphen effect, Peierls[6] considered the quantization of essentially free electrons in a magnetic field and showed that all metals should exhibit the effect under conditions such that $\mu H > kT$. However, for fields and temperatures attainable in the laboratory ($\sim$1°K, $\sim 10^4$ gauss), $\mu H \not> kT$ unless the effective mass of some of the conduction electrons is abnormally small. As this is just the condition for large normal diamagnetism, Peierls concluded that the effect would only be observable in metals exhibiting large diamagnetism.

Blackman[7] and Landau[8] extended Peierls' theory by considering the particular electronic structure of bismuth. Fair quantitative agreement with experimental data was obtained by assuming that the electrons responsible for the fluctuations in susceptibility were only 1 percent of those contributing to the large diamagnetism at higher temperatures and therefore large diamagnetism is not an essential condition for the occurrence of the de Haas-van Alphen effect. As to predicting additional occurrences of the effect, the theory is inadequate since it depends on a more detailed account of the particular electronic structures of other metals than is presently available.

That the de Haas-van Alphen effect might be observed in zinc was suggested by an experiment performed in 1939 by Lazarev *et al.*[9] who found an anomalous field dependence of resistance for zinc single crystals. Schubnikov and de Haas[10] had discovered that in addition to a field dependence of susceptibility, bismuth also exhibited a peculiar field dependence of resistance at low temperatures consisting in maxima and minima superimposed on the normal increase in resistance with increase in magnetic field. The theory which Davydov and Pomeranchuk[11] developed to account for this phenomenon, indicates that the re-

* Part of a dissertation submitted in 1947 to the faculty of the Graduate School of Yale University in candidacy for the degree of Doctor of Philosophy.

** Now at the Institute for the Study of Metals, University of Chicago, Chicago, Illinois.

*** Assisted by the ONR under contract N6ori-44.

[1] W. J. de Haas and P. M. van Alphen, Comm. Phys. Lab. Leiden, Nos. 208d, 212a (1930).

[2] W. J. de Haas and P. M. van Alphen, Comm. Phys. Lab. Leiden, No. 225b (1933).

[3] D. Shoenberg and Z. M. Uddin, Proc. Roy. Soc. **A156**, 687, 701 (1936).

[4] D. Shoenberg, Proc. Roy. Soc. **A170**, 341 (1939).

[5] D. Shoenberg and Z. M. Uddin, Proc. Camb. Phil. Soc. **32**, 499 (1936).

[6] R. Peierls, Zeits. f. Physik **81**, 186 (1933).

[7] M. Blackman, Proc. Roy. Soc. **A166**, 1 (1938).

[8] L. Landau, by private communication to Shoenberg. See reference 4.

[9] B. G. Lazarev, N. M. Nachimovich, and E. A. Parfenova, Comptes Rendus (URSS) **24**, 855 (1939).

[10] L. Schubnikov and W. J. de Haas, Comm. Phys. Lab. Leiden, Nos. 207a, 207d (1930).

[11] B. Davydov and I. Pomeranchuk, J. Phys. (U.S.S.R.) **2**, 147 (1940).

TABLE I. Values of susceptibility for zinc at room temperature.

	$-\chi_{\parallel}\times10^6$	$-\chi_{\perp}\times10^6$	$\bar{\chi}\times10^6$	$\chi_{\parallel}/\chi_{\perp}$
McLennan, Ruedy, and Cohen[a]	0.190	0.145	0.160	1.31
Rao[b]	0.202	0.149	0.167	1.36
Endo[c]	polycrystal		0.126	
de Haas and van Alphen[d]	polycrystal		0.143	
Specimen *A*	0.169	0.124	0.139	1.36
Specimen *B*	0.169	0.124	0.139	1.36
Specimen *C*	polycrystal		0.141	

[a] McLennan, Ruedy, and Cohen, Proc. Roy. Soc. **A121**, 9 (1928).
[b] S. R. Rao, Proc. Ind. Acad. Sci, 4, 186 (1936).
[c] H. Endo, Sci. Tohoku Imp. Univ. 14, 479 (1925).
[d] See reference 2.

sistance fluctuations should be accompanied by a marked de Haas-van Alphen effect.

Lazarev's[9] experiment showed a similar field dependence of resistance for zinc single crystals. In the case of zinc however, it occurs for only one orientation of the crystal with respect to the magnetic field and is not observable for deviations of as little as 5 percent from the one orientation. This indicated that the de Haas-van Alphen effect might be observable in zinc single crystals although it was not found in previous measurements[2] on polycrystals. Accordingly, a preliminary investigation of zinc single crystals was made at liquid hydrogen temperatures. Initial results were reported in an earlier communication.[12] The present paper gives a more extensive account of this research.

EXPERIMENTAL PROCEDURE

Single crystals of zinc were grown using metal from two different sources. Specimen *A* was prepared from Eimer and Amend chemical purity zinc shot with total impurities given as less than 0.01 percent and iron impurities as 0.003 percent. Specimen *B* was prepared from Johnson, Matthey & Company "H. S." brand zinc rods for which spectrographic analysis indicated total impurities of less than 0.0001 percent. Crystal *A* was grown by allowing a bead of the molten metal, sealed under a vacuum in a Pyrex tube, to cool slowly in an electric furnace. Crystal *B* was grown by the Bridgman[13] method whereby a Pyrex tube containing a polycrystalline rod of the metal and sealed under a vacuum, was slowly lowered out of an electric furnace. Orientation was determined by cleavage. A polycrystal, specimen *C*, was prepared from the higher purity material by rapid quenching from the melting point. The mass of the specimens ranged from 0.5 to 0.7 g and the maximum dimension of the largest crystal was 0.6 cm.

Susceptibilities were determined by the Faraday method in which the force on a small specimen in an inhomogeneous field is given by $F=\chi m H_x(\partial H_x/\partial z)$, where χ is the susceptibility per unit mass, m the mass of the specimen, H_x the horizontal magnetic field and $\partial H_x/\partial z$ the gradient of the field in the vertical direction. The field varied by about 10 percent over the volume of the specimen. It was found that this amount of variation did not appreciably effect the results for the range of fields used (3 to 10 kilogauss). Absolute values of susceptibility were determined in terms of a polycrystalline bismuth standard of the same dimensions as the specimen. The susceptibility of the bismuth standard was known to be $(-1.31\pm0.01)\times10^{-6}$.

To minimize the error of placement in changing specimens, specially designed pole pieces were used similar to those employed by Foex and Forrer.[14] With these poles, the force varied by less than ±1 percent for a ±0.3 cm displacement of the specimen. As the position of the specimen could easily be reproduced to 0.005 cm, the error from this source was negligible.

In the expression for the magnetic force given above, χ is the susceptibility in the direction of the field. For a single crystal, the magnetization does not generally coincide with the direction of the applied field. If as is usually the case, the magnetization is a linear vector function of the field, then for crystals with the hexagonal symmetry of zinc, the measured value of susceptibility is related to the principal susceptibilities $\chi_{\parallel}$ (in the direction of the hexagonal axis) and $\chi_{\perp}$ (at right angles to the hexagonal axis) by the expression

$$\chi=(\chi_{\parallel}\sin^2\phi+\chi_{\perp}\cos^2\phi)\cos^2\theta+\chi_{\perp}\sin^2\theta, \qquad (1)$$

where ϕ is the angle between the hexagonal axis and the vertical z direction and θ is the angle between the

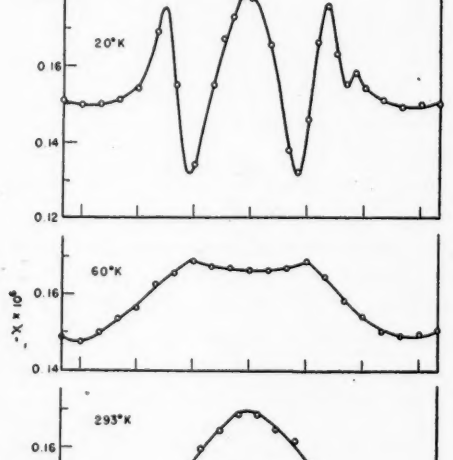

FIG. 1. Variation of the susceptibility of a zinc single crystal with angular orientation for $\phi=90°$ and $H=8.25$ kilogauss at 293°K, 60°K, and 20°K.

[12] J. A. Marcus, Phys. Rev. 71, 559 (1947).
[13] P. W. Bridgman, Proc. Am. Acad. Arts Sci. **60**, 305 (1925).
[14] G. Foex and R. Forrer, J. de Phys. 7, 180 (1926).

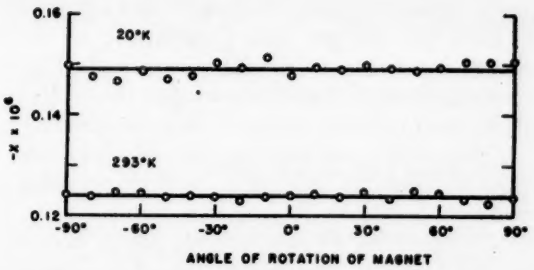

FIG. 2. Variation of the susceptibility of a zinc single crystal with angular orientation for $\phi=0°$ and $H=8.25$ kilogauss at 293°K and 20°K.

field and the projection of the hexagonal axis on the horizontal $x-y$ plane.

The present measurements were made with $\phi=90°$ or 0° so that

$$\chi=\chi_{\parallel}\cos^2\theta+\chi_{\perp}\sin^2\theta, \tag{2}$$

or

$$\chi=\chi_{\perp}, \tag{3}$$

respectively. For either mode of suspension, rotation of the magnet permitted variation of θ through 360°. Where $\phi=90°$, χ varies sinusoidally with θ and the principal susceptibilities were determined from the maxima and minima which occur at $\theta=0°$ and 90°, respectively.

Where the susceptibility is field dependent, the magnetization is not a linear vector function of the field and Eq. (1) is not valid. Therefore, if χ is measured as a function of θ in a constant field, any field dependence of χ will be apparent as deviations from (2) and (3), providing a convenient method for detecting the de Haas-van Alphen effect. Following this procedure in the initial measurements, only $\chi_{\parallel}$ was found to be field dependent. The field dependence of $\chi_{\parallel}$ was then studied by varying the field for the fixed orientation $\phi=90°$ and $\theta=0°$.

The forces, which ranged from 0.2 to 5 dynes, were measured by means of a Sucksmith[15] ring balance constructed by S. H. Browne[16] for measurements at liquid nitrogen temperatures. The only modification required was a more sensitive ring since Browne's had been designed for the measurement of considerably larger forces. With a ring 9 cm in diameter formed from a strip of phosphor bronze 0.20 cm wide and 0.010 cm thick, the sensitivity was 1 dyne per mm deflection of the optical image. The position of the image could be read to 0.001 mm but mechanical vibrations and a slow drift in the zero position due to thermal effects limited the accuracy of the force measurements to ± 0.01 dyne under average working conditions.

The specimen was suspended from the balance ring by a quartz fiber 0.01 cm in diameter. No correction was made for the magnetic force due to the suspension alone as it was less than 1 percent of the total force.

To eliminate the large magnetic effect of oxygen at low temperatures, the balance was evacuated and then filled with helium gas at a pressure of about 30 cm of mercury to provide thermal equilibrium between the specimen and the surrounding bath.

The low temperatures were obtained by using liquid hydrogen and nitrogen and were determined from the vapor pressures.

RESULTS AND DISCUSSION

Principal susceptibilities of the specimens used, measured at room temperature, are given in Table I along with the determinations of other investigators. For single crystals, the mean values of susceptibility, $\bar{\chi}$, were calculated from $\bar{\chi}=\frac{1}{3}(\chi_{\parallel}+2\chi_{\perp})$. The estimated error in our absolute values is less than 4 percent and similar estimates are given by the other investigators. Such large discrepancies between the individual values characterize most of the available data concerned with magnetic properties of metals and has usually been attributed to the presence of impurities. However, the anisotropy given by $\chi_{\parallel}/\chi_{\perp}$ (which is independent of the calibration errors) varies by less than 4 percent and it seems unlikely that impurities present in sufficient amounts to account for the large discrepancies in the individual values of $\chi_{\parallel}$ and $\chi_{\perp}$ should have so little effect on the ratio.

Since the data on both single crystals employed in the present investigation were in substantial agreement, the specimens will not be distinguished in stating the results.

Figure 1 shows the variation of χ with θ for $\phi=90°$ and $H=8.25$ kilogauss at the temperatures 293°K, 60°K, and 20°K. At 293°K, the variation is sinusoidal

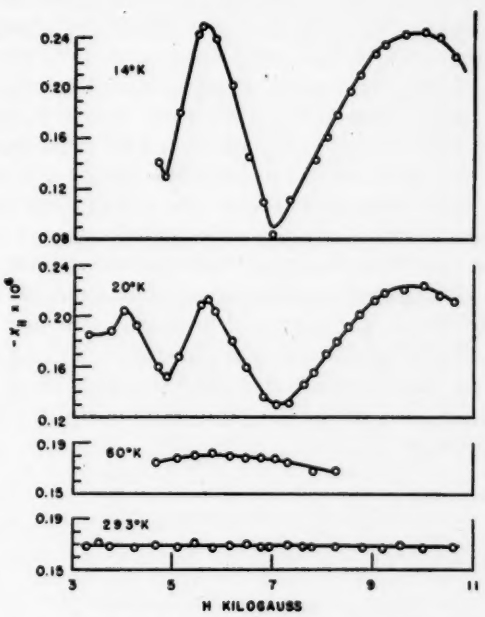

FIG. 3. Variation of $\chi_{\parallel}$ with magnetic field at 293°K, 60°K, 20°K, and 14°K.

[15] W. Sucksmith, Phil. Mag. 8, 158 (1929).
[16] S. H. Browne and C. T. Lane, Phys. Rev. 60, 899 (1941).

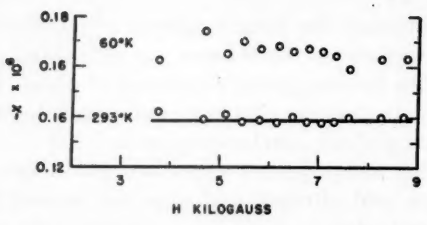

FIG. 4. Variation of the susceptibility of a zinc polycrystal with magnetic field at 293°K and 20°K.

as expected from Eq. (2); at 60°K some departure from Eq. (2) is apparent and at 20°K the effect is pronounced, indicating a marked field dependence of susceptibility. Additional rotation curves at liquid nitrogen temperatures showed that above 64°K, the deviation from Eq. (2) was less than the experimental error.

Variation of χ with θ for $\phi=0°$ and $H=8.25$ kilogauss at 293°K and 20°K is shown in Fig. 2. At both temperatures the susceptibility is isotropic in the basal plane (the greater spread at 20°K being due to an increase in vibration due to boiling of liquid hydrogen). The latter result together with the rotation curves for $\phi=90°$ indicate that the field dependence is confined to $\chi_{\parallel}$. This was confirmed by measurements of $\chi_{\parallel}$ and $\chi_{\perp}$ in fields ranging from 3 to 10.5 kilogauss.

The field dependence of $\chi_{\parallel}$ at 293°K, 60°K, 20°K, and 14°K is plotted in Fig. 3. While at 293°K, $\chi_{\parallel}$ is independent of the field, the curve at 20°K shows the marked oscillations characteristic of the de Haas-van Alphen effect. At 20°K and 14°K, the positions of the maxima and minima occur at approximately the same field strengths; the amplitude on the other hand is considerably increased with decrease in temperature. Thus, between the minimum at 7.1 kilogauss and the maximum at 9.8 kilogauss, the difference in susceptibility of 0.09×10^{-6} at 20°K increases to 0.162×10^{-6} at 14°K. If the increase in amplitude with temperature decrease continues at the same rate, then in the neighborhood of 4°K, the minima should be paramagnetic. At 60°K, $\chi_{\parallel}$ is still field dependent though the oscillations have smoothed out to the extent that the de Haas-van Alphen effect is no longer obvious.

The complicated form of the rotation curve at 20°K (Fig. 1) suggested that the effect might average out for a polycrystal. The results of measurements on a polycrystalline specimen are shown in Fig. 4. The specimen may not have been a true polycrystal since the average grain size was about 0.5 mm. However, the rotation curve at room temperature showed only a small deviation from the straight line. Comparison of the field dependence curve at 20°K with the corresponding curve for a single crystal (Fig. 3) shows that the de Haas-van Alphen effect is hardly apparent in measurements made on a polycrystal, accounting for de Haas and van Alphen's[2] failure to observe it in their previous measurements.

It is interesting to compare the above results with those for bismuth. In bismuth the effect is somewhat more complicated as the susceptibility is independent of the field only when the field is parallel to the trigonal axis. The field dependence occurs in a plane perpendicular to the trigonal axis, the periodicity being different in directions parallel and perpendicular to a binary axis. In both metals, the oscillations take place about a mean diamagnetic value, the spacing and amplitude increasing with increasing field. The amplitude is greater for bismuth than zinc but in zinc the oscillations constitute a greater fractional change in the mean value of susceptibility and as aforementioned, it seems likely that some of the minima may become paramagnetic at about 4°K. Bismuth remains diamagnetic to 2°K and Blackman[7] concluded that only a small fraction of the electrons responsible for the large mean value of diamagnetism contribute to the de Haas-van Alphen effect. No such conclusion can be drawn in the case of zinc as the mean diamagnetism is less than that of free zinc ions (-0.23×10^{-6}) and the net effect of the electrons must be paramagnetic.

For both metals, the magnitude of the oscillations decreases with temperature increase. In zinc, some field dependence is observed at temperatures as high as 64°K while for bismuth, no field dependence is observed above 35°K.

The observation of the de Haas-van Alphen effect in zinc single crystals, together with the previous discovery by Lazarev[9] of an anomalous field dependence of resistance support the contention of Davydov and Pomeranchuk[11] that the two effects are closely related. This is further borne out by the failure to observe either of these effects in cadmium despite its zinc-like electronic structure: Lazarev[9] found no resistance anomaly for cadmium; in the course of the present investigation the susceptibility of cadmium was measured at 14°K but no field dependence was observed.

The author wishes to thank Professor C. T. Lane, who suggested this problem, for his advice and encouragement. He is also indebted to Dr. Henry Fairbank for his very generous assistance.

Non-Equilibrium States in Helium II

WILLIAM BAND AND LOTHAR MEYER
Institute for the Study of Metals, University of Chicago, Chicago, Illinois
(Received April 1, 1949)

It is shown that second sound is thermodynamically possible only in the absence of thermal equilibrium between the superfluid and normal component of He II. The tendency of the assembly to drop back irreversibly to the state of internal equilibrium within a certain time of relaxation provides a consistent account of the observed limitations of superfluidity and heat conductivity in liquid helium. As a consequence it is to be expected that the times of relaxation calculated from heat conductivity measurements should be identical with those which can be derived from Pellam's direct attenuation measurements in second sound. This expectation is confirmed within the accuracy of available data.

INTRODUCTION

MOST of the peculiar properties of helium II can be described in terms of the two-fluid model developed by Tisza.[1] According to this model helium II consists of two inter-penetrating fluids, one of which is the so-called superfluid (mass per unit volume ρ_s) and the other the normal fluid (mass per unit volume ρ_n). The sum $(\rho_s+\rho_n)$ is the total density ρ of the liquid. The superfluid can move with respect to the walls of the vessel up to a certain limiting critical speed without friction, while the normal fluid has a normal viscosity. The normal fluid carries almost the whole heat content of the liquid.

The extremely high heat conductivity of helium II[2] appears qualitatively in this model as caused by the flow of the normal fluid carrying the heat content down the temperature gradient, while this mass flow is compensated by an opposing stream of superfluid. The thermal resistance is in first approximation regarded as due to the viscosity of the normal fluid. This picture has been worked out quantitatively by F. London and P. Zilsel[3] for narrow slits and capillaries ($r\sim10^{-4}$ cm) where the mobility of the normal fluid is rather strongly limited by viscosity. They obtained the correct order of magnitude for the heat current, at least for certain widths of the slits used.

The heat current calculated in this way for wider capillaries $r=$ (0.01 to 0.1 cm) is greater than the observed currents by several orders of magnitude. This fact suggests that in these wider capillaries another type of resistance must be limiting the relative mobility of the two streams of fluid in the heat current. Another very significant peculiarity in the behavior of the heat currents in these wider capillaries is their almost exact proportionality with the cube root of the temperature gradient,[4] and this also suggests that the normal viscosity picture becomes inadequate.

It seems natural to consider this additional limitation on the heat current as due essentially to the same factors that limit the superfluidity of the superfluid at the critical velocity as observed in direct flow measurements of the "film" or through narrow slits.[5–7] This additional limitation, therefore, is inoperative so long as the viscosity of the normal fluid is able to limit the compensating flow of the superfluid to levels lower than its critical speed, as happens in narrow capillaries. In the wider capillaries the viscosity is unable to do this, and the new limitation becomes operative.

The velocity of flow of the normal fluid u_n in the heat current is easily calculated from the two fluid model.[8] If W is the heat current density and ϵ the thermal energy per unity mass of the normal fluid, u_n its mean velocity, we have

$$W=\epsilon\rho_n u_n. \tag{1a}$$

But $\epsilon\rho_n$ is to this approximation the heat content ρQ per unit volume, therefore

$$W=\rho Q u_n. \tag{1b}$$

The values of u_n calculated in this way from the measured values of Q and of W for temperature gradients of 0.001°/cm are not only approximately equal to the critical velocities observed in the superfluid flow of the "film" and through narrow slits (1μ or less), but depend on temperature in about the same manner (compare reference 8, Table I). Moreover the rate of flow of the "film" at velocities higher than the critical speed is not proportional to the pressure or temperature gradients producing it, but depends approximately in the same way as the heat currents on the cube root of the gradient.*

It has been suggested that this limitation of super-

[1] L. Tisza, Comtes Rendus **207**, 1035, 1186 (1938); J. Phys. Rad. 1, 165, 350 (1940); Phys. Rev. **72**, 838 (1947); Phys. Rev. **75**, 885 (1949).
[2] W. H. Keesom, *Helium* (Elzivier Amsterdam-New York, 1942), p. 282.
[3] F. London and P. R. Zilsel, Phys. Rev. **74**, 1148 (1948).
[4] Keesom, Saris, and Meyer, Physica **VII**, 817 (1940).
[5] J. G. Daunt and K. Mendelssohn, Proc. Roy. Soc. **A170**, 423 (1939).
[6] P. L. Kapitza, J. Phys. U.S.S.R. **5**, 59 (1941).
[7] L. Meyer and J. H. Mellink, Physica **13**, 197 (1947).
[8] W. Band and L. Meyer, Phys. Rev. **73**, 226 (1948).

* Atkins' observation (K. R. Atkins, Nature **185**, 925 (1948)) of anomalously high superfluid velocities appear to be essentially observations of super-critical speeds. The flow of superfluid from one chamber to the other was produced by supplying heat to the latter. As long as the flow velocity is below the critical speed the heat supplied is completely compensated by thermomechanical cooling due to the incoming superfluid. A temperature difference between the two chambers can appear only if the flow of superfluid is unable to compensate the supplied heat, i.e., when the critical velocity is exceeded. See Kapitza, reference 6 and Meyer and Mellink, reference 7.

fluidity is essentially a quantum effect, and that no understanding of the phenomenon will be possible until a rigorous quantum hydrodynamics has been set up.[9,10]

It has also been imagined that the limitation of superfluidity, and also the cube root law dependence of the heat current on the temperature gradient may be due to turbulence or some other higher order terms in the hydrodynamical equations for the two-fluid model, and that, therefore, any attempt to study the problem quantitatively was not likely to succeed.[1,3,11,**]

This paper aims to show that the limitation of superfluidity can be described in terms of perturbations of the thermodynamic equilibrium between the normal fluid and the superfluid whatever the eventual interpretation of the superfluid and of the "normal fluid" may be. The inevitable tendency of the mixture to return irreversibly to thermal equilibrium and the resulting dissipation of energy provide a consistent picture both of the attenuation of second sound and of the thermal resistance.

SECOND SOUND AND NON-EQUILIBRIUM STATES

Second sound was predicted by Tisza[1] from the two-fluid model on the basis of the following considerations: If the two-fluid components do not interact—in the sense that there is no internal viscosity associated with their relative motion—the mixture has an additional basic mode of oscillation in which the two components move in opposite phase with each other. The first basic mode of motion in which the two components move in phase with each other consists of compressional waves or "phonons": the concentration ρ_n/ρ of the mixture remains sensibly constant during these oscillations, and only the total density ρ varies. These are the acoustical modes of vibration and are identical with the longitudinal modes which play an important role in the theory of solids. In the second basic mode, "second sound" vibrations, the total density ρ remains fixed, (normal sound is absent) and only the concentration ρ_n/ρ undergoes periodic changes. The two parts of the fluid have opposite velocities at every point, so that this mode is possible only in the absence of momentum transfer between the two components.

However, there seems to be at first sight a serious difficulty with thermodynamics. Helium II is thermodynamically a one component system, and its state is completely determined by the two variables ρ and T, the total density and the temperature respectively. As the total density remains constant in second sound, there is only one free variable, the temperature. Therefore, the concentration ρ_n/ρ is uniquely defined by the temperature everywhere and local oscillations of this concentration in second sound would appear to be local oscillations of the temperature. In fact, Tisza originally called second sound "temperature waves."

The heat carried by the second sound waves, namely, by the excess concentration $\epsilon\Delta\rho_n$, is propagated with the wave. This heat would be traveling not only down but also up the temperature gradients without regard for the second law of thermodynamics. Consider an arrangement in which standing second sound waves are maintained between the source and a perfect heat reflector, and let there be at least one antinode A in the wave pattern. If it is correct to regard ρ_n and ρ_s as uniquely defined by the temperature, then T must be oscillating at A between two extremes, say T_0 and $T_1 > T_0$. The nodes meanwhile remain at a fixed temperature, say T. During one phase of the wave the temperature T at A is increasing from T towards T_1 and heat is flowing into the region around A through the nodes, and therefore, going up the temperature gradient. Meanwhile no work is being done on the liquid because the source of the second sound is simply an oscillatory heat supply and the density ρ remains ideally constant. If in fact T and ρ were the only independent variables this would be an obvious contradiction with the second law of thermodynamics. This complication cannot be avoided by ascribing infinite thermal conductivity to the liquid and regarding second sound as simply the limiting form of a Fourier heat wave: such a heat wave would have an infinite speed of propagation in the limit of infinite thermal conductivity, while if the speed were finite it would depend upon distance from the source in the well-known classical manner. (Compare reference 12.) Second sound definitely has a finite speed of propagation characteristic of the liquid at the temperature of interest, independent of the distance from the source.

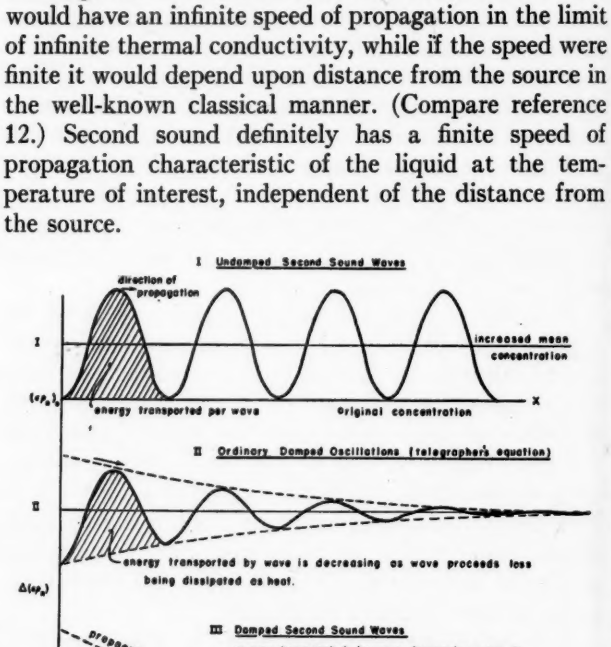
I Undamped Second Sound Waves
direction of propagation
increased mean concentration
energy transported per wave
original concentration
x
II Ordinary Damped Oscillations (telegrapher's equation)
energy transported by wave is decreasing as wave proceeds less being dissipated as heat.
III Damped Second Sound Waves
propagation
energy transported by wave, decreasing with x
concentration gradient to produce diffusion, increasing with x
mean concentration gradient, constant
uniform original concentration

FIG. 1. Table of wave motion.

[9] L. Landau, J. Phys. U.S.S.R. **5**, 71 (1941); **8**, 1 (1944); Phys. Rev. **75**, 884 (1949).

[10] H. S. Green, Proc. Roy. Soc. (London) **A194**, 244 (1948).

[11] C. J. Gorter, Phys. Rev. **74**, 1544 (1948).

** Recent statistical work on turbulence by Heisenberg (Proc. Roy. Soc. **A195**, 402 (1948)) may permit progress along this line of attack.

Possibly in an unconscious effort to escape from this dilemma several writers have stated, either explicitly or implicitly, that second sound does not carry heat, but only the kinetic energy of the relative motion of the two-fluid components.[3,12] In practice, however, second sound is always excited by an oscillatory heat source that never cools the liquid below the initial temperature during any phase of the oscillation; the heat supply is unidirectional and oscillates only between a minimum (possibly zero) and a maximum input. If the mean rate of heat input is W ergs/cm² sec., this thermal energy must be carried by the wave at the speed of its phase velocity V_s, there is a concentration of heat in excess of normal W/V_s ergs/cm² per cm of path. The amplitude of the heat wave measured from minimum to maximum heat content is $2W/V_s$ ergs/cm³. This statement is independent of any model, and simply follows from the experimental fact that heat supplied at the source is received at the detector with the phase velocity.

This point is so fundamental that we give in Appendix I a more detailed proof that the heat carried by second sound is large compared with the kinetic energy of the relative motion of the two-fluid components.

The answer to this apparent thermodynamic paradox is in fact almost trivial: namely, that at high enough frequencies T and ρ alone are not sufficient to specify the state of the liquid. The existence of second sound is possible only in the *absence* of thermal equilibrium between ρ_n and ρ_s; this provides the required extra degree of freedom and, in fact, renders the thermodynamical temperature T of the mixture as a whole essentially meaningless. This situation is already familiar in connection with Einstein's[12a] theory of dispersion of ordinary sound in a dissociating gas.[8] At low frequencies the dissociation equilibrium can follow the changes of pressure and temperature in the wave, but by increasing the frequency we must reach a situation in which the dissociation equilibrium cannot adjust itself rapidly enough to keep up with the sound vibrations. At still higher frequencies the two dissociating components behave as essentially independent fluids, their mutual thermal equilibrium never having time to readjust itself to the changes occurring in the wave. The concentration then becomes a third independent variable. Einstein showed that this mechanism would cause dispersion and attenuation of ordinary sound in the dissociating gas in a transition region at frequencies where the period of the wave nearly equals the time required for a perturbation from equilibrium to regress spontaneously, usually called the time of relaxation.

The two components of a dissociating gas do not lead to observable second sound even at high enough frequencies simply because internal viscosity hinders their relative motion: if such second sound existed it would probably be damped out too rapidly to be observed. But in He II the superfluidity of the low-energy component ensures the existence of second sound provided the frequency is high enough to inhibit the thermal equilibrium of the concentration.

If we can decrease the frequency so far that the wave period becomes comparable with or even longer than the relaxation time for the thermal equilibrium between the two parts of the fluid, then thermodynamics will enforce its restrictions and second sound will be damped out. At high frequency the concentration ρ_n/ρ varies in a manner that can be calculated from the equation of continuity applied to each fluid component separately, that is, assuming no transitions of particles between the two fluids and no coupling with temperature; at low frequency the concentration variations become uniquely determined by temperature variations and particles have to transfer from one component of the fluid to the other if they move relative to each other. The numerical evaluation of this effect is given in Appendix II.

This picture leads to the following wave equation, the "telegrapher's equation," for second sound applicable at all frequencies:[8]

$$\partial^2\rho_n/\partial t^2+\partial\rho_n/\partial t/\tau=V_s^{*2}\nabla^2\rho_n. \qquad (2)$$

In this equation the term $\dot{\rho}_n/\tau$ takes care of the dissipation of relative momentum due to transition of particles between the two fluids during their relative motion. The velocity V_s^* is a complex quantity[13] because of the irreversible relaxation towards equilibrium after perturbation, and its effect on the "elasticity constants" in the Hamiltonian. Essentially the same relaxation time τ appears*** in the detailed expression for V_s^*. If we were to neglect the relative momentum dissipation, and retain only the complex velocity, we would obtain the same effects as derived by Einstein for normal sound. Second sound waves would exist even at frequencies much lower than $1/\tau$ but with a different velocity of propagation. Attenuation would be present only in the transition region. The presence of the relative momentum dissipation, however, requires that when the maximum attenuation is reached, the wave equation degenerates into a diffusion equation. For still lower frequencies we then get only the classical Fourier type of heat wave (diffusion) without any true propagation of second sound, just as in the well-known solutions of the "telegrapher's equation."

HEAT TRANSFER AND ATTENUATION IN SECOND SOUND

Consider a second sound wave in which the density of normal fluid oscillates in the following manner: (See

[12] R. Dingle, Proc. Phys. Soc. (London) **61**, 9 (1948).
[12a] A. Einstein, Sitz. Berl. Akad. **1920**, 380.

[13] W. Band and L. Meyer, Phys. Rev. **74**, 386 (1948).
*** Dr. J. B. Garrison has drawn our attention to the desirability of a more generally rigorous treatment of the relaxation problem in a system that has three independent variables at high frequencies. Such a treatment would yield more than one relaxation time and possibly even modify the non-equilibrium elastic constants slightly.

TABLE I. Values of relaxation times.

T°K	$V_{s\infty}$ m/sec.	μ per cm	Second sound $\tau\times10^3$ sec. from μ	Steady heat flow $\tau\times10^{-3}$ sec. for $W=0.03$ cal./cm² sec.
2.18	4.25	3.0	0.4	—
2.15	8.05	1.0	0.6	—
2.10	12.25	0.3	1.35	1.1
2.0	16.69	0.15	2.0	2.4
1.9	18.68	0.10	2.7	2.7
1.8	19.90	0.07?	3.6?	2.2
1.7	20.35	0.05?	5.0?	1.5

Appendix I, Eqs. (6), (18).)

$$\Delta\rho_n=\Delta\rho_{n0}e^{-\mu x}\sin 2\pi\nu(t-x/V_s)+\Delta\rho_{n0}.$$

Then the rate of propagation of heat by this wave is

$$W_P=\epsilon_0\Delta\rho_{n0}e^{-\mu x}V_s. \tag{3}$$

Curve I of Fig. 1 illustrates the propagation when damping is neglected. The form (3) is familiar in electrical solutions of the "telegrapher's equation." In the electrical problem the dissipated energy is small compared with the thermal capacity of the conductor and we can safely neglect it (see curve II of Fig. 1); if it produces any effects on the wave, they are at most second order effects due to thermo-e.m.f.'s. Here, however, the attenuation of W_P appearing in (3) cannot be neglected. The primary wave itself is already essentially heat energy and the dissipated energy is neither changed in nature nor reduced by the "mechanical equivalent" factor, so a gradient must be set up to carry it away. Therefore, a concentration gradient of the normal fluid carrying the heat current has to be superposed on the concentration wave. The required arrangement is shown in curve III of Fig. 1. Here the lower envelope of the wave has a gradient which is everywhere proportional to the loss of energy from the wave, namely, to $W_{P0}(1-e^{-\mu x})$ where W_{P0} is the heat propagation at $x=0$. At great values of x the wave will have completely died out and the concentration gradient is such that it can carry the whole heat supplied to the system by a diffusion process in accordance with the equation:

$$W=-\tau V_s^2(d\epsilon\rho_n/dx). \tag{4}$$

The detailed proof of this is given in Appendix II.

A source of plane second sound waves propagated into an infinite medium must build up a mean temperature gradient large enough to take care of the entire heat flow. The wave may be regarded as a modulation of the resulting heat transport. The latter may be expressed either as excess heat content $\epsilon\Delta\rho_n$ propagated with the velocity of propagation of the wave, or as total heat content $\epsilon\rho_n$ transported with the mean speed $\bar{u}_n$ of the normal fluid down the temperature gradient. The two quantities are identical (see Appendix III).

However, if second sound is emitted from a finite (small) source into an infinite medium in a more-or-less parallel beam, the energy lost from the wave is dissipated more or less laterally, so that the liquid around the path of the beam is heated, avoiding the necessity of establishing a temperature gradient in the direction of propagation. In this situation we have to regard the propagation of heat as essentially that of excess heat content with speed V_s. It is in principle also possible to shoot second sound waves up a temperature gradient maintained against it. The thermal diffusion current is always down the effective temperature gradient, in whatever direction that may happen to be; the second sound merely superposes concentration waves on the concentration gradient. In none of these situation is there any difficulty with the laws of thermodynamics because the second sound wave essentially does not cause waves of thermodynamic equilibrium temperature.

Using this picture we were able to derive the approximate times of relaxation from the experimental evidence on second sound and thermal conductivities.[8,13] Recently Pellam[14] published data on the direct measurements of the attenuation of second sound. If the picture developed here is correct. Pellam's results should lead to the same values of the relaxation time as we derived from the heat conductivity measurements because the thermal diffusion current appears as the limiting case of completely damped second sound of zero frequency.

COMPARISON WITH OBSERVATION

The equation for high frequency second sound derived from the picture of the absence of internal equilibrium (see reference 13, Eqs. (C26) and (C27)), is

$$\ddot{U}_n+\dot{U}_n/\tau_1=V_{s\infty}^2\{1+1/2\pi i\nu\tau_3\}^{-1}\nabla^2U_n \tag{5}$$

where ν is the frequency,

$$1/\tau_3=(1/\tau_2)\{3-2\rho_n'Q/\rho_nC-S(\rho-\rho_n)/V_s^2\rho_n'\}, \tag{6}$$

and τ_1 is the relaxation time for the momentum exchange between oppositely moving streams of normal and superfluid components, while τ_2 is the relaxation time for the readjustment of the population towards thermal equilibrium between the two components. From the data on the quantities appearing in Eq. (6) we find that

$$\tau_3\doteqdot 4\tau_2 \tag{7}$$

to within about 5 percent at all temperatures of interest. It is, of course, not certain how τ_2 and τ_1 are related, but at least we can expect them to be the same order of magnitude and probably proportional to each other. The attenuation coefficient in cm^{-1} is now

$$\mu=1/\tau V_{s\infty} \tag{8}$$

where

$$1/\tau=\tfrac{1}{2}(1/4\tau_2+1/\tau_1). \tag{9}$$

[14] R. Pellam, Phys. Rev. **75**, 1183 (1949); **74**, 841 (1948).

Table I shows the results of using (8) to calculate τ from Pellam's data on the attenuation of second sound. The relation (8) is valid only if $2\pi\nu\tau \gg 1$, and this must be confirmed. The values of τ found are roughly between $4\cdot10^{-4}$ and $5\cdot10^{-3}$ sec. The frequency to be ascribed to Pellam's pulses is not very certain, but a safe minimum is obtained by assuming the time-length of each pulse to be a half period for the fundamental frequency in a Fourier analysis of the pulse form. This time length was reported as about 100 microsec., so it may be assumed that $\nu \geqslant 10^4$ sec.$^{-1}$. With these figures we find $2\pi\nu\tau > 10$ at least for all temperatures below 2.10°K where $\tau > 10^{-3}$. The accuracy nearer the lambda point may be doubtful.

Table I shows the times of relaxation derived for a heat current assumed to be $W = 0.03$ cal./cm^2 sec. which seems to be a reasonable value for the energy density in Pellam's waves. The values of τ derived in this way from Pellam's attenuation data are seen to be almost identical with the times calculated before from steady thermal currents. Unfortunately, there is no information available concerning the heat current density in Pellam's second sound waves. It is not even known whether the same power input was used at all the different temperatures. From Table I of a previous paper[15] and the fact that τ is inversely proportional to the square of the heat current we can calculate τ for any stated heat current. An even better agreement could be obtained between the two sets of figures if it were assumed that the heat current was only 0.02 cal./cm^2 sec. at the two lower temperatures recorded. The fact that Pellam's results for μ show a relatively wide scatter might indicate that the power input was not quite constant even at a given temperature.†

Note added in proof: Since communicating this paper we learned about several papers by V. P. Peshkov, Journal Experimental and Theoretical Physics, U.S.S.R. 18, 857, 867, and 951 (1948) on second sound and its attenuation. In these papers the discrepancy between the infinite heat conductivity in second sound and the finite heat resistance in steady state heat flow experiments representing effectively second sound of zero frequency is pointed out. This is exactly the problem the solution for which we have proposed above and in references 8 and 13. Furthermore Peshkov succeeded in producing second sound without superimposed heat flow by means of the "filtration" method. His result that in this case the attenuation is considerably smaller than when producing second sound in the usual manner by periodic heating must be considered as a qualitative confirmation of the above ideas.

ACKNOWLEDGMENTS

The writers are happy to thank Messrs. Zener, Long, Stout and Garrison for valuable discussions.

APPENDIX I

Heat Transfer and Kinetic Energy in Second Sound

At sufficiently high frequencies the wave equation for second sound is

$$\partial^2\mathbf{X}_n/\partial t^2+\partial\mathbf{X}_n/\partial t/\tau=V_s^{*2}\nabla\nabla\cdot\mathbf{X}_n \qquad \text{(I, 1)}$$

where

$$V_s^{*2}=V_s^2(1+1/2\pi i\nu\tau)^{-1}$$

is the complex velocity, V_s being the real velocity. The term in $1/\tau$ is due to momentum dissipation and the complex factor due to equilibrium relaxation. $\mathbf{X}_n$ is the vector of displacement of the normal fluid. Differentiate this equation with respect to time and we obtain the equation for the instantaneous velocity $\mathbf{U}_n$ of the normal fluid:

$$\ddot{\mathbf{U}}_n+\dot{\mathbf{U}}_n/\tau=V_s^{*2}\nabla\nabla\cdot\mathbf{U}_n. \qquad \text{(I, 2)}$$

Suppose the damping to be very small, then we can assume the normal fluid mass conserved:

$$\Delta\dot{\rho}_n/\rho_{n0}=-\nabla\cdot\mathbf{U}_n. \qquad \text{(I, 3)}$$

There is a phase factor correction when damping is appreciable. Use (I, 3) in (I, 2) to derive the equation for $\Delta\rho_n$:

$$\Delta(\partial^2\rho_n/\partial t^2)+\Delta(\partial\rho_n/\partial t)/\tau=V_s^{*2}\nabla\cdot\nabla(\Delta\rho_n). \qquad \text{(I, 4)}$$

Seeking a solution to (I, 2) which is consistent with (I, 3), we find to a first approximation

$$\mathbf{U}_n=\mathbf{U}_{n0}e^{-\mu x}\sin 2\pi\nu(t-x/V_s)+\mathbf{U}_{n1} \qquad \text{(I, 5)}$$

and

$$\Delta\rho_n=\Delta\rho_{n0}e^{-\mu x}\sin\{2\pi\nu(t-x/V_s)-\varphi\}+\Delta\rho_{n1} \qquad \text{(I, 6)}$$

where

$$\mu=1/\tau V_s \qquad \text{(I, 7)}$$

and

$$\Delta\rho_{n0}=U_{n0}\rho_{n0}/V_s. \qquad \text{(I, 8)}$$

The approximation is involved in small corrections on the V_s factor in (I, 7) and (I, 8) and in the evaluation of the small phase factor ϕ. $\mathbf{U}_{n1}$ and $\Delta\rho_{n1}$ are arbitrary constants which may, however, depend linearly on x and still satisfy the differential equations.

The heat entering per cm^2 per sec. at the source is given as a function of the time by

$$\mathbf{R}=\epsilon\rho_n\mathbf{U}_n, \qquad \text{(I, 9)}$$

where ϵ is the energy needed to excite a gram of superfluid arriving at the source into normal fluid leaving the

[15] L. Meyer and W. Band, Phys. Rev. 74, 394 (1948).

† There is indirect evidence that μ depended on the power input in the same way as the heat conductivity because Pellam reported that he could "over-drive" the second sound with resulting excitation of ordinary sound and undoubtedly greatly increased attenuation of the second sound. Experiments on the dependence of the attenuation on power input would be decisive for the present theory, because according to this theory τ depends on the heat current density, as shown by the fact that the heat current depends on the cube root of the temperature gradient (see references 8 and 15).

source, $\mathbf{U}_n$ is given by (I, 5) at $x=0$, and ρ_n is the normal component density given by (I, 6) at $x=0$ and

$$\rho_n=\rho_{n0}+\Delta\rho_n \tag{I, 10}$$

ρ_{n0} being the initial value of ρ_n.

The energy ϵ is also oscillating about a mean value ϵ_0, the amplitude of the oscillations being given by the ordered kinetic energy of the fluid components:

$$\epsilon=\epsilon_0+\Delta\epsilon \tag{I, 11}$$

where

$$\begin{aligned}\rho_{n0}\Delta\epsilon&=\tfrac{1}{2}(\rho_{n0}U_n^2+\rho_{s0}U_s^2)\\&=\tfrac{1}{2}\rho(\rho_{n0}/\rho_{s0})U_n^2.\end{aligned} \tag{I, 12}$$

First consider a wave in which $\mathbf{U}_{n1}=0$, so that the velocity oscillates about a zero mean value

$$\overline{\mathbf{U}}_n=0. \tag{I, 13}$$

The mean rate of heat supply at the source is then

$$\begin{aligned}\overline{\mathbf{R}}=\langle(\epsilon_0+\Delta\epsilon)(\rho_{n0}+\Delta\rho_n)\mathbf{U}_n\rangle_{Av}&=\epsilon_0\rho_{n0}\overline{\mathbf{U}}_n+\rho_{n0}\langle\Delta\epsilon\mathbf{U}_n\rangle_{Av}\\&+\epsilon_0\langle\Delta\rho_n\mathbf{U}_n\rangle_{Av}\text{ plus smaller terms.}\end{aligned} \tag{I, 14}$$

The first two of these terms vanish identically and for the third, using (I, 5) and (I, 6) we find

$$\overline{\mathbf{R}}=\tfrac{1}{2}\epsilon_0\Delta\rho_{n0}\mathbf{U}_{n0}. \tag{I, 15}$$

Because of (I, 8) this can be written in either of the forms

$$\bar{R}=\tfrac{1}{2}\epsilon_0\rho_{n0}U_{n0}^2/V_s$$

or

$$\bar{R}=\tfrac{1}{2}(\epsilon_0/\rho_{n0})(\Delta\rho_{n0})^2V_s. \tag{I, 16}$$

This is a second order of small quantities. This kind of wave receives heat from the source during one-half of the period and returns heat to the source during the other half. The net difference is enough to transmit the ordered kinetic energy of the wave (ϵ_0 is of the same order of magnitude as V_s^2). Of course the result (I, 16) is not exact because of the approximations present in (I, 5) and (I, 6); if the calculation were carried out exactly the equality of (I, 16) with the kinetic energy transport would have been exact. These approximations are of no importance for the larger first order energy transport that will be discussed next.

Calculations of the energy carried by second sound waves previously published,[9,12] have been confined to the above type of wave, in spite of the fact that actual second sound is produced by unilateral heat pulses.

In practice the source of second sound never receives heat from the liquid during any phase of the wave. It only supplies heat and maintains, therefore, a flow of heat into the liquid and the appropriate solutions of (I, 5) are those for which $\mathbf{U}_{n1}$, the arbitrary constant, is not zero. When $\mathbf{U}_{n1}$ is of the same order as $\mathbf{U}_{n0}$—or even equal to $\mathbf{U}_{n0}$, then the first term in the expression (I, 14) for the energy transport, becomes the dominant term and all the others are negligible, including the term responsible for the ordered kinetic energy. Thus we have now

$$\overline{\mathbf{R}}=\epsilon_0\rho_{n0}\mathbf{U}_{n1} \tag{I, 17}$$

To prevent R from ever being negative, as required by the experimental boundary conditions at the source, we have to take

$$\mathbf{U}_{n1}=\mathbf{U}_{n0}\quad\text{and}\quad\Delta\rho_{n1}=\Delta\rho_{n0} \tag{I, 18}$$

so that, using (I, 18) and (I, 8) we can write (I, 17) in the alternative form

$$\overline{\mathbf{R}}=\epsilon_0\Delta\rho_{n0}V_s. \tag{I, 19}$$

Comparison between (I, 19) and the second form of (I, 16) shows that this heat transmission is large compared with the ordered kinetic energy transmission in the ratio $\rho_{n0}/\Delta\rho_{n0}$, and this, of course, may easily be as high as 100:1.

The two alternative forms (I, 17) and (I, 19) illustrate the fact that it is, formally at least, quite arbitrary whether we regard the heat transport as a convection of the *total* heat content $\epsilon_0\rho_{n0}$ with the mean *drift* speed $\mathbf{U}_{n0}$, or as a propagation of *excess* heat content $\epsilon_0\Delta\rho_{n0}$ with the *phase* speed V_s.

APPENDIX II

Numerical Population Adjustments Due to Relaxation

If the liquid were merely not in equilibrium with its surroundings, but internally in thermal equilibrium, the variation of ρ_n could be considered as equivalent to a variation of temperature:

$$\Delta\rho_n=(d\rho_n/dT)\Delta T. \tag{II, 1}$$

Following Tisza, consider an adiabatic cylinder containing the liquid initially in equilibrium at temperature T. Let there be a porous piston in the cylinder that can be caused to move, and let the material of the piston be a perfect insulator. If the pistion is caused to oscillate *slowly* back and forth so that the superfluid passes freely from one side to the other through the pores, the liquid adjusts itself continuously on each side of the piston and we must find a temperature oscillation set up due to the thermomechanical effect.

Let the stroke of the piston be through a volume ΔV. The superfluid carries no heat—or rather we neglect it if it exists—and the energy balance on each side is very simple. A temperature difference ΔT develops and corresponding to this temperature difference there will be a pressure difference ΔP given by the fountain pressure relation

$$\Delta P=\rho S\Delta T. \tag{II, 2}$$

The conservation of energy in the volume V on one side of the piston where the total energy is, say Q, gives

$$\Delta(Q/V)=\rho C\Delta T \tag{II, 3}$$

where C is the specific heat. The amount of heat pro-

duced by the mechanical work done by the piston is the only source of heat in the volume V, so that

$$Q=-\tfrac{1}{2}\Delta P\Delta V. \qquad \text{(II, 4)}$$

This is of the second order of small quantities and may be neglected in comparison with the thermomechanical effect due to the flow of superfluid through the piston, represented by the other part of the variation in (II, 3). Thus (II, 3) gives

$$\Delta T=-(Q/\rho CV)(\Delta V/V). \qquad \text{(II, 5)}$$

As we are here considering slow oscillations the equilibrium variation of ρ_n is given by (1):

$$\Delta_e\rho_n=(d\rho_n/dT)\Delta T=-(Q/\rho CV)(d\rho_n/dT)(\Delta V/V). \qquad \text{(II, 6)}$$

We can write

$$(Q/V)=\epsilon\rho_n \quad \text{and} \quad \rho C=d(\epsilon\rho_n)/dT \qquad \text{(II, 7)}$$

so that (II, 6) becomes

$$\Delta_e\rho_n/\rho_n=-\{(\epsilon\rho_n')/(\epsilon\rho_n)'\}(\Delta V/V) \qquad \text{(II, 8)}$$

the primes indicating temperature derivatives.

On the other hand, if we assume rapid oscillations so that there is no time for population adjustments on either side of the piston we use the mass continuity equation for each fluid component, and at once obtain Tisza's equation

$$\Delta\rho_n/\rho_n=-\Delta V/V. \qquad \text{(II, 9)}$$

Comparison of (II, 8) and (II, 9) is very simple. We have roughly $\rho_n\propto T^6$ and $Q/V\propto T^7$ experimentally, so that

$$\Delta_e\rho_n/\rho_n=-(6/7)(\Delta V/V)=0.85(\Delta\rho_n/\rho_n). \qquad \text{(II, 10)}$$

APPENDIX III

Heat Transfer and Attenuation in Second Sound

The only part of (I, 9) that finally contributes to the mean heat transfer is

$$\mathbf{R}_t=\epsilon_0\rho_{n0}\mathbf{U}_n. \qquad \text{(III, 1)}$$

Using (I, 5) and (I, 18) in this we find

$$\mathbf{R}_t=\epsilon_0\rho_{n0}\mathbf{U}_{n0}\{1-e^{-\mu x}\sin 2\pi\nu(t-x/V_s)\} \qquad \text{(III, 2)}$$

and neglecting ϕ in (I, 6) and using (I, 8) again we find

$$\mathbf{R}_t=\epsilon_0\Delta\rho_n V_s. \qquad \text{(III, 3)}$$

We must, therefore, regard the heat propagated as having the same attenuation as $\Delta\rho_n$, and write for this rate of propagation the mean value of R_t at distance x, namely

$$\bar{R}_t=W_p=\epsilon_0\Delta\rho_{n0}e^{-\mu x}V_s \qquad \text{(III, 4)}$$

W_p is the propagation, and the loss from W_p with increasing x must be regarded as added to the diffusion current, so that at distance x the total diffusion current —considered also as traveling in the same direction as the wave—is

$$W_d=\epsilon_0\Delta\rho_{n0}V_s(1-e^{-\mu x}). \qquad \text{(III, 5)}$$

This diffusion current demands the presence of a slope in the heat content Q or $\epsilon_0\rho_{n0}$. The figure in the text showed the curve of Q superposed on a sloping axis determined by the condition that the curve tangent to the minima in the wave shall everywhere have a slope proportional to the value of W_d at the point.

Consider an infinite slab lying between the planes $x=0$ and $x=L$, with a plane source at $x=0$ and receiver at $x=L$. Let the axis of the wave be represented by the straight line in the ρ_n, x graph:

$$Q=\epsilon_0\rho_{n0}+\epsilon_0\Delta\rho_{n0}\{1+\mu^*(L-x)\}, \qquad \text{(III, 6)}$$

where μ^* is to be determined by the stated condition. The tangent to the minima of the wave $\epsilon_0\Delta\rho_n$ then has the equation

$$Q_{\min}=\epsilon_0\rho_{n0}+\epsilon_0\Delta\rho_{n0}\{1+\mu^*(L-x)-e^{-\mu x}\} \qquad \text{(III, 7)}$$

and this has the slope

$$dQ_{\min}/dx=-\mu\epsilon_0\Delta\rho_{n0}(\mu^*/\mu-e^{-\mu x}). \qquad \text{(III, 8)}$$

Comparing this with (III, 5) we see at once that the required condition can be met only by writing $\mu=\mu^*$. This yields the relation

$$W_d=-(V_s/\mu)(dQ_{\min}/dx)=-\tau V_s^2(dQ_{\min}/dx). \qquad \text{(III, 9)}$$

This result is identical with the diffusion equation derived previously from the low frequency limit of the wave equation, namely, the diffusion equation:

$$\dot{\rho}_n/\tau=V_{s0}^2\nabla\cdot\nabla\rho_n. \qquad \text{(III, 10)}$$

The only difference is in the value of V_s.

Excitation Functions for (α, n), $(\alpha, 2n)$, and $(\alpha, 3n)$ Reactions on Indium*

GEORGES M. TEMMER**
Department of Physics, University of California, Berkeley, California

WHEN In^{115}, whose isotopic abundance is 95.5 percent, is bombarded with α-particles, the capture process followed by the emission of one, two, or three neutrons leads to antimony isotopes of mass numbers 118, 117, and 116, respectively. Activities in the first two mentioned Sb isotopes have been reported by Coleman and Pool,[1] who obtained them by an (α, n) reaction on indium and deuteron bombardment of tin. Because of the ten stable tin isotopes, the isotopic assignment could only be made tentatively.

The α-particles of the Berkeley 60-inch cyclotron (37 Mev) produce sufficient excitation in the compound nucleus to permit the evaporation of one, two, and three neutrons. Hence, activities in the (α, n), $(\alpha, 2n)$, and $(\alpha, 3n)$ products were found and identified chemically as antimony, and by Calutron analysis as being mass numbers 116, 117, and 118. The periods found for Sb^{118} and Sb^{117} (5.1 hours and 2.8 hours) agree with those reported by Coleman and Pool. Sb^{116} decays with a 60-minute half-life. Reactions on In^{113} were not detected because of its low abundance.

These three periods are too close together to permit their satisfactory resolution from composite decay curves for the establishment of excitation curves. In order to separate the periods more effectively, use was made of a magnetic lens β-ray spectrometer of the Siegbahn type[2] constructed by Mr. R. W. Hayward. The momentum spectra of β-rays emitted by indium foils activated by 36-Mev and 22-Mev α-particles were scanned in an effort to locate salient features of the radiations of the three Sb isotopes (Fig. 1). The peak in the solid curve decay with the 2.8-hour period belonging to Sb^{117} and is produced by the conversion of a 156-kev γ-ray in the K-shell of Sn. The conversion peak

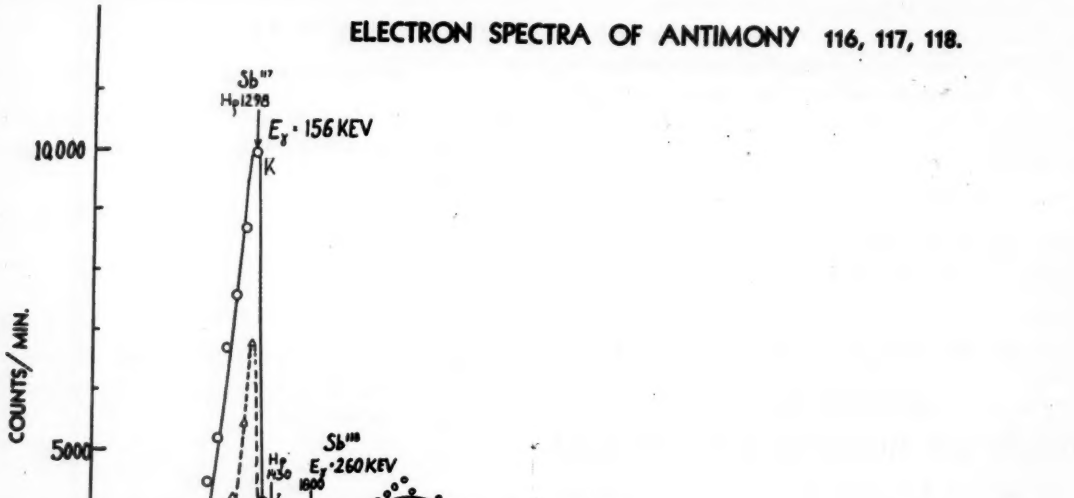

FIG. 1. β-spectra of α-induced Sb activities. Abscissa is proportional to momentum, ordinate is in arbitrary units of activity. Solid curve is for 36-Mev alphas, dashed curve for 22-Mev alphas.

* A preliminary report of the results in this paper was presented at the Berkeley meeting of the American Physical Society (Phys. Rev. 75, 1464 (1949)).

** AEC Pre-Doctoral Fellow.

[1] K. D. Coleman and M. L. Pool, Phys. Rev. 72, 1070 (1947).

[2] J. K. Siegbahn, Phil. Mag. 37, 162 (1946).

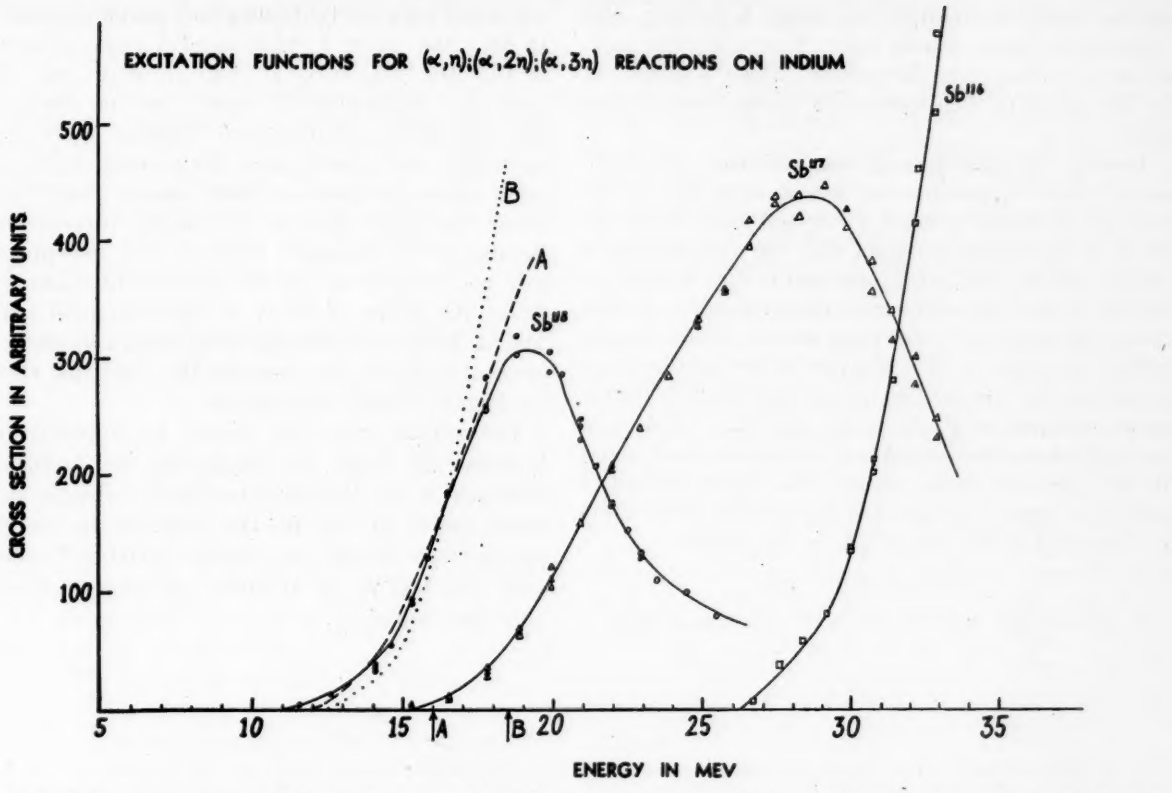

FIG. 2. Excitation curves for α-particle reactions on indium. The cross sections in arbitrary units (also arbitrary in relation to each other) are plotted against the α-particle energy in Mev. Circles indicate $In^{115}(\alpha, n)Sb^{118}$, triangles indicate $In^{115}(\alpha, 2n)Sb^{117}$, squares indicate the Coulomb barrier heights for $r_0=1.5$ and $r_0=1.3(R=r_0A^{\frac{1}{3}}\times10^{-13}$ cm), and curves A and B are the corresponding theoretical capture cross sections.

of $H\rho=1800$ in the dashed curve corresponds to a 260-kev γ-ray decaying with the half-life of Sb^{118}. Sb^{116} was identified with the positron continuum with an upper energy limit of about 1.45 Mev. By means of an electron-positron discriminator (helical baffle), it was found that no continuous β^--spectrum is present, as is to be expected for neutron-deficient isotopes. Hence, the two other isotopes (Sb^{118} and Sb^{117}) must decay primarily by K-capture.

To obtain the excitation functions, the stacked-foil technique was used, bombarding foils of indium evaporated to a thickness of about 5 mg/cm^2 upon quarter-mil foil. This was necessitated by the low melting point of metallic indium (155°C). In this way, steps of about 1 Mev in α-particle energy were obtained. Ten foils at a time were mounted in the spectrometer with a special wheel assembly permitting any one of the foils to be rotated internally to the source position, while at the same time shielding all others behind a Pb baffle. This device proved to be essential for the performance of the experiment because of the short periods involved.

A magnetic field in the spectrometer corresponding to 1-Mev electrons was selected to follow the positron activity. The procedure used to obtain the excitation curves was to set the field on the conversion peaks (or point of the continuum) and then to sweep through the ten foils, thus getting counting rates proportional to the cross sections at the various foil energies. The usual procedure would have been to follow the decay of these points in time and to extrapolate back to time zero. This, however, would have entailed greater uncertainties due to lack of reproducibility of current settings, and was unnecessary because of the almost pure decay of the points selected on the spectrum. In this manner the curves shown in Fig. 2 were obtained. They were compounded from several overlapping bombardments, as well as from data from the same run taken at various times, and normalized. The alpha-particle energy was obtained from semi-empirical range-energy curves for α-particles in aluminum and silver which is close enough to indium for the purpose ($Z=47$ *vs.* $Z=49$). The vertical scales of the three excitation curves bear no relation to each other since decay schemes and conversion coefficients are not known.

The energy values are uncertain because of the inherent spread of about 1 Mev of the uncollimated cyclotron beam (uncollimated because of need for high intensity). An additional uncertainty is introduced by non-uniformity of the foils and straggling, estimated at 0.5 Mev.

The errors along the ordinate are mostly due to slight variations in magnet current from the peak positions, as well as variations in geometry for the various foils

at the source, accounting for about 5 percent, plus counting statistics, usually below 5 percent. The overall error is thus about 10 percent, which is borne out by the spread of the experimental points from various runs.

Results of a possible (α, p) reaction could not be observed since the product tin isotope is stable. At any rate, for an atomic number $Z=50$ and near the threshold it is reasonable to expect that the contribution of protons will be quite small compared to that of neutrons because of the Coulomb barrier penetration factor. The rising portion of the (α, n) cross section should thus be mainly governed by the behavior of the capture cross section for the bombarding α-particles, which in turn is mainly determined by the penetration factor as long as the excitation of the compound nucleus lies above about 10 Mev and the levels overlap. The curves labeled A and B are theoretical values of the capture cross section as calculated by Weisskopf.[3] A nuclear radius

$$R=r_0A^{\frac{1}{3}}\times 10^{-13}\text{ cm}$$

was used, with $r_0=1.5$ leading to Coulomb barrier A at 16 Mev and curve A, while $r_0=1.3$ leads to barrier B at 18.5 Mev and curve B (Fig. 2). While one cannot select one or the other of these curves on the basis of this experiment, their general behavior is in general agreement with theory over the portion of the (α, n) curve up to the point of inflection at about 16 Mev where the competition of the $(\alpha, 2n)$ process sets in. Because of the unknown ratio of these two processes, it is not possible to add the two contributions constituting the modes of decay of the compound nucleus. The $(\alpha, 2n)$ mode is brought down in turn by the $(\alpha, 3n)$ process, beginning at about 26 Mev and still rising at the highest energy investigated.

The author wishes to express his appreciation to Professor E. Segrè for suggesting the problem, to Professor A. C. Helmholz for many valuable suggestions, and to Mr. R. W. Hayward for the use of the spectrometer. Thanks are also due the 60-inch cyclotron crew and Dr. W. L. Whitson and associates for the mass-spectrography.

[3] V. F. Weisskopf, MDDC 1175, p. 105 (Los Alamos Notes).

Letters to the Editor

PUBLICATION of brief reports of important discoveries in physics may be secured by addressing them to this department. The closing date for this department is five weeks prior to the date of issue. No proof will be sent to the authors. The Board of Editors does not hold itself responsible for the opinions expressed by the correspondents. Communications should not exceed 600 words in length.

Anomalous Magnetic Moments of Nucleons

S. D. DRELL
Physics Department, University of Illinois, Urbana, Illinois
May 31, 1949

IN this note we report an extension of previous work[1] to the calculation of the anomalous magnetic moments of nucleons. The interaction between quantized Dirac nucleon fields, quantized scalar and pseudoscalar meson fields, and an applied magnetic field is investigated by third-order perturbation theory in a manner similar to that recorded in reference 1. With the same notation, we have for the term in the Hamiltonian density which describes the first-order interaction of the meson-nucleon fields with an applied vector potential, **A**,

$$^{e}\mathcal{H}=ie\mathbf{A}\cdot(\psi^{*}\mathbf{grad}\psi-\psi\mathbf{grad}\psi^{*})-e\Psi_{P}^{*}\boldsymbol{\alpha}\cdot\mathbf{A}\Psi_{P}.$$

The meson-nucleon coupling terms appear in Eqs. (6) and (7) of reference 1 for a scalar meson field. The β-matrix there is replaced by $i\beta\gamma_5$ for a pseudoscalar field with pseudoscalar coupling.

We summarize our results as follows:

$$\mu_P-1=(g^2/4\pi)(\tfrac{1}{3}\pi)\mu_{\mathrm{I}};\ \mu_N=(g^2/4\pi)(\tfrac{1}{3}\pi)(-\mu_{\mathrm{I}}+\mu_{\mathrm{II}});$$
(charged meson theory)

$$\mu_P-1=(g'^2/4\pi)(\tfrac{1}{3}\pi)(2\mu_{\mathrm{I}}+\mu_{\mathrm{II}});\ \mu_N=(g'^2/4\pi)(1/\pi)(-\mu_{\mathrm{I}}+\mu_{\mathrm{II}});$$
(symmetric meson theory)

$$\mu_P-1=(g''^2/4\pi)(\tfrac{1}{3}\pi)\mu_{\mathrm{II}};\ \mu_N=0;\ \text{neutral meson theory)}$$

where

$$\mu_{\mathrm{I}}=\left[(\tfrac{3}{2})-a^2-(1-3a^2+a^4)\ln 1/a-(5-5a^2+a^4)\frac{a\cos^{-1}a/2}{(4-a^2)^{\frac{1}{2}}}\right]$$
$$\pm\left[1-(1-a^2)\ln 1/a-(3-a^2)\frac{a\cos^{-1}a/2}{(4-a^2)^{\frac{1}{2}}}\right]$$

represents that part of the moment contributed by a virtual intermediate meson cloud of positive electric charge, and

$$\mu_{\mathrm{II}}=\left[\tfrac{1}{2}-a^2+(2a^2-a^4)\ln 1/a-(2-4a^2+a^4)\frac{a\cos^{-1}a/2}{(4-a^2)^{\frac{1}{2}}}\right]$$
$$\pm\left[1+a^2\ln 1/a-(2-a^2)\frac{a\cos^{-1}a/2}{(4-a^2)^{\frac{1}{2}}}\right]$$

is the contribution of the virtual intermediate charged nucleon states. The plus sign is for scalar mesons, the minus sign for pseudoscalar ones, and a is the ratio of meson mass to nucleon mass.

With proper adjustments in notation these results agree with those obtained by different means by Luttinger,[2] Slotnick[3] and Case[4] for pseudoscalar theories, and by Case for a scalar meson field. Numerical results appear below for mesons of mass 300 m_e.

	Scalar	*Pseudoscalar*
Charged meson theory	$\mu_N=+.49(g^2/4\pi)$ $\mu_P-1=-.30(g^2/4\pi)$	$\mu_N=-.13(g^2/4\pi)$ $\mu_P-1=+.054(g^2/4\pi)$
Symmetric meson theory	$\mu_N=+.98(g'^2/4\pi)$ $\mu_P-1=-.42(g'^2/4\pi)$	$\mu_N=-.26(g'^2/4\pi)$ $\mu_P-1=+.034(g'^2/4\pi)$.

Moments obtained from the scalar calculation are of wrong sign and too small in magnitude[1] for $g^2/4\pi=0.30$ and $g'^2/4\pi=0.30$. The pseudoscalar theory yields moments of appropriate sign. If one chooses $g^2/4\pi\approx 36$, on the basis of questionable nuclear force arguments,[5] the anomalies are of proper magnitude for the protons, but too large in the neutron case because of exaggerated contributions from the charged intermediate nucleon states. Investigation of fourth-order interactions between nucleons which are important in the pseudoscalar theory has led Bethe[6] to suggest $g^2/4\pi\approx 4$. This has the effect that magnetic moment anomalies resulting from a pseudoscalar theory are also too small. It would appear to be necessary to investigate higher order effects in order to ascertain if contributions from a fifth-order calculation are large compared with these third-order results, as are the fourth-order effects in Bethe's calculation, relative to the second-order ones.

As recently discussed by French and Weisskopf[7] in the analogous calculations for electrons and a quantum field, one encounters a set of terms which may be written as $c[\boldsymbol{\alpha}\cdot\mathbf{A}]_{\mathrm{av}}$. In our calculations contributions to c come from interactions of **A** with both charged mesons and nucleons. By a careful integration of the individually diverging terms which contribute to it, we have also found that this term vanishes, as it must for covariance.

Of the four possible charge and mass renormalizations for protons and neutrons, only the proton mass renormalization must be taken into account in the calculation of the moments. Schemes according to which a proton pair is created, and then the same pair annihilated, contribute nil. They are analogous to the vacuum polarization terms of quantum electrodynamics. The proton mass renormalization is handled similarly to Feynman's[8] treatment for the quantum field. Neutron mass renormalization is a higher order effect since a neutron core has no direct interaction with electromagnetic fields.

Details of this calculation are to be found in the University of Illinois Ph.D. thesis of S. D. Drell, 1949.

We wish to thank Professor S. M. Dancoff for his continued guidance and interest.

[1] S. M. Dancoff and S. D. Drell, Phys. Rev. **76**, 205 (1949).
[2] J. M. Luttinger (Helv. Phys. Acta **21**, 483 (1948)) has performed a second-order perturbation calculation, treating nucleons and mesons in a uniform magnetic field as his zero order stationary states.
[3] M. Slotnick, Phys. Rev. **75**, 1295 (1949); Slotnick and Heitler, Phys. Rev. **75**, 1645 (1949) has calculated the spin-orbit coupling in an electrostatic field.
[4] K. M. Case (Phys. Rev. **74**, 1884 (1948); **76**, 1 (1949)) has performed this calculation in the framework of the Schwinger-Tomonaga-Dyson formalism.
[5] F. Villars, Helv. Phys. Acta **20**, 476 (1947).
[6] H. A. Bethe, Phys. Rev. **76**, 191 (1949).
[7] J. B. French and V. F. Weisskopf, Phys. Rev. **75**, 1240 (1949).
[8] R. P. Feynman, Phys. Rev. **74**, 1430 (1948).

Temperature Equilibrium in a Stationary Gravitational Field

H. A. BUCHDAHL
Physics Department, University of Tasmania, Hobart, Tasmania
June 13, 1949

IT has been shown by Tolman and Ehrenfest[1] that the distribution of proper temperature T_0 of matter in thermodynamic equilibrium situated in a static gravitational field whose metric is

$$ds^2=g_{ik}dx^i dx^k+g_{44}(dx^4)^2,\quad (i,k=1,2,3),\qquad (1)$$

is described by the relation

$$T_0(g_{44})^{\frac{1}{2}}=\text{const.}\qquad (2)$$

In (1) x^4 is the 'time,' and $\partial g_{ik}/\partial x^4=\partial g_{44}/\partial x^4\equiv 0$. By the method of *TE* it is very easily shown that (2) continues to hold in a *stationary*

gravitational field, that is, a field whose metric is of the form

$$ds^2=g_{\mu\nu}dx^\mu dx^\nu, \quad (\mu,\nu=1,\cdots,4), \tag{3}$$

with $\partial g_{\mu\nu}/\partial x^4\equiv 0$.

The energy momentum tensor is, as before, given by

$$\left.\begin{aligned} T^{\mu\nu}&={}'T^{\mu\nu}+{}''T^{\mu\nu},\\ {}'T^{\mu\nu}&=-g^{\mu\nu}p_0,\\ {}''T^{\mu\nu}&\begin{cases}=(\rho_{00}+p_0)(dx^4/ds)^2=(\rho_{00}+p_0)/g_{44}, & (\mu=\nu=4)\\ =0 \text{ (all other components)}, \end{cases}\end{aligned}\right\} \tag{4}$$

where

since $dx^i/ds=0$; note that now $g^{44}\neq 1/g_{44}$. The equation expressing the vanishing of the covariant derivative of $T_\mu{}^\nu$ may be written

$$T^\nu{}_{i;\nu}={}'T^\nu{}_{i;\nu}+{}''T^\nu{}_{i;\nu}=-\frac{\partial p_0}{\partial x^i}$$
$$+\tfrac{1}{2}{}''T^{\mu\nu}\frac{\partial g_{\mu\nu}}{\partial x^i}-\frac{1}{(-g)^{\frac{1}{2}}}\frac{\partial[(-g''T_i{}^\nu)^{\frac{1}{2}}]}{\partial x^\nu}=0. \tag{5}$$

It follows immediately from (4) that the last term of (5) vanishes, while the second term gives $[(\rho_{00}+p_0)/2g_{44}][\partial g_{44}/\partial x^i]$, so that (5) reduces to

$$\frac{\partial p_0}{\partial x^i}+\tfrac{1}{2}(\rho_{00}+p_0)\frac{\partial \log g_{44}}{\partial x^i}=0. \tag{6}$$

But (6) is identical with Eq. (26) in *TE*; so that the relation (2) follows as before.

[1] R. C. Tolman and P. Ehrenfest. Phys. Rev. **36**, 1791 (1930). This will be referred to as 'TE'.

Apparent Straggling of $_{16}S^{35}$ Beta-Particles in Glass*

MARY JANE A. LINKER
North Carolina State College of Engineering, Raleigh, North Carolina
AND
F. T. ROGERS, JR.,
U. S. Naval Ordnance Test Station, Inyokern, California
May 26, 1949

WHEN a beam of particles having kinetic energies in unit range of E, enters a solid normally to its surface, the particles suffer scattering and collisional losses of energy at fluctuating rates while traversing the solid; consequently the projected (on the normal direction) ranges of the particles, r, are more or less dispersed about some mean value R in accord with a suitable statistical frequency distribution. For alpha-particles in air, for example, scattering does not appreciably affect the distribution function and it has the Gaussian form[1]

$$W=\exp-[(r-R)/\rho]^2\Big/\int_0^\infty \exp-[(r-R)/\rho]^2, \tag{1}$$

where ρ is the coefficient of straggling. The object of the present investigation is to find out whether Eq. (1) can apply to the passage of beta-particles through a thin slab of glass; in this case scattering is large, so that ρ might be expected to be far greater than for alpha-particles. Equation (1) leads to a coefficient of transmission given by

$$\tau(E)=\int_{(t-R)/\rho}^\infty e^{-z^2}dx\Big/\int_{-R/\rho}^\infty e^{-z^2}dx, \tag{2}$$

for a slab of thickness t; and for ρ comparable to or greater than R,

$$\rho\cong(t-kE^2)/\text{erfi}^{-1}(1-2\tau). \tag{3}$$

In getting Eq. (3), R was replaced by kE^2 according to the energy-range relation; k is a constant.

To obtain data for use in Eq. (3), the beta-particle spectrum from the decay of $_{16}S^{35}$ was measured, using a glass Geiger-Müller counter with a nominal window thickness of 0.001 cm and superficial mass of 2.5 mg/cm^2. This radioactive material was the separated, reactor-made isotope, and was obtained from the Isotope Division of the AEC's Oak Ridge Operations, at Oak Ridge, Tennessee. Spectra from several active sources, prepared[2] under the guidance of Dr. Arthur Roe, were measured with an electrostatic analyzer designed (after Backus)[3] by Mr. S. J. Bame. Column 2 of Table I shows the energy distribution in this spectrum as observed through the 0.001 cm of glass; because of the weakness of sources used, these entries may be uncertain by several percent. Column 3 presents the true spectrum as computed from the theory of Fermi[4] according to the experimental studies of Cook, Langer, and Price,[5] and of Albert and Wu.[6] Column 4 lists the effective transmission at the respective energies.

TABLE I. Data on straggling of beta-particles.

E (kev)	$O(E)$ (arbitrary units)	$I(E)$ (arbitrary units)	$\tau(E)$	ρ, (cm)
35	12	132	0.09	5.1×10^{-4}
40	25	133	0.19	5.2
42.5	31	133	0.24	4.6
45	43	132	0.33	4.5
47.5	66	132	0.50	—
50	75	130	0.57	4.8
52.5	93	128	0.73	4.0
55	114	126	0.91	3.1
57.5	123	123	1.00	4.1
60	120	121	0.99	3.2
62.5	113	118	0.97	5.0×10^{-4}

From a curve of τ *vs.* E, E was found to be 48.5 kev for $\tau=50$ percent; hence from the energy-range relation, 0.001 cm$=k$(48.5 kev),[2] k was found to be 4.255×10^{-7} cm/kev.[2] This enabled the computation of ρ from the data, by Eq. (3); the results are shown in column 5 of Table I. The test of the applicability of Eq. (1) in this case, is in the values of ρ. Although there is evidence of a trend in the ρ-values, it does not seem significant in view of the appreciable uncertainties in $O(E)$; therefore this study indicates that $\rho=4.4\times10^{-4}$ cm, with an A.D. of 0.6×10^{-4} cm. The sensible constancy of ρ-values as here obtained, is rather surprising when the complexity of the process of apparent straggling is considered; but it does indicate that the simple Eq. (1) can describe the phenomenon, at least for energies barely appropriate to penetration.

* The experimental work here reported was carried out in the research laboratories of The University of North Carolina in Chapel Hill, North Carolina, during the academic years 1947–1948 and 1948–1949. The authors are particularly indebted to Messrs. N. Di Costanzo and R. Morris for their excellent shop-work in construction of the electrostatic analyzer.
[1] E. Rutherford, J. Chadwick, and C. D. Ellis, *Radiations from Radioactive Substances* (Cambridge University Press, London, 1930), pp. 112 *et seq.*
[2] The preparation of active sources was carried out in the new laboratory for radio-biological research at The University of North Carolina. The Division of Biology and Medicine of the AEC provided, through the ONR, a portion of the funds for this laboratory.
[3] J. Backus, Phys. Rev. **68**, 59 (1945).
[4] E. J. Konopinski, Rev. Mod. Phys. **15**, 209 (1943).
[5] Cook, Langer, and Price, Jr., Phys. Rev. **73**, 1395 (1948).
[6] R. D. Albert and C. S. Wu, Phys. Rev. **74**, 847 (1948).

Energy Release in Beryllium and Lithium Reactions with Protons

A. V. TOLLESTRUP, W. A. FOWLER, AND C. C. LAURITSEN
Kellogg Radiation Laboratory, California Institute of Technology, Pasadena, California
June 9, 1949

MEASUREMENTS have been made on the energy released in the reactions:

$$Be^9+H^1\rightarrow Li^6+He^4+Q_1, \tag{1}$$
$$Be^9+H^1\rightarrow Be^8+D^2+Q_2, \tag{2}$$
$$Be^8\rightarrow 2He^4+Q_2', \tag{2'}$$
$$Li^6+H^1\rightarrow He^3+He^4+Q_3. \tag{3}$$

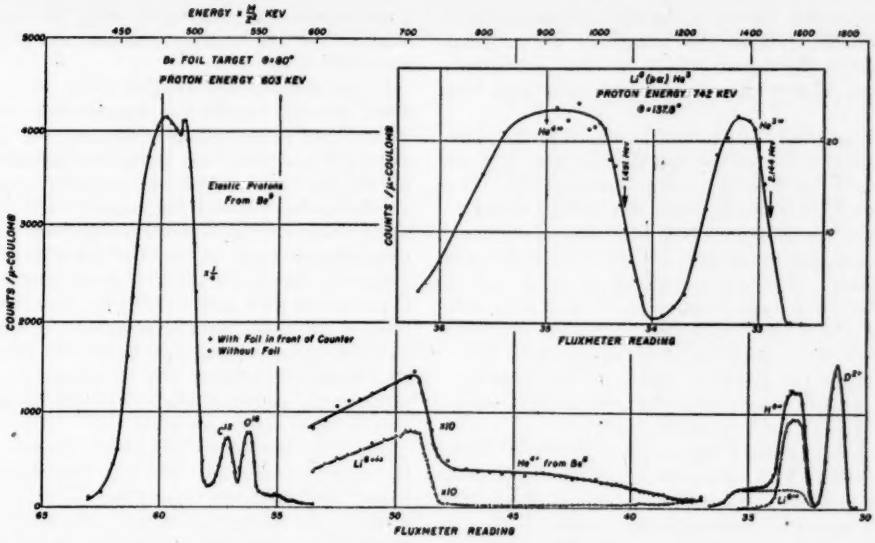

FIG. 1. Momentum analysis of the ions produced in the bombardment of Be^9 by protons. Inset: momentum analysis of the products of the reaction $Li^6(p\alpha)He^3$.

Protons monoenergetic to better than 0.03 percent were obtained from an electrostatic accelerator and analyzer previously described.[1] The analyzer was calibrated by measurements on the strong gamma-ray resonance in $F^{19}(p\alpha', \gamma)O^{16}$ which has been carefully standardized at 873.5 kev.[2] The targets used in studying reactions (1) and (2) were beryllium foils which were 10–20 kev thick for fast protons. The target for reaction (3) was produced by evaporating a thin lithium layer on copper in vacuum.

The energy of the ions produced in the reactions was accurately determined by a double-focusing magnetic spectrograph.[3] Reactions (1) and (2) were studied at two angles of observation in laboratory coordinates, 80.0° and 137.8°, while reaction (3) was studied only at 137.8°. The angles were measured directly and the angular aperture in each case was 6.6° in the plane in which the particles were deflected. The spectrograph field was determined by a null reading fluxmeter[4] and could be held constant to 0.05 percent and reproduced to ±0.15 percent. The fluxmeter was calibrated by observing protons of known energy scattered elastically from copper, beryllium, carbon, and oxygen. The energy of the scattered particles varies with angle for the light elements, and thus the consistency of the measurements was a verification of the direct measurement of the angle.

The scintillation counter used to detect the particles was arranged so that thin aluminum foils of known stopping power could be introduced directly in front of the ZnS screen. This made it possible to separate ions of different charge and energy that appeared at the same value of the magnetic field. For particles of energy greater than 100 kev, a plateau is exhibited in the integral spectrum of pulses from the scintillation counter. It was possible to set the discriminator bias high enough to eliminate all the dark current pulses, and still be operating on the plateau. It was verified with an ionization chamber that the plateau represented a counting efficiency of close to 100 percent.

Figure 1 shows data obtained by bombarding a 15-kev thick beryllium foil with 603-kev protons. The angle of observation was 80.0°. The peak at a fluxmeter reading of 60 mv* is elastically scattered protons from the beryllium. At readings of 57 mv and 58 mv the peaks due to elastically scattered protons from O^{16} and C^{12}, respectively, appear. Very thin carbon and oxygen layers were found on both the beryllium and lithium targets. Using the heights of the peaks it is possible to estimate the thickness of the layers from the cross sections for Rutherford scattering. The energies of all particles involved in any reaction were corrected for energy loss in these layers. The total carbon and oxygen layer in the curve shown is 0.44 kev thick normal to the target for 603-kve protons.

The alpha-particles from reaction (1) appear at 33 mv. They are superimposed on the doubly ionized Li^6 ions from the same reaction.** These two groups were separated by means of foils inserted in front of the ZnS screen. The triply ionized Li^6 ions from this reaction are observed at about 50 mv. The singly ionized He^4 and Li^6 ions could not be observed in the spectrograph with the maximum available field. The three groups of ions that were measured give three independent determinations of Q_1.

The deuterons from reaction (2) appear at 32 mv and Q_2 is calculated, using the energy of these particles. The Be^8 residual nucleus formed in reaction (2) recoils with a momentum equal and opposite to that of the deuteron in the center-of-mass system. Because of its short half-life, it disintegrates before it can travel far enough to make collisions and hence slow down. Since it disintegrates while in motion, the resultant two alpha-particles generate a continuous energy distribution. This is shown extending from 37 mv to 48 mv. The doubly ionized Li^6 peak gave some interference and foils were again used to separate the particles. The spectrum $N(E_\alpha)$ plotted against E_α is shown in Fig. 2. The

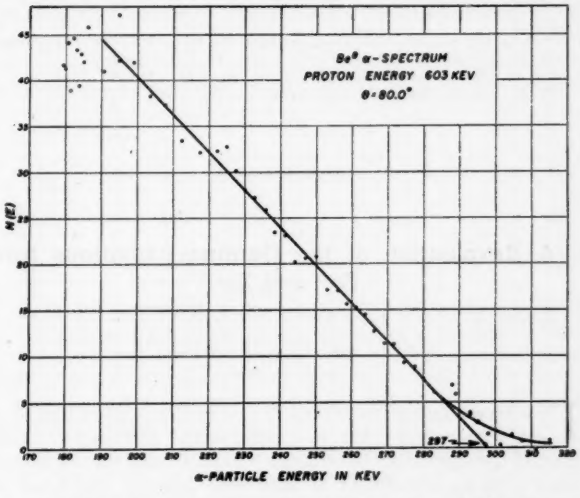

FIG. 2. Distribution in energy of the alpha-particles resulting from the disintegration of Be^8 produced in the reaction $Be^9(pd)Be^8$.

linearity of the curve within 150 kev of the end point is in accordance with theoretical expectations. The "fillet" near the end point can be accounted for by the angular window of the spectrograph. The extrapolated end point of this spectrum was used along with Q_2 to calculate Q_2'.

The curves obtained from reaction (3) are shown in the insert in Fig. 1. Both the doubly ionized He^4 and He^3 ions were detected and both groups were used in the energy determination. The reaction was studied at 742- and 1237-kev bombarding energy.

In the calculations, the midpoint of the front edge of the peaks was taken as corresponding to particles leaving the front surfaces of the target at the mean entrance angle of the spectrograph. Small corrections for relativity and surface layers have been made in each case. The errors were calculated by compounding the estimated systematic errors with the observed statistical errors which were very small. The probable systematic errors assumed were 0.3° in the angle of observation, 0.3 percent in observed energy, and 0.2 percent in the bombarding energy.

Q_1 is found to be 2.121 ± 0.012 Mev, Q_2 is 0.558 ± 0.003 Mev, while Q_3 is 4.017 ± 0.022. These are both somewhat higher than the measurements of Rosario,[5] and Perlow.[6] Q'_2 is 89 ± 5 kev, which is to be compared with Hemmendinger's value of 102 ± 10 after his value is corrected for the gamma-ray recoil.[7] A combination of the above Q values with those of $D(dp)H^3$ and $D(dn)He^3$, which have Q-values of 4.036 ± 0.022 Mev and 3.265 ± 0.018 Mev, respectively,[8] and the binding energy of the deuteron, 2.237 ± 0.007 Mev[9] makes it possible to calculate the energy release in the reactions $Li^6(nH^3)He^4$ and $Be^9(\gamma n)Be^8$. We find for the first reaction $Q=4.788\pm0.023$ Mev and for the second, $Q=-1.679\pm0.008$ Mev. The ratio of the Q-value of $H^2(\gamma n)H^1$ to that of $Be^9(\gamma n)Be^8$ is 1.332 ± 0.010, which is in agreement with the measurement of Waldman and Miller[10] who find 1.338 ± 0.004. The recently determined ranges of the particles in the Li^6 reaction[11] give the following two points on the range energy relations: 0.912-Mev protons have a range of 2.00 ± 0.02 cm and 2.058-Mev alpha-particles have a range 1.04 ± 0.02 cm in air at N.T.P.

We should like to thank Mr. Robert G. Thomas for his help in obtaining the data on beryllium. This work was assisted by the joint program of the ONR and the AEC.

* Fluxmeter readings are proportional to the (charge)/(momentum) of the observed particles.

** The particles and residual nuclei produced in a reaction at a given angle have approximately the same momentum. Hence, the ions of the two products with the same charge overlap in a momentum analysis made by a magnetic field. This is quite different than in an analysis by range measurements.

[1] Fowler, Lauritsen, and Lauritsen, Rev. Sci. Inst. **18**, 818 (1947).
[2] Herb, Snowdon, and Sala, Phys. Rev. **75**, 246 (1949).
[3] Snyder, Lauritsen, Fowler, and Rubin, Phys. Rev. **74**, 1564(A) (1948).
[4] C. C. Lauritsen and T. Lauritsen, Rev. Sci. Inst. **19**, 916 (1948).
[5] Leticia del Rosario, Phys. Rev. **74**, 304 (1948).
[6] G. J. Perlow, Phys. Rev. **58**, 218 (1940).
[7] A. Hemmendinger, Phys. Rev. **73**, 806 (1948); Phys. Rev. **74**, 1267 (1949).
[8] Tollestrup, Jenkins, Fowler, and Lauritsen, Phys. Rev. **75**, 1947 (1949).
[9] R. E. Bell and L. G. Elliott, Phys. Rev. **74**, 1552 (1948).
[10] B. Waldman and W. C. Miller, Phys. Rev. **74**, 1225(A) (1948).
[11] J. K. Bøggild and L. Minnhagen, Phys. Rev. **75**, 782 (1949).

A Revaluation of the Gamma-Radiations from Co^{60} and Zn^{65}

ERLING N. JENSEN, L. JACKSON LASLETT, AND WILLIAM W. PRATT
*Institute for Atomic Research and Department of Physics, Iowa State College, Ames, Iowa**
June 22, 1949

IN a recent paper[1] we described briefly the construction of an iron-free magnetic lens spectrometer and discussed the character of the corrections to be applied to gamma-ray measurements made with an instrument of that type. Energy values for the gamma-radiations from Co^{60} and Zn^{65}, obtained by measurement of photoelectric conversion lines, were reported. Calibration of the spectrometer was effected through the use of photoelectrons produced by annihilation radiation and of conversion electrons from ThB (*F*-line).

It has since become possible for us to obtain sources which would permit comparative measurements of the internal conversion line corresponding to the 2.62 Mev gamma-ray of ThC″ and the *F*-line from ThB. Such a comparison was considered desirable, since it would afford a definitive check of the presumed proportionality between the focused momenta and the currents in the spectrometer. Upon learning from Dr. T. Lauritsen that spectrometer work[2] at the California Institute of Technology indicated energies for the Co^{60} gamma-radiations approximately 15 kev higher than those cited by us,[1] we undertook to perform this check of our instrument *in conjunction with* a remeasurement of the photoelectric conversion lines from Co^{60}. This work has confirmed the linearity of the instrument but has led to a revised value of the spectrometer constant which is almost one percent greater than that found in our earlier work.

Based on momentum values of 1385 and 10,000 gauss-cm for the internal conversion electrons from ThB and ThC″, respectively,[3] and with the corrections for the photoelectric radiator made in the manner previously described,[1] our recent measurements lead to energies of 1.16_9 and 1.33_1 Mev for the gamma-radiations from Co^{60}. It is believed that these new values are more reliable than those given by us previously, as the stability of the spectrometer has been improved since the earlier data were obtained. These revised values are consistent with those determined by Hornyak *et al.*,[2] and with the precision wave-length measurements which have now been reported by Lind, Brown, and DuMond.[4] The values we have now obtained, when used in conjunction with previously reported[5] data obtained from a *composite* source in which *both* Co^{60} and Zn^{65} activities were present, leads to a revised value of 1.11_8 Mev for the Zn^{65} gamma-ray.

It should be mentioned that our corrections for the energy loss experienced by the electrons in the photoelectric converter are based[1] on the *average* energy loss by collision and, in the energy range with which we are concerned here, disregard complicating scattering effects. It is understood that the results of a more elaborate analysis have been used in the work of Hornyak *et al.*,[2] and lead to corrections appreciably smaller than those which we have been led to apply.

* Paper No. 72 from the Institute for Atomic Research. Work was performed at the Ames Laboratory of the AEC.

[1] Jensen, Laslett, and Pratt, Phys. Rev. **75**, 458 (1949).
[2] Hornyak, Lauritsen, and Rasmussen, *Gamma-Ray Measurements with a Magnetic Lens Spectrometer*, Phys. Rev. (to be published). We are indebted to Dr. Lauritsen for his courtesy in sending us a copy of the manuscript for this paper in advance of its publication and for discussing with us some aspects of the work.
[3] In computing the calibration constant of the spectrometer, the results of the ThB measurements were assigned twice the weight given to the data for the weaker ThC″ conversion line.
[4] D. A. Lind, J. R. Brown, and J. W. M. DuMond, Bull. Am. Phys. Soc. **24**, No. 6, paper F4 (1949).
[5] Jensen, Laslett, and Pratt, Phys. Rev. **73**, 529 (1948).

Ferro-electric Properties of WO_3

B. T. MATTHIAS
Bell Telephone Laboratories, Murray Hill, New Jersey
June 23, 1949

WE have recently grown single crystals of WO_3 and have found that these crystals appear to show ferro-electric behavior. The crystal structure of WO_3 may be looked at as being similar to a perovskite structure with the omission of the cations at the cube corners of the unit cell. That is, we may view WO_3 as derived from $BaTiO_3$ by the complete omission of the Ba-ions and the substitution of W for Ti. The ionic radius[1] of W^{+6} is 0.62 A and we therefore see that the WO_6 octahedra obey the empirical rule for the occurrence of ferro-electricity in perovskite-type structures

which we reported in an earlier communication in connection with the discovery of several ferro-electric columbates and tantalates.[2]

The crystals as grown from very pure tungstic acid vary in color from dark yellow to green. They are triclinic and show a marked domain structure very similar to that of ferro-electrics in the perovskite crystal system.

In the case of WO_3, however, the differences of lattice constants in different directions amount to about 5 percent whereas in the perovskite system they are near 1 percent. With a small external pressure the entire domain pattern in WO_3 can be shifted or changed, without damage to the crystal. Consequently the crystals appear to be very soft, nearly plastic.

The electric conductivity of the single crystals at room temperature is extremely high, which may have some connection with the occurrence of coloration in the crystals. It is not clear whether the color is due to slight chemical reduction or Na impurities. Pressed samples fired at much lower temperatures retained their light color and gave comparatively small losses and dielectric constants of the order of 10^3.

Dielectric measurements on the single crystals can be easily made, however, at liquid air temperature. There the losses are small and no longer interfere with the dielectric measurements. Preliminary results indicate a hysteresis loop and a dielectric constant between 100 and 300. This value is high compared to other ferro-electrics at the same temperature.

[1] Pauling and Goldschmidt.
[2] B. T. Matthias, Phys. Rev. **75**, 1771 (1949).

On the $\gamma-\gamma$-Angular Correlation in Pd^{106}

DANIEL S. LING, JR.
University of Kansas, Lawrence Kansas
AND
DAVID L. FALKOFF
University of Notre Dame, Notre Dame, Indiana*
June 20, 1949

MEASUREMENTS of $\gamma-\gamma$-correlations in excited states of Ni^{60}, Ti^{46}, Mg^{24}, Ba^{134}, Sr^{88}, and Pd^{106} have been reported by Deutsch and co-workers. Of these, all but Sr^{88} and Pd^{106} can be satisfactorily fitted with theory[2] by assuming that the γ-rays are either pure dipole or quadrupole radiation and by assigning to the nuclear states involved spins consistent with such other information as is available from measurements on internal conversion or β-decay. In general, the angular correlation theory by itself is not sufficient to make any unique assignment of multipole orders or of nuclear quantum numbers.

We have developed[3] the extension of the theory of $\gamma-\gamma$-angular correlations for the case in which one of the transitions is a mixture of magnetic dipole and electric quadrupole radiation and the other either pure dipole or quadrupole radiation. With it one can explain the observed correlation in Sr^{88} which could not be explained by assuming pure multipole transitions. The discussion of this and the interference effects accompanying such mixtures will be given elsewhere.[4] We discuss here some consequences of the application of this theory to the experimental data on the $\gamma-\gamma$-angular correlation in Pd^{106}. These data seem quite reliable having been independently reproduced by Deutsch and Wiedenbeck[5] with and without a strong applied magnetic field.

Pd^{106} being an even-even nucleus, its ground state may be taken as having zero spin. Because of the $\cos^4\theta$-term in the measured correlation function, neither transition can be pure dipole. A mixture of dipole and quadrupole radiation in one or both transitions would still be consistent with this $\cos^4\theta$-dependence. However, such mixtures are allowed only when $\Delta J=0, \pm 1$. Since quadrupole radiation is forbidden for $0\rightarrow 0$ or $0\rightarrow 1$ transitions and we have already ruled out pure dipole transitions, the least possible spin for the intermediate state must be $J=2$, and this choice would force pure quadrupole radiation for the lower transition. Similarly, for the upper (initial to intermediate state) γ-transition, the lowest multipoles possible are either pure quadrupole or a mixture of electric quadrupole and magnetic dipole. Deutsch[1] has already pointed out that the data cannot be fitted when both transitions are pure quadrupole. Since the assumption of a mixed transition made possible good agreement with experiment in the case of Sr^{88}, we attempted to interpret the data for Pd^{106} with a dipole-quadrupole mixture for the upper transition, the lower transition being taken as pure quadrupole. We find that agreement with experiment cannot be obtained. It follows, therefore, subject only to the reasonable assumption that the ground state has spin zero, that at least one of the successive rays must be of octupole or higher order.

A proposed disintegration scheme for Pd^{106} and its parent Ru^{106} has been given by Peacock.[6] Our arguments, while limiting the possible multipole orders of the γ-rays, do not otherwise affect his decay scheme except to exclude $J=1$ for the intermediate state in Pd^{106}.

This example illustrates the value of the angular correlation theory for nuclear spectroscopy, but it also makes clear the need for extending the calculations to higher multipoles.

* Supported in part by the joint program of the AEC and ONR at the University of Notre Dame.
[1] E. L. Brady and M. Deutsch, Phys. Rev. **72**, 870 (1947); **74**, 1541 (1948); M. Deutsch and F. Metzger, Phys. Rev. **74**, 1542 (1948).
[2] D. R. Hamilton, Phys. Rev. **58**, 122 (1940).
[3] D. S. Ling and D. L. Falkoff, Phys. Rev. **74**, 1224 (1948).
[4] Phys. Rev. in preparation.
[5] M. Deutsch and M. L. Wiedenbeck, private communication.
[6] W. C. Peacock, Phys. Rev. **72**, 1049 (1947).

The Magnetic Susceptibilities of Some Tetravalent Uranium Fluorides*

NORMAN ELLIOTT
Brookhaven National Laboratory, Upton, Long Island, New York
June 23, 1949

THE magnetic susceptibilities of UF_4, KUF_5, K_2UF_6, and Na_3UF_7 have been measured by the Gouy method over a temperature range of approximately 74°K to 300°K.

UF_4 was prepared from UO_2 by treatment with anhydrous HF. The complex salts were prepared by the fusion of UF_4 with stoichiometric quantities of the alkali or alkaline earth fluorides. This was done in a platinum crucible in an HF atmosphere, as described by Zachariasen.[1] Observation through a microscope showed them to be homogeneous. Uranium analyses were carried out on all the salts.

The susceptibility measurements were made over a two-month period on three or more samples of each compound, and during that time remained sensibly constant. If structural changes were taking place in any of the compounds, which might well be the case when one considers the method of preparation, this was not revealed by an effect on the susceptibilities.

With the exception of K_2UF_6, these substances obeyed the Curie-Weiss law $x=C/(T+\theta)$ over the whole temperature range of the investigation. K_2UF_6 followed the Curie-Weiss law down to 198°K, but deviated below this temperature. At 76°K its susceptibility is 8.6 percent smaller than that given by the Curie-Weiss equation. The experimental data are given in Table I.

The tetravalent uranium ion is thought to contain two $5f$ electrons, and so be in a $^3H_4$ state. The theoretical moment for a free ion in this configuration has been calculated by Van Vleck[2] to be 3.58 Bohr magnetons. It is seen from the table that the experimentally calculated moments are reasonably close to this value.

TABLE I. Susceptibilities of tetravalent uranium fluorides.

Compound	C	θ	μ
UF_4†	1.36	147°	3.30β
KUF_5	1.30	122°	3.30
K_3UF_8	1.47	108°	3.45
$CaUF_6$	1.31	101°	3.25
Na_3UF_7	1.45	290°	3.40

The large values found for the Weiss temperature in all these compounds make one hesitate to give the usual interpretation to the Curie constant, however, and experiments are in progress at this laboratory to obtain further information on the nature of the Weiss temperatures observed in these salts.

* Research conducted at Brookhaven National Laboratory under an AEC contract.

[1] W. H. Zachariasen, J. Am. Chem. Soc. **70**, 2147 (1948).

† In a previous letter to the editor the Curie constant for UF_4 was erroneously reported to have the value 1.00 (N. Elliott, Phys. Rev. **74**, 498 (1948)).

[2] J. H. Van Vleck, *Theory of Electric and Magnetic Susceptibilities* (Oxford University Press, New York).

Interaction of Mesons with the Electromagnetic Field

W. H. FURRY AND M. NEUMAN
Harvard University, Cambridge, Massachusetts
June 10, 1949

IN terms of the formalism of Duffin and Kemmer,[1] a Lorentz gauge and charge invariant theory of the interaction of a meson with an electromagnetic field has been formulated. It was found that a possible interaction Hamiltonian is of the form

$$H=-\frac{1}{c}j_\mu A_\mu+\frac{e^2}{mc^2}M_{\mu\nu}A_\mu A_\nu, \tag{1}$$

where

$$j_\mu=(iec/2)(\bar\psi\beta^\mu\psi-\bar\phi\beta^\mu\phi)$$
$$M_{\mu\nu}=\tfrac{1}{2}[\bar\psi\beta^\mu(\beta_N{}^2+1)\beta^\nu\psi+\bar\phi\beta^\mu(\beta_N{}^2+1)\beta^\nu\phi]$$
$$\phi=C\bar\psi;\ \bar\beta^\mu=-C^{-1}\beta^\mu C;\ C^+=C^{-1};\ \bar C=C.$$
$$\beta_N=N_\mu\beta_\mu$$

and N_μ is a unit vector normal to the surface. By means of the method used by Schwinger,[2] the longitudinal components of the electromagnetic field were eliminated from the Hamiltonian leaving it in the form

$$H=-(1/c)j_\mu A_\mu+(e^2/mc^2)M_{\mu\nu}A_\mu A_\nu+(\tfrac{1}{2}c)j_N V_N \tag{2}$$

with

$$V_N=N_\mu V_\nu=N_\mu\int\frac{\partial D(x-x')}{\partial x_\mu'}\frac{j_\lambda(x')}{c}d\sigma_\lambda'$$

$(N_\lambda\partial/\partial x_\lambda)^2D(x)=D(x)$; A_μ is the 4-vector of the pure radiation field. The terms linear in A_μ were then removed by means of a unitary transformation and the resulting second-order Hamiltonian analyzed into vacuum, photon, meson self-energy terms and terms representing the coupling of photons with mesons and the interaction between mesons. The explicit dependence on the orientation of the space-like surface present in (1) and (2) is exactly compensated in all these terms by the terms containing the derivatives of the signum function entering into the definition of $\Delta(X)$. The vacuum self-energy was shown to be a constant; the photon self-energy could be taken to vanish, if certain ambiguous integrals were suitably evaluated; the meson self-energy terms when transformed back to the original Kemmer equation could be interpreted as mass correction terms having the values

$$(\delta\kappa/\kappa)=(\alpha/12\pi)[6(P_mP_0/\kappa^2)+11\ln((P_0+P_m)/\kappa)-\tfrac{7}{8}]$$
$$(\delta\kappa/\kappa)=(3\alpha/4\pi)[(P_mP_0/\kappa^2)+\ln((P_0+P_m)/\kappa)-\tfrac{1}{8}]$$

in the representation of rank 10 and 5 respectively, where P_m is the maximum momentum of the virtual quanta and $P_0=(P_m{}^2+\kappa^2)^{\frac{1}{2}}$.

The polarization of the mesic vacuum by a given current distribution was also investigated. For a scalar meson the polarization kernel is of second order in the derivatives. The polarization kernel of the vector meson consists of two terms, separately conserved and gauge invariant. The first is formally identical with the polarization kernel of a spinless particle, the second is of fourth order in the derivatives. As a result, in the first term (and in the case of the scalar meson) the factor multiplying J_μ, and in the second term the factors multiplying J_μ and $\Box^2J_\mu$ are divergent. The physical concept of charge ormalization provides some justification for regarding the terms proportional to J_μ as unobservable and hence the infinities multiplying them as innocuous. It is suggested that because of the high order derivatives present in the second term of the polarization kernel of the vector meson, the formal strategy of dealing with infinities be extended to the term $\Box^2J_\mu$, even though the physical reason for this may not be too clear at present. Thus the current associated specifically with the vector meson would be regarded as observable beginning with derivatives of the external potential of higher order than those appearing in the polarization kernel, the formal procedure being the same as that used in the case of the electron and scalar meson. Explicitly stated, the formulas are:

$$\delta J_\mu=\delta J_\mu{}^{(0)}\quad\text{(for a scalar particle)}$$
$$\delta J_\mu=\delta J_\mu{}^{(0)}+\delta J_\mu{}^{(1)}\quad\text{(for the vector meson)}$$
$$\delta J_\mu{}^{(0)}=-(e^2/\hbar)\int\kappa_{\mu\nu}{}^{(0)}(x-x')A_\nu(x')d\omega'$$
$$\kappa_{\mu\nu}{}^{(0)}(x)=[\Delta^{(1)}(\partial^2\bar\Delta/\partial x_\mu\partial x_\nu)+\bar\Delta(\partial^2\Delta^{(1)}/\partial x_\mu\partial x_\nu)]$$
$$-[(\partial\Delta^{(1)}/\partial x_\mu)(\partial\bar\Delta/\partial x_\nu)+(\partial\Delta^{(1)}/\partial x_\nu)(\partial\bar\Delta/\partial x_\mu)]$$
$$+\delta_{\mu\nu}\Delta^{(1)}(x)\delta(x)$$
$$\kappa_{\mu\nu}{}^{(1)}(x)=\kappa^{-2}(\partial^2\Delta^{(1)}(x)/\partial x_\mu\partial x_\nu)\delta(x)$$
$$+\kappa^{-2}[(\partial^2\bar\Delta/\partial x_\mu\partial x_\sigma)(\partial^2\Delta^{(1)}/\partial x_\nu\partial x_\sigma)$$
$$+(\partial^2\bar\Delta/\partial x_\nu\partial x_\sigma)(\partial^2\Delta^{(1)}/\partial x_\mu\partial x_\sigma)]$$
$$-[(\partial\Delta^{(1)}/\partial x_\mu)(\partial\bar\Delta/\partial x_\nu)+(\partial\Delta^{(1)}/\partial x_\nu)(\partial\bar\Delta/\partial x_\mu)]$$
$$+\kappa^{-2}\delta_{\mu\nu}[\kappa^4\Delta^{(1)}\bar\Delta-(\partial^2\bar\Delta/\partial x_\lambda\partial x_\sigma)(\partial^2\Delta^{(1)}/\partial x_\lambda\partial x_\sigma)]$$
$$\langle\delta J_\mu{}^{(0)}\rangle_{\rm vac}=(-\alpha/6\pi)[\ln((P_0+P_m)/\kappa)-1]J_\mu$$
$$-(\alpha/24\pi)\int F_2(x-x')\kappa^{-2}\Box'^2J_\mu(x')d\omega'$$
$$\langle\delta J_\mu{}^{(1)}\rangle_{\rm vac}=-(\alpha/6\pi)[(P_0P_m/\kappa^2)-4\log((P_0+P_m)/\kappa)+3]J_\mu$$
$$-(\alpha/6\pi)[\log((P_0+P_m)/\kappa)-(27/20)]\kappa^{-2}\Box^2J_\mu$$
$$-(\alpha/16\pi)\int[F_2(x-x')-\tfrac{1}{3}F_3(x-x')]$$
$$\times(\kappa^{-2}\Box'^2)^2J_\mu(x')d\omega'$$

where $F_n(x)$ is defined by

$$F_n=16\kappa^3\int_0^1 dv\frac{v^{2n}}{(1-v^2)^2}\bar\Delta\left[\frac{2x}{(1-v^2)^{\frac{1}{2}}}\right].$$

According to the suggestion made here the second term of $\delta J_\mu{}^{(0)}$ and the third of $\delta J_\mu{}^{(1)}$ would be regarded as physically significant, corresponding to the formal fact that $K^{(0)}$ is of second- and $K^{(1)}$ of fourth order in the derivatives.

[1] N. Kemmer, Proc. Roy. Soc. **173A**, 91 (1939).
[2] J. Schwinger, Phys. Rev. **74**, 1439 (1948); Phys. Rev. **75**, 651 (1949).

Electromagnetic Induction in a Superconductor

A. WEXLER AND W. S. CORAK
Westinghouse Research Laboratories, East Pittsburgh, Pennsylvania
June 20, 1949

RECENTLY, Houston and Squire[1] reported the results of an experiment in which a Faraday disk of lead, in the form of a flattened spheroid, was investigated above and below the superconductive transition temperature. They found that the induced electromotive force remained practically unchanged as the transition range was traversed. On the basis of the "Meissner effect",[2] however, the electromotive force should have dropped to zero

when the lead became superconducting. These results seem to cast doubt upon the general validity of the supposed fundamental property of superconductors, namely, the zero value for the magnetic induction, B, within a substance when it is in the superconducting state.

Because of the fundamental nature of this experiment, we investigated the problem under isothermal conditions which facilitate precision measurements and eliminate errors due to temperature gradients. A lead sphere, one inch in diameter, was studied at *ca.* 4.2°K through the measurement of the induced electromotive force, between the axis and the periphery of the sphere, as a function of the applied magnetic field, H, in the direction of the axis of rotation, the rotational speed being maintained constant. Thus far, two speeds have been used: 200 r.p.m. and 350 r.p.m. The results were entirely in accord with the concept of the inability of a magnetic field to reside within a superconductor. As H was increased from zero, the induced voltage remained zero until the field reached a value $H=\frac{2}{3}H_c$. In the transition range, the voltage increased linearly with the field up to the critical field, $H=H_c$, attaining at this point a value in agreement with that deduced from the laws of electromagnetic induction for a conductor of permeability unity. Thus at 200 r.p.m. and at 4.180°K, corresponding to $H_c=552$ oersteds, the measured e.m.f. was 91 microvolts. The e.m.f. *versus* field curve was reversible except for a small hysteresis corresponding to a "frozen-in" flux of about 8 percent of the value obtaining within the specimen at $H=H_c$.

Auxiliary experiments in which the sphere was cooled in the presence of a magnetic field, in contrast to our aforementioned experiments, confirmed the transition to a state wherein the magnetic induction is zero. Under these conditions, the measured e.m.f. was only 17 percent of the value to be expected of a normal conductor, and was 7 percent of the e.m.f. observed at $H=H_c$. In addition, qualitative experiments involving temperature changes under conditions of constant rotational speed and applied magnetic field resulted in e.m.f. changes of the type to be expected from the variation of B with temperature.

The e.m.f. *versus* H transition curves should be entirely equivalent to those of B *versus* H. This was confirmed by measurements of B *versus* H by the conventional method described by Keeley and Mendelssohn.[3] All of our data are consistent and give values of H_c in very close agreement with the carefully determined critical data of Daunt and Mendelssohn.[4]

More extensive measurements, covering higher rotational speeds, will be reported in detail in the near future.

[1] W. V. Houston and C. F. Squire, Science **109**, 439 (1949).
[2] W. Meissner and R. Ochsenfeld, Naturwiss. **21**, 787 (1933).
[3] T. C. Keeley and K. Mendelssohn, Proc. Roy. Soc. London **A154**, 378 (1936).
[4] J. G. Daunt and K. Mendelssohn, Proc. Roy. Soc. London **A160**, 127 (1937).

Thompson Scattering and the Hole Theory

D. S. Kothari and F. C. Auluck
University of Delhi, Delhi, India
June 20, 1949

It is well known that the original Dirac theory and the "hole" theory give identical values for the scattering (electromagnetic waves) cross section of an (isolated) electron—in the "original" theory the negative energy states are assumed to be all vacant whereas in the hole theory they are all occupied. The type of divergence, however, of the electron self-energy is different in the two cases. Recently, while examining the problem of the effect of radiation field on the electromagnetic shift of the s-level of the H-atom, we were led, incidentally, to consider how the scattering cross section for a free electron becomes modified when it belongs to an assembly of a degenerate Fermi-Dirac gas. It was immediately obvious that the cross section for this case is affected differently according to whether the original theory or the hold theory is used. For instance, in the non-relativistic case (Thompson scattering) the scattering cross section is practically unaffected in the original theory whereas this is not so in the hole theory. In the case of the hole theory, the scattering cross section tends to vanish for photons of wave-length λ_0, where λ_0 is the minimum de Broglie wave-length for the fermi distribution for the degenerate electron gas.

We were, therefore, greatly interested to see a recent note by Halpern and Hall[1] on the coherent scattering of radiation and negative energy states. They have considered the scattering cross section of neutral atoms originally calculated by Waller, assuming the negative energy state to be unoccupied, and find that, in the case of the hole theory, the results of Waller need modification. As Halpern and Hall conclude, the results obtained indicate that not only the proof concerning the equivalence of the two versions of the theory is erroneous, but also that the two theories lead to different predictions concerning experimental results. The point that the hole theory and the original theory do not lead to identical results has been often overlooked. It is therefore worth while to draw attention to the fact that even for Thompson scattering the results are identical only when we consider an isolated electron, but they are different if the electron is the constituent of a degenerate gas. (In the case of non-degeneracy the difference is negligible.)

[1] O. Halpern and H. Hall, Phys. Rev. **75**, 910 (1949).

Quadrupole Moment of Sb^{121} and Sb^{123}

K. Murakawa and S. Suwa
Institute of Science and Technology, Komaba, Meguroku, Tokyo, Japan
June 15, 1949

In order to find the value of the quadrupole moment of Sb^{121} and Sb^{123}, the hyperfine structure of the spectrum of Sb II was studied. This was excited in an aluminum hollow cathode discharge tube which was filled with neon of a few mm Hg pressure. The cathode contained some powdered antimony and was cooled with water. The fine structure was examined by the use of two glass Lummer plates (thickness=10 mm and 4.7 mm), a quartz Lummer plate (thickness=4.4 mm), and a Fabry-Pérot etalon.

$\lambda 5640(5p6s^3P_2-5p6p^3S_1)$ was found to have the following structure: 0(10), 0.072(8), 0.222(8)*, 0.315(6), 0.351(6), 0.403(4)*, 0.484(7)*, 0.616(7)*, 0.672(2), 0.736(3) cm^{-1}, where numbers in brackets represent visually estimated intensities. The approximate structure of this line was calculated by Badami by assuming the nuclear spins[1] $I=5/2$ for Sb^{121} and $I=7/2$ for Sb^{123}. Comparison of the observed structure with the calculated one shows that the components marked with * are blends and are not suited for determining the hyperfine levels. From the observed structure we obtain the hyperfine separations of the term $5p6s^3P_2(Sb^{121})$:

$$F_{\frac{7}{2}}^{\frac{9}{2}}-F=0.315\ cm^{-1}$$
$$F_{\frac{1}{2}}^{\frac{5}{2}}-F=0.736+\text{total separation of } 5p6p^3S_1$$
$$=0.736+0.135=0.871\ cm^{-1}.$$

If we assume that the position of the hyperfine structure levels of a term is represented by $E=E_0+(A/2)C+C(C+1)$ where A and B are the fine structure constant and the quadrupole constant respectively and $C=F(F+1)-I(I+1)-J(J+1)$, we obtain from the above mentioned separations the values of the constants:

$$5p6s^3P_2(Sb^{121}):\quad A=0.0674,\quad B=-0.000086.$$

The value of the quadrupole moment Q can be calculated by the formula which is due to Casimir[2]:

$$=\frac{BZ_iH}{\delta R'}I(2I-1)44370\cdot10^{-24}\ cm^2,$$

in which H and R' are relativity correction factors, δ is the doublet separation of the p-electron, and $Z_i=Z-4$ for a p-electron. Putting $B=-0.00086$, $Z_i=47$, $H=1.06$, $\delta=6140$, $R'=1.10$ in the formula, we obtain

$$Q^{121}=(-0.3\pm0.2)\cdot10^{-24}\text{ cm}^2,$$

the uncertainty coming partly from the probable error of our measurement and partly from inaccuracy of the theoretical formula for Q. The structure of λ5640 is too complicated to find suitable resolved components of Sb^{123}.

Tomboulian and Bacher[3] measured the hyperfine structure of λ5895, and found that Sb^{122} has a quadrupole moment, but they could not determine the absolute value, since the classification of this line was unknown. We have classified this line as $5p6s^3P_1-5p6p^3P_0$, so that from the measurement of Tomboulian and Bacher the constant A and B of the term $5p6s^3P_1$ can now be deduced and are found to be:

$$Sb^{123}:\quad A=0.1054,\quad B=0.000127,$$
$$Sb^{121}:\quad A=0.1940,\quad B\approx0.00004.$$

The value of Q can be calculated by the formula[2]

$$Q=\frac{BZ_iHI(2I-1)\cdot14790}{\delta(R'\cdot c_1{}^2-2.83\cdot Sc_1c_2)_i}\cdot10^{-24}\text{ cm}^2,$$

in which S is a relativity correction factor, and c_1 and c_2 are coupling constants of the term $5p6s^3P_1$. Putting $S=1.17$, $H=1.06$, $c_1=0.99666$, $c_2=-0.08189$ and the value of B for Sb^{123} mentioned above in the formula we obtain

$$Q^{123}=(-1.2\pm0.2)\cdot10^{-24}\text{ cm}^2.$$

According to the above mentioned authors, the quadrupole effect of Sb^{121} in λ5895 is too small to deduce the value of Q^{121}.

[1] J. S. Badami, Zeits. f. Physik **79**, 206 (1932); M. F. Crawford and Bateson, Can. J. Research **10**, 693 (1934).
[2] H. Casimir, Verh. Teylers Tweede Genootschap., Haarlem **11** (1936).
[3] D. H. Tomboulian and R. F. Bacher, Phys. Rev. **58**, 52 (1940).

The Magnetic Moment of B^{11}

DONALD A. ANDERSON*
Radiation Laboratory, McGill University, Montreal, Canada
June 13, 1949

THE gyromagnetic ratio of B^{11} has been compared with that of the proton by measuring the ratio of their Larmor precession frequencies in the same magnetic field. The ratio of the resonant frequencies is:

$$\frac{\nu_B}{\nu_P}=0.320827\pm0.000004.$$

Making a small diamagnetic correction,[1,2] assuming a spin of $\frac{3}{2}$, and using the value 2.79352±0.031 percent for the proton moment,[3] one gets for the B^{11} moment

$$\mu_B=2.68939\pm0.031\text{ percent nuclear magnetons.}$$

Both resonances were observed in a supersaturated solution of potassium metaborate prepared by mixing 8 g of H_3BO_3 with a 10 cc boiling solution of 7 g of KOH. An absorption method with a simple regenerative circuit was used at 30 mc for the proton, and the induction method for the boron, the resonances being displayed on an oscilloscope in the usual way. A single switch made possible the switching from one resonance to the other in approximately 3 seconds. All known first-order errors except in the calibration of the secondary frequency standard were eliminated by making the resonances coincide first on one side and then on the other side of the center of the sweep display, using the fore-sweep resonance on one side and the back-sweep resonance on the other for the B^{11}. In this solution, T_1 for B^{11} is approximately 0.01 second, so that the resonance reverses for each fore and back sweep of the 60 c.p.s. display giving an oscilloscope pattern symmetrical about the center point. The chief error arises from the breadth of resonance and fluctuations of the magnetic field whose average value was regulated to <1 part in 10^4.

For the frequency determinations, reference was made to a stable crystal controlled standard. A second very stable oscillator operating at 10 mc had a sufficiently strong 3rd harmonic to pull the gently oscillating regenerative receiver into synchronism with it. The oscillator for the B^{11} induction, conveniently near at ~9.6 mc, was checked from the calibrated dial of the secondary standard.

The induction apparatus features the following: The push-pull oscillator and the induction coil which it supplies comprises a radiofrequency system balanced to ground to decrease capacitive coupling to the receiver coil. The receiver coil consists of two equal sections wound oppositely and in parallel aiding, so that the outside grounded ends tend to shield the inner ends which are connected to the center of the receiver coax. Theoretically this construction also balances out voltage induced by any flux parallel to the main magnetic field. The magnetic coupling between the coils is minimized by micrometer adjustment of the angle between their axes. The mechanism consists of a ball-and-socket-like arrangement in which the receiver coil is supported on the end of an adjustable probe inside the induction coil, the specially shaped polystyrene coil-forms of each forming the bearing. The voltage induced in the receiver coil is reduced to a few millivolts thereby making possible the observation of a signal of a few microvolts when the oscillator modulation is approximately 0.01 percent. A three-stage T.R.F. receiver, diode detector and audio amplifier were used for the induction signal.

Some indication of T_2 and a rough check on Bloch's formula for amplitude of an induction signal were obtained for the B^{11}. Experimentally, the resonance width was 3.2 gauss (at 0.707 maximum amplitude), and the resonance amplitude $6.2\mu\nu\pm40$ percent. A large fraction of the width is accounted for by the induction field 2 H_1, but at least we deduce

$$T_2>10^{-4}\text{ sec.}$$

The greatest amplitude expected with optimum relaxation times is $6.0\mu\nu$, which would be obtained if $T_1=T_2$. We conclude that conditions in this solution are about optimum for observation of induction and that $T_2\rightarrow T_1$.

Appreciation is expressed to Dr. J. S. Foster who suggested and encouraged the work. The suggestions of Mr. D. Hunten and his efforts in building some of the equipment are acknowledged as well as those of others of the Radiation Laboratory Staff. Gratitude is due to the National Research Council, Ottawa, for the award of three studentships during the course of the work.

* Now with Canadian Marconi Company, Montreal.
[1] W. E. Lamb, Phys. Rev. **60**, 817 (1941).
[2] Bloch, Nicodemus, and Staub, Phys. Rev. **74**, 1025 (1948).
[3] H. Taub and P. Kusch, Phys. Rev. **75**, 1326A (1949).
[4] F. Bloch, Phys. Rev. **70**, 460 (1946).

Erratum: The Scattering of Slow Neutrons by Paramagnetic Crystals

[Phys. Rev. **75**, 895 (1949)]

I. W. RUDERMAN, W. W. HAVENS, JR., T. I. TAYLOR, AND L. J. RAINWATER
Columbia University, New York, New York
June 13, 1949

THE following typographical error has been noted in the above paper:

Page 895, column 1, last line

for "$\alpha/k=6\pi/r_0\lambda$" read instead
"$\alpha/k=3\lambda/2\pi r_0$."

Gamma-Radiation from Na^{22} and Co^{60}

DAVID E. ALBURGER
Brookhaven National Laboratory, Upton, New York*
June 23, 1949

TECHNIQUES of gamma-ray measurement using the lens spectrometer have been applied to the radiation occuring in 3y Na^{22} decay. As shown by Good, Peaslee, and Deutsch,[1] the Na^{22} nucleus emits a positron of 0.575-Mev maximum energy followed by a single gamma-ray of 1.30±0.03 Mev from the residual Ne^{22} nucleus. The mass of Na^{22} has been calculated in Rosenfeld's tables[2] by adding the mass equivalent of these two energies plus $2m_0c^2$ to the mass of Ne^{22}. The accuracy of the mass difference has been limited by the gamma-ray value.

The experimental method used is due to Hornyak, Lauritsen, and Rasmussen[3] and was first described by Dr. Lauritsen at the 1949 Washington American Physical Society meeting. It consists of converting the gamma-radiation photoelectrically in thin foils of a heavy element such as thorium and taking the extrapolated upper energy edge end point of the photoelectron distribution as a direct measure of electron momentum. The end point is found to be nearly independent of converter thickness and avoids the difficulties of correcting for scattering and energy loss in the converter when the momentum is referred to the position of the curve maximum.

The Brookhaven lens spectrometer[4] was used to observe photoelectrons from 21.5-mg/cm² lead, 14-mg/cm² thorium, and 44-mg/cm² uranium foils. Calibration values taken from the extrapolated front edge of K-shell photoelectrons due to Na^{22} positron annihilation radiation were in close agreement for the three converters. Regulation of the lens coil current was maintained to better than 0.1 percent by a Lawson and Tyler type photoelectric regulator.[5] This operates from a current shunt and employs a 10-turn Helipot for reference voltage to control the current in field of an exciter generator. Frequent checks on current linearity and stability of the system were made by measuring the voltage developed across a second shunt with a Leeds and Northrup Type K potentiometer.

The Na^{22} source was formed in the DTM Carnegie cyclotron by the reaction $Mg^{24}(d\alpha)Na^{22}$ and separated by the Chemistry Department of this Laboratory. The active NaCl solution was deposited in a 0.85-cm diameter brass source capsule to which the converters were attached. A complete curve of the gamma-ray secondary electron spectrum using the 21.5-mg/cm² Pb foil is shown in Fig. 1. The inner K and L photoelectrons of large intensity are due to the 0.5108-Mev positron annihilation radiation and the outer K and L peaks correspond to transition gamma-rays. These are superposed on a double Compton distribution background. In general, only the two K peaks were measured. The average value of five final measurements using the three converters previously mentioned was 1.277±0.004 Mev for the gamma-ray energy. This falls within the limits assigned by Good, Peaslee, and Deutsch. Using a probable error of 10 kev in the positron end point,[6] the $Na^{22}-Ne^{22}$ mass difference may now be placed at 0.003087±0.000011 Mev.

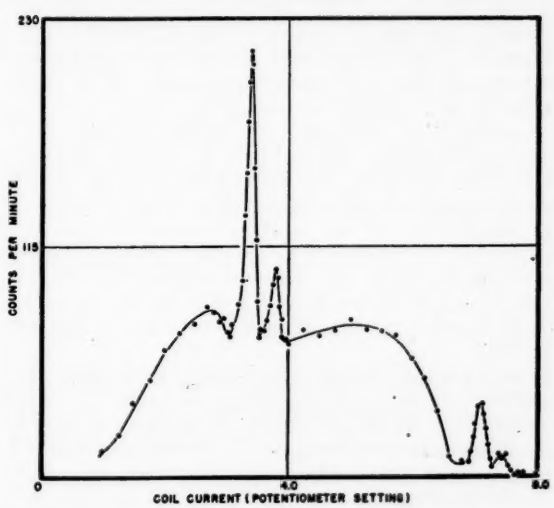

FIG. 1. Na^{22} gamma-ray secondary electron spectrum using a 21.5-mg/cm² Pb converter.

As a check on the method the gamma-rays of Co^{60} were investigated and energies of 1.175±0.006 Mev and 1.332±0.005 Mev obtained. These agree well with the new crystal spectrometer measurements of Lind, Brown, and DuMond,[7] namely, 1.1711 ±0.0010 Mev and 1.3318±0.0010 Mev but are definitely higher beyond the experimental limits than the values of Jensen, Laslett, and Pratt.[8] **

The author is indebted to Dr. W. Rubinson for the loan of the chemically separated Na^{22} sample.

* Research carried out under contract with the AEC.
[1] Good, Peaslee, and Deutsch, Phys. Rev. **69**, 313 (1946).
[2] L. Rosenfeld, *Nuclear Forces II* (Interscience Publishers, Inc., New York, 1949).
[3] Hornyak, Lauritsen, and Rasmussen, Phys. Rev. (in press). The author is grateful to Dr. Lauritsen for forwarding a copy of their paper in advance of publication.
[4] D. E. Alburger, Phys. Rev. **75**, 1442 (1949).
[5] J. J. Lawson and A. W. Tyler, Rev. Sci. Inst. **10**, 304 (1939). The actual circuit used is a modified version designed by Dr. G. Wadey.
[6] M. Deutsch, private communication.
[7] Lind, Brown, and DuMond, Bull. Am. Phys. Soc. **24**, No. 6, 12 (1949). The value 1.1171 in this reference is apparently a misprint and should be 1.1711 to agree with the wave-length in x.u.
[8] Jensen, Laslett, and Pratt, Phys. Rev. **75**, 458 (1949).
** See, however, the Letter to the Editor by Jensen, Laslett, and Pratt in this issue.

The Nuclear Spin and Magnetic Moment of Cs^{137}*

LUTHER DAVIS, JR.
Research Laboratory of Electronics, Massachusetts Institute of Technology, Cambridge, Massachusetts
June 13, 1949

THE decay scheme of Cs^{137} has recently been reported by Townsend, Cleland, and Hughes[1] in which they remark upon the desirability of determining the spin of this isotope. The atomic beam magnetic resonance method[2] as used by Zacharias[3] to determine the nuclear spin and magnetic moment of K^{40} has been used to determine the nuclear spin and magnetic moment of Cs^{137}.

Of the $Cs^{137}Cl$ obtained from the Isotopes Division of the Atomic Energy Commission, 210 microcuries in dilution of one part in one thousand with $Cs^{133}Cl$ were placed in the oven together with a slight excess of NaN_3. Upon decomposition of the azide, the sodium displaced the cesium in the chloride to furnish an atomic cesium beam. A fourteen-hour run was required for the present determination with the evaporation of 4×10^{-9} mole of Cs^{137} from the oven resulting in transition intensities for that isotope of several hundred atoms per second.

Because of the high frequencies of the hyperfine structure $\Delta\nu$ of both Cs^{133} and Cs^{137}, only $\Delta F=0$ transitions were observed having $\Delta m_F=\pm1$. These transitions permit direct comparison of g_F for the two isotopes. Search was made for transitions, having set the magnetic field (as determined by the Cs^{133} line) and radiofrequency for transitions corresponding to $I=1/2, 3/2, \cdots, 23/2$ with the mass spectrometer set for mass number 137. No resonances were observed except for $I=7/2$ which, because of the resolution of the mass spectrometer for this mass separation and number being only 0.4 percent, could be due to both cesium isotopes or to Cs^{133} alone. If both isotopes have the same spin but not identical nuclear magnetic moments, raising the value of the homogeneous magnetic field increases the separation between the transition frequencies because of the difference in $\Delta\nu$ until a value is reached where the resonances may be resolved. This procedure was followed until at 257 gauss two peaks were observed at about 96

Mc/sec., spaced some 700 kc/sec. apart, having the proper relative intensities in the two mass positions for the dilutions used. As the second peak did not appear in the mass 133 position, it must be associated with some other isotope rather than a spurious effect in the apparatus. The resolution of the mass spectrometer being only 10 percent for a spacing of two mass numbers at this mass number, it is possible that Cs^{135} present in abundance ten times as great as Cs^{137} could produce such an effect. However, the fission yield of these two isotopes should be about the same, so that such confusion seems highly improbable, leading us to assign the spin of 7/2 to Cs^{137}. The use of a mass spectrometer of higher resolution will allow observations to be made at the Cs^{135} position because of the diminished Cs^{133} background, permitting the determination that the observed transitions do not result from Cs^{135} and very likely permit observation of peaks due to that isotope.

The $\Delta F=0$ transitions of both isotopes were followed out to about 1100 gauss permitting an evaluation of the h.f.s. $\Delta\nu$ to an accuracy limited primarily by the instability of the homogeneous field. The results show that the spin of Cs^{137} is 7/2 in units of $h/2\pi$ and its h.f.s. $\Delta\nu$ is 10,128±15 Mc/sec. By comparison with the value of the nuclear magnetic moment of Cs^{133} given by Kusch, Millman, and Ravi,[4] we obtain for Cs^{137} a nuclear magnetic moment of 2.837±0.010 nuclear magnetons. The sign of this nuclear moment was determined to be positive in just the way used by Zacharias for K^{40}.

I am indebted to Mr. C. W. Zabel for his help in both this and the Na^{22} experiment during the run when time was of such importance; to Dr. D. E. Nagle for the design and construction of the apparatus adapted for use in this experiment; and to Professor J. R. Zacharias who suggested the problem and with whom repeated discussion of the problems involved made possible the conclusion of this experiment.

* This work has been supported in part by the Signal Corps, the Air Materiel Command, and the ONR.

[1] Townsend, Cleland, and Hughes, Phys. Rev. **74**, 499 (1948).
[2] Kusch, Millman, and Rabi, Phys. Rev. **57**, 765 (1940).
[3] J. R. Zacharias, Phys. Rev. **61**, 967 (1942).
[4] Kusch, Millman, and Rabi, Phys. Rev. **55**, 1176 (1939).

The Neutrons from the Disintegration of Sodium by Deuterons†

C. E. MANDEVILLE
Bartol Research Foundation of the Franklin Institute, Swarthmore, Pennsylvania
June 17, 1949

THE nuclear energy levels of Mg^{24} have been studied rather extensively with the aid of several different nuclear reactions. Inelastic lines have been observed in the scattering of fast protons by magnesium[1–3] and in the scattering of fast neutrons by magnesium;[4] levels[5] are also excited by beta-disintegration of Na^{24}. There is some uncertainty in the levels indicated by the two gamma-rays of Na^{24}, since the order of emission of the successive gamma-rays is not known. As yet unexplored as an indicator of nuclear energy levels of Mg^{24} has been the energy spectrum of the neutrons emitted when sodium is irradiated by deuterons. The nuclear reaction is

$$Na^{23}+D\rightarrow Mg^{24}+n^1+Q.$$

The Q-value corresponding to the formation of Mg^{24} in its ground state can be calculated from the masses[6] as 8.88 Mev. This rather large quantity of energy immediately suggests the possibility of forming Mg^{24} in highly excited energy levels to be marked by the presence of group structure in the neutron spectrum. To ascertain the distribution in energy of the neutrons, a thick target of metallic sodium was bombarded by 5.6-microampere hours of deuterons of energy 1.4 Mev in the Bartol Van de Graaff generator. The neutrons were detected by production of recoil protons in Ilford C_2 photographic emulsions located 9 cm from the target and at 90° to the incident beam. A total of 1450 acceptable tracks were measured. Track lengths were measured in the calibrated eyepiece of a compound microscope. An acceptance angle of twelve degrees in the forward direction was used throughout, and proper allowance was made for shrinkage of the plates on development. Using plates of emulsion thickness 100 microns, the energy distribution of Fig. 1 was obtained. Owing to the difficulty of finding acceptable long tracks, measurements were not extended beyond 8.5 Mev in the 100-micron emulsions. Four neutron groups are in evidence in Fig. 1 having peaks at 0.64, 1.70, 2.70, and 6.1 Mev. The actual neutron distribution, corrected for variation with energy of the $n-p$ scattering cross section and for the probability of finding an acceptable recoil proton track corresponding to a given energy, is shown by the broken line. In order to obtain data in the vicinity of 10 Mev and to improve statistical accuracy as a whole in the region of higher energies, the energy interval between 4.2 Mev and 10.5 Mev was surveyed with C_2 emulsions of thickness 200 microns. The distribution in energy is shown in Fig. 2 where neutron groups are to be found with apparent peaks at 6.1, 8.5, 8.9, 9.3, and 10.1 Mev. As in the case of Fig. 1, the corrected distribution is indicated by the broken line.

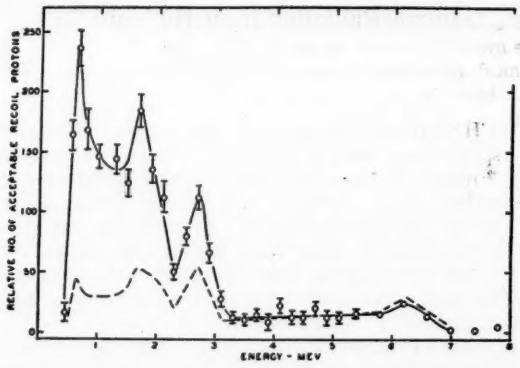

FIG. 1. Energy distribution to 8.5 Mev of the recoil protons projected in the forward direction by the neutrons from the disintegration of sodium by deuterons. The broken line is the corrected distribution. Corrections for variation with energy of acceptance probability and the neutron-proton scattering cross section were made. Emulsion thickness 100 microns.

The neutron group at 0.64 Mev is dismissed as very probably the monochromatic neutrons of the reaction $C^{12}(D,n)N^{13}$. The Q-values calculated from the remaining groups are 9.23, 8.40, 7.99, 7.57, 5.07, 1.53, and 0.59 Mev. In calculating the Q-values, the observed energies of the neutron groups were used, but the customary two percent additive correction introduced by the acceptance angle has not been made. With the omission of this correction, the calibration curve of Powell and Ochialini[7] was found to give precise agreement with known energy values of neutron groups such as the monochromatic neutrons of the deuteron-deuterium reaction. It is convenient that the level spacings of the residual nucleus depend on differences between the Q-values and not upon their absolute values. The above-cited Q-values indicate energy levels in Mg^{24} at 0.83, 1.24, 1.66, 4.16, 7.70, and 8.64 Mev. It may be argued that the 1.24-Mev−1.66-Mev doublet is actually a single level, and indeed it was hoped that this would be the case. However, although the data in the vicinity of a neutron energy of 8.5 Mev grouped according to several different energy interval sizes, the doublet structure seemed to persist.

Returning to the question of the order of emission of the gamma-rays of Na^{24}, it is first noted that the level at 4.16 Mev is consistent with the known cascade emission of the two gamma-rays. Moreover, the levels in the vicinity of 1.4 Mev suggest that the 1.38-Mev quantum is the second of the two emitted quanta. A salient feature of the distribution curve of Fig. 2 is that no neutron group appears which corresponds to an excitation level at 2.76 Mev, thus favoring a disintegration scheme in which the 1.38-Mev

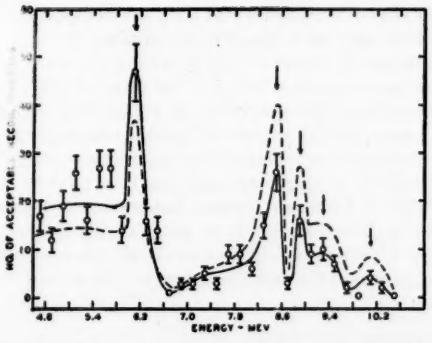

FIG. 2. Energy distribution (observed and corrected) ranging from 4.2 Mev to 10.5 Mev of the recoil protons projected in the forward direction by the neutrons from sodium irradiated by deuterons. Emulsion thickness 200 microns.

gamma-ray follows the 2.76-Mev gamma-ray. In the various proton scattering experiments, weak proton groups have appeared which correspond to levels between 2.0 Mev and 2.8 Mev. However, for reasons of intensity, these levels may be related to Mg^{25} or Mg^{26}. Separated magnesium isotopes have not as yet been employed in scattering experiments. The data of the present experiment are completely unambiguous, because Na^{23} is the single stable isotope of sodium. It is, of course, likely that other neutron groups may emerge at different angles of observation and different bombarding energies. The nuclear energy levels of Mg^{24} as determined by several different methods are summarized in Table I.

TABLE I. Nuclear energy levels of Mg^{24}.

Neutron scattering	Proton scattering Rochester, 1941	Proton scattering Rochester, 1943	Proton scattering Princeton, 1948	Disintegration of Na^{24}	$Na^{23}+D\rightarrow Mg^{24}+n'+Q$
			1.00		0.83
1.30		1.32	1.33		1.24
	1.37			1.38	
			1.54, 1.58		1.66
			1.98(?)		
	2.80	2.74	2.64(?)		
		3.88	3.97		
	4.07		4.17	4.14	4.16
			5.51		
			7.32		7.70
			8.30		8.64

The writer wishes to express his appreciation to Dr. E. L. Hudspeth and Mr. C. P. Swann of Bartol for many interesting discussions regarding the photographic plate technique and for the use of the Van de Graaff generator.

† Assisted by the joint program of the ONR and the AEC.

[1] T. R. Wilkins, Phys. Rev. **60**, 365 (1941).
[2] R. H. Dicke and J. Marshall, Phys. Rev. **63**, 86 (1943).
[3] H. W. Fulbright and R. R. Bush, Phys. Rev. **74**, 1323 (1948).
[4] Little, Long, and Mandeville, Phys. Rev. **69**, 414 (1946).
[5] Elliott, Deutsch, and Roberts, Phys. Rev. **63**, 386 (1943).
[6] H. A. Bethe, *Elementary Nuclear Theory* (John Wiley & Sons Inc., New York, 1947).
[7] C. F. Powell and G. P. S. Ochialini, *Nuclear Physics in Photographs* (Oxford University Press, New York, 1947).

Erratum: On the Difficulty of the Meson Theory of Nuclear Forces

[Phys. Rev. **75**, 1101 (1949)]

GENTARO ARAKI
Department of Industrial Chemistry, Kyoto University, Kyoto, Japan

FOR Eq. (1) read

$$W_{BA}=-\Sigma_I H'_{BI}H'_{IA}/(E_I-E_A). \qquad (1)$$

Decay Scheme of Te^{125m}

J. C. BOWE AND GERTRUDE SCHARFF-GOLDHABER
*Department of Physics, University of Illinois, Urbana, Illinois**

June 20, 1949

A STUDY of Te^{125m} (58 days) with a 180° magnetic beta-ray spectrograph[1] had shown that besides the K, L and M conversion lines of the 109.3 kev transition, a weak line of 31 kev electrons was present. With a more intense source of Te^{125m}, Hill[2] succeeded recently in photographing a second weak line, thus identifying the first and the second line as L and M conversion electrons, respectively, of a 35.4 kev transition.

The present investigation was undertaken to decide the role of this transition in the decay scheme of Te^{125m} in order to be able to assign the spin change between the metastable state and the ground state which is of particular interest in this case.[3]

We have carried out the following experiments:

1. By the fluorescence method previously described[4] we have detected unconverted photons corresponding to the 35.4 kev transition. We observed characteristic fluorescence from reflectors made of various iodine compounds, but not from reflectors made of caesium or barium compounds. This is to be expected for a 35.4 kev photon. A comparison of the intensity of the fluorescence from iodine with that obtained from silver, where the Te K x-ray lines are critically absorbed, showed that approximately 15 unconverted gamma-rays are emitted per 100 K x-rays. This result was confirmed by Mr. Katz by means of critical absorption instead of fluorescence.[5]

2. Using two krypton filled Eck and Krebs counters and a coincidence circuit with a resolving time of 0.2 microseconds, we found photon-photon coincidences which were strongly reduced by insertion of Ag absorbers between the source and one of the counters. This result taken together with the fact that no line corresponding to the difference 109.3 kev−35.4 kev=73.9 kev has been observed either converted or unconverted, indicates that the 35.4 kev transition succeeds the 109.3 kev transition.

An estimate of the K shell conversion coefficient can be made from the photon-photon coincidence rate observed. The absolute efficiency for K x-rays of the region in which we are interested was obtained by using a Te^{121} source, where K electron capture from the 17 day ground state leads to an excited state of 610 kev in Sb^{121} which decays promptly to the ground state.[6] If it is assumed that each 610 kev gamma-ray is preceded by K electron capture (thus ignoring small contributions from capture of electrons in higher orbits), the absolute efficiency ϵ for detecting K shell holes (equal to the efficiency of detecting K x-rays multiplied with the fluorescence yield) is obtained. If we further assume that the unconverted gamma-ray is detected by our Kr counter approximately as efficiently as a K hole and that the fractions η_{K_1} of the 109.3 kev radiation and η_{K_2} of the 35.4 kev radiation are converted in the K shell, the following relation holds:

$$A=\frac{\eta_{K_1}\times\frac{N_{12}}{N_1}}{2\eta_{K_1}\epsilon-\frac{N_{12}}{N_1}}.$$

Where A denotes $(\eta_{K_2}+\gamma_2)$, γ_2 being the fraction of unconverted gamma-rays per 35.4 kev transition and N_{12}/N_1 the number of coincidences per single count for the Te^{125m} source measured in a geometry identical to that used for the determination of ϵ. For η_{K_1} we used the previously determined value 0.54[1]. Our coincidence experiments yielded the following values:

$$\epsilon=(1.1\pm0.1)\times10^{-3}$$

$$\frac{N_{12}}{N_1}=(0.8\pm0.1)\times10^{-3}$$

from which it follows that A is close to 1.

TABLE I. Theoretical lifetimes and conversion coefficients.

	$\frac{N_{e_K}}{N_\gamma}$	$\frac{N_{e_L}}{N_\gamma}$	$\tau^{a,b}$	$\eta_{K_2}{}^b$	$\frac{N_\gamma{}^b}{N_e+N_\gamma}$
Electric dipole	3	0.41	9.6×10^{-13} sec.	0.68	0.23
Magnetic dipole	6.8	0.63	1.3×10^{-6} sec.	0.80	0.12
Electric quadrupole	17	36	2.0×10^{-7} sec.	0.31	0.018
Present work			$<5\times10^{-8}$ sec.	0.6–0.8	0.15–0.20

[a] Expected lifetime of excited state, corrected for internal conversion.
[b] For the calculation of these values conversion for shells higher than the L-shell has been neglected.

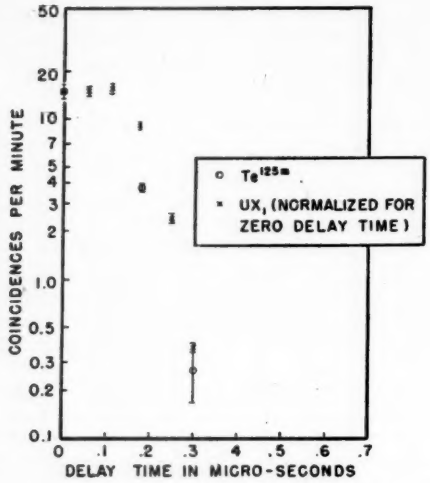

FIG. 1. Delayed photon-photon coincidences from Te^{125m}.

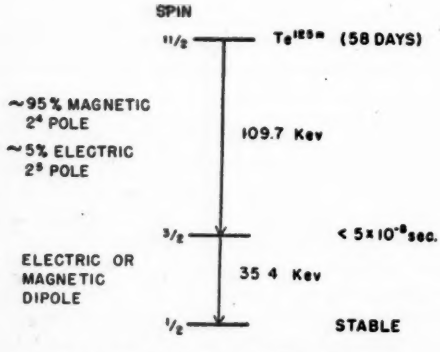

FIG. 2. Proposed decay scheme of Te^{125m}.

Values for ηK_2 between 0.6 and 0.8 and for γ_2 between 0.15 and 0.20 are best compatible with all the data.

3. An attempt was made to measure the lifetime of the 35.4 kev transition. Figure 1 shows the number of photon-photon coincidences, consisting of the coincidences between K x-rays of the 109.3 kev transition and either K x-rays or the unconverted gamma-rays of the 35.4 kev transition, as a function of the delay between two Eck and Krebs counters. The technique used was the same as that described by Bittencourt and Goldhaber.[6] For comparison a "zero-delay" curve obtained by shooting UX_1 beta-rays through both counters is given. No noticeable delay was found, and we can estimate that the half-life is $<5\times10^{-8}$ seconds.

Table I shows the theoretical lifetimes and conversion coefficients[7] to be expected for the 35.4 kev transition, with either an electric dipole or magnetic dipole transition or an electric quadrupole transition. In the last line the experimental results are given.

It is seen that the experimental data are compatible with the first two cases, although the lifetime appears to be somewhat short for a magnetic dipole transition. However, since theoretical lifetimes are uncertain by a factor of the order of 100 this is not sufficient to rule out the possibility of a magnetic dipole transition.[8] The assumption of an electric quadrupole transition, on the other hand, seems to be definitely in disagreement with our data.

The spin of Te^{125} in its ground state has been recently measured by Mr. Fowles[9] in Professor Jenkins' Laboratory at Berkeley, and found to be $\frac{1}{2}$. This permits us to propose the following decay scheme (Fig. 2), which is definitive as far as spin assignments are concerned, but leaves the parity change for the second transition still indefinite.

* Supported jointly by ONR and AEC.
[1] Hill, Scharff-Goldhaber, and Friedlander, Phys. Rev. **75**, 324 (1949).
[2] R. D. Hill, Phys. Rev. **76**, 186 (1949).
[3] Friedlander, Goldhaber, and Scharff-Goldhaber, Phys. Rev. **74**, 981 (1948).
[4] R. D. O'Neal and G. Scharff-Goldhaber, Phys. Rev. **62**, 83 (1942).
[5] R. Katz, unpublished.
[6] P. T. Bittencourt and M. Goldhaber, Phys. Rev. **70**, 780 (1946).
[7] M. H. Hebb and E. Nelson, Phys. Rev. **58**, 486 (1940); S. D. Drell, Phys. Rev. **75**, 132 (1949); P. Axel and S. M. Dancoff, in course of publication.
[8] It may be pointed out here that present ideas on the nuclear shell model seem to favor a magnetic dipole transition in this case (see R. D. Hill's discussion for Te^{123}, reference 2).
[9] Private communication from Professor A. C. Helmholz.

On the Energy Band Structure of Insulators

G. H. WANNIER
Bell Telephone Laboratories, Murray Hill, New Jersey
June 16, 1949

IT is a well-known fact that an insulator may become an n- or p-type semiconductor upon the introduction of a sufficient number of impurities. These "donors" and "acceptors" are known to stabilize the location of the Fermi level close to the conduction band or the uppermost filled band. Discussions of these phenomena often imply that the Fermi level of a good insulator is located in the center of the forbidden band. This letter wants to point out that this last possibility is rather remote and that an attempt to realize it is more likely to lead to uncontrolled spatial oscillations of the Fermi level between its n and p positions.

If we take, for instance, the case of diamond, we find that the product of electron and hole densities equals 10^{-8} cm^{-6}. Thus the electrons and holes which tend to stabilize the Fermi level in the center of the forbidden band are far too small in number to have any influence. Their role is restricted entirely to preventing the entry of the Fermi level into the filled or empty band. Within the forbidden region itself the location of the level becomes thus entirely dependent on the crystal imperfections and becomes subject to the fluctuations which they undergo. If we assume, for instance, that there exists, at a certain place, a number of low lying acceptors (as might be found in the neighborhood of a crack) then we will find that these acceptors will tend to attract negative charge. This negative charge cannot be supplied by the filled band unless the Fermi level approaches the latter closely. Thus the region acquires a net negative charge whose field lines must end up on the same donor impurity in the neighborhood. The potential which the negative region thus acquires is about equal to

$$V=-\frac{ne}{\epsilon a}+\frac{ne}{\epsilon d}$$

where n is the number of negative charges making up the imperfection, a the linear dimension of the region and d the mean distance to compensating positive charges. It is reasonable to assume $d\sim10^{-5}$, $a\sim10^{-8}$ and n a few units. The voltage thus obtained is considerably larger than 3.5 volts. The actual voltage drop will of course stop at the latter figure or earlier either because the

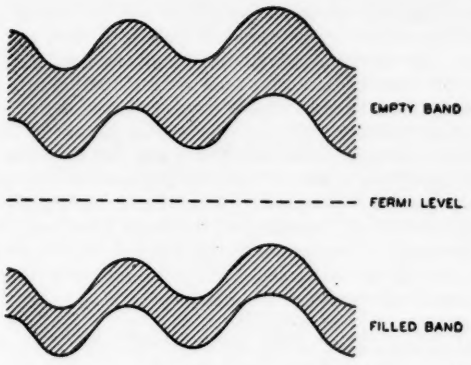

FIG. 1.

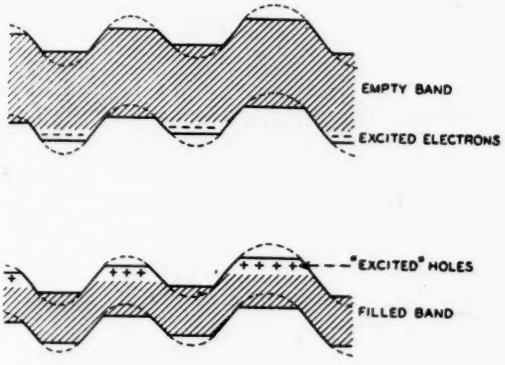

FIG. 2.

Fermi level has dropped below the acceptor levels or because it has approached the filled band sufficiently closely to form localized holes. In either case the Fermi level has been upset by the imperfection. The disturbance calculated here is localized, but this will not be the case for surface type imperfections which are suggested by some experiments.[1]

We arrive thus at a picture of an insulator as having a band structure whose height varies somewhat like a roller coaster (Fig. 1). Now let such material be flooded with electron hole pairs either by a rise in the temperature or by light or electron bombardment. The electron hole pairs produced will flow into the regions of unbalanced charge and gradually straighten out the band structure (Fig. 2). The conduction properties of the material will thus improve beyond what can be explained as primary photo-current. We have therefore a reasoning which offers a possibility of explaining the secondary photo-current observed in many insulators.[2]

The writer is indebted to Dr. P. W. Anderson for some clarifying discussions on the subject.

[1] Rose, Weimer, and Forgue, Phys. Rev. **76**, 179 (1949).
[2] Gudden and Pohl, Zeits. f. Physik. **6**, 248 (1921). F. C. Nix, Rev. Mod. Phys. **4**, 742 (1932). N. F. Mott and R. W. Gurney, Electronic Properties in Ionic Crystals, p. 185.

Computed Binding Energies of Some Light Nuclei

J. SAMUEL SMART
Naval Ordnance Laboratory, White Oak, Silver Spring, Maryland
June 13, 1949

A QUANTITATIVE theory of the mass defects of light nuclei was first proposed by Wigner.[1] Shortly thereafter, Barkas[2] employed Wigner's theory to compute the atomic masses of about 150 nuclear species with A 50. His method was to determine certain functions empirically from experimental data on a few nuclei, and then to use these functions in computing masses for the remainder. In this way, good agreements with experimental values were obtained for both stable and unstable nuclei.

Since the publication of Barkas' paper, some of the accepted mass values used by him in evaluating the binding energy functions have changed considerably. In particular, the experimental masses of the sulfur isotopes have been revised downward about 1.3 mMU, due to the accurate measurements of Okuda and Ogata.[3] For this reason, it is of interest to redetermine the main binding energy function, Eo, using experimental values listed in Bethe's text.[4] The results are shown in Fig. 1. In order to depict more clearly the variations in binding energy with A, the quantity $-Eo-8A$ is plotted as ordinate. To avoid using any more empirical constants than necessary in determining Eo, only points obtained from the experimental mass values of the $A=4n$, (000), nuclei are plotted. For these nuclear species, the atomic mass may be written

$$M(\text{mMU})=1008.5A+\frac{125}{A}+Eo. \qquad (1)$$

The resulting curve indicates that closed shells occur at masses 20 and 32. The existence of a closed shell at Ne^{20} has been suggested by Wigner, Barkas, and others, but the evidence for S^{32} has apparently not been reported before. However, M. G. Mayer[5] has recently suggested that the experimental facts concerning shell structure in heavy nuclei can be explained better by jj-coupling than by Russell-Saunders coupling. If one assumes that the $2s$ level in nuclei lies below the $3d$, then the jj-coupling theory predicts closed shells for 10 and 16 neutrons and protons, or for Ne^{20}

TABLE I. Comparison of calculated and experimental mass values.

Nucleus	Experimental	Calculated (corr.)
O^{19}	19.0093	19.0102
O^{20}		20.0125
F^{22}		22.0103
Na^{26}		25.9998
Al^{30}		29.9903
P^{34}	33.9826	33.9829
Cl^{38}	37.979	37.9777

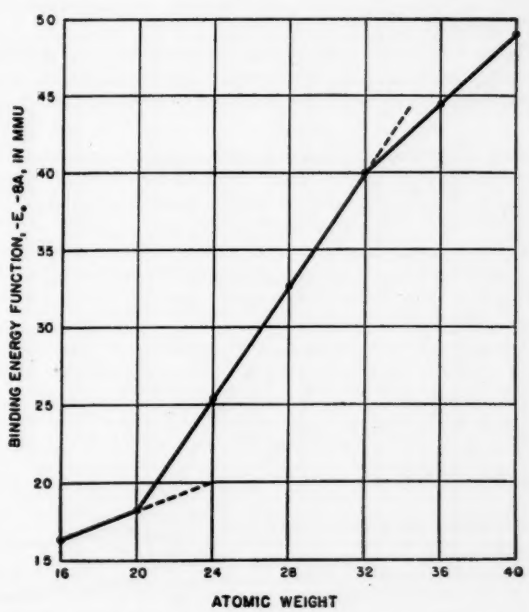

FIG. 1. The binding energy function, $-Eo-8A$, plotted as a function of A for the $n\alpha$-nuclei.

and S^{32}. We note that the average binding energy per particle for the three shells is, respectively, 8.3, 9.3, and 8.6 Mev.

In connection with the computed mass values of Barkas,[2] there are several misprints and errors which have apparently been propagated widely throughout the literature. The values for O^{19} and O^{20} seem to be in error, along with the entire group of $A=4n+2$, $T=2$ nuclei, for which the wrong symmetry character was used in making the calculations. In Table I, corrected values are reported for these nuclei and compared with probable experimental values taken from the table of isotopes prepared by Seaborg and Perlman.[6] The agreement is improved in every case. A more comprehensive study of the agreement of the Wigner theory with new experimental data of β-decay energies and Q-values will be presented by the author in the future.

[1] E. P. Wigner, Phys. Rev. **51**, 106, 947 (1937).
[2] W. H. Barkas, Phys. Rev. **55**, 691 (1939).
[3] T. Okuda and K. Ogata, Phys. Rev. **60**, 690 (1941).
[4] H. A. Bethe, *Elementary Nuclear Theory* (John Wiley & Sons, Inc., New York, 1947).
[5] M. G. Mayer, Phys. Rev. **76**, 185 (1949).
[6] G. T. Seaborg and I. Perlman, Rev. Mod. Phys. **20**, 585 (1948).

Angular Distribution of Annihilation Radiation

S. DeBenedetti, C. E. Cowan, and W. R. Konneker
Department of Physics, Washington University, St. Louis, Missouri*
June 15, 1949

While testing with annihilation radiation a circuit selecting the coincident pulses from two scintillation counters, it was realized that the angular correlation between the two annihilation photons could easily be measured with far greater accuracy than previously reported.[1] As a consequence, we performed several measurements on the angular distribution of the two photons, using sources of Cu^{64} surrounded by a gold absorber in which the positrons were stopped.

During the final measurements, whose results are reported in Fig. 1, the distance between the source and either detector was 120 cm. The source and detectors were aligned on the same horizontal line by means of a cathetometer, which was also used to measure the vertical displacements of one of the detectors. The detectors, seen from the source, subtended a vertical angle of 4×10^{-3} rad, while the source, seen from the detectors, covered an angle about ten times smaller.

The zero on the abscissas of Fig. 1. corresponds to the position where the source and the upper surfaces of the detectors were in the same horizontal line. The coincidence rate has a maximum for a negative abscissa, corresponding to the position where the line joining the centers of the detectors passes through the source. The fact that the counting rate does not vanish for positive displacements definitely indicates that the annihilation gamma-rays are not always emitted in exactly opposite directions.

If one approximates with an exponential the tail of the curve for positive abscissas, one obtains for the average value of the momentum of the center of mass of the annihilating pairs approximately 0.9×10^{-2} in units of mc. This is remarkably close to the value of 0.8×10^{-2} obtained by Dumond, Lind, and Watson,[2] from the shape of the annihilation line from a Cu absorber.

A more detailed description of the experiment and a more complete theoretical discussion is under preparation.

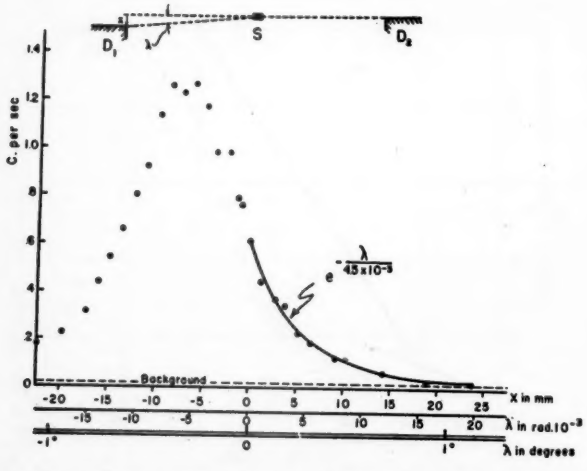

FIG. 1. Gamma-gamma-coincidences as a function of the position of one of the detectors.

* Assisted by the joint program of the ONR and the AEC.
[1] R. Beringer and C. G. Montgomery, Phys. Rev. **61**, 222 (1942).
[2] Dumond, Lind, and Watson, Phys. Rev. **75**, 1226 (1949).

Erratum: The Second Viscosity of Liquids

[Phys. Rev. **75**, 1415 (1949)]

L. N. Liebermann
University of California Marine Physical Laboratory, San Diego, California

THE values for n' given in column 5 of Table I are incorrect and should be deleted. It was intended that this column be derived by multiplication of columns 3 and 4 and the correct values are easily obtainable in this way.

Anomalous Adsorption of Helium at Liquid Helium Temperatures

Earl A. Long and Lothar Meyer
Institute for the Study of Metals, University of Chicago, Chicago, Illinois
June 9, 1949

During measurements on the distribution of He^3 between gas and adsorbed film for dilute mixtures of He^3 and He^4 adsorbed on jeweler's rouge (Fe_2O_3) in the He *II* region,[1] we encountered equilibrium pressures markedly different from those previously reported.[2] We, therefore, made preliminary measurements of the adsorption isotherms for He^4.

The adsorbent was 0.81 g of Fe_2O_3, of surface area 1.7 m^2, as determined from a Kr isotherm at 90.2°K.

The data are shown in Fig. 1, in which the volume adsorbed in S.T.P. cc is plotted against the ratio of the measured equilibrium pressure P to the saturation pressure P_0 of the bulk liquid He at the measuring temperature. The dotted curve is the isotherm at 2.45°K; the solid curve is for all measured temperatures below T_λ, namely, 2.11°, 1.78°, and 1.53°K.[3]

The data present several unusual features:

(1) The He *II* isotherms are identical, within our error of 2 percent between 1.53° and 2.11°K, and from 25 to 80 percent saturation. Consequently, the heat of vaporization of the adsorbed He in this region must equal that of the bulk liquid (see also Frederikse, reference 3). As the adsorbed He is in thermal equilibrium with vapor at $P<P_0$, this result requires that the entropy of the adsorbed layers be higher than that of liquid He, as predicted several years ago by Kramers.[4] The heat of adsorption would have to be changed by about twice our experimental error in order to account for the apparent entropy difference.

(2) Application of the simple BET theory[5] shows that the volume adsorbed in the first layer (v_m) is much larger than that calculated from surface areas and the liquid density, as already shown by Schaeffer *et al.*[6] from their data for carbon black at 4.2°K. We find for v_m about 0.9 cc/m², four times the value calculated from the liquid density, and corresponding to an atomic spacing in solid He under several hundred atmospheres pressure. The data of Schweers[7] at small P/P_0 also fit a BET plot, giving about the same v_m on glass and O_2 below 2.5°K, and yield also the value of Schaeffer *et al.* (v_m=0.57 cc/m²) at the b.p. It seems, therefore, certain that the first adsorbed layer on most surfaces is highly compressed.

Schweers' stated result, that the adsorption energy drops by *ca.* 50 cal./mole in building up the first four layers, must now be re-interpreted as representing the work of compression necessary to complete the mono-layer.[8]

(3) The He *II* isotherms show anomalously high adsorption, starting at $P/P_0\sim0.7$, and increasing enormously at high saturations. We reached the limiting value of 40 cc/m² with a distinctly lower equilibrium pressure than P_0. This value yields a minimum film thickness of ~160 atomic layers, on the reasonable assumption of liquid-type spacing (4A) for all but the first few layers.[9]

We consider this anomalous adsorption as due to the formation of the Rollin film. Previously widely differing results[10] on the film thickness are explainable because of the extreme sensitivity of the film thickness to percent saturation.

We observed some indication of slight hysteresis in desorption above P/P_0=0.9 below T_λ, whereas in all other parts of the isotherm the equilibrium pressures were identical in adsorption and desorption.

The isotherm at 2.45°K yields a v_m=0.9 cc/m², the same as below T_λ, but shows distinctly smaller adsorption above P/P_0 ~0.20, reaching saturation with ~30 layers adsorbed.

The two methods proposed by Harkins and Jura[11] for plotting adsorption data ($\log P/P_0$ *vs.* $1/v^2$, and the "film pressure" π *vs.* the area σ available per atom adsorbed) show a distinct break at $P/P_0\sim0.7$, in a manner which in their treatment would indicate a two-dimensional second-order transition. This, along with the disappearance of the effects above T_λ, suggests that the phenomenon is cooperative, and of the same character as the λ-point in bulk liquid He.

We plan to investigate in more detail the anomalous density of the first adsorbed layers, the "transition" at $P/P_0\sim0.7$ with the resulting high adsorption, and the entropy of the system as a function of the number of adsorbed layers.

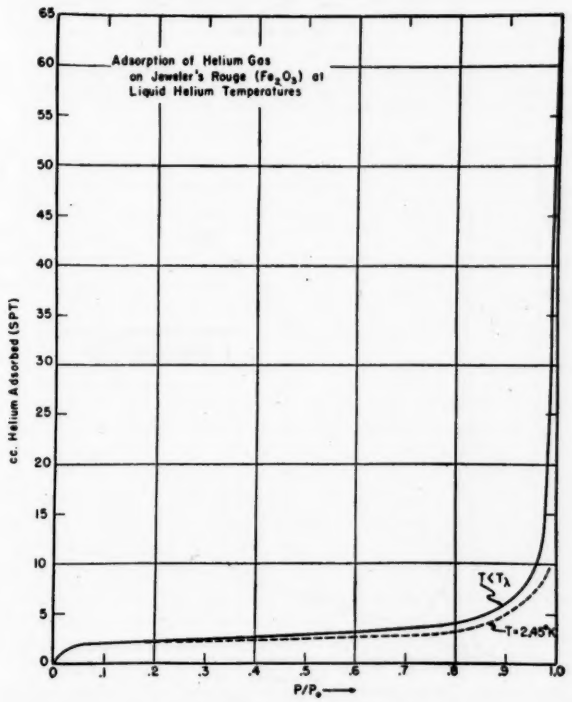

FIG. 1.

[1] Measurements made in collaboration with Professor A. O. C. Nier and Mr. B. B. McInteer, Department of Physics, University of Minnesota.
[2] J. Kistemaker, Leiden Comm. No. 271-b.
[3] The He *II* results are in good agreement with unpublished data of H. P. R. Frederikse, Leiden, who kindly sent us his data on the isotherms between 1.39° and 1.99°K, up to 85 percent saturation. We are indebted to him for these data, and for the manuscript of his communication to Physica on the specific heat of adsorbed He on Fe_2O_3, prior to publication.
[4] H. A. Kramers, personal communication to L. M.
[5] Brunauer, Emmett, and Teller, J. Am. Chem. Soc. **60**, 309 (1938).
[6] Schaeffer, Smith, and Wendell, J. Am. Chem. Soc. **71**, 863 (1949).
[7] J. Schweers, Thesis, Leiden, 1941.
[8] Suggested by W. Band.
[9] Kistemaker's statement that the number of adsorbed layers does not increase over ~30 layers, above $P/P_0\sim0.9$, is due to his method of evaluation, only valid below $P/P_0\sim0.8$, as it assumes the number of adsorbed layers to be equal in the two adsorption bulbs he compares. His original data show the effect we observed.
[10] See W. H. Keesom, *Helium*, Elsevier Publishing Company, Inc., New York, 1942) pp. 292–308.
[11] See Geo. Jura and W. D. Harkins, J. Am. Chem. Soc. **68**, 1941 (1946).

Anomalous Adsorption of Helium at Liquid Helium Temperatures

WILLIAM BAND
Institute for the Study of Metals, University of Chicago, Chicago, Illinois
June 13, 1949

THE results reported recently[1] under the above title by Earl A. Long and Lothar Meyer raise the following question: The "Brunauer-Emmett-Teller" theory[2] assumes that the saturation number of atoms in each monolayer is a constant and should be roughly equal to the number to be expected from the interatomic spacing in the liquid phase. However, by applying the B.E.T. isotherm to their observed adsorption for helium, Long and Meyer find that in the neighborhood of the lambda-temperature the saturation number in the first monolayer is about four times that expected from the liquid density. Schaeffer *et al.*[3] similarly found about twice the expected number at the boiling point temperature. Can these results be considered real, or are they simply an indication that the B.E.T. theory breaks down completely?

The density of liquid helium is unusually low at these temperatures because of the zero point energy, and it is, therefore, physically reasonable to suppose that the potential energy of adsorption can compress the first, and perhaps partly also the second monolayer to be adsorbed. Moreover the measurements by Frederikse[4] on the specific heat of an amount of adsorbed helium that corresponds to the first (compressed) monolayer, are actually consistent with that of a two-dimensional Debye solid with a characteristic temperature of about 18°K. It is, therefore, reasonable to consider the film at low pressures as immobilized, and to apply the following generalization of the B.E.T. theory: Let the number of sites available to the second monolayer be only some fraction α_1 of the number of atoms adsorbed in the first monolayer, the number of sites available to the third monolayer be another fraction α_2 of the number of atoms adsorbed in the second layer, and so on. This problem can be solved by the methods introduced by T. L. Hill.[5] In the simplest case where only one anomalous monolayer is present, i.e., $\alpha_1<1$, while α_2 etc. are all=1, the resulting adsorption isotherm is a simple generalization of the B.E.T. equation.

$$(V_1/V)\{x/(1-x)\}=\{x+\beta_1(1-x)^{\alpha_1}\}/\{1-x(1-\alpha_1)\}, \quad (1)$$

where $x=P/P_0$ is the ratio between the gas pressure and the saturated vapor pressure, V is the volume (at STP) of gas adsorbed, V_1 is the volume of gas that would just fill the first monolayer at its saturation density, $\alpha_1 V_1$ is the saturation volume for the second monolayer and must equal the value calculated from the normal liquid spacing, β_1 is the usual function of the heat of adsorption of the 1st monolayer ϵ_1 and the heat of evaporation $-\epsilon_L$,

$$\beta_1=\exp\{-(\epsilon_1-\epsilon_L)/kT\}.$$

If x is sufficiently small compared with unity (1) reduces to the following first approximation,

$$(V_1/V)\{x/(1-x)\}=\beta_1+x(1+\beta_1-2\alpha_1\beta_1). \qquad (2)$$

In practice β_1 is of the order 0.005, so that (2) is practically identical in form with the ordinary B.E.T. isotherm, but leaves V_1 free to be greater than the value given by the liquid density.

By admitting two anomalous monolayers, the isotherm becomes much more complicated, but it remains true that at small x it reduces practically to the same form (2). It may, therefore, be concluded that the anomalously high values of V_1 yielded by the ordinary B.E.T. plot are real, and indicate only that the B.E.T. theory requires generalization in the above manner.

The additional parameters present with two anomalous monolayers allow a much better fit between theory and observation in the case of the isotherms above the lambda-point, but do not reduce the discrepancy below T_λ, where the adsorption is already measurably greater than the maximum theoretical value at 20 percent saturation, or about four monolayers. A rough estimate of the order of magnitude of the cooperative energy ϵ_c required to account for this excess adsorption can be obtained as follows. If an attraction is included in the partition function of the assembly by means of a simple Boltzman factor for each monolayer, the adsorption isotherm is found to be the same as before, but on an x-scale reduced in the ratio $e^{\epsilon_c/kT}$. Such an isotherm would give formally an infinite adsorption at a pressure actually less than saturation, and if the cooperative energy is chosen about 0.07 cal. per mole it fits the data below T_λ at least as well as the corresponding isotherm (without the cooperative factor) fits the data above T_λ.

It is proposed to develop the above theory for isotopic mixtures, and details will be published later.

[1] E. A. Long and L. Meyer, Phys. Rev., preceding letter.
[2] S. Brunauer, *The Absorption of Gases and Vapors* (Princeton University Press, Princeton, New Jersey, 1943).
[3] Schaeffer, Smith, and Wendell, J. Am. Chem. Soc. **71**, 863 (1949).
[4] See footnote 3 in reference 1 above.
[5] T. L. Hill, J. Chem. Phys. **4**, 263 (1946); **4**, 268 (1946); **15**, 767 (1947).

Neutron Irradiated Semiconductors

W. E. JOHNSON* AND K. LARK-HOROVITZ**
Oak Ridge National Laboratory, Oak Ridge, Tennessee
June 13, 1949

GERMANIUM semiconductors after bombardment with deuterons or alpha-particles show[1] permanent changes in their electrical properties: the resistivity of P-type germanium decreases, indicating the production of acceptors[2] due to the bombardment, and N-type germanium becomes converted to P-type. The original state can be reproduced by heat treatment, indicating that the observed effects are not due to transmutations, but primarily due to lattice displacements, creating vacancies and interstitial atoms. If this explanation is correct, it is expected to find similar changes due to neutron bombardment.

Various samples of Ge semiconductors, with known impurity type and content[2] were exposed in the Oak Ridge reactor and the conductivity was measured during exposure as a function of irradiation: P-type samples show an increase in conductivity, as expected from the results of cyclotron irradiation (Fig. 1*a*).

N-type material shows a decrease in conductivity which reaches a minimum, and then increases steadily with continuing bombardment (Fig. 1*b*). Hall effect measurements[2] after bombardment indicate that the material has been converted to P-type. These experiments indicate also that neutron bombardment produces acceptors, creating additional holes; thus the conductivity of P-type material increases whereas the conductivity of N-type material first decreases, as electrons are removed from the conduction band, but increases again as hole conduction becomes prominent.

Exposure of germanium point contact rectifiers of the 1N34 and 1N38 type shows[3] that at 3 volt forward bias, where spreading resistance is primarily responsible for the resistance measured, the behavior is the same as the one observed for bulk resistivity

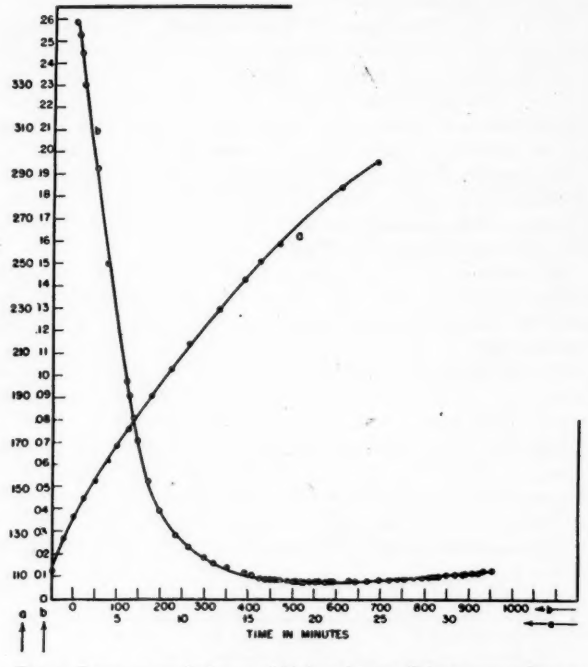

FIG. 1. Curve *a*: conductance of high resistance P-type germanium as a function of the time of irradiation. Curve *b*: conductance of N-type germanium as a function of time of irradiation.

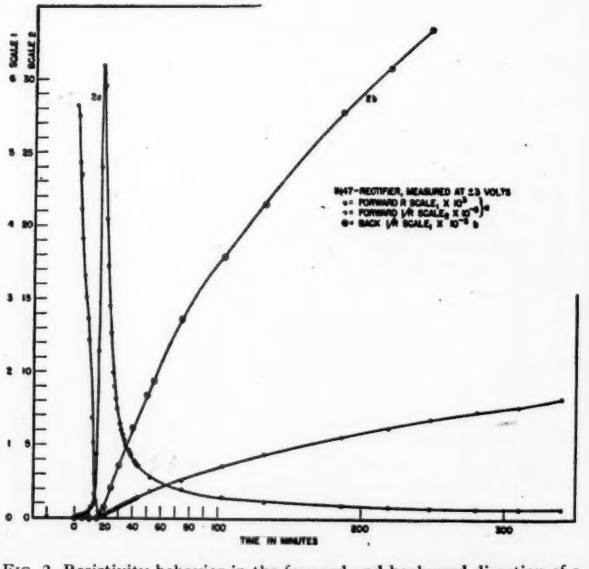

FIG. 2. Resistivity behavior in the forward and backward direction of a contact rectifier as a function of the time of irradiation.

(Fig. 2*a*). At forward bias of less than 0.18V and for bias in the back direction the resistance is determined primarily by the barrier resistance of the rectifier and since this barrier in an N-type rectifier is transparent for holes a decrease of resistance is expected and is actually observed (Fig. 2*b*).

The rectifier shows after prolonged irradiation ohmic behavior, but when reassembled with an aluminum point shows the behavior of a P-type rectifier.

When exposed in cadmium shields, the samples reach the point of minimum conductance at larger nvt values than in a graphite torpedo. Heat treatment reproduces the original behavior observed before neutron irradiation as in the case of deuteron and alpha-bombardment.

Silicon samples both N- and P-type show an increase in resistivity in a similar way, as has been observed with deuteron bombarded silicon samples. Heat treatment restores the original resistivity values; it also shows that deep lying traps of about 0.5 ev above the full band are produced, removing electrons and holes, thus producing poorly conducting material.

Preliminary experiments on Si-rectifiers (IN 21) Cu_2O semiconductors in bulk and rectifiers, Se bulk material and rectifiers, all show a behavior similar to the one observed for silicon samples discussed above.

* Now at Atomic Power Division, Westinghouse Electric Corporation.
** Purdue University; Consultant O.R.N.L.
[1] Lark-Horovitz, Bleuler, Davis, and Tendam, Phys. Rev. **73**, 1256 (1948).
[2] We are indebted to members of the Purdue Semiconductor Laboratory: V. Bottom, J. W. Cleland, R. E. Davis, and J. C. Thornhill, for the preparation of the samples and the Hall-effect measurements before and after irradiation.
[3] Davis, Johnson, Lark-Horovitz, and Siegel, Phys. Rev. **74**, 1255 (1948); AECD 2054 (1948).

Nuclear Magnetic Moments from Microwave Spectra: I^{127} and I^{129}

WALTER GORDY AND O. R. GILLIAM
Department of Physics, Duke University, Durham, North Carolina*
AND
RALPH LIVINGSTON
*Oak Ridge National Laboratory,** Oak Ridge, Tennessee*
June 14, 1949

THE effects of a magnetic field on the hyperfine structure of the $J=2\rightarrow3$ transition of CH_3I^{127} and CH_3I^{129} have been studied. The Zeeman components of several F transitions of these molecules were completely or partially resolved. Observations were made with a coiled wave guide cell in such a way that the magnetic field was parallel to the E vector of the radiation. This allowed detection of the p components, $\Delta M_F=0$ transitions, without complications from the s components, $\Delta M_F=\pm1$ transitions. The field strengths used in the study ranged from 1160 gauss to 3700 gauss.

The nuclear magnetic moment of I^{127} has already been determined by Pound,[1] using the nuclear resonance method, to a greater accuracy than can be reached by the present method. The remeasurement of this moment, however, helps to evaluate the accuracy obtainable with the microwave method. In Table I are listed the results obtained on different CH_3I^{127} transitions. The average value for $\mu(I^{127})$ from these data is 2.792, which, when corrected for diamagnetic effects[2] of the extranuclear electrons of the iodine, is 2.810. The mean deviation from this value is 0.062, or 2.2 percent. The value obtained by Pound is 2.8122 ± 0.003.

In Table I are also given results on two transitions of CH_3I^{129}, one of which is shown in Fig. 1. When diamagnetic corrections are made, our preliminary values*** for the I^{129} nuclear g-factor and magnetic moment are 0.783 and 2.74, respectively. We believe these to be accurate to about five percent. The major factor limiting the accuracy is the incomplete resolution of the transitions used. Small errors may also arise from the measurement of the strength of the magnetic field. The $3/2\rightarrow1/2$ transition, since it splits into a wide doublet, should be more favorable for these determinations. Unfortunately, this line, though detectable, was too weak to be measured when split by the magnetic field. We hope, with later improvements of the spectrometer, to measure the magnetic moment of I^{129} to an accuracy of one percent.

TABLE I. Nuclear magnetic moments as calculated from several observed Zeeman effects in the CH_3I spectrum, $J=2\rightarrow3$.

Isotope	K	F transition	H gauss	Separation Mc	μ[a] nuclear magnetons
	0	1/2→1/2	1160	4.07	2.878
	0	1/2→1/2	2320	7.70	2.723
	0	1/2→1/2	3010	10.17	2.773
I^{127}	1	1/2→1/2	3010	10.47	2.853
	1	1/2→1/2	3180	10.64	2.745
	0	3/2→3/2	2600	5.22[b]	2.743
	1	3/2→3/2	2600	5.19[b]	2.728
	0	5/2→5/2	3000	4.28[c]	2.89
				Average	2.792
I^{129}	1	9/2→9/2	3700	2.25[c]	2.78
	1	7/2→7/2	3700	2.64[c]	2.66
				Average	2.72

[a] These values are not corrected for diamagnetic effects.
[b] These separations represent the total spacing of the multiplet.
[c] These separations are for peaks containing unresolved components (see Fig. 1).

So far as we know, this is the first determination of an unknown nuclear magnetic moment with the microwave method.**** This method, though not so precise as the molecular beam method or the nuclear resonance method, is particularly well suited to the study of rare or radioactive nuclei. Less than 10^{-5} g of I^{129} was needed for each series of measurements. Previously, the Zeeman effect on the microwave spectrum of ammonia has been observed by Coles and Good[3] and by Jen.[4] The latter observer also studied the Zeeman effect in methyl chloride.[4]

The theory used for the Zeeman effect of the hyperfine structure is that developed for atomic spectra by Back and Goudsmit[5] and previously applied to molecular spectra by Jen.[4] In the present work, the effects caused by the molecular magnetic moment were considered to be negligible. The theory fits all observations satisfactorily except those for the $F=5/2\rightarrow7/2$ transitions of CH_3I^{127}. Here, an anomaly was detected which appears to result from a breaking down of the nuclear quadrupole coupling by the applied magnetic field.† This is being studied further.

The magnetic moment of I^{129} with the previously measured spin[6] of 7/2 allows an assignment of the state of the last proton in the I^{129} nucleus as $5g^-$, according to the Nordheim[7] scheme. The mag-

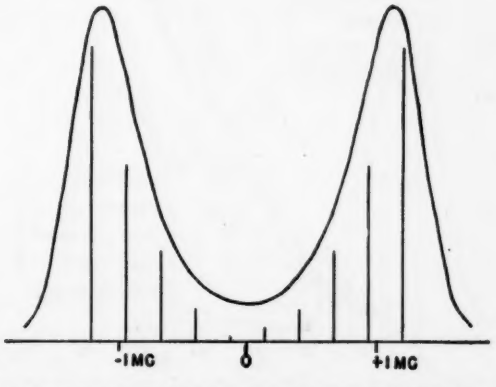

FIG. 1. Zeeman splitting of the hyperfine structure of the $J=2\rightarrow3$ transition of CH_3I^{129}. $F=9/2\rightarrow9/2$. $\Delta M_F=0$. Separation of the observed peaks is 2.25 mc/sec. $H=3700$ gauss. Bars represent calculated lines; curve represents the observed spectrum.

netic moment of 2.74 and the spin of 7/2, with the theory of Inglis,[8] indicate that the orbital and spin vectors of the odd proton in the nucleus are opposed, $I=l-\frac{1}{2}$. Thus, the nuclear orbital momentum, l, equals four.

We wish to acknowledge the help of Mr. George Parker and Mr. Gordon Hebert, of the Chemistry Division, Oak Ridge National Laboratory, who isolated the I^{129} from fission material.

* The work at this institution was supported by Contract No. W-19-122-ac-35 with the U. S. Air Forces, Cambridge Field Station.
** The work at Oak Ridge National Laboratory was performed under Contract No. W-7405, eng 26 for the Atomic Energy Project.
*** The sign of the magnetic moment is not obtained directly from the experiment because the Zeeman patterns are symmetrical. However, since the I^{129} nucleus has an odd number of protons and an even number of neutrons, a positive sign for μ is reasonable in view of the large spin value and the large magnitude of μ.
**** After this note was written, Dr. C. K. Jen informed us by private communication that he has measured the nuclear magnetic moment of S^{33} with the microwave method.
† This effect is analogous to the Paschen-Back effect in atomic fine structure and to the Back-Goudsmit effect in atomic hyperfine structure.

[1] R. V. Pound, Phys. Rev. **73**, 1112 (1948).
[2] W. E. Lamb, Jr., Phys. Rev. **60**, 817 (1941); J. B. M. Kellogg and S. Millman, Rev. Mod. Phys. **18**, 342 (1946).
[3] D. K. Coles and W. E. Good, Phys. Rev. **70**, 979 (1946).
[4] C. K. Jen, Phys. Rev. **74**, 1396 (1948).
[5] E. Back and S. A. Goudsmit, Zeits. f. Physik **47**, 174 (1928).
[6] Livingston, Gilliam, and Gordy, Phys. Rev. **76**, 149 (1949).
[7] L. W. Nordheim, Phys. Rev. **75**, 1297 (1949).
[8] D. R. Inglis, Phys. Rev. **53**, 470 (1938).

Latitude Dependence at 30,000 Feet of Penetrating Particles Slowed Down After Traversing 15 cm of Lead*

MARCELLO CONVERSI**
Institute for Nuclear Studies, University of Chicago, Chicago, Illinois
June 20, 1949

IN two recent B-29 expeditions from China Lake (California) to Lima, Peru, and to Fairbanks, Alaska, experiments have been carried out to investigate the composition of ionizing cosmic rays slowed down after traversing a certain thickness of lead. Mesons were separated from other ionizing particles with the counter arrangement sketched in the left side of Fig. 1. Counters A_1, A_2 (A_2 being two counters in parallel), and A_3 were in coincidence with counters B_1 plus B_2 (two in parallel), B_2 and B_2 plus B_3,

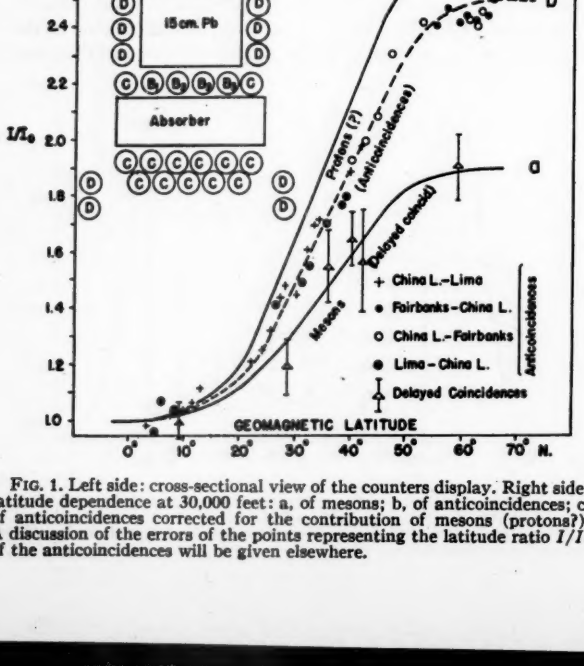

FIG. 1. Left side: cross-sectional view of the counters display. Right side: latitude dependence at 30,000 feet: a, of mesons; b, of anticoincidences; c, of anticoincidences corrected for the contribution of mesons (protons?). A discussion of the errors of the points representing the latitude ratio I/I_0 of the anticoincidences will be given elsewhere.

TABLE I. Results of measurements of delayed coincidences with graphite absorber at 30,000 feet at several latitudes. Mesons observed belong to the momentum range 315 to 348 Mev/C.

Average geomagnetic latitude (North)		9.0°N	28.5°	35.5°	40.0°	42.0°	59.0°
Duration of observation (minutes)	(Δt)	350	298	220	290	142	220
Delayed coincidences per hour due to mesons disintegrating in the time interval	1.14 to 3.94 μsec.	27.5 ±2.4	32.0 ±3.2	38.5 ±3.5	42.8 ±4.5	*	50.7 ±5.0
	2.12 to 4.92 μsec.	17.4 ±1.7	17.6 ±1.9	26.6 ±2.7	28.1 ±2.4	24.2 ±3.2	33.3 ±3.0
	3.10 to 5.90 μsec.	10.4 ±1.3	11.6 ±1.5	*	17.2 ±1.9	16.1 ±2.5	18.3 ±2.2
	4.08 to 6.88 μsec.	6.5 ±1.05	6.45 ±1.25	*	11.6 ±1.55	10.5 ±2.1	13.4 ±1.9
Extrapolated delayed coincid. per hour	(N)	46.5 ±2.7	53.5 ±4.4	72.0 ±6.0	76.9 ±4.5	73.2 ±8.6	89.1 ±5.2
Latitude ratio	(I/I_0)	1.00 ±0.06	1.14 ±0.095	1.55 ±0.13	1.65 ±0.095	1.57 ±0.185	1.91 ±0.11

* Not recorded.

respectively. All these double coincidences, added by means of a mixer, will be indicated as (AB). A 10-cm thick block of graphite surrounded by a group of counters, C, was placed below counters B and used as an absorber for the particles coming within the solid angle corresponding to the coincidences (AB). Counters C covered this solid angle. They were at the same time in "delayed coincidence" and in "anticoincidence" with respect to the coincidences (AB), while counters D were only used as additional anticoincidence counters. The delayed coincidences were registered by four "channels" of the same "time width" $\Delta\theta$ (2.8 μsec.), so that four points of the decay curve of mesons slowed down in the absorber were obtained simultaneously. The minimum delay for which a delayed coincidence was registered in the first channel was 1.14 μsec. The time distance between each channel and the next one was 0.98 μsec. For the apparatus employed, spurious delayed coincidences could practically occur only for random events in which an anticoincidence ($AB-C$) was followed after a short time by a single discharge (C) of counters C.*** Examples of decay curves obtained at altitude have been shown in a previous paper.[1]

By extrapolation of the decay curve to the zero time, one obtains the number, N, of mesons stopped per unit time in the absorber and which disintegrate between 0 and $\Delta\theta$ into electrons striking counters C. If p is the average value of the probability for the decay electrons of mesons, stopped in the absorber, to strike counters C, the number, M, of mesons stopped in the absorber after traversing the counter telescope is

$$M=N/p(1-\exp(-\Delta\theta/\tau)). \quad (1)$$

Events were registered as anticoincidences when no anticoincidence counter fired within 1.1 μsec. before or 7.8 μsec. after the arrival of a particle producing a coincidence (AB). Since the probability for an ordinary meson to disintegrate more than 7.8 μsec. after it has been stopped is less than 3 percent, the intensity, I_a, of the "true anticoincidences" (difference between the anticoincidences registered with and without absorber) is

$$I_a=(1-p)M+X, \quad (2)$$

where X represents the contribution due to particles which did not give rise, within 7.8 μsec. after they had been stopped in the absorber, to emission of secondary ionizing particles striking counters C.

In order to obtain the value of p, measurements with and without graphite absorber have been performed in Chicago, before and after the flights, with supplementary 5 cm and 20 cm of lead above counters A. From the results of these measurements the same value, 0.29 ± 0.015, is obtained in both cases for p, through Eqs. (1) and (2), if X is assumed to be negligible in these conditions.

The results concerning the latitude dependence of the delayed coincidences registered at 30,000 feet with absorber are summarized in Table I. The last line of the table contains the ratio ("latitude ratio," I/I_0) between the value of N obtained at each latitude and near the equator (9° North). Curve a in Fig. 1 represents these data. The results concerning the anticoincidences are graphically represented in the same way (namely, as latitude ratio I/I_0) by the points of curve b, curve c, which represents the latitude dependence of the X component, is obtained, through Eqs. (1) and (2), from the other two curves. If the X particles were protons, they should have a momentum of about 1 Bev/c to penetrate the 15 cm Pb interposed between counters A and B. A latitude ratio of 2.8 between the highest latitude and the equator for protons of such a momentum seems to be reasonable if compared with the latitude dependence recently observed for "stars"[2] and for small "bursts."[3] Further arguments which support the view that the X component is made up essentially of protons will be given in a future paper.

* Supported by the joint program of the ONR and the AEC.
** On leave from the University of Rome, Italy.
*** A small correction for the spurious delayed coincidences produced in the first channel by the spontaneous lags of counters C has been introduced on the basis of measurements taken in flight without absorber. A detailed account of all corrections introduced will be given in a complete report of this research.

[1] M. Conversi, Phys. Rev. **76**, 311 (1949).
[2] Lord, Schein, and Vidale, Phys. Rev. **76**, 171 (1949).
[3] J. A. Simpson, private communication.

Electron Gun Emission and X-Ray Output for Three Betatrons

W. F. Westendorp and F. R. Elder
General Electric Research Laboratory, Schenectady, New York
June 9, 1949

In a recent publication[1] a new theory was presented for the process of capture of electrons in the betatron. In an attempt to check this theory, measurements were made on three different betatrons of x-ray output *versus* electron emission from the gun. The results are interesting because of the great differences between curves plotted for different machines and because of the change of the shape of the curves with gun voltage. In one respect all the curves confirm qualitatively an important point of the theory namely for the greater portion of the curves the x-ray output varies as the gun electron emission current to a power larger than one.

All x-ray measurements were referred to Victoreen thimbles in one-eighth inch lead jackets and special checks were made on the location of the x-ray beam by means of films at different distances in order to exclude errors from stray electrons. The direct readings were taken on x-ray ionization chamber monitors calibrated with the Victoreen instrument.

In all three machines the magnetic field varies inversely proportional to the three-quarters power of the radius over most of the region between gun and target.

The curves shown at the left in Fig. 1 were taken on the 100-Mev betatron[2] which operates at 60 cycles per second and has a pumped vacuum tube. The orbit diameter is 66 inches, the free vacuum space is 3.4 inches high by 4.6 inches wide, corresponding respectively to relative apertures of 0.052 and 0.07. An improved electron gun with a barium aluminate cathode was used. During its long life of more than one thousand hours the x-ray output had dropped from 2300 roentgens per minute at 1 meter to the present figures principally on account of reduced spark over potential. The voltage pulse is a half-sine wave of 10 microsecond duration.

The curves in the middle of Fig. 1 were taken on the 50-Mev biased betatron[3] operating at 180 cycles per second with a sealed off vacuum tube. The orbit diameter is 23 inches, the free vacuum space is 1.63 in.×2.21 in. corresponding to relative apertures of 0.071 and 0.096 respectively. The gun has an improved focusing cup with a conventional coiled tungsten filament and a fourth electrode of adjustable potential which permits directional adjustment of the beam. The voltage pulse wave form is very nearly a half-sine wave of 5 microsecond base width.

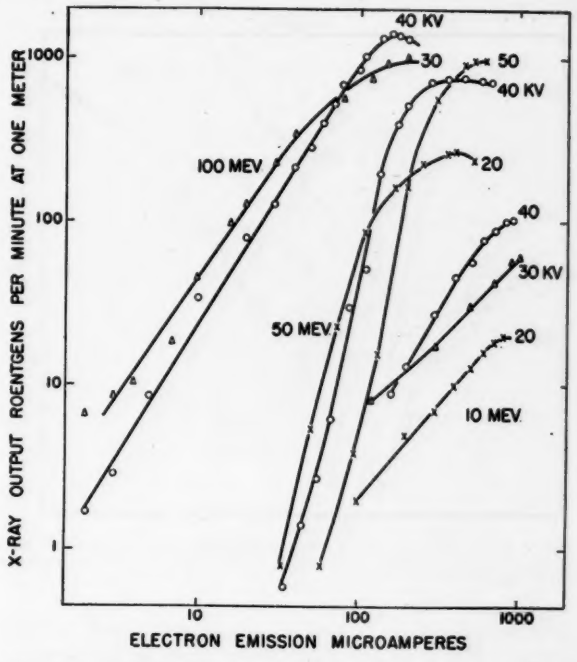

FIG. 1. Logarithmic plot of x-ray output *versus* electron gun emission for a 100-Mev, a 50-Mev and a 10-Mev betatron, at different gun voltages ranging from 20 to 50 kilovolts.

On the right in Fig. 1 are shown the data obtained with an industrial 10-Mev betatron operating at 1920 cycles per second. The orbit diameter is 10.5 in.; the free vacuum space is 1.7 in. ×2.33 in. with consequent relative apertures of 0.16 and 0.22. The tube is sealed off and has an electron gun like the one in the 50-Mev biased betatron. The gun voltage pulse has a waveform with a base of 6 microseconds and a flat top of 2 microseconds.

The steepest slopes of the curves as drawn are in descending order of gun voltage for the 100-Mev machine 1.6 and 1.45, for the 50-Mev machine 5.7, 5.0, and 4.3, and for the 10-Mev machine 1.7, 1.1, and 1.2. For all three machines the maximum x-ray output obtainable with excess emission available at a given gun voltage varies very nearly as the 1.25 power of the gun voltage.

[1] D. W. Kerst, Phys. Rev. **74**, 503 (1948).
[2] W. F. Westendorp and E. E. Charlton, J. App. Phys. **16**, 581 (1945).
[3] W. F. Westendorp, J. App. Phys. **16**, 657 (1945); Phys. Rev. **71**, 271 (1947).

The Superconducting Torus

R. L. Dolecek and Jules de Launay
Naval Research Laboratory, Washington, D. C.
June 10, 1949

A RECENT exact solution of the electrodynamic behavior of a superconducting torus by one of the authors,[1] presents the opportunity of discussing the effect of changes in torus dimensions on the hysteresis loop obtained by magnetic cycling.

Figure 1 is the hysteresis loop to be expected for a superconducting torus with s, the ratio of mean radius of toroidal ring to radius of toroidal wire, equal to four. Shoenberg[2] in studying the properties of a superconducting torus used a torus for which $s=4$. Within experimental error his results are in agreement with Fig. 1.

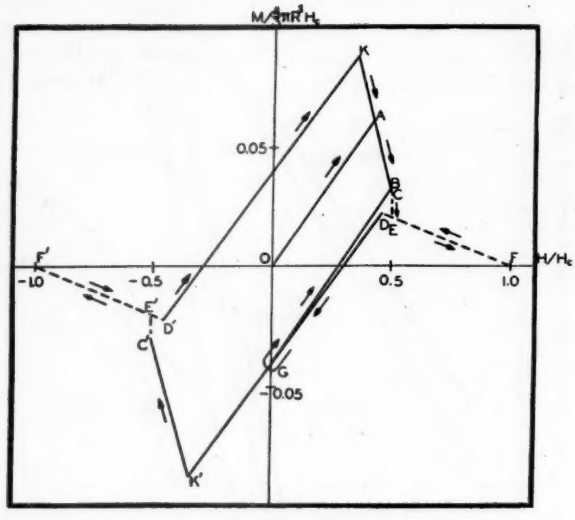

FIG. 1. Behavior of a torus ($s=4$) in a magnetic cycle. The symbols used are: M, magnetic moment; R, mean radius of ring; H_c, critical magnetic field; H, applied field.

Experiments with tori for which the geometrical factor s ranged in value from 6 to 33 have been conducted by McLennan *et al.*,[3] Schubnikow and Chotkewitsch,[4] and Grassmann and Eicke.[5] Their experimental data are in reasonable agreement with the theoretical formulas.[1] Thus it is felt that the interpretation of the hysteresis loop as outlined by Shoenberg[6] is essentially correct.

All investigations to date have been performed using tori for which s is relatively large. Of interest is the departures to be expected for the case of thick tori. Figure 2 is the hysteresis loop expected to be obtained upon the magnetic cycling of a superconducting torus for which $s=1.4$. Of immediate note are: (1) The increase in the value of H/H_c for the point C at which the torus, in increasing field, enters the intermediate state. The usually quoted value of $H/H_c=\frac{1}{2}$ for the point C is correct only for very large values of s. (2) The large increase in current change occurring (C to E) when the torus passes from the superconducting state to the intermediate state. (3) The large decrease in H/H_c (E to D) for which the torus again becomes superconducting in decreasing field.

These features suggest that tori having small values of s should be used when it is wished to study the intermediate state.

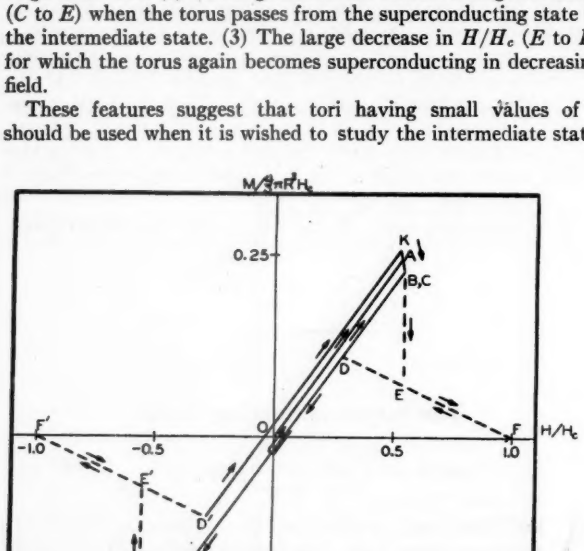

FIG. 2. Behavior of a torus ($s=1.4$) in a magnetic cycle. The symbols used have the same meaning as in Fig. 1.

On the other hand, tori of large s are more suitable for the determination of critical fields with minimum complication by the intermediate state. Along lines OA and KC, the material is completely superconducting[6] and since theoretically, the value of H/H_c at the point A is specified in terms of the geometry of the torus, a determination of the intersection point A would serve for the accurate determination of the critical field.

[1] J. de Launay, *Electrodynamics of a Superconducting Torus*, Naval Research Laboratory Technical Report No. P-3441, May 1949.
[2] D. Shoenberg, Proc. Roy. Soc. **155**, 712 (1936).
[3] McLennan, Allen, and Wilhelm, Phil. Mag. **14**, 168 (1932).
[4] L. W. Schubnikow and W. I. Chotkewitsch, Phys. Zeits. Sow. Union **10**, 231 (1936).
[5] P. Grassmann and H. Eicke, Phys. Zeits. **38**, 429 (1937).
[6] D. Shoenberg, *Superconductivity* (Cambridge University Press, London, 1938), Chapter IV.

An Observation of Non-Rayleigh Scattering of the Infra-Red Solar Spectrum by the Earth's Atmosphere

ARTHUR ADEL
Arizona State College, Flagstaff, Arizona
June 13, 1949

WHILE engaged in the measurement of 10-micron ozonosphere radiation at Holloman Air Force Base, Alamogordo, New Mexico, in the spring of 1948,[1] the author chanced to observe the intense, scattered infra-red solar spectrum coming from the sky in the neighborhood of the sun.

It appears worthwhile to call attention to these observations because the relative intensities depart strikingly from the Rayleigh distribution.

Figure 1 compares a series of five consecutive observations of the sky-scattered, rock salt prismatic solar spectrum ($S1$, $S2$, $S3$, $S4$, $S5$), from 1 to 4 microns, with the spectrum of direct sunlight (DO) over the same wave-length interval.[2] The direct and the scattered spectra alike were recorded with a Perkin-Elmer spectrometer set at slit width $\frac{1}{2}$ mm. Further, they constitute a related

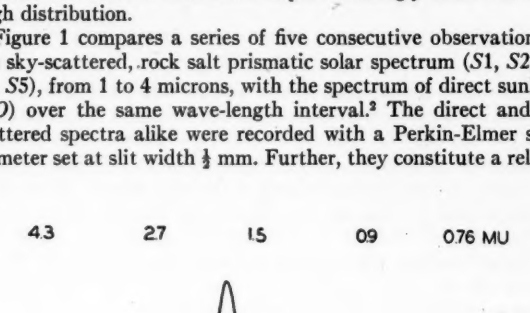

FIG. 1. Comparison of the near infra-red solar and sky spectra.

series. The direct solar spectrum was recorded at 1332 hours, M.S.T., April 12, 1948, following which the coelostat was halted and the solar image was allowed to drift off the slit. With the solar image safely out of the way, the sky-scatter series was begun, and the observations were made at the following times, M.S.T.:

*S*1–1347 hours
*S*2–1351
*S*3–1355
*S*4–1359
*S*5–1403

Thus, the portions of the sky observed were, respectively, 4, 5, 6, 7, and 8 degrees removed from the sun.

It will be clear from a cursory inspection of the comparison that the sky-scattered spectrum, although relatively poorer than the direct spectrum in the longer wave-lengths, is by no means as much poorer as might be expected. The comparison suggests the inverse first power for these particular observations rather than the inverse fourth.

[1] Arthur Adel, Phys. Rev. **75**, 133 (1949).
[2] The relative intensities of the direct solar radiation and the sky-scattered radiation are separated by a factor of many hundreds. We are concerned, however, with the relative intensities within the sky-scattered spectrum itself as compared with the relative intensities within the direct solar spectrum.

Large Cosmic Stars in Electron Sensitive Emulsions

E. Pickup and L. Voyvodic
Physics Division, National Research Council, Ottawa, Canada
June 10, 1949

IN examining some Ilford G5 emulsions, flown for 185 hours at an average height of 14,000 feet, examples of μ-meson decay were observed, showing that the emulsion was sensitive to minimum ionization. It is also apparent that many of the stars show tracks which could not have been detected with the C2 emulsion previously used.

It is the purpose of this note to discuss some interesting large stars we have found. One case is that of a 31-pronged star containing a downward cone of at least 4 light tracks.[1] A mosaic of photomicrographs of this event is shown in Fig. 1, which also includes mosaics of a μ-meson decay, a section of a star-producing meson, 2000 microns from the end of its range (energy about 9 Mev) which could only have been detected under good conditions in C2 emulsions.[2] This latter may be compared with the star fragments thus indicating the extra tracks visible in the new emulsion. There are 7 light tracks, including the cone, and at least 4 others, which may not have been recorded on C2 emulsions.

The downward cone[3] is extremely interesting. Two tracks leave the emulsion very soon as indicated on the mosaic, but two continue at a small angle (0.64°) without being scattered, until one emerges after 3000 microns, the other after 8000 microns. The ionization is sensibly the same along these tracks and is 25±2 grains/100 microns.

The grain density along random straight, thin tracks traversing this and other plates of the same batch varied between 21 and 25 grains/100 microns for different tracks. The correction for background grains for these minimum ionization tracks was 3 grains/100 microns. There appears to be no evidence for a systematic variation of grain density with depth in the emulsion.[4] In general, the characteristics of the Ilford G5 emulsions appear to be very similar to the Kodak NT4 as reported by the Bristol Group,[1] showing approximately the same grain density along the minimum ionization tracks and analogous grain density *versus* range curves for mesons. Thus the grain density of the long star tracks may be assumed to be very nearly minimum.

It seems unlikely that the particles can be electrons, and the only alternative would be protons or mesons. If they are protons

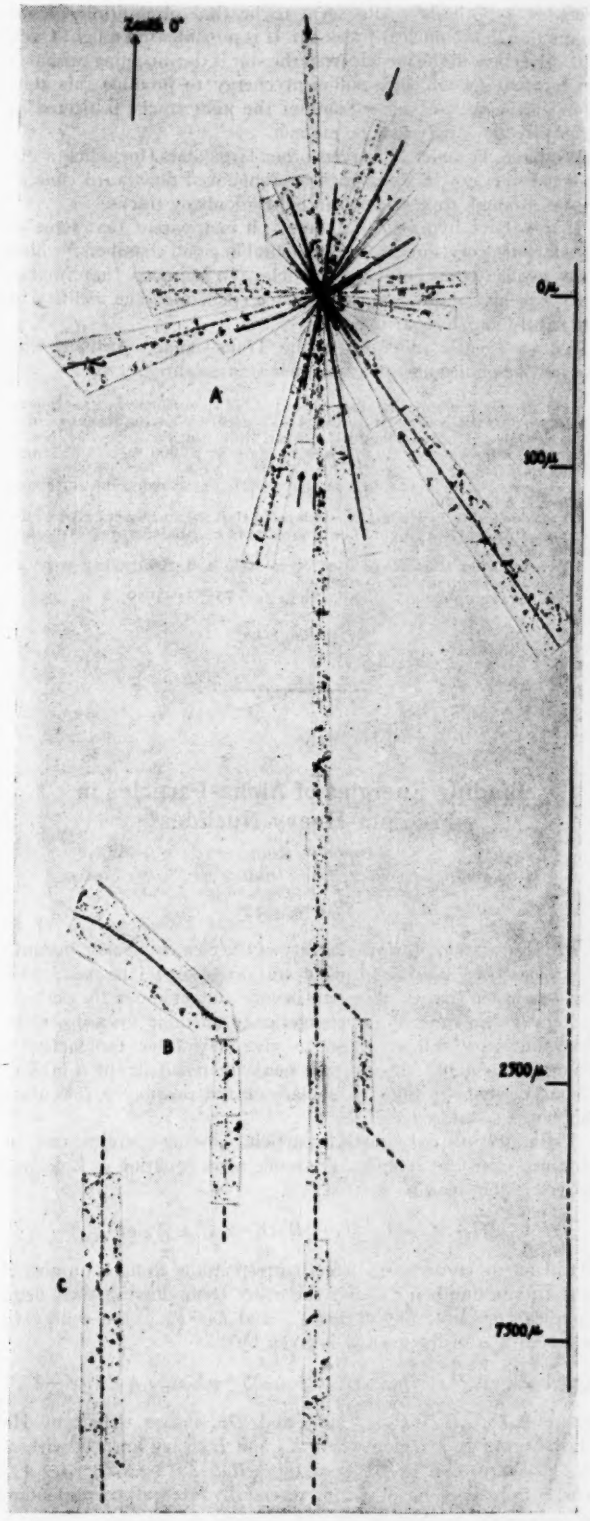

FIG. 1. Mosaics of photomicrographs showing events in Ilford G5 emulsions. A: 31-pronged star with downward cone of light tracks. Selected sections of two long tracks are shown, the tracks at 2500 microns being relatively, correctly spaced. Arrows indicate some other light tracks. B: μ-meson electron decay. C: section showing grain density of 9-Mev π-meson.

they would have to be extremely energetic and this again appears unlikely, although it cannot definitely be ruled out yet. The most probable hypothesis would seem to be that of multiple meson production in the nuclear break-up. It is possible that a light track almost vertical in the mosaic from the star is the incoming primary. An incident proton with sufficient energy to produce this star, would leave such a track. Some of the light tracks projected in other directions may also be mesons.

We have, however, observed other large stars, including a 30-pronged one, not showing such a pronounced downward cone as above although they do contain lightly ionizing tracks.

If the above hypothesis is correct, it is apparent that some of the stars are very similar to those found in cloud chambers,[5] which show associated penetrating particles. It is hoped that further work will give more definite evidence concerning the identity of the lightly ionizing particles.

We are greatly indebted to the Trans-Canada Airlines, who carried the emulsions for us on their transatlantic service.

[1] The presence of cones in stars in Kodak NT4 emulsions was mentioned recently by Brown *et al.*, Nature **163**, 47, 82 (1949). We have also just noted the results of J. Hornbostel and E. Salant, Bull. Am. Phys. Soc. **24**, No. 5, 25 (1949), who observe these cones in stars at 93,000 feet in Eastman NTB3 emulsions.

[2] All these events were found in the same batch of emulsions, although not in the same plate.

[3] The cone is downward on the assumption that the star was formed whilst the aircraft was in level flight. The approximate zenithal direction is marked on Fig. 1.

[4] The emulsion thicknesses used were 100μ and 200μ. They were all developed by the temperature method.

[5] See, for example, C. Y. Chao, Phys. Rev. **75**, 581 (1949).

Binding Energies of Alpha-Particles in Medium-Heavy Nuclides*

TRUMAN P. KOHMAN**
*Metallurgical Laboratory*** *and Institute for Nuclear Studies, The University of Chicago, Chicago, Illinois*
June 16, 1949

THE question of the α-stability of the elements below bismuth has been considered on several occasions in the past,[1] with the conclusion that the elements beyond the middle of the periodic system are on the average energetically unstable toward α-emission, but not sufficiently so to give detectable radioactivity. Fluctuations about this average behavior result in the α-lability of one or more isotopes of samarium and possibly a few other "missing" β-stable nuclides.[2]

Estimates of individual α-particle binding-energies can be obtained from the "empirical" atomic mass equation of Bohr and Wheeler.[3] This can be written:

$$M(A,Z)=A+D_A+\tfrac{1}{2}B_A(Z-Z_A)^2\pm\tfrac{1}{2}\delta_A \text{ or } 0,$$

D_A being the mean mass defect corresponding to mass number A and atomic number Z_A, and the other terms having their usual significance.[3] Assuming $B_A=B_{A-4}$ and $\delta_A=\delta_{A-4}$, the energy Q_α released by α-disintegration is given by:

$$Q_\alpha(A,Z)=\Delta_4D_A-D_{\mathrm{He}}-\tfrac{1}{2}B_A(2-\Delta_4Z_A)^2+B_A(2-\Delta_4Z_A)(Z-Z_A),$$

where $\Delta_4D_A=D_A-D_{A-4}$, etc., and D_{He}=mass defect of He^4 (3.61 Mev).[4] In a region where Z_A and D_A vary linearly with A, the last term can be replaced by $-B_A\Delta_1Z_A(2-\Delta_4Z_A)(A-A_Z)$, where A_Z is the value of A (not necessarily integral) corresponding to maximum β-stability for the element of atomic number Z. The approximately linear variation of α-disintegration energy with Z among isobars and with A among isotopes is responsible for many of the observed regularities among the known α-emitters,[5] and is illustrated in Fig. 1 by the plotted α-disintegration energies of Th and U.

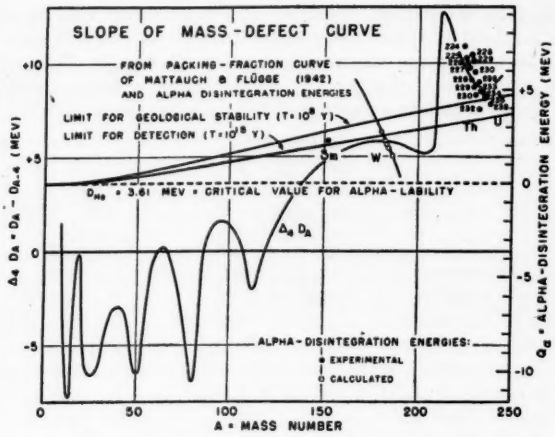

FIG. 1. Slope of the mass-defect curve. α-disintegration energies are plotted against the scale at the right.

The principal term determining the magnitude of Q_α is Δ_4D_A, a measure of the slope of the mass defect curve. Figure 1 gives a plot of Δ_4D_A *versus* A obtained from the packing-fraction curve of Mattauch and Flügge[6] up to mass number 206, at which point it is joined to a curve derived from an analysis of α-disintegration energies. The shape of the curve in the region $50\lesssim A\lesssim 200$ is poorly determined by the data; there is possibly a peak in the vicinity of $A=150$ which may account for the α-activity of samarium.

Evidently most nuclides above $A=140$ are energetically capable of emitting α-particles, and are only stabilized by the nuclear potential barrier resulting from the high charge. The effect of the barrier has been calculated using the simple one-body theory,[7] and is shown on the diagram by the two sloping lines. The lower indicates the α-disintegration energy corresponding to the maximum half-life which can be detected by present methods, $\sim 10^{18}$ years, and the upper corresponds to the minimum half-life for geological stability, $\sim 10^8$ years. Between these lie the primary natural α-emitters, U^{238}, U^{235}, Th^{232}, and Sm^{152}.

As a result of the last term in Q_α, sufficiently light isotopes of elements in the region from the rare earth elements to Pb should exhibit α-activity. Among the β-stable nuclides, this term can become largest for the even elements, and it has already been suggested[2] that some β-stable nuclides (in addition to Sm^{146}) may be missing in nature as a result of α-decay. Since the present experimental upper limits for α-activity for most β-stable nuclides correspond to lifetimes of only 10^{12} to 10^{14} years, it is possible that the lighter naturally occurring isotopes of some of the even elements in this region may possess detectable α-activity.[8]

Far to the neutron deficient side of the β-stability region α-activity should be an important mode of decay. As A becomes smaller for a given Z, the lifetimes against electron capture or positron emission will also decrease, but less rapidly, so β-decay will probably be the predominant mode except for large neutron deficiencies. By nuclear bombardments with very energetic photons[9] and ions,[10] which are known to result in the formation of highly neutron-deficient nuclides, it should be possible to observe artificial α-activity in medium-heavy elements.[11]

Calculated α-disintegration energies of the isotopes of W, as a typical element in this region, are shown in Fig. 1, the circles representing the β-stable isotopes and the line through them the locus of the β-labile ones. Such calculations are subject to large uncertainty, and are only meant to be suggestive. An analysis of presently available data pertaining to mass defects in this region is in progress in order to improve the basis for these calculations.

Conversely, measurements of α-disintegration energies below bismuth would improve our knowledge of the mass-defect curve.

Experiments along the lines suggested in this letter are being planned.

* Declassified by AEC as AECD-2060. Presented at the Madison, Wisconsin, meeting of the American Physical Society, June 21, 1948 (Phys. Rev. **74**, 1259 (1948)).

** Present address: Department of Chemistry, Carnegie Institute of Technology, Pittsburgh, Pennsylvania.

*** Part of this work was done in 1946 at the Metallurgical Laboratory, under the auspices of the Manhattan Engineer District, Contract No. W-7401-Eng-37.

[1] G. Gamow, Proc. Roy. Soc. London **A126**, 632 (1930), *Constitution of Atomic Nuclei and Radioactivity* (Oxford University Press, London, 1931), p. 15–21, Zeits. f. Physik **89**, 592 (1934), *Structure of Atomic Nuclei and Nuclear Transformations* (Oxford University Press, London, 1937), p. 7, 38–45, 48–52; W. Heisenberg, Zeits. f. Physik. **77**, 1 (1932); A. Landé, Phys. Rev. **43**, 620, 624 (1933); E. D. Eastman, Phys. Rev. **46**, 1, 238 (1934); H. A. Bethe and R. F. Bacher, Rev. Mod. Phys. **8**, 82 (1936), section 8, 30; C. F. v.Weizsäcker, *Die Atomkerne* (Akademische Verlagsgesellschaft, Leipzig, 1937), p. 34–35, 101–102; A. J. Dempster, Phys. Rev. **53**, 869 (1938); Hahn, Flügge, and Mattauch, Physik. Zeits. **41**, 1 (1940); E. Feenberg, Rev. Mod. Phys. **19**, 239 (1947).

[2] T. P. Kohman, Phys. Rev. **73**, 16 (1948).

[3] N. Bohr and J. A. Wheeler, Phys. Rev. **56**, 426 (1939).

[4] An alternate expression is given by Feenberg (reference 1, Eq. (65)).

[5] For example, K. Fajans, *Radioelements and Isotopes* (McGraw-Hill Book Company, Inc., New York, 1931), Chapter I; Perlman, Ghiorso, and Seaborg, Phys. Rev. **74**, 1730 (1948).

[6] J. Mattauch and S. Flügge, *Nuclear Physics Tables* (Verlag Julius Springer, Berlin, 1942; Interscience Publishers, Inc., New York, 1946), plate 1.

[7] R. W. Gurney and E. U. Condon, Nature **122**, 439 (1928); G. Gamow, Zeits. f. Physik **51**, 204 (1928). For computation, the formulation of H. A. Bethe, Rev. Mod. Phys. **9**, 69 (1937), section 66, was used.

[8] According to the present considerations, Gd^{152} should not have the special α-lability suggested for it by Feenberg (reference 1). K. K. Keller and K. B. Mather (Phys. Rev. **74**, 624 (1948)) were unable to detect α-activity in natural gadolinium. Ti^{44} and Zr^{88}, in which N. E. Ballou (Phys. Rev. **75**, 1105 (1949)) unsuccessfully sought α-activity, would be expected to be stable against α-decay.

[9] G. C. Baldwin and G. S. Klaiber, Phys. Rev. **70**, 259 (1946).

[10] Seaborg, Cunningham, Hopkins, Lindner, Miller, O'Connor, Perlman, and Thompson, Phys. Rev. **72**, 739, 740 (1947); D. H. Templeton, U. S. AEC Doc. 1525 (1947).

[11] Templeton (reference 10) observed short α-periods in light isotopes of Bi and Po and inferred that "the very light isotopes of the lighter elements" might also be α-active.

The τ-Meson

NORBERT WAGNER AND D. COOPER
Department of Physics, University of Maryland, College Park, Maryland

June 13, 1949

THREE particles of mass about 725 electron masses have been found in an Ilford C2 emulsion exposed to cosmic radiation at high altitude. Mesons of masses in this range have been reported,[1] but the number observed has been small and the mass determinations inadequate to definitely establish the existence of the particle. In the present experiment, high mass resolution has been achieved by minimizing the fading of the latent image and confining the observations to a single plate.

Ilford C2 plates, wrapped in a paper heat insulating envelope, were exposed to cosmic radiation for 6 hours at 90,000 to 100,000 ft. The temperature variation near the envelope during the flight was about 10°C. The plates were developed using a two bath process similar to that described by Blau and DeFelice.[2] Fifty-six mesons of residual range greater than 200 microns, including two $\pi-\mu$-decays, have been found in the single plate that has been analyzed.

One of the 725 m_e particles originated in a very high energy nuclear disintegration (Fig. 1, point *A*). Eighteen tracks emerge from this disintegration near the center of the 200-micron emulsion, but only the track τ and a 23-micron track of a particle heavier than an alpha-particle end in the emulsion. The characteristics of the track τ indicate that the particle reached the end of its range and was captured at *B*. Grain counting established that the short-range particle from *B* was at least as heavy as a proton, and the other product, although it passed out of the emulsion, was heavier than the meson. No nuclear events were associated with the other two 725-m_e particles, although both appeared to have reached the end of their range.

FIG. 1. τ-particle track of length 700 microns originating in disintegration *A* and initiating the secondary event at *B*.

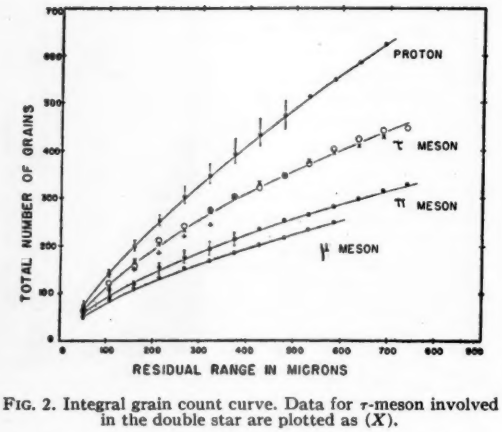

FIG. 2. Integral grain count curve. Data for τ-meson involved in the double star are plotted as (X).

Grain counting[3] was used to determine the mass of the τ-particles. The plot of Fig. 2 shows the integral grain count in 50-micron intervals from the end of the track *versus* residual range. The error lines on the points give the maximum range of the individual observations on at least five tracks, not the probable error. Taking the mass of the π-meson to be 286 m_e, the mass of the τ-meson was determined from the data of Fig. 2 to be 725 ± 40 m_e (Computations on the same basis: 1880 ± 90 m_e for the proton and 205 ± 50 m_e for the μ-meson.) Scattering measurements gave 1500 ± 1000 m_e for the mass of the τ-meson. The scattering measurements are not considered to be reliable, since the measurements on protons, π-mesons, and μ-mesons gave inconsistent results.

These results indicate that the τ-meson carries a single positive or negative charge. They give no indication of more than one particle of mass between that of the π-meson and the proton. It is suggested that the rarity and instability of the τ-meson may not be as great as previously indicated.

[1] C. R. LePrince-Ringuet, Rev. Mod. Phys. **21**, 42 (1949); A. I. Alichanian and A. I. Alichanow, Nature **163**, 761 (1949); Brown, Camerini, Fowler, Muirhead, and Powell, Nature **163**, 82 (1949); J. G. Retallack, and R. B. Brode, Phys. Rev. **75**, 1716 (1949); H. Yagoda, private communication.
[2] M. Blau and C. DeFelice, Phys. Rev. **74**, 1198 (1948).
[3] J. H. Webb, Phys. Rev. **74**, 511 (1948).

Proceedings of the American Physical Society

Minutes of the Semi-Centennial Meeting at Cambridge, June 16–18, 1949

THE 293rd meeting of the American Physical Society was held on Thursday, Friday, and Saturday, June 16, 17, and 18, 1949, in the buildings of Harvard University and the Massachusetts Institute of Technology in Cambridge, Massachusetts. This was designated as the Semi-Centennial Meeting of the Society, and comprised ceremonial features and speeches in commemoration of the foundation of the Society and the first fifty years of its history. The Society was organized on May 20, 1899 by a group of some forty physicists; six of them—Wilder L. Bancroft, Bergen Davis, Frederick L. Bedell, Marcia A. Keith, Isabelle Stone, and F. A. Waterman—are living, but unfortunately none of these was able to be present at this celebration. (Of those who are known to have been present at the first "regular" meeting of the Society —that of October 28, 1899—G. B. Pegram and L. P. Wheeler attended this meeting, and quite probably others were there.) Five hundred and ninety-three people registered, making this by far our largest summer meeting except for that of June 1946 when a great deal of work in nuclear physics emerged from classification. The Local Committee, headed by Otto Oldenberg and comprising Norman Ramsey, Roger Hickman, John C. Slater, A. E. Benfield, and many who helped them, handled its difficult work admirably well. The weather was warm and humid but might have been worse.

The Ceremonial Session was held on Thursday afternoon in Sanders Theatre. Together with the Past Presidents and present officers of the Society, and with some of the elder members of the Society and with the Local Committee, the delegates of eight scientific societies sat on the stage: in their conspicuous position they were severely tried by the sultry heat, for which ordeal the apologies of the Society are due and herewith tendered. President Loomis opened the session with felicitous words, and called then upon the eight delegates to present the messages of their Societies: the American Philosophical Society (A. B. Hastings), the National Academy of Sciences (F. O. Schmitt), the Physical Society, London (W. B. Mann), the Netherlands Physical Society (J. de Boer), the Japanese Physical Society (H. Yukawa), the American Mathematical Society (Hassler Whitney), the American Chemical Society (G. B. Kistiakowsky), the American Institute of Physics and its Founder Societies (G. R. Harrison). The President then read the messages of the following Societies: the Physical Societies of Denmark, Finland, France, Sweden, and Switzerland; the American Institute of Electrical Engineers, the American Society of Civil Engineers, the American Society of Mechanical Engineers, the Institute of the Aeronautical Sciences, the Institute of Radio Engineers, Sigma Pi Sigma; and personal messages from Niels Bohr and Max von Laue. Messages from the five German physical societies and from the American Institute of Mining and Metallurgical Engineers arrived too late for reading, but will be preserved in the archives of the Society. After these greetings were communicated to the audience, G. B. Pegram spoke on the early years of the Society, G. F. Hull, Sr., on some of its early meetings, and K. K. Darrow on the recent years of the Society.

On Friday morning in Sanders Theatre was held a General Session comprising addresses by E. U. Condon on the development of American physics, by C. G. Suits on physics in industry, and by President F. W. Loomis on the future of physics.

On Friday afternoon in Sanders Theatre the Chairmen of our four Divisions spoke on their respective fields. These Chairmen are Louis Malter (Division of Electron Physics), J. W. Liska (Division of High-Polymer Physics), William Shockley (Division of Solid-State Physics), and H. L. Dryden (Division of Fluid Dynamics). They were followed by J. S. Foster who reviewed the story of physics in Canada.

Invited papers on the general programme were given by Howard Aiken, E. O. Hulburt, R. A. Millikan, Julian Schwinger, M. S. Vallarta, and E. Bright Wilson, Vallarta speaking as representative of Mexico. A Symposium on linear accelerators consisted of three papers by Wolfgang Panofsky, R. F. Post, and J. C. Slater. A Symposium was held throughout Saturday by our Division of Electron Physics. The titles of all of these papers are given hereinafter.

The banquet of the Society was held on the Friday evening in the Ballroom of the Continental Hotel. With President Loomis twelve Past Presidents of the American Physical Society sat at the Speakers' Table: they were Henry Crew (President in 1909 and 1910), R. A. Millikan (1916 and 1917), K. T. Compton (1927 and 1928), W. F. G. Swann (1931 and 1932), P. D. Foote (1933), H. M. Randall (1937), John Zeleny (1940), G. B. Pegram (1941), P. W. Bridgman (1942), A. W. Hull (1943), Harvey Fletcher (1945), and E. U. Condon (1946). All spoke, too briefly. No such gathering of notable

physicists at one table has been seen in our time, perhaps no other will be seen before our Centennial. Especial gratitude is due to Henry Crew, who at the age of ninety made the long journey from Evanston to take part in this meeting, and evoked before the audience his memories of Helmholtz and Kirchhoff, Brace and Rowland from 1883. It is no pleasure to record that fewer than two hundred attended this unique banquet. In general, too few by far of our members feel the obligation to be present at what, in these days of simultaneous sessions, is normally the only function of our meetings at which all can be together.

The Society has lost through death, according to reports reaching this office, A. E. Bowen (Red Bank, New Jersey), J. P. Cooley (Palisades, New York), P. F. Hammond (University of Wyoming), W. W. Hansen (F, Stanford University), J. K. L. MacDonald (Inyokern), and J. A. Vargus (Inyokern), the last two having died in an airplane crash while on their way to our Berkeley meeting.

The Council met on Thursday morning.

Elected to Fellowship: Ernst Billig, W. L. Bond, J. R. Haynes, E. A. Hiedemann, A. V. Hollenberg, Vivian A. Johnson, Thomas Lauritsen, M. B. Sampson, L. R. Walker, R. G. Wilkinson, and Chien-Shiung Wu.

Elected to Membership: Elihu Abrahams, Bruce L. Adams, Harold R. Allan, Casper J. Aronson, Raphael F. Aronson, Benjamin L. Averbach, William W. Balwanz, Murray L. Barasch, Peter T. Barrett, Joe R. Beeler Jr., John Tyers Beher, Pasquale Bencivenga, Leon Bess, George H. Best, Egil K. Bjornerud, Richard C. Bradley, Ernest C. Briggs, Jr., Arthur S. Brill, Nicholas E. Broderick, Paul Brodt, Daniel P. Brooks, Robert J. Brousseau, Albert Brown, André Bruaux, John H. Bryant, David S. Bunbury, Charles Patrick Cadenhead, Edward W. Cannon, Richard R. Carlson, Edward F. Carr, William W. Carter, William R. Champion, Edwin J. Chernosky, Henry Chessin, H. N. Clarkson, Clarence M. Connelly, William A. Conrad, James E. Corry, Jr., Christopher Dean, Hervasio G. De Carvalho, Joseph J. Devaney, S. S. Dharmatti, Vernon H. Dibeler, Margarete Ehrlich, Richard W. Fink, Charles B. Fisk, Siegfried W. Fluegge, Stephen G. Gasiorowicz, R. E. Gibson, William S. Gilbert, Paul W. Gilles, John P. Gould, Howard Greenberg, Alan Adams Grometstein, Manfred Grunberg, Robert N. H. Haslam, Edward D. Havens, Jr., Charles H. Heuer, Richard J. Hirsch, Sidney Hoffman, Norman H. Horowitz, Howard S. Jarrett, Betsy M. Jones, Byron E. Keene, *William D. Kennedy, Geoffrey Knight, Jr., Jonathan H. Knox, Eli Kogos, John Kostolos, Jr., Walter H. Kruschwitz, James E. Kupperian, Jr., Dieter Kurath, Benjamin Lax, Daniel Leenov, Wayne Lowry Lees, Rannzo Leo, Stanley L. Leonard, John C. Lindsay, Ralph Livingston, Hans Walter Loeb, Harvey I. Lundy, Geraldean L. Lynn, Esteban F. R. Manfredi, Marvin Masel, Edward A. Mason, Frank D. Mason, Kurt L. Mayer, Benjamin T. McClure, Dale J. Meier, C. Howard Mellor, Harold W. Miller, Henry Thomas Minden, George R. Mitchell, George Davies Monk, C. Frank Mooney, Walter J. Moore, Cecile Morette, F. Hayder Morgan, Russell H. Morgan, Peter A. Morris, Mark P. Morse, Jr., Philip M. Mostov, Raymond J. Munick, Charles A. Murison, William Frederick Nash, John H. Neiler, Roger Newman, Richard Edwin Norberg, Carlos Obregon, Jack E. Oliver, Akshayabat Pande, Kenneth John Parry, Maynard D. Pearson, Robert H. Penfield, Sam R. Peoples, Earl M. Pollock, Charles E. Porter, Jr., Dwight C. Pound, Jerome Pressman, Wolfgang Ramm, Robert B. Raphael, Haskell A. Reich, Howard M. Robbins, Donald Murray Roberts, Fred W. Roberts, Robert C. Rohr, David Rosenfeld, Norbert Rosenzweig, Bernd Ross, Steven W. Ross, Wallace R. Rushin, Irving Sacks, Paul G. Saper, Matrala L. N. Sastri, William F. Schreiber, James F. Sears, Howard H. Seliger, David Shansky, Elmer M. Sharp, Joseph Silverman, Robert L. Small, Albert E. Smith, Joseph Sperrazza, Gordon L. Squires, Philip L. Stocklin, Ralph E. Sturm, John G. Teasdale, Walter F. Titus, Albert B. Tonik, Otto C. Turchan, Edwin M. Vahghn, Charles E. Van Albert, William M. Visscher, Garvin L. Von Eschen, Arthur A. Vuylsteke, Sidney Walovnick, William E. Water, Jr., Otto A. Weinreich, Eric A. Weiss, Wilfrid B. Whalley, Herman H. Wieder, Robert Lee Wild, Robert R. Williamson, Harvey Winston, Robert J. Wohl, Hiroshi Yamauchi, Paul M. Yavorsky, Myron Youdin Arnold Zellner, and Elmer L. Zimmerman.

* This man appeared on the Washington Agenda, but his second sponsor was not a member and he was not elected.

The Tellers have reported that the two Amendments to the Constitution of the American Physical Society submitted to the membership last February were carried by large majorities. Their texts will appear in a later issue of the Bulletin.

KARL K. DARROW, *Secretary*
American Physical Society,
Columbia University,
New York 27, New York

Ceremonial Session

Opening words by F. W. LOOMIS, *University of Illinois.*

Messages of greeting and felicitation from foreign and American scientific societies (listed elsewhere in these Minutes).

The early years of the American Physical Society. G. B. PEGRAM, *Columbia University.*

Early meetings of the American Physical Society. G. F. HULL, SR., *Dartmouth College.*

The recent years of the American Physical Society. K. K. DARROW, *Bell Telephone Laboratories.*

General Session

The development of American physics. E. U. CONDON, *National Bureau of Standards.*

Physics in industry. C. G. SUITS, *General Electric Company.*

The future of physics. F. W. LOOMIS, *University of Illinois.*

Speeches by the Chairmen of the Four Divisions

LOUIS MALTER, *RCA Laboratories* (Division of Electron Physics).

J. W. LISKA, *Firestone Tire and Rubber Company* (Division of High-Polymer Physics).

WILLIAM SHOCKLEY, *Bell Telephone Laboratories* (Division of Solid-State Physics).

H. L. DRYDEN, *National Advisory Committee for Aeronautics* (Division of Fluid Dynamics).

Symposium on Linear Accelerators

WOLFGANG PANOFSKY, *University of California, Berkeley.*
R. F. POST, *Stanford University.*
J. C. SLATER, *Massachusetts Institute of Technology.*

Other Invited Papers

The uses of computing machines. HOWARD AIKEN, *Harvard University.*

The light of the night sky. E. O. HULBURT, *Naval Research Laboratory.*

Recollections of the American Physical Society. R. A. MILLIKAN, *California Institute of Technology.*

Quantum electrodynamics. JULIAN SCHWINGER, *Harvard University.*

The sun and cosmic rays. M. S. VALLARTA, *University of Mexico.*

Molecular spectroscopy and molecular structure. E. BRIGHT WILSON, *Harvard University.*

Symposium of the Division of Electron Physics

Studies of electrons in gases by high frequency techniques. SANBORN C. BROWN, *M.I.T.*

Ionospheric measurements employing a voltage-scanning probe. W. G. DOW, *University of Michigan.*

The Townsend discharge on a micro-second time-scale. J. A. HORNBECK, *Bell Telephone Laboratories.*

Space-charge effects in electron beams and their reduction by positive-ion trapping. E. G. LINDER AND K. G. HERNQVIST, *R.C.A.*

Recent experimental results and theoretical interpretations on ionic phosphors. F. E. WILLIAMS, *General Electric.*

Studies of thermionic emission, photoelectric emission and conductivity of oxide-coated cathodes. W. B. NOTTINGHAM, *M.I.T.*

Photoelectric studies on the energy structure of barium oxide. L. APKER, E. TAFT, AND J. DICKEY, *General Electric.*

Deflection defocusing in cathode-ray tubes and methods for correction. R. G. E. HUTTER, L. H. MCKEE, AND S. W. HARRISON, *Sylvania.*

Beta-Ray Emitters; Nuclear Apparatus

A1. Radioactive Materials as X-Ray Sources. H. F. GUNLOCK, *Ohio State University.*—X-rays resulting from orbital capture or from internal conversion identify, by their wave-length, the radioactive element emitting them and the particular electronic levels involved. Various means for determining the wave-length are discussed and their use is illustrated in the study of the decay schemes of Pd^{103} and the Rh^{103} isomer. Examples of the use of x-ray emitting material as a source in radiography are given.

A2. The Effect of C^{14}, Ca^{45}, P^{32}, I^{131}, and Zn^{65} on Photographic Emulsions.* DANIEL STEINBERG** AND A. K. SOLOMON, *Harvard Medical School.*—The density response of photographic emulsions to five biologically important radioisotopes has been determined (C^{14}, Ca^{45}, P^{32}, I^{131}, and Zn^{65}). A set of eight sources of graded intensity was prepared for each isotope, and commercially available films (Eastman No-screen x-ray film, Type M stripping film, Type K industrial x-ray film, and NTB stripping film) were exposed for measured intervals to the eight sources. Exposure-density curves are presented, exposure being expressed in terms of total atomic disintegrations per square centimeter of film during the period of film source contact. Sensitivity and contrast are presented for each emulsion isotope combination in the form of characteristic curves. Photographic effectiveness is observed to decrease with increasing maximum energy of the radiation of the isotope. However, no simple quantitative correlation is observed between sensitivity and E_{max}. The reciprocity law has been checked in the case of Zn^{65} for exposures varying from 1 to 200 hours and found valid (Type M stripping film).

$\log_{10}$ exposure at density 0.1 above background.

Film	C^{14}	Ca^{45}	I^{131}	P^{32}	Zn^{65}
Eastman No-screen x-ray	6.16	6.42	6.70	7.11	7.96
Eastman Type M stripping	7.39	7.84	8.35	8.75	9.47

* This work has been supported in part by the ONR and the AEC.
** Postdoctorate Fellow, National Institute of Health.

A3. On the Excited States of Li^7.* MICHEL TER-POGOSSIAN, J. EUGENE ROBINSON, AND HAROLD GODDARD, *Washington University.* (Introduced by A. L. Hughes.)—In a recent unpublished note, H. Primakoff and E. Feenberg suggested the possibility of the existence of two closely spaced excited states in Li^7. This hypothesis appears necessary because of the selection rules in the Be^7 decay and the $B^{10}(n, \alpha)Li^{7*}$ reaction. The first step made to test this hypothesis was to compare the energies of the γ-radiations emitted in the transitions $Li^{7*} \rightarrow Li^7$ for different methods of producing Li^{7*}. The energy of the γ-radiation emitted after the K capture in Be^7 was carefully compared, in a high resolution beta-ray spectrometer, with the energy of the γ-radiation emitted by Au-198 (energy accurately measured by DuMond and his group). This comparison gave the energy of 478.6 ± 0.5 kev. This value is very close to the energy obtained by Elliott and Bell (478.5 ± 1.5 kev) for the gamma-radiation following the (n, α) reaction on B-10, using the same Au comparison line. If these two excited states of Li^7 are different they are not separated by more than 2 kev.

* This work was assisted by the joint program of the ONR and AEC.

A4. K Capture of Be^7 and the Excited State of Li^7.* R. M. WILLIAMSON AND H. T. RICHARDS, *University of Wisconsin.*—The fraction of Be^7 K capture to the 478 kev excited state of Li^7 has been experimentally determined to be 0.107 ± 0.02. The experimental method consisted in measuring the number of Be^7 atoms by counting neutrons from the $Li^7(p, n)Be^7$ reaction, and in observing the subsequent number of 478 kev gammas by use of a counter calibrated by beta-gamma coincidences from Au^{198}. Implications concerning the character of the 478 kev Li^7 level are discussed.

* This work was supported in part by the Wisconsin Alumni Research Foundation and in part by the AEC.

A5. Disintegration Energy of Al^{29}.* L. SEIDLITZ, E. BLEULER, AND D. J. TENDAM, *Purdue University.*—A discussion by Barkas[1] shows that the mass difference between Al^{28} and Si^{28} is about 1.5 Mev higher than expected from the decay energies of adjacent nuclei with the same symmetry (Na^{24}, $F^{20} \cdots$, P^{32}, $Cl^{36} \cdots$). If this is due to the closure of a shell for Si^{28}, a similar anomaly might be expected for the transition $Al^{29} - Si^{29}$ ($T_{\frac{1}{2}} = 6.6$ min.). Al^{29} was produced by bombarding Mg with the α-particles of the Purdue cyclotron. Absorption and coincidence measurements show a β^--spectrum of 2.4 Mev upper limit, accompanied by γ-radiation in cascade. Indications of a partial β^--spectrum of lower energy and of a cascade of γ-rays are present. Tentative decay schemes yield a total disintegration energy between 3 and 3.5 Mev. The comparison of the decay energies of corresponding nuclei (Ne^{23} 4.3, Na^{25} 3.7, Mg^{27} 2.64, Al^{29} 3–3.5, Si^{31} 1.8, P^{33} ?, S^{35} 0.167 Mev) indicates a similar anomaly in the mass difference $Al^{29} - Si^{29}$ as found for $Al^{28} - Si^{28}$.

* Supported by the ONR.
[1] W. H. Barkas, Phys. Rev. **72**, 346 (1947).

A6. The Forbidden Beta-Spectra of Sr^{89}, Sr^{90}, and Y^{90}. F. B. SHULL, C. H. BRADEN, AND L. SLACK, *Washington University.*—The spectrum "shape" for a forbidden beta-transition cannot be uniquely predicted except in special cases where restricted selection rules are satisfied. Konopinski and Uhlenbeck[1] have shown that one such special transition involves a

spin change of 2 units and a change of parity, provided Gamow-Teller rules govern the beta process. The expected distribution differs from that for an allowed transition by a factor $G\sim(W_0-W)^2+(W^2-1)$. Changes of parity for the beta-transitions of Sr^{89}, Sr^{90}, and Y^{90} are expected on the basis of the nuclear shell model.[2] In view of the *ft* values, these are first-forbidden by G-T rules, and the relatively large magnitude of $(W_0^2-1)ft$ in each instance favors a spin change of 2 units.[2,3] All three spectra have been measured in a double-focusing spectrometer. When analyzed as "allowed" Fermi-Kurie plots, all three display the characteristic upward bulge introduced by the factor G for energies above $W_0/2$. When analyzed as "forbidden" FK plots (i.e., after G is divided out), all three are satisfyingly straight.

[1] E. J. Konopinski and G. E. Uhlenbeck, Phys. Rev. **60**, 308 (1941).
[2] E. Feenberg and K. C. Hammack, Phys. Rev. (in press).
[3] F. B. Shull and E. Feenberg, Phys. Rev. (in press).

A7. The Forbidden Beta-Spectra of Sr^{89} and Y^{90}. H. CLAY PRICE, JR. AND LAWRENCE M. LANGER, *Indiana University.*—Because of the remarkable agreement between theory and experiment found recently[1] in the forbidden beta-transition of Y^{89}, it was thought desirable to examine the spectrum of Sr^{89}. This transition, in spite of its large comparative half-life, is also predicted by the nuclear shell structure analysis[2] to be once forbidden with a spin change of two units and parity change. The source, obtained from Oak Ridge, had in addition to the Sr^{89}, an activity of about 5 percent due to Sr^{90} in secular equilibrium with Y^{90}. Spectra were obtained with and without chemical extraction of the Y^{90}. Measurements were made in the high resolution 40 cm radius of curvature spectrometer with a source of about 0.01 mg/cm² average thickness. It is found that both Sr^{89} and Y^{90} yield forbidden spectra whose shapes are accounted for by the factor $a\sim[W^2-1+(W_0-W)^2]$. This indicates that according to Gamow-Teller selection rules both transitions are indeed once forbidden with parity change and spin change of 2, in agreement with the predictions of the shell model. The end points are: Sr^{89}, 1.463±0.005 Mev; Y^{90}, 2.180±0.008 Mev. This work has been assisted by a grant from the Frederick Gardner Cottrell Fund of the Research Corporation and by the joint program of ONR and AEC.

[1] Lawrence M. Langer and H. Clay Price, Jr., Phys. Rev. **75**, 1109 (1949).
[2] E. Feenberg and K. C. Hammack, private communication.

A8. The Beta-Spectrum of Silver-110. WERNER S. EMMERICH AND J. D. KURBATOV, *Ohio State University.*—The disintegration of Ag 110 into the isobars Cd 110 and Pd 110 was studied in a Wilson cloud chamber. Purified Ag 110 of high specific activity was mounted in the center of the chamber on very thin Zapon film, and pictures of tracks were taken in air and in helium at atmospheric pressures in magnetic fields of 372.5 and 149 gauss. A Kurie plot produced a straight line in the range of 150 to 550 kev indicating the presence of a continuous electron spectrum with an upper energy limit of 0.59 Mev. Upon subtraction of the theoretical component of this spectrum and recalculation of the remainder, evidence was obtained for the existence of a second continuous spectrum with an upper energy limit of 90±10 kev. The intensities of the two continuous spectra were found to be of the same order of magnitude which indicates, considering the careful mounting of the source, that the low energy spectrum is not due to back scattering. The presence of converted electron groups of 0.1, 0.6, 0.9, 1.2, and 1.5 Mev was observed. Monochromatic groups near 0.3 Mev were not well defined. Several single positrons and pairs were found. Howèver, the number of positrons, for which pairs could not be established, did not exceed 0.2 percent of the observed electrons of the beta-spectra.

A9. Radioactive Tin 111. R. A. HINSHAW, *Muskingum College.*—A radioactive isotope of a half-life of 35.0±0.5 minutes has been found in the tin fraction of cadmium bombarded in the cyclotron with 20 Mev alpha-particles.* Using electromagnetically enriched cadmium** the assignment can be made to Sn 111. Positrons of 1.45 Mev and x-rays are observed.

* Acknowledgment is gratefully made for support received from the Ohio State University Development Fund and the Graduate School.
** Supplied by the Y-12 plant, Carbide and Carbon Corporation through the Isotopes Division, USAEC, Oak Ridge, Tennessee.

A10. Radiations from Indium (114) and Barium (140).* C. E. MANDEVILLE AND E. SHAPIRO, *Bartol Research Foundation.*—The 72-second In^{114} activity, in equilibrium with its 48-day isomeric parent, was induced in metallic indium irradiated by slow neutrons in the Oak Ridge pile. Chemical separations were performed for the removal of Ag, Ca, Cu, Fe, Ni, and Pb as possible impurities. The beta-rays have a maximum energy of 1.89 Mev as measured by aluminum absorption, and the maximum gamma-ray energy is 0.90 Mev as determined by coincidence absorption. A lead absorption curve gives quantum energies of 0.15 Mev and 0.70 Mev. Beta-gamma coincidence data show that the harder gamma-rays are associated with less than 5 percent of the nuclear beta-rays. A gamma-gamma-coincidence rate of 0.25×10^{-3} coincidence per gamma-ray was noted. Fission-produced Ba^{140} emits beta-rays of maximum energy 0.91 Mev. Lead absorption curves observed continuously for 90 hours during growth of La^{140} reveal the presence of 0.14 Mev and 0.6 Mev quanta emitted by Ba^{140}. Beta-gamma coincidence measurements show that the beta-spectrum of Ba^{140} is complex.

* Assisted by the joint program of ONR and AEC.

A11. Studies on Synthetic LiF as a Scintillation Detector of Heavy Particles and Quanta. E. C. FARMER, H. B. MOORE, AND CLARK GOODMAN, *Massachusetts Institute of Technology.** —Studies have been made on synthetic LiF as a scintillation detector of heavy particles and quanta, particularly in view of its possibility as a high efficiency detector of thermal neutrons. Most of the results reported were obtained with a crystal of LiF grown in vacuum. Measurements were taken with the crystal, photomultiplier tube (1P28) and paraffin block cooled with solid CO_2, using three different sources: a Co^{60} gamma-source, a Po-Be neutron source and a Po alpha-source. The results for thermal neutrons were obtained by difference, with and without a boron shield around the crystal. Calculations from counting rate extrapolated to zero pulse height give an efficiency of 9.5 percent for thermal neutrons, 11 percent for Po α's and 1.6 percent for Co^{60} gammas. The duration of the light pulse from LiF is $\leq1\mu$sec. with no noticeable "after" pulses. Comparison runs were made on the three types of synthetic LiF (vacuum, ammonia, and air grown) using the alpha- and gamma-sources. Because of differences in size, relative efficiencies for the different type crystals were not attempted; however, there does not seem to be any marked difference between them.

* This is a joint undertaking of M.I.T. and ONR.

A12. Ring Focus in a Thin Magnetic Lens Beta-Ray Spectrometer. JOSEPH M. KELLER, ERNEST KOENIGSBERG, AND ARTHUR PASKIN, *Iowa State College.*—Various writers[1] have suggested an improvement in resolution of a magnetic lens type beta-ray spectrometer if a suitably located annular orifice is used for momentum discrimination. Primarily to study the application of "ring focus" selection to a thin lens spectrometer, we have calculated the electron trajectories for the Iowa State College spectrometer.[2] The differential equation of the orbit, for zero angular momentum about the symmetry axis, was integrated numerically on International Business Machines to yield a set of trajectories starting from a point source on the axis. For a fixed range of initial electron directions, different positions of ring focus occur (all at nearly the same

radius) for different values of electron momentum per unit magnetizing current. The calculated trajectories are used to predict line shapes. Effects of a finite source diameter and of finite angular momenta are estimated by perturbation methods.

* This work was supported by AEC.
[1] C. M. Witcher, Phys. Rev. **60**, 32 (1941); S. Frankel, Phys. Rev. **73**, 804 (1948).
[2] E. N. Jensen, L. J. Laslett, and W. W. Pratt, Phys. Rev. **75**, 458 (1949).

A13. Constant Sensitivity Gamma-Ray Detector.* J. PINE AND R. SHERR, *Princeton University.*—For many experiments it would be desirable to use a gamma-ray detector whose sensitivity is independent of energy. The scintillation counter offers this possibility. The larger absorption of softer radiation is compensated for by the smaller average pulses so that the bias curves for different energies might cross at some small bias. Accordingly, anthracene and NaI were investigated. Absolute efficiencies were obtained by comparison with a copper Geiger counter. The integral bias curves did not cross and the efficiencies exceeded the theoretical values at low bias. The latter effect has been reported by Hofstadter and is presumably due to radiation scattered into the detector. The absence of cross-over in the integral bias curves may also be caused by this effect. However, the differential bias curves for a single NaI crystal were found to cross at a particular bias which was far removed from the region of excessive efficiency. For our arrangement a 5-volt single channel discriminator would give an efficiency of detection of 1.1 percent for energies between 0.510 and 1.24 Mev. Preliminary measurements indicate the same efficiency for 1.8 Mev radiation.

* Supported in part by the joint program of ONR and AEC.

A14. A Micro Calorimeter Suitable for Study of Easily Absorbed Nuclear Radiations.* C. V. CANNON** AND G. H. JENKS, *Oak Ridge National Laboratory.*—A calorimeter, which can be applied to the measurement of radio-active decay energies when easily absorbed radiations are involved, has been designed and constructed. The calorimeter is of an isothermal type, operating at the temperature of liquid nitrogen and using the rate of vaporization of nitrogen, under constant pressure, as a measure of the heat input. Calibration of the calorimeter was carried out by means of a resistance heater. The sensitivity of the calorimeter is such that heat inputs as low as 7×10^{-6} cal./sec. can be measured with an accuracy of 1 percent. Reference is made to the application of the calorimeter to the study of the decay of P^{32} [1] and of tritium.[2]

[1] Zumwalt, Cannon, Jenks, Peacock, and Gunning, Science **107**, 47 (1948).
[2] Jenks, Ghormley, and Sweeton, Phys. Rev. **75**, 701 (1949).
* This document is based on work performed under contract for AEC.
** Present address: Department of Physics, University of Washington, Seattle, Washington.

Papers Not Classed Elsewhere

B1. Collimation Error in Small Angle X-Ray Scattering. K. L. YUDOWITCH, *Florida State University.*—It has been indicated[1] in small angle x-ray scattering experiments that excessive collimation error may be introduced by the use of an incident beam of finite cross section. To account for this error the usual procedure[2] has been multiple integrations for rays reaching a single point on the film from any position along the width or height of each slit. However, the common effect from both a finite slit width and height and a skew incident beam is a range of scattering angle ($\delta\epsilon$). The multiple integrations over each slit dimension are thus reduced to a single integration over scattering angle, which entails first finding the limits of scattering angle. The assumption of a constant distribution of intensity throughout the range, allows $\delta\epsilon$ to be taken as a measure of the collimation error. Minimization of $\delta\epsilon$ then leads to a quartic equation whose solution yields optimum values of slit height-to-width ratio or eccentricity. Determination of this optimum slit eccentricity is prerequisite to best results in small angle x-ray scattering.

[1] K. L. Yudowitch, J. App. Phys. **20**, 174 (1949).
[2] C. G. Shull and L. C. Roess, J. App. Phys. **18**, 295 (1949).

B2. Design of Small, Self-quenching, G-M Counters. C. V. ROBINSON, *Harvard Medical School.*—Several small self-quenching G-M counters have been constructed recently by the author for use in medical research. The diameters are in the range from 2 to 6 mm and the mixtures consist of argon and ether* or argon and ethyl acetate. The research connected with the design of these counters will be discussed and details of construction shown.

* C. V. Robinson and R. E. Peterson, Rev. Sci. Inst. **19**, 911 (1948).

B3. An Extension of a Theory of Magnetic Amplifiers. ROBERT T. BEYER AND MING-YI WEI, *Brown University.*—A theory of operation of certain magnetic amplifiers, previously presented,[1] has been extended, in the case of secondaries with infinite a.c. impedance to be valid for large input currents. The second harmonic output is shown to deviate from linearity and pass through a maximum as the direct current is increased. Some experimental evidence is given to support the calculations. The influence of a third harmonic term in the primary current (which has hitherto been considered as a pure sine wave), has also been investigated. It is shown that for small input currents no serious error is introduced by neglecting the higher harmonic.

[1] J. A. Krumhansl and R. T. Beyer, J. App. Phys. **20**, 432 (1949).

B4. Influence of Molecular Structure of Lubricant on the Variation of Incremental Friction Coefficient with Speed. J. T. BURWELL AND C. D. STRANG, *Massachusetts Institute of Technology.*—The incremental friction coefficient, defined as $\Delta F/\Delta W$ rather than F/W, where F is the friction force and W the applied load was shown in a previous paper[1] to be independent of all fluid viscous effects. Its variation with speed is found to be characteristic of the lubricant for various types of straight long-chain lubricant molecules. With non-polar hydrocarbon molecules it is found to decrease over the whole range of speed from 0.100 cm/sec. to 75.7 cm/sec. For various straight-chain polar molecules such as fatty acids, esters, metal soaps and alcohols the coefficient is independent of speed at the low end of the range but decreases at the higher speeds. For a series of normal alcohols the coefficient at any speed decreases with chain length up to dodecanol after which it is constant. The similarity is noted between the shape of the friction *vs.* speed curve and that of the curve of structural viscosity *vs.* rate of shear curve predicted by Umstätter[2] on the basis of Maxwell's relaxation relation. Hence, the decrease of this friction coefficient with speed may be due to a shear-induced orientation in the molecular monolayers of lubricant on the rubbing surfaces.

[1] J. T. Burwell and C. D. Strang: J. App. Phys. **20**, 79 (1949).
[2] H. Umstätter, Die Technik, **1**, 46 (1946); Koll. Zeits., **103**, 7 (1943).

B5. The Propagation Modes of a Helix.* WILLIAM SOLLFREY, *New York University.*—Previous researches on the helix have made simplifying approximations about the nature of the boundary conditions. In this paper the field equations and boundary conditions are formulated exactly. They are then solved by an expansion in powers of the ratio of the thickness of the wire to the distance between turns. The method used consists of introducing a new coordinate system, which is such that a helical wire of circular cross-section is a surface in which one coordinate is constant. Maxwell's equations and the electromagnetic boundary conditions are expressed in terms of this system. Since non-orthogonal coordinates are involved, the equations cannot be solved exactly, but a perturbation procedure may be applied as indicated above.

The result of the analysis is to show that there is a principal mode, which propagates with the free space velocity of light in the direction of the wire. The characteristics of this mode are studied, and they are compared successfully with experiment.

* This research was performed under the sponsorship of the Watson Laboratories of the U. S. Air Force under contract with New York University.

B6. Application of a Variational Principle to Biconical Antennas.* C. T. TAI, *Harvard University.*—A theoretical examination is made of the impedance of a biconical antenna, based upon a variational method due to Schwinger. In the present analysis, an integral equation to determine the aperture field is first obtained by matching the tangential electric and magnetic fields along the boundary sphere. Using this integral equation, the effective terminating admittance of the antenna can be expressed in a form that is stationary with respect to small variations in the aperture field. It is shown that the zeroth-order solution of the admittance function thus obtained is the same as the one that Smith derived by neglecting all the high order waves in the interior region except the principal mode. For small-angle cones, the present formulation yields the same exact solution obtained previously, based upon several different methods. The paper also contains a discussion of the first-order approximate solution which is applicable to both small- and wide-angle cones. The analysis includes a discussion of the Ritz method to determine very accurately the characteristic values and characteristic functions for a given cone.

* Supported by ONR.

B7. Terminal Impedance and Generalized Two-Wire Line Theory. K. TOMIYASU AND RONOLD KING, *Harvard University.*—Conventional transmission line theory takes no account of variations in the parameters of the line and of coupling near a terminating impedor or near any change in its uniform properties. A general theory is derived which substitutes for these effects a simple terminal zone network of lumped series and shunt elements which may be evaluated for each type of termination or discontinuity. The apparent terminal impedance, Z_{sa} (which is the impedance actually measured on a lossless line at one-half wave-length from the termination) consists of this network in combination with the theoretical, isolated impedance, Z_s, of the load. Application of the theory to terminations consisting of an open end, a bridge end, a line continuing at an angle, and antennas oriented in the plane of the line and in the plane perpendicular to the line, is outlined.

B8. Jacobian Thermodynamics. F. H. CRAWFORD, *Williams College.*—The author has discussed the utility of Jacobians in thermodynamic theory.[1] The results have been extended to the case of n-variable systems where it is necessary to divide all possible systems into: (a) *unrestricted* and (b) restricted systems (i.e., those having certain variables of limited functional dependence). In either case Clausius' equation $dU=TdS+dW$ is the starting point, with dW expressed as $(n-1)$ separate work terms of the form $Fd\theta$. This gives $2n$ variables on the right, where in case (a), *any* n may be taken as independent. If we set up the Jacobian, J_0, of the remaining n dependent variables with respect to the independent set, according to certain simple rules, then J_0 is a determinant of n^2 derivatives, *symmetric* about the main diagonal. The symmetry is a very concise expression of the general Maxwell relations and means that J_0 contains the $n(n+1)/2$ independent derivatives adequate for a complete thermodynamic discussion. In case (b), certain derivatives will vanish, alone if in the main diagonal, otherwise in pairs; hence a fewer number of derivatives must be measured experimentally to enable others to be determined.

[1] Phys. Rev. 72, 521A (1947); Am. J. Phys. 17, 1–5 (1948); Proc. Am. Acad. (in press).

B9. The Temperature Distribution in an Accreting Medium Containing a Source of Heat. A. E. BENFIELD, *Harvard University.*—Using the mathematical theory of the conduction of heat in solids, the temperature (as a function of distance and time) is calculated for an accreting semi-infinite medium which contains a uniformly distributed source of heat. The medium is initially all at a uniform temperature; the free surface of the medium, at which accretion occurs at a steady velocity v, is held at this initial uniform temperature, while the temperature in the interior of the medium increases due to the heat which is being generated there at the constant rate of A heat units per unit time per unit volume. It is found that, as time goes on, the temperature gradient approaches a steady value, $A/c\rho v$, where c is the specific heat of the medium and ρ is its density. The solution of the problem involves a Laplace transform that is not tabulated in the usual references.[1]

[1] See A. E. Benfield, Quart. App. Math. 6, 4, 439–443 (January, 1949).

Electrical Phenomena in Gases

C1. Afterglow of Nitrogen and Argon in Low-Density Supersonic Streams. THOMAS W. WILLIAMS AND JAMES M. BENSON, *NACA—Langley.*—An investigation will be described in which the phenomena of afterglow were utilized in a way suggested by J. Kaplan to make visible the low density supersonic flows of several gases, including nitrogen, oxygen, air, and argon. Photographs of the afterglow in the flow about wedges will be shown and compared with corresponding schlieren photographs for densities of the stream corresponding to static pressures in the order of 1 mm of mercury. The afterglow is effective in visualizing shock waves and other features of the flow at low densities where it is difficult or impracticable to obtain comparable results with schlieren, shadowgraph, or interferometer methods. The Lewis-Rayleigh afterglow of nitrogen[1,2] in particular is suggested for further use in this way to visualize the supersonic flow in streams having a density sufficiently low for the ratio of Mach number to Reynolds number to be a significant parameter.[3]

[1] S. K. Mitra, Active Nitrogen, a New Theory (Indian Press, Calcutta, 1943).
[2] J. Kaplan, Active Nitrogen, Phys. Rev. 73 No. 5 494–6, March 1, 1948.
[3] Thomas W. Williams and James M. Benson, Preliminary Investigation of the Use of Afterglow for Visualizing Low-Density Compressible Flows, NACA RM No. L9A24a, 1949

C2. Recombination Spectrum and Electron Density Measurements in Neon Afterglows.* R. B. HOLT, J. M. RICHARDSON, B. HOWLAND, AND B. T. MCCLURE, *Harvard University.*—The spectrum emitted by the recombination of positive ions and electrons in the afterglow of a pulsed microwave discharge through neon has been studied as a function of time. Electron density measurements on the plasma were made by the cavity resonant frequency shift method of S. C. Brown and co-workers.[1] The *relative* intensities of several strong lines in the spectrum remains essentially constant during the afterglow, while the *relative* intensities of several others show systematic changes. A recombination coefficient can be calculated on the basis of the observed variation of intensity as a function of time for any individual line, provided that the electron density is measured at some particular time. This technique allows measurements at electron densities much too high to be observed directly by the microwave method. The recombination coefficient obtained for positive ions and electrons in neon varies somewhat with the spectral line and the region of the afterglow chosen for the computation, but is on the order of 10^{-7} cc/ion-sec., in reasonable agreement with the value found at lower electron densities by the microwave method by Brown and co-workers.

* Supported by the ONR.
[1] Massachusetts Institute of Technology, Research Laboratory of Electronics, Technical Report No. 66.

C3. Measurements of Electron-Ion Recombination in Diatomic Gases.* MANFRED A. BIONDI AND SANBORN C. BROWN, *Massachusetts Institute of Technology.*—Previous measurements of recombination coefficients[1] which were made in the monatomic gases have been extended to the diatomic gases H_2, N_2, and O_2. The recombination of electrons with monatomic ions involves the radiation of energy as the process by which a stable combined atom is formed. This process seems to be of secondary importance in the case of recombination of electrons with diatomic ions. This latter recombination evidently is made stable by the absorption of the electron's kinetic energy in vibration and rotation levels of the diatomic molecule. Support of this hypothesis is found in the fact that for electrons and ions of 0.04 e.v. average energy, the recombination coefficient for H_2 is $\alpha=2.5\times10^{-6}$ (ions/cc$-$sec.)$^{-1}$ while for helium the value of α is only 1.7×10^{-8} (ions/cc$-$sec.)$^{-1}$. The variation of α with gas pressure and temperature has been studied.

* This work has been supported in part by the Signal Corps, the Air Materiel Command and ONR.

[1] M. A. Biondi and S. C. Brown, "Measurements of Positive Ion-Electron Recombination"—paper presented at A.P.S. Meeting, Washington, D. C. in April, 1949.

C4. Measurements on the Imprisonment of Resonance Radiation in Mercury Vapor. D. ALPERT, A. O. MCCOUBREY, AND T. HOLSTEIN, *Westinghouse Research Laboratories.*—The rate of escape of imprisoned resonance radiation was determined by measuring the rate at which resonance radiation emerged from a column of mercury vapor after a beam of exciting light was cut off. The emerging scattered light was detected by a photomultiplier and the resulting decay signal displayed on a properly synchronized oscilloscope. Measurements of the decay time, T, were carried out over a range of vapor densities, N, from 3×10^{14} to 2×10^{15} atoms per cc. In the region of Doppler broadening ($N<3\times10^{15}$/cc) the measurements are in good agreement with theory.[1] In the density range between 3×10^{16} and 10^{17}/cc, two time constants were observed. Above this range, the longer decay process, which is perhaps to be attributed to the presence of excited molecules, predominates.

[1] T. Holstein, Phys. Rev. **72**, 1212 (1947).

C5. Self-Broadening of Monatomic Resonance Lines. T. HOLSTEIN, *Westinghouse Research Laboratories.*—The self-broadening of the resonance lines of monatomic gases is treated from the standpoint of the statistical theory of Kuhn and Margenau. In the calculations, explicit account is taken of the degeneracy of excited and ground states. The results apply to the wings of a resonance line, for which the statistical theory should be valid and for which frequency shifts due to binary collisions alone need be considered. One obtains for the spectral distribution a symmetrical "dispersion" expression of the form

$$P(\nu)=\mu[(Ne^2f)/(2\pi m\nu_0)]/(\nu-\nu_0)^2,$$

where N is the density of normal atoms, f the absorption oscillator strength of the line, and μ a dimensionless function of the optical transition involved. In particular, for transitions of the type $(^1S_0-^{1,3}P_1)$, $(^2S_{1/2}-^2P_{1/2})$, and $(^2S_{1/2}-^2P_{3/2})$, μ takes on values 2/9, 1/3, and 0.2561, respectively. The theory is compared with measurements[1,2] on the self-broadening of alkali resonance doublets.

[1] Shang-Yi Ch'en, Phys. Rev. **58**, 884 (1940) (Rubidium).
[2] Chris Gregory, Phys. Rev. **61**, 465 (1942) (Caesium).

C7. A Method for Determining the Average Energy of Electrons in a Gas Discharge.* LAWRENCE J. VARNERIN, JR. AND SANBORN C. BROWN, *Massachusetts Institute of Technology.*—The gas in a resonant cavity will break down when the losses of electrons to the walls are replaced by ionization in the body of the gas. With an a-c field applied, the breakdown depends upon the coefficient of diffusion of electrons, D. If a small d-c sweeping field is applied, it will depend, as well, upon the coefficient of mobility of electrons, μ. Breakdown measurements with d-c fields and without d-c fields applied then permit a determination of the ratio D/μ. This quantity is a direct measure of the average energy of electrons in a gas. It is given, as well, by the ratio of the first Townsend ionization coefficient η, to the a-c ionization coefficient, ζ. Results for helium will be presented.

* This work has been supported in part by the Signal Corps, the Air Materiel Command, and ONR.

C8. High Frequency Breakdown in Magnetic Field.* BENJAMIN LAX AND SANBORN C. BROWN, *Massachusetts Institute of Technology.*—The condition for breakdown in a gas is expressed as a balance between the number of electrons produced by ionization and those lost by diffusion. A magnetic field which is transverse to the applied microwave field has two principal effects upon the electrons in a gas discharge. The energy transferred to the electron between collisions from a constant electric field shows a resonance character whose maximum occurs when the "cyclotron" frequency is equal to r-f frequency. The second effect is a reduction in the diffusion of the electrons to the walls. These effects become more and more significant at lower pressures, resulting in startling reduction of breakdown voltages near resonance. A brief description of the apparatus and the methods used in obtaining the experimental results will be presented. The results observed in air and helium will be shown. The curves for the latter gas are compared with those obtained theoretically.

* This work has been supported in part by the Signal Corps, the Air Materiel Command, and ONR.

C9. Electric Breakdown in CO_2 from Low Pressures to the Liquid State.* D. R. YOUNG, *Massachusetts Institute of Technology.*—Carbon dioxide, with a critical temperature of 31°C, allows the investigation of the change from the gaseous to the liquid type of electric breakdown during a continuous change in the density. Paschen's similarity law has been verified at low pressures. At high pressures, small departures are observed for long gap-lengths and large departures for small gap-lengths. Simultaneously the scatter of the breakdown voltage becomes independent of illumination and the breakdown strength dependent on the cathode material. This seems to be due to the onset of field emission. Measurements of pre-breakdown currents have yielded values for the Townsend first coefficient (α) as well as for the field emission constants. For small gap-lengths the current is higher than predicted by the normal field emission equation, indicating some new process which becomes effective at short gap distances. The transition from gas to the liquid state does not produce a discontinuous change of the breakdown voltage.

* Sponsored by ONR, the Army Signal Corps, and the Air Force under contract N5 ori-07801.

C10. Measurement of Temperatures in Complex Flame Structures by High Resolution Spectroscopy of the Sodium *D*-Lines, I. F. P. BUNDY AND H. M. STRONG, *General Electric Company.*—Sodium atoms in a flame of reasonable thermodynamic equilibrium radiate and absorb as thermally excited oscillators in equilibrium with the flame gases. Therefore, the brightness at any particular wave-length within the intensity contour of a sodium line depends only on the temperature and the emissivity of the flame for that particular wave-length, and the black body brightness is the observed brightness divided by the emissivity. The brightness may be measured by photographic densitometry, and the brightness scale calibrated by use of a standard uniform flame or arc of known temperature. The necessary high resolving power is conveniently at-

tained by use of an interferometer. The emissivity may be determined by comparing the brightness of the mirrored and unmirrored flame or by measurements of the spectral line width. Some of the advantages of the method are that the temperature distribution in a complex flame structure can be mapped from one photograph, the temperatures of submerged zones can be determined with considerable accuracy, and the temperatures of flames hotter than can be matched with conventional comparison lamps can be measured. The method is subject to the usual difficulties of high resolution spectroscopy and photographic densitometry.

C11. Measurement of Temperatures in Complex Flame Structures by High Resolution Spectroscopy of the Sodium *D*-Lines, II. H. M. STRONG AND F. P. BUNDY, *General Electric Company.*—The measurement of flame temperature by the conventional sodium line reversal method does not enable one to analyze the temperature structure in a complex flame or to measure temperatures higher than that of the hottest incandescent comparison radiator obtainable, the carbon arc. This method makes use of the sodium line reversal principle but uses a bright sodium vapor lamp as the comparison radiator. The observation of the match point is made photographically through a Fabry-Perot interferometer instead of the visual low resolving power spectroscope. The sodium lines are then fully resolved. Reversal temperatures can be observed for different parts of the flame structure. The photographs also enable one to measure the absorption by the flame at selected positions on the sodium line contour. The reversal temperatures together with absorption data enable one to compute the temperatures of inner zones of the flame. This method requires the photographic measurement of intensity and is attended by the usual difficulties in measurements of this kind.

Semi-Conductors, Phosphors, Ferroelectricity, Ferromagnetism

D1. Thermionic Emission of (BaSr)O without Metallic Support. GEORGE E. MOORE, *Bell Telephone Laboratories.*—To define problems associated with oxide cathodes, experiments have been performed in this laboratory on systems analogous to the oxide cathode but simpler physically and chemically. D. E. Wooldridge suggested the present experiment intended to eliminate effects associated with support metals, such as interface phenomena and various products of chemical interaction between (BaSr)O and support metal (including impurities); effects often thought responsible for high emission in oxide cathodes. The ideal sought is (Ba Sr)O isolated from foreign metal but in a structure permitting thermionic observations. To achieve this ideal, (Ba Sr)O applied to the outer surface of an internally heated MgO ceramic 1 mm thick, is capacitatively coupled to a Mo electrode inside the MgO and connected to the voltage source. No reaction apparently occurs between MgO and (Ba Sr)O and this structure is believed an approximation to the ideal desired. Although some questions require further investigation, emissions between 3 and 10 ma/cm² at 850°C have been observed in early experiments. Although low relative to the usual oxide cathode, this is enormous compared either to clean refractory metals or to the uncoated ceramic. To avoid charging effects, emission was measured in microsecond pulses using a high gain wide-band amplifier developed by R. W. Hull.

D2. Secondary Emission from Silicon and Germanium Oxides. H. E. MENDENHALL, *Bell Telephone Laboratories.*—Thin films of evaporated silica about 100A thick have been studied as secondary electron emitters. When backed by commercially pure platinum and after heating from 700° to 1000°C, a secondary emission ratio of 4.5 at 500 volts bombarding energy is developed. When backed by pure tantalum that had previously been outgassed to 2000°, the highest δ obtainable was only 1.59 at 650 volts due possibly to the lack of impurity activators. A very pure germanium oxide film sprayed on well outgassed tantalum showed charging of the surface when bombarded at room temperature. The highest δ observed was 1.35 at 500 volts energy at a target temperature of 850°C. Upon heating to 1150°C for over 10 hours the film which was 1 mg/cm² in thickness evaporated off leaving the $\delta=1.31$ at 650 volts at any temperature from room temperature up to 850°C. The crossover voltages for δ equal to unity were now 282 and 2850 close to reported characteristics for clean tantalum. The work was continued with "pure" germanium dioxide backed with commercially pure platinum to obtain a greater supply of activators. After heating to 700° and 850°C for about an hour, secondary emission ratios from 5 to 6 were obtained at about 700 volts bombarding energy.

D3. Electron Injection in *P*-Type Germanium.* RALPH BRAY, *Purdue University.*—Decreases in resistance of *N*-type germanium under high field pulse conditions[1] are apparently due to the injection of holes from the positive contact.[2] To explain similar resistance decreases[1] in *P*-type germanium, the voltage distribution along the sample was determined by probe methods when five microsecond constant current pulses were applied through soldered end contacts. The largest and most rapid resistance changes were found near the negative contact, indicating *that electrons are injected from the negative contact.* Only small negative space charge was measured, indicating that the hole density increases to compensate for increased electron density. Hall effect measurements using high field pulses corroborate the increased electron concentration. Superimposing a transverse magnetic field, *H*, produces magnetoresistive effects which are largest near the positive contact, indicating that *H* decreases the electron penetration depth. This may be due to deflection of the holes and electrons to the same surface, increasing the local concentration there, and hence the recombination rate. A *P*-type transistor was made using negative emitter and positive collector electrodes, in application of the electron injection effect.

* Work supported by Signal Corps.
[1] Ralph Bray, Phys. Rev. 74, 1218 (1948); Bray, Lark-Horovitz, and Smith 72, 530 (1947).
[2] E. J. Ryder and W. Shockley, Phys. Rev. 75, 310 (1949).

D4. The Barrier Layer on *P*-Type Germanium.* H. Y. FAN AND R. BRAY, *Purdue University.*—Surface states on high resistivity *N*-type germanium appear to fix the Fermi level at the surface close to the top of the full band. This produces a *P*-type surface inversion layer, and makes possible a large inward flow of holes in the forward direction.[1] The large increase in conductivity produced by electron injection in *P*-type germanium[2] ($\rho\sim 2$ ohm-cm) with soldered contacts, suggests that in this case the Fermi level at the surface is close to the bottom of the empty band, producing an *N*-type inversion layer. *P*-type rectification and photovoltaic effects[3] have been obtained with certain soft metal whiskers on etched high resistivity samples indicating that also in these cases the Fermi level at the contact is not close to the full band. However tungsten whiskers give poor rectification. According to contact potential measurements by Benzer[1] the Fermi levels at free, etched surfaces of *P*- and *N*-type germanium samples in air lie within 0.1 ev of each other. The barrier layer in *P*-type germanium therefore seems to be influenced by the metal contact.

* Work supported by Signal Corps.
[1] J. Bardeen and W. H. Brattain, Phys. Rev. 75, 1208 (1949).
[2] Ralph Bray, see companion abstract.
[3] R. Bray and K. Lark-Horovitz, Phys. Rev. 71, 141 (1947).

D5. The *P*-Type Germanium Transistor. W. G. PFANN AND J. H. SCAFF, *Bell Telephone Laboratories.*—The transistor effect described by Bardeen and Brattain for *n*-type germanium[1] has been found in *p*-type germanium. In the *p*-germanium transistor the emitted carriers are electrons and the collector is biased positively with respect to the base, in contrast to the *n*-type device wherein the carriers are holes and the collector is biased negatively. As in the *n*-germanium transistor amplification of power occurs both by impedance step-up and by current multiplication ($\alpha>1$). *p*-germanium of moderately high resistivity was used. It was produced by the thermal conversion of high back voltage *n*-germanium.[2] Preparation of the germanium surface and electrical forming followed generally procedures described for high back voltage germanium rectifiers.[3] The point-contact electrodes were of phosphor bronze. As compared with the *n*-germanium transistor, α's[1] were lower and cut-off frequencies were higher. The latter may be attributed in part to the fact that the mobility of electrons in germanium is higher than that of holes.

[1] J. Bardeen and W. H. Brattain, Phys. Rev. **74**, 230 (1948).
[2] J. H. Scaff and H. C. Theuerer, NDRC Report 14Sr1408-555, October 24, 1945.
[3] Torrey and Whitmer, *Crystal Rectifiers* (McGraw-Hill Book Company, Inc., New York, 1946).

D6. Electrical Properties of Crystal Grain Boundaries in Germanium. G. L. PEARSON, *Bell Telephone Laboratories.*—As ordinarily prepared high back voltage germanium ingots contain numerous crystals oriented in varied directions. A study of the electrical properties of the grain boundaries in *n*-type material indicate a high localized resistance which shows a reverse saturation characteristic when the applied potential is poled in either direction. When illuminated by a fine spot of light a photo-current is produced which reverses in direction as the light spot is moved across the boundary. The direction is such that electrons flow away from the boundary (holes flow toward the boundary). After the sample has been converted to *p*-type by heat treatment the localized resistance at the grain boundary is gone and the photo-current is that of a homogeneous sample. These data are consistent with the idea that the boundary represents a concentration of acceptor centers. It is possible that these centers are due not to chemical impurities but instead to misfit between the crystals. The presence of such a layer of *p*-type material would account for both the rectifying and photoelectric effects observed when the rest of the material is *n*-type. After conversion to *p*-type, the layer would become a thin region of low resistance which would be difficult to detect.

D7. Modulation of the Resistance of a Germanium Filament by Hole Injection. W. SHOCKLEY, G. L. PEARSON, M. SPARKS, AND W. H. BRATTAIN, *Bell Telephone Laboratories.*—When an emitter point contact to *n*-type germanium operates in the forward direction, a substantial fraction of the current consists of holes. We have been able to determine this fraction and also to measure the lifetime of the holes by injecting holes into a thin filament of germanium having a cross-section of about 0.01 cm$\times$0.01 cm. In addition to the current injected by the emitter near one end of the filament, an additional current flows from end to end sweeping the holes into one end of the filament. The space charge of the holes is compensated by an increased concentration of electrons and the net increase in carriers lowers the resistance of the filament. From measurements of the lowered resistance, the added concentrations of holes and electrons and the individual contributions of holes and electrons to the current can be found. From these measurements we conclude that for several cases the emitter current is more than 90 percent holes and that the hole lifetime is about 0.8 microseconds. The holes probably recombine on the surface and longer lifetimes would be found in larger structures. Filamentary transistors utilizing this resistance modulation have operated with point and $p-n$ junction emitters.

D8. Effect of X-Rays on the Absorption and Luminescence of Alkali Halide Phosphors. JAMES H. SCHULMAN, ROBERT J. GINTHER, CLIFFORD C. KLICK, AND LYLE W. EVANS,* *Naval Research Laboratory.*—Experiments on the effect of x-rays on the luminescence of alkali halide phosphors are reported. Particularly interesting phenomena were found with NaCl:(Pb+Mn) previously shown to be a sensitized luminescent system (excitation peaks, 2500A–2900A; emission peak in orange-red).[1] In addition to *F*-center coloration and a long-lived phosphorescence, *X*-irradiation produces the following changes in phosphor properties: (1) the phosphor no longer is excited by the above mentioned ultraviolet wave-lengths; (2) a grey coloration remains after the *F*-centers are bleached by light; (3) a red luminescence is excited by irradiation into the *F*-band immediately after x-ray treatment. The first two effects are permanent; the last, transitory. Transmission measurements show that x-rays erase the Pb^{+2}-induced ultraviolet absorption band. "Killing" of the original u.v.-excited luminescence is thus due to a change in state of the Pb^{+2} sensitizer, the grey visible absorption indicating this change to be: $Pb^{+2}\rightarrow Pb^{0}$. Heating removes the grey coloration and restores the characteristic Pb^{+2} ultraviolet absorption band. Making use of the first two effects above, permanent *X*-radiograms can be obtained on NaCl:(Pb+Mn) screens.

[1] Schulman, Burstein, Evans, Ginther, and White, Bull. Am. Phys. Soc. **24** (No. 4), 25 (1949), paper Q1.
* Present Address: Sylvania Electric Products, Inc. Emporium, Pennsylvania.

D9. Spontaneous Polarization of $BaTiO_3$ Single-Domain Crystals.* W. J. MERZ, *Massachusetts Institute of Technology.*—The spontaneous polarization P of $BaTiO_3$ single-domain crystals was measured as a function of temperature. At the Curie point, P_s increases with decreasing temperature as it does for KH_2PO_4, but much steeper than the Langevin theory predicts. Analogous to the other ferroelectrics one finds the spontaneous polarization and the crystal lattice deformation correlated in that $\Delta a/a$ and $\Delta c/c$ are proportional to P_s^2. This is explained by the fact that the piezoelectric constants d_{31} and d_{33} are zero above the Curie point and proportional to P_s below it. At lower temperatures P_s is smaller than expected, apparently due to antiparallel domains and internal strains. This argument is substantiated by the behavior of the birefringence Δn which is exactly proportional to $\Delta c/c$ but not to P_s^2 in this lower temperature region. At the transition point near 0°C a sudden drop of P_s of about $1/\sqrt{2}$ proves again the assumption that this transition results from a change of the polar axis from [001] to [011]. A further drop of P_s occurs at the −80°C transition when the polar axis changes to [111].

* Sponsored by ONR, the Army Signal Corps, and the Air Force under contract.

D10. Dependence of the Intensity of Magnetization and the Curie Point of Certain Iron Oxides Upon the Ratio of Fe^{++}/Fe^{+++}.* LOUIS R. MAXWELL AND J. SAMUEL SMART, *Naval Ordnance Laboratory,* AND STEPHAN BRUNAUER, *Bureau of Ordnance.*—The saturation intensity of magnetization (I_s) of certain unreduced iron oxide catalysts having variable ratios (γ) of Fe^{++}/Fe^{+++} was measured[1] at room temperature with a High-H Permeameter[2] at a maximum applied field of 10,000 Oersteds. Starting at $\gamma=0.352$, I_s was found to increase with increasing γ to a maximum at $\gamma=0.50$, agreeing with the known value for magnetite, and then decrease to a small value of I_s for large γ. Extrapolating back to $\gamma=0$, I_s agrees approximately with the value for cubic Fe_2O_3. The value found for I_s at $\gamma=0.352$ is in agreement with Néel's theory[3] of "ferrimagnetism" as applied to Fe_2O_3 and Fe_3O_4. Curie Point (θ) deter-

minations[4] made at an applied field of 3000 Oersteds for γ from 0.352 to 1.276 showed θ to be constant to within a few degrees and to have the same value as for pure magnetite (about 583°C).

* Work partially supported by ONR.
[1] Measurements of the intensity of magnetization were made at the National Bureau of Standards under the direction of Mr. R. L. Sanford.
[2] The apparatus used is described by R. L. Sanford and E. G. Bennett, J. Res. N.B.S. 26, January 1941.
[3] Louis Néel, Annales de Physique 3, 137 (1948).
[4] For the method used see L. R. Maxwell and S. Brunauer, Bull. Am. Phys. Soc. 24 (No. 4), 21 (1949).

D11. Magnetic and Electric Properties of Magnetite Single Crystals.* C. A. DOMENICALI, *Massachusetts Institute of Technology.*—Magnetite, according to previous investigators (Weiss, Verwey and de Boer, Okamura, Li, and others), has a low temperature transition (*ca.* −160°C), in which region its properties change abruptly. The magnetic and electric behavior of natural and synthetic single crystals has been investigated by the author, especially in this transition range. Besides substantiating the earlier findings, a number of additional effects have been observed of which the following seem to be the most interesting: (1) the behavior of the magnetization in the transition region depends upon the magnetic treatment while cooling through the transition, and is different for different crystallographic directions; (2) after cooling through the transition region in zero external magnetic field, all three principal crystallographic directions become difficult to magnetize; (3) Barkhausen experiments for temperatures below the transition show that most of the magnetization may result from domain rotation; (4) there is only a very small Barkhausen effect noticeable in the vicinity of −145°C, where the crystal becomes magnetically isotropic; the noise increases greatly as the transition is approached; and (5) the longitudinal saturation magnetostriction along [111] appears to change upon cooling through the transition.

* Sponsored by ONR, the Army Signal Corps, and the Air Force under contract.

D12. Fringe Fields of Ferromagnetic Domains. L. MARTON AND S. H. LACHENBRUCH, *National Bureau of Standards.*—Experiments have been undertaken to determine quantitatively, by electron optical means, the field emerging from single domain walls in ferromagnetic substances. The method used is the bright-field shadow technique,[1] an outgrowth of the electron optical "Schlieren" method described earlier.[2] A more or less parallel beam of electrons was passed normal to the edge of a single crystal of cobalt.[3] The faces of the crystal intersect at right angles and are oriented at 45° to the beam. Measurements were taken on the shadow patterns so obtained, and the approximate fringe field calculations were based upon certain simplifying assumptions, namely, (1) that the domain boundaries are rectangular, (2) that adjacent domain surfaces have uniformly distributed magnetic properties, (3) that the domain walls have finite thickness. Quantitative values of fringe fields will be reported.

[1] J. App. Phys. 19, 863 (1948).
[2] Phys. Rev. 73, 1475 (1948).
[3] Cobalt crystal on loan from Dr. R. M. Bozorth, Bell Telephone Laboratories.

Theoretical Physics and Some Experimental Nuclear Physics

H1. The Helium Wave Equation. JAMES H. BARTLETT, *University of Illinois.*—The wave equation for the normal state of helium has been written by Gronwall in the form $\nabla^2\psi+(1/z)(\partial\psi/\partial z)+(1/4r)(E-V)\psi=0$. If we let $\psi=e^F$, and $s=r^{\frac{1}{2}}$, it is possible to find a formal series for F in ascending powers of s, namely $F=F_1s+F_2s^2\cdots$. An analytical expression for F_1 has been found, and a possible F_2 has been calculated numerically. This procedure gets one away from the origin, and the integration can be continued outwards indefinitely, provided we are given E and two other adjustable parameters. The function ψ will have a node if E is greater than the lowest eigenvalue, and no node if E is below it. This enables us to enclose the lowest eigenvalue between two bounds, and to make their separation as small as we wish. Practical satisfaction of the boundary condition on ψ will be achieved by pushing the node outwards to larger and larger distances.

H2. A Field Formalism without Self-Action. T. A. WELTON, *University of Pennsylvania.*—It appears possible to interpret all physically real corrections to electrodynamic phenomena as arising from the action of the zero-point fluctuations of the electromagnetic field on the variables of the electron-positron field, or the reverse. If this is true, it seems somewhat pointless to use a formalism which contains other, unwanted effects, which must later be subtracted. A formalism has been developed in which a quantized electromagnetic field is allowed to act on the electron-positron field, but the motion of the quantized field is not affected by the charge-current vector. Instead, the interaction of particles is accounted for by a time-symmetric, unquantized interaction plus the quantized "free" field. The spontaneous emission probability is given in a trivial way. It seems likely that an improved treatment of the electron-positron field can be given along the same lines. For lack of such a treatment, however, the time-symmetric subtraction for the induced charge and current, previously described by this author,[1] has been used to accomplish the same result in a natural fashion. The mean-square fluctuation in position for a free electron is being calculated according to this formalism, and the result for the Lamb shift will be reported.

[1] T. A. Welton, Phys. Rev. 75, 1321 (1949).

H3. Internal Coordinates of a Particle. H. C. CORBEN, *Carnegie Institute of Technology.*—If we ascribe to a particle four internal coordinates X^α and conjugate momenta P_α and suppose the particle to be a four-dimensional oscillator, its internal state $\psi(X^\alpha)$ is an eigenfunction of $(P_\alpha P^\alpha+s)\psi=m^2\psi$, where $s=X_\alpha X^\alpha$, the unit of length λ being related to the force constant of the oscillator. For $s>0$, well-behaved solutions for $l=0,\ \frac{1}{2},\ 1,\ \frac{3}{2},\ 2$ are $(\psi_{nl})_{\alpha\beta\ldots}=\Pi_{\alpha\beta\ldots}s^le^{-s/2}L_{n+l}^{2l+1}(s)$, where $\Pi_{\alpha\beta\ldots}$ is the product of $2l$ unit orthogonal four vectors and $n+l$ is an integer $\geqslant 2l+1$. For given n, there are four independent solutions for $l=\frac{1}{2}$, six for $l=1$ etc., with parity $(-1)^{2l}$. If an internal spin operator is defined by $L_{\alpha\beta}=\frac{1}{2}(X_\alpha P_\beta-X_\beta P_\alpha)$ these correspond to particles of spin $l\hbar$. The exponential factor indicates that the particle is spread out in the neighborhood of the light cone through its center by an interval of order λ, requiring for its complete specification the ingoing and outgoing waves physically needed to observe it. The eigenvalues m are $2\pi(n'+l)^{\frac{1}{2}}e^2\lambda^{-1}c^{-2}$, where n' assumes positive integral values. The stable elementary particles do not fit into this simple model and it is not possible from this to determine λ.

H4. The Spin Dependence of Nuclear Forces. ALEX E. S. GREEN, *University of Cincinnati.*—If two fermions are coupled five vectorially (scalar+four vector) with a five vector field then the chief explicit interaction will be $V_{ab}=(1-\beta_a\beta_b-\boldsymbol{\alpha}_a\cdot\boldsymbol{\alpha}_b)J$. This simple Diracian form has the following interesting properties: (a) The non-relativistic terms cancel; (b) Its Pauli equivalent to the order v^2/c^2 contains static, spin-spin, and tensor interactions as well as velocity dependent interactions; (c) The detailed physical conclusions deduced from it will be very sensitive to effects which are small compared to J. Numerous possible small effects will be discussed. Some of them lead to interactions which appear suitable for nucleons. Thus the strong spin dependence of nuclear forces may be due to relativistic forces which become important if the large non-

relativistic forces tend to cancel. Although conceptually simple this approach unfortunately brings to the fore the host of unsolved problems associated with relativistic effects. The greatest of these, namely the divergent interactions and infinite self energies, do not arise however, if J is our generalized meson potential (Phys. Rev. in press).

H5. Internal Pair Formation. M. E. ROSE, *Oak Ridge National Laboratory.*—The electron-positron angular correlation and total conversion coefficient has been calculated for internal pair formation and for arbitrary multipole order of the electric and magnetic radiation fields. The Born approximation is used and in the region of greatest experimental interest, $Z \lesssim 40$ and gamma-ray energy $\lesssim 2.5$ Mev, the consequent error should be negligible. Numerical results for multipole fields of order 2^l with $l=1-5$ show that the ratio of total number of pairs formed with the angle between the particles equal to 0 (or a convenient small angle) and $\pi/2$ is sufficiently sensitive with l to determine multipole order. The total pair formation coefficient, in the region of interest, is of order 10^{-3} but is not quite so sensitive with l.

H6. Positon Theory. FREDERIK J. BELINFANTE, *Purdue University.*—From the conventional expressions of Dirac's electron theory for charge, energy and momentum densities and currents, in positon theory usually certain trivial infinite c-numbers are subtracted. For the proof of the Lorentz-invariance of the commutation relation in the quantum theory of wave fields, one often makes use of the fact that infinitesimal Lorentz-transformations can be represented by commutations with a certain operator. The commutation of a c-number with such operator, however, gives zero. Thus the infinite c-numbers subtracted in positon theory would behave like scalars, contrary to the tensor-behavior of the quantities in question. Thus these quantities cannot properly be considered as behaving like tensors both with *and* without subtraction. Fortunately, a direct check shows their correct tensor behavior *after* these subtractions. Statements about the transformation-behavior of the conventional *un*corrected expressions may then be considered as meaningless, since those quantities themselves by their divergence are meaningless. It might only be objected that also *after* the subtraction of these *trivial* infinities so many *other* infinities remain to be subtracted by some of the *ad hoc* methods proposed for such purposes, that even the proof of the tensor-character of the "corrected" expressions remains doubtful.

H7. Capture of μ^- Mesons by Deuterons. IRVING STEIN AND L. I. SCHIFF, *Stanford University.*—An investigation of the capture reaction of a μ^- (light) meson by a deuteron to yield two neutrons and a neutrino has been started, with the object of determining the dependence of the absolute rate of reaction and the emitted neutron spectrum on the meson coupling, the neutron-proton interaction and the neutron-neutron interaction. A preliminary result has been obtained, for the simplest case of scalar coupling when meson and neutrino are Dirac particles, under the assumption of zero range of nucleon interactions. Low but unequal neutron energies are favored in this case, and the life time for capture (ignoring decay) of a meson in its lowest Bohr orbit about a deuteron is about seven times that for a meson similarly bound to a proton.

H8. On the Vector Meson-Photon Interaction. GEORGE J. YEVICK, *Stevens Institute of Technology.*—Using the powerful methods developed by Feynman, we shall discuss the mass-term as the simplest illustration of these methods for the interaction between vector mesons and photons. The calculations are somewhat involved because of the complicated nature of the interaction Hamiltonian.[1] The relation of these considerations with the conventional second-order perturbation theory will be discussed.

[1] Kanesawa and Tomonaga, Prog. Theo. Phys. 3, 101 (1948).

H9. Nutation of the Nuclear Magnetic Moment.* ERWIN L. HAHN, *University of Illinois.*—Transient oscillations predicted by the quantum mechanical treatment[1] of a free spin in a large D.C. magnetic field H_0 and small perturbing r-f field H_1 have been experimentally confirmed in the liquid state using the method of nuclear induction.[2] An ensemble of spins, when suddenly subjected to an r-f field H_1 (which is left on) at angular frequency ω, behaves like a nutating classical macroscopic magnetic moment[3] if ω has the resonance value γH_0. In the coordinate system rotating at frequency ω a precession of the magnetic moment takes place about the r-f field H_1 (stationary in this system) at frequency $\omega_1=\gamma H_1$, which is seen as a nutation in the laboratory system. Nutation frequencies have been measured from as low as 5 c.p.s. up to 1 kc for the H^1 and F^{19} nuclei in various liquid compounds. The time rate of decay of the nutations gives information about spin-spin coupling within molecules, revealing the nature of the chemical bond, independent of external field inhomogeneities. For H_1 intensities sufficiently large, nutation signals with periods shorter than the phase memory time T_2 are larger in amplitude than steady state resonance signals.

* Work done under auspices of ONR.
[1] I. I. Rabi, Phys. Rev. 51, 652 (1937).
[2] Bloembergen, Purcell, and Pound, Phys. Rev. 73, 679 (1948).
[3] N. Bloembergen, *Nuclear Magnetic Relaxation* (Monograph published by Martinus Nijhoff, The Hague, 1948).

H10. Nuclear Gyromagnetic Ratios. WILLIAM H. CHAMBERS AND DUDLEY WILLIAMS, *Ohio State University.*—Using the super-regenerative oscillator techniques described in earlier reports, we have observed radiofrequency resonance absorption peaks for Be^9, P^{31}, Cl^{35}, Rb^{85}, Cs^{133}, and La^{139} in a magnetic field in which the proton resonance is observed simultaneously. Preliminary results are given below:

Nucleus	Resonance Frequency / Resonance Frequency of Proton
$_4Be^9$	0.14034 ±0.00007
$_{15}P^{31}$	0.40498 ±0.00011
$_{17}Cl^{35}$	0.09799 ±0.00007
$_{37}Rb^{85}$	0.09661 ±0.00004
$_{55}Cs^{133}$	0.13093 ±0.00014
$_{57}La^{139}$	0.14116 ±0.00014

H11. Proton-Proton Scattering Experiment at 250 Mev. CHARLES L. OXLEY, *University of Rochester.*—Apparatus has been developed for use in the tank of the Rochester synchro-cyclotron to measure proton-proton scattering with the undeflected beam. A polyethylene target is used with coincidence counters detecting the scattered and recoil $p-p$ protons according to the scheme of Wilson and Creutz.[1] The counters are of scintillation type with light pipes to phototubes in the region of low fringing field. A measure of the incident beam of protons is obtained by observing the beta activity induced in the target by the reaction[2,3] $C^{12}(p, pn)C^{11}$. Preliminary experiments at full cyclotron energy (240 Mev) and at a laboratory scattering angle of forty-five degrees show that the $p-p$ scattering is detected efficiently against background. Cross sections relative to the carbon cross section will be presented. The apparatus is being redesigned to cover a range of scattering angles. Provision will also be made to move the target and counters to smaller cyclotron radii, thus covering the energy range down to about 100 Mev. This work is supported by the joint program of the ONR and AEC.

[1] R. R. Wilson and E. C. Creutz, Phys. Rev. 71, 339 (1947).
[2] W. W. Chupp and E. M. McMillan, Phys. Rev. 72, 873 (1947).
[3] E. M. McMillan and R. D. Miller, Phys. Rev. 73, 80 (1948).

H12. Self-Absorption and Backscattering of Soft Beta-Radiations.* L. E. GLENDENIN, *Massachusetts Institute of Technology*, AND A. K. SOLOMON, *Harvard Medical School.*—Self-absorption and backscattering effects of the soft β-radiations of S^{35} (0.17 Mev) and Ca^{45} (0.26 Mev) have been investigated, using isotopes obtained from Oak Ridge. By comparison of weightless sources evaporated on thin collodion films ($\sim$20 μg/cm^2) with identical sources on "infinitely thick" backings of various metals (Be, Al, Fe, Cd, Pb), the variation of backscattering with atomic number was determined. As first noted by Yaffe, a marked increase (factor of $\sim$1.5) in backscattering was observed when the source was evaporated directly on the metal surface as compared with an equal source first evaporated on a thin collodion film and then placed against the metal, e.g., for S^{35} on Pb a backscattering effect of 90 percent was obtained in the former case as compared with 60 percent in the latter. Self-scattering (internal backscattering) as a function of the average atomic number of the sample was also determined for S^{35} by intercomparison of the counting rates of thick samples of benzidine sulfate (average $Z=4.5$), $BaSO_4$ (average $Z=17.3$), and $PbSO_4$ (average $Z=21.7$). The self-scattering effect is in approximate agreement with the backscattering curve for sources evaporated directly on metals. The self-absorption coefficient for Ca^{45} in $CaCO_3$ mounted on glass, Al, Fe, and Cu is 0.09 ± 0.01 cm^2/mg. The coefficient for S^{35} in benzidine sulfate mounted on Be ($Z=4$) is uniformly 0.18 ± 0.01, whereas on Al ($Z=13$) the coefficient is initially 0.22 ± 0.01 (due to enhanced reflection by the Al), dropping to 0.18 for sample thicknesses >6 mg/cm^2.

* This work has been supported in part by ONR and AEC.

H13. The Lifetime of Positrons in Matter. JAMES W. SHEARER AND MARTIN DEUTSCH, *Massachusetts Institute of Technology.*—Delayed emission of annihilation radiation has been observed when positrons from Na^{22} are stopped in various gases. The time of creation of each positron was marked by the 1.3 Mev nuclear gamma-ray from Na^{22}. Delay times between 1.8×10^{-7} and 6×10^{-7} sec. were used. Preliminary results for the mean life τ are listed below together with the apparent electron cross section σ in terms of $\sigma_0=\tau r_0^2 c$. The fact that σ has about twice the Born approximation value σ_0 is probably due to the attraction between positron and electron. The tendency for σ to decrease with increasing pressure may be connected with the slowing down mechanism at very low energies or perhaps to the formation of positronium:

Gas	$\tau\times10^7$	σ/σ_0
N_2 0.5 atm.	2.6 ± 0.3	2.8
1 atm.	1.5 ± 0.15	2.4
2 atm.	1.0 ± 0.15	1.8
A 0.5 atm.	2.9 ± 0.6	1.9
1 atm.	1.6 ± 0.3	1.8
2 atm.	1.3 ± 0.2	1.1
CH_4 1.5 atm.	1.3 ± 0.15	2.7

* Supported in part by the joint program of the AEC and ONR.

H14. Multiply Scattered γ-Rays: Angular Distribution.* L. V. SPENCER AND FANNIE JENKINS, *National Bureau of Standards.* (Introduced by U. Fano.)—In an investigation of the angular distribution of multiple scattered gamma-rays, the case of an infinite medium filled uniformly with a mono-directional source is considered. The solution is given by an expansion in zonal harmonics the coefficients of which are determined by solving integral equations of the following form: $\mu(\lambda)N_l(\lambda)=\int^{\lambda}_{\lambda_0}d\phi_{\lambda'\lambda}N_l(\lambda')P_l(1-\lambda+\lambda')d\lambda'+P_l(1-\lambda+\lambda_0)d\phi_{\lambda_0\lambda}$, where λ is the wave-length in compton units, $d\phi_{\lambda'\lambda}$ is the differential compton scattering cross section, $N_l(\lambda)$ is the coefficient of the l'th harmonic, and $\mu(\lambda)$ is the total absorption coefficient. Numerical computations have been made for aluminum, $\lambda_0=0.1$. These show that the solution for $\lambda>2$ has a maximum approximately at $\theta=\cos^{-1}\times(-3+\lambda-\lambda_0)$ which behaves like a wave traveling back and forth between the poles as λ increases, superposed on a continually increasing isotropic distribution. A simple qualitative explanation can be given for this result. Computations for heavier materials are in progress.

* Work supported by an ONR grant.

Nuclear Physics, Mostly Neutron Physics

J1. A Search for Some Rare Stable Isotopes.* HENRY E. DUCKWORTH, ROBERT F. BLACK, AND RICHARD F. WOODCOCK, *Wesleyan University.*—The Wesleyan University double-focusing mass spectrograph has been used to search for rare stable isotopes of a number of the heavier elements. A brief description will be given of the mass spectrograph and of the experimental procedure employed in this search. Mass spectra will be shown for zirconium, palladium, tellurium, gadolinium, tungsten, and lead.

* This work has been done under contract with the AEC.

J2. Nuclear Energy Levels in N^{15} and N^{16}. L. D. WYLY, *Yale University.**—The reported mass values for N^{16} have shown large discrepancies as determined from the β-decay of N^{16} and from the $F^{19}(n\alpha)N^{16}$ reaction. Ammonia, enriched to 61.5 percent in N^{15}, has been bombarded with deuterons to obtain the Q values of the $N^{15}(dp)N^{16}$ reaction. A ground state Q value of 0.21 ± 0.15 Mev was obtained, thereby giving a N^{16} mass of 16.01121 ± 0.00023 MU. The Q values for the associated $N^{14}(dp)N^{15}$ reaction were also determined and are listed in Table I, together with the relative intensity as obtained at 90° for a deuteron energy of 3.32 Mev.

TABLE I.

Mev	Relative intensity
8.61 ± 0.1	1
3.29 ± 0.1	5
2.30 ± 0.1	2
1.38 ± 0.1	25.0

* Assisted by the Joint Program of the ONR and the AEC.

J3. The Reactions $N^{14}(n,p)C^{14}$ and $He^3(n,p)H^3$ and the Neutron-Hydrogen Mass Difference. W. FRANZEN,[1] J. HALPERN, AND W. E. STEPHENS, *University of Pennsylvania.*[2]—The pulse height distributions arising from the reactions $N^{14}(n,p)$ and $He^3(n,p)$ induced by slow neutrons have been studied in a cylindrical ionization chamber containing a purified mixture of 2 atmos. A$+\frac{1}{10}$ atmos. $N_2+\frac{1}{2}$ atmos. He ($He^3/He^4=4.9\times10^{-5}$). The distributions due to $N^{14}(n,p)$ and $He^3(n,p)$ are well resolved, the ratio of total ionizations being 1.217. In a separate experiment, the ratio of the total ionizations due to $N^{14}(n,p)$ to that of Po-α-particles was found to increase by 3 percent as the concentration of N_2 in nitrogen-argon mixtures was increased from 10 percent to 100 percent. If proportionality between energy and total ionization in pure argon is assumed, the energy equivalent of the ionization produced by $N^{14}(n,p)$ compared to that produced by Po-α-particles is 628 ± 4 kev, whereas a similar comparison for $He^3(n,p)$ yields 764 ± 10 kev. The ratio of these values agrees with the ratio of the total ionizations due to the two reactions obtained when observed simultaneously, and their difference agrees with the β-end points of C^{14} and H^3. If possible systematic errors due to the assumption of a constant energy per ion in argon are disregarded and the ionization is assumed to give the Q values for the reactions, these results give $n-H=783\pm4$ kev, in good agreement with several recent measurements.

[1] Mary Amanda Wood Research Associate.
[2] Supported partly by the joint program of the ONR and AEC and aided by a grant from the Committee on Advancement of Research of the University of Pennsylvania.

J4. Neutron Distributions in Cylindrical Geometry. HENRY FAUL AND CLARK GOODMAN, *Massachusetts Institute of Technology.**—Thermal and cadmium difference neutron distributions from a 1-g Ra-Be source have been measured with indium detectors in pipes (4 to 8 in. in diameter) surrounded by water and by brines of various concentrations (effectively infinite media). The results are of interest in the design of orifices in nuclear shields and in the logging of oil wells. The axial neutron distribution in the empty pipes is closely approximated by a simple exponential at distances greater than 15 cm from the source. Slowing-down and absorption in an average barite drilling mud and in water are almost identical. A 2-in. layer of water (or mud) between the logging probe and the geological formation effectively obscures the influence of the formation, and two $\frac{1}{4}$-in. layers of iron separated by $\frac{1}{4}$ in. of water produce a similar effect. Two coaxial iron pipes (4-in. and 5-in.) surrounded by saturated brine reduce the thermal distribution to within a few percent of the resonance flux. The net hydrogen content of the formation can be estimated roughly from the resonance data. A single probe can be designed to measure the intensity and slope of both thermal and epithermal neutron distributions. The high thermal capture cross section of chlorine permits identification of brine in a reservoir rock behind casing under favorable conditions.

* This is a joint undertaking of the Massachusetts Institute of Technology and the ONR.

J5. Determination of the Phase of Scattering of Neutrons and of Incoherent Residual Scattering Cross Sections. P. J. BENDT AND I. W. RUDERMAN, *Columbia University.*—The phase in which neutrons are scattered by various elements, and the coherent scattering cross sections of these elements, have up to now been obtained principally by measurements of the intensities of Bragg reflections from suitable crystals. For such measurements a crystal spectrometer and an intense neutron source such as a pile are needed. We wish to point out that similar information can be obtained more readily and directly from transmission experiments. In a typical experiment, the Columbia neutron velocity spectrometer was used to obtain transmission curves for two pure elements and for a substitutional solid solution of the two, for neutron wave-lengths up to and beyond the cut-off wave-length for Bragg reflections, λ_c. The cross section *vs.* neutron wave-length curves in the region beyond λ_c, when extrapolated to zero wave-length, give directly the residual incoherent scattering cross sections, σ_r. The temperature-dependent part of σ_r may be determined by repeating the transmission experiments at liquid nitrogen temperature. The value of σ_r for the solid solution shows whether the two constituent elements scatter neutrons in the same or in opposite phases, and gives information about order-disorder in the alloy. The Cu-Ni, Mn-Ni, and Mn-Fe systems are now being studied.

J6. Reflection of Neutrons from Magnetized Mirrors. D. J. HUGHES AND M. T. BURGY, *Argonne National Laboratory.*—In a recent investigation of small angle scattering of neutrons in iron[1] the observed deviations were explained as the magnetic refraction of neutrons at domain boundaries. According to this explanation there should be two indices of refraction for neutrons in iron, and the possibility exists of demonstrating this double refraction in a more striking way and of using it for the production of polarized neutrons. The present work was designed to measure the indices of refraction in iron by obtaining two critical angles for reflection from an iron mirror and to investigate the possibility of producing highly polarized beams of neutrons by reflection. BeO-filtered neutrons (4.4A) were used to increase the expected critical angles to 14.2 and 30.7 minutes for the two spin states. The two critical angles have been observed and are in good quantitative agreement with theory. The reflection as a function of magnetization direction shows that the classical electron-neutron interaction originally used by Bloch[2] is incorrect. Reflection of the polarized neutrons produced by one magnetized mirror have been reflected from a second mirror to measure the polarization.

[1] Hughes, Burgy, Heller, and Wallace, Phys. Rev. **75**, 565 (1949).
[2] F. Bloch, Phys. Rev. **50**, 259 (1936); **51**, 994 (1937).

J7. Neutron Spectra from (p, n) Reactions with 16-Mev Protons.* P. C. GUGELOT AND M. G. WHITE, *Princeton University.*—By means of track length measurements of proton recoils in photographic emulsions neutron spectra are obtained from different elements bombarded by 16-Mev protons. About 1-Mev thick targets of Be, Al, Fe, and Au have been investigated. For each reaction *ca.* 2000 tracks are measured and special exposures made to obtain information about the background of scattered neutrons which might distort the spectra and to be able to estimate the reliability of the method. The neutron spectra can be represented by $dN/dE=\text{const.}\times Ee^{-E/kT}$ for neutron energies $E>2$ Mev. The values for kT decrease from 2.4 Mev for Be, 1.1 Mev for Al, 0.94 Mev for Fe to 0.77 Mev for Au. The Be neutron spectrum consists of two parts; for neutron energies >4.5 Mev, $kT=2.4$ Mev and for neutrons slower than 4.5 Mev, $kT=0.9$ Mev. A preliminary exposure with a Be target bombarded by 8-Mev protons indicates that kT may decrease with decreasing energy of the incoming proton. This behavior may show that properties other than the level-density of the residual nucleus are necessary to explain the general form of these spectra.

* Supported in part by the Joint Program of the ONR and the AEC.

J8. Evidence for Broad Nuclear Energy Levels in Lead.* R. K. ADAIR, H. H. BARSCHALL, C. K. BOCKELMAN, R. L. HENKEL, AND R. E. PETERSON, *University of Wisconsin.*—The total neutron cross section of lead was measured over an energy range of from 30 to 750 kev, using an energy spread of 10 kev. Certain interesting energy intervals were investigated with an energy resolution of about 5 kev. The cross section was determined by means of simple transmission measurements as previously described.[1] The lead cross section diminishes from 12 *b* at 30 kev to 6 *b* at 750 kev. Three distinct peaks were resolved, which appear to have a natural width of the order of 5 kev. They are attributed to elastic scattering resonances, most likely resulting from energy levels in Pb^{209}, the compound nucleus formed from the closed shell nucleus Pb^{208}. Two of the peaks, at 350 and 525 kev, are preceded by dips, explained as the result of destructive interference between resonance and potential scattering. No evidence was found for such a dip before the 725-kev peak. No peaks were found in bismuth, which was surveyed from 30 to 600 kev with a neutron energy spread of 10 kev.

* This work was supported in part by the AEC.
[1] Adair, Barschall, Bockelman, and Sala, Phys. Rev. **75**, 1124 (1949).

J9. Fast Neutrons from Bombardment with the Cyclotron Particles.* A. J. ALLEN AND J. F. NECHAJ, *University of Pittsburgh*, AND K. H. SUN AND B. JENNINGS, *Westinghouse Research Laboratories.*—The total fast neutron yield, N, from thick Be, Al, Cd, Au, and Bi targets bombarded by 15-Mev deuterons, measured with a $S^{32}(n, p)P^{32}$ detector,[1] was found to be $(19, 6.4, 1.2, 0.22, \text{and } 0.14)\times 10^9$/sec./$\mu$A, respectively. As a rule of thumb, N may be estimated within a factor of two from the nuclear charge, Z, of the target by the relation: $\log N=10.25-0.022Z$. The angular distribution (0° to ±160°) shows a pronounced forward peak with angular widths at half-intensity of 42°, 42°, 98°, 102°, and 119° respectively (in the laboratory system). The total yields for <7.5-Mev protons and 30-Mev alphas on thick Be are $(0.086 \text{ and } 14)\times 10^9$/sec./$\mu$A and the angular widths 70° and 80°, respectively. The presence of a strong peak in the forward direction only is common in all cases studied, irrespective of the type of bombarding particles

and target. These measurements are being extended to targets of other monoisotopic nuclei as well as commonly used elements.

* Assisted by ONR, AEC, and Research Corporation.
[1] Allen, Nechaj, Sun, and Jennings, Bull. Am. Phys. Soc. **24**, No. 4, 36 (1949).

J10. Neutron Spectrum from $N^{15}(d, n)$.* EMMETT L. HUDSPETH AND CHARLES P. SWANN, *Bartol Research Foundation.*—Gas targets of normal and of N^{15}-enriched N_2O have been bombarded with 1.2-Mev deuterons, and the neutron spectra have been observed on photographic plates placed at 0° to the bombarding beam. Two groups previously reported[1] from $N^{14}(d, n)$ were observed, with evidence for the production at our bombarding voltage of a third group of lower energy. Neutron groups from $N^{15}(d, n)$ were observed at 11 Mev and at approximately 4.5 Mev. The latter group was broader and several times as intense as the group at 11 Mev. There is evidence for a third group at 2.5 Mev, but it may belong entirely to the N^{14} reaction. Excited states of O^{16} in the vicinity of 6.5 Mev are well known from studies by other experimenters of the reaction $F^{19}(p, \alpha)$ and from the β-decay[2] of N^{16}. Our results reveal these levels (unresolved), and no lower excited state is observed.

* Assisted by the Joint Program of ONR and AEC.
[1] Stephens, Djanab, and Bonner, Phys. Rev. **52**, 1079 (1937).
[2] H. S. Sommers, Jr., and R. Sherr, Phys. Rev. **69**, 21 (1946).

J11. Isotopic Spectra of Lead. THURSTON E. MANNING, *Yale University.*—Using a sample[1] of lead sulfate from lead enriched to 27 percent in the isotope 204, the isotopic shifts of several blue and ultraviolet lines in the spectrum of neutral lead have been examined. The source used in these investigations, a hollow cathode tube especially designed to use and conserve small amounts of valuable material, will be described. The shifts are of the order of 0.08 wave numbers between successive even isotopes. Analysis with a crystalline quartz Lummer plate of 200-mm length and 7.34-mm thickness shows that the 204–206 shift is in some cases smaller than the 206–208 shift by perhaps 10 percent of the smaller (e.g., for λ4058 the shifts are 0.07 and 0.08 wave numbers). Such results confirm conclusions previously drawn from shifts of the odd-numbered isotopes that the isotopic shifts in heavy elements cannot be explained in any case by the mass difference alone, as has sometimes been suggested; the results will be discussed from the viewpoint of the nuclear volume effect utilized by Rosenthal and Breit.

[1] Supplied by the Carbide and Carbon Chemicals Corporation and allocated by the Isotopes Division, U. S. AEC.

Papers Not Classed Elsewhere

K2. Extinction Coefficients for Oxygen in the Schumann Region. R. J. LANG AND A. R. J. STEPHENSON, *University of Alberta.*—Absorption measurements have been made in oxygen up to pressures of one atmosphere in the region between 2050 and 1600A by means of a 3-meter vacuum spectrograph. The gas was contained in a Pyrex glass cell with fluorite ends which was placed just behind the slit. The source used was a spark in an atmosphere of nitrogen, and a spectrum very rich in lines was obtained from tungsten steel electrodes. Most of the known bands of oxygen in the region were found and a few new members. By using the oxygen at different pressures it is found that Beer's law does not hold.

K3. On Exchange Energy in He_3 Assemblies. LOUIS GOLDSTEIN AND MAX GOLDSTEIN, *Los Alamos Scientific Laboratory.*—An account will be given of a series of studies on the role of the identity exchange energy in He_3 assemblies at liquid He_3 densities. Using, at the highest density, assumedly near the one realized at absolute zero, the free atom individual wave functions together with the well-known He-He mutual potential energy, one finds that the exchange energy alone favors the parallel alignment of all the nuclear spins (the latter being $\hbar/2$). However, the smaller free particle kinetic energy associated with the state of balanced spins as compared with the same quantity in the all-spin parallel state compensates, in this crude model, for the favorable all-spin parallel exchange energy excess over the balanced spin state exchange energy. Hence, in this free particle approximation liquid He_3 has no nuclear ferromagnetism. Clearly, no definite conclusion can be drawn from the free particle model as to the actual magnetic properties of liquid He_3. Other He models are being studied.

K4. Rotational Dispersion of Ultrasonics in Deuterium and Hydrogen.* JAMES L. STEWART AND ELLEN S. STEWART, *Rutgers University.*—Dispersion in the velocity and the associated absorption peak for ultrasonics, caused by the failure of the rotational degrees of freedom to follow the temperature cycle, were observed first in hydrogen and have now been discovered in deuterium. Measurements at 303°K in commercial deuterium ($\simeq$0.5 percent impurity) show that the dispersion starts at four megacycles per atmosphere and continues to about 100 Mc/atmos., the velocity increasing 9 percent above the classical value. These determinations were made using a variable-path ultrasonic interferometer with a crystal of frequency 1.95 Mc. The pressure was varied from one atmosphere to 0.02 atmos. The dispersion region centers about 20 Mc/atmos. compared with less than 10 Mc/atmos. for purer hydrogen. The authors have also found a marked dependence of the dispersion frequency on very small amounts of impurity in the case of hydrogen. This probably applies to deuterium also, making any comparison between the two premature until the large amount of impurity in deuterium has been removed. Since the hydrogen impurity in deuterium, which amounts to 0.2 percent, cannot be readily removed, it may limit the significance of any comparison. Quantitative data on the deuterium and hydrogen velocity and absorption curves will be presented and their theoretical interpretation discussed.

* This work was supported by the Rutgers University Research Council.

K5. Bioelectric Potential Transients Accompanying Closing Movements of the Lobes of Venus' Fly-Trap. OTTO STUHLMAN, JR., *University of North Carolina.*—The method used for measuring the bioelectric potentials is a modified Wheatstone bridge arrangement designed by Burr, Lane, and Nims for measuring slow changes in mammalian potentials. Contact potentials of the electrodes across which the bioelectrical potentials are measured was minimized by using a pair of Ag-AgCl reversible electrodes in dilute KCl, terminating in a glass capillary containing a small asbestos-fiber wick, which served as the contact electrode on the surface of the plant where the e.m.f. originated. Closure of the trap-like structure at the end of the spatulated petiole of Venus' Fly-Trap normally follows when any one of the spike-like trigger hairs or the irritable inner epidermis is stimulated. The speed of closure depends on the pattern of excitation, which was hypothesized to originate as a localized destruction of the degree of polarization, which progressively spreads as an equipotential electrical wave front, propagated over the surface of the lobe at about 3.0 cm per sec. The excitatory wave front was found to be a negative potential of about 0.05 volt for summer growth or as low as 0.01 volt for winter growth plants. It is measurable as a diphasic or monophasic potential pulse depending on the position of the nonpolarizable electrodes. The exact shape, speed, and origin of the electrical impulse is being explored with the aid of an oscillograph.

K6. Solar Position Calculator. DONALD W. DUNIPACE, *Libby-Owens-Ford Glass Company.*—The important effect of

the sun on our lives is well known. A primary factor in its influence is its position with respect to a given location on the earth. Two calculators have been developed which give geometric relations between the sun and various geographic locations for any time of the day and year. One calculator can be set up to give such quantities as altitude, air mass, direction, and angle of incidence on walls facing north, east, south, or west. This calculator consists of a transparent overlay on an opaque underlay, and the patterns can be constructed by using elliptical, circular, and straight lines. The other calculator gives angles pertinent to architectural designs. For accuracy, convenience, and speed of operation, these calculators are comparable to a slide rule.

K7. Pentode Counting or Control Ring.* BENJAMIN L. MOORE, *Harvard University.*—The 6AS6 pentode has a suppressor grid voltage plate current characteristic similar to that of the control grid, and has been used in a counting or control ring whose input is essentially independent of amplitude and wave shape. The basic element of this ring is two pentodes connected as a direct coupled type trigger pair using the screen grids as the plates. A number of these trigger pairs are arranged in a ring with the two tubes of each trigger pair opposite each other. The plate of each tube is connected to the screen of the next tube in the ring. If initially the first n tubes are conducting, then the next n tubes must be non-conducting. By applying positive pulses alternately to the suppressor grids of all odd tubes and then to all even tubes, the ring will step once for each pulse. Control voltages corresponding to one or more states of the ring may be obtained very easily.

* This work was supported by the Bureau of Ordnance, U.S. Navy.

K8. A Static Storage System Utilizing Magnetic Retentivity.* W. D. WOO AND AN WANG, *Harvard University.* (Introduced by B. L. Moore.)—Magnetic cores with a rectangular hysteresis loop[1] have been used in a storage system which requires no mechanical motion. The binary digit "1" is stored as a positive residual flux, and the binary digit "0" as a residual flux in the opposite direction. When a negative probing field is applied to the core, a large voltage is induced in another winding if the digit stored has been a "1," and very small voltage if it has been a "0." The induced voltage in the former case is large enough to magnetize another core of identical construction. Binary digits can thus be transferred from one core into another. If two such cores are arranged in a pair, one binary digit can be transferred back and forth between them. If many cores are arranged in series, binary digits can be advanced along the line. The present upper limit of the speed of propagation is about 30,000 to 40,000 digits per second, and there is no lower limit.

* This work has been supported by the United States Air Force.
[1] The cores are furnished through the courtesy of Allegheny Ludlum Steel Corporation.

K10. Ion Exchange and Chromatography. H. L. FINSTON AND R. M. DYER, *Ohio State University.*—The ion exchange techniques developed in the Manhattan project, and described in detail by Ketelle and Boyd[1] have been tried and found to yield excellent results with mixtures of rare earth activities of moderately long half-lives. The time involved in this procedure, however, made certain modifications necessary in order to work with activities of shorter half-life. It was found that a short column of "Dowex 50" could be extruded after first being frozen. A sample of Tm was bombarded for 6 hours with deuterons in the cyclotron, dissolved and adsorbed at the top of a column 21 cm long with a cross section of 0.28 sq. cm. The column was operated for 5 hours, and then extruded. The column was cut into short lengths and the distribution of activity determined. Four definitely different fractions were obtained. In another investigation the chromatographic method of separation described by Schwab and Jockers[2] has been applied to a separation of Cr, V, and Mn produced by a deuteron bombardment of Cr. Three fractions were obtained with characteristics corresponding to those of Cr, V, and Mn, respectively.

[1] Ketelle and Boyd, J. Am. Chem. Soc. 69, 2800 (1947).
[2] Schwab and Jockers, Angew. Chem. 50, 546 (1937).

K11. Use of the Density-Gradient Tube in the Study of Finely Divided Materials. WILLIAM H. OTTO, *Owens-Corning Fiberglas Corporation.*—A vertical linear density gradient is established in a glass tube by the diffusion of liquids or solutions of different density and can be maintained in a stable condition for prolonged periods. The device is particularly useful in the density determination of finely divided materials or samples of extremely low mass such as fine glass fibers and provides a means for the study of the density distribution of a mixed-density sample. The application of the density-gradient tube to the study of glass fibers is discussed with particular regard to density differences between the bulk glass and the glass fiber form.

K12. Presentation of Mass Spectra with a Cathode-Ray Oscillograph. J. W. TOWNSEND, JR., *Williams College.*—A new approach to electronic presentation of mass spectra with a cathode-ray oscillograph has been undertaken. Previously this has been achieved by sweeping the accelerating potential of the mass spectrometer with a sawtooth voltage, and detecting the resultant ion currents by means of d.c. or pulse amplifiers. In the new system, the rate of production of ions in a conventional Nier type 60° spectrometer is modulated by a 1000 c.p.s. voltage, and the ion current at the collector detected by a specially designed a.c. amplifier. This amplifier is composed of two parts, a low noise preamplifier employing a miniature "acorn" type pentode mounted as close to the collector as possible, and a main amplifier whose band pass is restricted to 100 c.p.s. by a feed-back network. The 10-c.p.s. sawtooth voltage, of sufficient amplitude to cover the desired range of masses, is synchronized with the horizontal sweep of the oscillograph, while the amplifier output is applied to the vertical plates. Results have been encouraging. It is possible to detect peaks as small as 4×10^{-14} ampere, with good linearity and resolution. The system has been especially valuable in adjusting and focusing the newly completed spectrometer.

Magnetic Resonance; Non-Metallic Solids

L1. The Optical Detection of Radiofrequency Resonance.* F. BITTER, *Massachusetts Institute of Technology.*—Calculations are made of the frequency, intensity, and polarization of the light emitted by an atom in a doublet P to a doublet S transition in a weak magnetic field having an oscillating component. Near resonance, or when the frequency of the oscillating component approaches the Larmor frequency of one of the two states involved in the radiation process, all of the quantities calculated are modified. Qualitatively similar results are to be expected for other transitions. Observations in very weak fields would be of particular interest because they would give information on nuclear as well as atomic g-factors. Under such conditions, the Zeeman components will, in general, not be resolvable, and the only observable effect will be a change in the polarization of the edges of a spectral line at resonance. It is further shown that very small changes in this polarization structure are theoretically detectable.

* This research has been supported in part by the Signal Corps, the Air Materiel Command, and ONR.

L2. Some Measurements of Nuclear Spin-Lattice Relaxation Times in Solids. E. H. TURNER, A. M. SACHS, AND E. M. PURCELL, *Harvard University.*—Nuclear spin-lattice relaxa-

tion[1] was studied as a function of field strength and temperature to obtain information about the relaxation mechanism in crystals. Relaxation times, T_1, greater than 5 seconds were found by observing at low power the growth of the center of a previously "saturated" absorption line. For T_1 less than 30 seconds, a saturation curve method[1] was used. For substances with a long T_1, the rate of approach to equilibrium at low fields was studied by adiabatic changes between the low field and a field suitable for measurements. Substances which were investigated include ice, benzene, and sucrose. One sample of ice had the longest T_1 observed to date: 210 min. at 88°K. Benzene exhibited a minimum in its T_1 *versus* temperature curve qualitatively similar to the minima described in the next paper. The T_1 of a single sucrose crystal was proportional to field strength and decreased fast with increasing temperature. Interpretation of the results will be discussed.

[1] Bloembergen, Purcell, and Pound, Phys. Rev. **73**, 679 (1948).

L3. A Study of Internal Motion in Ammonium Salts by Nuclear Spin-Lattice Relaxation Time Measurements. A. M. SACHS, E. H. TURNER, AND E. M. PURCELL, *Harvard University.*—Gutowsky and Pake* have reported sharp line-width transitions in ammonium salts at temperatures 100° or more below the specific heat anomalies. Using methods outlined in the preceding paper, we have measured nuclear spin-lattice relaxation times (T_1) of some ammonium salts from 85°K to 270°K at 14.2 and 30 mc/sec. Sharply defined minima of T^1 are found at temperatures from 45° to 75° above the line-width transitions, with the minima of the 30-mc/sec. curves occurring approximately 9° above those of the 14.2-mc/sec. curves. Assuming relative motion of protons as the relaxation mechanism, the characteristic time of this motion, τ_c, has been deduced from the general formula of Bloembergen, Purcell, and Pound** and the experimental data. The result is described by $\tau_c = A \exp(a/T)$. All of the data, including the temperature of the line-width transition, are consistent with a single choice of the constants A and a for each salt. For example, in NH_4Br, $a = 1700$ deg., $A = 1.2 \times 10^{-13}$ sec. A discussion will be given in terms of barrier penetration by NH_4 tetrahedra.

* H. S. Gutowsky and G. E. Pake, J. Chem. Phys. **16**, 1164 (1948).
** Bloembergen, Purcell, and Pound, Phys. Rev. **73**, 699 (1948).

L4. Measurements of Spin-Lattice Relaxation Times in Paramagnetic Solids by the Saturation Method. C. P. SLICHTER* AND E. M. PURCELL, *Harvard University.*—The measurement of spin-lattice relaxation times, T_1, in paramagnetic solids has been performed extensively at low temperatures by the study of absorption or dispersion at frequencies of the order of $1/2\pi T_1$.[1] We have extended the measurement of T_1 at room and dry ice temperatures by studying saturation in the absorption of microwave energy at the Larmor frequency in analogy to the experiments of Bloembergen, Purcell, and Pound.[2] The sample was held in a resonant cavity terminating one arm of a magic tee bridge. Since a pulsed magnetron was used to generate the high microwave magnetic fields (~30 gauss) needed to saturate the samples, slight modifications were made in conventional bridge techniques because of transient effects associated with the short pulses and high Q cavity. Relaxation times ($\sim 10^{-8}$ sec.) have been determined for manganese ammonium sulfate, manganese sulfate, and copper sulfate both at room temperature and at −78°C, and at room temperature for a free radical kindly supplied by the Bell Laboratories.

* Socony Vacuum Predoctoral Fellow in Chemical Physics.
[1] C. J. Gorter, *Paramagnetic Relaxation* (Elsevier Publishing Company, New York, 1948).
[2] Bloembergen, Purcell, and Pound, Phys. Rev. **73**, 679 (1948).

L5. Hyperfine Structure of the Paramagnetic Resonance Spectrum of Cobalt. B. BLEANEY AND D. J. E. INGRAM, *Clarendon Laboratory, Oxford.* (Introduced by E. M. Purcell.)—Following the discovery of Penrose[1] that the paramagnetic resonance spectrum of diluted copper potassium sulphate shows a hyperfine structure, measurements have been made on a mixed crystal of cobalt and zinc ammonium sulphate containing Co:Zn in the ratio 1:1000. The Co^{++} ion is found to have exact tetragonal symmetry within the experimental error, with a single electronic transition whose g-value varies from 3.0, perpendicular, to 6.2 parallel to the tetragonal axis. The absorption line is split up into eight unequally spaced components due to the nuclear spin (7/2) of Co^{59}. The over-all separation of the *h.f.s.* varies from 0.14 kg to 0.67 kg, having the same anisotropy as the crystalline electric field. The half-width at half-intensity of the lines is about 7 gauss, most of which is attributed to the protons of the water of crystallization. At 90°K the line width is about 1400 gauss, corresponding to a spin-lattice relaxation time of 7×10^{-12} sec. ($=\rho/2\pi$ in Gorter's[2] nomenclature).

[1] Penrose, unpublished owing to illness of author.
[2] J. Gorter, *Paramagnetic Relaxation*, Elsevier Publishing Company, New York, 1948).

L6. The Solids Condensed from Carbon Monoxide by Alpha-Particles. JOHN H. L. WATSON, *Edsel B. Ford Institute for Medical Research;* MARCEL VANPEE, *University of Minnesota;* AND S. C. LIND, *Carbide and Carbon Chemicals Corporation.*—An electron microscopic and x-ray diffraction study was made of the residues formed by bombardment by alpha-rays from radon of carbon monoxide gas. Carbon monoxide, when polymerized by alpha-rays from radon exhibits a particulate structure. The particles have recognizable shape and have nearly the same dimensions in all directions. There are two components in the residue. The first are solid particles which are rigid aggregates of graphitic flakes. The second is a viscous liquid material which surrounds the particles, may exist within them, and often joins them one to the other by short necks. The mean diameter of the material taken from the base of the flask is about 0.5 and from the neck of the flask about 0.41 micron. About 15 percent of the silhouette images of the particles appear hexagonal in shape. The percentage of particles having this shape is undoubtedly even higher than this, since non-hexagonal images often are accompanied by hexagonal shadows. The approximate uniformity of particle dimensions in all directions and the increase in particle size toward the base of the flask indicate that they are formed and grow in the gas phase, and that the larger ones fall out under gravity.

L7. Thermal Conductivity and Heat Capacity of Beryllium Carbide. CHARLES E. TEETER, JR., *Fairchild Engine & Airplane Corporation.*—Beryllium carbide is an interesting substance which has recently become available in laboratory quantities. Among its physical properties which are being studied at NEPA are thermal conductivity and heat capacity. The thermal conductivity of a hollow cylinder of beryllium carbide was measured in a preliminary fashion by a radial heat flow method. A central globar heater was used to raise the inside of the cylinder to temperatures up to 950°C (1740°F). This inside temperature, as well as the temperature of the outside, was measured by thermocouples and the thermal conductivity calculated by the conventional formula. Further experiments are continuing to improve the accuracy. The heat capacity of beryllium carbide in powdered form was measured by a modification of the so-called "drop method." Capsules of refractory metals (copper was first used, than stainless steel, and finally nickel) were heated in a furnace and dropped into a copper block in a water calorimeter. To correct for heat losses during the drop, empty capsules were heated to various temperatures, and dropped in a similar manner. Results were obtained for the enthalpy and mean heat capacity from room

temperature to 200–1100°C (392–2012°F). From the smoothed curve for the enthalpy, the heat capacity, C_p, was calculated.

L8. A Model for the Plastic Flow of Oriented Nylon Fibers. JOHN KAUFFMAN AND WALLER GEORGE, *Naval Research Laboratory.*—Studies of the changes in broadening shown by x-ray fiber patterns have been associated with the stress-strain relation for highly oriented Nylon fibers (Type 200). The angular broadening of the equatorial spots reduces with increasing strain up to the inflection point of the stress-strain curve. For larger strains this broadening increases at a decreasing rate. The radial broadening of these spots remains essentially constant up to the strain at the inflection, then increases at a decreasing rate to rupture. Assuming a crystallite model, these data indicate that the initial straining is accompanied by the rotation of crystallites toward positions parallel to the fiber axis. This process appears to terminate in the inflection region of the stress-strain curve and is replaced by a process of crystallite breakup. The broadening in the later phase of straining is analogous to that found recently by Patterson and Orowan[1] for aluminum and copper deformed in torsion.

[1] Patterson and Orowan, Nature **162**, 991 (1948).

L9. X-Ray Analysis of Clays for Quantity of Montmorillonite. L. H. SIMONS,[1] D. F. WEEKES, AND J. G. POTTER, *A. and M. College of Texas.*—The crystalline structure of montmorillonite, $(Al_2O_3, Fe_2O_3, 3MgO)\cdot 4SiO_2 + nH_2O$, is laminar, permitting water to penetrate between unit layers, and add to the structure in a stepwise manner, sometimes to the extent that the volume is increased by a factor of thirty. The characteristically large variation in basal spacing with moisture permits the positive identification of montmorillonite by x-ray diffraction methods but has made difficult its quantitative determination by such methods. No other satisfactory method for the quantitative analysis of montmorillonite in clays is known. A sequence of treatments has been developed in this laboratory whereby the basal spacing of montmorillonite in clays can be stabilized to an extent that quantitative analyses can be made with a Geiger counter recording x-ray diffraction spectrometer. The treatments involve calcium saturating the sample, dehydration, and then bringing the sample to a reproducible moisture content in a humidifier employing sodium tartrate as the humidifying agent.

[1] Now at Humble Research Laboratory.

L10. On the Vibrational Spectrum of Crystals. W. A. BOWERS, *University of North Carolina.*—A formula has been derived for the distribution of frequencies of transverse vibrations of a plane square lattice, with nearest and next-nearest neighbor interactions. Although this case is of no direct physical significance, it is interesting as a check on the various methods of approximating the crystalline frequency distribution which have been proposed. We find that the numerical methods used by Blackman,[1] and later by Fine, Leighton, and others give a good approximation; the method of Montroll,[2] which is based on a calculation of the moments of the distribution function, also gives a reasonable approximation; but the method recently proposed by Houston[3] introduces spurious peaks into the distribution function which seriously distort its shape. We find also that in this two-dimensional case, the only peak in the distribution diverges only logarithmically instead of in the inverse square root fashion found in the linear chain. In the case of a three-dimensional crystal with vibration into a fourth dimension or degree of freedom (physical nature unknown!) we find no infinities at all.

[1] M. Blackman, Proc. Roy. Soc. **148**, 365, 384 (1935).
[2] E. Montroll, J. Chem. Phys. **10**, 218 (1942); **11**, 481 (1943).
[3] W. V. Houston, Rev. Mod. Phys. **20**, 161 (1948).

L11. Studies of the Vibrational Characteristics of a Piezoid.* CHARLES R. MINGINS, CARL A. STEVENS, AND DAVID W. MACLEOD, JR., *Tufts College.*—The characteristics of a vibrating piezoelectric crystal are investigated by means of a system of applying mechanical constraints to the surfaces with a probing device, meanwhile observing the variations produced with a response spectrometer. Different manners of mounting the plate and of providing the exciting field require different arrangements for scanning with the probing mechanism. Many modes of the thickness-shear family for rotated-Y cuts of quartz have been studied by this method. The 1,1,3 and 1,3,1 modes of this family are generally found to be very pronounced, but the coupling of these with other modes, such as certain of the higher orders of face shears and $X_{y'}$ flexures, does not have any appreciable effect upon the functioning of the principal mode. Plates of various shapes have been studied, and different cuts are receiving attention. Other methods of investigation are used to supplement and to check the results.

* This work is sponsored by the Frequency Control Branch of the Signal Corps.

L12. Dynamic Measurement of Electro-optic Coefficients in ADP Crystals. R. O'B. CARPENTER, *Baird Associates, Inc.*—Both the electro-optic coefficients r_{41} and r_{63} in ammonium dihydrogen phosphate crystals have been measured as a function of wave-length. Although r_{63} has been measured in several tetragonal crystals by various workers, r_{41} has not been observed, except by Dr. Hans Jaffe of the Brush Development Company of Cleveland, because the small effect is largely masked by the natural birefringence. Under a field in the x direction of 6 kv/cm, the "fast" and "slow" directions of vibration are rotated 5×10^{-4} radian, while the change in $n_1 - n_2$ is a very small effect proportional to the square of the field. By applying an alternating field to a crystal in a suitably arranged polarimeter, the rotation of the vibration direction introduces a small modulation in the transmitted light intensity, which is detected by a photo-cell and sharply tuned amplifier. The equipment is capable of detecting a rotation of 10^{-7} radian, or, in a different optical arrangement, a retardation change of 10^{-7} wave, which is considerably more sensitive than visual optical compensator methods. Other crystals are being obtained for measurement and a program of frequency response measurements is being undertaken. The coefficient e_{63} in ADP measured at frequencies above the piezoelectric fundamental vibration frequency is about one-half the low frequency value. The difference is accounted for by the piezoelectric deformation at low frequencies and the photoelastic effect, using the presently accepted values for these coefficients.

Cosmic Rays; Nuclear Emulsions

P1. Cosmic-Ray Variations at High Altitudes Resulting from Meteorological Variations.* W. F. G. SWANN AND STEPHEN H. FORBES, *Bartol Research Foundation.*—K. M. Kupferberg has called attention to latitude and seasonal variation of cosmic-ray intensity resulting from variations of the distance between the layer of mesotron production and the place of observation, which distance operates through mean-life on the cosmic-ray intensity. We have developed an expression for the percentage change of intensity at any altitude resulting from unit change in the aforesaid distance, this expression taking into account the energy distribution function and the lower limit of energy as determined by the energy necessary to penetrate the apparatus. Data supplied by the Weather Bureau show that observations extending over a single day may experience a change of 100 meters or even more in the aforesaid distance. Our calculations show that with a change of 100 meters at an altitude of 30,000 ft. with a lower energy limit determined by 9 cm of lead, the effect on the

cosmic-ray intensity amounts to 2.1 percent. With a lower limit determined by 18 cm of lead, the effect is 1.8 percent.

* Assisted by the Joint Program of ONR and AEC.

P2. Penetrating Power of Extensive Shower Particles.* L. D. WHITE, G. G. HARRIS, AND GEORGE T. REYNOLDS, *Princeton University.*—Previously reported experiments[1] to measure the absorption in load of particles associated with sea level extensive cosmic ray showers have been continued. In these experiments an extensive shower is selected by means of master coincidence trays of Geiger counters separated by a distance of about 4.5 meters. This master coincidence gates 6 other channels of Geiger counter trays under various thicknesses of lead, so that several lead thicknesses can be investigated simultaneously. A cloud chamber was placed on top of 11 inches of lead over one of the counter trays, and some pictures were obtained of the particles which might have tripped these counters. The absorption curve obtained for the extensive shower particles agrees well with the earlier results[1] and the recent results of Cocconi.[2] The fraction of particles able to penetrate 11 inches of lead is found to be 0.018 ± 0.005.

* Supported by joint program of ONR and AEC.
[1] Reynolds and Hardin, Phys. Rev. **74**, 1549 (1948).
[2] Cocconi, Tongiorgi, and Greisen, Phys. Rev. **75**, 1063 (1949).

P3. The Positive Excess in the Mesotron Spectrum.* ROBERT B. BRODE, *University of California, Berkeley.*—A Geiger counter experiment has been devised that measures the number of positive and negative particles in the energy band between 1.4 and 2.0 Bev. The particles are deflected through two feet of iron in which a field of 14,000 gauss is maintained by Alnico permanent magnets. The field in the Alnico blocks is reversed at regular intervals and the entire apparatus inverted at other intervals. By either of these procedures the sensitivity of a counter system to positive or negative particles is interchanged. The apparatus, operated at an elevation of 100 meters above sea level, has given 1.37 ± 0.04 as the ratio of positive to negative particles. This is appreciably higher than the value of 1.20 ± 0.04 given by previous[1] Geiger counter observations.

* Assisted by the joint program of ONR and AEC.
[1] Bernardini, Conversi, Pancini, Scrocco, and Wick, Phys. Rev. **68**, 109 (1945).

P4. Examples of Meson Production and Absorption.* R. L. COOL, E. C. FOWLER, AND J. C. STREET, *Harvard University.*—An 18-inch cloud chamber containing 3 lead plates, about 1 cm each, and 8 aluminum foils, 0.020 cm thick, has been operated for five months at Climax, Colorado (11,200 ft.). Some 24,000 expansions have been photographed, 7,000 random, 12,000 anti-coincidence for stopped mesons, and 5,000 with a simple shower selector. Particles in the lower energy range can, in many cases, be identified by study of the ionization, range and scattering. Five interactions have been observed in which, it is believed, mesons were produced. One of these is believed to show 2 mesons from one center. Twenty-three cases of mesons stopping in the thin foils have been identified. Of these, 10 show decay electrons, 12 show no additional track at the end point, one has a dense track coming back from the end point and stopping in the adjacent foil. The frequency of these events, not selected by counters, is in reasonable agreement with photo-plate data.

* Assisted by the joint program of ONR and AEC.

P5. Spontaneous Decay Rate of Heavy Mesons. L. I. SCHIFF, *Stanford University.*—The assumption[1] of direct interactions between nucleons and light mesons (μ), and between nucleons and electrons (e), leads to heavy meson (π) decay as a second-order process through the intermediate nucleon field, quite apart from any direct $\pi-\mu$ or $\pi-e$ coupling. The computed probabilities for both decay processes diverge in the same way. If the divergent integrals are cut off in the relativistic region, the computed life times have the order of magnitude but are somewhat shorter than the observed life time for $\pi-\mu$ decay. The ratio of the computed life times for $\pi-\mu$ and $\pi-e$ decay does not involve the divergent integral, and is approximately equal to four. This seems to disagree with experimental results at Berkeley, in which few if any $\pi-e$ decays are observed. Thus if the direct couplings of nucleons with μ and e are accepted, one must (1) also postulate a direct $\pi-\mu$ coupling, and (2) so interpret the divergent integrals that they are much smaller than they are when the relativistic cut off is used.

[1] J. Tiomno and J. A. Wheeler, Rev. Mod. Phys. **21**, 153 (1949).

P6. High Energy Events at High Altitude.* J. HORNBOSTEL AND E. O. SALANT, *Brookhaven National Laboratory.*—At 93,000 feet, production of many-pronged stars in nuclear emulsions at 31° geomagnetic latitude (cut-off 8 Bev) is about 0.3 production at 57°. Cross section for disintegration of Ag and Br nuclei by primaries is 0.5 (± 0.3) of geometrical cross section. On minimum ionization plates (Eastman NTB3), about 40 percent of these show, in addition to customary heavy, unoriented tracks, a broom-like bundle of relativistic particles fanning out downwards. In many of such broom events, the star has a single minimum ionization track in the hemisphere above it; this track is consistent in energy and location with being due to the incident particle. The broom consists, on the average, of 5 (but sometimes as high as 15) light tracks, within a cone of 120°; two-thirds of these tracks have true minimum ionization. Reasons for regarding the collimated events, in part at least, as creation of fast mesons by primaries of energy greater than cut-off are presented. We particularly thank ONR and officers and men of USS Saipan.

* Research carried out at the Brookhaven National Laboratory under the auspices of AEC.

P7. Measurements and Interpretation on the "Showers" Associated with Stars in Nuclear Emulsions.* L. S. OSBORNE AND B. T. FELD, *Massachusetts Institute of Technology.*—In Eastman NTB3 emulsions, exposed as described in the previous abstract, an appreciable fraction of the nuclear disintegrations emit, in addition to the isotropically distributed, low energy evaporation products, a group (shower) of particles of relativistic energies, confined within a relatively narrow cone of angles in the downward direction. We have observed, in one star, 18 fast particles within a cone of 63° apex; 15 lie within 33°. In this event, the "cone" is really a "whiskbroom," of maximum angle quoted above. The spread along the minor axis is 10–15°. Of the 18 particles, 11 have grain densities corresponding to minimum ionization. The largest grain density corresponds to a kinetic energy of ~ 0.2 rest energy. It can be shown that the "slow" particles are certainly not electrons. Other showers studied have smaller multiplicity and do not show the "whiskbroom" effect. Measurements of multiplicity, angular spread, and grain counts have been made on a number of such showers. Evidence concerning the nature of the shower particles will be discussed. An interpretation of the data is attempted on the basis of the assumption that a shower results from a nucleon-nucleon collision, in which the nucleons lose most of their kinetic energy (in the cm system) by the multiple production of π-mesons.

* Assisted by the joint program of ONR and AEC.

P8. Energy Degeneration of Cosmic-Ray Primaries. F. J. MILFORD AND L. L. FOLDY, *Case Institute of Technology.*—Under the assumption that a meson-producing collision be-

tween two nucleons at relativistic energies is completely inelastic and that the cross-section is independent of energy, one may calculate the energy degeneration of the primary cosmic rays (assumed to be protons) and the energy spectrum of the high energy nucleons as a function of the depth in the atmosphere for any primary spectrum. Binding of nucleons into nuclei is neglected except for the "shadow effect" on the mean-free-path. An analytic solution is readily obtained for the energy spectrum as a function of depth for kinetic energies greater than 1 Bev, where ionization energy loss is negligible, and $v \simeq c$. For an incident power law differential energy spectrum $N(E)=kE^{-s}$, the same power spectrum is preserved for energies $E \gg t^{1/(s-1)}-2$ where t is the depth in mean-free-paths, but deviations toward greater populations occur for energies below this limit. Calculations are in progress for an incident power law energy spectrum with low energy cut-off to represent the geomagnetic cut-off. Measurements of the energy spectrum of nucleons in the energy range from 1 Bev. to the geomagnetic cut-off at various depths should provide a fairly sensitive test for the postulated assumptions concerning meson-producing collisions.

P9. Rotating Illumination Method of Locating Stars in Nuclear Track Plates.* E. H. LAND AND W. A. SHURCLIFF, *Polaroid Corporation.*—Stars are usually found by bright-field microscope method affording limited field of view and requiring continual focusing up and down. Ordinary dark-field illumination fails due to background scattering by fog grains. A rotating-azimuth planar illumination scheme has been developed which provides good contrast for finding stars in emulsions whose fog background is not excessive. The dark-field illuminating rays, roughly in a single vertical plane, are 20° to 45° from the vertical and intersect in the horizontal emulsion. Tracks perpendicular to the illuminating plane gleam; others are almost invisible. As the illuminating plane rotates at 1 r.p.s. all tracks gleam successively. Magnification as low as 50× is permissible, affording a field of 3 mm diameter. Since effective depth of field is roughly 100 microns, continual focusing is unnecessary even for 200-micron emulsions. The nuclear track group at Brookhaven has not found the method applicable to differentiating tracks of different type or to locating individual tracks in very foggy emulsions, but reports five-fold faster locating of stars in favorable cases of minimum ionization plates.

* Work performed under contract with Brookhaven National Laboratory.

P10. Background Eradication of Thick-Layered Nuclear Emulsions. M. WIENER, *National Bureau of Standards* AND H. YAGODA, *National Institute of Health.*—A method for eradicating accumulated background on Ilford C-2 Plates, 100–200 microns thick without reducing their sensitivity to medium ionizing particles is described. The method involves a mild oxidation of the emulsion by air saturated with water vapor at 35°C for a period of about 16 hours. The plates are then dried and are ready for experimental exposure. Analysis of grain counts shows no loss of sensitivity in proton tracks over their last 200 microns range when the plates are developed with a mild hydroquinone developer. Complete eradication of background alpha tracks and stars is secured as well as destruction of latent images of the less ionizing proton recoils instigated by external neutron bombardment. Grain density studies on proton tracks located at different depths in the emulsion indicate substantially uniform sensitivity after eradication except for the uppermost 50 microns which develop with about a 10 percent reduction in mean grain density as compared with tracks deep within the recording medium.

Metal Physics

Q1. Electronic Phase Transition in Iron at Extreme Pressures. W. M. ELSASSER AND I. ISENBERG, *University of Pennsylvania.*—Bridgman[1] found a pronounced phase transition in metallic cesium at 45000 atm. Compression up to this point is $V/V_0=0.51$; in the transition $\Delta V/V_0=-0.056$. According to Sternheimer's theory[2] the valence electron changes here from the 6*s* to a 5*d* orbital. There are theoretical indications that similar transitions occur in other metals at pressures well beyond laboratory range. There exists, *inside* the earth's core, a well established seismic discontinuity at $p=3.1\cdot10^6$ atm. V/V_0 and $\Delta V/V_0$ are known with moderate accuracy; they are similar to those in Cs. Interpretation, if any, has been *ad hoc*, as a transition between liquid and solid iron. We find that a $4s-3d$ electronic transition leaving iron in a $(3d)^8$ configuration might lead to a quite satisfactory explanation. So far the theoretical data are rather crude and do not as yet permit the quantitative identification toward which we are working. The difficulties of interpreting the discontinuity are very serious on the other hand, if one abandons the current assumption that the main constituent of the core is iron throughout.

[1] P. W. Bridgman, Proc. Am. Acad. Arts Sci. **76**, 55 (1948).
[2] R. M. Sternheimer, Phys. Rev. **75**, 888 (1949); detailed paper in print.

Q2. Martensitic Transformations in Iron-Nickel. ANDREW W. MCREYNOLDS, *Brookhaven National Laboratories.*—Transformations of crystal structure in solids occur either by a diffusion growth process or by a martensitic transition, characterized by practically instantaneous formation of plates of the new phase. Electrical and direct visual observations on Fe-Ni 71-29 alloys have been made in connection with studies of effects of strain on the transformation, and show that: (1) Quenching to a temperature in the range below −30°C results in instantaneous partial transformation followed by isothermal transformation for several minutes at decreasing rate, approaching an amount characteristic of temperature. (2) Such isothermal transformation following quenching continues at any temperature up to 20°C. The martensitic character of the isothermal transition has been verified by visual observation of the formation of plates during reheating. (3) During continuous cooling, transformation occurs initially in large steps, each representing transformation of an appreciable fraction of the total volume, and each being accompanied by instantaneous appearance of large complexes of many plates extending across many grains. Subsequent transformation occurs as smaller complexes or individual needles in the remaining interstices.

Q3. Surface Impedance of Metals at 24000 Mc/sec.* W. B. NOWAK AND J. C. SLATER, *Massachusetts Institute of Technology.*—The skin conductivity Σ,[1] of copper, silver, tin, and lead has been measured at 24000 Mc/sec. from 300°K to 4°K, and follows the theory[2] qualitatively. Surface roughness, rather than cold work, oxide layers, etc., largely accounts for low absolute values of Σ, particularly at low temperatures, and no essential disagreement with theory is found that is not explicable by roughness. Low temperature asymptotic values of Σ (in mhos) are: 93.5 for the best copper surface, 61.8 for electropolished copper, 59.8 for electropolished silver, 68.4 for tin cast against glass, and 46.5 for finely machined lead. A semi-theoretical surface roughness correction factor, applied to Σ, raises the values to 103.4 mhos for the best copper, 89.6 for electropolished copper, 74.8 for electropolished silver, and 88.4 for lead. The value of Σ for tin agrees well with unpublished results of I. Simon at 9000 Mc/sec., thus checking the theoretical frequency dependence of Σ. Computed values for the number of free electrons per atom are discussed.

* This work has been supported in part by the Signal Corps, Air Materiel Command, and ONR.
[1] A. B. Pippard, Proc. Roy. Soc. **A191**, 385 (1947).
[2] G. E. H. Reuter and E. H. Sondheimer, Proc. Roy. Soc. **A195**, 336 (1948).

Q4. Lattice Energy, Lattice Constant and Compressibility of Metallic Copper and Silver. THOMAS P. MERRITT AND ROYAL M. FRYE, *Boston University*.—A careful investigation of previous quantum mechanical treatments of lattice energy, lattice constant and compressibility of metallic copper and silver has been made. Serious discrepancies prompted a renewal of calculations, the results of which indicate the error to exist in the previous calculations for copper. The results of the present work together with earlier investigations and experimental determinations are given in Table I.

TABLE I

	Cohesive energy	Lattice constant	Compressibility
Copper			
Theoretical (as determined in this work)	112 kg cal./mole	1.98A	0.0082×10^{-11} cm²/dyne
Experimental	71.0	3.6	0.070×10^{-11}
K. Fuchs (Reported)	34.1	4.2	0.069×10^{-11}
(From his graphs)	34.1	4.6	0.545×10^{-11}
Silver			
Theoretical (as determined in this work)	71.8 kg cal./mole	2.57A	0.035×10^{-11} cm²/dyne
Experimental	64.5	4.03	0.090×10^{-11}
R. C. Gunter	95.8	2.72	(0.056×10^{-11})

Q5. Elastic Constants of Single Crystals of Nickel. W. P. MASON, R. M. BOZORTH, H. J. MCSKIMIN, J. G. WALKER, *Bell Telephone Laboratories*.—Measurements have been made of the elastic constants of nickel, using two specimens of single crystals grown by slow cooling of the melt. Planes were cut parallel to (100) and (110) within less than one degree as determined with x-rays. Thin crystals of quartz were cemented to these surfaces and velocities of elastic waves determined by pulsing methods. In a more satisfactory arrangement two fused silica rods were fastened to opposite sides of a nickel crystal with the interposition of polystyrene films a quarter wave-length thick, and quartz crystals were placed at the other ends of the rods. The longitudinal or shear wave excited by one of the crystals was reflected multiply in the nickel and detected by the other crystal. The pulses were made longer than the time between reflections and the pulsing frequency adjusted until all pulses added in phase, and the velocity then calculated from this frequency. Results are: $c_{11}=2.50$, $c_{12}=1.60$, $c_{44}=1.185$, all times 10^{12}. The anisotropy factor, $2c_{44}/(c_{11}-c_{12})$, is 2.63. In the longitudinal [100] wave at 10 Mc/sec., $Q=300$. The decrement (π/Q) increases approximately as f, indicating magnetic damping from micro eddy currents.

Q6. Strain Rate Effects in Polycrystalline Cadmium Wire. RICHARD LATORRE AND WALLER GEORGE, *Naval Research Laboratory*.—The strength of polycrystalline high purity cadmium wire (".005 diameter) strained at controlled rates from 10^{-6} to 10^{-2} sec.$^{-1}$ shows a rapid increase for true strain rates between $10^{-5}-10^{-3}$ sec.$^{-1}$. Through this region the rupture load varies from approximately 20 g to 60 g. Load-strain curves show, in general, a region from small to medium "homogeneous" strains where the load resisting deformation remains essentially constant. For larger strains, at strain rates greater than 10^{-3} this load increases with strain. For strain rates below 10^{-5} the load drops with increasing strain. The time during which the resistant load is essentially constant varies from about 20 sec. at strain rates of 10^{-3} to about 2400 sec. at 10^{-5} sec.$^{-1}$. The former time is, to order of magnitude comparable, to the "incubation times" recently reported by Wood for mild steel.[1] Our data suggest that the nucleation mechanisms in cadmium for strain softening may be different from those for strain hardening (work hardening). Other features of the stress-strain relationship at constant true straining rates appear quite analogous to those obtained for single crystals.[2,3]

[1] D. S. Wood, Second Symposium on Plasticity, Brown Univ., April 1949.
[2] E. N. da C. Andrade and R. Roscoe, Proc. Phys. Soc. (London) **49**, 152 (1937).
[3] W. Boas and S. Schmid, Zeits. f. Physik **54**, 16 (1929); *ibid.* **61**, 767 (1930).

Q7. Anomalous Internal Friction Associated with the Precipitation of Cu in Plastically Deformed Al-Cu Alloys. T'ING-SUI KÊ, *University of Chicago*.—Anomalous internal friction at small stress levels has been observed in plastically deformed aluminum-copper alloys heat-treated short of complete recrystallization. The temperature range within which such anomalous internal friction was observed is −5 to 125°C in the case of aluminum specimens containing ½ percent of copper. At each temperature within the range, the anomalous effect first increases and then decreases with the aging time at that temperature. This effect is shown to be associated with the precipitation of Cu from the solid solution with aluminum. It seems to be correlated with the well-known phenomena of precipitation hardening except that it proceeds at a much faster rate. The internal friction associated with this effect is anomalous in the following aspects: (1) At a given temperature, it first increases and then decreases with decreasing stress amplitude; (2) the value of internal friction at a given temperature is temporarily reduced by previous vibration. The frequency of vibration used was about one cycle per second in torsion and the maximum shearing strain on the specimen was about 10^{-5}. The physical origin of this internal friction and its implications will be discussed.

Q8. The Increase in the Resistivity of Ordered $AuCu_3$ Produced by Single Slip. T. H. BLEWITT* AND J. S. KOEHLER, *Carnegie Institute of Technology*.—Single crystals of $AuCu_3$ were produced in a high vacuum by the Bridgman method using 99.999 percent pure copper and gold. The tensile specimens of ⅛" diameter (ASTM specifications) were homogenized and ordered. The electrical resistances were measured potentiometrically from 90 to 300 degrees absolute. Residual resistances were obtained by fitting Gruneisen's equation using Matthiesson's rule. It was found that the characteristic temperature of the undeformed specimens was 275 degrees with a residual resistance of 1.36 micro-ohm centimeters. Upon deformation the residual resistance does not change; for a bicrystal, at 30 percent shear strain (15 percent elongation) the residual resistance changes by about 1 percent with no change being apparent in the characteristic temperature. Dahl[1] deformed polycrystals and obtained much larger resistance changes. The stress-strain curves obtained were in substantial agreement with those of Sachs and Weerts.[2] Calculations made using Taylor's theory of deformation and a variation of Muto's treatment of the resistance of disorder gave resistance changes many times larger than those observed.

* AEC Fellow in the Physical Sciences. Supported by ONR.
[1] O. Dahl, w. Metallkunde **28**, 133 (1936).
[2] G. Sacks and J. Weerts, Zeits. f. Physik **67** (1931).

Q9. Grain Boundary Diffusion. M. R. ACHTER AND R. SMOLUCHOWSKI, *Carnegie Institute of Technology*.—One of the least known parts of a polycrystalline material is its grain boundary. As an indication of the degree of perfection of and the mobility of atoms in, the boundary layer, diffusion along the grain boundaries is being studied by means of x-ray, electrographic, and microscopic methods. Preliminary results indicate that the rate of diffusion is influenced by the relative orientations of the two grains forming the boundary. This behavior would be predicted from a study of a rough model of a grain boundary, and agrees with the fact that a grain boundary between two fixed grains has a preferred orientation

of lowest energy. From the rough data, it has been possible to obtain a comparison of the rates of grain boundary diffusion to the rates of volume diffusion in the case of silver diffusing into copper. This estimate, made on copper in which all grains had one cubic axis almost parallel to the direction of diffusion, indicates that the activation energy for the grain boundary diffusion is 20,000 calories smaller than that for the volume diffusion.*

* Work done under contract with the AEC.

Q10. Mechanism of Ordering in Co-Pt. J. B. NEWKIRK AND R. SMOLUCHOWSKI, *Carnegie Institute of Technology.*—As part of a study of the influence of order on magnetic properties, a detailed investigation of atomic ordering in the ferromagnetic Co-Pt (50-50) alloy is being continued.* X-ray studies are being made on powders and single crystals. The results show that ordered and disordered phases can coexist, thus indicating that the reaction is of a heterogeneous character. It is believed that at least with the tetragonal type ordered lattice this is a general characteristic, all indications to the contrary being due to the inadequacy of the experimental methods. The structure of the surface material appears to influence the critical temperature of that layer or the rate at which the ordering reaction can take place there. Microscopic evidence indicates the existence of a fine structure within the grains which resembles polygonalization or mosaic structure observed in pure metals. A possible relation of this structure to order is considered. Single crystal work shows the presence of lattice strains and aperiodic regions (order-disorder layers) which are parallel to the (111) planes. This is in agreement with the minimum strain condition of the tetragonal ordered structure.

* Work done under contract with the AEC.

Q11. Magnetostriction and Order in $FeNi_3$. J. E. GOLDMAN, *Westinghouse Research Laboratories.*—The magnetostriction of the alloy $FeNi_3$ was measured as a function of the state of order. The strain gauge technique previously described was employed for this purpose.[1,2] Samples of the 76.5 percent nickel vacuum melted alloy $3\times3\times0.05$ cm were cut and measurements were made in both long directions in order to eliminate errors due to the possible non-randomness of the initial domain distribution. The ordered samples were heated to 600°C for 24 hours and then cooled through the critical temperature at the rate of 2°C per hour to 300°C. The disordered samples were measured in the cold worked state after a cold reduction of 75 percent. The saturation magnetostriction is found to increase by more than 100 percent on ordering. The magnitude of the magnetostriction in the cold worked sample is 1.9×10^{-6} and in the annealed sample is 4.15×10^{-6}. The latter value is in closer agreement with the value reported by various investigators for an alloy of this approximate composition which may indicate that most of these investigators employed at least partially ordered samples.

[1] J. E. Goldman, Phys. Rev. **72**, 529 (1947).
[2] J. E. Goldman and R. Smoluchowski, Phys. Rev. **75**, 140 (1949).

Q12. Rate of Self-Diffusion in Single and Polycrystals of Silver.* D. TURNBULL, *General Electric Research Laboratory.*—At comparatively high temperatures (800–950°C) the self-diffusion coefficients, D, in single and polycrystalline silver specimens were found in good agreement with those measured by Johnson[1] on large-grained silver specimens. In the low temperature range (500–600°C) D for single crystals agreed closely with the values calculated from the relation valid at high temperatures which was: $D=0.90\exp(-46{,}000/RT)$ cm^2 $sec.^{-1}$. Also in this temperature range D for single crystals slow-cooled from high temperatures agreed, within experimental errors, with D for single crystals rapidly cooled from high temperatures. The apparent D for fine-grained silver (mean linear grain dimension = 1.36 mils.) was much larger than for single crystals in the low temperature range and followed the relation: $D=2.3\times10^{-5}\exp(-26{,}100/RT)$.

* This work was sponsored by the Research Division of the AEC.
[1] W. A. Johnson, Trans. A.I.M.E. **143**, 107 (1941).

Molecular Spectra, Mostly Microwave

R1. Rotational Magnetic Moments for H_2O and HDO. C. K. JEN, *Harvard University.*—The rotational g-factors for H_2O and HDO have been studied by observing the Zeeman splitting of their rotation lines in the microwave spectrum. For the σ-components of the $5_{-1}-6_{-5}$ line of H_2O (22,235.22 mc/sec.), the Zeeman splitting resolved into a doublet pattern for a field as low as 300 oersteds. The doublet separation was found to be a linear function of the field except that each doublet component became continuously weaker and broader with increasing field and was hardly recognizable beyond 2500 oersteds. The measurement gave for this line $g'=h\Delta\nu/\beta H_0=0.586\pm0.012$, where $\Delta\nu$ = frequency displacement of each doublet component, h = Planck's constant, β = nuclear magneton, and H_0 = magnetic field. The Zeeman patterns for the $4_{-3}-3_1$ line (20,460.40 mc/sec.) and the 5_0-5_1 line (22,307.67 mc/sec.) of HDO were similar to that of the above-mentioned H_2O line as regards doublet appearance and linearity with magnetic field. However, the 5_0-5_1 line showed a sharp doublet pattern for fields as high as 7000 oersteds, whereas the $4_{-3}-3_1$ line pattern became unrecognizably diffuse for fields above 3000 oersteds. The measured g'-values for HDO lines are $g'(4_{-3}-3_1)=0.413\pm0.008$ and $g'(5_0-5_1)=0.465\pm0.009$. It is noteworthy that the ratio of $g'(H_2O)$ to $g'(HDO)$ is close to the ratio of the reduced mass $\mu(HD)$ to $\mu(H_2)$. This suggests that the rotation of the hydrogen or deuterium atoms contributes a large proportion of the molecular g-factor for a water molecule.

* Supported by ONR contract.

R2. On the Limits of Validity of the Van Vleck-Weisskopf Line Shape Formula.* P. W. ANDERSON, *Bell Telephone Laboratories.*—By use of the Einstein relations the line shape in gaseous absorption can be derived rigorously from that for spontaneous emission, $I(\nu)$. $I(\nu)$ is given, if the translational motion of the emitting molecules can be assumed to be classical, by the well-known Fourier integral formula or by a more rigorous variation thereof derived by the author.† The solution of either type of Fourier integral for sufficiently low pressures is the standard dispersion line shape. The Einstein relations applied to the correct dispersion shape give the Van Vleck-Weisskopf line shape at microwave frequencies. The conditions under which this line shape fails can be two-fold: either the low-pressure solution of the Fourier integral fails, or the classical treatment of translational motion becomes invalid. Reasons are advanced which indicate that the latter is always the case at frequency differences from the line center of greater than kT/h.

* J. H. Van Vleck and V. F. Weisskopf, Rev. Mod. Phys. **17**, 227 (1945).
† Unpublished.

R3. The Radiofrequency Spectrum of $Rb^{85}F$ and $Rb^{87}F$. VERNON HUGHES, LUDWIG GRABNER, AND I. I. RABI, *Columbia University.*—The radiofrequency spectrum of $Rb^{85}F$ and $Rb^{87}F$ had been studied by the molecular beam electrical resonance method.[1,2] The main features of the spectrum for either isotope are predicted from a Hamiltonian:[2,3]

$$H=+\frac{\hbar^2}{2A}\mathbf{J}^2-\boldsymbol{\mu}\cdot\mathbf{E}-\frac{e^2q_1'Q_1}{I_1(2I_1-1)(2J-1)(2J+3)}\times\{3(\mathbf{I}_1\cdot\mathbf{J})^2+\tfrac{3}{2}(\mathbf{I}_1\cdot\mathbf{J})-\mathbf{I}_1^2\mathbf{J}^2\}.$$

However, a splitting of the lines is observed, which suggests that a small interaction of the form $c_2 I_2 \cdot J$ be added to this Hamiltonian.[2,3] (I_2 is spin of F.) The data are:

		$\lvert e^2q_1'Q_1\rvert$	
J	V	$Rb^{85}F$ (mc/sec.)	$Rb^{87}F$ (mc/sec.)
1	0	35.158±0.06	17.000±0.02
1	1	34.772±0.06	16.814±0.02
1	2	34.358±0.06	16.600±0.02
1	3	33.997±0.06	
1	4	33.597±0.06	

where J=rotational quantum number, V=vibrational quantum number, $e^2q_1'Q_1$=quadrupole interaction constant of Rb in RbF. An "extra" line was observed and is tentatively believed to be a two-quantum process.

[1] H. K. Hughes, Phys. Rev. **72**, 614 (1947).
[2] J. W. Trischka, Phys. Rev. **74**, 718 (1948).
[3] W. A. Nierenberg *et al.*, Phys. Rev. **73**, 1430 (1948).

R4. The Radiofrequency Spectrum of $K^{39}F$. LUDWIG GRABNER, VERNON HUGHES, AND I. I. RABI, *Columbia University.*—The radiofrequency spectrum of $K^{39}F$ has been studied by the molecular beam electrical resonance method.[1,2] The Hamiltonian is:[3]

$$H=+\frac{\hbar^2}{2A}\mathbf{J}^2-\boldsymbol{\mu}\cdot\mathbf{E}-\frac{e^2q_1'Q_1}{I_1(2I_1-1)(2J-1)(2J+3)}\times\{3(\mathbf{I}_1\cdot\mathbf{J})^2+\tfrac{3}{2}(\mathbf{I}_1\cdot\mathbf{J})-\mathbf{I}_1^2\mathbf{J}^2\}.$$

The data are:

J	V	$-e^2q_1'Q_1$ (mc/sec.)
1	0	3.969±0.02
1	1	3.914±0.02
1	2	3.872±0.02
1	3	3.829±0.02
2	0	3.964±0.02
2	1	3.914±0.02
2	2	3.863±0.02

where J=rotational quantum number, V=vibrational quantum number, $e^2q_1'Q_1$=electrical quadrupole interaction constant of K^{39} in $K^{39}F$.

[1] H. K. Hughes, Phys. Rev. **72**, 614 (1947).
[2] J. W. Trischka, Phys. Rev. **74**, 718 (1948).
[3] W. A. Nierenberg *et al.*, Phys. Rev. **73**, 1430 (1948).

R5. The Molecular Structure and Dipole Moment of Chlorosilane.* B. P. DAILEY, J. M. MAYS, AND C. H. TOWNES, *Columbia University.*—Three previously unreported lines arising from the $J=1\rightarrow2$ rotational transitions of the rarer isotopic species of chlorosilane, $Si^{29}H_3Cl^{35}$, $Si^{29}H_3Cl^{37}$, and $Si^{30}H_3Cl^{35}$, have been observed. The transitions involving Si^{29} are being studied further. The accurately measured $Si^{30}H_3Cl^{35}$ frequency combined with those of Sharbaugh[1] gives the following values of Bo in Mc/sec.=$Si^{28}H_3Cl^{35}$, 6,673.8; $Si^{28}H_3Cl^{37}$, 6,512.4; $Si^{30}H_3Cl^{35}$, 6,485.8. From these data, the molecular parameters, uncorrected for zero-point vibrations, Si-Cl distance 2.05A, Si-H 1.50A, and H-Si-H angle 110° 57′, are obtained. These are to be compared with the previous values[1] 2.035A, 1.456A, and 103° 57′, respectively. The new H-Si-H angle is seen to be slightly larger than the tetrahedral angle of 109° 28′, and very close to the values reported for the methyl halides by Gordy.[2] In addition, measurement of the Stark displacement of the $J=1\rightarrow2$, $F=5/2$, $7/2$, $K=1$ line of $Si^{28}H_3Cl^{35}$ as a function of field strength yields a dipole moment of 1.311 Debye units, as compared with the earlier value of 1.284±0.005 obtained from polarization measurements.[3]

* Work supported jointly by the Signal Corps and ONR.
[1] A. Sharbaugh, Phys. Rev. **74**, 1870(L) (1948).
[2] Gordy, Simmons, and Smith. Phys. Rev. **74**, 243 (1948).
[3] Brockway and Coop, Trans. Faraday Soc. **34**, 1429 (1938).

R6. Dipole Moments from Microwave Spectra.* C. H. TOWNES, R. G. SHULMAN, AND B. P. DAILEY, *Columbia University.*—The dipole moments of several molecules have been determined by measurements of the Stark splitting of the quadrupole components of rotational transitions in the microwave region. A Stark modulation microwave spectroscope was used and the method and calibrations have been reported.[1] On the basis of the theory of Low and Townes[2] the splittings of the first-order lines of AsF_3 and CH_3I were calculated. By selecting the transition observed it was possible to find the splitting as a solution of a second order equation. The calculations for the highest values of F and M are the simplest for these molecules and also for the second-order Stark splitting of CH_3Cl^{35} which was calculated by Fano's[3] method. In all cases the accuracy was greater than one percent. The moments of $N^{15}N^{14}O^{16}$ and CH_3CF_3 were also measured and the values given below in Debye units. $CH_3Cl^{35}\mu=1.871\pm0.005$; $CH_3I\mu=1.658\pm0.014$; $AsF_3\mu=2.834\pm0.025$; $CH_3CF_3\mu=2.35\pm0.02$; $N^{15}N^{14}O^{16}\mu=0.167\pm0.002$.

* Work supported jointly by the Signal Corps and ONR.
[1] R. G. Shulman and C. H. Townes, Phys. Rev. **75**, 1318 (1949).
[2] W. Low and C. H. Townes, Phys. Rev. **75**, 1319 (1949).
[3] U. Fano, J. Research Nat. Bur. of Stand. **40**, 215 (1948).

R7. Microwave Spectrum of Formaldehyde.* R. B. LAWRANCE, R. L. KYHL,** AND M. W. P. STRANDBERG, *Massachusetts Institute of Technology.*—H_2CO is a slightly asymmetric rotor whose absorption spectrum has been extensively studied in the infra-red[1,2] and ultraviolet.[3] The asymmetry removes the symmetric-top K degeneracy, giving a wealth of $\Delta J=0$ lines in the accessible microwave region. Bragg and Sharbaugh[4] have identified four of these pure rotation lines in the region 18,300–27,500 megacycles. We have explored the region 14,000–73,000 megacycles, with some gaps. Our measurements of the $0_{00}\rightarrow1_{01}$ line and the homologous series $2_{12}\rightarrow2_{11}\cdots5_{15}\rightarrow5_{14}$ give exceedingly accurate values of the reciprocal moments b and c. Several lines from each of the K_{-1} sequences 2, 3, and 4 have been measured and afford rather accurate centrifugal-distortion corrections. In several lines, the effective dipole moment has been evaluated by means of the Stark effect.

* This research has been supported in part by the Signal Corps, the Air Materiel Command, and ONR.
** Now at Stanford University.
[1] H. H. Nielsen, Phys. Rev. **46**, 117 (1934).
[2] E. S. Ebers and H. H. Nielsen, J. Chem. Phys. **5**, 822 (1937).
[3] G. H. Dieke and G. B. Kistiakowsky, Phys. Rev. **45**, 4 (1934).
[4] Private communication, since published in Phys. Rev. **75**, 1774 (1949).

R8. The Microwave Spectrum of Chloroacetylene and Deuterochloroacetylene. A. A. WESTENBERG, J. H. GOLDSTEIN, AND E. B. WILSON, JR.—The $J=1\rightarrow2$ pure rotational transitions in the linear molecules $H-C\equiv C-Cl^{35}$, $H-C\equiv C-Cl^{37}$, $D-C\equiv C-Cl^{35}$, and $D-C\equiv C-Cl^{37}$ have been observed using a Stark Modulation microwave spectrograph. The frequencies of the principal components (5/2→7/2) of the multiplets are 22738.6$_8$, 22290.8$_5$, 20749.7$_6$, and 20338.2$_9$ megacycles, respectively. The quadrupole hyperfine structure has been analyzed in the usual manner, yielding values for the nuclear quadrupole coupling constants of −79.67, −62.75, −79.66, and −63.12 (mc), respectively. By comparison, the values for $Cl^{35}CN$ and $Cl^{37}CN$ are −83.4 and −65.3. The observed Stark effect is in good agreement with that calculated for a linear molecule with a single quadrupolar nucleus. This leads to a calculated value for the dipole moment of 0.44 ±0.01D. The previously reported value is 0.44±0.01D. Bond distances calculated are H—C=1.052±0.001A, C—C=1.211 ±0.001A, and C−Cl=1.632±0.001A. The previously reported electron diffraction results are C−C=1.21±0.04A and C−Cl =1.68±0.04A. Both the bond distances and the quadrupole coupling constant indicate the presence of important resonating structures in the molecule.

R9. A Reinvestigation of the Vibration Spectrum of Nitrogen Dioxide. M. KENT WILSON, *Harvard University* AND RICHARD M. BADGER, *California Institute of Technology.*—The infra-red spectrum of nitrogen dioxide was investigated under

prism dispersion between 1.5 and 25μ. The weak symmetric valence vibration, heretofore unreported in the infra-red, was found near 1306 cm^{-1} and the center of the bending vibration was located near 755 cm^{-1}. This latter value is in contrast to the value of 648 cm^{-1} previously reported.[1] These observed infra-red frequencies are in good agreement with the values of 1319 cm^{-1} and 749 cm^{-1} which were found to occur in the temperature-sensitive ultraviolet bands of nitrogen dioxide.[2] Both ν_1 and ν_2 exhibit doublet structures with rotational spacing of about 15 cm^{-1}. This spacing leads to a value of A″–B″ in close agreement with that calculated for the obtuse angled structure as determined by electron diffraction.[3] Several infra-red bands ascribed to nitrogen dioxide have been shown by their temperature dependence to belong to nitrogen tetroxide.

[1] R. Schaffert, J. Chem. Phys. **1**, 507 (1933).
[2] Harris, King, Benedict, and Pearse, J. Chem. Phys. **8**, 765 (1940).
[3] Claesson, Donohue, and Schomaker, J. Chem. Phys. **16**, 207 (1948).

R10. Isotopic Frequencies in the Microwave Spectra of OCS and CH_3Cl. D. Bianco, G. Matlack, and A. Roberts, *State University of Iowa.*—Additional isotopic lines have been observed in the microwave spectra of OCS and CH_3Cl. In OCS, a sample enriched in O^{18} (kindly provided by Professor A. O. C. Nier of the University of Minnesota) yielded the following new lines:

Isotope	V_1 V_2 V_3	Frequencies of 1→2 trans.
$O^{18}C^{12}S^{32}$	1 0 0	22754.6 ±0.2 mc
	0 1 0	22871.28±0.1
	0 1 0	22848.70±0.1
$O^{18}C^{13}S^{32}$	0 0 0	22763.8 ±0.2
$O^{18}C^{12}S^{34}$	0 0 0	22239.6 ±0.2

The excited vibrational lines provide proof that the vibration-rotation constant α_1 varies inversely as the $\frac{3}{2}$ power of the total mass. The quadrupole coupling of the O^{17} line has been determined to be not more than 1 mc. In CH_3Cl, triplets have been observed due to the chlorine quadrupole splitting of the 0→1 transitions of $C^{13}H_3Cl^{35,37}$, $C^{12}H_2DCl^{35,37}$, and $C^{12}HD_2Cl^{35,37}$. Accurate values of the frequencies will be presented.

* Supported in part by ONR.

R11. Quadrupole Interactions in Pressure Broadening of Ammonia Inversion Spectrum by Non-Polar Gases.* William V. Smith and Raydeen Howard.—We have measured the N_2-NH_3, O_2-NH_3, and CO_2-NH_3 collision cross sections from the pressure broadening of the ammonia inversion spectrum, finding values relative to the NH_3-NH_3 cross section of 0.202, 0.115, and 0.455. The first two values check Bleaney and Penrose's values,[1] confirming the large cross section for nitrogen. The value for CO_2 may be compared with their value of 0.296 for CS_2 which, with its larger polarizability might be expected to have the larger cross section. The anomalous cross sections of N_2 and CO_2 can be explained on the assumption that these molecules have permanent quadrupole moments of, respectively, 0.06×10^{-16} and 0.29×10^{-16} cm^2. Interaction of the quadrupole and dipole, with an r^{-4} law rather than the r^{-6} law of polarizable molecules gives the required interaction energy at the observed cross section. The triple bond of N_2 with its abnormally large energy of formation suggests a high electronic density between the two nuclei—hence a quadrupole moment. The lower quadrupole moment of CS_2 compared to CO_2 is to be expected from the small difference in electronegativity of carbon and sulfur.

* The research described in this report was supported by Contract No. W-19-122-ac-35 with the Air Forces, Air Materiel Command, Cambridge Field Station.

R12. The Infra-Red Spectrum of Benzene at Liquid-Helium Temperature. R. M. Hainer and Gilbert W. King, *Arthur D. Little, Inc.*—The infra-red absorption spectrum of solid benzene has been investigated between 1200 and 660 cm^{-1} at 4°K, the temperature of liquid helium. These data were obtained with a low-temperature infra-red transmission cell recently described.[1] The sample was deposited from the gas phase and did not scatter infra-red. Bands were found at 1171 (weak), 1145 (w), 1141 (w), 1037.$_5$ (strong), 1033 (s), 1009 (medium), 986.$_5$ (m), 978 (m), 974.$_5$ (m), 706 (s), 680 (v.s.) cm^{-1}. The pairs 1145–1141, 1038–1033, 978–975 cm^{-1} appear to be frequencies degenerate in the isolated molecule, split on the average by 4 cm^{-1} by the crystalline field. Slit widths at 1160, 1000, and 700 cm^{-1} were 3.5, 2.5, and 1.6 cm^{-1} respectively. The half-widths of the bands are in all cases greater. The band at 1171 is absent at 278°K, is apparent at 60°K, then decreases in intensity as the temperature is lowered to 4°K. Recent interpretations[2-4] of the spectrum of benzene are not entirely supported by these results.

[1] McMahon, Hainer, and King, Phys. Rev. **75**, 1320 (1949).
[2] R. D. Mair and D. F. Hornig, Phys. Rev. **75**, 1283 (1949).
[3] C. K. Ingold *et al.*, J. Chem. Soc. 222 (1946).
[4] B. L. Crawford and F. A. Miller, J. Chem. Phys. **17**, 249 (1949).

R13. An Empirical Formula for the Refractive Indices of Infra-Red Dispersing Materials. Gilbert W. King, *Arthur D. Little, Inc.*—D. S. McKinney and R. A. Friedel[1] have shown the calibration curve of a Perkin-Elmer spectrometer can be expressed as a linear relation between the rotation (ϕ) of the wave-length shaft and the quantity $u=1/\nu^2-\nu_0^2$, ν_0 being the first reststrahlen. Since the conditions of dispersion are essentially those of minimum deviation, this result leads to the following empirical formula for the refractive index: $\sin^{-1}n=-k_1u+k_0$ which fits the refractive indices of the common dispersing media within 50 parts per million over the useful range in a spectrometer. For purposes of calibration of wave-length and resolving power the properties of the refracting medium are thus described completely by the single parameter k_1. The calibration curve can be written $(\phi-\phi_0)=2Gk_1u$. Here $G(=798.8)$ is the gear ratio[2] between the wave-length shaft and Littrow mirror and is independent of the prism used. Suitable values of k_1 for KCl, NaCl, CaF_2, LiF are 0.01308, 0.02414, 0.07945, and 0.160×10^6 radians cm^{-2} respectively. Calibration curves from this formula agree within experimental error of locating peaks with those obtained from measurements of known spectra.

[1] D. S. McKinney and R. A. Friedel, J. Opt. Soc. Am. **38**, 222 (1948).
[2] Obtained by private communication with Dr. Van Zandt Williams of the Perkin-Elmer Corporation.

SUPPLEMENTARY PROGRAMME

SP1. Brownian Motion in Liquids.* Frederik J. Belinfante, *Purdue University.*—A simple derivation of Einstein's equation for Brownian motion is given, in which the motion is regarded as the superposition of motions due to single collisions. Correlations between collisions are taken into account only roughly by a phenomenological friction law. For sufficiently large particles one can take Stokes' law for this. The number of thermal collisions against a particle of 0.2μ diameter is about $10^{17}\sim10^{19}$ sec.$^{-1}$, but the number of collisions giving an appreciable impulse to the particle is many times smaller, as simultaneous collisions from different directions tend to neutralize the impulses. Even thus, the number of "effective" collisions during the "relaxation time" of about $10^{-11}\sim10^{-8}$ sec. (time in which velocity is about halved by

friction) is about 10^7, and each such collision alters the velocity only slightly. Thus the actual motion is no zigzag, but is irregularly curved. For very small particles Stokes' law will break down for Brownian motion; the higher the viscosity of the liquid, the sooner this breakdown occurs. (For instance, for glycerin at room temperature, Stokes' law is already inapplicable for particles of 1μ.) Details will appear in the American Journal of Physics.

* To be presented at the end of Session B if the Chairman rules that time permits.

SP2. An Experimental Limit for the Inequality of the Electron and Proton Charges.* VERNON HUGHES, *Columbia University*.—The charge on the CsI molecule is proven to be less than 6.5×10^{-22} e.s.u. or 1.4×10^{-12} of the electronic charge by a deflection experiment on a beam of CsI molecules passing through a homogeneous electric field. This implies that the magnitude of the proton charge equals that of the electron charge to at least 1.3 parts in 10^{14}. By measurement of the charge of a mass of deionized gas, Piccard and Kessler proved that the ratio of the electron charge to the proton charge is $(-1\pm5\cdot10^{-21})$.[1]

* To be presented at the end of Session J if the Chairman rules that time permits.

[1] A. Piccard and E. Kessler, Archives des Sciences Physiques et Naturelles 7, 340 (1925).

SP3. A Theoretical Treatment of Neutron Attenuation in Thick Shields.* S. W. W. SHOR, *Massachusetts Institute of Technology*.†—By application of statistical sampling concepts to the Monte Carlo method, a procedure for computing neutron attenuation through very thick shields has been developed. This method allows computation of the fast flux transmitted through a thick plane shield with the aid of a desk calculator, a table of random numbers, and a table of logarithms. The equation actually being solved in the case of a plane slab is $\gamma(\partial\phi/\partial z)=-\mu\phi+\int_\mu^{\mu_0}\int_\gamma K(\mu,\mu',\gamma,\gamma')\phi d\mu' d\gamma'$. Substitution of $\Phi=\phi e^{\alpha z}$ makes it possible to solve for $e^{\alpha z}$ times the actual flux through the slab. This transformation, apparently devised by Herman Kahn, and John von Neumann's "Russian Roulette" are combined to minimize variance of the transmitted flux. A sample computation was made assuming a beam of fast neutrons incident normally on a plane slab of tungsten about 25 relaxation lengths thick. The computation gave the flux transmitted after one or more collisions with a statistical probable error of less than 10 percent, and required five man-days to complete.

* This is a joint undertaking of M.I.T. and ONR.

† To be presented at the end of Session J if the Chairman rules that time permits.

Author Index to Papers Presented at the Cambridge Meeting

Achter, M. R. and R. Smoluchowski—No. Q9
Adair, R. K., H. H. Barschall, C. K. Bockelman, R. L. Henkel, and R. E Peterson—No. J8
Aiken, Howard—No. I2
Allen, A. J., J. F. Nechaj, K. H. Sun, and B. Jennings—No. J9
Alpert, D., A. O. McCoubrey, and T. Holstein—No. C4
Alvarez, L. W.—No. S1
Anderson, P. W.—No. R2
Apker, L., E. Taft, and J. Dickey—No. O3
Bartlett, James H.—No. H1
Belinfante, Frederik J.—Nos. H6, SP1
Bendt, P. J. and I. W. Ruderman—No. J5
Benfield, A. E.—No. B9
Beyer, Robert T. and Ming-Yi Wei—No. B3
Bianco, D., G. Matlack, and A. Roberts—No. R10
Biondi, Manfred A. and Sanborn C. Brown—No. C3
Bitter, F.—No. L1
Bleaney, B. and D. J. E. Ingram—No. L5
Blewitt, T. H. and J. S. Koehler—No. Q8
Bowers, W. A.—No. L10
Bray, Ralph—No. D3
Brode, Robert B.—No. P3
Bundy, F. P. and H. M. Strong—No. C10
Burwell, J. T. and C. D. Strang—No. B4
Brown, Sanborn C.—No. N1
Cannon, C. V. and G. H. Jenks—No. A14
Carpenter, R. O'B—No. L12
Chambers, William H. and Dudley Williams—No. H10
Conant, J. B.—No. E1
Condon, E. U.—No. F1
Cool, R. L., E. C. Fowler, and J. C. Street—No. P4
Corben, H. C.—No. H3
Crawford, F. H.—No. B8
Dailey B. P. J. M. Mays and C. H. Townes—No. R5
Darrow, K. K.—No. E5
Domenicali, C. A.—No. D11
Dow, W. G.—No. N2
Dryden, H. L.—No. G4
Duckworth, Henry E., Robert F. Black, and Richard F. Woodcock—No. J1
Dunipace, Donald W.—No. K6
Elsasser, W. M. and I. Isenberg—No. Q1
Emmerich, Werner S. and J. D. Kurbatov—No. A8
Fan, H. Y. and R. Bray—No. D4
Farmer, E. C., H. B. Moore, and Clark Goodman—No. A11
Faul, Henry and Clark Goodman—No. J4
Finston, H. L. and R. M. Dyer—No. K10
Foster, J. S.—No. G5
Franzen, W., J. Halpern, and W. E. Stephens—No. J3
Glendenin, L. E. and A. K. Solomon—No. H12
Goldman, J. E.—No. Q11
Goldstein, Louis and Max Goldstein—No. K3
Grabner, Ludwig, Vernon Hughes, and I. I. Rabi—No. R4
Green, Alex E. S.—No. H4
Gugelot, P. C. and M. G. White—No. J7
Gunlock, H. F.—No. A1
Hahn, Erwin L.—No. H9
Hainer, R. M. and Gilbert W. King—No. R12
Hinshaw, R. A.—No. A9
Holstein, T.—No. C5
Holt, R. B., J. M. Richardson, B. Howland, and B. T. McClure—No. C2
Hornbeck, J. A.—No. N3
Hornbostel, J. and E. O. Salant—No. P6
Hudspeth, Emmett L. and Charles P. Swann—No. J10
Hughes, D. J. and M. T. Burgy—No. J6
Hughes, Vernon—No. SP2
Hughes, Vernon, Ludwig Grabner, and I. I. Rabi—No. R3
Hulburt, E. O.—No. K1
Hull, G. F., Sr.—No. E4
Hutter, R. G. E., L. H. McKee, and S. W. Harrison—No. O4
Jen, C. K.—No. R1
Kauffman, John and Waller George—No. L8
Kê, T'ing-Sui—No. Q7
Keller, Joseph M., Ernest Koenigsberg, and Arthur Paskin—No. A12
King, Gilbert W.—No. R13
Land, E. H. and W. A. Shurcliff—No. P9
Lang, R. J. and A. R. J. Stephenson—No. K2
LaTorre, Richard and Waller George—No. Q6
Lawrance, R. B., R. L. Kyhl, and M. W. P. Strandberg—No. R7
Lax, Benjamin and Sanborn C. Brown—No. C8
Linder, E. G. and K. G. Hernqvist—No. N4
Liska, J. W.—No. G2
Loomis, F. W.—No. F3
McReynolds, Andrew W.—No. Q2
Malter, Louis—No. G1
Mandeville, C. E. and E. Shapiro—No. A10
Manning, Thurston E.—No. J11

Marton, L. and S. H. Lachenbruch—No. D12
Mason, W. P., R. M. Bozorth, H. J. McSkimin, and J. G. Walker—No. Q5
Maxwell, Louis R., J. Samuel Smart, and Stephan Brunauer—No. D10
Mendenhall, H. E.—No. D2
Merritt, Thomas P. and Royal M. Frye—No. Q4
Merz, W. J.—No. D9
Milford, F. J. and L. L. Foldy—No. P8
Millikan, R. A.—No. I1
Mingins, Charles R., Carl A. Stevens, and David W. MacLeod, Jr.—No. L11
Moore, Benjamin L.—No. K7
Moore, George E.—No. D1
Newkirk, J. B. and R. Smoluchowski—No. Q10
Nottingham, W. B.—No. O2
Nowak, W. B. and J. C. Slater—No. Q3
Osborne, L. S. and B. T. Feld—No. P7
Otto, William H.—No. K11
Owen, G. E.—No. K9
Oxley, Charles L.—No. H11
Pearson, G. L.—No. D6
Pegram, G. B.—No. E3
Pfann, W. G. and J. H. Scaff—No. D5
Pine, J. and R. Sherr—No. A13
Post, R. F.—No. S2
Price, H. Clay, Jr. and Lawrence M. Langer—No. A7
Robinson, C. V.—No. B2
Rose, M. E.—No. H5
Sachs, A. M., E. H. Turner, and E. M. Purcell—No. L3
Schiff, L. I.—No. P5
Schwinger, J.—No. B10
Schulman, James H., Robert J. Ginther, Clifford C. Klick, and Lyle W. Evans—No. D8
Seidlitz, L., E. Bleuler, and D. J. Tendam—No. A5
Shearer, James W. and Martin Deutsch—No. H13
Shockley, William—No. G3
Shockley, W., G. L. Pearson, M. Sparks, and W. H. Brattain—No. D7
Shor, S. W. W.—No. SP3
Shull, F. B., C. H. Braden, and L. Slack—No. A6
Simons, L. H., D. F. Weekes, and J. G. Potter—No. L9
Slater, J. C.—No. S3
Slichter, C. P. and E. M. Purcell—No. L4
Smith, William V. and Raydeen Howard—No. R11
Sollfrey, William—No. B5
Spencer, L. V. and Fannie Jenkins—No. H14
Stein, Irving and L. I. Schiff—No. H7
Steinberg, Daniel and A. K. Solomon—No. A2
Stewart, A. B.—No. C6
Stewart, James L. and Ellen S. Stewart—No. K4
Strong, H. M. and F. P. Bundy—No. C11
Stuhlman, Otto, Jr.—No. K5
Suits, C. G.—No. F2
Swann, W. F. G. and Stephen H. Forbes—No. P1
Tai, C. T.—No. B6
Teeter, Charles E., Jr.—No. L7
Ter-Pogossian, Michel, J. Eugene Robinson, and Harold Goddard—No. A3
Tomiyasu, K. and Ronald King—No. B7
Townes, C. H., R. G. Shulman, and B. P. Dailey—No. R6
Townsend, J. W., Jr.—No. K12
Turnbull, D.—No. Q12
Turner, E. H., A. M. Sachs, and E. M. Purcell—No. L2
Vallarta, N. S.—No. P11
Varnerin, Lawrence J., Jr. and Sanborn C. Brown—No. C7
Watson, John H. L., Marcel Vanpee, and S. C. Lind—No. L6
Welton, T. A.—No. H2
Westenberg, A. A., J. H. Goldstein, and E. B. Wilson, Jr.—No. R8
White, L. D., G. G. Harris, and George T. Reynolds—No. P2
Wiener, M. and H. Yagoda—No. P10
Williams, F. E.—No. O1
Williams, Thomas W. and James M. Benson—No. C1
Williamson, R. M. and H. T. Richards—No. A4
Wilson, E. Bright—No. I3
Wilson, M. Kent and Richard M. Badger—No. R9
Woo, W. D. and An Wang—No. K8
Wyly, L. D.—No. J2
Young, D. R.—No. C9
Yevick, George J.—No. H8
Yudowitch ,K. L.—No. B1

The Names of Those Who Met on 20 May 1899 to Organize the American Physical Society

This list is not derived from any document contemporary with the event. Ernest Merritt, first Secretary and ninth President of the Society, published it in the Review of Scientific Instruments in March 1934 with the words "so far as can be found from the records." The list is not complete, for on a reprint once in the possession of the present Secretary there were three or four other names added with pen by Dr. Merritt. Any intimations of names which should be added to this list will be gratefully received at the office of the Society.

CLEVELAND ABBE
JOSEPH S. AMES
WILLIAM C. ANDREWS
WILDER D. BANCROFT[1]
CARL BARUS
FREDERICK E. BEACH
FREDERICK BEDELL[2]
HENRY A. BUMSTEAD
HENRY S. CARHART
LEROY C. COOLEY
MORRIS B. CRAWFORD
BERGEN DAVIS[3]
WILLIAM S. DAY
THOMAS W. EDMONDSON
WILLIAM HALLOCK
CHARLES S. HASTINGS
DANIEL W. HERING
GEORGE A. HOADLEY
MARCIA A. KEITH[4]
ARTHUR L. KIMBALL
A. STANLEY MACKENZIE
WILLIAM F. MAGIE
HOWARD MCCLENAHAN
ERNEST MERRITT
ALBERT A. MICHELSON
EDWARD L. NICHOLS
HERSCHEL C. PARKER
B. OSGOOD PEIRCE
MICHEL I. PUPIN
HENRY A. ROWLAND
JOHN S. SHEARER
ALLISON W. SLOCUM
ISABELLE STONE[5]
ELIHU THOMSON
CHARLES C. TROWBRIDGE
FRANK L. TUFTS
FRANK A. WATERMAN[6]
ARTHUR G. WEBSTER

[1] Now living at Ithaca, New York.
[2] Now living in Pasadena, California.
[3] Now living in New York City.
[4] Now living in Braintree, Massachusetts.
[5] Now living in Ponce, Puerto Rico.
[6] Now living in Northampton, Massachusetts.